Analysing the role of SAL1/PAP retrograde signalling within the circadian system of *Arabidopsis thaliana*

By

Suzanne Litthauer

A thesis submitted for the degree of Doctor of Philosophy

School of Biological Sciences

University of Essex

September, 2017

Abstract

Plants have developed an internal timing mechanism, the circadian system, that serves to synchronise physiological and metabolic functions with daily, predictable cues such as dawn and dusk. This endogenous oscillator is comprised of biochemical and transcriptional rhythms that are entrained by environmental signals, particularly light and temperature, through the action of input pathways. The circadian system provides plants with an adaptive advantage, and techniques that allow *in vivo* monitoring of circadian rhythms give valuable insights into the components and mechanisms employed by plants to optimally respond to abiotic signals. This study shows that chlorophyll *a* fluorescence imaging can be used to describe circadian rhythms of PSII operating efficiency (F_q'/F_m') in the chloroplasts of *Arabidopsis thaliana*. These circadian rhythms in F_q'/F_m' are influenced by the well-defined rhythmic transcriptional feedback loops that comprise the central oscillator in the nucleus, and are maintained under constant blue light by the action of phototropin photoreceptors. Using chlorophyll *a* fluorescence imaging, the chloroplast-localised enzyme SAL1 was identified as impacting circadian oscillations both in chloroplasts and in the nucleus. SAL1 is a redox-sensitive component of the SAL1-PAP-XRN retrograde signalling pathway, and influences nuclear gene expression in response to stress by modulating the levels of its substrate, 3'-phosphoadenosine 5'-phosphate (PAP). PAP accumulates in chloroplasts under abiotic stress and inhibits the activity of 5'→3' exoribonucleases (XRNs). This study shows that genetically inducing the SAL1-PAP-XRN pathway in plants lacking SAL1 function induces a long circadian period in a blue light-dependent manner. Application of exogenous PAP or osmotic stress lengthens circadian period, and period lengthening correlates with increases in endogenous PAP levels. Furthermore, plants lacking functional XRNs exhibit a similar long circadian period phenotype. The SAL1-PAP-XRN pathway is therefore proposed to regulate nuclear circadian rhythms in response to changes in chloroplast redox poise, and serves as a possible link between molecular timekeeping and abiotic stress response mechanisms.

Acknowledgements

I am grateful to the University of Essex School of Biological Sciences, The Oppenheimer Memorial Trust (South Africa) and the Gen Foundation for the financial support that made this research possible. A special thank you to Dr Matthew A. Jones for facilitating this work, and for making an immeasurable contribution towards my scientific education through guidance and training. Thank you to Prof Christine A. Raines, Prof Tracy Lawson, Dr Phillip Davey, and Dr Ulrike Bechtold for valuable input throughout the course of this research. Thanks also to Mr Martin Battle and other members of the Jones Lab, as well as to Dr Lauren Headland, Dr Patricia E. Lopez Calcagno, Dr Sunitha Subramaniam and everyone else in Lab 5.36 for their kindness and help throughout these four years. A special thank you to Dr Stuart Fisk for his near-unlimited patience and technical assistance with the HPLC, as well as to Prof Philip Mullineaux, Dr Philippe Laissue and Dr Marino Exposito Rodriguez for their input and assistance with the HyPer biosensor and confocal imaging.

None of this would be possible without the support of family and friends, in Essex and at home. A special thank you to Michael, who remained patient and managed to keep me sane through it all, and to Alida, Lize and Maatje for their frequent messages of encouragement. *'n Enorme dankie aan Mamma en Pappa vir ondersteuning (emosioneel en finansieël), wysheid en geduld, en aan Ouma vir haar liefde en gebede. Ek sou dit nie sonder julle kon doen nie. Ek is oneindig dankbaar vir die geleenthede wat die Vader aan my gegee het, en ek hoop dat ek ten volle daarvan gebruik maak.* This work is dedicated to my grandfather, Nassau Strydom, who many years ago opened my eyes to the wonder and beauty of the natural world.

Publications

Sections of this thesis have been published in the following peer-reviewed journal articles:

Litthauer, S., Battle, M.W., and Jones, M.A. (2016). Phototropins do not alter accumulation of evening-phased circadian transcripts under blue light. *Plant Signal Behav* **11**: e1126029.

Litthauer, S., Battle, M.W., Lawson, T., and Jones, M.A. (2015). Phototropins maintain robust circadian oscillation of PSII operating efficiency under blue light. *Plant J* **83**: 1034–1045.

Contents

Chapter 2: Materials and methods

List of tables and figures

Abbreviations

The following abbreviations are used throughout this thesis	
35S	Cauliflower mosaic virus *35S* promoter
ABA	Abscisic acid
APK	ADENOSINE-5'-PHOSPHOSULFATE KINASE
apk1 apk2	*apk1-1 apk2-1*
apk1 apk2 fou8	*apk1-1 apk2-1 fou8*
APX2	ASCORBATE PEROXIDASE 2
ATP	Adenosine triphosphate
BRASS	Biological Rhythms Analysis Software System
BSA	Bovine serum albumin
CCA1	CIRCADIAN CLOCK ASSOCIATED 1
CCR2	COLD CIRCADIAN REGULATED 2
cDNA	Complementary DNA
CO_2	Carbon dioxide
cry	Cryptochrome
DF	Delayed fluorescence
dH_2O	Distilled water
DNA	Deoxyribonucleic acid
dNTPs	Deoxyribonucleotide triphosphates
ELF	EARLY FLOWERING
FFT-NLLS	Fast Fourier Transform Non-Linear Least Squares
F_q'/F_m'	PSII operating efficiency
FRP	Free-running period
gDNA	Genomic DNA
GFP	Green fluorescent protein
GI	GIGANTEA
HPLC	High-performance liquid chromatography
HSF	HEAT SHOCK FACTOR
kDa	Kilodaltons
LHY	LATE ELONGATED HYPOCOTYL
LUC	LUCIFERASE
mRNA	Messenger ribonucleic acid
MS	Murashige and Skoog basal mineral salts
NDPK	NUCLEOSIDE DIPHOSPHATE KINASE

NLS	Nuclear localisation signal
nm	Nanometers
NPH	NONPHOTOTROPIC HYPOCOTYL
OD	Optical density
p1p2	*phot1-5 phot2-1*
PAP	3’-phosphoadenosine 5’-phosphate
PAPS	3’-phosphoadenosine 5’-phosphosulfate
PCR	Polymerase chain reaction
phot	Phototropin
phy	Phytochrome
PP2a	SERINE/THREONINE PROTEIN PHOSPHATASE 2A
PRR	PSEUDO-RESPONSE REGULATOR
PSII	Photosystem II
qRT-PCR	Real-time quantitative reverse transcription-polymerase chain reaction
RAE	Relative amplitude error
RNA	Ribonucleic acid
ROS	Reactive oxygen species
SDS	Sodium dodecyl sulfate
SDS-PAGE	SDS-polyacrylamide gel electrophoresis
SIG	SIGMA FACTOR
STN7	STT7 HOMOLOGUE
T-DNA	Transfer-DNA
TOC	TIMING OF CAB1
U	Units
UBQ	Ubiquitin
UV	Ultraviolet
v/v	volume/volume
w/v	weight/volume
XRN	5'→3' EXORIBONUCLEASE
xrn23	*xrn2-1 xrn3-3*
xrn234	*xrn2-1 xrn3-3 xrn4-6*

Chapter 1

Circadian regulation and retrograde signalling mechanisms in *Arabidopsis*

1.1. The evolution of universal cellular timekeeping mechanisms

Since the emergence of life ~3.7 billion years ago, terrestrial organisms have lived and evolved under predictable, regular daily cycles created by the 24-hour rhythm of the Earth's rotation (Hut and Beersma, 2011). Organisms that aligned their physiology and behaviour with these predictable changes were provided competitive advantages. As a result, most organisms have developed internal timing mechanisms that serve to synchronise their cellular chemistry with the daily rhythmic fluctuations of environmental cues such as light and temperature (Hut and Beersma, 2011). Circadian rhythms are considered to be a feature of almost all living cells (Edgar et al., 2012; Reddy and Rey, 2014). Cyanobacteria contain what is thought to be the oldest known molecular clock: a core phosphorylation oscillator that consists of a three-gene cluster (*kaiABC*) thought to have evolved approximately 1,000 Mya (Dvornyk et al., 2003; Edgar et al., 2012). In the alga *Gonyaulax polyedra*, rhythms in cell division, protein turnover and photosynthetic capacity are under control of the circadian system (Hastings, 2007), as are rhythms in luminescent glow in dinoflagellates (Hastings, 2013). Similarly, the fungus *Neurospora crassa* exhibits circadian regulation in conidiation rhythms (Sulzman et al., 1984). Circadian rhythms have also been described in higher organisms, including rhythms in locomotion and eclosion in *Drosophila melanogaster* (Pittendrigh, 1954; Tataroglu and Emery, 2014), activity levels in mice (Eckel-Mahan and Sassone-Corsi, 2015), and body temperature and sleep-wake cycles in humans (Aschoff, 1965; Czeisler et al., 1980). While the specific components of molecular clocks differ among different species, these ubiquitous circadian systems are thought to have evolved from a common molecular origin (O'Neill et al., 2011;

Edgar et al., 2012). The emergence of photosynthetic bacteria lead to the accumulation of molecular oxygen, culminating in the Great Oxidation Event ~2.5 billion years ago (Edgar et al., 2012). As a result, the ability to survive cycles of oxidative stress may have been an adaptive advantage in newly aerobic environments (Edgar et al., 2012). Indeed, rhythmic oxidation-reduction cycles of peroxiredoxins have been discovered in both human red blood cells (O'Neill and Reddy, 2011) and in a unicellular alga (O'Neill et al., 2011), and these peroxiredoxin proteins are conserved across Archaea, Bacteria and Eukaryota (Edgar et al., 2012).

This chapter will provide an overview of the characteristics of circadian rhythms in plants and the adaptive advantage provided by these rhythms, as well as the communication of environmental signals to the cellular mechanisms of the plant cell.

1.2. Monitoring and characterising circadian rhythms

Simplistically, circadian clocks can be described as biological networks that cycle autonomously in constant conditions (Hsu and Harmer, 2014). The networks consist of components that are phased to specific times of the day, with the phased components regulating each other through a complex network of feedback loops. Input pathways relay signals from the environment to the central oscillator to entrain the clock, and the clock in turn produces a large number of rhythmic outputs to regulate numerous pathways, including growth and metabolic processes (Hsu and Harmer, 2014). Circadian clocks not only allow organisms to synchronise their cellular processes with the rhythms of the external environment, but also provide a timing mechanism for the measurement of day length, allowing the organism to follow the change of seasons (Devlin and Kay, 2001).

1.2.1. Methods for monitoring circadian rhythms in plants

The rhythmic outputs (circadian rhythms) that are generated by circadian clocks can be observed either at the whole-organism level (e.g. emergence of *Drosophila* adults from puparia (Pittendrigh, 1954)) or at a cellular level (e.g. expression patterns of clock-regulated genes in *Arabidopsis thaliana* (Covington et al., 2008)). The first recorded observations of daily rhythms in plants date back to the 4th century BC, when Androsthenes of Thasos, admiral of Alexander the Great, described daily movements of leaves of the tamarind tree, *Tamarindus indicus* (Bretzl, 1903; McClung, 2006). The first indication that these rhythms are endogenous only came centuries later, when the French astronomer de Mairan observed that daily opening and closing of *Mimosa pudica* leaves persist in constant darkness (De Mairan, 1729; McClung, 2006). More than a century passed before these rhythms in leaf movement were described as truly endogenous and capable of inversion by reversing the alternation of light and dark (Candolle, 1832; McClung, 2006). The term 'circadian' was first coined in the 1950s to describe rhythms that are self-sustained under constant conditions (Golombek and Rosenstein, 2010).

Rhythms in leaf movement remain a useful reporter for measuring circadian rhythms in plants, and have been implemented in studying the circadian systems of a range of plant species including *Arabidopsis thaliana* (Engelmann et al., 1992; Thain et al., 2004), *Brassica rapa* (Xie et al., 2015), *Phaseolus vulgaris* (common bean) (Kiyosawa, 1979) and *Samanea saman* (Rain Tree) (Satter et al., 1974). Oscillations in leaf position can be mediated by specialized motor organs (the pulvini) through changes in cell volume, or can occur due to different growth velocities of the adaxial and abaxial halves of the leaf, causing the positions of young leaves and cotyledons to rise and fall over the course of 24 hours (Kiyosawa, 1979; Uehlein and Kaldenhoff, 2008; Farré, 2012). In both cases, leaf movement is associated with the circadian regulation of cellular water potential and rates of membrane water permeability, which may be facilitated by membrane aquaporins (Uehlein and Kaldenhoff, 2008; Farré, 2012). While circadian oscillations in hypocotyl and petiole elongation can also be utilised for monitoring

circadian rhythms, analysis of leaf movement is preferred due to the robustness of the assay and the ease of measurement (Tindall et al., 2015). Advancements in digital photography technology has provided low-cost digital cameras suitable for imaging, while computer-automated image capture and automated leaf tracking systems allow monitoring of leaf movements in a growth chamber continuously over the course of numerous days. Leaf movement assays therefore provide a non-invasive, high-throughput method for measuring circadian rhythms in a range of plant species without the need for transgenic plants. However, the method cannot be used on plant species with sessile leaves, which includes all major cereal crops (Tindall et al., 2015). Furthermore, circadian leaf movement ceases in mature leaves in *Arabidopsis*, leaving a limited window of approximately one week for circadian analysis (Edwards and Millar, 2007).

Carbon fixation has long been known as a circadian output in photosynthetic organisms, and plants exhibit circadian oscillations in transpiration, stomatal conductance and carbon fixation (Neeb, 1952; Schon, 1955; Hennessey and Field, 1991; Nassoury et al., 2001). Carbon assimilation has been used to reliably monitor circadian rhythms in a wide variety of plants, including *Arabidopsis* (Somers et al., 1998b), *Phaseolus vulgaris* L. (red kidney bean) (Hennessey and Field, 1991), and the Crassulacean acid metabolism (CAM) plant *Kalanchoë fedtschenkoi* (Dever et al., 2015). Carbon assimilation is measured through infra-red gas exchange analysis, which involves growing whole (or partial) plants in chambers with controlled atmospheric composition, and allows rapid analysis of photosynthetic rates at high resolution (Tindall et al., 2015). While gas exchange methods allow analysis of circadian rhythms in most plant species, the assay does not provide insight into the complex factors (from control of gene expression to regulation of stomatal conductance and growth) underlying the circadian control of carbon fixation (Tindall et al., 2015).

More recently, imaging techniques to monitor circadian rhythms have been developed that utilise the light emitted by plants. It has long been known that chlorophyll has the ability not only to absorb light, but also to dissipate some of the energy as fluorescence (Arnold and

Davidson, 1954; Goltsev et al., 2003). Measuring chlorophyll *a* fluorescence (also called variable or prompt fluorescence) is an established, versatile and non-invasive technique that can provide insight into Photosystem II (PSII) photochemistry, linear electron flux and carbon assimilation in many different plant species (Goltsev et al., 2003; Baker, 2008). Peak fluorescence emission occurs in the red region of the light spectrum (685nm) and extends into the infra-red region (around 800 nm) (Krause and Weis, 1991). Upon illumination of a leaf, light is absorbed by the chlorophylls associated with PSII, and the excitation energy is harnessed by reaction centres of the photosystems to drive the primary photochemical reactions and initiate photosynthetic energy conversion (Butler, 1978; Barber, 2009). Transfer of excitation energy from PSII is achieved via the occurrence of a charge separation between the chlorophyll *a* molecule P680 in the first excited singlet state (P680*) and the intermediate acceptor pheophytin *a* (Pheo), resulting in the formation of a radical pair state $P680^{*+}Pheo^{*-}$ (Barber, 2009). This is followed by rapid transfer of one electron from $Pheo^{*-}$ to plastoquinone Q_A, the primary quinone electron acceptor bound to the D2 protein of PSII, and subsequent transfer of the electron to the plastoquinone Q_B bound to the D2 protein of the reaction centre. The charge separation at the radical pair $P680^{*+}Pheo^{*-}$ upon illumination creates a highly active oxidant ($P680^{+}$), which receives an electron from a secondary donor – a tyrosine residue (Z) of the D1 protein. The oxidized tyrosine donor (Z^{+}) in turn is reduced by an electron generated from the splitting of water at the oxygen evolving centre, and the electron subsequently transferred to Q_B (Barber, 2009). Under optimal conditions in low light, more than 90% of the absorbed light quanta are utilized for photochemistry, but a minor fraction of the energy derived from the deactivation of excited pigments is lost either through emission of fluorescence from chlorophyll *a*, or through loss as heat (Butler, 1978; Baker, 2008). Photochemistry, chlorophyll fluorescence and heat loss are competing processes, and chlorophyll fluorescence is reduced (quenched) either through effective use of energy for photosynthesis (photochemical quenching) or through heat loss (nonphotochemical quenching). Minimum fluorescence occurs when all the PSII reaction centres are "open", that is where Q_A in the PSII reaction centre is oxidised and capable of photochemical reduction (such as in a leaf kept in the dark). In contrast,

reaction centres are "closed" when Q_A is fully reduced, preventing stable charge separation of $P680^*$ and resulting in maximum fluorescence yield (Butler, 1978; Baker, 2008). To quantify the fractions of fluorescence quenching that are due to photochemical and nonphotochemical quenching, respectively, a light-addition technique is used (Figure 1.1; Table 1.1) (Baker, 2008). For a leaf grown in the dark (dark-adapted), in which Q_A of all PSII reaction centres is optimally oxidised, the minimal level of fluorescence (F_0) is determined by exposing the leaf to a weak, nonactinic modulated measuring beam (so as not to cause reduction of Q_A) and capturing the fluorescence emission using a charged coupled device (CCD) camera. The maximum fluorescence yield (F_m) is determined by exposing the leaf to a brief (less than 1 second), bright, saturating light pulse of high photosynthetically active photon flux density (PPFD), sufficiently intense to maximally reduce Q_A in all PSII reaction centres. These parameters can be used to calculate the quantum yield (quantum efficiency) of PSII, which is a measure of the number of molecules that undergo photoconversion per photon absorbed. In the absence of photorespiration, the quantum yield of PSII photochemistry is directly related to the quantum yield of carbon assimilation by the leaf. The difference between F_m and F_0 is defined as the variable fluorescence, F_v and the ratio of F_v/F_m can be used to estimate the maximum efficiency at which light absorbed by PSII is used for the reduction of Q_A (maximum quantum efficiency of PSII). Interestingly, F_v/F_m has been shown to decrease in plants exposed to abiotic and biotic stresses, which could be due to increased nonphotochemical quenching caused by photoinactivation or oxidative damage and loss of PSII reaction centres (Baker, 2008). Chlorophyll *a* fluorescence parameters can also be determined for plants grown in continuous light, a routine requirement when employing an assay to measure circadian rhythms (Baker, 2008; Tindall et al., 2015). A leaf grown in constant actinic light has PSII reaction centres that are partially closed, and emits fluorescence at a level *F'* (Baker, 2008). Upon application of a saturating pulse that maximally reduces Q_A, the leaf's fluorescence emission will rise to the maximum fluorescence level F_m'. The fraction of fluorescence quenching that occurs as a result of PSII photochemistry (F_q') can be determined by calculating the difference between F_m' and *F'*.

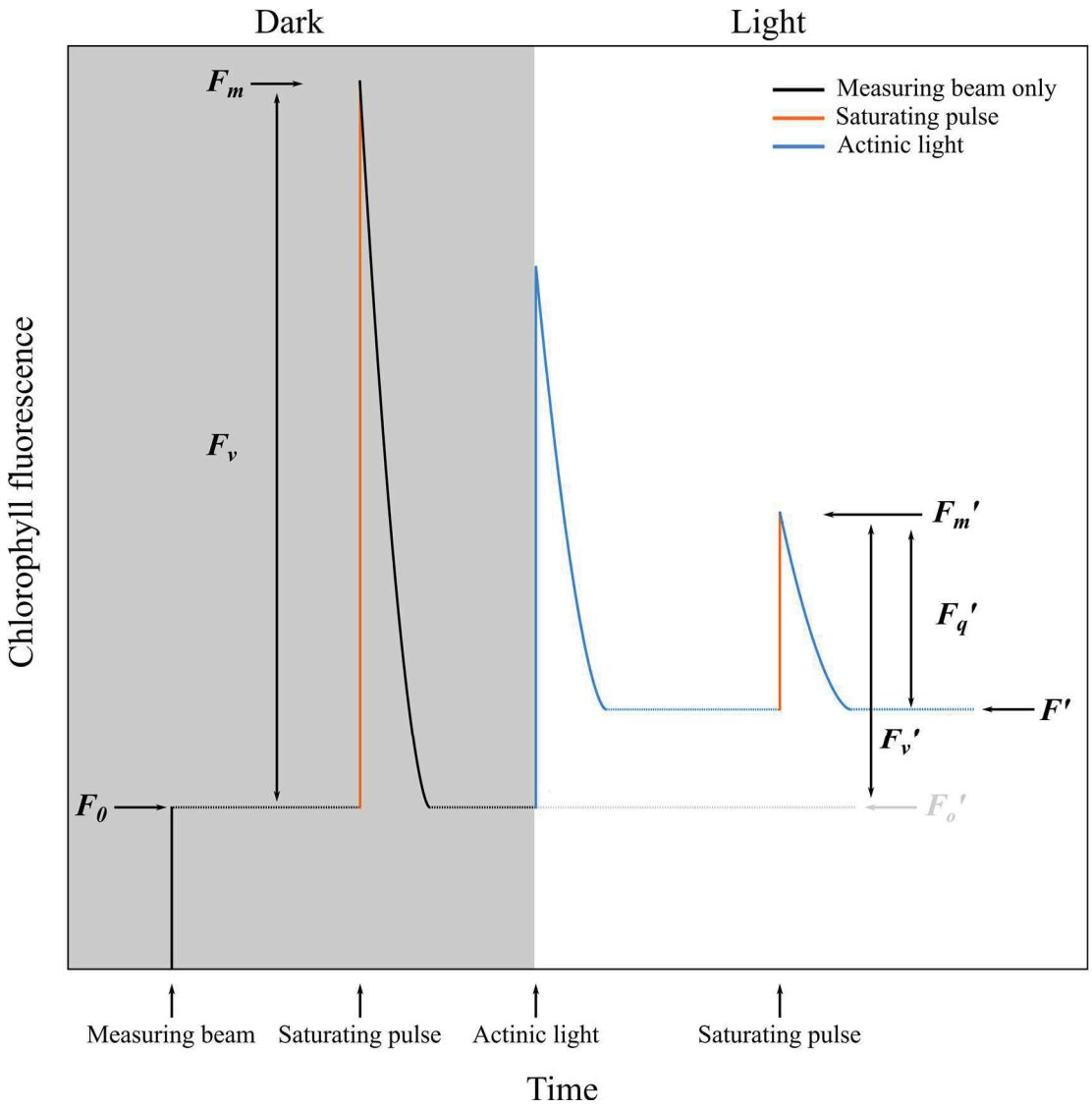

Figure 1.1 Graphical representation of chlorophyll *a* fluorescence quenching parameters. Chlorophyll *a* fluorescence parameters are determined for a leaf using a light-addition technique. Parameters are obtained from a leaf in a dark-adapted state by exposure of the leaf to a weak measuring beam (black line) to obtain minimal fluorescence (with Q_A maximally oxidised; F_0), followed by brief exposure (≤1 s duration) to a saturating light pulse (orange line) that maximally reduces Q_A and provides maximal fluorescence (F_m). A leaf under actinic light (blue line) produces fluorescence emission (F'), while exposure to the saturating light pulse (orange line) provides the maximal fluorescence parameter (F_m') for a leaf under actinic light. Variable fluorescence is calculated from the dark-adapted leaf ($F_v = F_m - F_o$) or from an illuminated leaf ($F_v' = F_m' - F_0'$). F_0' can be obtained from a light-adapted leaf by exposure to far-red light, which preferentially excites PSI and oxidises plastoquinone and Q_A associated with PSII. Fluorescence that is quenched from F_m' to F' by PSII photochemistry is calculated in an illuminated leaf ($F_q' = F_m' - F'$). (Figure adapted from Baker, 2008).

Table 1.1 Chlorophyll *a* fluorescence parameters

Parameter	Description
F, F'	Fluorescence emission from a dark- or light-adapted leaf, respectively.
F_0	Minimal fluorescence from a dark-adapted leaf. Level of fluorescence when Q_A is maximally oxidised (PSII centers "open").
F_m, F_m'	Maximal fluorescence from a dark- or light-adapted leaf, respectively. Level of fluorescence when Q_A is maximally reduced (PSII centers "closed").
F_v, F_v'	Variable fluorescence from a dark- and light-adapted leaf, respectively. Demonstrates the ability of Q_A to be reduced.
F_q'	Defined by F_m'-F'. Represents photochemical quenching of fluorescence by open PSII centers.
F_v/F_m	Maximum quantum efficiency of PSII photochemistry. Maximal efficiency at which light absorbed by PSII is used for reduction of Q_A.
F_q'/F_m'	PSII operating efficiency. Estimates the efficiency with which light absorbed by PSII is used for reduction of Q_A.
F_v'/F_m'	PSII maximum efficiency. Estimates the PSII operating efficiency if Q_A is fully oxidised (PSII centers "open").
F_q'/F_v'	PSII efficiency factor. Nonlinearly related to the proportion of PSII centers that are "open".
NPQ	Nonphotochemical quenching. Estimates the nonphotochemical quenching of fluorescence from F_m to F_m'.

Selected parameters used in chlorophyll *a* fluorescence studies of PSII photochemistry. (Table reproduced from Baker, 2008)

Furthermore, the ratio F_q'/F_m' (ϕ_{PSII}) is theoretically proportional to the quantum yield of PSII photochemistry under the constant actinic light of the growth condition. PSII quantum yield of a leaf in actinic light is equivalent to the quantum yield of linear electron flux through the PSII reaction centres. As a result, F_q'/F_m' is regarded as a measure of the PSII operating efficiency – the efficiency at which light absorbed by PSII is used for the reduction of Q_A at a specific PPFD. In contrast, the parameter F_v'/F_m' estimates PSII operating efficiency if all the PSII centres are "open" (PSII maximum efficiency) at a specific PPFD, while the PSII efficiency factor (F_q'/F_v') relates to the number of "open" PSII centres (Baker, 2008). Chlorophyll *a* fluorescence imaging has been used to monitor circadian rhythms in detached leaves of the crassulacean acid metabolism (CAM) plant *Kalanchoë daigremontiana*, with F_q'/F_m' cycling with circadian rhythm under constant light conditions in these leaves (Rascher et al., 2001; Wyka et al., 2005). Chlorophyll *a* fluorescence imaging therefore has the potential to serve as a well-defined, non-invasive circadian imaging assay that could be expanded for use in other plant species.

In addition to variable (prompt) fluorescence, PSII also emits delayed chlorophyll fluorescence, which is detected upon transfer of light-grown plants to darkness (Goltsev et al., 2003). Although prompt and delayed fluorescence signals are emitted from the same population of chlorophyll molecules of PSII antenna complexes, the underlying mechanisms differ and the signals provide information about different fundamental processes within the photosynthetic apparatus (Baker, 2008; Gould et al., 2009; Tindall et al., 2015). While the exact mechanism of delayed fluorescence (DF) is not completely understood, it is thought to occur during normal photosynthesis due to charge recombination between $P680^+$ and pheophytin *a* upon transfer of an electron from $Pheo^-$ to Q_A, resulting in re-excitation of the P680 complex and the release of a photon as P680* returns to the ground state (Mimuro et al., 2007; Gould et al., 2009). Only ~0.03% of absorbed light energy is re-emitted through DF, which emits light at 720 nm and occurs with a lifetime of 2-4 ns (Arnold and Davidson, 1954; Goltsev et al., 2003; Gould et al., 2009). DF decays rapidly (within 50 seconds) upon transferral of plants to the dark, and the

decay kinetics of DF in the time range of several microseconds after light excitation is thought to occur due to charge recombination of $Z^{+}PQ^{-}_{A}$. While the rate of decay is not affected by the circadian clock, the absolute amount of DF is under circadian control (Gould et al., 2009). Delayed fluorescence can be measured in a growth chamber with an accurately controlled light source, using a low light CCD camera system with long exposure times (normally 1 minute). Since DF decays to near-undetectable levels within a minute, image capture must be performed over exactly the same period following lights-off (Gould et al., 2009; Tindall et al., 2015). Delayed fluorescence imaging has been employed as a circadian assay to study rhythms in a variety of plants, including *Arabidopsis*, *Lactuca sativa* (lettuce), *Hordeum vulgare* (barley), *Zea mays* (maize), *Kalanchoë fedtschenko* and *Picea abies* (Norway spruce) (Gould et al., 2009; Gyllenstrand et al., 2014). While the exact nature of circadian control of DF is not understood, analysis of DF does provide an easy, high-throughput and universal method for monitoring circadian rhythms in a broad range of plant species without the need for transgenics (Tindall et al., 2015).

Leaf movement assays, gas exchange analysis, and variable and delayed fluorescence imaging are useful techniques that allow analysis of circadian rhythms in most, if not all, plants, yet these methods are indirect assays that monitor overall circadian health (Tindall et al., 2015). Often, direct assays of gene expression are required to study the effect of a specific process or gene within the circadian system. Quantitative reverse transcription PCR (qRT-PCR) is used extensively in circadian studies to monitor the rhythms in transcript accumulation for specific genes of interest over a sampling time course (Martin-Tryon et al., 2006; Hsu et al., 2013; Tindall et al., 2015). In addition, micro-arrays and RNA-seq technology allow the study of rhythms in global mRNA abundance and splicing patterns over time (Harmer et al., 2000; Filichkin et al., 2010; Tindall et al., 2015). However, these molecular techniques are time consuming and often costly, and involve frequent sampling over numerous days with limited resolution (Tindall et al., 2015). Sampling is also destructive, and rhythms cannot be analysed *in vivo.* The need for a simple, non-invasive, high-throughput assay for analysing the spatial

and temporal expression of target genes was met through the development of imaging assays using transgenic luciferase reporters (Millar et al., 1992b). Firefly luciferase is a monomeric, ~62kDa enzyme which catalyses the monooxidation of D-luciferin in the presence of ATP and O_2 (and Mg^{2+}) yielding the fluorescent product oxyluciferin and CO_2 (Sherf and Wood, 1994; Smale, 2010). Plants are transformed with reporter constructs consisting of the firefly luciferase gene fused to the promoter region of a circadian-controlled gene of choice (Millar et al., 1992a). Prior to imaging, plants are dosed with D-luciferin, which can diffuse through cellular membranes (Sherf and Wood, 1994). Under normal conditions, O_2 and ATP are present in excess in the plant cell, and the amount of bioluminescence observed is directly proportional to the amount of active luciferase protein present in the cell (Smale, 2010; Tindall et al., 2015). In addition, luciferase is an unstable enzyme that rapidly loses function, and the amount of active luciferin is directly related to the rate of luciferase expression. These properties make luciferase an ideal reporter for studying clock-controlled expression over time (Tindall et al., 2015). Luciferase imaging assays can be performed in growth chambers with controlled lighting, using the same low light CCD camera systems used for capturing DF, with exposure times exceeding 10 minutes following lights-off (Millar et al., 1992a). With recent improvements in the sensitivity of low light camera systems, luciferase assays have been used to monitor circadian rhythms in individual cells of the duck-weed *Lemma gibba*, providing spatio-temporal information of gene expression at high resolution (Muranaka et al., 2013). In addition, split-luciferase assays have been used to study tissue-specific clock elements in *Arabidopsis*: with expression of the C-terminal half of the luciferase protein driven by a clock promoter and the N-terminal half of luciferase driven by a tissue-specific promoter, active luciferase was produced only when both constructs were expressed in the same cell (Endo et al., 2014). Despite the clear advantages provided by the development of high-throughput, high resolution luciferase assays in plants, the technique is reliant on the need to introduce transgenic luciferase constructs into plants, a process which is time-consuming and limits the technique for use only in transformable species (Tindall et al., 2015).

1.2.2. Characteristics of circadian rhythms

Circadian rhythms can be represented as sinusoidal waves with a period, amplitude and phase (Figure 1.2), and have four defining characteristics (Pittendrigh, 1992; Dunlap, 1999; Harmer, 2009). Firstly, circadian rhythms are endogenous and self-sustaining, continue in constant ("free-running") conditions and are therefore not just passive reactions to the periodicity of the environment (Aschoff, 1963; Pittendrigh, 1992). Secondly, circadian rhythms cycle with a frequency that differs from that of a periodic environmental signal, and exhibit intrinsic periods of approximately (but never exactly) 24 hours (Pittendrigh, 1992; Dunlap, 1999). These rhythms can be reset (the time of onset of the rhythms changed) by certain environmental cues (Dunlap, 1999; Harmer, 2009). Lastly, circadian rhythms occur with the same period over a range of physiological temperatures. Temperature compensation of the clock prevents it from running faster under warmer temperatures, or slower under colder temperatures (Dunlap, 1999; Harmer, 2009).

In circadian biology, an external "entraining" signal capable of resetting the clock is referred to as a Zeitgeber ("time-giver"), with the time of onset of the last Zeitgeber regarded as "Zeitgeber time 0 (ZT0)" (Zerr et al., 1990). Under entraining conditions (where an environmental input signal is present), the circadian system adjusts its free-running period (τ) to the similar, but different period (T) of the Zeitgeber, thereby synchronising with the rhythmic external signal (Pittendrigh, 1992). As a result, the oscillator's period is changed from τ to T in the entrained steady state (Pittendrigh, 1992). The organism is entrained to a unique phase relative to the phase of the Zeitgeber, known as the phase of entrainment (Aschoff, 1963; Millar, 2003). While circadian rhythms in plants and animals are easily entrained to a 24 hour cycle, entrainment to a period as short as 18 hours or as long as 28-30 hours is possible (Bunning, 1973). In nature, an organism's circadian clock will be reset daily by a combination of external cues (Millar, 2004).

A

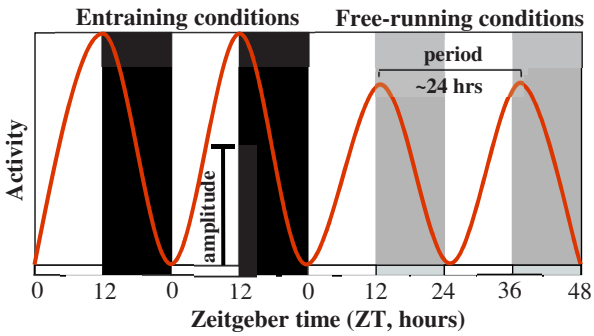

B

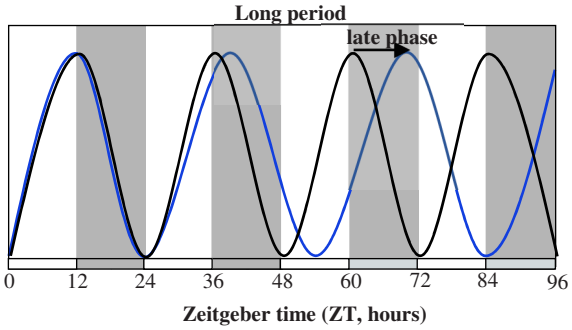

Loss of function		Overexpression	
prr7	*prmt5*	*PRR3*	*ELF3*
prr9	*skip*	*PRR5*	*RVE8*
rve8	*stipl1*	*PRR7*	*NOX*
ztl	*lnk1/lnk2*		

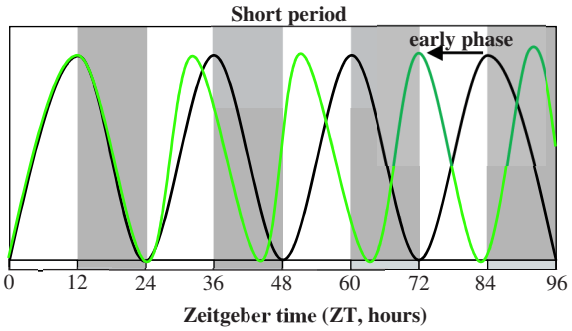

Loss of function			Overexpression
cca1	*prr3*	*jmjd5*	*GI*
lhy	*prr5*	*lwd1/lwd2*	*PRR9*
gi	*toc1*	*lip1*	*JMJD5*
nox	*det1*		

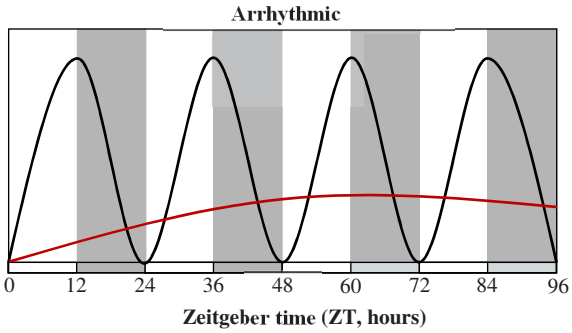

Loss of function	Overexpression	
elf3	*CCA1*	*LUX*
elf4	*LHY*	*TOC1*
lux	*CHE*	

Figure 1.2 Basic properties of circadian clock outputs under entraining and constant light conditions. (A) A rhythmic circadian output represented as a cosine wave with period, amplitude and phase. Activity of the biological process is plotted on the y-axis. The Zeitgeber time (ZT), plotted on the x-axis, is measured in hours from the last onset of light. White bars indicate light, black bars indicate dark, and grey bars indicate subjective darkness under constant light conditions. Under entraining conditions of 12h:12h light:dark cycles, the period of the rhythmic output corresponds to the exactly 24 hour period of the Zeitgeber. Under free--running conditions, the endogenous period of the oscillator (approximately, but not exactly 24 hours) becomes apparent. **(B)** Graphical representations of circadian outputs from mutants with long-period, short-period and arrhythmic circadian rhythms under free-running conditions, with phase shifts indicated as appropriate. White bars and grey bars indicate subjective day and subjective night, respectively. Tables providing examples of mutations in *Arabidopsis* that result in long-period, short-period or arrhythmic circadian period phenotypes, are shown. (Figures adapted from Nagel and Kay, 2012; Hsu and Harmer; 2014).

As a result, the circadian period of approximately 24 hours (τ) is synchronised with (entrained to) one or several Zeitgebers in the external environment that have a period (T) of precisely 24 hours due to the period of the earth's rotation (Aschoff, 1963; Pittendrigh, 1992). The adjustment of circadian period to that of the environment is necessary even if the endogenous period is very close to 24 hours (Golombek and Rosenstein, 2010). Under prolonged exposure to free-running conditions, the endogenous period will gradually diverge from the period of the natural cycles until the phase differences are inadequate for survival. For example, a circadian system with an endogenous phase shifted by 0.1 hours compared to the natural cycles will result in a 1 hour advancement after 10 days in free-run and a shift from day-active to nocturnal after 3 months (Golombek and Rosenstein, 2010).

Daily cycles of temperature can entrain circadian systems in some organisms, yet day-night changes in light serve as the strongest entraining signal (Pittendrigh, 1992). The appearance of light at dawn and the disappearance of light at dusk cause adjustments to the phase of the clock on a daily basis to keep the endogenous period synchronised with the day-night cycles of the environment (Devlin and Kay, 2001). However, it is important to note that circadian clocks are not merely hourglass timers that count down from an initial Zeitgeber at a constant rate (Millar, 2004). The time and duration of the light signal also affects the period of the oscillator (Golombek and Rosenstein, 2010). Circadian clocks regulate the sensitivity of their response to a Zeitgeber depending on the time of day the stimulus is applied (referred to as 'gating') (Devlin, 2002). In *Arabidopsis* plants placed in free-run, a pulse of light given before subjective dawn will advance the phase of the clock, setting the clock to an 'earlier' time (Covington et al., 2001; Devlin and Kay, 2001). A similar pulse of light applied after subjective dusk will delay the phase of the clock (setting it to a 'later' time), while the same pulse applied in the middle of the subjective day will have no effect. The phase shift in response to a stimulus applied at different times across the circadian cycle can be plotted on a phase response curve (PRC), providing insight into the sensitivity of the specific circadian system and identifying the times at which the same stimulus can induce phase delays, advances or no change at all

(Dunlap, 1999). The PRC regions in which the largest phase shifts can occur provide windows for entrainment by "skeleton photoperiods" – single light pulses given at dawn and at dusk, with the time between the pulses delimiting the boundaries of the subjective day and subjective night (Golombek and Rosenstein, 2010). In general, a prolonged pulse of irradiation is required to reset the clock, which prevents small fluctuations in light level from causing large changes in phase (Devlin and Kay, 2001). When entraining an organism in a laboratory setting using pulses of light, the severity of the response is determined by the total amount of light, regardless of whether this light is given as a very bright pulse for a short period of time or as a prolonged (≤45 min) pulse of dim light (Devlin and Kay, 2001). The intensity of the light signal also affects the circadian period under constant conditions (Aschoff, 1979). According to Aschoff's rule, the period of circadian rhythms in plants and day-active animals kept under constant light conditions is inversely proportional to the environmental light intensity. Therefore, increased intensities of illumination cause shortened circadian period in plants, but result in lengthened circadian period in nocturnal animals (Aschoff, 1979).

As mentioned, the phase of entrainment depends on the difference in period between the Zeitgebers (T) and the endogenous oscillator (τ) (Aschoff, 1963; Millar, 2004). In natural conditions, plants are subjected to prolonged periods of irradiation, and the phase of entrainment is the net effect of phase advances in the morning and phase delays in the late afternoon (Devlin and Kay, 2001). The most physiologically relevant variable is the alteration in photoperiod (the duration of illumination in a light:dark cycles) (Millar, 2004). The circadian system senses changes in photoperiod, allowing the plant to regulate seasonal processes such as flowering or senescence (McClung, 2006). In addition, outputs of the clock can be regulated to occur at the correct phase of the day:night cycle (time of day) despite a change in day length (Edwards et al., 2010). For example, the expression of the *CAB* genes encoding the chlorophyll a/b-binding proteins in *Arabidopsis* exhibit robust circadian rhythms under constant light, yet under entraining conditions the phase of peak expression is delayed under long days and advanced under short days, thus always peaking in the middle of the day regardless of day

length (Edwards et al., 2010). *Arabidopsis* is a "long-day plant" which flowers under long photoperiods, and regarded as "dawn-dominant": large changes in photoperiod length result in comparatively small changes in the phase of gene expression rhythms relative to dawn, indicating that the rhythms are more susceptible to the "dawn" signal and exhibit a limited response to the "dusk" signal. This is in contrast to the "dusk-tracking", "short-day plant" *Ipomoea nil* (Morning Glory) which flowers under shortening day lengths and which, when grown under constant light, only flowers upon transfer to an interval of constant darkness mimicking a long night (Edwards et al., 2010).

1.3. Cellular timekeeping improves fitness in plants

Although signals such as dawn and dusk or tidal movements act as rhythmic environmental cues, the coupling of an organism's responses to an endogenous, autonomous timing is advantageous (Golombek and Rosenstein, 2010). In some instances, such as at extreme latitudes, environmental variables remain virtually stable, yet these cues may not always be reliable enough to adequately steer behaviour. An hour glass-like timer that simply responds to external signals is also by its very nature reactive, while an endogenous timer allows an organism to anticipate and predict changes and to respond optimally to future challenges. For example, cold or frost is likely associated with dusk, while high light or heat stress occurs during the day (Jones, 2009; Golombek and Rosenstein, 2010). Lastly, an endogenous clock allows for the overall synchronisation of the various biological components that function in a living organism (Golombek and Rosenstein, 2010).

The advantages provided by a circadian system have been described in a variety of species. In humans, misalignment between internal circadian rhythm and the rhythms of the environment (such as observed in jet lag or shift work) has numerous adverse consequences, including an association with increased risk of cancer and metabolic or mental disease (Hastings et al., 2003). Competition experiments performed on wild-type and mutagenized strains of

cyanobacteria with different clock properties showed that strains compete most effectively when the period of their internal biological oscillator is similar to that of the environmental cycle (Ouyang et al., 1998; Woelfle et al., 2004). This advantage is not simply due to an "intrinsic value", as the advantage is visible only in rhythmic environments, and not under constant conditions (Woelfle et al., 2004). Similarly in *Arabidopsis*, both wild-type and long- and short-circadian period mutants grow faster, fix more carbon, contain more chlorophyll and survive better when their circadian period is matched to the period of the environment, compared to plants for which the circadian periods are desynchronised from the environment (Dodd et al., 2005). This is perhaps not surprising, as microarray analysis has indicated that approximately one-third of expressed genes in *Arabidopsis* are regulated by the circadian system at transcriptional level (Covington et al., 2008). In addition, over 70% of the 88 protein-coding genes encoded by the chloroplast genome can be regulated by the circadian system (Noordally et al., 2013). Among the circadian-regulated genes in the *Arabidopsis* genome are genes involved in the light-harvesting reactions of photosynthesis, genes involved in carbon, nitrogen and sulfur pathways, as well as genes involved in developmental processes including cell elongation, cell wall biosynthesis, and flowering (Harmer et al., 2000). Furthermore, a number of genes involved in classical plant hormone pathways and abiotic stress are regulated by the circadian system in *Arabidopsis* (Covington et al., 2008). Interestingly, circadian control of gene expression in *Arabidopsis* extends beyond gene transcription to include regulation of translation rate (Missra et al., 2015). Prior to protein synthesis, transcripts are recruited to ribosomes to form polysomes, and the rate of translation of a given transcript depends on the transcript abundance, the proportion of transcript present in polysomes (ribosome occupancy), the number of ribosomes present on the transcript (ribosome loading) and the speed of progression along the transcript (Piques et al., 2009). While rhythms in ribosome abundance are not observed, global cycles of ribosome loading have been reported over the course of the light:dark cycle (Piques et al., 2009; Pal et al., 2013; Missra et al., 2015). Approximately one in seven mRNAs exhibit robust cycles of ribosome loading, and include mRNAs involved in ribosome biogenesis, synthesis of the inner mitochondrial membrane and the photosynthetic

apparatus. In addition, these cycles of ribosome loading are controlled in part by the circadian system, and are substantially altered upon disruption of the circadian clock (Missra et al., 2015)

The effect of circadian regulation on the daily functioning of plants is apparent not only at the level of gene expression, but also at metabolic and physiological levels. Circadian regulation of light harvesting has been described in higher plants, as is demonstrated by circadian oscillations in DF (Gould et al., 2009; Dodd et al., 2014). In the legume species *Pisum sativum*, *in vitro* monitoring of O_2 production from isolated mesophyll cells (using an oxygen-sensitive electrode) revealed circadian rhythms in light-induced O_2 evolution (Lonergan, 1981). Furthermore, circadian rhythms in uncoupled, light-induced whole-electron flow have been observed in isolated chloroplasts from three legume species, using an *in vitro* H_2O to methyl viologen assay (Lonergan, 1981). As mentioned previously, the CAM plant *Kalanchoë daigremontiana* exhibits circadian oscillations in the operating efficiency of PSII (F_q'/F_m'; ϕPSII) in isolated leaves (Wyka et al., 2005). In addition, diurnal cycles of Rubisco carbamylation in *K. deigremontiana* continue under constant light conditions, and correlate with diurnal changes in Rubisco activity and the rate of carbon fixation (Maxwell et al., 1999). Circadian gating of plant responsiveness to light and hormone signalling allows for maximal sensitivity to light during the day, and maximal sensitivity to the phytohormones auxin and gibberellin at night (Millar and Kay, 1996; Covington and Harmer, 2007; Arana et al., 2011; Atamian et al., 2016). In addition, the abundance of light signalling components and hormones are regulated both by the circadian clock and by light, and the complex integration of light and temperature sensing, hormone signalling, circadian regulation and circadian gating results in daily rhythms in growth and organ expansion (Nozue et al., 2007; Müller et al., 2014; Atamian et al., 2016). Since the direction and intensity of sunlight changes with predictable rhythm during the day, coordination between directional growth pathways and the circadian clock could result in optimal light capture and performance during the course of the day (Atamian et al., 2016). One example of such a directional growth pathway is phototropism, a process that integrates blue light sensing and auxin response pathways to allow alignment of photosynthetic

organs with the direction of light (Briggs, 2014). Heliotropism, or solar tracking, is a kind of phototropism observed in the *Helianthus annuus* (common sunflower) which coordinates light-signalling pathways and circadian regulation to optimise plant performance in natural conditions (Atamian et al., 2016). Young sunflowers track the sun from east to west during the day, and reorient during the night to face east in anticipation of the oncoming dawn. In contrast, movement ceases in mature plants, with flower heads facing eastward. Solar tracking in young plants occurs due to differential elongation on opposite sides of stems, with growth rates on the east side higher during the day and very low at night, contrasting with growth rates on the west side that are low during the day and higher during the night. This antiphasic growth is regulated by differential expression of auxin-sensitive genes involved in phototropism and is under circadian control, continuing for several days under constant overhead lighting. Furthermore, the gradual cessation of westward movement toward the final stages of flower development is possibly due to circadian gating of plant responses to light (with plants responding more strongly to light activation of phototropism during the morning than at any other time of the day), combined with decreased elongation rates as plants reach maturity. The permanent eastward orientation of mature flowers promotes pollinator visits, with flowers artificially orientated westward experiencing approximately five-fold fewer pollinator visits. Interestingly, eastward-facing flower heads warm up more quickly in the morning than westward-facing flowers. Artificial warming of westward-facing flowers with heaters improved pollinator visits of these flowers (although visits were still fewer than for eastward-facing flowers), suggesting that upon interception of morning solar radiation, both light and heat improves attractiveness of flowers to pollinators (Atamian et al., 2016)

In *Arabidopsis*, the circadian clock also controls the availability of carbohydrate for growth at night (Graf et al., 2010). During the day, sugars produced by photosynthesis can be used to directly fuel growth, or can be stored in the chloroplasts as starch to be used as a source of carbohydrate during the night (Lu et al., 2005; Graf et al., 2010). Circadian regulation of growth responses results in repression of growth during the day and peak shoot growth towards the

end of the night, allowing growth to coincide with maximum water availability (Walter et al., 2009). By timing growth to occur towards the end of the night, carbohydrates produced during the day are favoured for storage, and the depletion of carbon sources before the next dawn is prevented. Indeed, starch degradation occurs at a linear rate during the night in *Arabidopsis* leaves, and is timed such that ~95% of the stored starch is depleted by dawn (Smith and Stitt, 2007; Graf et al., 2010). The accurate timing of starch degradation is vital to plant growth, and artificial extension of the night beyond normal dawn causes a pronounced decrease in growth rate. In addition, growth under short-day conditions leads to increased accumulation of starch, and mutants that are unable to store starch or degrade it very slowly exhibit limited growth rates compared to wild-type plants, unless grown under very long days (Gibon et al., 2004; Smith and Stitt, 2007). Plants are able to very rapidly adjust the rate of starch degradation in response to an unexpectedly early or late onset of night (Graf et al., 2010). Plants grown under long-day conditions and subjected to darkness after only 8 hours of light exhibit an immediate and pronounced decrease in starch degradation rate. Similarly, plants grown under short day conditions exhibit accelerated starch degradation upon exposure to a 16-hour light period (Lu et al., 2005; Graf et al., 2010). While the levels of starch-degrading proteins do not cycle rhythmically under light:dark cycles, constant light or constant darkness, cellular levels of maltose (but not of starch, glucose or sucrose) cycle with strong circadian rhythms under constant light conditions (Lu et al., 2005). Growing plants under abnormal day lengths (such as 28 hours) results in depletion of starch ~24 hours after dawn and a subsequent reduction in growth (Graf et al., 2010). In addition, mutants with shortened circadian period exhibit exhausted starch supplies at the time of early dawn as anticipated by the fast-running oscillator, rather than at the actual dawn of the light:dark cycle. Therefore, the circadian clock plays an important role in timing the degradation of stored starch during the night, ensuring that carbohydrate availability for growth is maintained until the next anticipated dawn. (Graf et al., 2010).

1.4. Circadian regulation of flowering

The advantages obtained by synchronising internal biological processes to the rhythms of the environment are not limited merely to daily processes, but extend to longer term, seasonal processes as well (Hsu and Harmer, 2014; Millar, 2016). Many plants optimise reproductive success by aligning their flowering time to seasonal changes (Green et al., 2002; Song et al., 2015). Plants that grow in lower latitudes tend to flower in response to short days, thereby avoiding extreme summer heat. In contrast, plants growing in more temperate climates often flower in response to long days, allowing these plants to flower and set seed before the onset of winter (Thomas and Vince-Prue, 1997; Green et al., 2002). The process through which plants use information on photoperiod to regulate flowering under certain day length conditions can be described by means of the external coincidence model (Pittendrigh and Minis, 1964; Song et al., 2015). The external coincidence model as originally described consists of two factors: a hypothetical enzyme that is present throughout the day, but is activated only in the presence of light, and a hypothetical substrate of which the levels oscillate throughout the day and which induces a photoperiodic response when processed. The photoperiodic response is triggered only when the peak of substrate coincides with the presence of the enzyme. Levels/expression patterns of the substrate are regulated by the circadian clock, and the clock is reset by changes in light and temperature. Since the time of resetting changes over the course of the year, slight phase shifts occur in the oscillations of the substrate. As a result, the phases of maximal substrate are different under long- and short-day conditions (Pittendrigh and Minis, 1964; Song et al., 2015). The external coincidence model is well demonstrated in the flowering mechanisms of *Arabidopsis*, barley, wheat and rice (Song et al., 2015). In many plant species, the timing of flowering depends largely on seasonal changes in the expression levels of the gene *FLOWERING LOCUS T* (*FT*). The *FT* gene product is synthesised in the leaves, where photoperiod is sensed, and moves to the shoot apexes to induce flowering. In the long-day plant *Arabidopsis*, *FT* expression is induced to high levels under long day conditions, while short-day conditions lead to very low levels of *FT* expression (Kobayashi et al., 1999). The induction

of *FT* expression under long days is regulated by the transcription factor CONSTANS (CO), which directly activates *FT* expression (Samach et al., 2000; Valverde et al., 2004). The activity of CO protein is restricted to the afternoon of long days through coordination of circadian clock regulation of *CO* transcription and photoreceptor regulation of CO activity (Samach et al., 2000; Suárez-López et al., 2001; Valverde et al., 2004; Song et al., 2015). Expression of *CO* is regulated by the circadian clock, with transcripts occurring from the late afternoon to night. Transcription of *CO* is repressed in the morning by CYCLING DOF FACTORs (CDFs) which play an important role in allowing *Arabidopsis* plants to differentiate between long days and short days, and *CDF* expression is accurately timed through complex circadian mechanisms (Imaizumi et al., 2005; Sawa et al., 2007; Song et al., 2015). Morning-phased clock components induce *CDF* expression, while afternoon-phased components repress *CDF* expression, thereby restricting *CDF* expression to the mornings. Furthermore, CDF protein is degraded by clock-controlled proteins that are expressed at highest levels and activated at the end of the day in long days (but not in short days) (Sawa et al., 2007; Song et al., 2015). In addition to circadian regulation of *CO* expression, stabilization of CO protein is dependent on light signalling pathways. Red light signalling modulates degradation of CO to occur in the morning and during the night in both long and short days, preventing flowering under short days (Liu et al., 2008b; Lazaro et al., 2012; Song et al., 2015). In contrast, blue and far-red light signalling mechanisms cause an increase in CO protein abundance, thereby allowing CO to accumulate only in the late afternoon in long days (Valverde et al., 2004; Song et al., 2015). Combined, these activator, repressor and protein degradation mechanisms coordinate with the circadian system to ensure that peak *CO* expression coincides with light primarily in the summer (long days), when CO protein is stabilized and *FT* expression occurs (Song et al., 2015).

1.5. Natural variation in plant circadian rhythms

While photoperiod is the most reliable signal indicating the time of year, the relationship between photoperiod and season depends on latitude (Hut and Beersma, 2011). Seasonal changes in the environment become more severe at latitudes closer to the poles, and the amplitude of environmental temperature rhythms increases with latitude. As a result, species that occur across a broad range of latitudes must adapt to annual changes of both temperature and photoperiod to optimize the timing of reproduction. In some species this has led to latitudinal differences in the characteristics of their circadian systems, suggesting that the circadian system's ability to respond to changes in photoperiod generates selective pressure. In *Arabidopsis*, considerable natural variation is evident in the period, amplitude and phase of circadian rhythms among 150 natural accessions (Michael et al., 2003). A latitudinal cline is observed in the endogenous period of *Arabidopsis*, with the period length correlating strongly with day length at the latitude of origin such that plants at higher latitudes exhibit longer circadian period (Michael et al., 2003; Hut and Beersma, 2011). The longer period of *Arabidopsis* enhances its ability to track dawn, allowing improved seasonal responsiveness at high latitudes where sharp increases in day length occur during spring (Michael et al., 2003). In addition, the lengthened period at higher latitudes serves to delay flowering until later in the season, avoiding cold weather in late spring (which is more common at higher latitudes) and reduce damage by herbivores when *Arabidopsis* might be one of few species available during early spring. Optimal flowering time is vital to the success of crops in modern agriculture, and the circadian system has emerged as a promising target for breeding and developing crops for improved production in different environments (Murphy et al., 2011; Gawroński et al., 2014; Millar, 2016). In crop domestication, early flowering or reduced photoperiod sensitivity are often breeding targets (Zakhrabekova et al., 2012; Boden et al., 2014). While early flowering may limit productivity in highly fertile areas due to inefficient use of the entire growing season, it does allow cultivation in low-yielding, marginal environments with short seasons, which constitutes the majority of land used for agriculture (Zakhrabekova et al., 2012). In addition,

plants with reduced photoperiod sensitivity has allowed for the migration of crops to latitudes where daylengths might otherwise inhibit flowering (Boden et al., 2014). Variation in flowering time has been attributed to allelic variation in core circadian clock gene homologs, such as in brassica (Xie et al., 2015), wheat (Gawroński et al., 2014), sorghum (Murphy et al., 2011), rice (Izawa et al., 2011) and pea (Weller et al., 2012); or due to variation in alleles of downstream, clock-regulated genes, such as in beet (Dally et al., 2014; Millar, 2016). In barley, the northward migration of cultivated barley from the Fertile Crescent to Scotland and Scandinavia is associated with selection of single-gene mutations in core circadian clock genes that alter flowering time (Jones et al., 2008; Boden et al., 2014; Millar, 2016). Wild barley is early flowering under long days and late flowering under short days (Turner, 2005; Faure et al., 2012). The long-day photoperiod response of barley is affected by *Ppd-H1*, a *PRR* gene homologous to the morning-phased *Arabidopsis* clock gene *PRR7* (see Section 1.6). Mutation in *Ppd-H1* has no effect on flowering time under short days, but results in delayed flowering under long days. This late-flowering phenotype (which is associated with reduced expression levels of the barley *FT* homologue, *HvFT1*) provides an advantage in environments with long growth seasons (Turner, 2005; Faure et al., 2012). In contrast, mutation in the barley *EARLY MATURITY8* (*EAM8*), an orthologue of the *Arabidopsis* clock gene *ELF3* (see Section 1.6) results in an early-flowering, day-neutral phenotype (Faure et al., 2012; Zakhrabekova et al., 2012; Boden et al., 2014). The resultant rapid flowering under either short days or long days are advantageous for cultivation in short growth seasons, such as those in Scandinavia, and as a result a number of spontaneous and induced *eam8* spring barley varieties are available commercially (Faure et al., 2012; Zakhrabekova et al., 2012; Boden et al., 2014). Interestingly, a recent study of circadian rhythms in cultivated tomato (*Solanum lycopersicum*) and its wild ancestor *Solanum pimpinellifolium* indicated that the circadian clock of tomato has slowed down during domestication (Müller et al., 2016). Circadian rhythms in cultivated tomato cycle with a period 2 hours longer, and with a phase delayed by more than 3 hours, compared to that of *S. pimpinellifolium*. In addition, cultivated tomato exhibit lower gene expression amplitudes than the ancestor, suggesting a weaker circadian clock in domesticated varieties. The phase

delay observed in domesticated species relates to a gene homolous to the *Arabidopsis EID1*, a negatively-acting component involved in the phytochrome signalling cascade. Interestingly, distant related green-fruited wild tomato species exhibits circadian rhythms with similar phase, but even shorter period compared to *S. pimpinellifoliumi.* Domestication of tomatoes is thought to have begun in Ecuador and Peru, with deceleration of the clock occurring in a stepwise manner. The delayed phase is apparent in the earliest domesticated Ecuadorian types, while the long period emerged during the later steps of domestication in Mesoamerican varieties. The long period and late phase became fixed only in the modern cultivars brought to Europe approximately 500 years ago, suggesting the selection of plants with slower circadian rhythms that are better adapted to the long summer days encountered as it was moved to areas further from the equator (Müller et al., 2016).

1.6. The *Arabidopsis thaliana* circadian clock as a model system

Extensive research has been done on the workings of the circadian system in *Arabidopsis*, with both genetic and biochemical studies playing important roles in revealing the architecture of the system (Nagel and Kay, 2012). The *Arabidopsis* circadian system has historically been described as a central oscillator consisting of core transcriptional feedback loops, which in turn generate rhythmic outputs via specific signalling pathways (Harmer, 2009). However, it is becoming increasingly apparent that the *Arabidopsis* clock is a complex system, consisting of an interconnected network of transcriptional and translational feedback loops (Millar, 2016; Sanchez and Kay, 2016). Some clock genes have multiple functions, acting within the central oscillator as well as in input and output pathways, while clock outputs can be directly regulated by input pathways (Nagel and Kay, 2012; Hsu and Harmer, 2014). More recently, the *Arabidopsis* circadian system is described simplistically as a four-component “repressilator” (or “quadripressilator”), a gene circuit consisting of a ring of inhibitors in which the expression of each gene inhibits the earlier-expressed gene (Figure 1.3a) (Nakamichi, 2011; Pokhilko et

al., 2012; Millar, 2016). More than 20 components associated with the clock have been identified in *Arabidopsis* (a simplified diagram is presented in Figure 1.3b), with different rhythmically-expressed clock genes acting at specific times of day to regulate the expression of other clock-related genes at transcriptional and post-transcriptional level (Nakamichi, 2011; Nagel and Kay, 2012; Hsu and Harmer, 2014; Sanchez and Kay, 2016). Constitutive overexpression or loss of function of these components can impact the period or rhythmicity of the observed circadian rhythms (Figure 1.2b and Table 1.2).

1.6.1. Transcriptional loops in the Arabidopsis clock network

The first transcriptional regulatory feedback loop involves the morning-phased components CIRCADIAN CLOCK ASSOCIATED1 (CCA1) and LATE ELONGATED HYPOCOTYL (LHY), two morning-phased transcription factors that contain a single MYB DNA-binding domain (Alabadí et al., 2001). *CCA1* and *LHY* transcription begins to rise in the middle of the night and peaks at dawn, with cycles in protein levels well synchronised with transcript level rhythms (Alabadí et al., 2001). The expression of *CCA1* is activated by LIGHT-REGULATED WD1 (LWD1), a nuclear-localised protein for which transcription peaks at dusk (Wang et al., 2011; Wu et al., 2016). In order to act as activator of *CCA1* expression, LWD1 interacts with TEOSINTE BRANCHED 1-CYCLOIDEA-PCF20 (TCP20) and TCP22 proteins, and the resulting LWD-TCP complex binds to the TCP binding site on the *CCA1* promoter (Wu et al., 2016). CCA1 and LHY proteins are expressed mainly in leaves and stems and co-localise in the nucleus where they can interact to form both heterodimers and CCA1 homodimers (Lu et al., 2009; Yakir et al., 2009). Furthermore, CCA1 and LHY have partially redundant functions, inhibiting the expression of the evening-phased component *TIMING OF CAB EXPRESSION1/PSEUDO-RESPONSE REGULATOR1 (TOC1/PRR1)* (Alabadí et al., 2001). In addition to *TOC1*, CCA1 and LHY also inhibit expression of a number of other evening-phased genes (Nagel and Kay, 2012; Hsu and Harmer, 2014). -

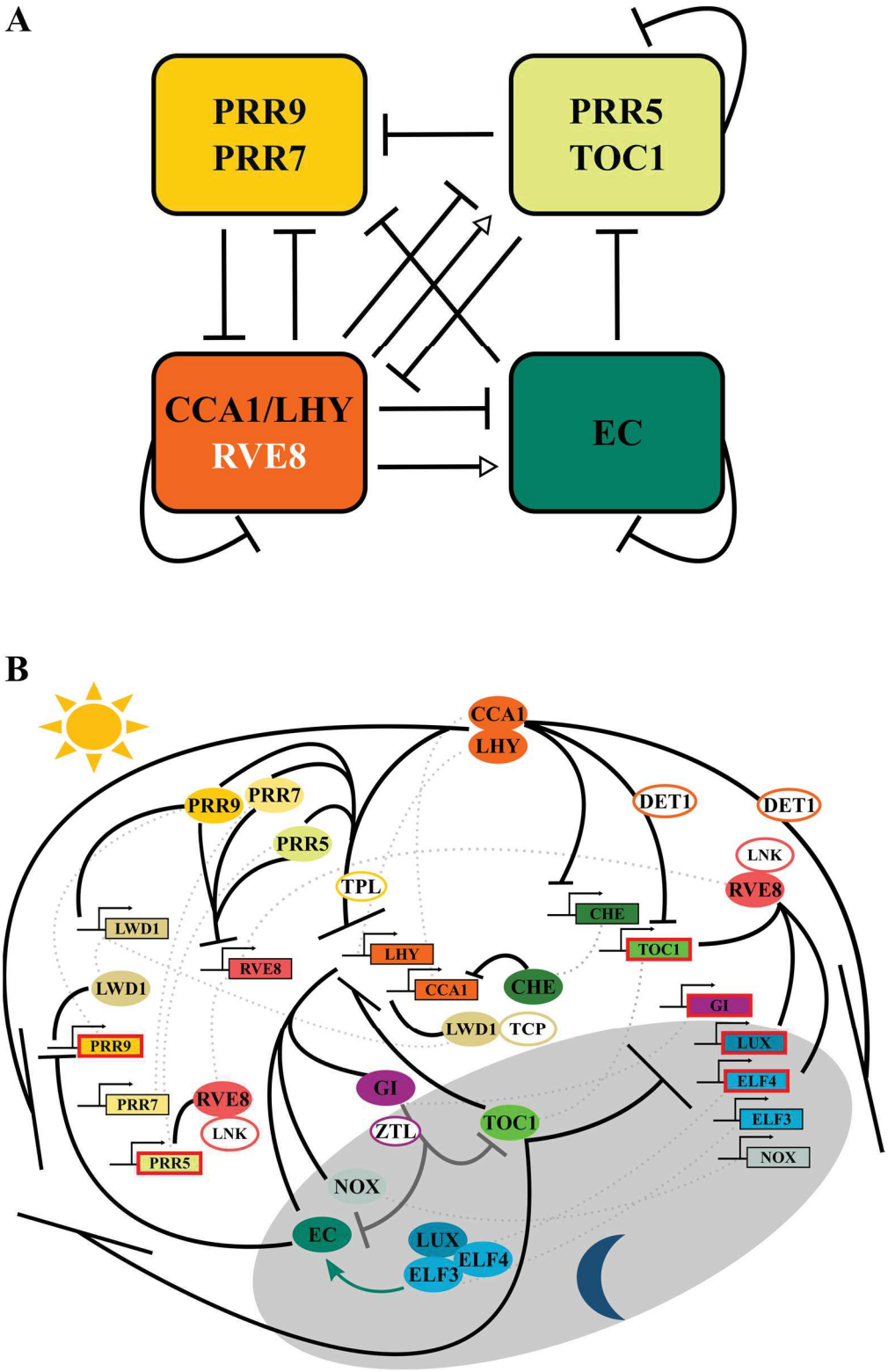

Figure 1.3 Simplified representation of the circadian clock in *Arabidopsis*. (A) Schematic representation of the four component repressilator circuit (quadripressilator) consisting of a ring of suppressors, with RVE8 as an activator. **(B)** Schematic representation of the transcription/translation feedback loops of the *Arabidopsis* circadian system, with day-phased and night-phased components shown. Boxes indicate genes and ovals indicate the respective proteins, connected with grey dotted lines for clarity. Genes with EEs in their promoters are marked with red boxes. Black arrows indicate activation or suppression as appropriate. (Figures adapted from Nagel and Kay, 2012; Hsu and Harmer; 2014; Millar et al., 2016).

Table 1.2 Components of the *Arabidopsis* circadian system and their effect on circadian rhythms

Gene	Time of day	Function	Circadian phenotype of mutant	
			Loss-of-function	Overexpression
CCA1	Morning	Transcription factor	Short period (partially redundant with *LHY*)	Arrhythmic
LHY	Morning	Transcription factor	Short period (partially redundant with *CCA1*)	Arrhythmic
PRR9	Morning	Transcription factor	Long period (partially redundant with *PRR7* and *PRR5*)	Short period
PRR7	Morning	Transcription factor	Long period (partially redundant with *PRR9* and *PRR5*)	Long period
GI	Day	Interacts with numerous proteins	Short period	Short period
RVE8	Afternoon	Transcription factor	Long period (partially redundant with *RVE4* and *RVE6*)	Long period
PRR5	Afternoon	Transcription factor	Short period (partially redundant with *PRR9* and *PRR7*)	Long period
LWD1/2	Afternoon /Evening	Nuclear protein	Short period (*LWD1* redundant with *LWD2*)	
PRR3	Evening	Transcription factor	Short period	Long period
TOC1	Evening	Transcription factor	Short period	Arrhythmic
CHE	Evening	Transcription factor	No phenotype	Arrhythmic
LUX	Evening	Transcription factor	Arrhythmic under constant light	Arrhythmic
NOX	Evening	Transcription factor	No phenotype/short period	Long period
ELF3	Evening	Transcription regulator	Arrhythmic under constant light	Long period
ELF4	Evening	Transcription regulator	Arrhythmic under constant light	
ZTL	Evening	F-box protein, blue light receptor	Long period	
STIPL1	-	Component of spliceosome	Long period	
LNK2	-	Nuclear protein	Long period (redundant with *LNK1*)	
JMJD5	-	Histone demethylase	Short period	Short period
LIP1	-	Small GTPase	Short period	
TPL1	-	Tup1 corepressor	Long period or arrhythmic (redundant with other members of TPL/TPR family)	Long period

Selected components of the *Arabidopsis* circadian system that affect the period or rhythmicity of circadian rhythms upon mutation. Name of gene, the time of day of activity and function of gene product, as well as the effect of loss of function and constitutive overexpression on circadian rhythms are shown (Nagel and Kay, 2012; Hsu and Harmer, 2014).

These include the nuclear localised MYB-like transcription factor *LUX ARRHYTHMO* (*LUX*) (Hazen et al., 2005); *BROTHER OF LUX ARRHYTHMO* (*BOA* or *NOX*), a nuclear-localised GARP family transcription factor expressed in all plant tissues with particular abundance in flowers (Dai et al., 2011; Helfer et al., 2011); *GIGANTEA* (*GI*), a nuclear-localised protein with diverse functions and protein interactions (Locke et al., 2006; Song et al., 2014); *EARLY FLOWERING 3* (*ELF3*) and *ELF4*, two unrelated novel nuclear-localised transcription regulators (Herrero et al., 2012) and the nuclear-localised TCP transcription factor *CCA1 HIKING EXPEDITION* (*CHE*) (Pruneda-Paz et al., 2009). In each case, repression of transcription by CCA1 and LHY depends on the recruitment of DEETIOLATED1 (DET1), a nuclear protein component of the evolutionarily conserved COP10-DET1-DDB1 (CDD) protein complex involved in photomorphogenesis (Lau et al., 2011). DET1, which acts as a transcriptional repressor, physically interacts with CCA1 and LHY and binds to the promoter of CCA1/LHY target genes in a CCA1/LHY-dependent manner (Lau *et al*., 2011). Association of DET1 to target promoters occurs via the evening element (EE) motif - a nine-nucleotide absolutely conserved circadian clock regulatory element present in the promoters of numerous evening-phased clock regulated genes (Harmer et al., 2000; Lau et al., 2011). Interestingly, CCA1 and LHY proteins also repress their own and each other's expression, possibly by forming interactions with other transcription factors (Adams et al., 2015).

TOC1 is part of a five-member, nuclear-localised PSEUDO-RESPONSE REGULATOR (PRR) family which is characterised as containing two domains – the N-terminal pseudoreceiver (PR) domain and the DNA-binding CONSTANS (CO)-like CCT domain at the C-terminal (Strayer et al., 2000; Matsushika et al., 2000; Wenkel et al., 2006). The N-terminal PR domain allows homo- and heterodimerisation between PRR proteins as well as interactions with other proteins. The repressing function of TOC1 is widespread, and occurs through direct binding of the C-terminal CCT domain to a *cis*-element termed T1ME (TOC1 morning element), which is present in the promoters of target genes (Gendron et al., 2012). *TOC1* transcripts and protein oscillate 12 hours out of phase with both LHY and CCA1, and the

nuclear-localised, evening-expressed TOC1 protein represses the expression of *CCA1* and *LHY* genes by direct binding of the CCR domain to the target promoters (Gendron et al., 2012; Pokhilko et al., 2012). In contrast, the evening-phased transcription factor CHE inhibits only the expression of *CCA1* (Pruneda-Paz et al., 2009). TOC1 also interacts with CHE, which in turn binds to the *CCA1* promoter, thereby establishing another molecular linkage between TOC1 and *CCA1* regulation. Interestingly, *NOX* also binds to the promoter of *CCA1*, but acts as an activator of *CCA1* expression (Dai et al., 2011).

The regulatory module containing *CCA1* and *LHY* is interlocked with two additional loops, the first of which involves the day-phased members of the PRR family (Farré et al., 2005; Farré and Liu, 2013). Members of the *PRR* family are expressed sequentially from morning to night, with transcription of *PRR9* peaking just after dawn, followed by *PRR7* in the morning, *PRR5* in the afternoon, and *PRR3* and *TOC1* (*PRR1*) in the evening (Matsushika et al., 2000). In addition to acting as transcriptional repressors of the evening-phased PRR *TOC1*, CCA1 and LHY also inhibit the expression of the day-phased PRRs *PRR9*, *PRR7* and *PRR5* (Adams et al., 2015; Kamioka et al., 2016). CCA1 and LHY protein levels peak a few hours before *PRR9* and *PRR7* transcription peaks (Farré et al., 2005), and the proteins repress expression of the *PRR*s by binding directly to the *PRR9* and *PRR7* promoters. *PRR7* has three CCA1 binding sites (CBS, a circadian clock regulatory element highly related to the EE motif), while the *PRR9* promoter contains an EE upstream of the transcription start site (Farré et al., 2005; Adams et al., 2015).

The importance of PRRs in regulating clock function is demonstrated by the circadian phenotype of the *prr5 prr7 prr9* triple mutant, which is arrhythmic under constant conditions (Nakamichi *et al*., 2005). The functions of *PRR5*, *PRR7* and *PPR9* are partially redundant, yet all three proteins collectively play an important part in maintaining circadian rhythms as they are expressed at different times of day. *PRR9*, *PRR7* and *PRR5* actively repress expression of *CCA1* and *LHY* through association with promoter their regions. Transcript abundance for each of the five members of the *PRR* family peak sequentially from shortly after dawn to

approximately dusk, with corresponding protein cycling with a slightly lagging phase relative to transcript, which allows repression of *CCA1* and *LHY* from morning until midnight and limiting expression of CCA1 and LHY only in a small portion of the day (Nakamichi et al., 2005; Fujiwara et al., 2008; Pokhilko et al., 2012). Repression of *CCA1* and *LHY* expression by the three PRR proteins relies on interaction with members of the Groucho/Tip1 corepressor family, TOPLESS/TOPLESS-RELATED (TPL/TPR) (Wang et al., 2013). TPL/TPR proteins specifically interact with PRR9, PRR7 and PRR5 and bind to the promoters of *CCA1* and *LHY* to repress transcription. In addition, a complex of PRR9 and TPL interacts with histone deacetylase 6 (HDA6), with the resulting PRR-TL-HDA complex also binding to promoters of *CCA1* and LHY to repress transcription. The five members of the TPL/TPR family are functionally redundant, and mutants in which all TPL/TPR functionality is reduced mimic the arrhythmic phenotype of *prr5 prr7 prr9* mutants (Wang et al., 2013).

The repressive function of the PRRs extend further to include *REVEILLE8/LHY and CCA1-like 5* (*RVE8*/*LCL5*), a MYB-like transcription factor highly related to CCA1 and LHY, as target (Rawat et al., 2011; Hsu et al., 2013). Like CCA1 and LHY, the RVE transcription factors have been shown to bind to the EE motif of target promoters (Harmer et al., 2000; Rawat et al., 2011). Expression of the homologues *RVE1*, *RVE2* and *RVE7* are controlled by the circadian system, yet disrupting the function of these proteins does not impact circadian rhythms (Kuno, 2003; Zhang et al., 2007; Rawat et al., 2009). While RVE1, RVE2 and RVE7 do not play a role in regulating core circadian rhythms, they do play a role in regulating circadian outputs such as auxin signalling and flowering (Kuno, 2003; Zhang et al., 2007; Rawat et al., 2009). In contrast, RVE4, RVE6 and RVE8 are central, partially redundant components of the circadian oscillator (Rawat et al., 2011; Hsu et al., 2013). Transcription levels of *RVE8* peak at dawn (similar to *CCA1* and *LHY* transcription patterns) yet unlike CCA1 and LHY, RVE8 protein levels peak in the afternoon (Rawat et al., 2011). Like CCA1 and LHY, RVE8 binds specifically to the EE of target promoters, but acts as an activator of expression rather than a suppressor (Rawat et al., 2011; Hsu et al., 2013). RVE8 induces

numerous evening-phased genes, and activates expression of the evening clock components *PRR5*, *TOC1*, *PRR3*, *GI*, *LUX* and *ELF4* through binding to the EE (Hsu et al., 2013). The expression of *RVE8* is in turn suppressed directly by PRR5, as well as possibly by PRR7 and PRR9 (Nakamichi et al., 2010; Hsu et al., 2013). The negative feedback loop formed between RVE8 and the PRRs is also linked to CCA1/LHY-containing loops, as PRRs act in sequence to suppress expression of *CCA1* and *LHY* (Nakamichi et al., 2010; Pokhilko et al., 2012). In addition, the expression of *PRR9*, *PRR7* and *PRR5* is inhibited by the both the morning-phase CCA1 and LHY, and by the evening-phased PRR protein TOC1 by direct binding to the promoters (Gendron et al., 2012; Huang et al., 2012; Adams et al., 2015; Kamioka et al., 2016).

The final transcriptional feedback loop further links morning- and day-phased components to evening-phased clock components. As previously stated, *LUX* is an evening-phased MYB-like transcription factor for which expression is activated by RVE8 and suppressed by the morning-phased CCA1 and LHY, and by the evening-phased TOC1 (Hazen et al., 2005; Gendron et al., 2012; Huang et al., 2012; Hsu et al., 2013). LUX interacts with EARLY FLOWERING 3 (ELF3) and ELF4, two nuclear-localised proteins of unknown function, to form the Evening Complex (EC). The EC plays an important, central role in regulation of circadian rhythms, and loss of function of any one member of the evening complex results in plants becoming arrhythmic (Hazen et al., 2005; Herrero et al., 2012). The three members of the EC regulate the expression of a variety of clock genes by direct binding to the EE of target gene promoters (Harmer et al., 2000; Hazen et al., 2005; Herrero et al., 2012). LUX, ELF3 and ELF4 repress expression of day-phased *PRR9*, and LUX represses expression of itself, through direct binding to the EE element of the promoter regions (Helfer et al., 2011). The EC also forms a negative feedback loop with morning components CCA1 and LHY by promoting (through an indirect mechanism) *CCA1* and *LHY* expression, while CCA1 and LHY in turn repress expression of *LUX*, *ELF3* and *ELF4* (Kikis et al., 2005; Herrero et al., 2012; Nagel and Kay, 2012; Adams et al., 2015; Kamioka et al., 2016). In addition, expression of *LUX* and *ELF4* is also repressed by the evening-phased PRR TOC1 (Gendron et al., 2012; Huang et al., 2012) The LUX-

homologue NOX, which (like LUX) promotes expression of *CCA1* and forms a negative feedback loop with the morning component, can also interact with ELF3 and ELF4 (Dai et al., 2011).

1.6.2. Post-transcriptional regulation of circadian clock components in Arabidopsis

In addition to the complex network of transcription feedback loops discussed above, posttranscriptional mechanisms (such as alternative splicing) and posttranslational regulation (such as protein-protein interactions) play important roles in the circadian system (Seo and Mas, 2014; Nolte and Staiger, 2015). Alternative splicing (AS) of precursor mRNAs produces different mRNA variant transcripts from pre-mRNA from the same gene (Nolte and Staiger, 2015). These mRNA isoforms can give rise to protein variants with altered amino acid sequences or protein domains, which in turn could result in changes in activity, localisation, interaction with other proteins or posttranscriptional modifications. Alternatively, AS can result in the generation of mRNAs that contain premature termination codons (PTCs), which are targeted for degradation by nonsense-mediated decay (NMD) (Nolte and Staiger, 2015). Genome-wide mapping of alternative splicing in *Arabidopsis* using RNA sequencing revealed that approximately 42% of intron-containing genes in *Arabidopsis* are alternatively spliced (Filichkin et al., 2010). AS is prevalent among genes of the circadian system, with AS mRNA variants identified for the clock components *CCA1, LHY, TOC1, PRR3, PRR5, PRR7, PRR9, RVE4* and *RVE8* (Filichkin et al., 2010; James et al., 2012). Intron retention events have been reported in mRNAs of the CCA1/LHY-like subfamily of MYB transcription factors, while *RVE2* transcripts are alternatively spliced through the inclusion of a "poison cassette exon" (PCE), a PTC-containing cassette which leads to degradation of the transcript by NMD (Filichkin and Mockler, 2012). AS has been proposed as a mechanism through which the *Arabidopsis* circadian system regulates responses to environmental signals, particularly temperature-associated responses (Filichkin and Mockler, 2012; James et al., 2012; Nolte and

Staiger, 2015). A study investigating AS of clock genes *CCA1*, *LHY*, *TOC1*, *PRR3*, *PRR5*, *PRR7*, *PRR9*, *GI*, *ZTL* and *CHE* at different temperatures revealed extensive alternative splicing: 63 temperature-related AS events were identified for the set of 10 clock genes, with 15 AS events identified upon transfer of plants from ambient temperatures to 4 °C (James et al., 2012). Some of these identified AS events are shown to directly contribute to the abundance of transcripts by triggering NMD, and lower temperatures result in the accumulation of non-productive *LHY*, *PRR7* and *PRR5* transcripts. AS plays a particularly important role in regulating the expression of *LHY* and *CCA1* in response to changes in temperature (James et al., 2012). Shifting plants to low temperatures results in the accumulation of an alternative splice isoform of *LHY* in which intron 5, a long intron which occurs in the *LHY* gene after the two small exons (exons 4 and 5) that code for the Myb domain, is retained. This intron retention event results in the occurrence of a PTC in the *LHY* splice isoform, resulting in a decline in LHY protein levels at low temperature due to action of the NMD pathway (James et al., 2012). In contrast, retention of intron 4 in *CCA1* (which corresponds to intron 5 in *LHY*), decreases at low temperature (Filichkin and Mockler, 2012; James et al., 2012). Interestingly, this effect of temperature on AS and clock gene expression is reversible and can be detected irrespective of the direction of temperature change, suggesting a temperature response mechanism rather than a mere cold stress response (James et al., 2012). The *CCA1* variant transcript in which intron 4 is retained (*CCA1β*) has been linked to cold acclimation of the clock, possibly through self-regulation of CCA1 activity (Seo et al., 2012). The *CCA1β* transcript isoform can code for a variant of the CCA1 protein (CCA1β) that lacks the MYB-like DNA binding domain. It has been proposed that CCA1β interferes with CCA1 function by preventing formation of CCA1α (fully spliced) and LHY homodimers, as well as CCAα-LHY heterodimers. Low temperatures supress this alternative splicing of *CCA1*, and constitutive over-expression of *CCA1β* results in a shortening of circadian period also observed in *cca1 lhy* double mutants. Furthermore, overexpression of *CCA1β* leads to increased sensitivity to freezing, while *CCA1α* overexpressing lines exhibited enhanced tolerance to freezing. However, it remains to be

demonstrated whether the CCA1β variant of the CCA1 protein is expressed *in planta* (Seo et al., 2012).

A few instances of proteins involved in RNA processing affecting circadian rhythms have been reported in *Arabidopsis*. *PROTEIN ARGININGE METHYLTRANSFERASE 5* (*PRMT5*) encodes a type II protein arginine methyltransferase that is located in the nucleus and cytoplasm, and which catalyses the symmetric demethylation of arginine residues (Sanchez et al., 2010). Targets for this protein modification include components of the transcription complex and components of the spliceosome. PRMT5 is involved in the regulation of a variety of pre-mRNA splicing events, possibly by modulating 5'-splice-site recognition (Sanchez et al., 2010). The expression of *PRMT5* is rhythmic and regulated by the circadian clock, and PRMT5 is required for intact circadian rhythms (Hong et al., 2010). Loss of function in *prmt5* mutants causes a lengthening of circadian period, possibly due to effects on the alternative splicing and expression of the *PRR9* (Sanchez et al., 2010). Components of the spliceosome have also been shown to influence the circadian system. SM-like (LSM) proteins are components of the U6 small nuclear ribonucleoprotein (snRNP), one of five snRNPs that, along with several accessory factors, combine to form the large ribonucleoprotein complex of the spliceosome (Perez-Santángelo et al., 2014). Seven LSM proteins have been identified in *Arabidopsis*, and are targets of PRMT5 (Hong et al., 2010). Loss of the PRMT5 substrates LSM4 or LSM5 in the *lsm4* and *lsm5* mutants results in a lengthening of period (as is observed in *prmt5* mutants), along with changes in patterns of expression and splicing of clock genes, including intron retention events in *CCA1*, *PRR9* and *TOC1*. Interestingly, a subset of LSM proteins also regulate and maintain circadian rhythms in mammals, and are themselves regulate by the circadian system (Perez-Santángelo et al., 2014). Other splicing factors have also been identified as playing a role in circadian regulation. SNW/Ski-interacting protein (SKIP) is a splicing factor that physically interacts with the spliceosomal splicing factor Ser/Arg-rich protein 45 and associates with the pre-mRNA of various genes to regulate alternative splicing and mRNA maturation (Wang et al., 2012). SKIP is expressed globally and constitutively, and

regulates the alternative splicing of numerous clock genes, including *PRR9* and *PRR7*. Mutation of *SKIP* causes lengthening in circadian period and affects light sensitivity and temperature compensation of the clock (Wang et al., 2012). Similarly, SPLICEOSOMAL TIMEKEEPER LOCUS1 (STIPL1; also known as NTR1), a putative RNA binding protein and homologue of the spliceosomal proteins Ntr1p (yeast) and TFP11 (human) that are involved in spliceosome disassembly, also affects the *Arabidopsis* circadian system (Jones et al., 2012; Dolata et al., 2015). *stipl1* mutants exhibit a lengthened circadian period, likely linked to the accumulation of splice variants of numerous clock gene transcripts including *CCA1*, *LHY*, *PRR9*, *GI* and *TOC1* (Jones et al., 2012).

Regulation of protein degradation also plays an important role in the circadian system. LHY is rapidly degraded via the proteasome pathway, but interaction with DET1 stabilises LHY protein levels by preventing degradation (Song and Carré, 2005). The cytoplasmic blue light-sensing protein ZEITLUPE (ZTL, see Section 1.7.1.1) and its homologues, FLAVIN BINDING KELCH REPEAT F-BOX (FKF1) and LOV KELCH PROTEIN 2 (LKP2), mediate the regulation of protein turnover of TOC1 and PRR5 (Más et al., 2003; Baudry et al., 2010). ZTL (or FKF1 and LKP2 in the absence of ZTL) binds to TOC1 and PRR5 via its Light-Oxygen-Voltage (LOV) domain, thereby targeting the proteins for ubiquitination and proteasome-dependent degradation (Más et al., 2003; Kiba et al., 2007; Baudry et al., 2010). Interestingly, TOC1 and PRR5 are the only targets of ZTL interaction among the PRR family (Fujiwara et al., 2008). The ZTL-mediated degradation of protein is dark-dependent, and adds yet another layer to the complex mechanism through which the timing of TOC1 (and PRR5) is regulated (Más et al., 2003; Kiba et al., 2007). In plants grown under light:dark cycles, TOC1 protein is rapidly degraded after midnight and levels remain low until ~2 hours before dusk (Más et al., 2003). During the day, blue light induces the LOV domain of ZTL, which results in binding of ZTL to GI being favoured (Kiba et al., 2007; Kim et al., 2007). This protein-protein interaction between ZTL and GI protects TOC1 and PRR5 from ZTL-mediated degradation, and also stabilises ZTL by preventing the proteasome-dependent degradation of

ZTL. GI protein cycles with circadian rhythm, peaking late in the day, and is itself also degraded by the proteasome during the night in a dark-dependent manner (David et al., 2006). During the night, TOC1 interacts with PRR3, thereby preventing formation of the ZTL-TOC1 interaction and delaying degradation of TOC1 until the middle of the night (Para et al., 2007; Fujiwara et al., 2008). Furthermore, TOC1 and PRR5 interact via their conserved N-termini, resulting in increased TOC1 protein levels (by promoting nuclear import), increased subnuclear localisation of TOC1, and increased phosphorylation of the TOC1 N-terminus (Wang et al., 2010). Protein phosphorylation is yet another regulatory mechanism within this system. Phosphorylation of CCA1 by protein kinase Casein Kinase 2 is necessary for CCA1 to perform its function within the circadian oscillator, with phosphorylation allowing the formation of CCA1 dimers and the binding of DNA (Daniel et al., 2004). PRR7, PRR5, PRR3 and TOC1 are all phosphorylated progressively over the circadian cycle, with maximum phosphorylation of PRR5 and TOC1 occurring prior to degradation (Fujiwara et al., 2008). The highly phosphorylated forms of PRR5 and TOC1 interact optimally with ZTL, promoting their degradation, while phosphorylation of TOC1 and PRR3 are necessary for the TOC1-PRR3 interaction (Fujiwara et al., 2008).

1.6.3. Cell-, tissue-, and organ-specific elements of the Arabidopsis circadian system

Cellular- and subcellular localisation of clock elements adds yet another level of complexity to the regulation of the circadian system. In particular, GI has been shown to have separate functions depending on its location in the cell (Kim et al., 2013a). In the cytosol, GI stabilises ZTL by forming a ZTL-GI heterodimer in the blue light-induced protein-protein interaction described in Section 1.6.2 (Kiba et al., 2007; Kim et al., 2007). In the nucleus, GI regulates the expression of *CONSTANS* (*CO*) and *Flowering Locus T* (*FT*), which is required for accurate day-length measurements (Sawa et al., 2007; Sawa and Kay, 2011). Blue light-activation of the LOV domain of FKF1 allows the formation of a GI-FKF1 complex (Sawa et al., 2007). This

GI-FKF1 complex binds to the *CO* promoter, thereby preventing repression of *CO* expression by CYCLING DOF FACTOR 1 (CDF1) and facilitating the correct timing of *CO* expression under different day lengths. In addition, GI directly activates the expression of *FT* by binding to the *FT* promoter, and by interacting with three FT suppressors (Sawa and Kay, 2011). The subcellular distribution of GI is regulated by ZTL and ELF4 (Kim et al., 2013a, 2013b). The ZTL-GI interaction stabilises GI and enhances GI cytosolic localisation (Kim et al., 2013a). In contrast, ELF4 regulates the subnuclear distribution of GI (Kim et al., 2013b). ELF4 sequesters GI from the nucleoplasm to discrete nuclear bodies, thereby limiting the ability of GI to access chromatin, negatively regulating *CO* expression. The formation of these ELF4-GI nuclear bodies varies throughout the day, with punctate nuclear bodies mostly absent during the day and present by the end of the night, even under different day lengths (Kim et al., 2013b).

In contrast to the mammalian circadian system, where the central clock in the brain's suprachiasmatic nucleus is tightly coupled to other clocks in peripheral tissues, intercellular coupling of circadian clock processes in plants has long been described as weak or absent (Wenden et al., 2012; Endo et al., 2014). Rhythmic outputs, such as rhythms in free cytosolic calcium in tobacco or the rhythmic expression of circadian-regulated genes in *Arabidopsis*, lose amplitude (dampen) after prolonged time (~5 days) under free-running, constant light conditions (Sai and Johnson, 1999; Hall et al., 2002; Wenden et al., 2012). It is generally assumed that all plant cells contain essentially identical and cell-autonomous clocks, and coupling of multiple oscillators would require intercellular communication pathways (Bohn et al., 2001; James et al., 2008). Chlorophyll *a* fluorescence analysis of individual *Kalancho*ë *daigremontiana* leaves illustrates the concept of the circadian clock as an assembly of individual, weakly-coupled oscillators that operate independently in space and time (Rascher et al., 2001). Patches of tissue behave as individual oscillators and are weakly coupled, with increasing desynchronization resulting in dampening of overall observable F_q'/F_m' rhythms of the leaf in extended free-run (Rascher et al., 2001). The *Arabidopsis* circadian system is heterogeneous in clock gene expression among different cells, and intercellular coupling is

insufficient to prevent this cellular heterogeneity from resulting in desynchronization of circadian rhythms among cells. Desynchronised leaves can be rapidly resynchronised through application of entraining light:dark cycles, indicating that these cellular clocks are coupled far more strongly to external light:dark cycles than to each other (Wenden et al., 2012). Indeed, whole plans can be desynchronised by applying light-dark treatments to different locations of the same plant (Fukuda et al., 2007). The heterogeneity of rhythms in *K. daigremontiana* leaves does not correlate with tissue type, but is rather due to the dynamics of metabolite pools involved in CAM photosynthesis (Rascher et al., 2001). When monitoring rhythms in *Arabidopsis* through whole-plant assays, the dampening of rhythms has been attributed to spontaneous desynchronization among different cell types, with properties of the circadian clock differing among different plant tissue types (Thain et al., 2002; Wenden et al., 2012). Circadian rhythms in vascular tissues play an important role in regulating flowering, and activation of *FT* expression in leaf vascular tissue (phloem) induces flowering (Corbesier et al., 2007; Endo et al., 2014). Furthermore, GI acts mainly in vascular tissue, directly activating *FT*, and PRR3 expression is restricted to the vascular tissue where it binds to and stabilises TOC1, with TOC1 itself being more abundant in the vasculature of leaves (Para et al., 2007; Sawa and Kay, 2011). A combination of high-resolution tissue isolation techniques and split-luciferase imaging has revealed two distinct clocks with distinct global phases - one in the vasculature and one in the mesophyll (Endo et al., 2014). The two tissue clocks are coupled and regulate each other asymmetrically, with the vasculature exhibiting dominant regulation over the mesophyll clock. Mesophyll-enriched genes tend to be expressed in the morning, while vascular-rich genes tend to be expressed in the evening (Endo et al., 2014).

1.7. Communicating environmental signals to plant cells

Living cells sense signals from their environment, which can elicit direct responses or act to entrain circadian systems (Pittendrigh, 1992; Christie et al., 2015; de Souza et al., 2017). While

daily temperature cycles are an effective entraining signal for many circadian systems, particularly in poikilotherms, light is the most universal and important Zeitgeber in nature (Pittendrigh, 1992; Millar, 2016). In addition to serving as an entraining signal, light is a ubiquitous source of energy and acts as a stimulus that directs development, morphogenesis and physiology in plants (Christie et al., 2015). The intercellular coupling of circadian rhythms does not occur in isolation, and effective coordination of responses to environmental inputs such as light is achieved through tightly regulated inter- and intracellular communication networks (Chan et al., 2016b; de Souza et al., 2017; Millar, 2016). These communication networks often rely on interorganellar interactions that are controlled by anterograde (nucleus-to-organelle) and retrograde (organelle-to-nucleus) signalling, although interorganellar communication can occur without nuclear mediation (de Souza et al., 2017). Chloroplasts and mitochondria serve as the metabolic hubs of plant cells, with chloroplasts playing particularly varied roles by serving as the site of photosynthesis, synthesis of fatty acids, production of fatty-acid derivatives such as amino acids and starches, and as the site of hormone metabolism. In addition, chloroplasts act as sensors that sense environmental signals and perceive stress. As a result, chloroplasts (and mitochondria) produce retrograde signals to coordinate adaptive responses that require nuclear encoding (de Souza et al., 2017). This section will focus on the sensing of light signals from the environment, circadian regulation of light sensing and light-driven responses, and the communication of signals from chloroplasts via retrograde signalling in plant cells.

1.7.1. Sensing light from the environment

1.7.1.1. Light inputs through photoreceptor pathways

Plants sense and utilise light through the action of specialised photoreceptors (Christie et al., 2015; Galvão and Fankhauser, 2015). Photoreceptors are light-responsive proteins that typically contain a prosthetic cofactor or chromophore which allows the photoreceptor to

perceive and respond to changes in the intensity, quality, direction and duration of light (Rockwell et al., 2006; Chen and Chory, 2011). Five different photoreceptor systems have been identified in plants, each sensitive to specific wavelengths of light (Christie et al., 2015): cryptochromes (crys) (Chaves et al., 2011), phototropins (phots) (Christie, 2007) and members of the Zeitlupe (ZTL) family (Suetsugu and Wada, 2013) that respond to blue light (Christie et al., 2015), UV Resistance locus 8 (UVR8) that monitors ultraviolet B wavelengths (Jenkins, 2014), and phytochromes (phys) that respond to red and far-red light (Rockwell et al., 2006; Chen and Chory, 2011).

Cryptocromes. Cryptochromes are UV-A/blue photoreceptors that act as major regulators of growth and development and entrain the circadian clock (Liu et al., 2011b; Christie et al., 2015). *Arabidopsis* contains three cryptochromes (cry1-cry3) that have partially overlapping functions (Christie et al., 2015). Cry1 and cry2 are localised predominantly in the nucleus, and regulate seedling de-etiolation under blue light and photoperiodic flowering, respectively (Liu et al., 2011b; Christie et al., 2015). Cry3 is a cry-DASH protein that localises in mitochondria and chloroplasts and functions in DNA repair, repairing UV-induced damage in single-stranded DNA and in loop structures of double-stranded DNA (Kleine et al., 2003; Pokorny et al., 2008; Liu et al., 2011b). Cryptochromes are evolutionarily related to DNA photolyases and bind two chromophores: a two-electron carrier flavin adenine dinucleotide (FAD) non-covalently bound and functioning as the primary light sensor, and a pterin derivative 5,10-methenyltetrahydrofolate (MTHF) which harvests and transfers additional light energy to the FAD from the near UV region (Ahmad and Cashmore, 1993; Hoang et al., 2008; Christie et al., 2015). Cry1 and cry2 each consists of a N-terminus photolyase homology region (PHR) which binds FAD and mediates photosensing, and a cryptochrome C-terminus (CCT) domain, which is important in cryptochrome signalling and is absent in cry3 (Yang et al., 2000; Hoang et al., 2008; Yu et al., 2009). The exact mechanism of photoexcitation of cryptochromes is still debated (Liu et al., 2011b; Galvão and Fankhauser, 2015). In darkness, cryptochromes exist in a dark (ground) state, with the PHR and CCT domains in closed (inactive) conformation and

FAD in the oxidised state (Banerjee et al., 2007; Bouly et al., 2007; Liu et al., 2011b). According to the photoreduction cycle model, upon illumination with blue light FAD is reduce to semireduced $FADH^*$ and may be further reduced to $FADH_2$. The photoreduction of oxidized FAD to semireduced $FADH^*$ triggers a conformational change in the CCT domain to produce an open (active) conformation, resulting in subsequent signal transduction, and the reduced flavin is re-oxidised to complete the photocycle (Banerjee et al., 2007; Bouly et al., 2007; Liu et al., 2011b). An alternative model describes a circular electron shuttle whereby photoexcitation results in transfer of electrons from FAD^{*-} to bound ATP, facilitating phosphotransfer from ATP to the CCE domain and triggering the conformational changes necessary for signal transduction (Liu et al., 2010, 2011b). Phosphorylation of the CCT domain correlates with photoactivation and biological activity of cryptochromes, and both cry1 and cry2 are rapidly phosphorylated in etiolated seedlings upon exposure to blue light (Shalitin et al., 2002, 2003; Christie et al., 2015). The blue light-induced phosphorylation of cry2 also induces ubiquitination and subsequent degradation, demonstrating the functioning of cry2 in light-limiting conditions (Tan et al., 2013; Christie et al., 2015).

The regulation of plant development by cryptochromes largely involves mediating changes in gene expression in the nucleus, and two mechanisms of transcriptional control have been described for cryptochrome signalling (Liu et al., 2011b; Christie et al., 2015). The first involves indirect regulation of gene expression through post-transcriptional mechanisms involving the CONSTITUTIVE PHOTOMORPHOGENIC 1 (COP1)/SUPPRESSOR OF PHYA 1 (SPA) complex (Lian et al., 2011; Liu et al., 2011a; Zuo et al., 2011). The COP1-SPA1 complex acts as a substrate receptor for the CUL4-DDB1 E3 ubiquitin ligase complex, which is responsible for the degradation of proteins involved in photomorphogenic development (Liu et al., 2011b; Lau and Deng, 2012; Christie et al., 2015). Upon activation by blue light, cry1 and cry2 bind to SPA1 and suppress the action of the COP1-SPA1 complex. Specifically, interaction between COP1-SPA1 and cry1 prevents the COP1-mediated degradation of the basic leucine zipper (bZIP) transcription factors LONG HYPOCOTYL 5

(HY5) and HY5 HOMOLOGUE (HYH), and of the basic helix-loop-helix transcription factor LONG HYPOCOTYL IN FAR RED 1 (HFR1), all of which regulate the transcription of genes required for the de-etiolation response (Osterlund et al., 2000; Duek et al., 2004; Yang et al., 2005; Lee et al., 2007; Liu et al., 2011b). Similarly, cry2 interaction with the COP1-SPA1 complex prevents degradation of CO, allowing the accumulation of CO under blue light and initiation of flowering in long days (Liu et al., 2008b, 2011b). The second mechanism of cryptochrome signalling involves direct regulation of transcription by means of a blue light-dependent interaction between cry2 and the CRYPTOCHROME-INTERACTING BASIC-HELIX-LOOP-HELIX (CIB) transcription factors (Liu et al., 2008a, 2013). CIB transcription factors positively regulate flowering in a cry2-dependent manner, possibly through heterodimerisation and subsequent binding to the promoter region of *FT* (Liu et al., 2008a, 2013). While the exact mechanism of the cry2-CIB pathway is not well understood, it has been suggested that interaction with cry2 prevents ubiquitination and degradation of CIB proteins under blue light (Liu et al., 2011b).

Phototropins. Phototropins are blue-light-activated serine/threonine kinases that mediate a range of photoresponses, such as phototropism and stomatal movement, to optimise photosynthetic efficiency and promote growth (Christie et al., 1999; Takemiya, 2005; Christie et al., 2015). Higher plants, like *Arabidopsis,* contain two phototropins (phot1 and phot) that perform a range of overlapping and distinct functions (Takemiya, 2005; Liscum et al., 2014). phot1 and phot2 act redundantly to regulate hypocotyl and root phototropism under moderate light conditions, as well as stomatal opening, chloroplast movement, and leaf positioning and flattening (Kagawa et al., 2001; Kinoshita et al., 2001; Sakai et al., 2001; Sakamoto and Briggs, 2002; Inoue et al., 2008b; Liscum et al., 2014). Phot1 regulates hypocotyl phototropism over a range of light intensities, particularly under low intensity light, while phot2 regulates this response predominantly under higher fluence rates (Sakai et al., 2001). Similarly, phot1 and phot2 act redundantly to stimulate chloroplast positioning along cellular edges under low light conditions, while phot2 alone facilitates chloroplast and nuclear avoidance movements under

high light intensities (Kagawa et al., 2001; Sakai et al., 2001; Higa et al., 2014). Phot1 also regulates the rapid inhibition of hypocotyl elongation in etiolated seedlings in response to light, promotes mRNA destabilisation in etiolated seedlings under high light intensities, and regulates suppression of lateral root growth via an auxin-related pathway (Folta et al., 2003; Folta and Kaufman, 2003; Moni et al., 2015). Phot1 and phot2 are localised predominantly to the intracellular side of the plasma membrane in dark-grown seedlings, and can also localise to the outer membrane of chloroplasts (Sakamoto and Briggs, 2002; Kong et al., 2006, 2013). Upon long-term (>12h) exposure to blue light, phototropins autophosphorylate and are re-localised to intracellular locations, with a fraction of phot1 targeted to the cytosol while phot2 is re-localised to the Golgi apparatus (Sakamoto and Briggs, 2002; Kong et al., 2006; Inoue et al., 2008a; Kaiserli et al., 2009). While the relocalisation of phototropins under blue light is dependent upon some of the same autophosphorylation mechanisms that are required for phototropin function, it remains to be determined how this intracellular movement is involved in phototropin signalling (Liscum et al., 2014; Liscum, 2016).

Phototropins consist of an N-terminal photosensory region containing two repeated Light-Oxygen-Voltage domains, LOV1 and LOV2, and a C-terminal protein kinase domain (PKD) responsible for signal output (Tokutomi et al., 2008; Suetsugu and Wada, 2013; Liscum et al., 2014). LOV1 functions primarily to facilitate dimerisation of the phototropins, and has also been shown to affect the photoreactivity of the LOV2 domain (Salomon et al., 2004; Matsuoka and Tokutomi, 2005; Jones and Christie, 2008; Nakasako et al., 2008). In contrast, the LOV2 domain functions as the main regulator of the C-terminal PKD kinase activity through a novel blue light-induced derepression mechanism (Christie et al., 2002; Jones et al., 2007; Jones and Christie, 2008; Tokutomi et al., 2008; Liscum et al., 2014). In the dark (inactive state), each LOV domain binds oxidised flavin mononucleotide (FMN) noncovalently, which serves as a chromophore and strongly absorbs blue light (Christie et al., 1999, 2015). In this inactive state, the LOV2 domain is folded in such a way as to cause steric inhibition of the PKD kinase activity (Harper et al., 2003, 2004; Jones and Christie, 2008; Tokutomi et al., 2008). Upon irradiation

with blue light, a covalent bond is rapidly formed between FMN and a nearby conserved cysteine residue (Salomon et al., 2000; Liscum, 2016). The resulting FMN-cysteinyl adduct produces a spectral species that no longer absorbs blue light, and which represents the active signalling state that leads to photoreceptor activation. This photochemical reaction is rapidly and fully reversible in darkness, while thermal decay of the covalent adduct back to the dark state can occur over a longer time scale (Circolone et al., 2012; Christie et al., 2012b, 2015). The LOV2 domain contains a conserved glutamine residue which hydrogen-bonds to the FMN chromophore in darkness and which, upon blue light-induced formation of the FMN-cysteinyl adduct, undergoes a side chain rotation that temporarily alters the hydrogen bonding with FMN (Crosson and Moffat, 2001; Christie et al., 2015). The side chain rotation leads to structural changes in the phot protein that in turn result in the unfolding of a surface α-helix (J_α) present in a linker domain region between LOV2 and the PKD (Harper et al., 2003, 2004; Jones et al., 2007; Jones and Christie, 2008; Liscum et al., 2014). This unfolding of J_α causes the N-terminus to move and alleviate the steric repression of the PKD, promoting ATP binding and initiating receptor autophosphorylation (Pfeifer et al., 2010; Inoue et al., 2011; Liscum et al., 2014). Autophosphorylation of the phot occurs at multiple (>20) serine residues and is essential to phototropin function, with phosphorylated phot generally regarded as the activated version of the photoreceptor (Inoue et al., 2008a; Sullivan et al., 2008; Inoue et al., 2011; Liscum et al., 2014; Christie et al., 2015).

A variety of downstream, phot-interacting proteins have been described, and the discovery of phototropin substrate targets is ongoing (Liscum et al., 2014; Christie et al., 2015). Targets include proteins involved in phototropic responses, and proteins involved in auxin or ion transport. Among the proteins involved in phototropism is NONPHOTOTROPIC HYPOCOTYL3 (NPH3), the gene locus of which was first identified among four loci that result in impaired phototropic responses in etiolated *Arabidopsis* seedlings with loss-of-function mutations (Liscum and Briggs, 1995; Liscum et al., 2014). NPH3 is necessary for phot1-dependent phototropism under low blue light, as well for phot1/phot2-mediated

phototropic signalling under high intensity blue light (Motchoulski and Liscum, 1999; Roberts et al., 2011). The phototropic signalling capacity of NPH3 is regulated by phosphorylation state (Pedmale and Liscum, 2007; Liscum et al., 2014). In the dark, NPH3 is present mostly in a phosphorylated state, while illumination with blue light results in accumulation of dephosphorylated NPH3. The conversion of phosphorylated to dephosphorylated NPH3 is dependent on the presence of phot1, and prevention of this conversion disrupts phototropic responses (Pedmale and Liscum, 2007; Liscum et al., 2014). Like phot1, NPH3 associates with the plasma membrane, yet NPH3 does not relocalise under exposure to light (Motchoulski and Liscum, 1999). NPH3 interacts directly with phot1, with the C-terminal region of NPH3 binding to the LOV domain-containing N-terminal of phot1 (Motchoulski and Liscum, 1999; Inada et al., 2004). The regulation of phot1-mediated phototropic signalling by NPH3 likely occurs via the action of $CRL3^{NPH3}$, a complex formed upon the interaction between NPH3 and CULLIN3-based E3 ubiquitin ligase (CUL3) (Roberts et al., 2011). Indeed, normal phototropism in hypocotyls requires the presence of functional NPH3 and CUL3. CUL-based E3 complexes (also referred to as CULLIN-RING-ligases, CRLs) catalyse the final step in a three-enzyme process that results in the ubiquitination of a target protein (Komander, 2009; Roberts et al., 2011). Ubiquitination of a target protein can involve ligation of a single ubiquitin moiety to a single lysine residue (monoubiquitination), ligation of single ubiquitin moieties to multiple lysine residues (multiubiquitination), or the addition of poly-ubiquitin chains to one or more lysine residues (polyubiquitination) (Motchoulski and Liscum, 1999; Sakai et al., 2000; Pedmale and Liscum, 2007). While ubiquitination of proteins is most commonly associated with subsequent protein degradation, mono- and multiubiquitination is typically linked to proteasome-independent processes such as DNA repair, transcription, membrane protein endocytosis and subcellular protein trafficking (Komander, 2009; Roberts et al., 2011). Upon illumination with high-intensity light, $CRL3^{NPH3}$ facilitates the mono-, multi- and polyubiquitination of phot1 (Roberts et al., 2011). The polyubiquitination of phot1 leads to 26S proteasome-dependent degradation of phot1, a process which is also dependent on the activity of $CRL3^{NPH3}$ and which possibly serves to desensitize phototropic signalling. In contrast,

illumination with low-intensity blue light results in $CRL3^{NPH3}$-dependent mono- and multiubiquitination of phot1, thereby likely targeting phot1 for internalisation by an autophosphorylation-dependent, clathrin-associated endocytic mechanism (Roberts et al., 2011). Another protein suggested to play a role in the ubiquitination-dependent regulation of phototropism is ROOT PHOTOTROPISM2 (RPT2), a protein in the same family as NPH3 (Motchoulski and Liscum, 1999; Sakai et al., 2000; Pedmale and Liscum, 2007; Liscum et al., 2014). Loss of function in *RPT2* results in defective root phototropism, as well as defective hypocotyl phototropism under high-intensity blue light conditions where both phot1 and phot2 are active (Sakai et al., 2000). Like NPH3 and phots, RPT2 associates with the plasma membrane, and RPT2 interacts physically with both NPH3 and phot *in planta* (Inada et al., 2004). While the exact mechanism of RPT2 activity is not known, it has been proposed that RPT2 also interacts with CUL3 and that a separate $CRL3^{NPH3/RPT2}$ complex might mediate the polyubiquitination of phot1 under high blue light (Liscum et al., 2014).

Zeitlupe family. ZEITLUPE (ZTL), FLAVIN BINDING KELCH REPEAT F-BOX (FKF1) and LOV KELCH PROTEIN 2 (LKP2) comprise a family of LOV UV-A/blue light photoreceptors that play direct roles in post-transcriptional regulation of circadian and flowering components (described in Section 1.6.2) (Más et al., 2003; Baudry et al., 2010; Christie et al., 2015; Galvão and Fankhauser, 2015). The three ZTL members localise either in the cytosol or the nucleus, and overlap partially in function (Fornara et al., 2009; Baudry et al., 2010; Takase et al., 2011). *Arabidopsis ztl* mutants exhibit lengthened circadian rhythms (which are more severe in ZTL family double or triple mutants), while *fkf1* single mutants mostly show alterations in flowering time, and *lkp2* single mutants show minimal alterations in circadian and flowering regulation (Imaizumi et al., 2003; Baudry et al., 2010). While the protein structure of ZTL members is similar to that of cryptochromes and phototropins (with a N-terminal photosensory module located upstream from a C-terminal effector region), unlike phototropins, ZTL members contain only one LOV domain (Ito et al., 2012). Following the N-terminal LOV domain is an F-box (which associates with Skp Cullin F-box (SCF)-type E3

ubiquitin ligases involved in protein degradation) and six kelch repeats (which mediate heterodimerization between LKP2 and the other two ZTL family members) at the C-terminus (Takase et al., 2011; Ito et al., 2012). Similar to phototropins, ZTL members bind oxidised FMN as a chromophore at the LOV domain which, upon blue light illumination, forms a FMN-cysteinyl adduct within the protein (Imaizumi et al., 2003; Ito et al., 2012). Unlike phototropins, which undergo rapid reversion in the dark, FKF1 remains stable in the light-activated signalling state for days, while the adduct decay of activated ZTL occurs over hours (Zikihara et al., 2006; Pudasaini and Zoltowski, 2013). ZTL family members undergo light-mediated interactions with circadian and flowering components via protein-protein interactions that are facilitated by the LOV domain (Sawa et al., 2007; Fornara et al., 2009; Kim et al., 2013a; Christie et al., 2015). Degradation of TOC1 is mediated by ZTL and inhibited by blue light (Más et al., 2003; Kiba et al., 2007; Fujiwara et al., 2008). Interaction between ZTL and GI results in reciprocal stabilization of both proteins, and limits the action of the SCF-ZTL complex on its substrates targeted for degradation (Kim et al., 2007, 2013a). Similarly, FKF1 interacts with GI, yet this interaction promotes SCF-FKF1 activity (Sawa et al., 2007; Fornara et al., 2009) Furthermore, Cycling DOF factors (CDFs, that repress *CO* expression by direct binding to the promoter) interact with the kelch repeats of FKF1, further regulating flowering (Sawa et al., 2007; Fornara et al., 2009).

UVR8. UVR8 is a photoreceptor that occurs in the cytosol and nucleus, and which mediates photomorphogenic responses under low fluence rates of UV-B light (Jenkins, 2009; Rizzini et al., 2011). UV-B radiation (280 to 315 nm) does not drive photosynthesis, but has the potential to damage molecules, such as DNA, due to its relatively high energy (Jenkins, 2014; Galvão and Fankhauser, 2015). Plants employ a variety of protective mechanisms to shield against UV-B damage, including the production of reflective surface waxes and hairs and the synthesis of phenolic compounds that accumulate in the epidermal layer and absorb UV-B light, reducing transmittance to cells. Exposure to UV-B also initiates protective responses, including antioxidant- and DNA repair systems. In addition, low doses of UV-B light initiate a variety of

photomorphogenic responses (Jenkins, 2014). Among these, UVR8 mediates flavonoid biosynthesis, DNA repair, amelioration of oxidative damage, stomatal movement and phototropic bending (Brown et al., 2005; Favory et al., 2009; Fehér et al., 2011; Jenkins, 2014; Vandenbussche et al., 2014; Tossi et al., 2014). In addition, UVR8 mediates entrainment of the circadian clock by low-fluence-rate UV-B light (Jenkins, 2014). While the exact mechanism of UVR8 photoreception is not clear, insight has been gained into structural features important in UVR8 signalling (Jenkins, 2014; Galvão and Fankhauser, 2015). Instead of a cofactor chromophore, UVR8 senses light via a triad of closely packed tryptophan residues (Rizzini et al., 2011; Christie et al., 2012a; Wu et al., 2012). UVR8 exists as a homodimer in its ground state, maintained by salt-bridge interactions between charged amino acids (particularly arginines) at the dimer interface surface (Christie et al., 2012a; Wu et al., 2012). Upon illumination with UV-B light, the tryptophan pyramid at the dimer interface mediates disruption of the salt bridges, and the homodimer immediately dissociates into active monomers that initiate signalling (Rizzini et al., 2011; Christie et al., 2012a; Wu et al., 2012). This UV-B-induced monomerization is reversible, with UVR8 homodimers reforming and allowing continuous sensitivity to UV-B light (Christie et al., 2012a; Heijde and Ulm, 2013; Heijde et al., 2013). UVR8 mediates UV-B-induced responses mostly through gene expression, regulating the transcription of several hundred target genes in *Arabidopsis* seedlings. UVR8 signalling intersects with both cryptochrome and phytochrome signalling pathways (Cloix et al., 2012; Binkert et al., 2014; Jenkins, 2014; Galvão and Fankhauser, 2015; Hayes et al., 2017). Following UV-B-induced monomerization, the active UVR8 monomer accumulates in the nucleus and interacts with COP1, leading to the expression and stabilisation of the bZIP transcription factors HY5 and HYH (Cloix et al., 2012; Jenkins, 2014). HY5 and HYH in turn bind directly to the promoters of UV-B-responsive genes and to the promoter region of *HY5*, promoting transcriptional activation (Binkert et al., 2014; Galvão and Fankhauser, 2015). In addition, UVR8 has recently been shown to inhibit thermomorphogenesis, inhibiting auxin signalling and stem elongation at higher temperatures (Hayes et al., 2017). At higher temperatures, the UV-B-induced UVR8-COP1 interaction supresses transcript abundance of

the bHLH factor PIF4 (see section on phytochromes below), while in turn stabilising the bHLH factor HFR1 – an inhibiter of PIF4 function (Hayes et al., 2017).

Phytochromes. Phytochromes are homodimeric or heterodimeric proteins capable of sensing red (R) and far-red (FR) light. (Burgie and Vierstra, 2014; Galvão and Fankhauser, 2015). In plants, each subunit of phytochromes consists of an N-terminal photosensing module (PSM) that covalently binds to a phytochromobilin tetrapyrrole chromophore (PϕB), and a C-terminal output module (OPM) that is involved in dimerization and possibly in relaying light signals to downstream signalling events (Rockwell et al., 2006; Burgie and Vierstra, 2014). Phytochromes are synthesised in the cytoplasm as a biologically inactive, red-absorbing (Pr) form that converts to an active, far-red-absorbing (Pfr) form upon absorption of red light (Rockwell et al., 2006; Bae and Choi, 2008). The active Pfr form is converted back to the inactive Pr ground state rapidly upon irradiation with far-red light, or slowly through a thermal inversion process in the absence of light (dark reversion). While Pr and Pfr have absorption peaks at 667nm (red) and 730 nm (far-red), respectively, both forms absorb in far-red and red spectra as well (Casal et al., 2003). The structural aspects of phytochrome photoconversion have not yet been resolved, but it has been proposed that absorption of red light might cause photoisomerisation of the bilin, resulting in cleavage of the hydrogen bond between the bilin D-ring and a conserved histidine residue, and subsequent conformational changes (Burgie and Vierstra, 2014).

Plants are exposed to varying ratios of red and far-red light depending on factors such as canopy cover and soil depth (Legris et al., 2017). Green leaves reflect and transmit far-red light more efficiently than red light, while red light is absorbed by photosynthetic pigments. Therefore, plants growing in the shade of canopy cover are exposed to a low red/far red ratio than in open-field conditions, while the poor penetration of light through soil means buried seeds are exposed to very low levels of light (Legris et al., 2017). As a result, the ratio of red/far red light (and therefore the ratio of Pr/Pfr) impacts the level of light responsiveness and shade avoidance in plants (Rockwell et al., 2006; Casal, 2013; Legris et al., 2017). Pr/Pfr ratio is determined by

the light environment, the forward and reverse rates of photoconversion, and the rates of thermal interconversion between the two forms. *Arabidopsis* contains five different phytochromes (phyA-E) which are obligate dimers (Rockwell et al., 2006; Galvão and Fankhauser, 2015). These five phytochromes have both distinct and overlapping functions throughout the lifecycle, including mediation of germination, de-etiolation, stomata development, flowering transition, circadian regulation, senescence and shade avoidance. PhyA is the most unique of the plant phytochromes, as it is light-labile (stable in the Pr form) and acts in a specialised role as a far-red light sensor (Casal et al., 2014). In addition, PhyA has been shown to regulate chloroplast gene transcription in response to blue light or UV-A radiation in mature green leaves (Chun, 2001). PhyA is essential for de-etiolation in far-red-rich environments (such as in canopy shade) and it may have provided an adaptive advantage to early angiosperms during colonization of habitats that were dominated by gymnosperms and ferns (Mathews, 2005). Upon irradiation with red or far-red light, phyA rapidly localizes in the nucleus (Toledo-Ortiz et al., 2010). The translocation of phyA into the nucleus is vital to its function as FR sensor and, since phyA does not contain a nuclear localization signal, is depended on the physical interaction with the two functional homologs FAR-RED ELONGATED HYPOCOTYL1 (FHY1) and FHY1-LIKE (FHL) (Hiltbrunner et al., 2006). *PHYA* promoter activity is regulated by the circadian clock and peaks during the day, yet PhyA is rapidly degraded during the light period in day/night cycles (Sharrock and Clack, 2002; Casal et al., 2014). In addition, light down-regulates the abundance of phyA at transcriptional level (Jang et al., 2011; Sharrock and Clack, 2002; Casal et al., 2014). In contrast, phyB-E are light stable; and phyB is the predominant red light sensor in plants, with phyC, phyD and phyE in many cases functionally redundant to phyB (Rockwell et al., 2006). PhyB Pfr undergoes spontaneous thermal reversion, while dark-reversion of phyA is observed only in some *Arabidopsis* accessions (Casal et al., 2014; Legris et al., 2016). As observed in phyA, phyB converts to Pfr upon absorption of red light, and the Pfr form migrates to the nucleus and localises in nuclear bodies (photobodies) (Legris et al., 2017). This nuclear localisation is necessary to the function of phyB, and phyB activity (during de-etiolation) correlates with the

formation of large nuclear bodies. The spontaneous reversion of phyB Pfr to Pr means that maintaining a level of active Pfr is irradiance-dependent and, as phyB Pfr will gradually decrease in the dark, phyB provides a mechanism for sensing changes in irradiance and night length (Legris et al., 2017). PhyB has also been proposed as a point of entry for temperature signalling, as phyB thermal reversion rate increases with temperature (from 4-30 °C) (Legris et al., 2016, 2017).

Signalling downstream of phytochromes for regulation of growth occurs mainly through two interconnected branches: one branch involves the PHYTOCHROME INTERACTING FACTOR (PIF) transcription factors, while the other involves the transcription factor ELONGATED HYPOCOTYL 5 (HY5) and CONSTITUTIVE PHOTOPORPHOGENIC 1 (COP1) (Casal et al., 2014; Legris et al., 2017). PIFs are a fifteen-member family of nuclear-localised basic helix-loop-helix transcriptional regulators, of which seven (PIF1, PIF3, PIF4, PIF5, PIF6, PIF7 and PIF8) bind directly to the Pfr form of phyB in a red/far-red photoreversible fashion (Leivar and Monte, 2014). PIF1 and PIF3 also interact similarly with phyA Pfr (Casal et al., 2014). The direct physical binding of PIFs with phy Pfr results in rapid phosphorylation, ubiquitination and degradation of PIFs via the ubiquitin-proteasome system, and inhibits their binding to target gene promoters (Leivar and Quail, 2011; Legris et al., 2017). In the dark, such as in seedlings germinated in soil, phytochromes reside in the cytosol in the inactive Pr form, allowing accumulation of PIFs in the nucleus (Leivar and Quail, 2011; Leivar and Monte, 2014). The accumulated PIFs (particularly PIF1, PIF3, PIF4 and PIF5) promote skotomorphogenesis, facilitating growth to seek for light. Upon light exposure, the active Pfr form of phytochromes translocates to the nucleus and physically interacts with PIFs, resulting in a decrease in PIF levels and initiation of deetiolation (Leivar and Quail, 2011; Leivar and Monte, 2014). PIFs serve to integrate environmental and internal signals, including sugar-derived signalling, hormone signalling, light and temperature signalling, and retrograde signalling (Leivar and Monte, 2014; Legris et al., 2017; Martín et al., 2016; Soy et al., 2016; Zhu et al., 2016).. It has been suggested that the nuclear-localised photoreceptor system

regulates photomorphogenic development under moderate light, but that excessive light levels result in the induction of retrograde signalling mechanisms that serve to suppress such development, thereby providing protection against photo-oxidative damage (Martín et al., 2016). Indeed, PIF and ROS signalling pathways integrate antagonistically to regulate light-induced responses (Chen et al., 2013a; Martín et al., 2016).

The COP1-HY5 branch integrates phytochrome and cryptochrome signalling (Casal et al., 2014; Legris et al., 2017). During deetiolation, light-activated cryptochromes and phytochromes interact directly with COP1, interfering with the COP1-SPA1 interaction in the nucleus. This reduces COP1 activity and enhances stability of the transcription factor HY5, thereby promoting photosynthetic pigment accumulation and enhancing photomorphogenesis (Casal et al., 2014; Legris et al., 2017). HY5 is also seen as another entry point for temperature signalling, as HY5 stability is enhanced in the light, and by cold temperatures in dark-grown seedlings (Catalá et al., 2011). The COP1-HY5 and PIF branches of phytochrome signalling are also interconnected (Legris et al., 2017). In the dark or shade, COP1 activity promotes the degradation of LONG HYPOCOTYL IN FAR-RED (HFR1), an atypical bHLH protein that forms heterodimers with PIFs (especially PIF4) and prevents PIFs from activating transcription. In addition, HY5 is a strong antagonist of PIFs, and competition between PIF and HY5 for occupancy of common G-box elements forms a dynamic activation-suppression transcriptional module that is responsive to changes in both light and temperature (Toledo-Ortiz et al., 2014).

1.7.1.2. Circadian regulation of light harvesting and light responses

Light is one of the main external timing cues that entrains the clock, and it is therefore not surprising that the circadian system and light signalling networks are closely interlinked (Rugnone *et al*., 2013). Indeed, various clock input, output and core pathways intersect and interact (Hsu and Harmer, 2014). For example, while photoreceptors function to entrain the

clock, the expression of these photoreceptors is itself regulated by the circadian system (Harmer et al., 2000; Hsu and Harmer, 2014). Transcript abundance of cryptochromes, phototropins, UVR8 and phytochromes (phyA, phyB, phyC and phyE) cycles with circadian rhythm under constant light conditions (Harmer et al., 2000; Covington et al., 2008), while these photoreceptors in turn mediate light effects on the pace of the clock (Fankhauser and Staiger, 2002). Photoreceptors act redundantly to sustain circadian rhythms (Fankhauser and Staiger, 2002). The single mutants *ztl*, *cry1*, *cry2*, *phyA* or *phyB*, the double mutants *cry1 cry2*, *phyA phyB* and *cry1 phyA*, and the *phyA phyB phyC phyD phyE* quintuple mutant have extended circadian periods but are not arrhythmic (Somers et al., 1998a; Fankhauser and Staiger, 2002; Somers et al., 2000). Similarly, the *phyA phyB cry1 cry2* quadruple mutant is severely impaired for de-etiolation, but retains leaf movement rhythms that can entrain to different photoperiods. Extended darkness lengthens the period of nuclear circadian rhythms (up to 30-36 hour period) (Millar et al., 1995), while both blue light and red light contribute to the period shortening observed under higher fluence rates of light (Millar et al., 1995; Fankhauser and Staiger, 2002). Phytochromes contribute to the fluence rate-dependent shortening of circadian period in a redundant fashion (Hu et al., 2013; Hsu and Harmer, 2014), and the shortening of circadian period in response to increasing fluence rates occurs even in a *phyB* mutant (Jones et al., 2015). Interestingly, expression of a constitutively active version of phyB sustains robust circadian rhythms with ~24 hour period even in plants grown without light, yet results in a clock that is insensitive to light intensity (Jones et al., 2015). It has been suggested that far-red light absorbing phytochromes accelerate the pace of the clock, while the red-light absorbing form decreases the pace of the clock (Hsu and Harmer, 2014). Entrainment with far-red light (whereby phyA is expected to be the only active photoreceptor) results in elevated expression of evening-phased genes and decreased expression of morning genes, with ELF4 proposed as a target and mediator in these far-red light effects (Wenden et al., 2011). In addition, three positive regulators of phytochrome A signalling pathways, Far-red Elongated Hypocotyl 3 (FHY3), Far-red Impaired Response 1 (FAR1) and HY5, directly bind to the *ELF4* promoter, activating expression of *ELF4* during the day (Li et al., 2011).

Adding to the complexity of the system is the circadian gating of light inputs that entrain the oscillator (Millar, 2004; Greenham and McClung, 2015). In particular, the evening-phased clock components ELF3 and ELF4 function in the phytochrome-mediated light input pathway to the circadian clock (McWatters et al., 2000; Covington et al., 2001; Kikis et al., 2005; McWatters et al., 2007). ELF3 and ELF4 play pivotal roles in circadian gating by acting as negative regulators that repress the phytochrome-mediated light inputs to the central oscillator, with ELF3 directly interacting with phyB, and ELF4 acting downstream of ELF3 (McWatters et al., 2000; Covington et al., 2001; McWatters et al., 2007; Liu et al., 2001). *elf3* and *elf4* loss-of-function single mutants are arrhythmic in constant light, but maintain circadian rhythms in constant darkness (Covington et al., 2001; McWatters et al., 2007). In wild-type plants grown under constant light conditions, applications of red light or blue light pulses results in small phase advances and little resetting of the core clock when applied in the subjective morning, while light stimuli applied later in the subjective day elicits delays that continue to increase in magnitude, until the greatest phase shift occurs upon application of light stimuli during the subjective night, when ELF3 expression is at its highest (Covington et al., 2001). In the *elf3* mutant, application of red light pulses in the subjective night (when ELF3 expression in wild-type is maximal) causes even larger phase shifts or arrhythmia. ELF3 and ELF4 also feed back to antagonize light-mediated acute induction of circadian outputs such as expression of the nuclear gene *LIGHT-HARVESTING CHLOROPHYLL A/B* (*Lhcb*) *Lhcb1*1* (*CAB2*): the *elf3* null mutant is hypersensitive to the phytochrome-mediated acute induction of *CAB2* expression and blunts circadian gating of *CAB2* gene expression (McWatters et al., 2000; Covington et al., 2001). By timing levels of ELF3 and ELF4 for greatest expression at night, the sensitivity of the clock to light signals during the night is restricted, and allows for an efficient clock that is resistant to transitory fluctuations in light levels at night (such as change in cloud cover or stellar/lunar illumination) (Covington et al., 2001). While most light-induced genes in plants respond more strongly to light during the subjective day, a small number of these genes that are more strongly induced by light in the middle of the night (Rugnone et al., 2013). Among these are the clock genes *CCA1*, *PRR7* and *GI*, as well as four genes that belong to the small

family of *NIGHT LIGHT-INDUCIBLE AND CLOCK-REGULATED* (*LNK*) genes. *LNK1* and *LNK2* are circadian-regulated transcription factors that regulate light signalling and biological timing by activating transcription of numerous afternoon- and evening-phased clock-controlled genes (in particular *ELF4* and *PRR5*). *LNK1* and *LNK2* are morning-phased and are directly repressed by members of the *PRR* family (Rugnone et al., 2013). Indeed, adding to their role of regulating rhythms of the central oscillator, *PRR9* and *PRR7* have been reported as being instrumental in relaying light signals to the circadian clock (Farré *et al.*, 2005). While *prr9* and *prr7* mutants exhibit long period circadian rhythms under constant light, no effect on circadian rhythms is observed in these mutants under constant darkness. In contrast, the *prr7 prr9* double mutant exhibits a more severe period lengthening under constant blue light than under constant red, as well as arrhythmia in constant darkness (Farré et al., 2005). The E3 ubiquitin-ligase COP1 (the negative regulator of photomorphogenesis) also regulates light signalling to the central oscillator, with ELF3 and COP1 interacting to mediate day length signalling from cry2 to GI (Yu et al., 2008). COP1 mediates ubiquitination and degradation of ELF3, and, upon interaction with ELF3, results in destabilisation of GI (Yu et al., 2008).

In addition to gating light inputs, the circadian clock gates light signalling to output pathways such as hypocotyl growth (Nusinow et al., 2011; Hsu and Harmer, 2014; Zhu et al., 2016). The ELF3-ELF4-LUX evening complex is required for the proper rhythmic expression of growth-promoting *PIF4* and *PIF5* under diurnal conditions, with LUX targeting the complex to the promoters of *PIF4* and *PIF5* to suppress transcription in the early evening (Nusinow et al., 2011). Combined with the degradation of PIFs in the light, this interaction allows for maximal growth before dawn under diurnal conditions (Nusinow et al., 2011; Legris et al., 2017). Interestingly, the evening-phased components PRR5 and TOC1 mediate circadian gating of thermoresponsive growth (Zhu et al., 2016). Thermogenesis is mainly regulated by PIF4, and PRR5 and TOC1 bind to the *PIF4* promoter to prevent transcription of *PIF4*. In addition, TOC1 interacts directly with PIF4, thereby inactivating PIF4 and suppressing warm temperature-induced growth in the evening when TOC1 levels are high (Zhu et al., 2016).

The circadian system also regulates photosynthesis and carbohydrate metabolism, with many transcripts involved in photosynthesis (encoded from both the nuclear and chloroplast genomes) reported to be under circadian control (Covington et al., 2008; Dodd et al., 2015). One of the main mechanisms whereby the circadian clock regulates these two genomes is through SIGMA FACTOR 5 (SIG5) (Noordally et al., 2013). *Arabidopsis* encodes six sigma factors, all of which are circadian regulated. Some sigma factors (such as SIG2 and SIG6) are required for gene expression during chloroplast biogenesis, while others (such as SIG1 and SIG5) adjust the photosynthetic apparatus during steady-state photosynthesis. SIG5 is expressed in the nucleus, but upon import into the chloroplast acts as a subunit of the plastid RNA polymerase, generating circadian expression of several chloroplast genes involved in photosynthesis (Noordally et al., 2013). Expression of the two circadian regulated nuclear genes, *CAB2* and *CAB3*, are regulated by HY5 and CCA1 (Andronis et al., 2008). HY5 binds specifically to the G-box element of the *CAB3*, and absence of HY5 leads to shorter period in *CAB1* circadian expression. CCA1 binds to the promoters of both *Lhcb* genes via a designated CCA1-binding site, and also physically interact with HY5 and alters the binding activity of HY5 to the *Lchb* promoters (Andronis et al., 2008). Post-translational modification of reaction centre proteins are also reported to be under circadian control, particularly through the activity of STATE TRANSITIONS8 (STN8) and STT7 HOMOLOG (STN7), which mediate the light-dependent reversible phosphorylation of the D1 protein of PSII (Dodd et al., 2014). D1 undergoes phosphorylation, which is thought to optimize the PSII repair cycle, and changes in the phosphorylation state of D1 cycles with circadian rhythm. This suggest circadian control of the PSII repair cycle, possibly arising from the cycles observed for *STN7* transcription (Dodd et al., 2014). Clock-controlled output pathways can also act as clock input pathways (Hsu and Harmer, 2014; Dodd et al., 2015). Sucrose is known to affect the amplitude of clock gene expression, and can serve as a modulator of period length and an entrainment signal, resetting the clock in constant darkness (Knight et al., 2008; Dalchau et al., 2011; Hsu and Harmer, 2014). Furthermore, the rhythmic oscillations of endogenous sugars produced through photosynthesis can entrain the circadian system in *Arabidopsis* by regulating the gene

expression of circadian clock components early in the photoperiod (Haydon et al., 2013). In particular, photosynthetically derived sugars repress *PRR7* late in the photoperiod, leading to de-repression of *CCA1* (Haydon et al., 2013). Similarly, while iron homeostasis is under circadian control, iron in turn affects the pace of circadian oscillations: circadian period lengthens when iron becomes limiting, and gradually shortens upon increased application of external iron (Salomé et al., 2013; Chen et al., 2013b; Hong et al., 2013).

1.7.2. Chloroplast-to-nucleus retrograde signalling

1.7.2.1. Ca^{2+} and reactive oxygen species (ROS) as initiators of interorganellar communication

ROS and Ca^{2+} are well-known, evolutionarily conserved triggers of a wide range of molecular and biochemical responses in living organisms (de Souza et al., 2017). Changes in environmental conditions can result in the accumulation of ROS or in rapid spatial and temporal modulations of Ca^{2+} concentrations (known as Ca^{2+} signatures), and these molecules are often regarded as master switches that initiate processes involved in inter- and intracellular communication (de Souza et al., 2017). Cells have evolved mechanisms to differentially accumulate Ca^{2+} in distinct cellular compartments, and distinct Ca^{2+} signature profiles are produced in response to various stimuli (Tuteja and Mahajan, 2007; de Souza et al., 2017). Cytosolic Ca^{2+} in plant cells increases in response to various environmental signals (including abiotic and biotic stresses) and in response to developmental cues (Tuteja and Mahajan, 2007). Indeed, levels of cytosolic Ca^{2+} oscillate with diurnal and circadian rhythm in plants (Love et al., 2004). These oscillations are modulated by photoperiod and light intensity, and are proposed to act as second messengers conveying information about day length and light intensity to and from the clock (Love, 2004). The unique transient elevation of cytosolic Ca^{2+} in response to specific environmental or developmental cues results from the sub-cellular localisation and/or the phase, duration or magnitude of the changes in cytosolic Ca^{2+} (Tuteja

and Mahajan, 2007). Ca^{2+} signatures are well-known triggers of cellular signalling cascades, and the stimulus-specific changes in Ca^{2+} levels are sensed by several Ca^{2+}-binding proteins (such as calmodulin, calmodulin-like proteins, calcium-dependent protein kinases and calcium- and calmodulin-dependent protein kinases) that in turn transmit the signals to various downstream processes (Tuteja and Mahajan, 2007; Batistič and Kudla, 2012). Ca^{2+} also plays a role in rapid, long-distance signalling: upon exposure of *Arabidopsis* roots to salt stress, Ca^{2+} waves propagate from roots to shoots at rates of up to ~400 $\mu m.s^{-1}$ to elicit systemic molecular responses in target organs (Choi et al., 2014). It has been proposed that there is reciprocal interplay between Ca^{2+} and ROS, as ROS activates plastid calcium transporters, while Ca^{2+} signatures can induce ROS production (Pei et al., 2000; Takeda et al., 2008; Kimura et al., 2012). It has also been suggested that ROS and Ca^{2+} cooperate to relay rapid, long-distance signalling through the action of self-amplifying, cell-to-cell propagating ROS- Ca^{2+} waves (Choi et al., 2017; de Souza et al., 2017).

1.7.2.2. Reactive oxygen species (ROS)

Like other aerobic organisms, plants continuously generate ROS as byproducts of normal oxygen metabolism (Apel and Hirt, 2004; Das et al., 2015). The different ROS species, which include superoxide, singlet oxygen ($^1O_2$), the hydroxyl radical and hydrogen peroxide (H_2O_2, the most common and most stable ROS), differ in stability and cytotoxicity, and are generated in distinct compartments. In plants, ROS are produced mainly in the chloroplasts (as a result of light harvesting, photosynthetic electron transport and photochemistry), mitochondria (via respiratory electron transport), and peroxisomes (as byproducts of photorespiration), as well as in the cytoplasm and plasma membranes through the action of peroxidases (Das et al., 2015). Accumulation of ROS can cause oxidative damage to cellular components which, if not controlled, can result in further ROS production, cellular damage and cell death (Apel and Hirt, 2004; Das et al., 2015; de Souza et al., 2017). Plants therefore employ a variety of ROS-

scavenging antioxidant pathways, which can involve enzymatic (peroxidases, catalase and superoxide dismutase) and non-enzymatic (glutathione, ascorbate, flavonoids, alkaloids and carotenoids) mechanisms that are often confined to specific cellular compartments (Apel and Hirt, 2004; de Souza et al., 2017). Environmental stresses can disrupt the equilibrium between ROS production and scavenging. The "oxidative burst" observed in response to abiotic stress occurs mainly due to the action of NAPH-dependent oxidases, while ROS accumulation in response to abiotic stresses results mainly from the action of photodynamically-active molecules (such as chlorophyll precursors) and overreduction of electron transport chains (Apel and Hirt, 2004; Chi et al., 2015; de Souza et al., 2017). Despite the negative consequences of ROS reactivity, the instability of ROS, combined with the high rate of ROS production and scavenging, make ROS ideal candidates for signalling molecules (Apel and Hirt, 2004; de Souza et al., 2017). It has been proposed that the specific activity of ROS (or of ROS-oxidised components) in different cellular compartments could provide cells with the ability to interpret complex environmental signals (de Souza et al., 2017). Specifically, the interaction of different ROS species with proteins might result in protein modifications which in turn determine the specificity of a response (León, 2013). ROS also play a role in the synthesis of metabolites that themselves act as signals (discussed below) (Ramel et al., 2012). Production of the precursor to the signal molecule 3'-phosphoadenosine 5'-phosphate (PAP; see Section 1.7.2.7) relies on the availability of ATP, which itself is determined by the cell's redox potential and levels of ROS (Estavillo et al., 2011). In addition, the activity of SAL1, the enzyme involved in regulating PAP accumulation, is influenced by the redox state of plastids (Chan et al., 2016a). Similarly, the enzyme responsible for the reduction of the signal molecule MEcPP contains an iron-sulfur cluster in the catalytic site, rendering the enzyme highly sensitive to oxidative state and thereby providing an avenue by which levels of the molecular signal is influenced by ROS (Seemann et al., 2005; de Souza et al., 2017). ROS (specifically $^1O_2$) are also known to cause lipid peroxidation, which results in the production of free fatty acids and derivatives that act as signals in response to abiotic and biotic stress (Cecchini et al., 2015). ROS signalling pathways also intersect with photoreceptor signalling pathways (Chen et al., 2013a). Phytochromes,

cryptochromes and COP1 act upstream to regulate ROS signalling, with PIFs inhibiting ROS production and ROS-responsive gene expression in the light, while HY5 and HYH bind to and promote expression of ROS-responsive genes (Chen et al., 2013a).

In *Arabidopsis*, the production and scavenging of ROS have been shown to oscillate with a diurnal rhythm (Lai et al., 2012). In plants grown under 12-hour light:12-hour dark cycles, H_2O_2 and catalase levels peak at noon and reach the lowest levels at midnight, while 140 of 167 genes known to be involved in ROS production and scavenging exhibit similar daily rhythms. Interestingly, these oscillations of H_2O_2 and ROS-related gene transcript levels persist even in constant light, suggesting the ROS network is under circadian control. Plants with mutations in core circadian genes including *CCA1*, *LHY*, *ELF3*, *ELF4*, *PRR5* and *LUX* exhibit hypersensitivity to methyl viologen (MV) treatment, while the overexpression of *CCA1* has been linked to hyposensitivity to MV treatment in both light:dark cycles and constant light (Bowler et al., 1992; Lai et al., 2012). Furthermore, expression of the three catalases, *CAT1*, *CAT2* and *CAT3*, in response to oxidative stress is altered upon overexpression of *CCA1* or mutations in *CCA1* or *LHY*, and becomes arrhythmic in an *elf3* mutant (Lai et al., 2012). Evidence suggests that *CCA1* regulates the transcription of ROS genes even in the absence of oxidative stress, with 34% of genes grouped under numerous ROS GO categories known to be regulated by the circadian clock (Covington et al., 2008). Noteworthy changes in the time of day expression of the ROS-related genes *APX4*, *HSP182*, *PAL1, HSFA4A*, *MYB9* and the peroxidase *AT2G22420* are apparent in a *CCA1* over-expressing line and in *cca1-1/lhy-11* and *elf3-1* mutants (Lai et al., 2012). A set of 28 genes involved in ROS signalling have been shown to contain a putative EE and/or CCA-1 binding site in their upstream promoters, and chromatin immunoprecipitation-qPCR assays have been used to confirm that CCA1 directly regulates the expression of ROS genes *WRKY11*, *MYB59* and *ZAT12 in vivo*. There is thus a strong indication that regulation of ROS levels is coupled to the circadian clock with CCA1 playing a pivotal role, yet the exact mechanisms of these important ROS-related signalling pathways remain unknown (Lai et al., 2012). Linking ROS homeostasis to the circadian clock is almost intuitive.

By allowing the circadian control of ROS-scavenging mechanisms it is ensured that these energy-demanding pathways are activated only when needed, providing plants with the ability to anticipate oxidative stress according to daily rhythms (Lai et al., 2012). Furthermore, it may be advantageous to couple the production and scavenging of such an important signal molecule to the circadian clock (Lai et al., 2012).

1.7.2.3. gun mutants

Chloroplasts contain approximately 3,000 proteins, of which more than 95% are encoded in the nucleus (Koussevitzky et al., 2007). Chloroplast biogenesis therefore requires coordination of nuclear and chloroplast gene expression, with retrograde signals coupling chloroplast function with the transcription of certain nuclear-encoded proteins (Susek et al., 1993; de Souza et al., 2017)**.** The first evidence of such a plastid-nucleus retrograde signalling pathway was discovered in barley mutants with undifferentiated chloroplasts lacking ribosomes and with high sensitivity to photo-damage, and in which expression of nuclear-encoded, plastid-localised proteins was reduced (Bradbeer et al., 1979). Further study of the phenomenon led to the identification of the *genomes uncoupled* (*gun*) mutants in *Arabidopsis*, which are characterised by sustained expression of photosynthesis-related *Lhcb* and *RIBULOSE-1,5-BISPHOSPHATE CARBOXYLASE/OXYGENASE SMALL SUBUNIT* (*RBCS*) genes, even when chloroplast development is blocked by the application of norflurazon, an inhibitor of carotenoid biosynthesis (Susek et al., 1993). The *GUN1* gene encodes a plastid-localised protein that is a member of the P subfamily of pentatricopeptide repeat (PPR)-containing proteins. Unlike other PPR proteins, GUN1 also contains a DNA-binding SMR domain, and associates with sites of active plastid DNA transcription where it is thought to function in DNA repair and recombination (Koussevitzky et al., 2007). Promoters of genes with misregulated expression in *gun1* mutants are enriched for abscisic acid (ABA) response elements, and GUN1 acts upstream of, and is required for the expression of the nuclear-localised ABA-regulated

transcription factor ABSCISIC ACID INSENSITIVE 4 (ABI4). ABI4 can bind to the promoter of *Lhcb* to repress expression, and constitutive overexpression of ABI4 rescues the *gun1* mutant phenotype (Koussevitzky et al., 2007). In addition, retrograde signalling and phytochrome signalling pathways converge antagonistically via a GUN1-mediated signalling mechanism, with signals from the chloroplast repressing the light-induced expression of PIF-mediated genes involved in photomorphogenesis (Martín et al., 2016).

The remaining five *GUN* genes encode proteins that participate in tetrapyrrole biosynthetic pathways (de Souza et al., 2017). Intermediates of tetrapyrrole biosynthesis have been implicated in chloroplast-nucleus signalling, and the application of inhibitors of tetrapyrrole biosynthesis can lead to the repression of nuclear encoded genes, while inhibiting the synthesis of tetrapyrrole biosynthesis intermediates can lead to activation of nuclear-encoded genes (Oelmüller et al., 1986; Kobayashi et al., 2011). *GUN2* (*HY1*) and *GUN3* (*HY2*) code for a plastid heme oxygenase and a plastid-localised phytochromobilin synthase, respectively, both of which are involved in the heme branch of the tetrapyrrole metabolism pathway (Muramoto et al., 1999; Kohchi et al., 2001). Heme (Fe-protoporphyrin IX) has been proposed as a retrograde signal in algae (von Gromoff et al., 2008), and bilin metabolites are thought to function as signals in light-dependent chlorophyll accumulation responses in *Chlamydomonas reinhardi* (Duanmu et al., 2013). In *Arabidopsis*, upregulation of photosynthetic gene expression is observed in *gun6* mutants – a gain-of-function mutation in plastidial ferrochelatase I which causes increased heme synthesis (Woodson et al., 2011). *GUN4* and *GUN5* act at the chloroplast membranes to promote chlorophyll biosynthesis by promoting the synthesis of the chlorophyll precursor, Mg-protoporphyrin IX (Mg-protoIX) (Mochizuki et al., 2001; Larkin et al., 2003; Adhikari et al., 2011). *GUN5* encodes the large subunit of Mg-chelatase, the enzyme which commits porphyrins to chlorophyll biosynthesis by catalysing the insertion of Mg^{2+} into protoporphyrin to yield Mg-protoIX, and *GUN4* encodes a novel protein that activates Mg-chelatase, the enzyme that commits Mg-protoIX to chlorophyll biosynthesis (Mochizuki et al., 2001; Larkin et al., 2003). One of the most common porphyrins in nature,

Mg-protoIX has been shown to repress the expression of a number of nuclear-encode genes in *Chlamydomonas reinhardi*, and can mimic the light stimulus for nuclear gene expression when applied exogenously to cells in the dark (Johanningmeier and Howell, 1984; Kropat et al., 1997). Similarly in *Arabidopsis*, application of exogenous Mg-protoIX results in suppression of photosynthesis-associated nuclear genes (PhANGs, including *Lhcb*), and Mg-protoIX accumulates *in vivo* in response to norflurazon treatment (Strand et al., 2003; Kindgren et al., 2012). While the rapid rates of Mg-protoIX production and degradation would allow the metabolite to function as a signal, either directly or indirectly, the mechanism through which Mg-protoIX acts as a signal is not yet understood (Mochizuki et al., 2008). It has been proposed that Mg-ProtoIX binds Heat Shock 90 (HSP90)–type proteins and subsequently interacts with the transcription factor HY5, which in turn regulates expression of PhANGs (Lee et al., 2007; Kindgren et al., 2011). Mg-ProtoIX has also been shown to interact with Protein Phosphatase 5 (PAPP5), a type 5 serine/threonine protein phosphase that dephosphorylates biologically active Pfr phytochromes and enhances phytochrome-mediated responses (Barajas-López et al., 2013). In addition, it has been suggested that Mg-ProtoIX controls the expression of sigma factors SIG1-6 (Ankele et al., 2007). However, the mechanism of Mg-protoIX export from plastids remains unsolved, and there is no correlation between the expression of Mg-protoIX-sensitive nuclear genes and the *in vivo* steady state levels of Mg-protoIX, (or indeed for any other tetrapyrrole intermediates of chlorophyll biosynthesis) (Mochizuki et al., 2008; Moulin et al., 2008; Schlicke et al., 2014). Mg-protoIX is therefore thought to affect gene expression indirectly through alteration of the redox status of chloroplasts, or through directing tetrapyrrole flux towards the production of heme (Woodson et al., 2011; Schlicke et al., 2014). Alternatively, Mg-protoIX could act as a retrograde signal by controlling DNA replication. In primitive red algae, Mg-protoIX enables maintenance of plastids, as it is required for coordinating plastidial DNA replication events with nuclear DNA replication (Kobayashi et al., 2011). Plastid-derived Mg-protoIX activates DNA replication by preventing the ubiquitination of a G1 cyclin, a protein responsible for cell cycle progression (Tanaka and Hanaoka, 2013).

1.7.2.4. β-Cyclocitral

Carotenoids are the main quenchers of $^1O_2$ in chloroplast, and light stress induces the oxidation of the carotenoid β-carotene, leading to the production of various volatile β-carotene derivatives in chloroplasts (Ramel et al., 2012). One of these derivatives, β-cyclocitral, accumulates in *Arabidopsis* leaves in response to high light stress, and has been proposed as an intermediate in the $^1O_2$ signalling pathway that links the cytoplasm and nucleus during acclimation responses (Ramel et al., 2013; Lv et al., 2015). Treatment with exogenous β-cyclocitral is associated with increased tolerance to photooxidative stress and induces expression of a large set of nuclear-encoded $^1O_2$-responsive- and high light-responsive genes, including genes involved in detoxification mechanisms, hormone synthesis and signalling and plant defence (Ramel et al., 2012, 2013). In addition, application of exogenous β-cyclocitral impedes ROS production in chloroplasts and enhances the synthesis of salicylic acid (SA) via the ISOCHORISMATE SYNTHASE 1 (ICS1)-mediated isochorismate pathway (Lv et al., 2015). SA accumulation increases the nuclear localisation of SA signalling cofactor NONEXPRESSOR OF PATHOGENESIS-RELATED GENES 1 (NPR1), which in turn results in upregulation of $^1O_2$-responsive nuclear genes involved in detoxification, including *GLUTHATHIONE-S-TRANSFERASEs* (*GSTs*) (Lv et al., 2015).

1.7.2.5. 2-C-Methyl-D-erythritol 2,4-cyclodiphosphate (MEcPP)

MEcPP is a small metabolite that acts as a precursor of isoprenoids in the plastidial methylerythritol phosphate (MEP) pathway (Xiao et al., 2012). In *Arabidopsis*, MEcPP accumulates in response to a range of stresses, including high light stress, oxidative stress and wounding (to a lesser degree), and an increase in *in vitro* MEcPP correlates with the upregulation of specific nuclear stress-responsive genes. Among these upregulated genes are *HYDROPEROXIDE LYASE* (*HPL*) and *ICS1*, which results in increased SA levels. Increased SA levels can in turn enhance resistance to infection by the pathogen *Pseudomonas syringae*

(Xiao et al., 2012). It has been suggested that the MEcPP-signalling mechanism is evolutionarily conserved among species (de Souza et al., 2017). Genes involved in the plant MEP pathway are among a group of genes inherited from endosymbiotic ancestors and subsequently relocated to the nuclear genome (Bouvier et al., 2005), while oxidative stress-mediated induction of MEcPP levels has been reported in several bacterial strains (Ostrovsky et al., 1992, 1998). However, the exact mechanism of MEcPP signalling remains elusive. It has been suggested that MEcPP changes expression of stress-responsive genes by altering the functional organisation of chromatin structure, as MEcPP can directly disrupt interactions between histone H1-like (Hc1) protein and DNA in *Chlamydia trachomatis* (Grieshaber et al., 2004). MEcPP is also involved in the unfolded protein response (UPR), a cellular stress response related to the endoplasmic reticulum (ER) (de Souza et al., 2017). Almost a third of a cell's proteins are synthesized, folded, and secreted and redistributed in and from the ER (Hetz et al., 2015). Under stress conditions, due to the limited protein-folding capacity of the ER, the UPR serves as a regulatory process by which the load of proteins to the ER is decreased, while the capacity for folding and degradation of unfolded proteins is increased (Hetz et al., 2015). Accumulation of MEcPP induces the expression of a subset of genes involved in UPR, while application of exogenous MEcPP also increases transcript levels of these UPR genes within 15-30 minutes (Walley et al., 2015). A direct function of MEcPP in inducing UPR in the ER would rely on the import of MEcPP from plastids to the ER, which is suggested to occur through membrane contact sites that occur between the ER and chloroplasts (Prinz, 2014). Interestingly, application of exogenous SA has also been shown to active UPR (Nagashima et al., 2014).

MEcPP has been linked to the circadian regulation of growth and development in *Arabidopsis* (de Souza et al., 2017). In the mutant *constitutively expressing HPL* (*ceh1*), elevated levels of endogenous MEcPP accumulate, and the plants exhibit a dwarf phenotype and flower early (Wang and Dehesh, 2015). The elevated levels of MEcPP repress expression of *B-BOX DOMAIN PROTEIN 19* (*BBX19*), a positive regulator of growth and a negative regulator of

flowering time (Wang et al., 2014; Wang and Dehesh, 2015). Indeed, constitutive overexpression of *BBX19* restores growth and flowering time in the *ceh1* mutant (Zhang et al., 2015) The BBX family of proteins are zinc-finger transcription factors that are comprised of one or two B-box motifs at the N-terminal that often occur in combination with a C-terminal CCT (CONSTANS, CONSTANS-like, and TOC) domain (Wang et al., 2014). BBX19 is localised in the vasculature, and circadian-controlled expression of *BBX19* is antiphasic to the rhythmic expression of *FT* and *CO*. BBX19 and CO colocalise and interact in the nucleus, resulting in depletion of the active CO pool required for the transcription of *FT* and downstream flowering-promoting genes (Wang et al., 2014). In addition, BBX19 promotes hypocotyl growth through interaction with COP1 and ELF3 (Wang et al., 2015). BBX19 binds to and recruits ELF3 for degradation by COP1, which in turn prevents repression of *PIF4* and *PIF5* expression by ELF3. As such, MEcPP could play a role in the dynamic gating of the formation of the circadian evening complex, and the subsequent regulation of growth through the action of PIF4/5 (Wang et al., 2015).

1.7.2.6. Fatty acids

Fatty acids (FAs) are functionally and structurally cross-kingdom conserved macromolecules that act as constituents of cellular structures and, as well as in a variety of essential metabolic functions (Upchurch, 2008; Walley et al., 2013; de Souza et al., 2017). FAs have distinct characteristics, and the profile and concentration can change rapidly and transiently in response to stimuli. These changes can in turn affect membrane permeability, and alter biochemical events through modifying membrane composition and the activities of a variety of enzymes and signalling proteins. These characteristics allow FAs to act as signalling molecules in response to stimuli. In particular, the signalling action of free FAs released by certain lipases in response to stress and development stimuli is a well-established function (Upchurch, 2008; Walley et al., 2013; de Souza et al., 2017). Linolenic or linoleic acid accumulate rapidly in

response to pathogen attack, and the exogenous application of free linolenic or linoleic acid results in the rapid activation of Rapid Stress Response Element (RSRE), a stress-specific functional *cis*-element (Walley et al., 2013). Activation of RSRE also occurs upon treatment with arachidonic acid (a FA present in plant pathogens, but absent in the membrane lipids of higher plant cells), suggesting a function for FAs as interorganismal signalling molecules (Savchenko et al., 2010). Oleic acid has been shown to act as a retrograde signal to induce expression of nuclear-encoded resistance genes, and mutants deficient in the plastidial stearoyl-acyl carrier protein desaturase SS12 exhibit impaired oleic acid accumulation and impaired R (Resistance) gene expression patterns, which are restored upon restoration of endogenous oleic acid levels (Kachroo et al., 2004). Interestingly, oleic acid is also proposed to influence R genes through regulation of the synthesis of nitric oxide (NO) – a conserved cellular metabolite that occurs in a variety of organisms and is known to modify FAs and regulate disease physiology (Mandal et al., 2012).

Oxylipins are a class of modified FAs that result mainly from the oxidation of linoleic acid and linolenic acid (and arachidonic acid in animals), and that act as evolutionarily conserved signalling molecules in response to biotic and abiotic stress (de Souza et al., 2017). The most studied oxylipins are jasmonate and volatile C_6-aldehydes, which are produced by the two main competing branches of the oxylipin pathway, the allene oxide synthase (AOS) and hydroperoxide lyase (HPL) branches, respectively (Chehab et al., 2008). Volatile C_6-aldehydes act as inter- and intra-plant stress signals in defence against biotic stress (Chehab et al., 2008). Jasmonates (which include biologically active derivatives of jasmonic acid and biologically active intermediates in the pathway for jasmonic acid biosynthesis) are signalling molecules that regulate a diverse range of processes, including biotic and abiotic stress responses, wound responses and pollen maturation (Turner et al., 2002). Jasmonic acid (JA) synthesis requires the production and translocation of various lipid intermediates from the chloroplasts to the cytoplast, and later into peroxisomes (León, 2013). The AOS pathway produces 12-oxophytodienoic acid (12-OPDA) in the chloroplasts in repsonse to stress, as well as precursors

needed for the formation of jasmonates (jasmonic acid and methyl jasmonate) in the peroxisomes (Schaller and Stintzi, 2009). The JA-isoleucine conjugate, jasmonoyl-L-isoleucine (JA-Ile) is the active form of the hormone and faciliates the degradation of JASMONATE ZIM-DOMAIN (JAZ) transcriptional repressors (Sheard et al., 2010). The removal of these JAZ proteins releaves the suppression of gene transcriptioin of various defense-related genes. In tomato, this mechanism results in the JA-induced upregulation of proteinase inhibitors which are rapidly produced in response to tissue damage from herbivorous acitvity and act to disrupt the digestive processes in insect gut (Chen et al., 2005). 12-OPDA also act as a signalling molecule in a JA-independent manner, interacting with TGACG motif-binidng factors to alter gene expression and thereby affecting processes including stomatal closure in repsonse to drought, amino acid biosynthesis, and cellular redox homeostasis in stress responses (Park et al., 2013; Savchenko et al., 2014). Finally, the production of ROS in reponse to biotic and abiotic stress can result in lipid peroxidation and the subsequent generation of fragmented FAs and products such as azeleic acid (AZA) (Cecchini et al., 2015; de Souza et al., 2017). AZA is a metabolite essential for systemic acquired resistance and induced systemic resistance, and which acts through a mechanism involving lipid transfer protein homolgues that are localized at the ER or plasmodesmata, the chloroplast outer envelopes and the membrane contacts between these organelles (Cecchini et al., 2015; de Souza et al., 2017).

1.7.2.7. The SAL1-PAP-XRN pathway

In an attempt to understand the steps between the initiation of a signal by an environmental trigger and the perceived changes in gene expression in the nucleus, numerous screens have been performed to identify mutants that exhibit altered nuclear gene expression under oxidative stress (Xiong et al., 2001; Rossel et al., 2006; Estavillo et al., 2011). Of particular interest are mutants with lesions in the *SAL1* gene, also identified from parallel screens as *FIERY1/ALTERED EXPRESSION OF APX2*. The *Arabidopsis SAL1* gene (At5g63980) was first identified in a cDNA library constructed from roots of *Arabidopsis* exposed to NaCl, and

which was subsequently used to complement Na^+ and Li^+ sensitivities in yeast strains defective in Na^+ and Li^+ efflux mechanisms (Quintero et al., 1996). The first of the *Arabidopsis sal1* mutants, *fry1*, was identified in a genetic screen based on altered gene expression responses to ABA signalling (Xiong *et al*., 2001). *Arabidopsis SAL1* is homologous to the yeast *HAL2* gene, which encodes a salt-sensitive 3',5'-bisphosphate nucleotidase involved in conferring salt tolerance in yeast (Gil-Mascarell et al., 1999; Quintero et al., 1996). In subsequent studies, *sal1* mutants were shown to exhibit a variety of phenotypes, including slowed growth and altered leaf and root morphology (Gy et al., 2007; Hirsch et al., 2011), hypersensitivity to light or ABA (Xiong et al., 2001; Kim and von Arnim, 2009), altered sulfate- and fatty acid-metabolism (Rodriguez et al., 2010; Lee et al., 2012), increased RNA silencing triggers (Gy et al., 2007), and increased *APX2* expression and drought tolerance (Rossel et al., 2006; Wilson et al., 2009).

The SAL1 enzyme is expressed ubiquitously throughout plant tissues (Xiong et al., 2001; Estavillo et al., 2011). In *Arabidopsis* seedlings, *SAL1* expression is particularly pronounced in cotyledons and leaves, and to a lesser extent in primary roots, root hairs and lateral root caps, stems, and floral organs (Xiong et al., 2001; Zhang et al., 2011). In flowers, *SAL1* transcripts accumulate to highest level 4 days after flowering, followed by a subsequent decrease to lowest levels twelve days after flowering (Sato et al., 2011). *SAL1* expression is stronger in stamens and in seed coats (Zhang et al., 2011). There is also a tissue-specific element to the patterns of *SAL1* expression. In roots, *SAL1* is expressed in all root tissues, with highest levels in the pericycle and stele regions of mature primary roots (Hirsch et al., 2011). In leaves, *SAL1* expression is highest in the vascular tissue, with lower levels of expression in the mesophyll tissue (Estavillo et al., 2011).

SAL1 is encoded in the nucleus, but is localised in chloroplasts and mitochondria where it acts as a phosphatase to hydrolyse the phosphate group from both phosphonucleotides and inositol polyphosphates *in vitro* (Quintero et al., 1996; Xiong et al., 2001). While SAL1 exhibits phosphatase activity to both inositol 1,4,5-triphosphate (IP_3) and 3'-phosphoadenosine 5'-phosphate (PAP), PAP is regarded as the enzyme's *in vivo* substrate (Estavillo et al., 2011).

PAP is produced from 3'-phosphoadenosine 5'-phosphosulfate (PAPS), with PAPS acting as a sulfate donor for the synthesis of sulfated secondary metabolites such as glucosinolates, phytosulfokines, and certain hormones and flavonoids (Klein and Papenbrock, 2004; Mugford et al., 2009). PAPS is produced in plastids, but conversion to PAP occurs in the cytosol through the action of cytosol-localized sulfotransferases (SOTs) (Klein and Papenbrock, 2004; Mugford et al., 2009; Estavillo et al., 2011). These SOTs catalyse the transfer of a sulfonate group from PAPS to the appropriate hydroxyl group of numerous substrates to produce sulfate esters and sulfate conjugates, as well as PAP as by-product (Klein and Papenbrock, 2004). PAP in turn inhibits the activity of SOTs, thereby influencing sulfur flux through a negative feedback mechanism (Lee et al., 2012; Chan et al., 2013). Despite the formation of PAP through SOT activity in the cytosol, PAP has been shown to accumulate in chloroplasts and not in the cytosol (Estavillo et al., 2011). It has been proposed that the movement of both PAPS and PAP between the plastids and cytosol is facilitated by PAPS transporter 1 (PAPST1), an ADP/ATP carrier that localises to both the thylakoid and plastid envelope (Gigolashvili et al., 2012). In *Saccharomyces cerevisiae*, PAP has been shown to inhibit the activity of 5'→3' exoribonucleases (XRNs), with PAP concentration of 0.1 mM inhibiting the activity of the two yeast XRNs by 40%-65% (Dichtl et al., 1997). The inhibition of XRN activity by PAP *in vivo* has been proposed in *Arabidopsis* (Gy et al., 2007; Chen and Xiong, 2010; Hirsch et al., 2011; Estavillo et al., 2011). The XRN family of *Arabidopsis* consists of three members: XRN2 and XRN3 are localised in the nucleus and are homologues of Xm2p/Rat1p, while XRN4 is localised in the cytosol and is a functional homolog of *S. cerevisiae* Xm1p (Kastenmayer and Green, 2000; Gy et al., 2007). XRN2 is required in the primary cleavage of pre-ribosomal RNAs and, along with XRN3, displays activity towards excised hairpin loops that form part of miRNA transcripts (Gy et al., 2007; Kurihara et al., 2012). XRN4 is involved in mRNA decay by catalysing the degradation of the 3' cleavage products that result from the microRNA (miRNA)-mediated cleavage of mRNA targets (Souret et al., 2004; Gy et al., 2007). XRN4 is also necessary for ethylene signalling and functions by promoting the degradation of mRNAs of two proteins involved in the degradation of ETHYLENE INSENSITIVE 3, a transcription

factor involved in ethylene response (Potuschak et al., 2006). In addition, all three exoribonucleases act as RNA silencing suppressors, possibly through elimination of the free 5‘ ends of single-stranded RNA templates that are targets for RNA-dependent RNA polymerases (Gy et al., 2007; Kurihara et al., 2012).

Recently, analysis of the molecular structure of SAL1 through X-ray crystallography provided insight into the enzyme’s structural and functional characteristics (Figure 1.4a; Chan et al., 2016). SAL1 is a 37.5 kDa α/β protein that belongs to the carbohydrate phosphatase fold superfamily (Quintero et al., 1996; Chan et al., 2016a). SAL1 crystallizes as a dimer but occurs in a monomer-dimer equilibrium in solution, with dimerization affecting the catalytic activity of the enzyme (Chan et al., 2016a). Under reducing conditions (such as in the presence of DTT) SAL1 occurs as catalytically active monomers. In the presence of oxidisers such as DTT_{ox} or oxidised glutathione (glutathione disulfide, GSSG) SAL1 occurs in solution as a dimer, which dissociates with the addition of DTT. Dimerisation of SAL1 under oxidising conditions is facilitated by the formation of an intermolecular disulfide bond between a symmetrical pair of Cys119 side chains present on each monomer. Each SAL1 monomer contains a pair of cysteine residues (Cys169 and Cys190) also capable of forming an intramolecular disulfide bond (Figure 1.4a). The SAL1 monomer exhibits high catalytic activity towards PAP.

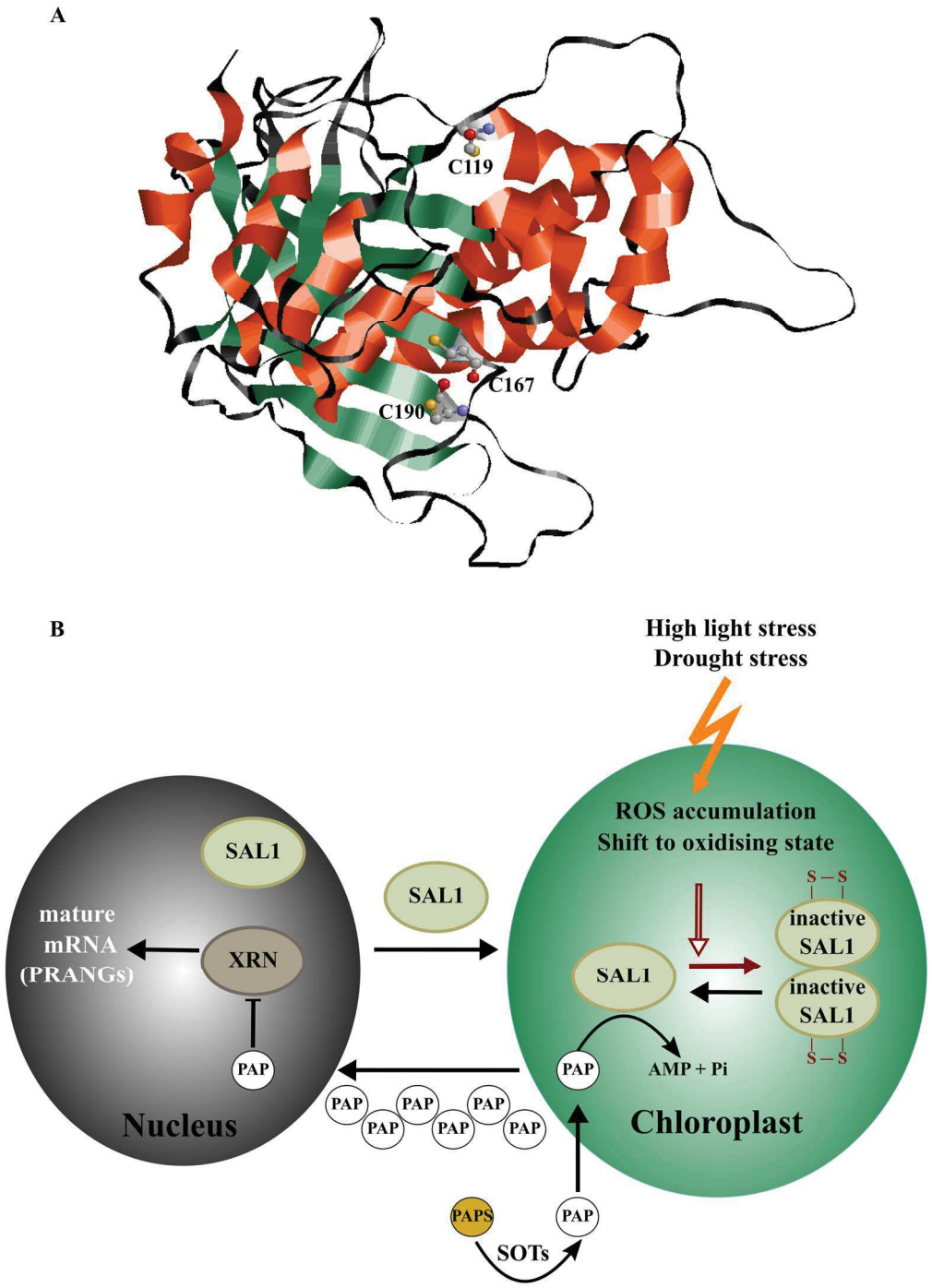

Figure 1.4 ***Arabidopsis*** **SAL1 and the SAL1/PAP/XRN retrograde signalling pathway. (A)** Cartoon of the molecular structure of a SAL1 monomer in a reducing environment. Cysteine residues C167 and C190, as well as C119 capable of forming intra- and intermolecular disulfide bonds, respectively, under oxidising conditions are indicated. α-helices shown in orange, β-sheets shown in green and loops shown in black. Cysteine residues shown as ball-and-stick diagrams. Diagram prepared from Protein Data Bank file PDB ID 5ESY (Chan et al., 2016a) using RasMol (Sayle, 1995). **(B)** The SAL/PAP/XRN retrograde signalling pathway (Estavillo et al., 2011; Chan et al., 2016a). SAL1 is encoded in the nucleus and localised in the chloroplasts due to the presence of a N-terminal chloroplastic transit peptide. In the cytosol, 3'-phosphoadenosine 5'-phosphate (PAP) is formed from the precursor 3'-phosphoadenosine 5'-phosphosulfate (PAPS) through the activity of cytosolic sulfotransferases (SOTs). PAP is formed in the cytosol, but accumulates in the chloroplasts where SAL1 catalyses the hydrolysis of PAP to AMP + Pi through its phosphatase activity. Under stress conditions such as high light or drought stress, the accumulation of ROS and other oxidising agents cause a shift in plastid redox poise. In this oxidising environment, SAL1 dimerises and is inactivated by the formation of inter- and intramolecular disulfide bonds between side chains of cysteine residues. Inactivation of SAL1 causes PAP to accumulate and act as a molecular signal from the chloroplasts to the nucleus. In the nucleus, PAP influences the expression of plastid redox associated nuclear genes (PRANGs) by inhibiting the activity of 5'→3'exoribonucleases.

In contrast, the SAL1 dimer has lower catalytic activity than the monomer, and increasing oxidation (increase in redox potential of the solution) correlates with a rapid loss of catalytic activity in the SAL1 dimer (Chan et al., 2016a).

Under abiotic and oxidative stress, the abundance of SAL1 protein in plant tissues does not change, but the catalytic activity of SAL1 towards PAP is downregulated through allosteric regulation (Chan et al., 2016a). In addition, PAP has been shown to accumulate significantly in wild-type plants within 1 hour of high light stress, and a 30-fold increase in PAP levels has been reported in Col-0 plants subjected 7 days of drought stress (Estavillo et al., 2011). SAL1 has therefore been proposed as a ROS- and redox-sensitive switch located in the chloroplasts, that regulates nuclear gene expression in response to environmental signals through the SAL1/PAP/XRN retrograde signalling pathway (Figure 1.4b) (Estavillo et al., 2011; Chan et al., 2016). Stress conditions such as high light stress or drought stress result in the rapid increased production of singlet oxygen ($^1O_2$) from Photosystem II (PSII) and superoxide (O_2^-) from Photosystem I (PSI) (Apel and Hirt, 2004). Superoxide radicals generated from PSI are rapidly converted within the chloroplast to H_2O_2 by superoxide dismutase (SOD), and H_2O_2 is in turn detoxified by thylakoidal and stromal ascorbate peroxidases (tAPX and sAPX), a reaction which results in the conversion of ascorbate to monodehydroascorbate (Asada, 1999; Apel and Hirt, 2004). Additional ROS scavenging reactions result in the production of $NADP^+$ and GSSG from the oxidation of NADPH and glutathione (GSH), respectively (Apel and Hirt, 2004). The accumulation of $^1O_2$, O_2^-, monodehydroascorbate, GSSG and $NADP^+$ changes the redox poise of the plastid, and in this oxidising environment the dimer-monomer equilibrium of SAL1 shifts towards dimerization (Apel and Hirt, 2004; Chan et al., 2016a). The dimerization of SAL1 occurs through formation of a Cys119-Cys119 intermolecular disulfide bond (Chan et al., 2016). The resulting conformational changes allow a second, intramolecular Cys167-Cys190 disulfide interaction to occur across two adjacent antiparallel β sheets in each monomer. The dimerisation and disulfide bond formation results in reduced mobility of key surface loops, including an active site loop, preventing the enzyme from adopting

conformational changes essential for activity and substrate binding. The inhibition of SAL1 results in the accumulation of PAP in chloroplasts, and PAP acts as a mobile signal influencing nuclear gene expression through the inhibition of XRNs (Estavillo et al., 2011; Chan et al., 2016a). Genes with altered expression as a result of PAP signalling are referred to as plastid redox associated nuclear genes (PRANGs), which include known stress marker genes such as *APX2* and *ZAT10* that are upregulated in response to abiotic stress or PAP accumulation (Rossel et al., 2006; Estavillo et al., 2011; Chan et al., 2016a). Through sufficient activation of ROS scavenging mechanisms, such as those involving APX2, glutathione peroxidase and dehydroascorbate reductase, the plastid redox state is restored and SAL1 dimers dissociated into catalytically active monomers capable of PAP hydrolysis (Estavillo et al., 2011; Chan et al., 2016a).

1.8. Conclusions and introduction to the study

Plants have evolved an abundance of adaptive strategies and mechanisms to cope with the inevitable changes and challenges of their environment. Among these is the evolution of an endogenous timing mechanism that emerged due to the predictable, rhythmic environmental changes that result from the 24-hour rhythms of the Earth's rotation. These circadian rhythms allow synchronisation of the cell's vast array of biological processes, and align the cell's biology with the rhythms of the environment, providing plants with an adaptive advantage. While the circadian system controls numerous processes, both daily and seasonal, the circadian clock does not function in isolation. Plants perceive a variety of environmental inputs, particularly in chloroplasts, and effective coordination of responses to these stimuli rely on interorganellar signalling systems such as chloroplast-to-nucleus retrograde signalling. While widespread attempts to identify the nature and mechanism of these signals have led to exciting discoveries of roles for various signal molecules, a broader understanding of how plants incorporate environmental signals, interorganellar signals and circadian regulation will provide

insight into how plants adapt and thrive in challenging environments. This study will focus on the role of chloroplast-to-nucleus retrograde signalling in circadian regulation in *Arabidopsis thaliana*.

Chapter 2

Material and Methods

2.1. Media and reagents prepared for use in this study

2.1.1. Murashige and Skoog media for Arabidopsis thaliana growth

Arabidopsis thaliana seedlings were grown on half-strength Murashige and Skoog basal mineral salts (0.5x MS) agar plates. 2.15 g/L Murashige and Skoog Basal Salt Mixture (Sigma-Aldrich, cat #M5519) was dissolved in dH_2O and pH adjusted to pH 5.7 using 1 M KOH solution (prepared in dH_2O). 0.8% (w/v) agar was added before sterilisation. In some cases, 0.5x MS media was supplemented with 3% (w/v) sucrose and 100 µg/mL Carbenicillin (Fisher Bioreagents, cat# BP2648-1). Media was sterilised by autoclaving at 121°C for 15 minutes.

For sulfate deficiency experiments, *Arabidopsis* seedlings were grown on sulfate-deficient media prepared according to the media formulation stipulated for Murashige and Skoog Basal Medium (Sigma-Aldrich, cat #M5519), but with all sulfates replaced by chlorides to consist of 10.31 mM NH_4NO_3, 0.05 mM H_3BO_3, 1.50 mM $CaCl_2$, 0.05 ρM $CoCl_2$, 0.05 ρM $CuCl_2$, 0.05 mM $C_{10}H_{14}N_2Na_2O_8$, 0.05 mM $FeCl_3$, 0.75 mM $MgCl_2$, 0.05 mM $MnCl_2$, 0.52 ρM Na_2MoO_4, 2.50 ρM KI, 9.40 mM KNO_3, 0.63 mM KH_2PO_4, 15 ρM $ZnCl_2$ and 0.8% agar. As a control, seedlings were grown on comparable media, but with $CuCl_2$, $FeCl_3$, $MgCl_2$, $MnCl_2$ and $ZnCl_2$ substituted with equimolar concentrations of $CuSO_4$, $FeSO_4$, $MgSO_4$, $MnSO_4$ and $ZnSO_4$, respectively. Media was prepared in ultrapure MilliQ H_2O, and pH adjusted to pH 5.7 using 1 M KOH solution prepared in ultrapure MilliQ H_2O.

2.1.2. Luria-Bertani (LB) media for Escherischia coli and Agrobcterium tumefaciens growth

E. coli and *Agrobacterium tumefaciens* strain GV3101 were cultured in Luria-Bertani media (10 g/L Casein Digest Peptone, 5 g/L Yeast Extract, 10 g/L NaCl). 25 g/L LB Broth High Salt Powder (Melford Laboratories Ltd., Ipswich, UK, cat# L1704) was dissolved in dH_2O and pH adjusted to pH 7.2 using 1 M NaOH solution (prepared in dH_2O). For LB agar, 0.8% (w/v) agar was added to LB broth before sterilisation. Media was sterilised by autoclaving at 121°C for 15 minutes.

2.1.3. Preparation of DEPC-treated water

Water used in RNA and first-strand cDNA preparations (Section 2.3) was treated with 0.1% diethylpyrocarbonate (DEPC, Sigma-Aldrich, cat# D5758) to inactive RNase enzyme activity prior to use. 100 µL DEPC was added to 100 mL Ultrapure MilliQ H_2O, properly mixed, aliquoted into working volumes and incubated overnight in the dark at room temperature. Following incubation, DEPC was inactivated by autoclaving at 121°C for 15 minutes.

2.1.4. Preparation of qPCR Reaction Mixture for qRT-PCR

qPCR Reaction Mixtures used for qRT-PCR were used as previously described (Martin-Tryon et al., 2006). 1 mL 2x qPCR Reaction Mixture stocks were prepared in ultrapure Milli-Q H_2O and contained 40 mM Tris-HCl pH 8.4 (prepared in ultrapure Milli-Q H_2O), 100 mM KCl (prepared in ultrapure Milli-Q H_2O), 6 mM $MgCl_2$ (prepared in ultrapure Milli-Q H_2O), 8% glycerol (99+%, Fisher Chemical, cat# G/0650/17), 20 nM Fluorescein (diluted with 1 M Tris-HCl pH p08.8 from a 1 mg/mL Fluorescein solution prepared in acetone; ACROS Organics™, cat# 119240250), 0.4x SYBR™ Green I Nucleic Acid Gel Stain (diluted in DMSO from a 10,000x solution, Invitrogen, UK), 0.1 mg/mL Bovine Serum Albumin (BSA, prepared in ultrapure Milli-Q H_2O; >98%, Sigma-Aldrich, cat# 05470) and 1.6 mM dNTP mix (10 mM of

each dNTP, prepared in DEPC-treated water; Thermo Scientific, cat# R0182). Solutions containing ultrapure Milli-Q H_2O, Tris-HCL pH 8.4, KCl, $MgCl_2$, Glycerol and BSA were treated with 365 nm UV light for two hours using a MINERALIGHT® Multiband UV lamp (UVP, Upland, USA, cat# UVGL-85) before addition of dNTP mix, SYBR Green I and Fluorescein (on ice). 1 mL 2x qPCR Reaction Mixture aliquots were stored at -20°C, with 750 µL dH2O, 5 µL 100 mM both forward and reverse primer (prepared in DEPC-treated water, and 40 µL Taq polymerase added prior to use (Section 2.3.4).

2.1.5. Purification of Taq DNA Polymerase I

Thermus aquaticus DNA Polymerase I (Taq) was purified according to a previously described method (Pluthero, 1993) and used in PCR and qRT-PCR analysis as reported previously (Martin-Tryon et al., 2006; Chen et al., 2015). The *Escherichia coli* (*E. coli*) Rosetta™ II strain was used as a host for the recombinant plasmid pTaq (Engelke et al., 1990) to overproduce the Taq DNA polymerase. Glycerol stocks of *E. coli* Rosetta™ II cells previously transformed with the pTaq plasmid were a gift from Dr M. A. Jones (University of Essex, UK). Glycerol stock was recovered by streaking out cells on a LB agar plate (see Section 2.1.2) containing 100 µg/mL Ampicillin (Melford Laboratories Ltd, Ipswich, UK, cat# A0104) and incubated overnight at 37°C, and a single colony used to inoculate 10 mL LB broth (see Section 2.1.2) containing 100 µg/mL Ampicillin. Following incubation overnight at 37°C with shaking at 180 rpm, 100 µL of the overnight culture was used to inoculate 1 L LB broth containing 100 µg/mL Ampicillin. This 1 L culture was incubated at 37°C with shaking until an OD_{600nm} of 0.8 was reached (approximately 11 hours), at which point IPTG (Sigma-Aldrich, UK, cat# I6758) was added to a final concentration of 124 mg/L to induce protein expression. After incubation at 37°C with shaking for 12 hours, cells were collected by centrifugation at 3,000 rpm for 30 minutes at 4°C and gently resuspended in 100 mL Buffer A (50 mM Tris-HCl pH 7.9, 50 mM Dextrose, 1 mM ethylene diaminetetra-acetic acid (EDTA)). Cells were pelleted by centrifugation at 3,000 rpm for 15 minutes and gently resuspended in 50 mL Buffer A

containing 4 mg/mL Lysozyme (Sigma-Aldrich, UK, cat# L6876). Mixtures were incubated at room temperature for 15 minutes, after which 50 mL Lysis Buffer (10 mM Tris-HCl pH 7.9, 50 mM KCl, 1 mM EDTA, 1 mM PMSF, 0.5% Tween-20, 0.5% Nonidet P40) was added and incubated at 75°C for 1 hour. Lysate was cleared by centrifugation at 10,000 rpm for 15 minutes at 4°C and transferred to a glass beaker. Protein was precipitated by adding 30 g ammonium sulfate ($(NH_4)_2SO_4$) to the cleared lysate slowly (over the course of 30 minutes) with gentle stirring at room temperature. Solution was incubated with stirring for a further 30 minutes at room temperature, and precipitated protein collected by centrifugation at 10,000 rpm for 15 minutes at 4°C. Protein was resuspended in 20 mL Buffer A and dialyzed against Storage Buffer (50 mM Tris-HCl pH 7.9, 50 mM KCl, 0.1 mM EDTA, 1 mM DTT, 50% glycerol, 0.5 mM phenylmethylsulfonyl fluoride (PMSF, Thermo Fisher Scientific, cat# 36978 PMSF)) using Slide-A-Lyzer™ 20K MWCO 30 mL Dialysis Cassettes (Thermo Fisher Scientific, UK, cat# 66003) as per manufacturer's instructions. Dialysis was performed at 4°C for 2 hours, after which Storage Buffer was replaced with fresh Storage Buffer. Dialysis was continued for another 2 hours at 4°C, with buffer again replaced with fresh Storage Buffer before dialysis was continued overnight at 4°C. Following dialysis, protein was diluted 1:1 with Storage Buffer.

To determine the optimal dilution of Taq to use, a sample of the protein extract was used to prepare a dilution series (1:0, 1:1, 1:3, 1:5, 1:7, 1:15, 1:31) using Storage Buffer. Activity of the Taq dilution series was tested using PCR (Section 2.3.3), and optimum Taq dilutions were tested with qRT-PCR as described in Section 2.3.4. The remaining purified Taq was diluted to the optimum dilution for both PCR and qRT-PCR use with Storage Buffer, aliquoted and stored at -20°C.

2.2. DNA preparation, cloning and manipulation

2.2.1. Agarose gel electrophoresis

DNA was analysed by horizontal agarose gel electrophoresis. Samples were combined with 1x DNA Loading Buffer (6% (v/v) glycerol, 0.2% (w/v) Ponceau S) and resolved on a 1% (w/v) agarose gel containing 1:10,000 dilution SafeView Nucleic Acid Stain (NBS Biologicals, Cambridgeshire, UK, cat# NBS-SV1) in TAE buffer (40 mM Tris pH 7.6, 1 mM EDTA, 20 mM acetic acid) at 100V. 5 µL GeneRuler 1kb DNA Ladder (Thermo Fisher Scientific, SM0313) or MassRuler DNA Ladder Mix (Thermo FisherScientific, SM0403) was analysed alongside 12 uL of sample. Gels were visualised under blue light using the GeneGenius Bioimaging system (Syngene, Synoptics Ltd., Cambridge, UK) per the manufacturer's instructions.

2.2.2. Quantification of nucleic acids

Purity and concentration of extracted total RNA, plasmids and genomic DNA were examined using the NanoDrop™ ND-1000 Spectrophotometer (Thermo Fisher Scientific, UK) with NanoDrop™ 1000 Operation Software as per the manufacturer's instructions. Absorbance of 2 µL sample at 230 nm, 260 nm and 280 nm was determined spectrophotometrically, with sample concentration in ng/µL based on absorbance at 260 nm using Beer's Law. The ratio of sample absorbance at 260 nm and 280 nm (260/280), as well as the ratio of absorbance at 260 nm and 230 nm (260/30) were used as indicators of nucleic acid purity. A 260/280 ratio of ~2 and a 260/280 ratio of 1.8-2.2 were regarded as indicating 'pure' RNA, with RNA re-precipitated before use if either 260/280 or 260/230 ratio was below 1.7. Similarly, a 260/280 ratio of ~1.8 and a 260/230 ratio of 1.8-2.2 was regarded as indicated 'pure' plasmid or genomic DNA.

2.2.3. Polymerase chain reaction (PCR)

Polymerase chain reaction (PCR) was routinely used to analyse plasmids in this study, as well to verify genotypes of *Arabidopsis* T-DNA insertion lines. PCR reactions were performed using an Applied Biosystems 2720 Thermal Cycler (Thermo Fisher Scientific, UK). Primers were designed using Primer3Plus (Untergasser et al., 2007). For genotyping of *Arabidopsis* T-DNA insertion lines, the SALK T-DNA verification primer design online tool was used (http://signal.salk.edu/tdnaprimers.2.html). Specificity of designed primer sets was confirmed using Primer Blast (Ye et al., 2012). Primers used in this study are listed in Appendix I.

Routine PCR reactions were set up (on ice) in thin-walled 200 µL PCR tubes in 20 µL volumes consisting of 2 µL 10x PCR buffer (500 mM KCl, 100 mM Tris-HCl pH 9.0, 15 mM $MgCl_2$, 1% Triton X-100), 2 µL dNTP mix (2.5 mM each, prepared in dH_2O, Thermo Scientific, cat# R0182), 2 µL 20 mM $MgCl_2$, 1 µL 10 µM forward primer, 1 µL 10 µM reverse primer, 1 µL Taq polymerase, 0.1 µg template DNA, dH_2O up to 20 µL final volume. PCR conditions for amplification with Taq polymerase were as follows: initial DNA denaturation at 94°C for 2 minutes; 40 cycles of DNA denaturation at 94°C for 30 seconds, primer annealing at T_a for 30 second, extension at 72°C for 30 seconds per 1 Kb template; final extension at 72°C for 7 minutes. Annealing time (T_a) depended on melting temperatures (T_m) of primers used, usually defined as T_a = lowest T_m – 5°C.

Amplification of gDNA (see Section 2.2.8) or cDNA (see Section 2.3.3) for transformation of *Arabidopsis thaliana* was performed using Phusion High-Fidelity DNA Polymerase (Thermo Fisher Scientific, UK, cat# F530S) as per manufacturer's instructions. 20 µL reactions were set up (on ice) in thin-walled 200 µL PCR tubes and consisted of 4 µL 5x Phusion HF Buffer, 0.4 µL dNTP mix (10 mM each, prepared in dH_2O), 1 µL 10 µM forward primer, 1 µL 10 µM reverse primer, 100 ng template DNA, 0.2 µL Phusion High-Fidelity DNA Polymerase (2U/µL).

The 3-step protocol for amplification with Phusion High-Fidelity DNA Polymerase was as follows: initial denaturation at 98°C for 30 seconds; 35 cycles of denaturation at 98°C for 10 seconds, primer annealing at T_a for 30 seconds, extension at 72°C for 30 seconds per 1 Kb template; final extension at 72°C for 10 minutes. Annealing time (T_a) depended on melting temperatures (T_m) of primers used, usually defined as T_a = lowest T_m – 5°C

2.2.4. Colony PCR

Positive transformants from cloning reactions (see Section 2.2.5) were identified using colony PCR. Following overnight incubation of transformed *E. coli* overnight at 37°C on selective LB-agar plates, single colonies were transferred to individual thin-walled 200 µL PCR tubes containing 5 µL dH_2O. A portion of each selected colony was re-streaked onto a selective LB-agar plate containing the appropriate antibiotic. PCR was performed using Taq polymerase in 20 µL reaction volumes consisting of 2 µL 10x PCR buffer, 2 µL dNTP mix, 2 µL 20 mM $MgCl_2$, 1 µL 10 µM forward primer, 1 µL 10 µM reverse primer, 1 µL Taq polymerase and dH_2O up to 20 µL final volume. PCR products were visualised using agarose gel electrophoresis as described in Section 2.2.1 to identify colonies containing the desired plasmid. Plasmids were isolated from overnight cultures of the positive colonies as described in Section 2.2.6.

2.2.5. Construction of plasmids for transformation of Arabidopsis thaliana

PCR products amplified with Phusion High-Fidelity DNA polymerase (see Section 2.2.3) were cloned into the pCR™8/GW/TOPO® entry vector using the pCR™8/GW/TOPO® TA® Cloning kit (Invitrogen, UK, cat# K2020-20) as per manufacturer's instructions. Following amplification with proofreading polymerase, 3' A-overhangs were added to PCR products as follows: to 20 µL PCR reaction, 1 µL Taq polymerase was added, reaction mixed well and incubated at 72°C for 10 minutes using an Applied Biosystems 2720 Thermal Cycler (Thermo

Fisher Scientific, UK). Reaction was placed on ice and immediately used in the TOPO® Cloning reaction consisting of 4 µL PCR product, 1 µL Salt Solution and 1 µL pCR™8/GW/TOPO® entry vector. After gentle mixing, reaction was incubated for 30 minutes at room temperature, placed on ice and used to transform One Shot® Top10 Chemically Competent *E. coli* (Invitrogen, UK, cat# C4040).

Transformation of *E. coli* was performed as follows: one vial of One Shot® Top10 *E. coli* cells was thawed on ice for 30 minutes. All 6 µL of the TOPO® Cloning reaction was added to the thawed cells, mixed gently and cells incubated on ice for 30 minutes. Cells were heat-shocked at 42°C for 30 seconds and cooled on ice for 2 minutes. 1 mL LB media was added and cells recovered by incubation at 37°C with shaking at 200 rpm for 1 hour. Cells were collected by centrifugation at 6,000 rpm for 5 minutes at room temperature and supernatant removed so that only approximately 50 µL remain. After resuspension in the remaining supernatant, transformed *E. coli* cells were plated on selective LB agar plates containing 100 µg/mL Spectinomycin (Melford Laboratories Ltd, Ipswich, UK, S0188). Cells were incubated overnight at 37°C, following which single colonies were selected, screened using colony PCR (see Section 2.2.4) using the primers GW1 and GW2 and each incubated in 10 mL selective LB media containing 100 µg/mL Spectinomycin. Cultures were incubated overnight at 37°C and plasmids isolated as described in Section 2.2.6. Quality and concentration of plasmid preparations were analysed spectrophotometrically as described in Section 2.2.2.

To generate an expression clone, Entry clone constructs isolated from successful transformants were used to transfer the gene of interest into Gateway® destination vectors using the Gateway® LR Clonase® II kit (Invitrogen, UK, cat# 11791) as per manufacturer's instructions. An Applied Biosystems 2720 Thermal Cycler (Thermo Fisher Scientific, UK) was used for incubation steps. LR reactions consisted of 125 ng Entry clone, 75 ng Destination vector and TE buffer (10 mM Tris-HCl pH 8.0, 1 mM EDTA pH 8.0) up to 4 µL total volume. 1 µL LR Clonase® was thawed on ice and added. Reactions were mixed well, briefly centrifuged and incubated at 25°C for one hour. LR reaction was terminated by adding 1 µL Proteinase K,

mixing and incubating at 37°C for 10 minutes. The complete LR clonase reaction was used to transform One Shot® Top10 Chemically Competent *E. coli* as described above. Expression clones were isolated from overnight *E. coli* cultures and screened using colony PCR as described. Sequence and direction of gene of interest in expression clones were verified by sequencing (see Section 2.2.7). Maps for all vectors and plasmids use in this study are given in Appendix II.

2.2.6. Isolation of plasmid DNA from Escherischia coli

Plasmid DNA was isolated from overnight *E. coli* cultures prepared in Section 2.2.5 according to the QIAprep Spin Miniprep Kit protocol (Qiagen, UK), with modifications. Cells were harvested from 5 mL cultures by centrifugation at 3,000 rpm for 15 minutes at 4°C. Supernatant was discarded and cells resuspended in 250 µL Resuspension Buffer P1 (50 mM Tris-HCl pH 8, 10 mM EDTA pH 8, 100 µg/mL RNase A). 250 µL Lysis Buffer P2 (0.2 M NaOH, 1% (w/v) SDS) was added, samples mixed gently by inverting 4-6 times and incubated at room temperature for 3-5 minutes (not more than 5 minutes) until suspension turned transparent and viscous. 350 µL Neutralisation Buffer N3 (4 M guanidine hydrochloride, 0.5 M sodium acetate) was added, reactions mixed gently by inverting 4-6 times and centrifuged at 13,000 rpm for 15 minutes at room temperature. Supernatant was transferred onto an EZ-10 DNA Mini Spin Column (NBS Biologicals, UK, cat# SD5005) and centrifuged at 13,000 rpm for 1 minute at room temperature. Flow-through was discarded. 750 µL Wash Buffer PE (10 mM Tris-HCl pH 7.5, 80% ethanol) was added to column and incubated at room temperature for 1-2 minutes before centrifugation at 13,000 rpm for 1 minute at room temperature. Flow-through was discarded and wash step with Buffer PE repeated. Flow-through was discarded and column centrifuged again at 13,000 rpm for 1 minute at room temperature to dry column. The blue column was transferred to a clean 1.5 mL microcentrifuge tube, after which 50 µL ultrapure MilliQ H_2O (heated to 55°C) was added to the column and incubated at room temperature for 5-10 minutes. Columns were centrifuged at 13,000 rpm for 1 minute at room temperature and

flow-through containing plasmid collected. Quality and concentration of plasmid preparations were analysed spectrophotometrically as described in Section 2.2.2.

2.2.7. Sanger sequencing of prepared plasmids and PCR products

DNA sequencing of PCR products and inserts in expression clones was completed through the Sanger Sequencing Service from Source Bioscience (Nottingham, UK) as per sample requirements. For sequencing of PCR product, the procedure was as follows: following PCR reaction (see Section 2.2.3), nucleotides were precipitated by adding 2 µL 3 M sodium acetate ($C_2H_3NaO_2$, prepared in dH_2O) and 40 µL 100% ethanol to the 20 µL PCR reaction. Reaction was thoroughly mixed and incubated at -80°C for 30 minutes. Precipitate was collected by centrifugation at 13,000 rpm for 30 minutes at 4°C, supernatant removed completely using pipettes, and pellets washed by adding 100 µL 70% ethanol (prepared in dH_2O). Following centrifugation at 13,000 rpm for 5 minutes at 4°C, supernatant was removed and wash step repeated using 100% ethanol. After final centrifugation at 13,000 rpm for 5 minutes at 4°C, supernatant was removed completely using pipettes and pellets dried by incubating open tubes on the bench at room temperature. Pellets were resuspended in 20 µL dH_2O by heating at 55°C for ten minutes, after which purity and concentration of sample were determined spectrophotometrically (see Section 2.2.2). 5 µL PCR product at >1 ng/µL per 100 bp product length was sent for sequencing. For sequencing of expression clones, 5 µL 100 ng/µL clean plasmid preparation (as determined spectrophotometrically) was provided. Where necessary, 5 µL each of 3.2 µM forward and/or reverse primer was also provided. Sequences were analysed using the software BioEdit (http://www.mbio.ncsu.edu/bioedit/bioedit.html).

2.2.8. Extraction of genomic DNA from Arabidopsis thaliana tissue

Genomic DNA was extracted from *Arabidopsis thaliana* tissue using cetyltrimethyl ammonium bromide (CTAB) with modifications to a previously described protocol (Clarke, 2009). 10-20 *Arabidopsis* seedlings were harvested, placed in a 1.5 mL microcentrifuge tube

containing two 2.0 mm diameter AISI 304 stainless steel balls (Dejay Distribution Ltd, Cornwall, UK) and snap-frozen in liquid nitrogen. Tissue was ground using a Qiagen Retsch MM300 Tissuelyser (Qiagen, UK) tissue disrupter, with metal plates chilled on ice prior to use, for 2 minutes at 30 rpm. Ground tissue was collected in bottom of the tube by brief centrifugation, resuspended in 300 µL CTAB buffer (2% CTAB, 1.4 M NaCl, 100 mM Tris-HCl pH 8, 20 mM EDTA), and heated at 65°C for 30 minutes. After cooling to room temperature, 300 µL chloroform was added, sample vortexed vigorously for 20 seconds and centrifuged at 13,000 rpm for 15 minutes at 4°C. To precipitate nucleic acids, aqueous phase was transferred to a clean 1.5 mL microcentrifuge tube containing 500 µL isopropanol, mixed by brief vortexing and precipitate pelleted by centrifuged at 13,000 rpm for 15 minutes at 4°C. Pellet was washed by adding 500 µL 10% ethanol (prepared in dH_2O) with repeated pipette aspirations until pellet is free-floating, centrifuged at 13,000 rpm for 10 minutes at 4°C, and supernatant removed using pipettes. Pellets were dried by incubating open microcentrifuge tubes at room temperature on the bench for 30 minutes. Pellets were resuspended in 30 µL dH_2O by heating at 55°C for ten minutes. Genomic DNA preparations were analysed spectrophotometrically as described in Section 2.2.2 and stored at -20°C.

2.3. RNA preparation and manipulation

2.3.1. Sampling and extraction of total RNA from Arabidopsis thaliana tissue

Total RNA was extracted from *Arabidopsis* tissue using TRI Reagent® (Sigma-Aldrich, UK, cat# T9424) with modifications to manufacturer's instructions. For each data point, at the indicated sampling time, 10-15 seedlings were collected in a 1.5 mL microcentrifuge tube containing two 2.0 mm diameter AISI 304 stainless steel balls (Dejay Distribution Ltd, Cornwall, UK) and snap-frozen in liquid nitrogen immediately upon sampling. Tissue was ground using a Qiagen Retsch MM300 Tissuelyser (Qiagen, UK) tissue disrupter, with metal plates chilled on dry ice prior to use, for 1 minute at 30 rpm, repeating if necessary until tissue

was properly ground. Following quick centrifugation at 13,000 rpm for 10 seconds at 4°C to collect ground tissue at the bottom of the tube, tissue was resuspended in 400 µL TRI Reagent® by brief vortexing, and incubated on ice for 2 minutes. 200 µL chloroform was added to each tube and samples were mixed gently by inversion for 20 seconds, followed by incubation at room temperature for 2 minutes and subsequent centrifugation at 13,000 rpm for 15 minutes at 4°C. Chloroform extraction was repeated by collecting aqueous phase and transferring to a new 1.5 mL microcentrifuge tube containing 200 µL chloroform, mixing gently by inversion for 20 seconds and incubating at room temperature for 2 minutes. Following centrifugation at 13,000 rpm for 15 minutes at 4°C, total RNA was precipitated by transferring aqueous phase to a new 1.5 mL microcentrifuge tube containing 500 µL isopropanol, mixed by inversion for 20 seconds, and incubated on ice for 20 minutes. Precipitate was collected by centrifugation at 13,000 rpm for 20 minutes at 4°C, and care taken to remove all supernatant using pipettes. Precipitate was washed by adding 500 µL 70% ethanol (prepared using DEPC-treated water) with repeated pipette aspirations until pellet was free-floating, followed by centrifugation at 13,000 rpm for 3 minutes at 4°C and removal of all supernatant using pipettes. The wash step was repeated using 500 µL 100% ethanol and samples centrifuged again at 13,000 rpm for 3 minutes at 4°C. Following total removal of supernatant using pipettes, pellets were dried by incubating open microcentrifuge tubes (covered with Hospitex soft medical tissue, Aero Healthcare, UK, cat# AN1035) on the bench at room temperature for 30 minutes. Once dry, pellets were resuspended in 30 µL DEPC-treated water through incubation at 55°C for ten minutes. Purity and concentration of extracted total RNA was determined spectrophotometrically (Section 2.2.2), and RNA re-precipitated using ethanol if not pure.

For re-precipitation of total RNA, 3 µL 3 M sodium acetate ($C_2H_3NaO_2$, prepared with DEPC-treated water) and 60 µL 100% ethanol were added to the RNA preparation, reactions mixed and briefly centrifuged, and incubated at -80°C for 30 minutes. Precipitates were pelleted by centrifugation at 13,000 rpm for 30 minutes at 4°C and al supernatant removed using pipettes. Precipitates were washed with 500 µL 70% ethanol (prepared in DEPC-treated water) with

repeated pipette aspirations until pellet was free-floating, followed by centrifugation at 13,000 rpm for 3 minutes at 4°C and removal of all supernatant using pipettes. Wash step was repeated using 100% ethanol. Following total removal of supernatant using pipettes, pellets were dried at room temperature for 30 minutes and resuspended in 30 µL DEPC-treated as described above. Purity and concentration of extracted total RNA was determined spectrophotometrically, and pure complete RNA preparations were stored at -80°C.

2.3.2. DNase treatment of extracted total RNA

Genomic DNA was removed from pure total RNA preparations by DNase treatment using Recombinant DNase I, RNase-free (DNase I, Thermo Fisher Scientific, UK, cat# EN0525) as per manufacturer's instructions. Reactions were set up in PCR tubes kept on Eppendorf® PCR Cooler iceless cold PCR tube racks (Sigma-Aldrich, UK, cat# Z606634) as follows: <1 µg total RNA, 1 µL 10x Reaction Buffer with $MgCl_2$, 1 µL DNase I (1U/µL), DEPC-treated water up to 10 µL total volume. Reactions were gently mixed, briefly centrifuged, and incubated at 37°C for 30 minutes. Following incubation, 1 µL 50 mM EDTA solution was added to each reaction, mixed, briefly centrifuged and DNase I inactivated by incubation at 65°C for 10 minutes. All incubation steps were performed using an Applied Biosystems 2720 Thermal Cycler (Thermo Fisher Scientific, UK).

2.3.3. First-strand cDNA synthesis

cDNA was synthesised from total mRNA by a two-step reaction using $Oligo(dT)_{18}$ primer (Sigma Aldrich, UK) and RevertAid Reverse Transcriptase (RT, Thermo Fisher Scientific, cat# EP0442) with modifications to manufacturer's instructions. Following DNase-treatment of total RNA preparations (see Section 2.3.2), 1.25 µL DEPC-treated water and 1 µL 0.5 µg/µL $Oligo(dT)_{18}$ (prepared in DEPC-treated water) were added to each 11 µL reaction from Section 2.3.2. Reactions were gently mixed, briefly centrifuged and incubated for 5 minutes at 65°C

followed by 1 minute at 4°C. 4 µL 5x Reaction Buffer, 2 µL dNTP mix (10 mM each prepared in DEPC-treated water, Thermo Scientific, cat# R0182) and 0.25 µL RT were added to each reaction, reactions gently mixed, briefly centrifuged and incubated for 60 minutes at 42°C, followed by termination of the reaction by heating at 70°C for 10 minutes. All reactions were kept cold during preparation on Eppendorf® PCR Cooler iceless cold PCR tube racks (Sigma-Aldrich, UK, cat# Z606634), and incubation steps performed using an Applied Biosystems 2720 Thermal Cycler (Thermo Fisher Scientific, UK).

2.3.4. Real-time quantitative RT-PCR (qRT-PCR)

qRT-PCR was performed using a CFX96 Touch Real-Time PCR Detection System (Biorad, UK) or a CFX Connect™ Real-Time PCR Detection System (Biorad,UK) with reaction setup as previously described (Martin-Tryon et al., 2006). Final reaction concentrations were as follows: 20 mM Tris-HCL pH 8.4, 50 mM KCl, 3 mM $MgCl_2$, 4% glycerol, 10 nM Fluorescein, 0.2x SYBR Green I, 0.05 mg/mL Bovine Serum Albumin, 0.8 µM dNTPs, 1.25 µM forward primer, 1.25 µM reverse primer, 0.2 uL Taq polymerase and 10% diluted cDNA. Reactions were set up in clear 96-well PCR microplates (Alpha Laboratories, UK, LW2216) kept cold on Eppendorf® PCR Cooler iceless cold PCR tube racks (Sigma-Aldrich, UK, cat# Z606634) by adding 17.5 µL 1x qPCR Reaction Mixture (see Section 2.1.4) and 2 µL diluted cDNA prepared in Section 2.3.3. PCR Microplates were sealed with clear adhesive PCR plate seals (Thermo Fisher Scientific, cat# AB-0558).

PCR conditions were as follows: Initial denaturation and DNA polymerase activation at 95°C for 2 minutes, 50 cycles consisting of denaturation at 95°C for 5 seconds, annealing at 60°C for 10 seconds and extension at 72°C for 5 seconds. Melt curve analysis from 65°C to 90 °C in 0.5 °C increments for 5 seconds was performed to verify the specificity of the amplification products. Primers were designed using Primer3Plus (Untergasser et al., 2007) and targeted to amplify products between 85-100 bp in length. Where possible, primer sets contained one

primer bridging an intron to prevent amplification of any contaminating genomic DNA remaining after DNase treatment of total RNA. Primer sets used in this study are given in Appendix I.

Samples were run in triplicate and a non-template control was included. Starting quantities were estimated from critical thresholds compared to the standard curve of amplification for each primer set. cDNA from samples were diluted 10x in dH_2O, with combined cDNA for standards diluted 2x with dH_2O. All qRT-PCR data presented were normalized to *PP2a* expression level

2.4. Protein gel electrophoresis

2.4.1. Protein extraction from Arabidopsis thaliana tissue

Protein was extracted from transgenic *Arabidopsis thaliana* transformed with *Agrobacterium* to analyse level of protein expression. 10-15 14-day old *Arabidopsis* seedlings were harvested, collected in a 1.5 mL microcentrifuge tube containing two 2.0 mm diameter AISI 304 stainless steel balls (Dejay Distribution Ltd, Cornwall, UK) and snap-frozen in liquid nitrogen immediately upon sampling. Tissue was ground using a Qiagen Retsch MM300 Tissuelyser (Qiagen, UK) tissue disrupter, with metal plates chilled on ice prior to use, for 45 seconds at 30 rpm. Tubes were briefly centrifuged at 13,000 rpm for 10 seconds at 4°C, and ground tissue resuspended in 200 µL cold Homogenisation buffer (25 mM MOPS, 0.25 M sucrose, 0.1 mM MgCl, 8 mM L-Cystine, 0.5 mM PMSF, 1 Complete Mini Protease Inhibitor Cocktail tablet (Roche) per 10 mL buffer) by vortexing for 45 seconds. Samples were centrifuged at 13,000 rpm for 20 minutes at 4°C, supernatant transferred to clean 1.5 mL microcentrifuge tube, and centrifugation step repeated.

Concentration of protein was determined using the Pierce™ Coomassie Plus™ (Bradford) Protein Assay (Thermo Fisher Scientific, UK, cat# 23238) as per manufacturer's instructions. Bradford assays were prepared at room temperature in Greiner 96-well clear multiwell plates

(Sigma-Aldrich, UK, cat# M2936). Reactions consisted of 245 µL Bradford reagent and 5 µL protein extract and were properly mixed by repeated pipette aspirations before analysis. Absorbance of samples at 595 nm was determined at room temperature using a SPECTROstar Omega Ultra-fast UV/Vis spectrum absorbance spectrometer microtitre plate reader (BMG LABTECH, Offenburg, Germany) and protein concentrations calculated using a standard curve prepared with Bovine Serum Albumin.

2.4.2. SDS-polyacrylamide gel electrophoresis (SDS-PAGE)

Protein extractions were analysed by SDS-PAGE with modifications to the original described protocol (Laemmli, 1970), using the Mini-PROTEAN® Electrophoresis System (Biorad, UK). Approximately 15 µg total protein was analysed for each sample, alongside either Precision Plus Protein™ Dual Colour standard (250 kDa-10 kDa; BioRad, UK, cat# 161-0374) or PageRuler™ Plus Prestained 10-250 kDa Protein Ladder (Thermo Fisher Scientific, UK, cat# 26619). Protein samples were denatured in 1x SDS Loading Buffer (50 mM Tris-HCl pH 6.8, 100 mM DTT, 2% (w/v) SDS, 0.1% (w/v) Bromophenol Blue, 10% (v/v) glycerol) by boiling for 10 minutes at 100°C. Denatured proteins were resolved on a 15% polyacrylamide separating gel (4.5 mL 30% (29:1) acrylamide:bis-acrylamide, 4.5 mL 1 M Tris-HCl pH 6.8, 2.8 mL dH_2O, 120 µL 10% (w/v) SDS, 60 µL 10% (w/v) ammonium persulfate, 8 µL TEMED) with 5% polyacrylamide stacking gel (1 mL 30% (29:1) acrylamide:bis-acrylamide, 1.32 mL 1 M Tris-HCl pH 6.8, 7.72 mL dH_2O, 120 µL 10% (w/v) SDS, 50 µL 10% (w/v) ammonium persulfate, 8 µL TEMED). Electrophoresis was performed at 200 V for 1 hour at room temperature in 1x Running Buffer (25 mM Tris, 250 mM glycine, 0.1% (w/v) SDS). Following electrophoresis, SDS-PAGE gels were either used for Immunoblot analysis (see Section 2.4.3) or stained for 2 hours at room temperature using InstantBlue Protein Stain (Expedeon, UK, cat# ISTB).

2.4.3. Immunoblot analysis of proteins

HyPer and SAL1-GFP were immunodetected by anti-GFP antibody (Abcam, UK, cat# ab290) at a 1:10,000 dilution, with anti-GFP primary antibody detected using the Anti-Rabbit IgG (H+L) HRP conjugate (Promega, UK, cat# W4011) at 1:4,000 dilution. As loading control, actin was immunodetected by anti-Actin primary antibody (Sigma-Aldrich, UK, cat# mAB1501) at a 1:2,000 dilution. Anti-actin primary antibody was detected using the Anti-Mouse IgG (H+L) HRP conjugate (Promega, UK, cat# W4021) at 1:4,000 dilution.

Following SDS-PAGE, protein was semi-dry transferred onto an Amersham Protran 0.45 µM nitrocellulose membrane (GE Healthcare Life Sciences UK, cat# 10600002) at 100 V for 1.5 hours at room temperature using cooled Transfer Buffer (25 mM Tris, 190 mM glycine. 20% (v/v) methanol). Membrane was stained using Ponceau Solution (0.2% (w/v) Ponceau S, 1% (v/v) acetic acid) to confirm successful transfer of proteins to membrane. Stain was removed, membranes rinsed with dH_2O and blocked for 1 hour at room temperature using 8% (w/v) skim milk powder dissolved in dH_2O. After blocking, primary antibody diluted in 8% milk power solution prepared in 1x PBST buffer (137 mM NaCl, 2.7 mM KCl, 0.88 mM KH_2PO_4, 2.15 mM Na_2HPO_4, 0.1% (v/v) Triton X-100, pH adjusted to pH 7.4 with HCl) was incubated with the membrane at the appropriate dilution overnight at 4°C. Membrane was washed in 1x PBSTT buffer (137 mM NaCl, 2.7 mM KCl, 0.88 mM KH_2PO_4, 2.15 mM Na_2HPO_4, 0.1% Triton X-100, 0.1% Tween-20, pH 7.4) for 5 minutes with shaking, and wash step repeated two more times. Secondary antibody prepared in 8% milk powder PBST solution at the appropriate dilution was incubated for 1 hour at room temperature, and membranes washed 5 times with 1x PBSTT as described above, and a final wash step with 1x PBS buffer (137 mM NaCl, 2.7 mM KCl, 0.88 mM KH_2PO_4, 2.15 mM Na_2HPO_4, pH 7.4). Horseradish peroxidase (HRP)-conjugated antibodies were visualised using the Pierce™ ECL Western Blotting Substrate as per manufacturer's instructions. Each membrane was incubated with 2 mL substrate for 5 minutes, and excess substrate removed before analysis. Chemiluminescence from membrane

was imaged by scanning with a Fusion FX imaging system (Vilber Lourmat, France), and images analysed using ImageJ.

2.5. Metabolite analysis

2.5.1. Extraction of PAP from Arabidopsis thaliana tissue

3'-phosphoadenosine 5'-phosphate (PAP) was extracted from whole seedlings based on a method previously described (Bürstenbinder et al., 2007). 150-300 mg tissue was collected in 2 mL Eppendorf® Safe-Lock microcentrifuge tubes (Sigma-Aldrich, UK, T2795), snap frozen in liquid nitrogen and weighed. Two 2.0 mm diameter AISI 304 stainless steel balls (Dejay Distribution Ltd, Cornwall, UK) were added to each tube and tissue ground using a Qiagen Retsch MM300 Tissuelyser (Qiagen, UK) tissue disrupter, with metal plates chilled on dry ice prior to use, for 1 minute at 30 rpm, repeating if necessary until all tissue was ground. After quick centrifugation at 13,000 rpm for 10 seconds at 4°C, tissue was resuspended in 0.1 M HCl (prepared in ultrapure MilliQ H_2O) with vortexing, and tubes incubated on ice for 15 minutes. Tubes were centrifuged at 13,000 rpm at 4°C for 5 min, supernatant collected in clean 2 mL Eppendorf® Safe-Lock microcentrifuge tubes, and centrifuged again. 150 µL of the supernatant was added to 770 µL cold CP buffer (620 mM citric acid and 760 mM Na_2HPO_4, pH 4, prepared in ultrapure MilliQ H_2O). Metabolites were derivitised using 80 µL ~50% (w/v) chloroacetaldehyde solution (Sigma-Aldrich, UK, cat# 317276) with incubation at 80°C for 10 min, and centrifuged for 45 minutes at 13,000 rpm at 4°C before HPLC analysis.

For standards, commercial standard for PAP (Santa Cruz Biotechnology, UK, cat# sc-210760) was used to prepare a dilution series in ultrapure MilliQ H_2O. For each dilution, 100 µL PAP solution was prepared in 1.5 mL microcentrifuge tubes (on ice) and 150 µL of each solution transferred to a tube containing cold CP buffer. PAP was derivitised using chloroacetaldehyde solution as described above and centrifuged for 45 min at 13,000 rpm at 4°C before HPLC analysis.

2.5.2. High Performance Liquid Chromatography (HPLC) analysis of PAP

Reverse-phase HPLC analysis of derivitised PAP extracts was performed based on a method described previously (Bürstenbinder et al., 2007; Estavillo et al., 2011). All buffers used were prepared using ultrapure MilliQ H_2O and filtered using Minisart® 0.2 µM syringe filters (Sartorius Stedim Biotech, cat# 10076891). Samples and standards were analysed in a randomised order.

20 µL of each derivitised PAP extract and 1 µL of each standard prepared in Section 2.5.1 was injected into an Agilent 1100 HPLC system connected to a FLD G1321A (Agilent) fluorescent detector. PAP was analysed by reverse-phase HPLC using a Luna 5 µm C18(2) 100 Å column (Phenomenex). Column was equilibrated for 0.2 minutes with 95% (v/v) of Buffer A (5.7 mM $[CH_3(CH_2)_3]_4NHSO_4$ and 30.5 mM KH_2PO_4, pH 5.8) and 5%(v/v) Buffer B (67% [v/v] acetonitrile and 33% [v/v] Buffer A), followed by a linear gradient for 53 minutes up to 50% (v/v) of Buffer B. Column was re-equilibrated for 7 minutes with 5% (v/v) buffer B before injection of the next sample. PAP concentration was calculated relative to a standard curve prepared from commercially available standard (Santa Cruz Biotechnology, cat# sc-210760), with 1 µL derivitised standard injected.

2.6. Plant material and growth conditions

2.6.1. Arabidopsis thaliana plant material

All wild type and transgenic lines used in this study were in the *Arabidopsis thaliana* Columbia-0 (Col-0) ecotype background. Single mutants *phot1-5* (*nph1-5*) and *phot2-1* (*npl-1*), deficient in PHOTOTROPIN 1 (NPH1/PHOT1) or PHOTOTROPIN 2 (NPL1/PHOT2) respectively, as well as the *nph3-1* and *nph3-102* single mutants deficient in NONPHOTOTROPIC HYPOCOTYL, and the *phot1-5 phot2-1* double mutant have been previously described (Liscum and Briggs, 1995; Huala et al., 1997; Sakai et al., 2001) and were gifts from Prof John M. Christie (University of Glasgow, UK). *alx8-1* (N66977) and *fry1-6*

(SALK_020882), both loss-of-function mutant alleles of *SAL1*, have been previously described (Rossel et al., 2006; Gy et al., 2007) and were re-isolated from seed provided by NASC (Scholl et al., 2000). The loss-of-function *SAL1* mutant allele *fou8*, the double mutant *apk1-1 apk2-1* deficient in both ADENOSINE-5'-PHOSPHOSULFATE KINASE 1 (APK1) and ADENOSINE-5'-PHOSPHOSULFATE KINASE 2 (APK2), as well as the triple mutant *apk1 apk2 fou8* have been previously reported (Mugford et al., 2009; Rodriguez et al., 2010) and were a kind gift from Prof. Edward E. Farmer (Université de Lausanne, Switzerland). Loss-of-function in EXORIBONUCLEASE 2 (XRN2) mutant allele *xrn2-1* (SALK_041148) and XRN3 mutant allele *xrn3-3* (SAIL_ 1172C07), as well as the double mutant *xrn2-1 xrn3-3* and the triple mutant *xrn2-1 xrn3-3 xrn4-6* have been reported previously (Gy et al., 2007; Hirsch et al., 2011) and were re-isolated from seed obtained from Prof. Philip M. Mullineaux (University of Essex, UK). XRN4 mutant alleles *xrn4-3* (SALK_014209) and *ein5-1* have been previously described (Roman et al., 1995; Gazzani et al., 2004) and were received from Dr Pascal Genschik and Dr Thomas Potuschak (CNRS, France). Loss-of-function in NUCLEOSIDE DIPHOSPHATE KINASE 3 (NDPK3) mutant allele *ndpk3-1* (SALK_138260C) were re-isolated from seed provided by NASC (Scholl et al., 2000). *fry1-6* transformed to express nuclear-localised SAL1 (ΔN-SAL1) has been previously reported (Kim and von Arnim, 2009) and was a gift from the Pogson laboratory (Australian National University, Australia). *alx8-1* transformed to express *35S::AHL:GFP* were received from Dr M. A. Jones (University of Essex, UK). *toc1*-4, a null *toc1* allele for the core clock components *TOC1* has been previously described (Hazen et al., 2005a; Jones and Harmer, 2011) and was received from the Harmer laboratory (University of California, Davis, USA).

Col-0 lines transformed for the expression of the biosensors HyPer1 (Belousov et al., 2006) and roGFP2 (Schwarzländer et al., 2008; Marty et al., 2009) were gifts from Dr M. A. Jones (University of Essex) and Dr. Markus Schwarzländer (Universität Bonn, Germany), respectively. Col-0 luciferase reporter lines *CCR2::LUC* (Martin-Tryon et al., 2006) and *CCA1::LUC2* (Jones et al., 2015) have been previously reported and were gifts from the

Harmer laboratory (University of California, Davis, USA) and Dr M. A. Jones (University of Essex, UK), respectively. *fry1-6 CCA1::LUC2* lines were generated by crossing *fry1-6* to the *CCA1::LUC2* line (Jones et al., 2015). Col-0 luciferase reported lines *CAB2::LUC+*, *CCA1::LUC+*, *GI::LUC+*, *LHY::LUC+* and *TOC1::LUC+* (Tindall et al., 2015) were a kind gift from Prof Anthony Hall (University of Liverpool, UK).

2.6.2. Surface sterilisation of Arabidopsis thaliana seeds

For growth on 0.5x MS plates, *Arabidopsis* seeds were surface sterilised using chlorine gas. In a glass dessicator jar, seeds were incubated for 3 hours in open 1.5 mL microcentrifuge tubes along with an open glass beaker containing 50 mL commercial 5% chlorine household bleach solution and 3 mL 37% HCl. After sterilisation, open tubes were placed in a sterile laminar flow hood for 5-10 minutes to remove remaining chlorine gas. 400 µL sterile dH_2O was added to each tube and seeds stored in the dark at 4°C for 2-3 days before sowing.

For larger volumes of *Arabidopsis* seeds, seeds were surface sterilised using ethanol. Working in a sterile laminar flow hood, seeds in sterile 15 mL tubes were washed with 5 mL 70% ethanol (prepared in sterile dH_2O) for 10 minutes, ethanol decanted, and wash step repeated with 5 mL 100% ethanol. Following sterilization, seeds were washed 4-5 times in 10 mL sterile dH_2O. Seeds were stored in 5 mL sterile dH_2O for 2-3 days at 4°C before use.

2.6.3. Entraining and free-run growth conditions of Arabidopsis thaliana

Surface-sterilised seed from *Arabidopsis* were sown on 0.5x MS plates and germinated under 60 µmol.m^{-2}.s^{-1} cool white fluorescent light (fluorescence spectrum peaks 434 nm, 544 nm and 610 nm) at 22°C in A1000 Adaptis chambers (Conviron Europe Ltd, Isleham, UK). Seedlings were entrained for 6, 10 or 12 days in 12 hours white light: 12 hours dark cycles (12h:12h) before being imaged or moved to constant light conditions. For entrainment under 16 hours white light: 8 hours dark cycles (16h:8h, long day conditions) or 8 hours white light: 16 hours dark cycles (8h:16h, short day conditions). Seedlings were grown at 22°C under cool white

phosphor-based LED light (blue luminescence emission peak at 442 nm, phosphorescence emission peak at 572 nm) in LMS Series 1A Cooled Incubators (LMS, UK)

For growth under free-run conditions, seedlings were moved to constant light conditions at subjective dawn following 10 or 12 days of entrainment in light:dark cycles. Free-run conditions were at 22°C under constant white light (cool white phosphor-based LED light; blue luminescence emission peak at 442 nm, phosphorescence emission peak at 572 nm), constant red light (monochromatic red LED light, 660 nm emission peak) or constant blue light (monochromatic blue LED light, 450 nm emission peak).

2.6.4. Transformation of Arabidopsis thaliana using Agrobacterium tumefaciens

For transformation with *Agrobacterium tumefaciens* (strain GV3101), *Arabidopsis thaliana* seeds were sown on wet soil, vernalized in the dark at 4°C for 3 days and germinated at 22°C in long day conditions under cool white fluorescent lighting (see Section 2.6.3) in Sanyo Fitotron plant growth cabinets (Sanyo Gallenkamp PLC, UK).

Agrobacterium were transformed with prepared expression clones (see Section 2.2.5) using a freeze/thaw method. 250 µL competent *Agrobacterium* cells (stored at -80°C) were thawed on ice, 20 µL plasmid preparation (See Section 2.2.6) added, and cells very briefly and gently mixed. Cells were incubated on ice for 30 minutes, transferred to liquid nitrogen for 5 minutes, and then incubated at 37°C for 5 minutes. 1 mL LB media was added, tubes sealed well and incubated at room temperature for 2-4 hours with gentle mixing. Cells were collected by centrifugation at 3,000 rpm for 5 minutes, resuspended in 50 µL supernatant and transferred to two LB agar plates containing 150 µg/mL rifampicin (prepared in methanol, Melford Laboratories Ltd; cat# R0146) and 15 µL/mL. Gentamycin (prepared in dH_2O, Melford Laboratories Ltd., Sigma-Aldrich, cat# G1914), as well as the appropriate antibiotic for the expression clone. Cells were incubated at 28°C for 2 days and overnight cultures prepared in LB broth containing the appropriate antibiotics.

At the first sign of bolting, *Arabidopsis* plants were transformed with overnight cultures *Agrobacterium* using a simplified floral dip method as previously described (Narusaka et al., 2010). Transformations were performed late afternoon. For every three plants to transform, 2 mL overnight transformed *Agrobacterium* culture was centrifuged at 3,000 rpm for 5 minutes at room temperature and cells resuspended in 300 µL inoculation solution (5% (w/v) sucrose, 0.02% (v/v) Silwet L-77). Using a pipette, flower buds were washed 5-6 times with inoculation solution containing cells. Plants were placed back in growth cabinets under long-day conditions, shaded from light until the next morning. Protocol was repeat every 3-4 days to treat new emerging buds. Seed from transformed *Arabidopsis* plants were collected, surface sterilised using ethanol (see Section 2.6.2) and positive transformants selected by sowing seed on 0.5x MS agar plates containing the appropriate herbicide.

2.7. Live imaging of *Arabidopsis thaliana* seedlings

2.7.1. Luciferase and delayed fluorescence imaging

Luciferase imaging was performed on 6- or 12-day old individual or grouped *Arabidopsis* seedlings grown on agar plates and entrained as described in Section 2.6.3. The day before imaging, plants were sprayed with 3 mM D-luciferin (prepared in filter sterilized 0.01% Triton X-100). Delayed fluorescence imaging was performed on 12-day old *Arabidopsis* seedlings grown on agar plates in groups of 10-15 seedlings.

Imaging was completed under free-run conditions for 5 days under the indicated fluence rates using either a Photek HRPCS5 system under monochromatic blue LED light (peak emission at 470nm) at the indicated fluence rate, or an Andor iKon-M CCD camera under monochromatic blue LED light (peak emission at 450nm) or monochromatic red LED light (peak emission at 660 nm). The Andor iKon-M CCD camera was controlled using µManager (Edelstein et al., 2010) before data was processed using ImageJ (Schneider et al., 2012). For luciferase and delayed fluorescence imaging, patterns of bioluminescence were fitted to cosine waves using

Fourier Fast Transform Non-Linear Least Squares analysis (FFT-NLLS, Plautz et al., 1997) to estimate circadian period length. Prior to FFT-NLLS analysis, baselines of data were detrended (luciferase imaging and delayed fluorescence data) and normalised (delayed fluorescence data). RAE is a measure of rhythmic robustness, with a value of 0 indicating an exact fit to a cosine wave (Plautz et al., 1997). Detrending, normalisation and FFT-NLLS analysis of data were performed using the Biological Rhythms Analysis Software System version 3 (BRASS; available from http:// www.amillar.org; Millar et al., 2010).

2.7.2. Chlorophyll fluorescence imaging

Chlorophyll fluorescence parameters were analysed in free-run conditions using a Fluorimager imaging system with automated camera control and image processing scripts provided by the manufacturer (Technologica Ltd, Colchester, UK, http://www.technologica.co.uk) as described previously (Litthauer et al., 2015). Individually spaced *Arabidopsis* seedlings were entrained for 12 days in 12h:12h light:dark cycles on agar plates (see Section 2.6.3) before transfer to imaging chamber. After transfer, plants were illuminated with 20 $\mu mol.m^{-2}.s^{-1}$ blue light using blue LEDs and measuring pulses of 5713 $\mu mol.m^{-2}.s^{-1}$ blue light applied for 800 milliseconds once per hour. Chlorophyll fluorescence was imaged using a Dolphin camera (Allied Vision Technologies, UK, http://www.alliedvision.com) through a long pass filter to exclude the blue light from the LEDs. Chlorophyll fluorescence parameter $(F_m'-F')/F_m'$ (also known as ϕ_{PSII} or F_q'/F_m') was determined as previously described (Baker, 2008) and patterns of F_q'/F_m' were fitted to cosine waves using FFT-NLLS analysis (Plautz et al., 1997) to estimate circadian parameters. Baselines of data were detrended prior to FFT-NLLS analysis. Detrending and FFT-NLLS analysis of data were performed using the Biological Rhythms Analysis Software System version 3 (BRASS; available from http:// www.amillar.org; Millar et al., 2010).

2.7.3. Confocal laser scanning microscopy

6-7 day old or 12-14 day old live *Arabidopsis* seedlings were imaged on microscope slides using a Nikon A1si confocal microscope with a CFI 10x Plan Fluor objective with numerical aperture (NA) 0.3 as described previously (Exposito-Rodriguez et al., 2013). Images were acquired using one-way sequential line scans of two excitation lines. Laser power was at 405 nm between 15 and 33, and at 488 nm between 7 and 17. Emission was collected with one detector at 540/30 nm, with a photomultiplier tube gain of 90-180. No offset was used, and pinhole size was set at 1.2 times the Airy disk size of the used objective. Image acquisition for roGFP2 plants were as described for HyPer1 plants, but with additional use of a Nikon LWD condenser lens with NA 0.52 in combination with the CFI 10x Plan Fluor and CFI 4x Plan Apo objectives with NA 0.3 and 0.2 respectively. Images were processed using ImageJ.

2.7.4. Application of exogenous PAP to Arabidopsis thaliana seedlings

12-day old seedlings were prepared for luciferase imaging (see Section 2.7.1) and imaged for one day before 1 mM PAP (prepared in 0.01% Triton X-100) was applied to seedlings at Zeitgeber (ZT) 29. Luciferase imaging was performed under constant blue light and circadian analysis completed as described in Section 2.7.1.

Chapter 3

Chlorophyll *a* fluorescence imaging as a tool to monitor circadian rhythms

3.1. Introduction

Light energy absorbed by the chlorophylls associated with Photosystem II (PSII) can be harnessed to drive photochemistry (photochemical quenching), or can be lost as heat (nonphotochemical quenching) or irradiated at a longer wavelength as chlorophyll fluorescence (Butler, 1978). Measuring chlorophyll *a* fluorescence is a well-established and non-invasive method used to monitor the photochemical and nonphotochemical processes in plants and algae (Baker, 2008). Under non-photorespiratory conditions, the parameters derived from modulated chlorophyll fluorescence yields allow the analysis of photosynthetic performance in leaves *in vivo*. In particular, the chlorophyll fluorescence parameter F_q'/F_m' ($\Delta F/F_m'$; ϕ_{PSII}) provides an estimate of PSII operating efficiency, or the efficiency with which actinic light absorbed by PSII is used for the reduction of plastoquinone Q_A (Baker, 2008).

In the Crassulacean acid metabolism (CAM) plant *Kalanchoë daigremontiana* F_q'/F_m' oscillates with circadian rhythm in individual leaves under constant light conditions (Wyka et al., 2005). This chapter examines fluctuations in F_q'/F_m' as a possible measure of circadian rhythms in whole *Arabidopsis thaliana* seedlings. In addition, the role of phototropins in maintaining oscillations in PSII operating efficiency is examined.

3.2. Results

3.2.1. Changes in PSII operating efficiency cycle with circadian rhythm in Arabidopsis thaliana Col-0 under constant dim blue light

Luciferase imaging is a non-invasive technique used for monitoring the spatial and temporal expression of genes *in vivo* (Millar et al., 1992b). In *Arabidopsis*, fusion of the luciferase reporter gene to the promoter region of a clock-regulated gene of interest allows real-time analysis of circadian rhythms *in planta* (Millar et al., 1992a). For example, rhythms in expression of the morning-phased core clock gene *CCA1* can be monitored by imaging 6-day old Col-0 luciferase reporter line *CCA1::LUC2* seedlings (Jones et al., 2015) under 20 µmol.m^{-2}.s^{-1} constant blue light for ~5 days (Figure 3.1a and d). Plotting averages of time series data (waveforms) for 10 individually imaged seedlings, bioluminescence from *CCA1:LUC2* activity was shown to peak 2 hours after dawn (Figure 3.1a) as previously described (Jones et al., 2015). Circadian period length was estimated by fitting waveforms to cosine waves using Fast Fourier Transform Non-Linear Least Squares (FFT-NLLS; Plautz et al., 1997). For each individual seedling, drift in the baseline of time series data was detrended and detrended data subjected to FFT-NLLS analysis using the Biological Rhythms Analysis Software System version 3 (BRASS; Millar et al., 2010). Baseline detrending is achieved by fitting a regression line through the time series data and subtracting the regression line from the curve, followed by addition of the mean of the regression line to the new curve (Millar et al., 2010). The curve-fitting FFT-NLLS algorithm is used to determine the rhythmic strength of time series data and to assign period, amplitude and phase to these rhythms in an automated manner (Millar et al., 2010). Through non-linear least-squares minimization, FFT-NLLS analysis determines the best-fit parameter values (period, amplitude phase and constant offset) for all statistically significant rhythmic components identified in a time series within a 95% confidence limit.

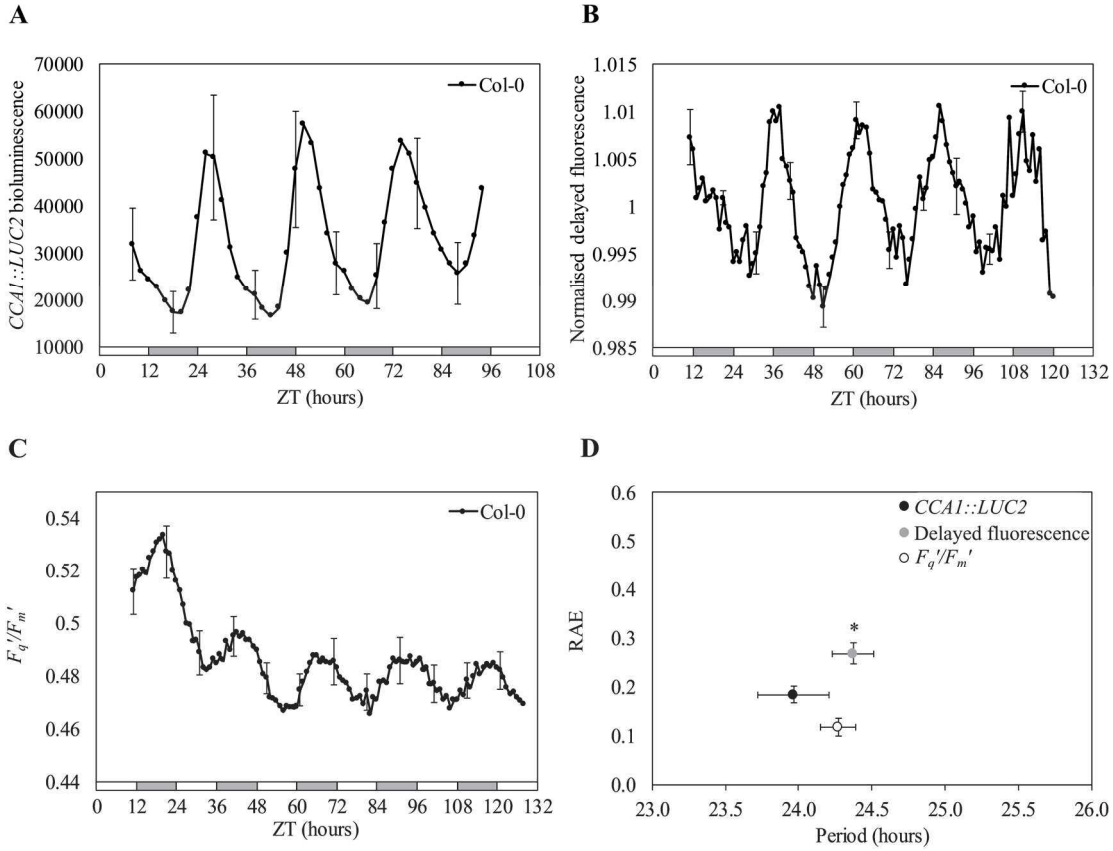

Figure 3.1 Monitoring circadian rhythms in whole *Arabidopsis thaliana* Col-0 seedlings through different live imaging techniques. **(A)** Waveforms of luciferase activity monitored in 6-day old Col-0 *CCA1::LUC2* seedlings in constant blue light. **(B)** Normalised and detrended delayed fluorescence waveforms in 12-day old Col-0 seedlings in constant blue light. **(C)** Waveforms of PSII operating efficiency (F_q'/F_m') oscillations monitored in 12-day old Col-0 seedlings under constant blue light. **(D)** Circadian period estimates of Col-0 seedlings plotted against Relative Amplitude Error (RAE) determined for luciferase imaging (*CCA1::LUC2*), delayed fluorescence or F_q'/F_m' rhythms. Seedlings were grown on 0.5x MS agar plates and entrained in 12h:12h light:dark cycles under 60 µmol.m^{-2}.s^{-1} white light for 6 days (luciferase imaging) or twelve days (delayed fluorescence and chlorophyll *a* fluorescence imaging) before imaging under 20 µmol.m^{-2}.s^{-1} constant blue light. White bars and grey bars indicate subjective day and subjective night, respectively. Period estimates and RAE were determined by fitting waveforms to cosine waves using Fourier Fast Transform Non-Linear Least Squares (FFT-NLLS; Plautz et al., 1997). RAE is a measure of rhythmic robustness, with a value of 0 indicating an exact fit to a cosine wave (Plautz et al., 1997). Data were detrended (luciferase and F_q'/F_m') or normalised and detrended (delayed fluorescence) prior to FFT-NLLS analysis (see Section 3.2.1). Error bars indicate standard error of the mean, with n=8-10. Waveforms are averages of time series data for seedlings used in analysis, with error bars shown every 10 hours for clarity. Data from one of three independent experiments are shown. Asterisk indicates statistically significant difference in RAE compared with luciferase imaging (p<0.01; Student's T-test).

Statistical significance is assessed by means of the Relative Amplitude Error (RAE), a ratio of the amplitude error to the most probable amplitude magnitude. RAE provides a measure of the robustness of the identified rhythms (how well time series data fit to a cosine function), and ranges from 0.0 to 1.0. A rhythmic component with RAE of 0.0 has infinite precision (perfect fit to a cosine wave), while RAE of 1.0 indicates that the error is equal to the most probable amplitude magnitude and that the rhythmic component is therefore not significant (Millar et al., 2010). Data for individual waveforms with RAE>0.6 were discarded and RAE-weighted means of period length and standard error were calculated and presented for each experiment. Bioluminescence from *CCA1:LUC2* activity was shown to cycle with ~24 hour period (23.97 ± 0.24 h; Figure 3.1d), as previously reported (Jones et al., 2015).

Delayed fluorescence imaging is another established technique used to monitor circadian rhythms in *Arabidopsis* (Gould et al., 2009). Delayed fluorescence, which is caused as a result of charge recombination in PSII post-illumination and is under control of the nuclear clock, was monitored in 12-day old Col-0 seedlings (clustered into groups of 10-15 seedlings) under 20 $\mu mol.m^{-2}.s^{-1}$ constant blue light for ~5 days. Using BRASS, time series data were normalised and baseline detrended before FFT-NLLS analysis was performed (Millar et al., 2010). Time series data for each individual cluster was normalised by calculating the average value for all points in the time series and dividing the value at each point by the average value for the series. Average of the normalised and detrended waveforms plotted peaked 2 hours after dusk (Figure 3.1b), with a RAE-weighted mean period of ~24 hours (24.37 ± 0.14 h) under constant blue light (Figure 3.1d)

Since the operating efficiency of PSII (F_q'/F_m') has been shown to cycle with circadian rhythm in detached *Kalanchoë daigrmontiana* leaves under constant light (Wyka et al., 2005), chlorophyll *a* fluorescence imaging was examined as an alternative method to measure circadian rhythms in whole *Arabidopsis* seedlings. Col-0 seedlings were grown on 0.5x MS agar plates for 12 days in 12h:12h light:dark cycles under 60 $\mu mol.m^{-2}.s^{-1}$ white light. Following entrainment, individual seedlings were imaged under 20 $\mu mol.m^{-2}.s^{-1}$ constant blue

light for ~5 days. Average F_q'/F_m' oscillated with circadian rhythm, with peak PSII operating efficiency reached approximately 4 hours before dawn (Figure 3.1c). FFT-NLLS analyses on baseline-detrended time series data revealed a RAE-weighted mean period of 24.27 ± 0.12 h (Figure 3.1d). Furthermore, rhythms in F_q'/F_m' were robust (RAE 0.12 ± 0.02) for the entire free-run period, with RAE significantly lower than for delayed fluorescence rhythms (RAE 0.27 ± 0.02; $p<0.01$, Student's T-test).

3.2.2. F_q'/F_m' rhythms are influenced by nuclear rhythms in a short-period circadian mutant

Since delayed fluorescence is under control of the nuclear circadian oscillator, DF provides a simple, high throughput assay that can characterise novel *Arabidopsis* circadian clock mutants (Gould et al., 2009). In order to determine if rhythms in F_q'/F_m' were under control of the nuclear circadian clock, and whether chlorophyll *a* fluorescence can therefore be used to identify *Arabidopsis* clock mutants, F_q'/F_m' rhythms in the circadian mutant *toc1-4* (Hazen et al., 2005a; Jones and Harmer, 2011) were analysed. TIMING OF CAB EXPRESSION 1 (TOC1) is a DNA-binding transcription factor and evening-phased core nuclear clock component (Alabadí et al., 2001; Gendron et al., 2012), and loss-of-function *toc1* mutants have been shown to exhibit short period in delayed fluorescence and nuclear clock rhythms (Somers et al., 1998; Gould et al., 2009). Seedlings were grown on 0.5x MS agar plates and entrained for 12 days in 12h:12h light:dark cycles under 60 $\mu mol.m^{-2}.s^{-1}$ white light. Individual entrained seedlings were imaged under 20 $\mu mol.m^{-2}.s^{-1}$ constant blue light for ~5 days. F_q'/F_m' oscillated in *toc1-4* mutants with robust circadian rhythm (RAE 0.24 ± 0.01) comparable to Col-0 (Figure 3.2a and b), while period length was significantly shorter in *toc1-4* (20.64 ± 0.08 h) compared to Col-0 ($p<0.001$, Student's T-test).

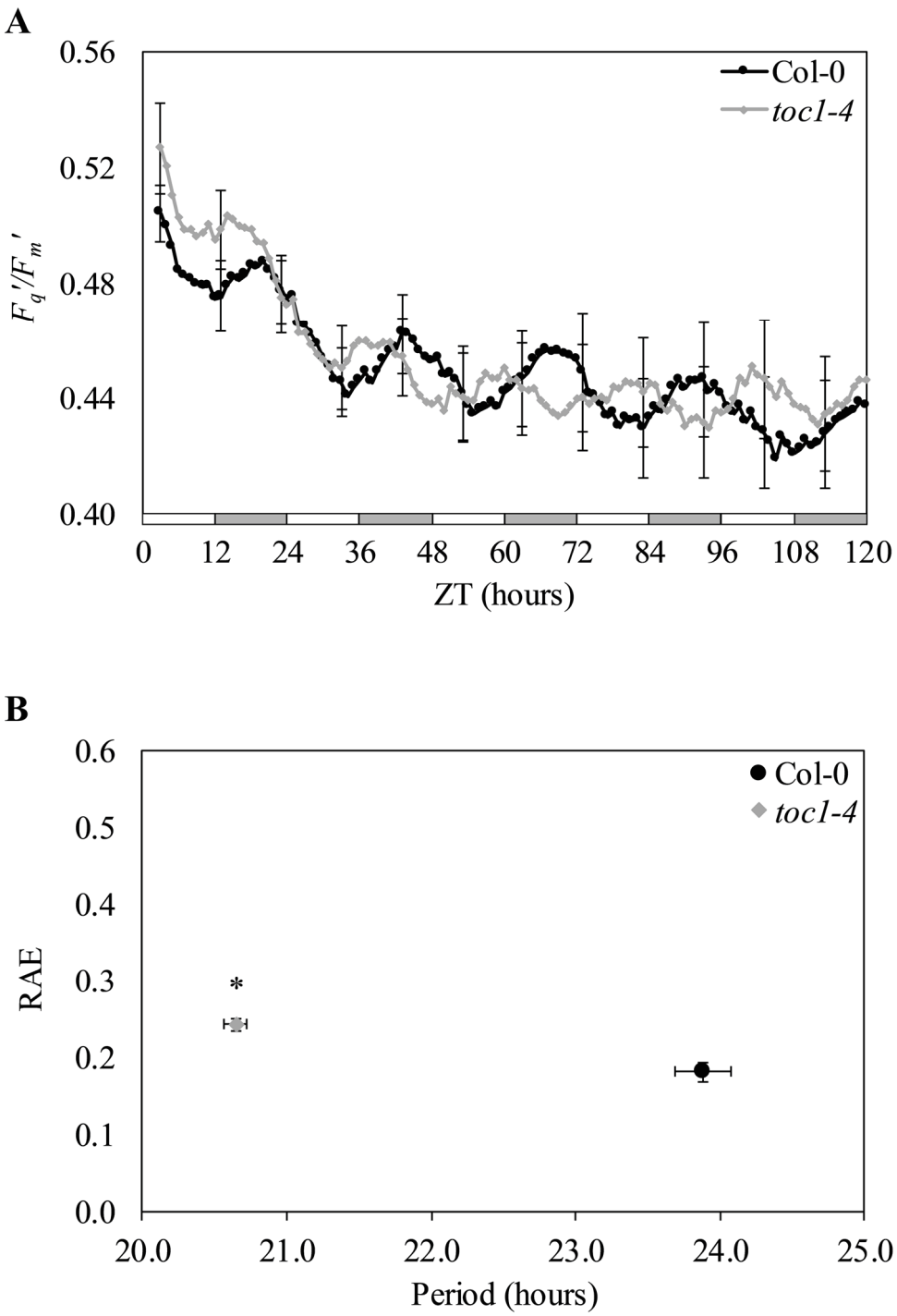

Figure 3.2 F_q'/F_m' rhythms in the short-period circadian mutant *toc1-4* under constant blue light. **(A)** Waveforms of F_q'/F_m' oscillations in Col-0 and *toc1*-4 seedlings. **(B)** Circadian period estimates of Col-0 and *toc1-4* seedlings plotted against Relative Amplitude Error (RAE) for F_q'/F_m' rhythms. Seedlings were grown on 0.5x MS agar plates and entrained in 12h:12h light:dark cycles under 60 µmol.m^{-2}.s^{-1} white light for 12 days before imaging under 20 µmol.m^{-2}.s^{-1} constant blue light. White bars and grey bars indicate subjective day and subjective night, respectively. Error bars indicate standard error of the mean, with n=8. For waveforms, error bars are shown every 10 hours for clarity. Data from one of two independent experiments are shown. Asterisk indicates statistically significant difference in period compared to Col-0 control (p<0.001; Student's T-test).

3.2.3. Loss of phototropin function affects amplitude, but not period, of F_q'/F_m' rhythms under constant blue light

Circadian clocks are entrained by environmental signals such as light and temperature, and numerous input pathways relay these signals to the central oscillator to keep the plant's endogenous rhythms synchronised with the exogenous rhythms of the environment (Hsu and Harmer, 2014). While phytochromes, cryptochromes and the ZEITLUPE family of proteins serve to input light signals to the circadian system, a role for phototropins has not yet been determined (Fankhauser and Staiger, 2002; Hsu and Harmer, 2014; Christie et al., 2015). Phototropins localise on the outer chloroplast membrane under blue light, and loss of phototropin function has been shown to affect hypocotyl phototropism (Liscum and Briggs, 1995; Sakai et al., 2001), leaf movement (Inoue et al., 2008), stomatal opening (Kinoshita et al., 2001; Doi et al., 2004) and chloroplast movement (Kagawa et al., 2001; Sakai et al., 2001). To determine whether phototropin activity affects the circadian oscillations of PSII operating efficiency, rhythms in F_q'/F_m' were analysed in phototropin mutants under constant blue light (Figure 3.3). Seedlings of Col-0, the phototropin single mutants *phot1-5* (Huala et al., 1997) and *phot2-1* (Sakai et al., 2001), and the phototropin double mutant *phot1-5 phot2-1* (*p1p2;* Sakai et al., 2001) were grown on 0.5x MS agar plates and entrained for 12 days in 12h:12h light:dark cycles under 60 $\mu mol.m^{-2}.s^{-1}$ white light. Individual seedlings were imaged under 20 $\mu mol.m^{-2}.s^{-1}$ constant blue light for ~5 days. No effect on period was observed in phototropin (phot) mutants, with F_q'/F_m' rhythms cycling with circadian period in Col-0 (23.30 ± 0.39 h), *phot1-5* (24.21 ± 0.29 h), *phot2-1* (23.74 ± 0.13 h) or *p1p2* (24.10 ± 0.38 h) seedlings (Figure 3.3a). Robust rhythms were maintained in Col-0 and in both *phot1-5* and *phot2-1* (Figure 3.3b). In comparison, F_q'/F_m' oscillations in *p1p2* dampened after 3 days of free-run, with reduced amplitude and significantly higher RAE compared to Col-0 ($p<0.01$, Student's T-test).

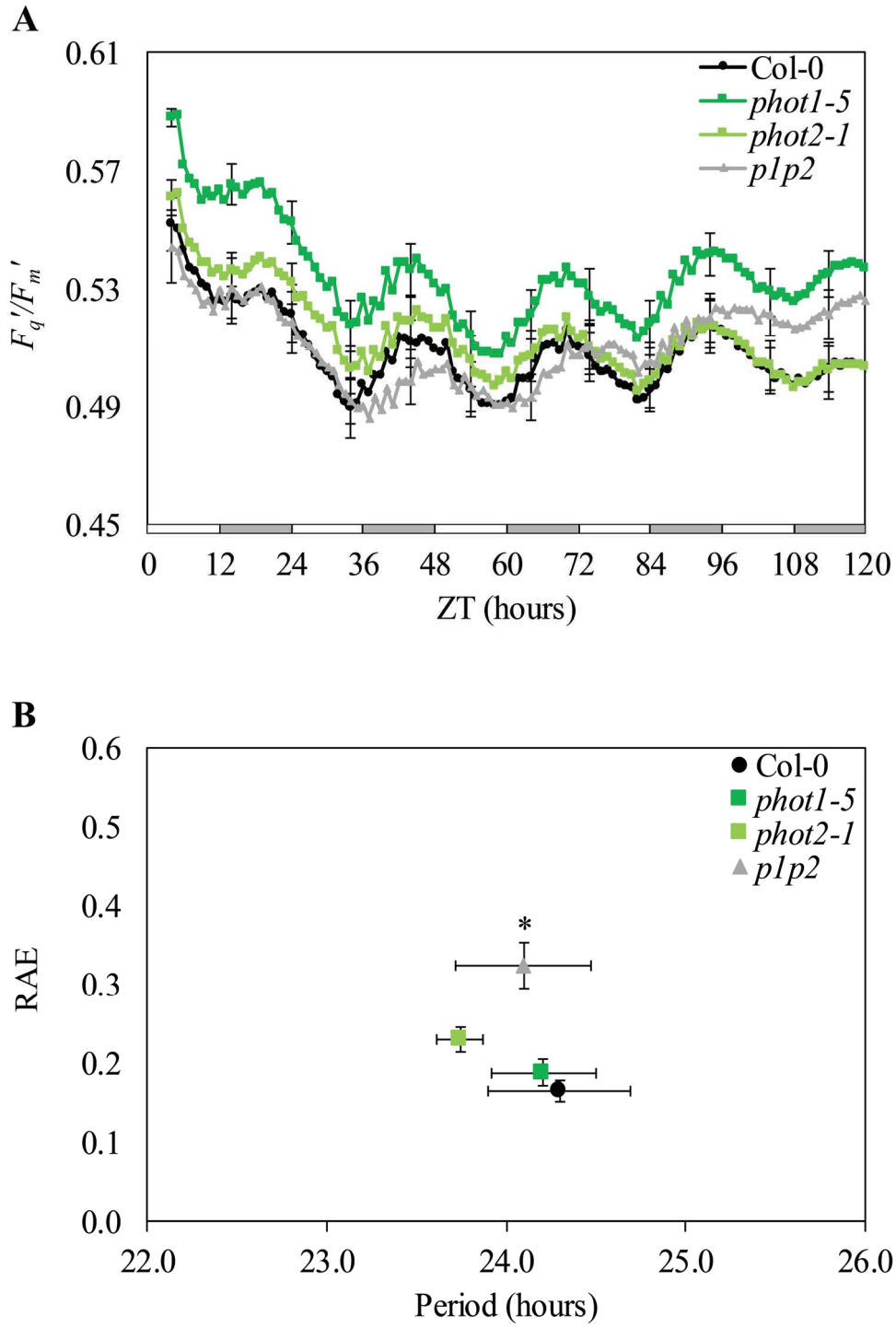

Figure 3.3 F_q'/F_m' rhythms in phototropin mutants under constant blue light. **(A)** Waveforms and **(B)** circadian period estimates and Relative Amplitude Error (RAE) of F_q'/F_m' rhythms Col-0 and *phot1-5*, *phot2-1* and *p1p1* phototropin mutant seedlings. Seedlings were grown on 0.5x MS agar plates and entrained in 12h:12h light:dark cycles under 60 µmol.m^{-2}.s^{-1} white light for 12 days before imaging under 20 µmol.m^{-2}.s^{-1} constant blue light. White bars and grey bars indicate subjective day and subjective night, respectively. Error bars indicate standard error of the mean, with n=10. For waveforms, error bars are shown every 10 hours for clarity. Data from one of two independent experiments are shown. Asterisk indicates statistically significant difference in RAE compared to Col-0 control (p<0.01; Student's T-test).

3.2.4. Delayed fluorescence rhythms remain intact in phot mutants under constant blue light

Since loss of phototropin function affected the robustness of F_q'/F_m' circadian oscillations, the effect of phototropins on delayed fluorescence rhythms was examined. Seedlings were grown on 0.5x MS agar plates in clusters of 10-15 and entrained for 12 days in 12h:12h light:dark cycles under 60 µmol.m^{-2}.s^{-1} white light before imaging under 20 µmol.m^{-2}.s^{-1} constant blue light (Figure 3.4). To determine whether loss of phototropin function affected amplitude of delayed fluorescence rhythms, baseline detrended time series data were analysed at first without normalisation to prevent possible masking of any loss in amplitude (Figure 3.4a and b). As observed for F_q'/F_m' oscillations, rhythms in delayed fluorescence cycled with an ~24 h period in Col-0 and *phot* mutants (Figure 3.4a and b). However, while a trend for higher RAE was observed in the *p1p2* mutant, no significant difference in RAE between Col-0 and *p1p2* was observed (Figure 3.4b). Since normalisation of delayed fluorescence data is recommended for greater accuracy in circadian parameter estimates (Gould et al., 2009; Millar et al., 2010), FFT-NLLS analysis was performed on normalised baseline detrended time series data as well (Figure 3.4c and d). Analysis of normalised data confirmed the ~24 h period of delayed fluorescence rhythms in *phot* mutants, and confirmed that these rhythms were maintained in *p1p2* across 5 days of free-run.

3.2.5. Core clock transcript accumulation is unaltered in phot mutants under constant blue light

As rhythms in F_q'/F_m' and DF are maintained by the nuclear circadian oscillator, qRT-PCR analysis of core clock transcripts was done to determine if nuclear rhythms are affected in *phot* mutants. Seedlings were grown on 0.5x MS agar plates and entrained for 10 days in 12h:12h light:dark cycles under 60 µmol.m^{-2}.s^{-1} white light before being transferred to 20 µmol.m^{-2}.s^{-1} constant blue light at subjective dawn (ZT0).

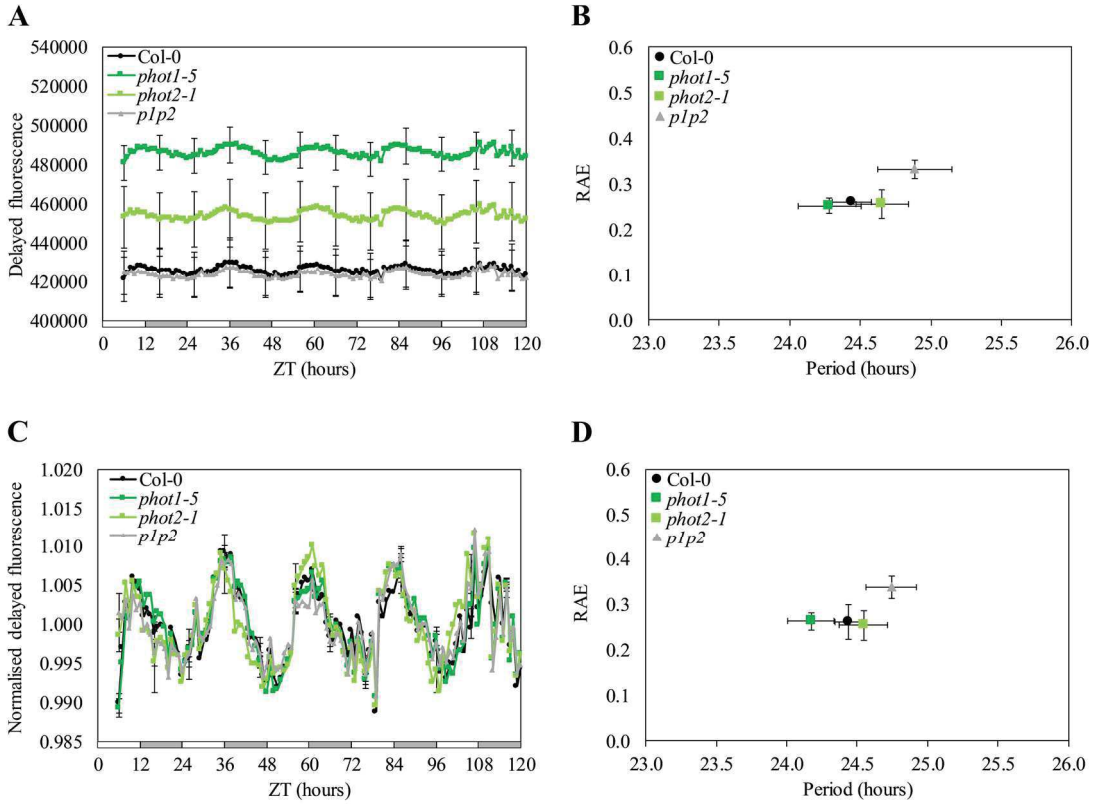

Figure 3.4 Delayed fluorescence rhythms in phototropin mutants under constant blue light. **(A,C)** Waveforms and **(C,D)** circadian period estimates plotted against Relative Amplitude Error (RAE) for **(A-B)** delayed fluorescence and **(C-D)** normalised delayed fluorescence in Col-0, *phot1-5*, *phot2-1* and *p1p2* under constant blue light. Seedlings were grown on 0.5x MS agar plates and entrained in 12h:12h light:dark cycles under 60 µmol.m^{-2}.s^{-1} white light for 12 days before imaging under 20 µmol.m^{-2}.s^{-1} constant blue light. White bars and grey bars indicate subjective day and subjective night, respectively. Error bars indicate standard error of the mean, with n=10. For waveforms, error bars are shown every 10 hours for clarity. Data from one of two independent experiments are shown.

After 48 hours in free-run conditions, 10-12 seedlings per genotype were harvested every three hours from subjective dawn (ZT48). cDNA was synthesised from extracted total mRNA and levels of transcripts for clock-controlled components analysed using qRT-PCR.

Accumulation of transcripts for morning-phased components remained unchanged in phot mutants (Figure 3.5). *CIRCADIAN CLOCK ASSOCIATED 1* (*CCA1*) and *LATE LONGATED HYPOCOTYL* (*LHY*) are two MYB-like transcription factors that from part of the core nuclear circadian oscillator, with transcript and protein levels highest in the morning (Alabadí et al., 2001; Harmer, 2009). In Col-0, *phot1-5*, *phot2-1* and *p1p2* transcripts of *CCA1* and *LHY* were phased to the morning, peaking at ZT51 (Figure 3.5a and b). Similarly, no phase shift was observed in *phot1*-5, *phot2-1* or *p1p2* for peak transcript levels of the transcription factor *PSEUDO-RESPONSE REGULATOR* (*PRR9*), a morning-phased core clock gene peaking shortly after dawn (ZT54; Figure 3.5c). Amplitude of *CCA1*, *LHY* and *PRR9* transcript levels remained unchanged in *phot1-5*, *phot2-1* and *p1p2.*

Similarly, no difference in phase or amplitude was observed for evening-phased clock transcripts in *phot1-5*, *phot2-1* or *p1p2* (Figure 3.6). *GIGANTEA* (*GI*), a clock component involved in post-transcriptional regulation within the circadian system (Kim et al., 2013), has transcripts phased to the evening (peaking at ZT60; Figure 3.6a). Transcripts for *COLD-CIRCADIAN RHYTHM- RNA BINDING 2* (*CCR2*), a glycine-rich RNA-binding protein often used for monitoring circadian rhythms through luciferase imaging (Kreps and Simon, 1997; Martin-Tryon et al., 2006), peak during the evening (ZT63; Figure 3.6b). Similarly, the transcription factor *TIMING OF CAB1 EXPRESSION* (*TOC1*) and the MYB-like transcription factor *LUX* which form part of the central oscillator (Helfer et al., 2011; Gendron et al., 2012), have transcripts peaking in the evening (ZT63; Figure 3.6c and d).

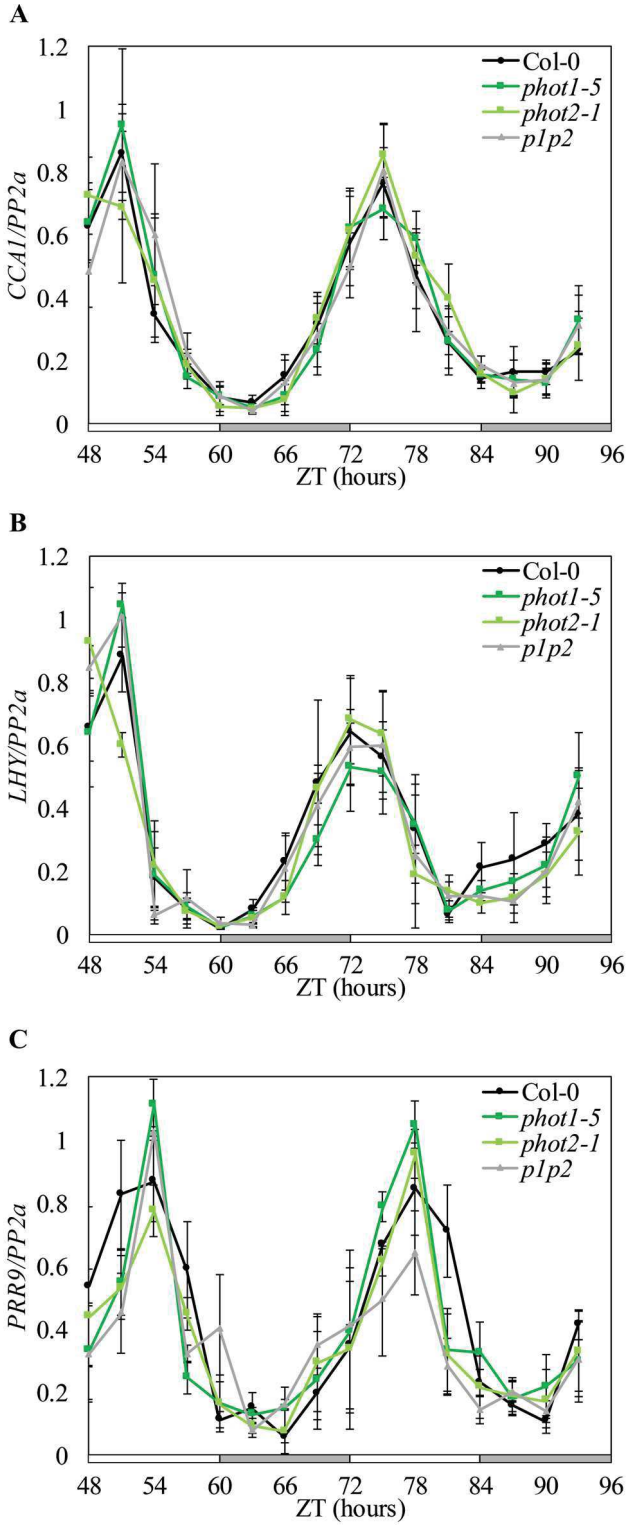

Figure 3.5 Expression of morning-phased circadian clock genes in phototropin mutants under constant blue light. qRT-PCR analysis of transcript accumulation for morning-phased core clock genes **(A)** *CCA1* **(B)** *LHY* and **(C)** *PRR9* in Col-0 and phototropin mutants *phot1-5*, *phot2-1* and *p1p2* under constant blue light. Seedlings were grown on 0.5x MS agar plates and entrained in 12h:12h light:dark cycles under 60 $\mu mol.m^{-2}.s^{-1}$ white light for 10 days before being transferred to 20 $\mu mol.m^{-2}.s^{-1}$ constant blue light at subjective dawn. After 48 hours in free-run, 10-12 seedlings were sampled and pooled, with sampling repeated every three hours for two days. Data for each gene were normalised to an internal control (*PP2a*) before being normalised to the peak of wild type expression. White bars and grey bars indicate subjective day and subjective night, respectively. Data are the average of three biological replicates. Error bars indicate standard error of the mean.

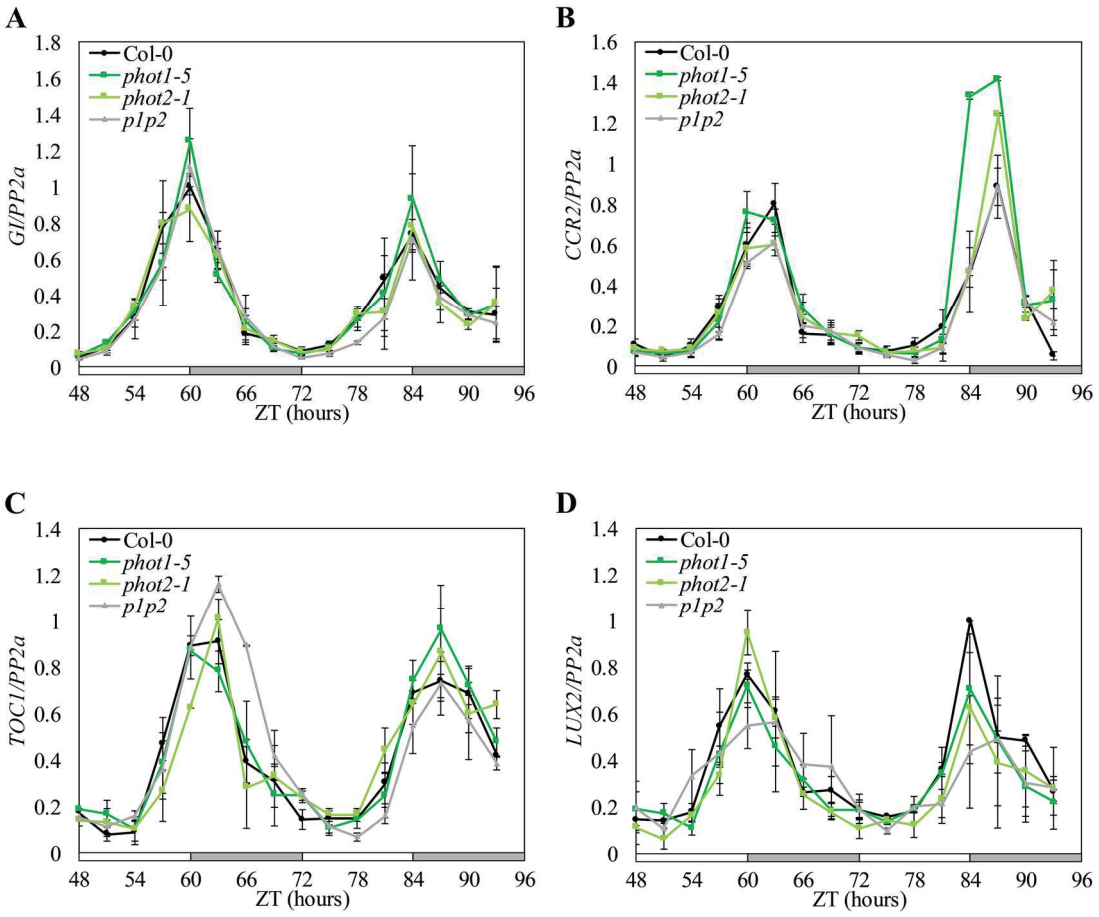

Figure 3.6 Expression of evening-phased circadian clock-regulated genes in phototropin mutants under constant blue light. qRT-PCR analysis of transcript accumulation for evening-phased clock-regulated genes **(A)** *GI* **(B)** *CCR2* **(C)** *TOC1* and **(D)** *LUX2* in Col-0 and phototropin mutants *phot1-5*, *phot2-1* and *p1p2* under constant blue light. Seedlings were grown on 0.5x MS agar plates and entrained in 12h:12h light:dark cycles under 60 $\mu mol.m^{-2}.s^{-1}$ white light for 10 days before being transferred to 20 $\mu mol.m^{-2}.s^{-1}$ constant blue light at subjective dawn. After 48 hours in free-run, 10-12 seedlings were sampled and pooled, with sampling repeated every three hours for two days. Data for each gene were normalised to an internal control (*PP2a*) before being normalised to the peak of wild type expression. White bars and grey bars indicate subjective day and subjective night, respectively. Data are the average of three biological replicates. Error bars indicate standard error of the mean.

3.2.6. NPH3 activity is not required to maintain chlorophyll a fluorescence rhythms under constant blue light

Phototropic growth responses mediated by phototropin signalling cascades are dependent on the activity of NONPHOTOTROPIC HYPOCOTYL 3 (NPH3), a plasma membrane-localised protein that functions as part of a Cullin 3-based E3 ubiquitin ligase complex and targets phot1 for ubiquitination following illumination with blue light (Folta and Spalding, 2001; Liscum et al., 2014). To determine whether NPH3 activity is involved in maintaining rhythms in chlorophyll fluorescence, F_q'/F_m' rhythms in *p1p2* and in the *nph3-1* (Liscum and Briggs, 1995) and *nph3-102* (Tsuchida-Mayama et al., 2008) mutant alleles were compared under constant blue light. Seedlings were entrained in 12h:12h light:dark cycles under 60 $\mu mol.m^{-2}.s^{-1}$ white light for 12 days before imaging under 20 $\mu mol.m^{-2}.s^{-1}$ constant blue light, as described previously. While F_q'/F_m' oscillations dampened in *p1p2* after 3 days of free-run, these rhythms were maintained in Col-0, and in both *nph3-1* and *nph3-102* (Figure 3.7a) Period lengths were also indistinguishable between Col-0 (24.17 ± 0.08 h), *nph3-1* (24.53 ± 0.23 h), *nph3-102* (24.13 ± 0.05 h) and *p1p2* (24.27 ± 0.11 h) (Figure 3.7b). Furthermore, oscillations in PSII efficiency factor (F_q'/F_v') in the *p1p2* mutant showed a similar loss in amplitude by day 4 of free-run, while these rhythms in *nph3-1* and *nph3-102* were indistinguishable from rhythms in Col-0, both with respect to period length and robustness (Figures 3.7c and d).

3.2.7. F_q'/F_m' rhythms in plants entrained under long or short photoperiods

In addition to synchronising metabolic and physiological responses to the daily rhythms of the environment, circadian rhythms also control longer-term, seasonal processes (Harmer, 2009; Hsu and Harmer, 2014; Flis et al., 2016). Interactions between circadian regulated components and light signalling pathways serve to sense day length (photoperiod) and regulate day length-specific responses, such as accelerated hypocotyl elongation under short-day conditions or induction of flowering under long-day conditions (Niwa et al., 2009; Song et al., 2015).

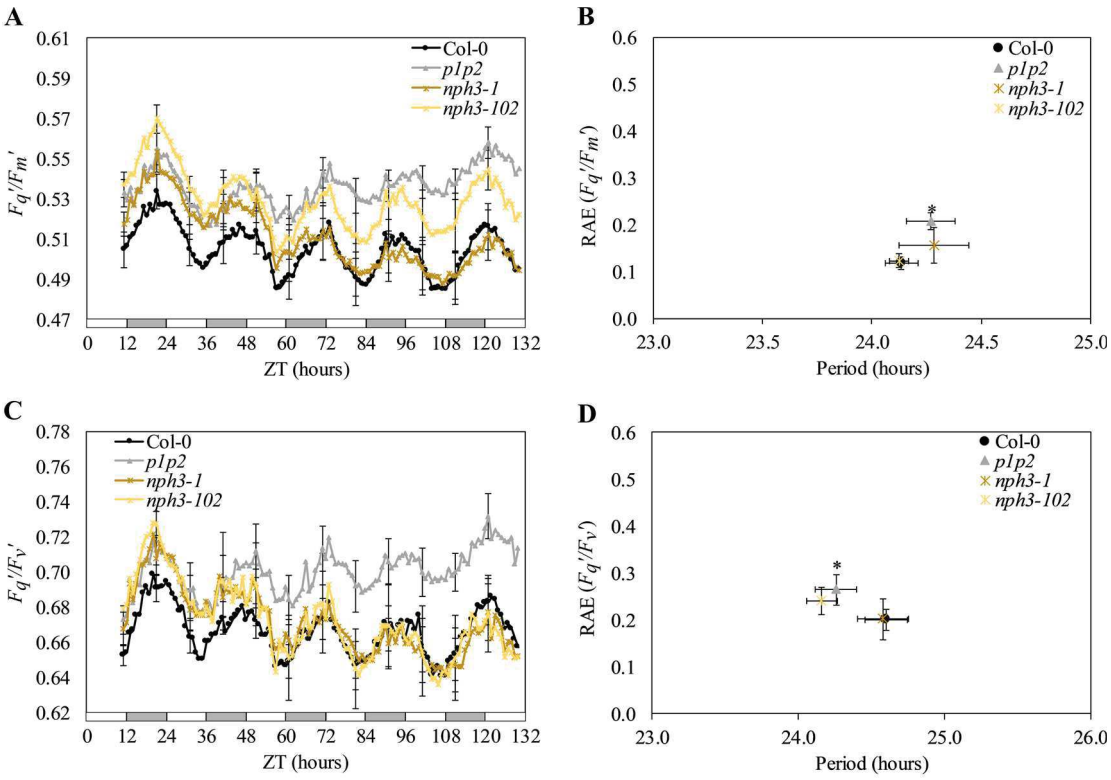

Figure 3.7 Rhythms in photosynthetic operating parameters in *nph3* mutants under constant blue light. (A,C) Waveforms and **(B,D)** circadian period estimates plotted against Relative Amplitude Error (RAE) of **(A-B)** $F_q'/F_m'$and **(C-D)** F_q'/F_v' rhythms in Col-0, phototropin mutant *p1p2* and *nph3* mutants *nph3-1* and *nph3-102*. Seedlings were grown on 0.5x MS agar plates and entrained in 12h:12h light:dark cycles under 60 µmol.m^{-2}.s^{-1} white light for 12 days before imaging under 20 µmol.m^{-2}.s^{-1} constant blue light. White bars and grey bars indicate subjective day and subjective night, respectively. Error bars indicate standard error of the mean, with n=10. For waveforms, error bars are shown every 10 hours for clarity. Data from one of two independent experiments are shown. Asterisks indicates statistically significant difference in RAE compared to Col-0 control (p<0.01; Student's T-test).

Since phototropins maintain amplitude of F_q'/F_m' rhythms under free-run in plants entrained under 12h:12h light:dark cycles (Figure 3.3), the effect of entrainment to different photoperiods was examined in Col-0, *p1p2* and *nph3-1*. Seedlings were entrained in either 8h:16h light:dark cycles (short days) or 16h:8h light:dark cycles (long days) under 60 $\mu mol.m^{-2}.s^{-1}$ white light for 12 days before imaging under 60 $\mu mol.m^{-2}.s^{-1}$ constant blue light. In Col-0, rhythms in F_q'/F_m' remained robust and continued to peak approximately two hours before subjective dawn, whether plants were entrained to short days (Figure 3.8a and b) or long days (Figure 3.8c and d). A phase shift in F_q'/F_m' rhythms was observed in *p1p2* after ~2 days of free run (Figure 3.8a and c), implying a longer period in these rhythms compared to Col-0. FFT-NLLS analysis was therefore performed to provide an indication of period length, even though plants were not entrained to symmetrical (12h:12h) light:dark cycles. Circadian period estimates for seedlings entrained under short days (Figure 3.8b) revealed a statistically significant longer period in *p1p2* mutants (24.53 ± 0.24 h) compared to Col-0 (23.10 ± 0.15 h; $p<0.01$, Student's T-test). Similarly, *p1p2* seedlings entrained under long days (Figure 3.8d) exhibited a statistically significant long period (25.29 ±0.19 h) compared to Col-0 (24.58 ± 0.23 h; $p<0.01$, Student's T-test). The loss of amplitude in F_q'/F_m' rhythms observed in *p1p2* mutants entrained under 12h:12h light:dark cycles (Figure 3.3) appeared absent in *p1p2* seedlings entrained under either short days (Figure 3.8a) or long days (Figure 3.8c). Even so, a significantly higher RAE was observed in *p1p2* compared to Col-0 in plants entrained under long days (Figure 3.3d; $p<0.001$, Student's T-test). However, no significant difference in RAE was observed for *p1p2* seedlings entrained under short days compared to Col--0 (Figure 3.8b). As was observed in plants entrained under 12h:12h light:dark cycles (Figure 3.7a and b), no significant difference in period length or RAE was observed in *nph3-1* mutants compared to Col-0 in seedlings entrained under either photoperiod (Figure 3.8b and d).

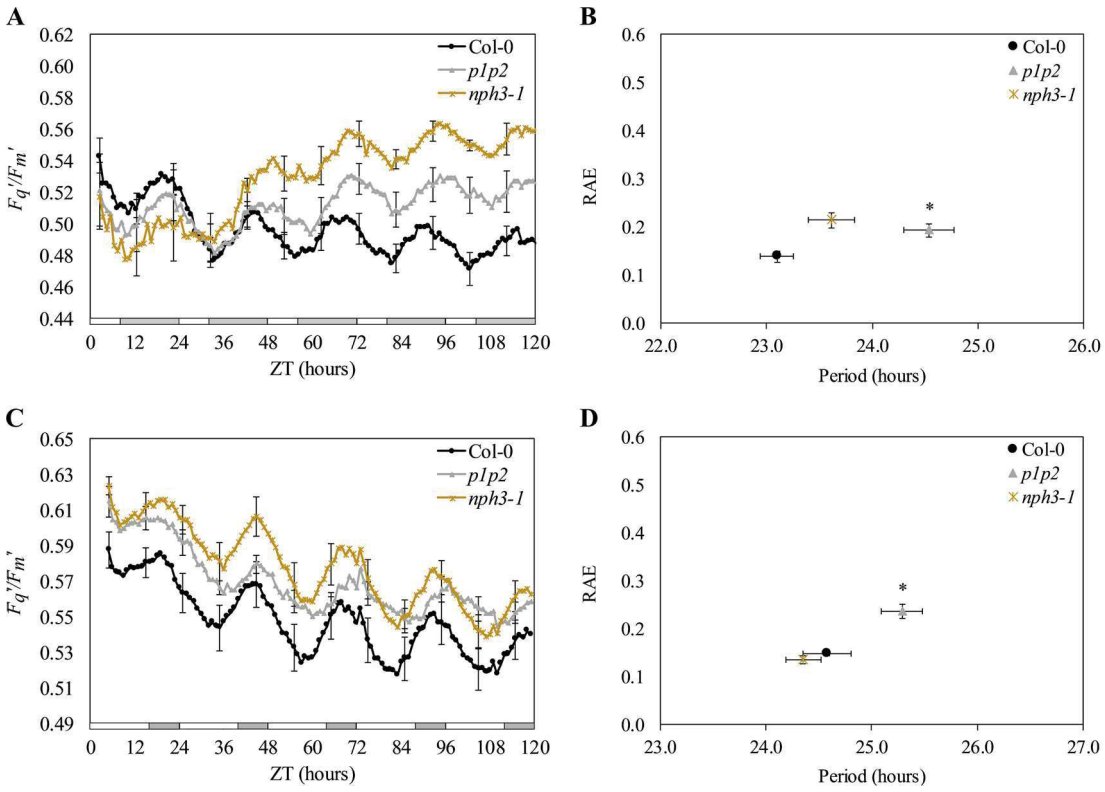

Figure 3.8 F_q'/F_m' rhythms in phototropin and *nph3* mutants entrained in long and short days. (A,C) Waveforms and **(B,D)** circadian period estimates plotted against Relative Amplitude Error (RAE) of F_q'/F_m' in Col-0, phototropin mutant *p1p2* and *nph3* mutant *nph3-1* seedlings entrained under **(A-B)** 8h:16h light:dark cycles or **(C-D)** 16h:8h light:dark cycles. Seedlings were grown on 0.5x MS agar plates and entrained in short or long photoperiods under 60 µmol.m^{-2}.s^{-1} white light for 12 days before imaging under 20 µmol.m^{-2}.s^{-1} constant blue light. White bars and grey bars indicate subjective day and subjective night, respectively. Error bars indicate standard error of the mean, with n=10. For waveforms, error bars are shown every 10 hours for clarity. Data from one of two independent experiments are shown. Asterisks indicates statistically significant difference in period compared to Col-0 control (p<0.01; Student's T-test).

3.3. Discussion

3.3.1. Fluctuations in PSII operating efficiency provides a measure of circadian rhythms in Arabidopsis

In *Arabidopsis*, the clock has been shown to regulate between 30% and 40% of genes expressed in seedlings, which include genes involved in photosynthesis (Covington et al., 2008). Furthermore, the transcription of numerous chloroplast genes is under control of the nuclear oscillator through the nuclear-encoded (and circadian regulated) sigma factors (Noordally et al., 2013). Circadian regulation of PSII repair has also been suggested, particularly with respect to the transcription of the D2 protein (regulated by SIG5) and phosphorylation of the D1 protein by STN7 (Noordally et al., 2013; Bonardi et al., 2005). The circadian system has also been shown to regulate CO_2 assimilation (Dodd et al., 2004) and starch degradation during the night (Graf et al., 2010). It is therefore not surprising that circadian regulation improves plant productivity, survival and even seed viability (Green et al., 2002; Dodd et al., 2005).

Delayed fluorescence and chlorophyll *a* fluorescence are two well-established techniques that can be used to analyse light emitted from PSII *in vivo* (Gould et al., 2009; Dodd et al., 2014; Baker, 2008). Although both delayed fluorescence and chlorophyll *a* fluorescence involve light emitted from PSII apparatus following illumination, the processes underlying these two phenomena are not the same. Following illumination, charge recombination between excited plastoquinone (Q_A) and P680 leads to the emission of a photon from the chlorophyll *a* associated with PSII (Gould et al., 2009). The resulting delayed fluorescence provides a high-throughput method to measure circadian rhythms in numerous higher plants, including *Arabidopsis*, barley, lettuce, maize and *Kalanchoë*, without the need for transgenics (Gould et al., 2009; Dodd et al., 2014). This chapter investigated whether the chlorophyll *a* fluorescence parameter F_q'/F_m' can be used as an alternative measure to monitor circadian rhythms in plants under constant light conditions. In addition to providing an additional non-invasive circadian assay, the chemistry underlying chlorophyll *a* fluorescence is much better understood than for delayed fluorescence (Baker, 2008; Gould et al., 2009) and might provide further insight into

the regulation of photosynthesis by the circadian clock. When plants are grown in constant light conditions, the difference between the fluorescence emission (F') and the maximal fluorescence (F_m'; the level of fluorescence when Q_A is maximally reduced) provides a measure for the photochemical quenching of fluorescence by PSII (F_q') (Baker, 2008). The ratiometric parameter F_q'/F_m' provides an estimate of the efficiency at which light absorbed by PSII is used for Q_A reduction (Baker, 2008). In this chapter, F_q'/F_m' was shown to cycle with circadian rhythm in whole *Arabidopsis* seedlings under constant dim blue light (Figure 3.1c and d). These rhythms in F_q'/F_m' can be more robust than DF rhythms (Figure 3.1d), and peak shortly before subjective dawn (Figure 3.1c). The phase of F_q'/F_m' rhythms in *Arabidopsis* occurs before stomatal opening, with stomatal opening peaking during the subjective morning (Litthauer et al., 2015). This suggests that F_q'/F_m' rhythms are not a direct consequence of stomatal opening. This is in contrast to F_q'/F_m' rhythms in detached *Kalanchoë daigremontiana* leaves, where circadian rhythms in F_q'/F_m' peak at subjective dusk and correlate with inverse rhythms in gas exchange (Wyka et al., 2005). The difference in phase could be due to the fact that *Kalanchoë daigremontiana* undergoes crassulacean acid metabolism (CAM), separating CO_2 absorption from incorporation in the Calvin cycle. Rhythms in F_q'/F_m' in *Arabidopsis* are also not due to leaf movement or shading artefacts. Firstly, the ratiometric nature of the F_q'/F_m' parameter should compensate for leaf and chloroplast movement (Brugnoli and Björkman, 1992). Secondly, rhythms in F_q'/F_m' continue in seedlings where leaf movement is restrained with wire mesh (Litthauer et al., 2015).

As has been reported for delayed fluorescence (Gould et al., 2009), rhythms in F_q'/F_m' are coupled to transcriptional rhythms in the nuclear oscillator, with intact nuclear rhythms necessary for circadian oscillations in F_q'/F_m'. In the short period mutant *toc1-4*, rhythms in F_q'/F_m' are robust, but with significantly shorter period than in Col-0 (Figure 3.2a and b). Similarly, long period rhythms in F_q'/F_m' have been reported in the long-period mutant *prr7-3*, while no F_q'/F_m' rhythms are observed in the arrhythmic mutant *lux-2* (Litthauer et al., 2015).

3.3.2. Phototropins maintain circadian oscillations in PSII operating efficiency under constant blue light

Since phototropins are known to localise on the outer membrane of chloroplasts upon illumination and play a role in actin-based chloroplast photorelocation (Kong et al., 2013), the effect of phototropin activity on F_q'/F_m' rhythms in 20 µmol.m^{-2}.s^{-1} constant blue light was examined. Loss of phototropin function had no effect on the period of F_q'/F_m' rhythms (Figure 3.3) or on the phase of transcript accumulation for morning- or evening-phased circadian genes (Figure 3.4 and Figure 3.5). These data confirmed previous reports that phototropins do not affect the nuclear circadian clock (Devlin and Kay, 2001; Kong et al., 2013). However, a loss of amplitude in F_q'/F_m' rhythms was observed in the *p1p2* mutant under after ~3 days of free-run under 20 µmol.m^{-2}.s^{-1}, with rhythms dampening to near arrhythmia towards the end of the 5-day free-run period (Figure 3.3). Interestingly, F_q'/F_m' rhythms are maintained in *p1p2* mutants imaged under 50 µmol.m^{-2}.s^{-1} (Litthauer et al., 2015), and no loss of amplitude in F_q'/F_m' rhythms was observed in the *phot1-5* or *phot2-1* single mutants under either 20 µmol.m^{-2}.s^{-1} or 50 µmol.m^{-2}.s^{-1} constant blue light (Figure 3.3; Litthauer et al., 2015). These data correspond with previous reports that the two phototropins redundantly mediate numerous responses and have different light sensitivities, including in regulation of chloroplast accumulation (Kong and Wada, 2011). The decrease of amplitude in F_q'/F_m' rhythms in *p1p2* under free run in the absence of any changes in clock gene transcription implies that the lost rhythmicity is due to processes within the chloroplast, and not due to changes in nuclear gene expression. Interestingly, phototropin function had no significant effect on delayed fluorescence rhythms in *phot* single mutants or the *p1p2* double mutant (Figure 3.4). These data, along with the observation that delayed fluorescence and F_q'/F_m' rhythms peak at different times of the day respectively (Figure 3.1), support the idea that different biological processes underlie these rhythms and that phototropin function affects only a subset of the circadian-regulated chloroplast responses. DF rhythms in the leaves of various *Kalanchoë* species cycle

with a circadian period that is shorter than that observed for F_q'/F_m', further suggesting that F_q'/F_m' and DF report distinct outputs from the circadian system (Malpas and Jones, 2016).

The loss of amplitude in F_q'/F_m' rhythms in the *p1p2* mutant under dim blue light needs further investigation. At the whole plant level, loss of amplitude in circadian rhythms under constant conditions can be attributed either to decreased amplitude of oscillations in individual cells, or due to a desynchronization of rhythms across different individual cells over time (Yakir et al., 2011). In *K. daigremontiana* leaves, the dampening of circadian oscillations in F_q'/F_m' has been attributed to desynchronization of individual, weakly-coupled oscillators that operate independently in space and time (Rascher et al., 2001; Wyka et al., 2005). Chlorophyll *a* fluorescence analysis of individual *Kalanchoë daigremontiana* leaves illustrates the concept of the circadian clock as an assembly of individual, weakly-coupled oscillators that operate independently in space and time (Rascher et al., 2001). In leaves grown under light:dark cycles, F_q'/F_m' averaged over the entire leaf surface shows small variations during the day. However, mapping the spatiotemporal distribution of F_q'/F_m' during this light stage of CAM photosynthesis shows strongly heterogeneous, isolated patches of F_q'/F_m' during the transition phase (Phase II of CAM) in the early light period. Heterogeneity is greatest when the rate of net carbon fixation is high (at low internal CO_2 concentration) and when the competing carboxylases, RUBISCO and phosphoenolpyruvate-carboxylase (PEPCase), are both active. In contrast, homogeneity in F_q'/F_m' is observed across the leaf surface during Phase III (remobilisation of malic acid from the vacuole and subsequent decarboxylation, followed by re-fixing of carbon by RUBISCO and assimilation via the Calvin cycle), when internal CO_2 concentrations are high due to decarboxylation of malic acid, stomata are closed and PEPCase is inhibited. During the transition from Phase III to Phase IV in the later light period, heterogeneity in F_q'/F_m' returns, occurring as wave fronts initiated at the leaf base and extending over the entire leaf. These wave fronts persist until the end of phase IV, when malic acid stores are exhausted and stomata open to allow uptake of CO_2 and subsequent direct assimilation by RUBISCO. The oscillations in F_q'/F_m' measured over the entire *Kalancoë* leaf

cycle in step with rhythms in carbon assimilation. The waveform of F_q'/F_m' exhibits sections of both fast and slow change, with a gradual increase in F_q'/F_m' occurring as carbon assimilation increases (from minimum) from approximately midday to midnight, followed by a rapid decline in F_q'/F_m' from maximum to minimum as carbon assimilation again reaches minimum at midday the following day. This rapid decline in total leaf F_q'/F_m' corresponds to isolated peaks in heterogeneity that occur as the weakly-coupled patches of tissue that act as individual oscillators become desynchronised. After minimum F_q'/F_m' is reached around midday, gradual resynchronisation of the individual oscillators occurs, which manifests as a gradual increase in F_q'/F_m' observed from midday to midnight. Under free-running conditions, however, the individual oscillators become increasingly desynchronised with increased time from the last Zeitgeber. After extensive free-run, some leaf regions exhibit increased amplitude in F_q'/F_m' rhythms while others cease to oscillate, with antiphasic oscillations even occurring among different patches of tissue. This desynchronization results in a decline in the amplitude of total leaf F_q'/F_m' and dampening of observable rhythms (Rascher et al., 2001). Further analysis needs to be done to determine whether the effect of phototropin function on the rhythms in PSII operating efficiency in *Arabidopsis* are due to changes in the light harvesting apparatus or through regulation of photochemistry. Alternatively, the effect of phototropin function on F_q'/F_m' rhythms could be indirect, through regulation of chloroplast accumulation (Kagawa et al., 2001; Sakai et al., 2001) or stomatal opening (Kinoshita et al., 2001; Doi et al., 2004). In a light-adapted leaf, the parameter F_q'/F_m' is calculated as the product of two fluorescence parameters, F_v'/F_m' and F_q'/F_v' (Baker, 2008). These parameters allow assessment of whether changes in PSII operating efficiency are due to changes in nonphotochemical quenching or due to the ability of an excited PSII reaction centre to drive electron transport. F_v'/F_m' estimates the maximum quantum yield of PSII photochemistry when Q_A is maximally oxidised and can therefore be used to assess the effect of nonphotochemical quenching on changes in PSII operating efficiency. In contrast, F_q'/F_v' provides an indication of the proportion of 'open' PSII centres where Q_A is oxidised, and estimates the fraction of the maximum PSII efficiency that is realized in the leaf (Baker, 2008). In *p1p2* mutants, loss in

amplitude occurred in rhythms of both F_q'/F_m' (Figure 3.3) and F_q'/F_v' (Figure 3.7c and d) after ~3 days of free-run, while rhythms were maintained in Col-0 and *phot* single mutants. Loss of F_q'/F_v' rhythms in *p1p2* suggests an effect of phototropin function on changes in proteins and components involved in photochemistry (Baker, 2008; Litthauer et al., 2015). Rhythms in F_v'/F_m' have also been shown to dampen in *p1p2* mutants, suggesting that both regulation of photochemistry and changes in the light harvesting apparatus are involved in the F_q'/F_m' rhythms observed in the *p1p2* mutant (Litthauer et al., 2015). In addition, F_v'/F_m' rhythms oscillate with a later phase (~2 h) in comparison to F_q'/F_v' rhythms in Col-0 under constant light conditions. This suggests that the organisation of components involved in light harvesting are not synchronised with the organisation of proteins involved in photochemical reactions (Litthauer et al., 2015).

Even though NPH3 has been reported as being required for phototropic responses under blue light (Inoue et al., 2008; Liscum et al., 2014), loss of NPH3 function had no effect on the period or amplitude of F_q'/F_m' rhythms under constant blue light (Figure 3.7a). In addition, no effect was observed on the parameter F_q'/F_v' (PSII efficiency factor; Figure 3.7). While rhythms in F_q'/F_v' dampened in the *p1p2* mutant, rhythms of F_q'/F_m' and F_q'/F_v' in *nph3* mutants were indistinguishable from WT (Figure 3.7a and b), suggesting that another signalling intermediate may be involved in regulation of PSII efficiency. This corresponds to previous reports that NPH3 is needed for only a subset of phototropin-regulated responses. During phot1-regulated phototropic responses, curvature, but not growth inhibition, relies on NPH3 activity (Folta and Spalding, 2001), while mediation of stomatal opening and chloroplast accumulation through phot1 also occurs without NPH3 involvement (Inoue et al., 2008).

3.3.3. Different photoperiods may affect the regulation of F_q'/F_m' rhythms by phototropins

When analysing rhythms in F_q'/F_m' in plants entrained in different photoperiods, it was revealed that F_q'/F_m' rhythms in Col-0 peak ~4 hours before subjective dawn whether plants

are entrained to 12h:12h (Figure 3.1c), 8h:16h (Figure 3.8a) or 16h:8h (Figure 3.8b) light:dark cycles prior to imaging. This corresponds to previous reports of circadian gene transcript analysis suggesting that the *Arabidopsis* clock as dawn-dominant (Flis et al., 2016; Millar, 2016). While F_q'/F_m' rhythms dampened in *p1p2* seedlings entrained to 12h photoperiods (Figure 3.3a), the loss of amplitude was less severe in plants entrained to long days (Figure 3.8c and d) and absent in plants entrained to short days (Figure 3.8a and b). Furthermore, while loss of phototropin function had no effect on F_q'/F_m' rhythms in plants entrained to 12h:12h light:dark cycles (Figure 3.3), F_q'/F_m' rhythms in *p1p2* mutants entrained to either short or long days exhibited significantly longer periods compared to Col-0 (Figure 3.8). Loss of NPH3 function had no effect on the amplitude or period of F_q'/F_m' rhythms in plants entrained in either long, short or 12-hour photoperiods (Figure 3.7 and Figure 3.8). These data suggest a possible role for phototropins in maintaining F_q'/F_m' rhythms in different photoperiods through a signalling cascade in which NPH3 is not involved. Since the sensing of photoperiods plays a key role synchronising plant responses to rhythms in seasonal changes (Song et al., 2015), these observations suggest that phototropins could function to regulate seasonal processes such as flowering, senescence or growth. Further analysis, including analysis of delayed fluorescence and accumulation of circadian-regulated gene transcripts in *phot* mutants under long- and short-day conditions, could reveal possible targets involved in phototopin regulation of circadian rhythms under different photoperiods.

This chapter has demonstrated that PSII operating efficiency is a rhythmic circadian output which is controlled by the nuclear central oscillator, and which maintains robust rhythms under a variety of photoperiods independent of leaf movement. In the following chapters, chlorophyll *a* fluorescence imaging, and in particular the parameter F_q'/F_m', will be used extensively to identify and characterise the circadian phenotypes of various mutants.

Chapter 4

The effect of *SAL1* activity on circadian rhythms

4.1. Introduction

Chloroplasts serve as sensors that detect signals from the environment, and regulate developmental and stress responses by changing the expression of both chloroplast- and nuclear-encoded genes (Chan et al., 2016b; Millar, 2016) Signalling between the nucleus and chloroplasts also plays an important role in circadian regulation of processes such as photosynthesis (Dodd et al., 2014; Belbin et al., 2017). The regulation of nuclear gene expression through chloroplast-nucleus retrograde signalling involves numerous pathways and cellular signals, including phosphoadenosines, carotenoid derivatives, isoprenes, tetrapyrroles, proteins and reactive oxygen species (Noordally et al., 2013; Chan et al., 2016b). One such pathway involves the activity of the redox-sensitive chloroplast-localised enzyme SAL1 (Estavillo et al., 2011; Chan et al., 2016a). In this chapter, the function of SAL1 in the circadian system of *Arabidopsis* is investigated.

4.2. Results

4.2.1. Loss-of-function mutations in SAL1

Mutations in *Arabidopsis SAL1* are highly pleotropic and *sal1* mutants have been identified in a variety of genetic screens, including screens for altered regulation of cold-induced gene expression (Lee et al., 1999), elevated expression of ABA- and osmotic stress-inducible genes (Xiong et al., 2001), elevated expression of *APX2* (Rossel et al., 2004), restoration of posttranscriptional gene silencing (Gy et al., 2007), altered regulation of photo-morphogenic processes including hypocotyl elongation and late flowering time (Kim and von Arnim, 2009),

altered leaf morphogenesis and venation patterning (Robles et al., 2010) and lateral root initiation (Chen and Xiong, 2010), as well as deregulation of the high affinity phosphate transporter *PHT1;4* (Hirsch et al., 2011) and of fatty acid oxygenation rates (Rodriguez et al., 2010). In addition, *sal1* mutants exhibit increased tolerance to drought and osmotic stress (Wilson et al., 2009; Estavillo et al., 2011), and accumulate significantly higher levels of PAP compared to wild-type, both in the absence and presence of abiotic stress (Chen et al., 2011; Estavillo et al., 2011; Lee et al., 2012).

In this study, analysis focused on the *sal1* null mutant alleles *alx8-1* (Rossel et al., 2006), *fry1-6* (Gy et al., 2007) and *fou8* (Rodriguez et al., 2010) (Figure 4.1a). *alx8-1* was identified in a screen for altered high light-induced expression of *APX2* performed on Col-0 carrying an *APX2:LUC* reporter gene and mutagenized with ethyl methanesulfonate (Rossel et al., 2006). *alx8-1* was described as a gain-of-function mutant with constitutively higher *APX2* expression compared to wild type (Rossel et al., 2006), and the *alx8-1* mutation was mapped to a single nucleotide change (G1226A) that results in a G217D amino acid substitution occurring on an internal β-sheet of unknown function (Wilson et al., 2009). *fry1-6* (SALK_020882) was first described in a study identifying SAL1 as an endogenous suppressor of posttranscriptional gene silencing, and the mutation was mapped to a T-DNA insertion in exon 3 that results in truncation of the SAL1 protein at amino acid position 71 (Gy et al., 2007). *fou8* was identified in a screen of ethyl methanesulfonate-mutagenised Col-0 as exhibiting higher rates of α-linolenic acid oxygenation (Rodriguez et al., 2010). The *fou8* mutation was mapped to a single nucleotide substitution (G531A) in the splicing donor sequence of intron 2, which results in the skipping of exon 2 during splicing (Rodriguez et al., 2010).

sal1 loss-of-function mutants exhibit obvious morphological characteristics that are more pronounced in adult plants than in seedlings (Figure 4.1b and c). At 7 days old, seedlings of *alx8-1* and *fry1-6* grown on 0.5x MS agar in 12h:12h light:dark cycles under 60 $\mu mol.m^{-2}.s^{-1}$ white light are slightly smaller, but strongly resemble Col-0 seedlings (Figure 4.1b).

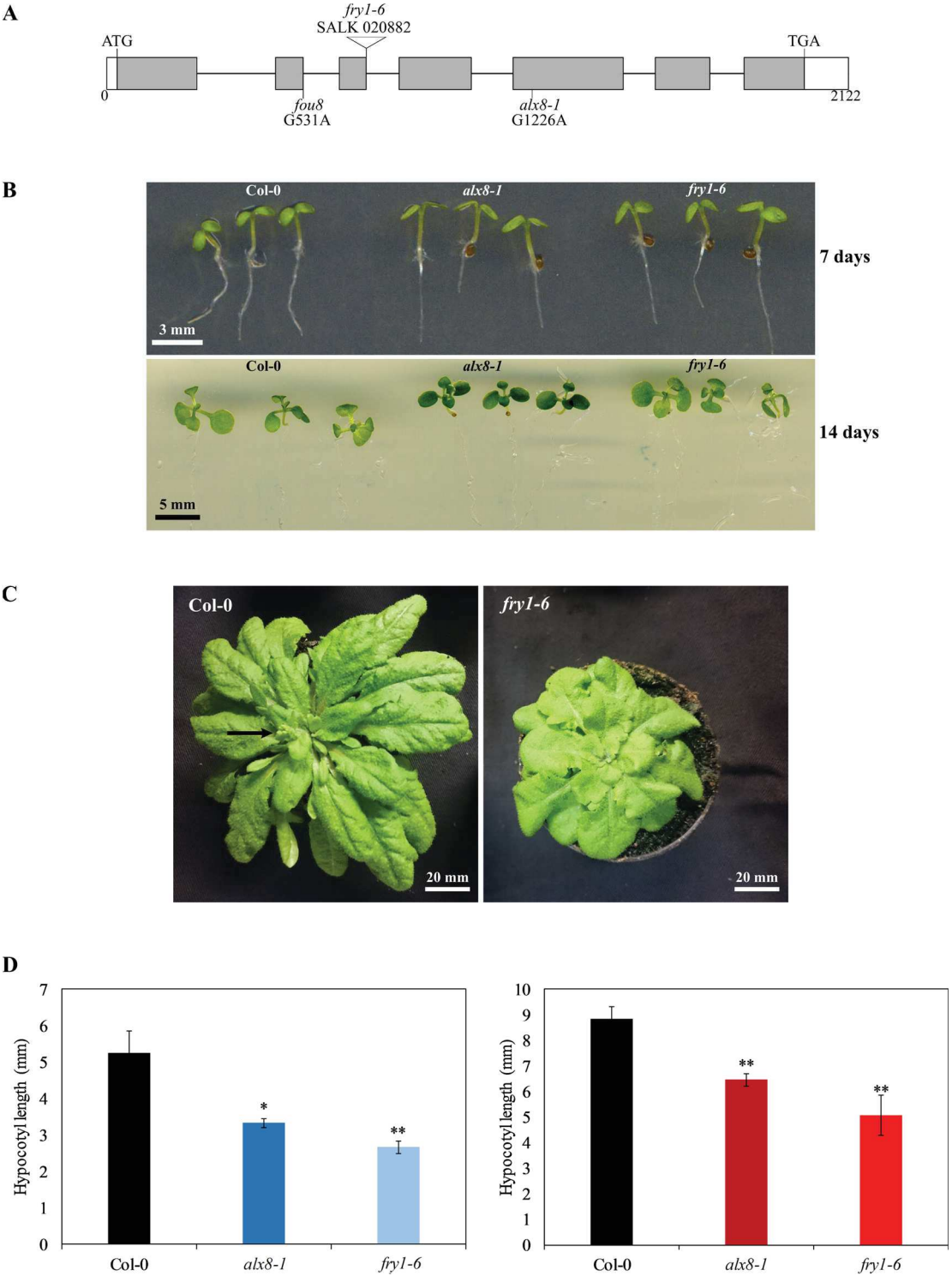

Figure 4.1 *sal1* loss-of-function mutations in *Arabidopsis* Col-0. (A) Schematic representation of the *Arabidopsis SAL1* gene showing positions of mutations for *alx8-1* (G1226A), *fry1-6* (T-DNA insertion at exon 3) and *fou8* (G531A). White blocks indicate UTR regions, with grey blocks and lines indicating exons and introns respectively. Start (ATG) and stop (TGA) codons shown. **(B)** Morphology of Col-0, *alx8-1* and *fry1-6* seedlings 7 days (top) and 14 days (bottom) after germination. Seedlings were grown on 0.5x MS agar plates in 12h:12h light:dark cycles under 60 $\mu mol.m^{-2}.s^{-1}$ white light. **(C)** Quantification of hypocotyl lengths of Col-0, *alx8-1* and *fry1-6* seedlings grown on 0.5x MS agar plates for 6 days under 5 $\mu mol.m^{-2}.s^{-1}$ constant blue light (left) or 10 $\mu mol.m^{-2}.s^{-1}$ constant red light (right). Error bars indicate standard error of the mean, with n>16. Asterisks indicate statistical significance compared to Col-0 control (** $p<0.001$; * $p<0.01$; Student's T-test) **(D)** Morphology of Col-0 and *fry1-6* after 7-8 weeks growth. Black arrow indicates position of inflorescence with buds in Col-0. Plants were grown on soil in 8h:16h light:dark cycles under 120 $\mu mol.m^{-2}.s^{-1}$ white light.

After 14 days of growth under the same conditions, the differences are more visible, with *sal1* mutant seedlings exhibiting shortened petioles and rounded leaves (Figure 4.1b). Morphological characteristics are much more pronounced in ~8-week old plants grown on soil in 8h:16h light:dark cycles under 120 $\mu mol.m^{-2}.s^{-1}$ white light (Figure 4.1d). In these older plants, *sal1* mutants such as *fry1-6* exhibit dwarfed rosettes, and shortened, rounder leaves with undulating surfaces and more lobed edges, as well as shortened petioles (Gy et al., 2007; Wilson et al., 2009; Hirsch et al., 2011). In addition, *fry1-6* flowers significantly later than Col-0, as has been reported for other *sal1*mutant alleles (Gy et al., 2007; Kim and von Arnim, 2009; Rodriguez et al., 2010). *fry1-6* seedlings have been reported as having shortened hypocotyls under both blue and red light (Kim and von Arnim, 2009). To analyse hypocotyl length in *sal1* seedlings, Col-0, *alx8-1* and *fry1-6* seedlings were grown on 0.5x MS agar plates for 6 days under 5 $\mu mol.m^{-2}.s^{-1}$ constant blue or 10 $\mu mol.m^{-2}.s^{-1}$ constant red light. Quantification of hypocotyl length revealed significantly shortened hypocotyls in *alx8-1* and *fry1-6* compared to Col-0 under constant blue and constant red light (Figure 4.1d). This corresponds to previous reports of *sal1* mutants exhibiting slower growth, shortened hypocotyls and petioles, limited primary root and lateral root growth, and shorter and rounder leaves (Xiong et al., 2001; Kim and von Arnim, 2009; Wilson et al., 2009; Hirsch et al., 2011).

4.2.2. SAL1 protein is present throughout the day, with no circadian rhythm in transcript accumulation

Transcript of *SAL1* is detectable in Col-0 at both dawn and dusk in plants grown under 16h:8h light:dark cycles (Figure 4.2a and b), which corresponds with previous reports (Wilson et al., 2009; Estavillo et al., 2011). qRT-PCR analysis can be used to distinguish between *alx8-1* and *fry1-6* by using primers targeted to either exons 3 and 4 (Figure 4.2a) or exons 6 and 7 (Figure 4.2b). Primer pairs were designed with one primer bridging an intron, such that one end of the primer is complementary to the 3′ end of one exon and the other end is complementary to the 5′ end of the next downstream exon.

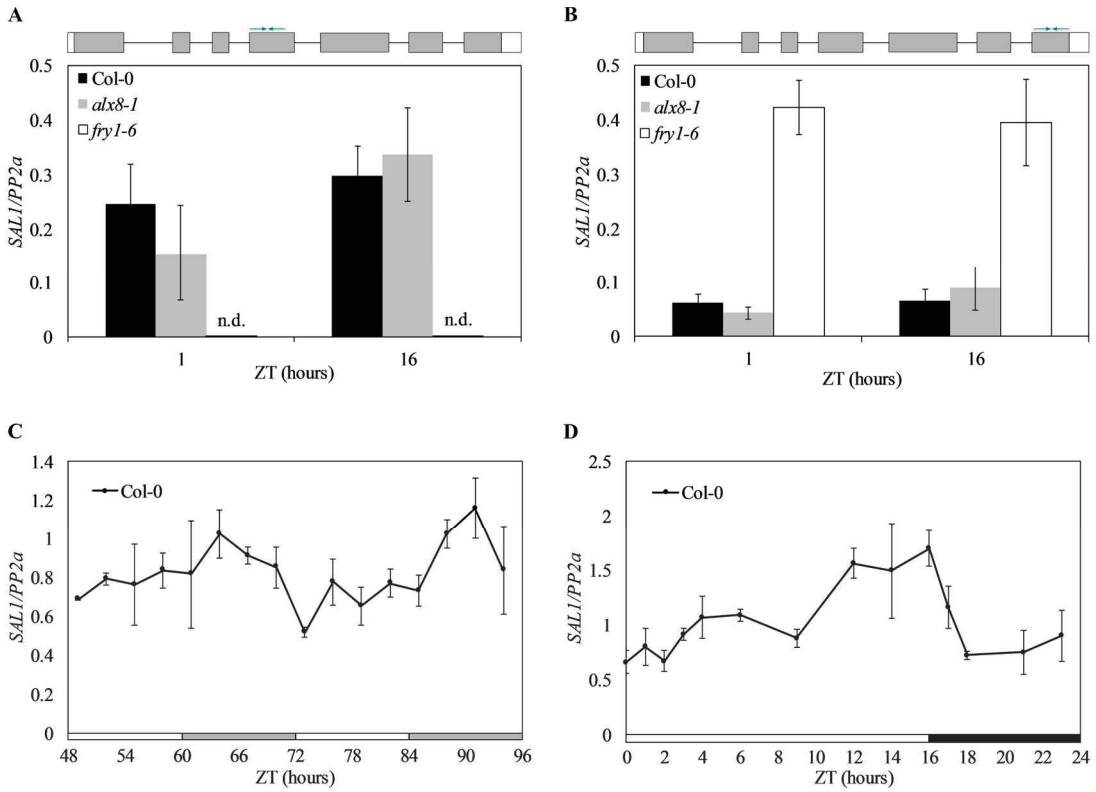

Figure 4.2 Transcription of *SAL1* in Col-0 and *sal1* mutants. (A-B) qRT-PCR analysis of *SAL1* transcript levels in Col-0, *alx8-1* and *fry1-6* at dawn (ZT0) and dusk (ZT16) respectively. Transcript levels were analysed using primers targeted to **(A)** exon 3 or **(B)** exon 7. Simplified gene diagrams of *SAL1* gene with arrows indicating positions of primer binding are shown. Data from one of three independent experiments are shown. Error bars indicate standard error of the mean for three technical replicates. **(C)** qRT-PCR analysis of *SAL1* transcript accumulation in Col-0 seedlings under constant white light. Transcript levels were analysed using primers targeted to exon 7. Seeding were entrained in 12h:12h light:dark cycles under 60 µmol.m^{-2}.s^{-1} white light for 10 days before being transferred to 60 µmol.m^{-2}.s^{-1} constant white light at subjective dawn. After 48 hours in free-run (ZT48), seedlings were sampled every 3 hours for 2 days. White bars and grey bars indicate subjective day and subjective night, respectively. **(D)** qRT-PCR analysis of *SAL1* transcript accumulation in Col-0 seedlings under long-day conditions. Seedlings were grown on 0.5x MS agar plates in 16h:8h light:dark cycles under 60 µmol.m^{-2}.s^{-1} white light for 12 days before sampling. White bars indicate light period, black bars indicate dark period. **(C-D)** Data are average of two independent experiments. Error bars indicate standard error of the mean. All data were normalised to an internal control (*PP2a*).

This allows for amplification to occur only if the primer binds to cDNA from a spliced mRNA transcript. Primers targeted to exons 3 and 4 detect no *SAL1* transcript in *fry1-6* due to the T-DNA insertion at exon 3, while primers targeted to exons 6 and 7 detects elevated levels of *SAL1* in *fry1-6*. Both primer pairs detect *SAL1* transcript in the *alx8-1* mutant allele (Figure 4.2a and b). Despite the presence of transcript, no SAL1 protein is detected in these mutants (Wilson et al., 2009; Estavillo et al., 2011).

While the abundance of *SAL1* transcript in Col-0 is reportedly not regulated by osmotic stress treatment (Xiong et al., 2001), light induction and dark repression of *SAL1* transcription has been reported (Kim and von Arnim, 2009). Previous cDNA microarray analysis of the early dark response in *Arabidopsis* seedlings identified repression of *SAL1* transcripts within 1 hour of transfer from constant light to dark (Kim and von Arnim, 2006). In addition, time series microarray studies have indicated rhythms in *SAL1* transcription under light:dark cycles in both long and short photoperiods, with less pronounced oscillations occurring under constant light conditions (Mockler et al., 2007). To determine whether transcription of *SAL1* is regulated by the circadian system, the accumulation of *SAL1* transcripts under constant light conditions was analysed in Col-0 using qRT-PCR. Seedlings were grown on 0.5x MS agar plates in 12h:12h light:dark cycles under 60 $\mu mol.m^{-2}.s^{-1}$ white light for 10 days and, following entrainment, were transferred to constant light conditions under 60 $\mu mol.m^{-2}.s^{-1}$ white light at subjective dawn (ZT0). After 48 hours of free run, 10-12 seedlings per time point were sampled from subjective dawn (ZT48) every 3 hours for two days. Transcripts were analysed using primers targeted to exon 7. A modest rhythm in *SAL1* transcript accumulation was observed under constant white light, with transcript levels lowest at subjective dawn and peaking during the subjective night (Figure 4.2c). Oscillations in *SAL1* transcript levels were also examined under light:dark cycles (Figure 4.2d). Seedlings were entrained on 0.5x MS agar plates in 16h:8h light:dark cycles under 60 $\mu mol.m^{-2}.s^{-1}$ white light for 12 days, and tissue (10-12 seedlings per timepoint) harvested from dawn (ZT0) the following day. A rhythm in *SAL1* transcript accumulation under long-day conditions was observed, with *SAL1* transcript levels increasing from dawn (ZT0)

throughout the 16 h photoperiod to reach peak transcript levels at dusk (ZT16), followed by a decrease in transcript level within 1 hour from dusk. These data correspond with the *SAL1* transcription dark response previously reported (Kim and von Arnim, 2006), as well as with *SAL1* transcription rhythms reported in long and short photoperiods, and in constant light conditions (Mockler et al., 2007).

Expression of SAL1 fused at the C-terminal to GFP and driven by the native *SAL1* promoter has been used successfully to study localisation of SAL1 protein and complementation of *sal1* phenotypes (Wilson et al., 2009; Rodriguez et al., 2010; Estavillo et al., 2011). In order to analyse the accumulation of SAL1 protein over time under dark:light cycles, *alx8-1* was transformed with a Gateway® plasmid construct for expression of a SAL1-GFP fusion under control of the native *SAL1* promoter (*alx8-1 SAL1::SAL1:*GFP; Appendix II). Protein time course analysis was performed on homozygous T3 seedlings of two independent *alx8-1 SAL1::SAL1:GFP* lines, one line (#1) expressing SAL1-GFP at higher levels and one line (#2) expressing SAL1-GFP at lower levels. Seedlings were grown on 0.5x MS agar plates in 16h:8h light:dark cycles under 60 $\mu mol.m^{-2}.s^{-1}$ white light for 12 days, and tissue (12-15 seedlings per timepoint) harvested from dawn (ZT0) on the 13th day. Immunoblot analysis was performed on total protein extracts using an anti-GFP antibody, and intensity of protein bands quantified (Figure 4.3a and b). SAL1-GFP protein was detected in both independent lines of *alx8-1 SAL1::SAL1:GFP* throughout the entire day (Figure 4.3a). Despite the increase in transcript levels towards the end of the 16 h photoperiod and a subsequent decrease in transcript levels occurring from dusk (Figure 4.2d), no obvious rhythm in protein levels was detected in either of the two *alx8-1 SAL1::SAL1:GFP* independent lines under entraining conditions (Figure 4.3a and b).

To confirm the subcellular localisation of the SAL protein, *alx8-1 SAL1::SAL1:GFP* seedlings were subjected to confocal laser microscopy imaging (Figure 4.4).

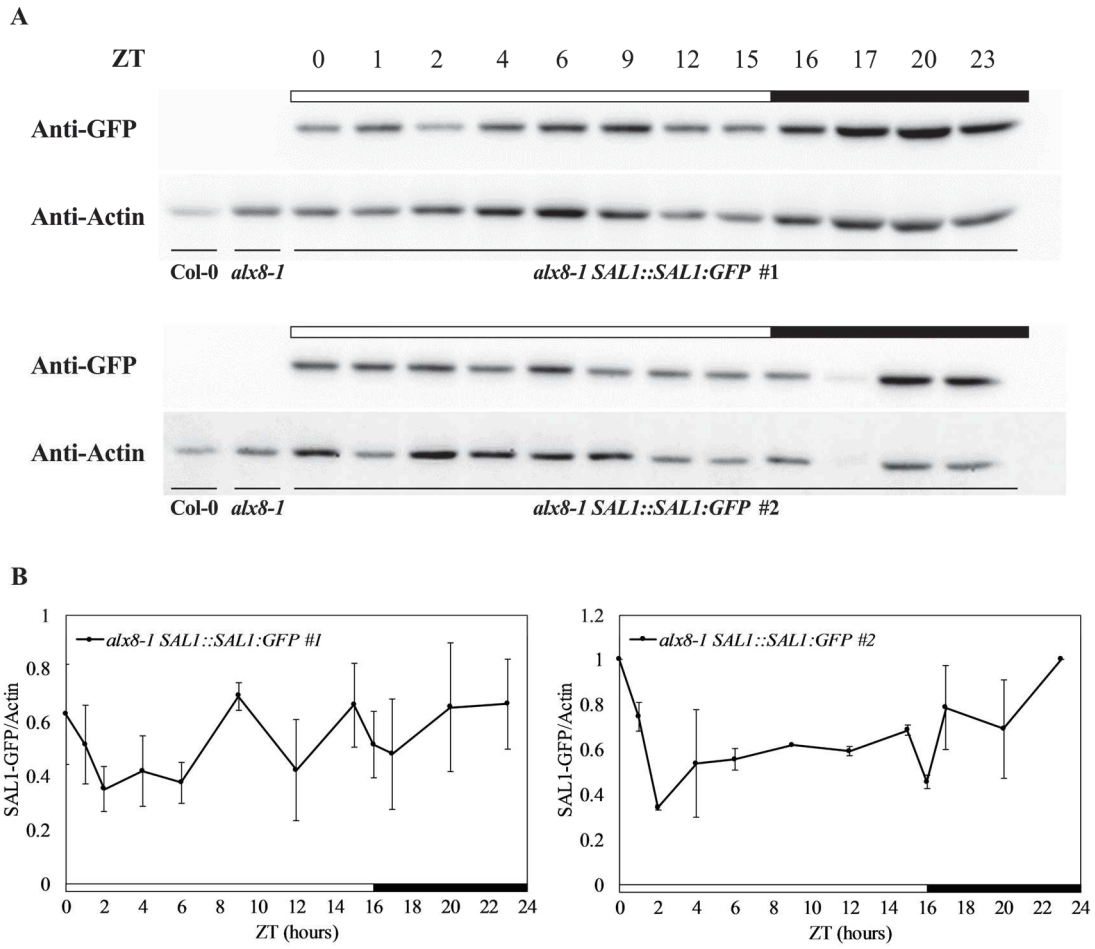

Figure 4.3 Rhythms of *SAL1* expression in Col-0 under long-day conditions. (A) Immunoblot analysis and **(B)** quantification of SAL-GFP levels under long-day conditions using an anti-GFP antibody in Col-0, *alx8-1* and two independent *alx8-1 SAL1::SAL1:GFP* lines, one with higher (#1, top) and one lower expression of SAL1-GFP (#2, bottom). Anti-Actin antibody used to detect actin levels for loading control. Seedlings were grown on 0.5x MS agar plates in 16h:8h light:dark cycles under 60 µmol.m^{-2}.s^{-1} white light for 12 days before sampling. White bars indicate light period, black bars indicate dark period. Immunoblots from one of two independent experiments are shown. Protein level quantification data are average of three independent experiments. Data were normalised to internal control (Actin). Error bars indicate standard error of the mean.

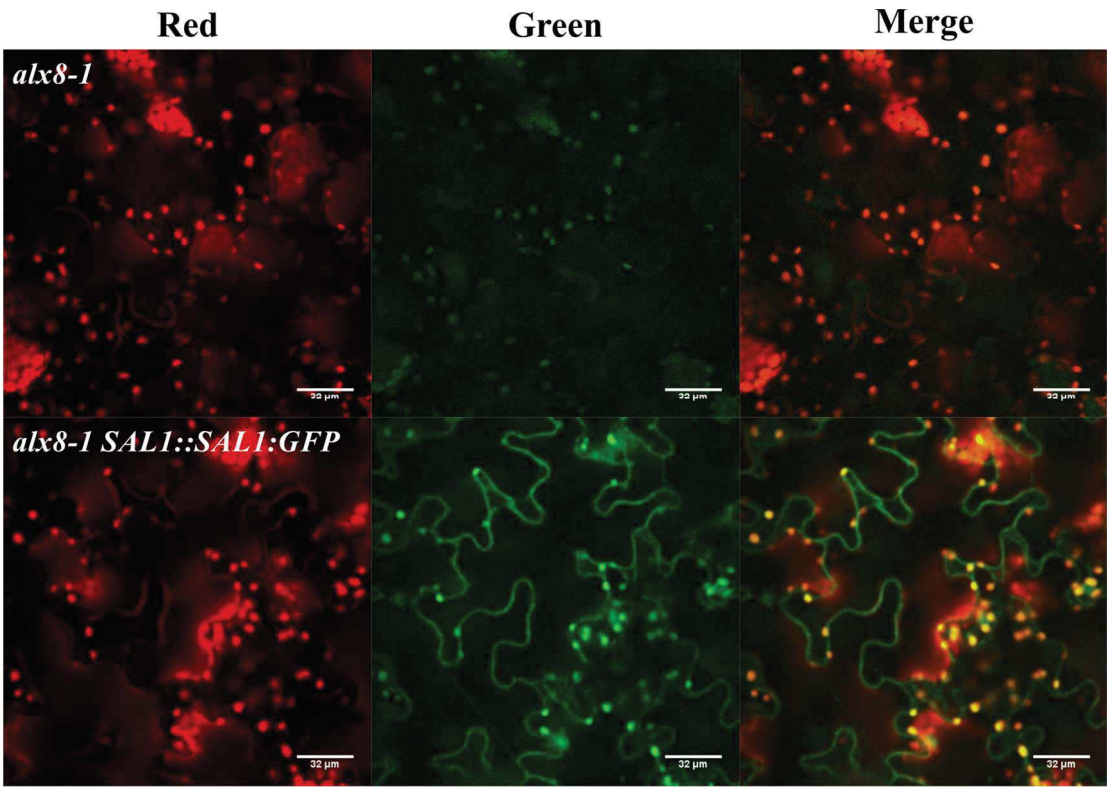

Figure 4.4 Subcellular localisation of SAL1-GFP. Confocal laser scanning microscopy images of leaves of Col-0 (top) and *alx8-1 SAL1::SAL1:GFP* (bottom) seedlings showing red (chlorophyll) channel, green (GFP) channel and merged images. Seedlings were grown on 0.5x MS media in 12h:12h light:dark cycles under 60 µmol.m^{-2}.s^{-1} white light for 12 days before imaging.

Seedlings were grown on 0.5x MS media for 12 days in 12h:12h light:dark cycles under 60 $\mu mol.m^{-2}.s^{-1}$ white light before leaves of intact seedlings were subjected to confocal microscopy imaging in the late afternoon. SAL1-GFP was detected in the chloroplasts and in the cytosol of *alx8-1SAL1::SAL:GFP* seedlings, as has been previously reported for *sal1* mutants (Zhang et al., 2011; Estavillo et al., 2011).

4.2.3. sal1 mutants exhibit long period rhythms in chloroplasts under constant blue light, but not under constant red light

Production and scavenging of ROS is regulated by both by diurnal cycles and the circadian clock, and the core clock gene *CCA1* regulates the coordinated transcription of ROS genes under non-stressed conditions (Lai et al., 2012). The sensitivity of SAL1 activity to the redox poise of the plastids (Chan et al., 2016a), combined with the late flowering phenotype exhibited by *sal1* mutants (Gy et al., 2007; Wilson et al., 2009; Rodriguez et al., 2010) suggests a possible role for SAL1 within the *Arabidopsis* circadian system.

In order to determine whether loss of *SAL1* function has an impact on the circadian system, F_q'/F_m' rhythms were monitored in the *sal1* mutant alleles *alx8-1*, *fry1-6* and *fou8* under constant blue light (Figure 4.5). Imaging was performed across three separate experiments, analysing one *sal1* mutant allele along with Col-0 in each case to allow analysis of >8 individual seedlings per genotype. Seedlings were grown on 0.5x MS agar plates and entrained for 12 days in 12h:12h light:dark cycles under 60 $\mu mol.m^{-2}.s^{-1}$ white light. Following entrainment, individual seedlings were imaged under 20 $\mu mol.m^{-2}.s^{-1}$ constant blue light for ~5 days. Circadian period estimates were determined through FFT-NLLS analysis of time series data using BRASS (Millar et al., 2010) as described in Chapter 3. Robust F_q'/F_m' rhythms were maintained across all 5 days of free-run in Col-0 and in all *sal1* mutant alleles, with no significant difference in RAE in *alx8-1* (0.15 ± 0.01; Figure 4.5a and b), *fry1-6* (0.13 ± 0.01; Figure 4.5c and d) or *fou8* (0.21 ± 0.02; Figure 4.5e and f) compared to Col-0.

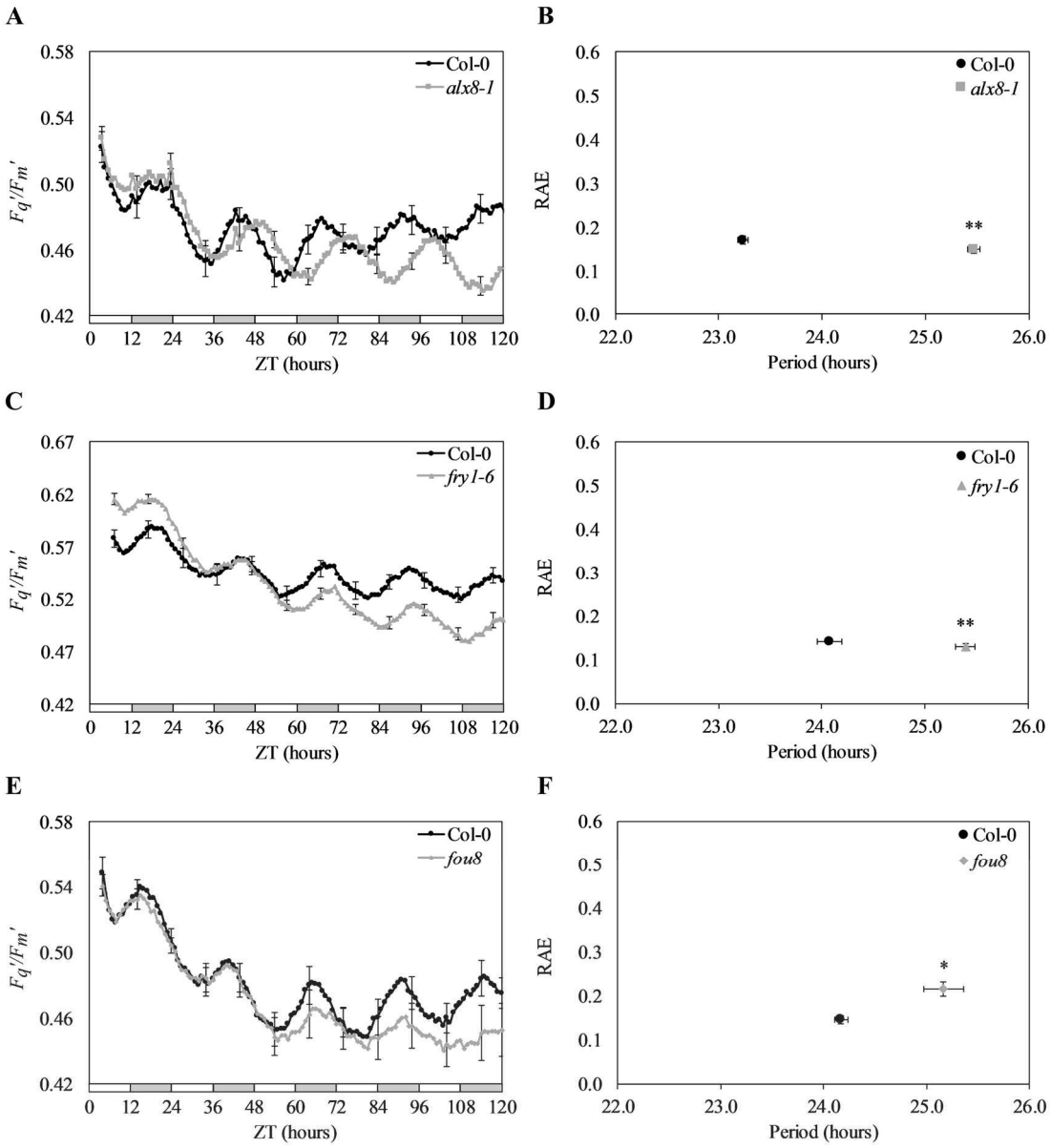

Figure 4.5 F_q'/F_m' rhythms in *sal1* mutants under constant blue light. **(A,C,E)** Waveforms and **(B,D,F)** circadian period estimates plotted against Relative Amplitude Error (RAE) for F_q'/F_m' oscillations in Col-0, **(A-B)** *alx8-1*, **(C-D)** *fry1-6* and **(D-E)** *fou8* seedlings under constant blue light. Seedlings were grown on 0.5x MS agar plates and entrained in 12h:12h light:dark cycles under 60 $\mu mol.m^{-2}.s^{-1}$ white light for 12 days before imaging under 20 $\mu mol.m^{-2}.s^{-1}$ constant blue light. White bars and grey bars indicate subjective day and subjective night, respectively. Error bars indicate standard error of the mean, with n>8. For waveforms, error bars are shown every 10 hours for clarity. RAE is a measure of rhythmic robustness, with a value of 0 indicating an exact fit to a cosine wave (Plautz et al., 1997). Data from one of three independent experiments are shown. Asterisks indicate statistically significant difference in period compared to Col-0 control (** $p<0.001$; * $p<0.01$; Student's T-test).

While F_q'/F_m' rhythms cycled with circadian period of ~24 h in Col-0 across all three experiments (Figure 4.5 b, d and f), a significantly longer period in F_q'/F_m' rhythms was observed in *alx8-1* (25.4 ± 0.06 h; Figure 4.5b) and *fry1-6* (25.39 ± 0.09 h; Figure 4.5d) compared to Col-0 (p<0.001; Student's T-test). While the period of F_q'/F_m' rhythms was also significantly longer in *fou8* (25.17 ± 0.19; Figure 4.5f) compared to Col-0 (p<0.01, Student's T-test), the long period was less pronounced than in *alx8-1* and *fry1-6*.

To confirm the effect of SAL1 activity on chloroplast circadian rhythms, rhythms in delayed fluorescence were monitored in Col-0, *alx8-1* and *fry1-6* under constant blue light. Seedlings were grown on 0.5x MS agar plates in clusters of 10-15 and entrained for 12 days in 12h:12h light:dark cycles under 60 µmol.m^{-2}.s^{-1} white light before imaging under 20 µmol.m^{-2}.s^{-1} constant blue light (Figure 4.6a and b). FFT-NLLS analysis was performed on time series data using BRASS (Millar et al., 2010) as described. As had been observed for F_q'/F_m' rhythms (Figure 4.5), rhythms in delayed fluorescence remained robust in Col-0, *alx8-1* and *fry1-6* with RAE<0.6 following ~5 days of free-run (Figure 4.6b). *sal1* mutant alleles did exhibit a significantly higher RAE (0.39 ± 0.03 for *alx8-1*, 0.34 ± 0.03 for *fry1-6*) compared to Col-0 (0.23 ± 0.02; p<0.001, Student's T-test). Period estimates for delayed fluorescence rhythms revealed significantly longer period in both *alx8-1* (25.09 ± 0.28 h) and *fry1-6* (25.07 ± 0.26 h) compared to Col-0 (23.83 ± 0.19 h; p<0.001, Student's T-test), confirming the long period of chloroplast rhythms in *sal1* mutants under constant blue light.

The *sal1* mutant allele *fry1-6* has been reported has being hypersensitive to both red and blue light, with shortened hypocotyls and petioles observed in *fry1-6* mutants under far-red and blue light conditions, and even more dramatically under monochromatic red light (Kim and von Arnim, 2009). To determine whether the long circadian period in chloroplast rhythms of *sal1* mutants is blue light specific, delayed fluorescence rhythms in *alx8-1* mutants were monitored under constant red light. Seedlings were grown as described for Figure 4.6a, and following entrainment were imaged under 30 µmol.m^{-2}.s^{-1} constant red light for ~ 5 days (Figure 4.6c and d).

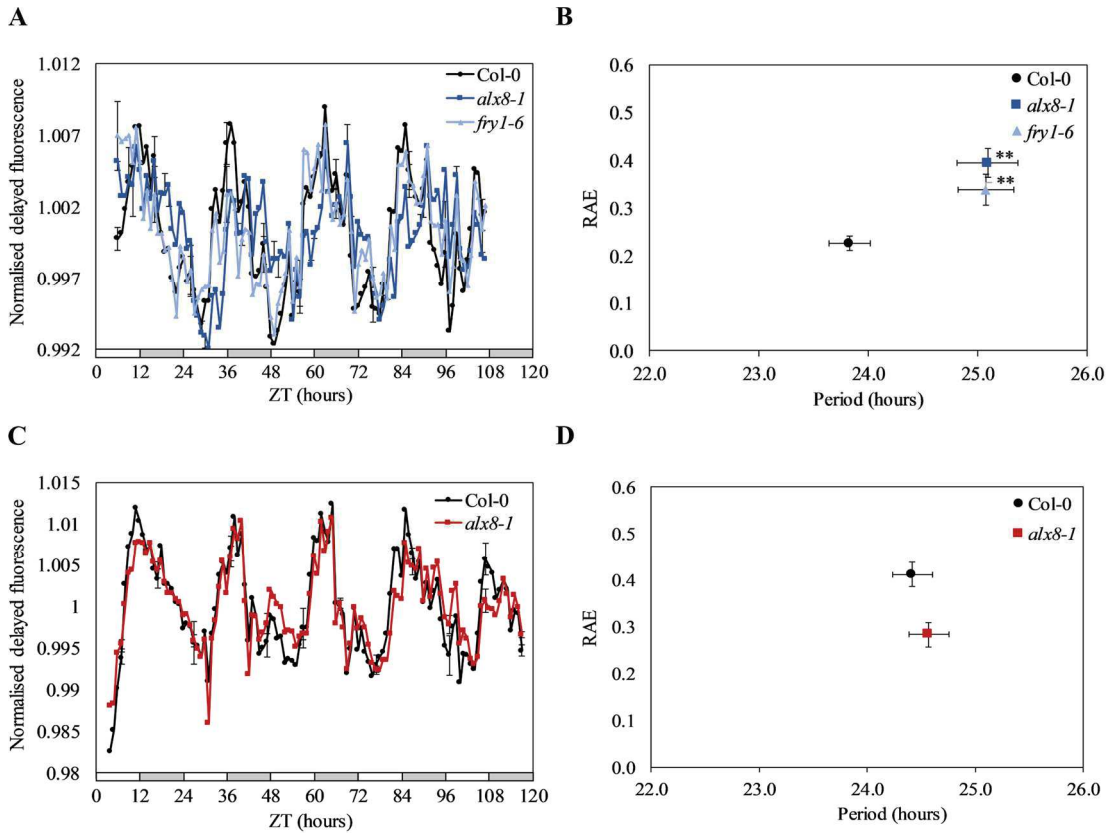

Figure 4.6 Delayed fluorescence rhythms in *sal1* mutants under constant blue and constant red light. (A,C) Waveforms and **(C,D)** circadian period estimates plotted against Relative Amplitude Error (RAE) for normalised delayed fluorescence rhythms in Col-0, *alx8-1* and *fry1-6* seedlings under **(A-B)** 20 µmol.m^{-2}.s^{-1} constant blue light and **(C-D) 3**0 µmol.m^{-2}.s^{-1} constant red light. Seedlings were grown on 0.5x MS agar plates and entrained in 12h:12h light:dark cycles under 60 µmol.m^{-2}.s^{-1} white light for 12 days before imaging under constant light. White bars and grey bars indicate subjective day and subjective night, respectively. Error bars indicate standard error of the mean, with n=10. For waveforms, error bars are shown every 10 hours for clarity. RAE is a measure of rhythmic robustness, with a value of 0 indicating an exact fit to a cosine wave (Plautz et al., 1997). Asterisks indicate statistically significant difference in period compared to Col-0 control (p<0.001; Student's T-test). Data from one of two independent experiments are shown.

Unlike *sal1* mutants grown under constant blue light, *alx8-1* mutants did not exhibit a longer period in delayed fluorescence rhythms (24.57 ± 0.18 h) compared to Col-0 (24.42 ± 0.19 h) under constant red light.

4.2.4. Loss of SAL1 function affects rhythms in CCA1 expression under constant blue light

Since rhythms in F_q'/F_m' and delayed fluorescence are affected by the nuclear circadian oscillator (Gould et al., 2009; Litthauer et al., 2015), rhythms in expression of the morning-phased nuclear core clock gene *CCA1* was examined using luciferase imaging. A *fry1-6 CCA1::LUC2* reporter line was obtained by crossing the *fry1-6* allele into a Col-0 reporter line expressing *LUCIFERASE2* under control of the *CCA1* promoter (Jones et al., 2015). To monitor rhythms in *CCA1* promoter activity under constant blue light, Col-0 *CCA1::LUC2* and *fry1-6 CCA1::LUC2* seedlings were grown on 0.5x MS agar plates for 6 days in 12h:12h light dark cycle under 60 µmol.m^{-2}.s^{-1} white light. Following entrainment, individual seedlings were imaged under 20 µmol.m^{-2}.s^{-1} constant blue light for ~5 days, and time series data subjected to FFT-NLLS analysis as described (Figure 4.7a and b). Bioluminescence from *CCA1::LUC2* activity cycled with robust circadian rhythm in Col-0, peaking shortly after dawn as previously described (Jones et al., 2015). *CCA1::LUC2* rhythms also cycled with robust circadian rhythm in *fry1-6*, with no loss in amplitude or significant difference in RAE compared to Col-0. A phase shift in peak *CCA1::LUC2* activity was observed in *fry1-6* within the first day of free-run, growing more pronounced on successive days under constant light conditions (Figure 4.7a). Circadian period estimates determined for *CCA1::LUC* rhythms (Figure 4.7b) were significantly longer in *fry1-6* (25.42 ± 0.04 h) than in Col-0 (23.65 ± 0.11 h; p<0.001, Student's T-test).

In order to determine whether the long period of *CCA1* expression in *fry1-6* was as a result of altered *CCA1* expression during entrainment, rhythms in *CCA1::LUC2* were monitored under light:dark cycles.

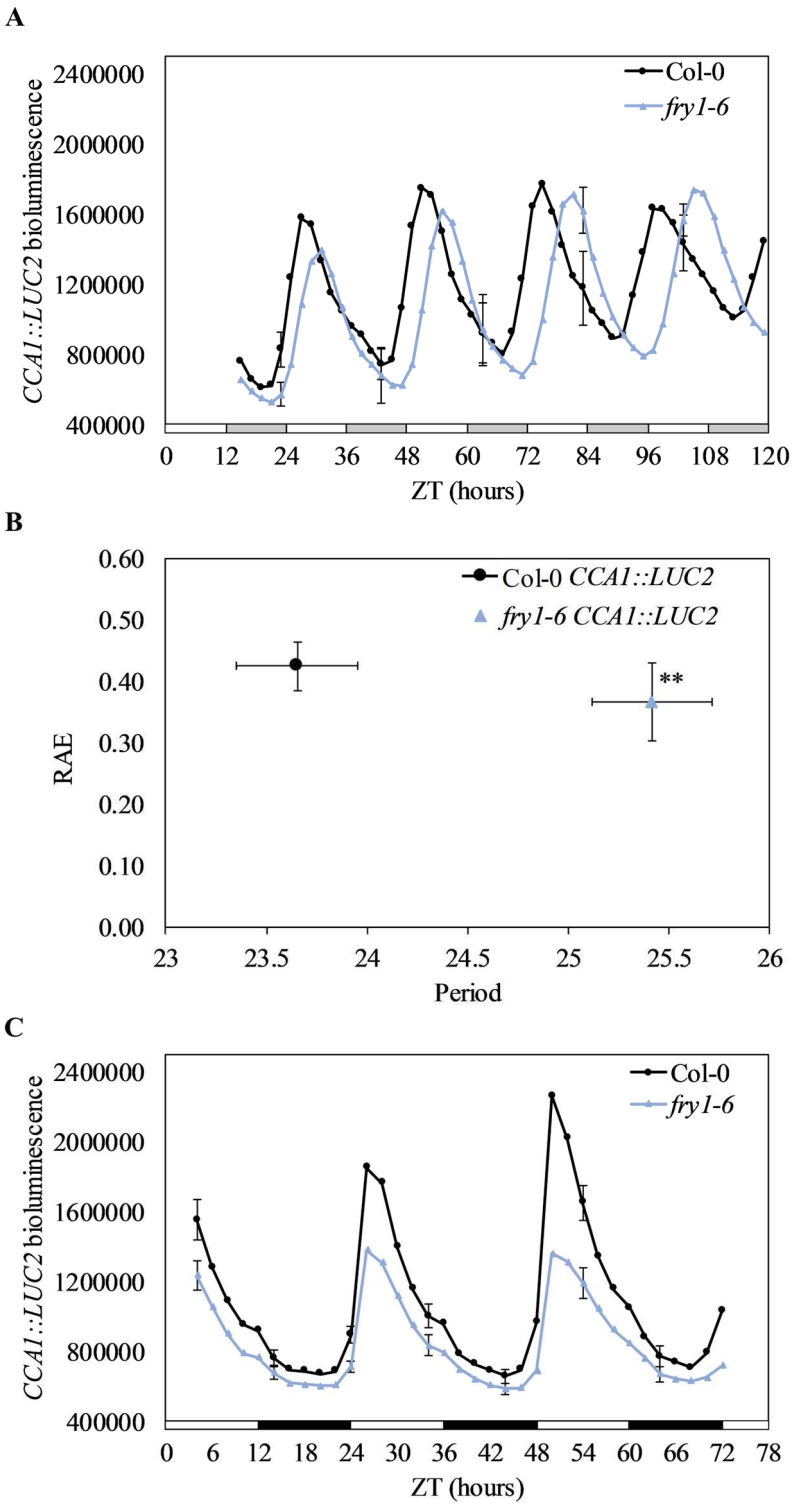

Figure 4.7 Rhythms in *CCA1* expression in *fry1-6* under constant light and entraining conditions. (A) Waveforms and **(B)** circadian period estimates plotted against Relative Amplitude Error (RAE) for luciferase activity monitored in Col-0 *CCA1::LUC2* and *fry1-6 CCA1::LUC2* seedlings under constant blue light. Seedlings were entrained on 0.5x MS agar plates and entrained in 12h:12h light:dark cycles under 60 µmol.m^{-2}.s^{-1} white light for 6 days before imaging under 20 µmol.m^{-2}.s^{-1} constant blue light. White bars and grey bars indicate subjective day and subjective night, respectively. **(C)** Waveforms of *CCA1::LUC2* activity in Col-0 and *fry1-6* in 12h:12h light dark cycles under 20 µmol.m^{-2}.s^{-1} blue light supplemented with 30 µmol.m^{-2}.s^{-1}red light. Seedlings were grown on 0.5x MS agar plates and entrained in 12h:12h light:dark cycles under 60 µmol.m^{-2}.s^{-1} white light for 6 days before imaging. White bars and black bars indicate light and dark periods, respectively. Error bars indicate standard error of the mean, with n=10. For waveforms, error bars shown every 10 hours for clarity. RAE is a measure of rhythmic robustness, with a value of 0 indicating an exact fit to a cosine wave (Plautz et al., 1997). Data from one of three independent experiments are shown. Asterisks indicate statistically significant difference in period compared to Col-0 control (p<0.001; Student's T-test).

Seedlings were grown on 0.5x MS agar plates for 6 days in 12h:12h light dark cycle under 60 µmol.m^{-2}.s^{-1} white light, and subsequently imaged in 12h:12h light:dark cycles under 20 µmol.m^{-2}.s^{-1} blue light supplemented with 30 µmol.m^{-2}.s^{-1} red light (Figure 4.7c). No phase shift in peak *CCA1::LUC2* activity was observed in *fry1-6*, with both Col-0 and *fry1-6* exhibiting peak *CCA1::LUC2* activity 2 hours after dawn. A decreased amplitude in peak bioluminescence was observed in *fry1-6*, but this could be due to the smaller size of individual *fry1-6* seedlings compared to Col-0 (Kim and von Arnim, 2009).

4.2.5. Complementation by SAL1 restores F_q'/F_m' rhythms in sal1 mutants

Previous studies have reported complementation of *sal1* morphological phenotypes by *SAL1* cDNA driven either by the CaMV 35S promoter (Kim and von Arnim, 2009; Chen et al., 2011; Hirsch et al., 2011) or the *SAL1* native promoter region (Kim and von Arnim, 2009; Wilson et al., 2009). To determine whether complementation by *SAL1* cDNA under control of the native *SAL1* promoter complements the long circadian period phenotype of a *sal1* mutant, *alx8-1* was transformed with a Gateway pGWB4 (Nakagawa et al., 2007) plasmid construct for expression of a SAL1-GFP fusion under control of the native *SAL1* promoter region (*alx8-1 SAL1::SAL1:GFP*; Appendix II). *F_q'/F_m'* rhythms in homozygous T3 *alx8-1 SAL1::SAL1:GFP* seedlings from three independent lines were monitored under constant blue light. Seedlings were grown on 0.5x MS agar plates and entrained in 12h:12h light:dark cycles under 60 µmol.m^{-2}.s^{-1} white light for 12 days before imaging under 20 µmol.m^{-2}.s^{-1} constant blue light (Figure 4.8). As observed previously (Figure 4.5a and b) *F_q'/F_m'* rhythms in *alx8-1* and Col-0 were robust with RAE<0.3 (Figure 4.8a and b), and a significantly longer period observed in *alx8-1* (24.68 ± 0.25 h) compared to Col-0 (23.54 ± 0.22 h; p<0.001, Student's T-test). This period lengthening of ~1 hour in *alx8-1* was absent in *alx8-1* seedlings expressing *SAL1-GFP* under control of the native *SAL1* promoter.

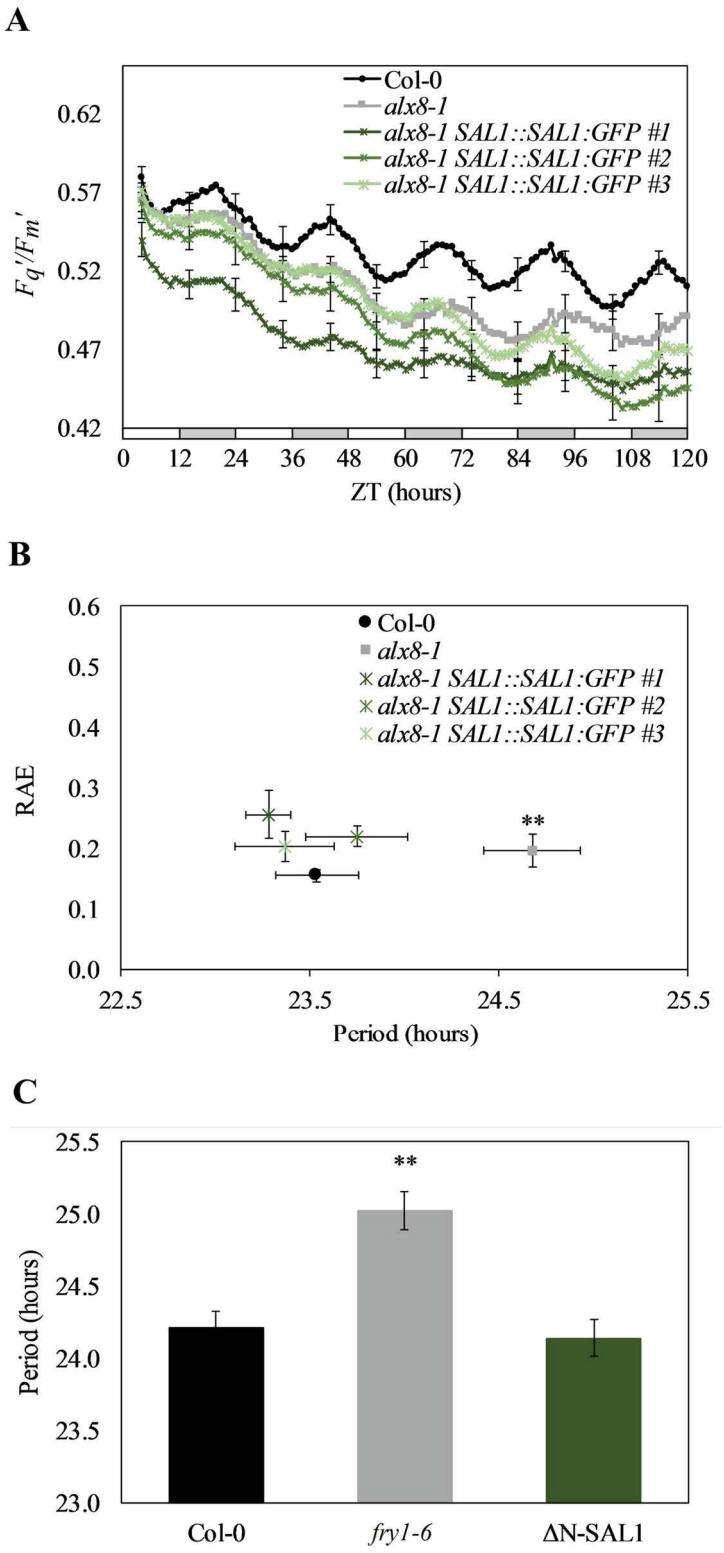

Figure 4.8 F_q'/F_m' rhythms in *sal1* mutants complemented with SAL1 or ΔN-SAL1 under constant blue light. **(A)** Waveforms and **(B)** circadian period estimates plotted against Relative Amplitude Error (RAE) for F_q'/F_m' oscillations in Col-0, *alx8-1* and three independent homozygous *alx8-1 SAL1::SAL1:GFP* lines under constant blue light. **(C)** Circadian period estimates for F_q'/F_m' oscillations in Col-0, *fry1-6* and *fry1-6* expressing SAL1-GFP in the nucleus and cytosol (ΔN-SAL1) under constant blue light. Seedlings were grown on 0.5x MS agar plates and entrained in 12h:12h light:dark cycles under 60 µmol.m^{-2}.s^{-1} white light for 12 days before imaging under 20 µmol.m^{-2}.s^{-1} constant blue light. White bars and grey bars indicate subjective day and subjective night, respectively. Error bars indicate standard error of the mean, with n=8. For waveforms, error bars are shown every 10 hours for clarity. RAE is a measure of rhythmic robustness, with a value of 0 indicating an exact fit to a cosine wave (Plautz et al., 1997). Data from one of three independent experiments are shown. Asterisk indicates statistically significant difference in period compared to Col-0 control (** p<0.001; * p<0.01 Student's T-test).

F_q'/F_m' rhythms were restored in all three independent lines of *alx8-1 SAL1::SAL1::GFP*, with circadian period estimates (23.28 ± 0.12 h for line #1; 23.75 ± 0.27 h for line #2; 23.37 ± 0.26 h for line #3) indicating no significant difference in period length compared to Col-0 (23.54 ± 0.22 h).

Although SAL1 is reported as accumulating and acting in the chloroplasts, targeting of SAL1 to the nucleus and cytosol of *fry1-6* has been shown to decrease PAP levels and result in complementation of *APX2* expression and morphological phenotypes (Kim and von Arnim, 2009; Estavillo et al., 2011). To determine whether SAL1 localised in the nucleus also complements the long period circadian phenotype of *fry1-6*, F_q'/F_m' rhythms were monitored in homozygous *fry1-6* seedlings expressing the cDNA of *SAL1* lacking the nucleotides coding the chloroplastic transit peptide and driven by the CaMV 35S promoter (ΔN-SAL1; Kim and Von Arnim, 2009). Upon complementation with nuclear-localised SAL1, F_q'/F_m' rhythms in *fry1-6* were restored (Figure 4.8c). While circadian period estimates were significantly longer in *fry1-6* (25.02 ± 0.13 h) compared to Col-0 (24.21 ± 0.12 h; $p<0.001$, Student's T-test), there was no significant difference in period length in ΔN-SAL1 seedlings (24.14 ± 0.13 h) compared to Col-0.

4.2.6. Loss of SAL1 function results in a late phase of core clock transcript accumulation under constant blue light

Inhibition of SAL1 activity (whether through oxidative stress or mutation) results in increased transcript levels for numerous plastid redox associated nuclear genes (PRANGs) involved in stress responses (Wilson et al., 2009; Estavillo et al., 2011; Chan et al., 2016a). Since SAL1 activity affects transcript levels of PRANGs, and rhythmic expression of nuclear clock gene *CCA1* is altered in *fry1-6* (Figure 4.7a and b), the effect of SAL1 activity on the accumulation of nuclear clock gene transcripts was analysed using qRT-PCR. Seedlings were grown on 0.5x MS agar plates in 12h:12h light:dark cycles under 60 $\mu mol.m^{-2}.s^{-1}$ white light for 10 days and,

following entrainment, were transferred to 20 µmol.m^{-2}.s^{-1} constant blue light at subjective dawn (ZT0). After 48 hours of free run, 10-12 seedlings per time point were sampled from subjective dawn (ZT48) every 3 hours for two days. Under constant blue light, rhythmic accumulation was observed for the nuclear clock gene transcripts *CCA1* and *LHY* (morning-phased) and *PRR9* and *GI* (evening-phased) in Col-0, *alx8-1* and *fry1-6* (Figure 4.9). A clear late phase (~6 hours) in peak transcript levels was observed for both morning- and evening-phased clock genes in *alx8-1* and *fry1-6* compared to Col-0, corresponding with the long period of rhythmic *CCA1* expression in *fry1-6* (Figure 4.7a and b).

Since delayed fluorescence oscillates with lengthened period in *alx8-1* under constant blue, but not under constant red light (Figure 4.6), the accumulation of clock gene transcripts under constant red light was also examined. Seedlings were entrained as described for Figure 4.9, with plants transferred to 30 µmol.m^{-2}.s^{-1} constant red light following entrainment. qRT-PCR analysis revealed rhythmic transcript accumulation for *CCA1*, *LHY*, *PRR9* and *GI* transcripts in Col-0, *alx8-1* and *fry1-6* (Figure 4.10). A late phase in peak transcript levels was observed for evening-phased clock genes in *alx8-1* and *fry1-6* compared to Col-0, but was less pronounced under constant red light than under constant blue light (~3 hours). Furthermore, the late phase in transcript accumulation of morning-phased components that was observed under constant blue light (Figure 4.9) was much less severe (or absent) in *sal1* seedlings under constant red light. These data corresponded with period estimates for rhythms in delayed fluorescence measured under constant blue and constant red light (Figure 4.6), which indicated period lengthening in *sal1* under constant blue light, but not under constant red. When viewed in combination with the long period of rhythms in F_q'/F_m' (Figure 4.5) and in *CCA1::LUC2* activity (Figure 4.7) observed in *sal1* mutants under constant blue light conditions, it was clear that the long circadian period phenotype of *sal1* less severe (or even absent) under constant red light compared to constant blue light.

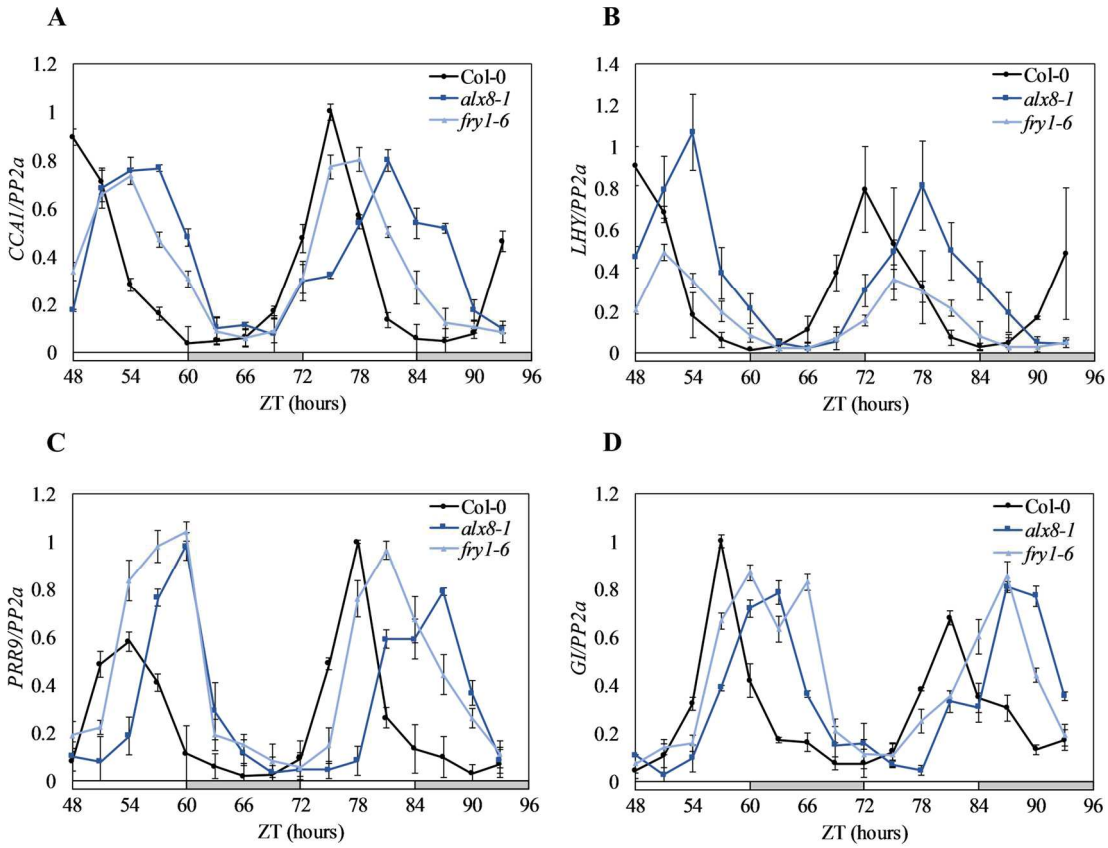

Figure 4.9 Expression of core nuclear circadian clock genes in *sal1* mutants under constant blue light. qRT-PCR analysis of transcript accumulation for morning-phased core clock genes **(A)** *CCA1* and **(B)** LHY, and evening-phased core clock genes **(C)** *PRR9* and **(D)** *GI* in Col-0 and *sal1* mutants *alx8-1* and *fry1-6* under constant blue light. Seedlings were grown on 0.5x MS agar plates and entrained in 12h:12h light:dark cycles under 60 µmol.m^{-2}.s^{-1} white light for 10 days before being transferred to 20 µmol.m^{-2}.s^{-1} constant blue light at subjective dawn. After 48 hours in free-run, 10-12 seedlings were sampled and pooled, with sampling repeated every three hours for two days. Data for each gene were normalised to an internal control (*PP2a*). White bars and grey bars indicate subjective day and subjective night, respectively. Data are the average of three biological replicates. Error bars indicate standard error of the mean.

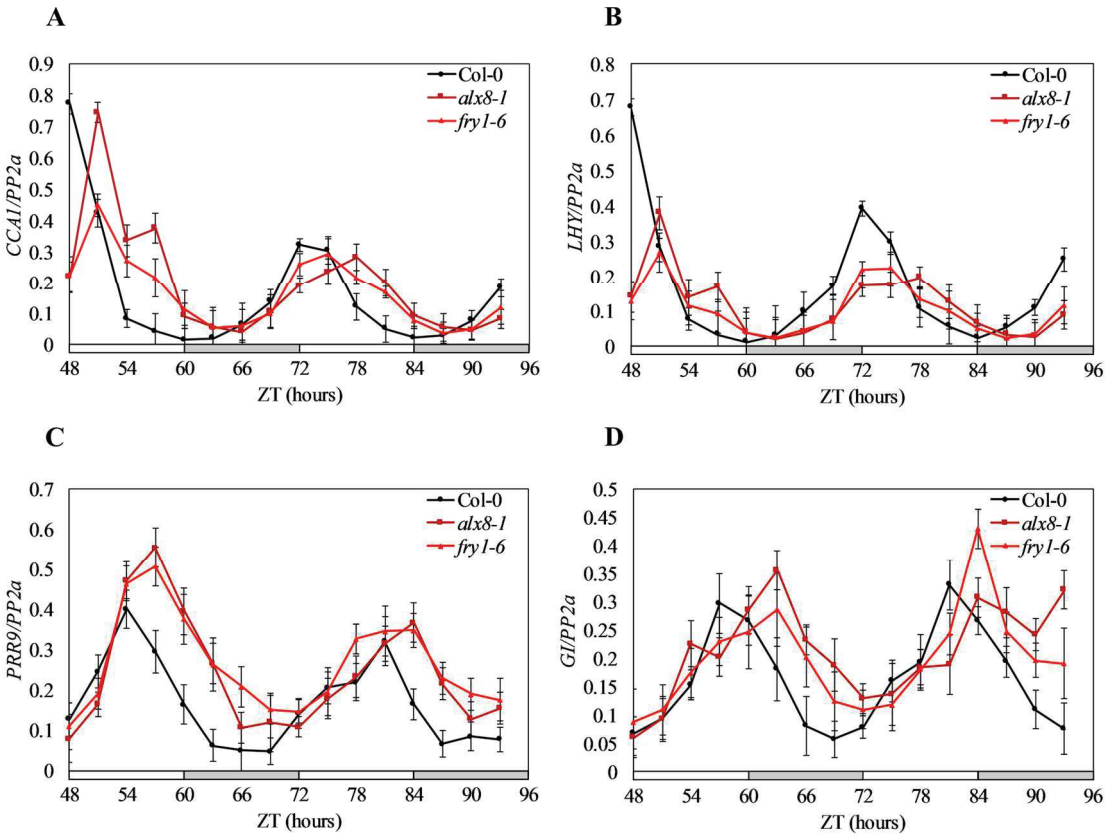

Figure 4.10 Expression of core nuclear circadian clock genes in *sal1* mutants under constant red light. qRT-PCR analysis of transcript accumulation for morning-phased core clock genes **(A)** *CCA1* and **(B)** LHY, and evening-phased clock genes **(C)** *PRR9* and **(D)** *GI* in Col-0 and *sal1* mutants *alx8-1* and *fry1-6* under constant red light. Seedlings were grown on 0.5x MS agar plates and entrained in 12h:12h light:dark cycles under 60 $\mu mol.m^{-2}.s^{-1}$ white light for 10 days before being transferred to 30 $\mu mol.m^{-2}.s^{-1}$ constant blue light at subjective dawn. After 48 hours in free-run, 10-12 seedlings were sampled and pooled, with sampling repeated every three hours for two days. Data for each gene were normalised to an internal control (*PP2a*). White bars and grey bars indicate subjective day and subjective night, respectively. Data are the average of two biological replicates. Error bars indicate standard error of the mean.

The mechanism of circadian regulation of chloroplast function can occur through the activity of nuclear-encoded chloroplast components such as SIG5 and STN7 (Dodd et al., 2014; Belbin et al., 2017). One of the mechanisms through which circadian regulation from the nucleus is communicated to the chloroplasts is through the action of SIGMA FACTOR5 (SIG5) (Noordally et al., 2013). SIG5 is a nuclear-encoded sigma factor that confers promoter specificity to the plastid-encoded plastid RNA polymerase (PEP), thereby regulating the transcription of a specific subset of chloroplast genes (Noordally et al., 2013; Belbin et al., 2017). Another mechanisms through which chloroplast function is regulated by nuclear gene expression is through the action of State Transition 7 (STT7 HOMOLOG, STN7), a protein kinase involved in the phosphorylation of the D1 protein of PSII (Bellafiore et al., 2005; Pesaresi et al., 2009). Transcription of *SIG5* and *STN7* in the nucleus are regulated by the circadian clock (Noordally et al., 2013; Dodd et al., 2014). To determine whether expression of *SIG5* and *STN7* are affected by SAL1 activity, accumulation of *SIG5* and *STN7* transcripts were analysed in *alx8-1* under constant blue light (Figure 4.11). Circadian oscillations in *SIG5* and *STN7* transcript abundance were observed in Col-0 with peak abundance at dawn (Figure 4.11a and b), as has been previously reported (Noordally et al., 2013; Dodd et al., 2014). Oscillations in transcript abundance were also observed in *alx8-1*, with transcripts of *SIG5* and *STN7* accumulating with a similar late phase in peak transcript abundance observed for core clock gene transcripts under constant blue light (Figure 4.9).

4.2.7. Constitutive overexpression of SAL1 has no effect on the rhythmic expression of CCR2 in Col-0 under constant light

Since loss of SAL1 function lengthens circadian rhythms in *sal1* mutants, the effect of SAL1 overexpression on the circadian system in Col-0 was examined. Circadian rhythms were analysed by monitoring rhythmic expression of the clock-regulated RNA-binding protein *CCR2* through luciferase imaging under constant blue light.

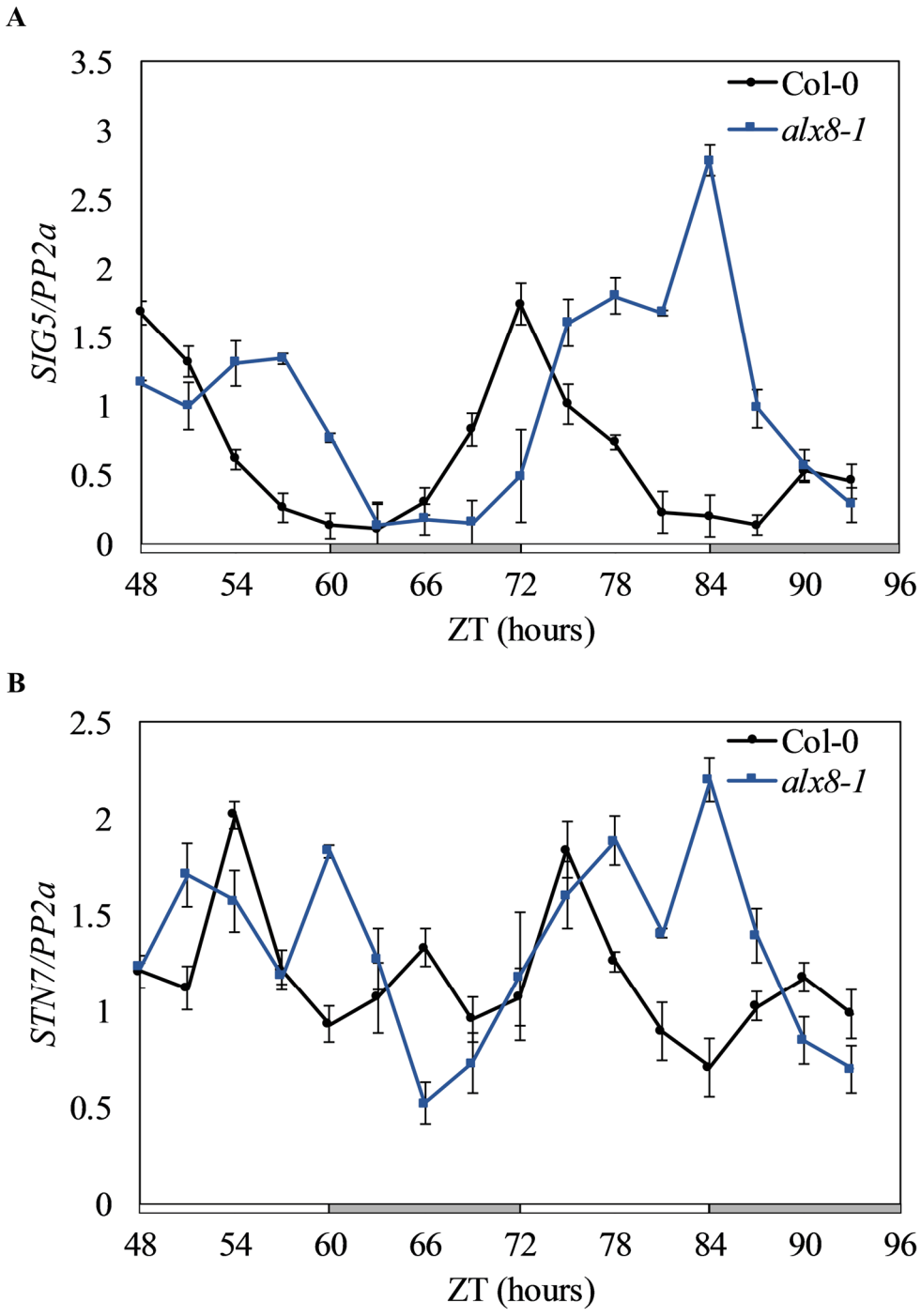

Figure 4.11 Rhythms in expression of *SIG5* and *STN7* in *sal1* mutants under constant blue light. qRT-PCR analysis of transcript accumulation for **(A)** *SIG5* and **(B)** *STN7* in Col-0 and *alx8-1* under constant blue light. Seedlings were grown on 0.5x MS agar plates and entrained in 12h:12h light:dark cycles under 60 µmol.m^{-2}.s^{-1} white light for 10 days before being transferred to 20 µmol.m^{-2}.s^{-1} constant blue light at subjective dawn. After 48 hours in free-run, 10-12 seedlings were sampled and pooled, with sampling repeated every three hours for two days. Data for each gene were normalised to an internal control (*PP2a*). White bars and grey bars indicate subjective day and subjective night, respectively. Data are representative of two biological replicates. Error bars indicate standard error of the mean.

Col-0 expressing the *CCR2::LUC* reporter gene construct (Strayer et al., 2000) was transformed with a pEarlyGate (Earley et al., 2006) plasmid construct for expression of a SAL1-GFP fusion under control of the CaMV 35S promoter (Col-0 *35S::SAL1:*GFP; Col-0 SAL-OX; Appendix II). Luciferase imaging was performed on homozygous T3 seedlings of three independent Col-0 *35S::SAL1:*GFP lines. Seedlings were grown on 0.5x MS agar plates for 6 days in 12h:12h light dark cycle under 60 $\mu mol.m^{-2}.s^{-1}$ white light. Following entrainment, seedlings (in groups of 5-10) were imaged under 20 $\mu mol.m^{-2}.s^{-1}$ constant blue light for ~5 days (Figure 4.12). Bioluminescence from *CCR2::LUC* activity cycled with robust circadian rhythm in Col-0 and Col-0 SAL1-OX (RAE<0.3; Figure 4.12a and b), peaking shortly after dusk as previously described (Martin-Tryon et al., 2006). No shift in peak *CCR2::LUC* activity was observed in Col-0 SAL1-OX across all 5 days of free run (Figure 4.12a). Circadian parameter estimates determined for *CCR2::LUC* rhythms revealed no significant difference in RAE or period in Col-0 SAL1-OX compared to Col-0 (Figure 4.12b), with *CCR2::LUC* rhythms oscillating with circadian period in Col-0 (23.71 ± 0.06 h), Col-0 SAL1-OX #1 (23.71 ± 0.10 h), Col-0 SAL1-OX #2 (23.73 ± 0.05 h) and Col-0 SAL1-OX #3 (23.93 ± 0.06 h).

4.3. Discussion

4.3.1. SAL1 protein accumulates in chloroplasts, and SAL expression is not a rhythmic clock output

Arabidopsis SAL1 is expressed ubiquitously in most plant organs (Xiong et al., 2001; Chen et al., 2011; Hirsch et al., 2011), and loss of function results in a range of morphological phenotypes, including slowed growth, altered leaf and root morphology, and hypersensitivity to light (Figure 4.1a, b and c; Gy et al., 2007; Kim and Von Arnim, 2009; Hirsch et al., 2011). The subcellular localisation of SAL1 has been a subject of debate.

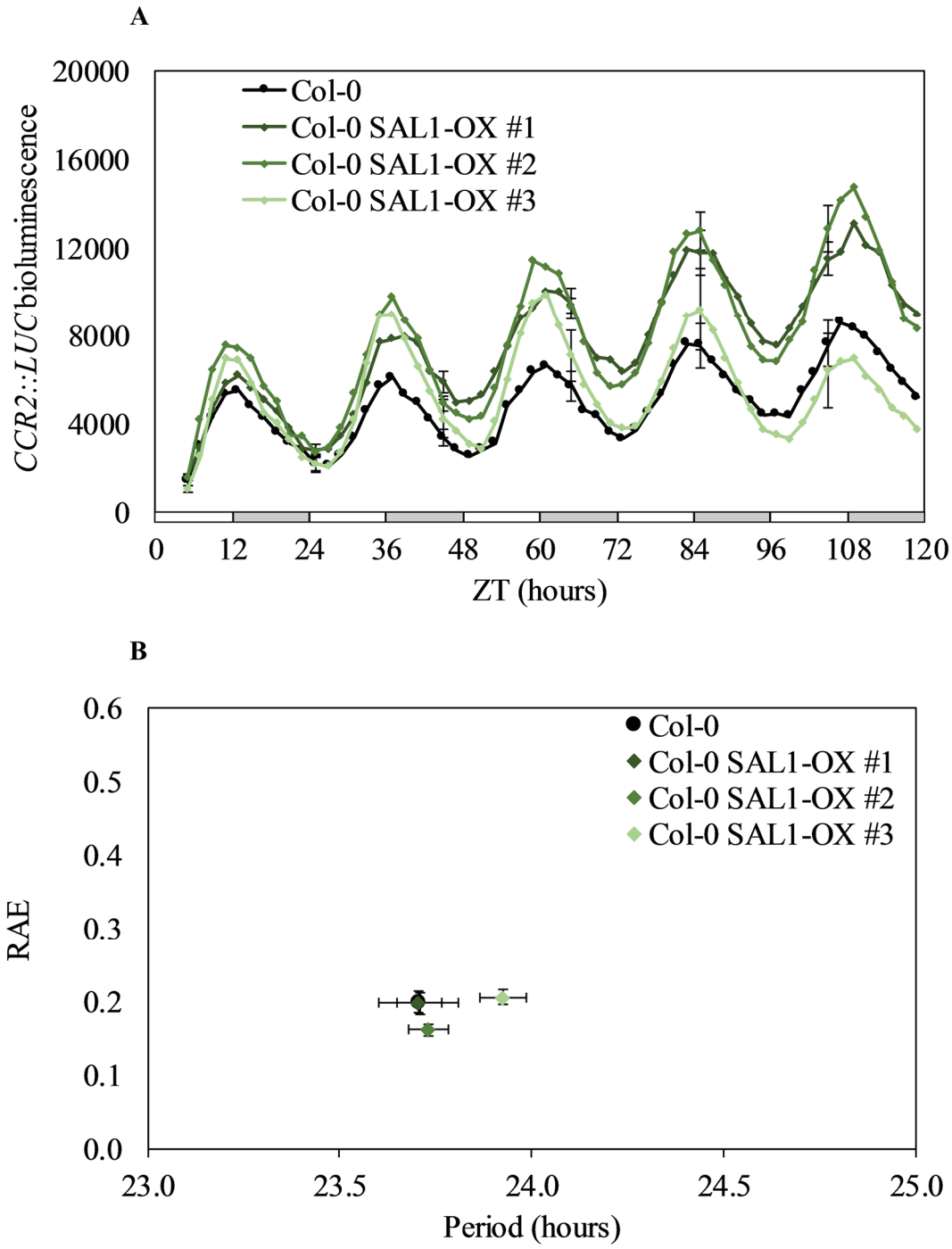

Figure 4.12 Rhythms in *CCR2* expression in Col-0 SAL1-OX lines under constant blue light. **(A)** Waveforms and **(B)** circadian period estimates plotted against Relative Amplitude Error (RAE) of *CCR2::LUC* luciferase activity monitored in Col-0 and three independent Col-0 SAL1-OX lines under constant blue light. Seedlings (in groups of 5-10) were grown on 0.5x MS agar plates and entrained in 12h:12h light:dark cycles under 60 µmol.m^{-2}.s^{-1} white light for 6 days before imaging under 20 µmol.m^{-2}.s^{-1}.constant blue light. White and grey bars indicate subjective day and subjective night, respectively. Error bars indicate standard error of the mean, with n=10. For waveforms, error bars shown every 10 hours for clarity. RAE is a measure of rhythmic robustness, with a value of 0 indicating an exact fit to a cosine wave (Plautz et al., 1997). Data from one of two independent experiments are shown.

Mass spectrometry analysis of the *Arabidopsis* stromal proteome identified SAL1 as a chloroplast-localised protein (Peltier, 2005), and transient expression of a SAL1 fused at the C-terminus with GFP (SAL1-GFP) in onion epidermal cells identified SAL1 as being present in the chloroplasts (Rodriguez et al., 2010). Reports of expression of SAL1-GFP fusion in stable *Arabidopsis* lines revealed localization to the cytoplasm (Zhang et al., 2011) or plastids (Chen et al., 2011) of roots, as well as to chloroplasts and unidentified small organelles (Chen et al., 2011). A tripartite approach to establishing the subcellular localization of SAL1 involving both stable and transient transformation of *Arabidopsis* using SAL1-GFP fusion, as well as immunological detection of native SAL1 protein in purified chloroplastic and mitochondrial fractions of Col-0 leaves, revealed accumulation of the SAL1 protein in chloroplasts and mitochondria (Estavillo et al., 2011). Through this method, no SAL1 protein was detected in the cytosolic fraction or in nuclei. Furthermore, expression of SAL1 without the N-terminal signal peptide results in localization to the cytosol and nuclei (Kim and von Arnim, 2009; Chen et al., 2011). In this chapter, stable expression of a SAL1-GPF fusion in *alx8-1* revealed localisation of SAL1-GFP in both the chloroplasts and the cytosol (Figure 4.4). However, these data must be interpreted with caution, as it is not clear whether *SAL1* is overexpressed or over-accumulates in the transgenic lines used. Indeed, the observations in this study further demonstrate the need for a combined approach in determining the subcellular localisation of proteins (Estavillo et al., 2011). *SAL1* transcript abundance exhibits no rhythm under constant white light and a modest rhythm under dark:light cycles, with transcript levels increasing throughout the day and peaking at dusk under long-day conditions (Figure 4.2). Despite this pattern in *SAL1* transcript accumulation, there is no rhythm in SAL1 protein accumulation under long-day conditions (Figure 4.3).

4.3.2. SAL1 activity affects the circadian system under constant blue light

Although SAL1 expression is not regulated by the circadian system, activity of SAL1 affects circadian rhythms in chloroplasts. In *sal1* mutants, loss of SAL1 activity lengthens the period

of F_q'/F_m' and delayed fluorescence rhythms under constant blue light (Figure 4.5 and 4.6). This long period circadian phenotype of *sal1* mutants appears to be limited to blue light, as a lengthening in period of delayed fluorescence rhythms is not observed in a *sal1* mutant under constant red light (Figure 4.6). These data are in contrast with a previous study which reported that *sal1* mutants exhibit shortened hypocotyls both under constant blue and constant red light (Figure 4.1d; Kim and Von Arnim, 2009).

The long period in rhythmic expression of the nuclear clock gene *CCA1* under constant blue light (Figure 4.7a and b) indicates that the altered chloroplast rhythms in *sal1* mutants are not merely a direct result of SAL1 activity in chloroplasts, and that the effect of SAL1 activity on circadian rhythms is not limited to these organelles. Indeed, expression of *SAL1* targeted either to the plastids (Figure 4.8a and b) or to the nucleus and cytosol (ΔN-SAL1; Figure 4.8c) of a *sal1* mutant restores rhythms in F_q'/F_m', confirming that activity of SAL1 in either the chloroplasts or nucleus complements the *sal1* phenotype as previously reported (Estavillo et al., 2011). The effect of SAL1 activity on nuclear clock components is not limited to *CCA1* promoter activity. Analysis of transcript accumulation in *sal1* mutants indicated a late phase in peak transcript accumulation for both morning-phased (*CCA1* and *LHY*) and evening-phased (*PRR9* and *GI*) clock transcripts under constant blue light (Figure 4.9), corresponding to the long period in F_q'/F_m' (Figure 4.5), delayed fluorescence (Figure 4.6) and *CCA1::LUC2* rhythms (Figure 4.7a and b) observed under constant blue light. As had been observed for rhythms in delayed fluorescence (Figure 4.6), these altered circadian rhythms in transcript accumulation in *sal1* are a blue light-specific phenotype. A less severe phase shift in peak transcript accumulation is observed for evening-phased core clock transcripts in *sal1* mutants grown under constant red light compared to constant blue light, while no late phase is observed for accumulation of transcripts of morning-phased clock genes (Figure 4.10). Interestingly, *CCA1* promoter activity is only affected in *sal1* mutants under free-run (constant blue light), with no effect of SAL1 activity on patterns of *CCA1* expression under entraining conditions (Figure 4.6b). These data suggest a need for further analysis of the effect of SAL1 activity on

circadian rhythms under different light qualities and regimes, which will be discussed in Chapter 6.

4.3.3. The effect of SAL1 on nuclear circadian rhythms suggests involvement of an interorganellar signalling mechanism

Since the chloroplast-localised SAL1 enzyme affects circadian rhythms not only in chloroplasts but also in the nucleus, the involvement of communication between these two organelles must be investigated. Rhythms in chloroplasts, as monitored through delayed fluorescence and chlorophyll *a* fluorescence, are regulated by the rhythmic expression of clock-regulated genes in the nucleus (Chapter 3; Gould et al., 2009; Litthauer et al., 2015). Numerous pathways that facilitate communication between chloroplasts and the nucleus have been described, and the SAL1/PAP pathway does not function in isolation (Chan et al., 2016b). Two of these mechanisms, involving activity of nuclear-encoded chloroplast components SIG5 and STN7, have been implicated in circadian regulation of chloroplast function from the nucleus (Noordally et al., 2013; Belbin et al., 2017; Dodd et al., 2014). In *sal1* mutants, a late phase in transcript accumulation is observed for *SIG5* and *STN7* (Figure 4.11), which corresponds to the late phase in core clock transcripts and long period phenotypes observed in *sal1*. This indicates that signalling via SIG5 and STN7 remains intact and under circadian control in *sal1* mutants, and suggests that these mechanisms are not directly involved in the *sal1* circadian phenotype.

It has been reported that neither *SAL1* transcript levels (Xiong et al., 2001) nor SAL1 protein levels (Chan et al., 2016a) change significantly in response to abiotic stress. Previous reports have shown that overexpression of SAL1 under control of the 35S promoter in Col-0 has no effect on salt stress tolerance in plants (Chen et al., 2011), which corresponds with the observation in the current study that constitutive overexpression of SAL1 in Col-0 had no effect on the period or amplitude of rhythms in *CCR2::LUC* activity (Figure 4.12). SAL1 exhibits high enzymatic activity both as pure protein and in plant cell extracts (Quintero et al., 1996;

Chen et al., 2011; Chan et al., 2016a), and the sensitivity of SAL1 activity to oxidising environments implies allosteric regulation of SAL1 activity via the redox poise of the plastid (Chan et al., 2016a). These findings suggest that allosteric regulation of SAL1 activity plays a more important role than SAL1 protein levels in mediating function *in vivo*. Indeed, while SAL1 protein is not expressed with a clear diurnal rhythm (Figure 4.2 and 4.3), the time-of-day-specific oscillations of ROS production and scavenging, along with the diurnal and circadian regulation of ROS-responsive genes (Lai et al., 2012), could provide a mechanism through which SAL1 acts within the circadian system.

This chapter has demonstrated that the chloroplast-localised enzyme SAL1 acts within the *Arabidopsis* circadian system, influencing rhythms in chloroplasts and the nucleus. Since SAL1 has been described as modulating the activity of both the XRN family of exoribonucleases and sulfur metabolism (Rodriguez et al., 2010; Chen et al., 2011; Estavillo et al., 2011; Lee et al., 2012), the mechanism through which SAL1 acts within the circadian system will be further investigated in Chapter 5.

Chapter 5

The effect of 5'→3' exoribonuclease (XRN) activity on circadian rhythms

5.1. Introduction

Circadian regulation is in part achieved through the rhythmic modulation of gene expression, and the processing of mRNA plays an important role in the circadian system (Millar, 2016; Nolte and Staiger, 2015). In *Arabidopsis,* SAL1 activity has been shown to affect sulfur metabolism (Rodriguez et al., 2010; Lee et al., 2012), as well as the function of 5'→3' exoribonucleases (XRNs) (Gy et al., 2007; Estavillo et al., 2011; Kurihara et al., 2012). Indeed, redox regulation of SAL1 has been proposed as a metabolic mechanism through which both sulfur assimilation and nuclear gene expression can be controlled (Chan et al., 2016a, 2016b). To further understand the mechanism through which SAL1 influences circadian rhythms, this chapter investigates the role of altered sulfur metabolism and XRN activity in the circadian system.

5.2. Results

5.2.1. Sulfate deficiency does not cause lengthening of circadian period

Sulfur is an element essential to plant growth and survival, and total loss of sulfur assimilation is lethal to plants (Mugford et al., 2010). In nature, sulfur is most commonly present in its most oxidised form as sulfate (SO_4^{2-}) (Kopriva et al., 2012; Takahashi et al., 2011). The influx of sulfate into plant cells occurs against the gradient of membrane potential and is facilitated through plasma membrane-bound high-affinity sulfate transporters (SULTR; Figure 5.1a).

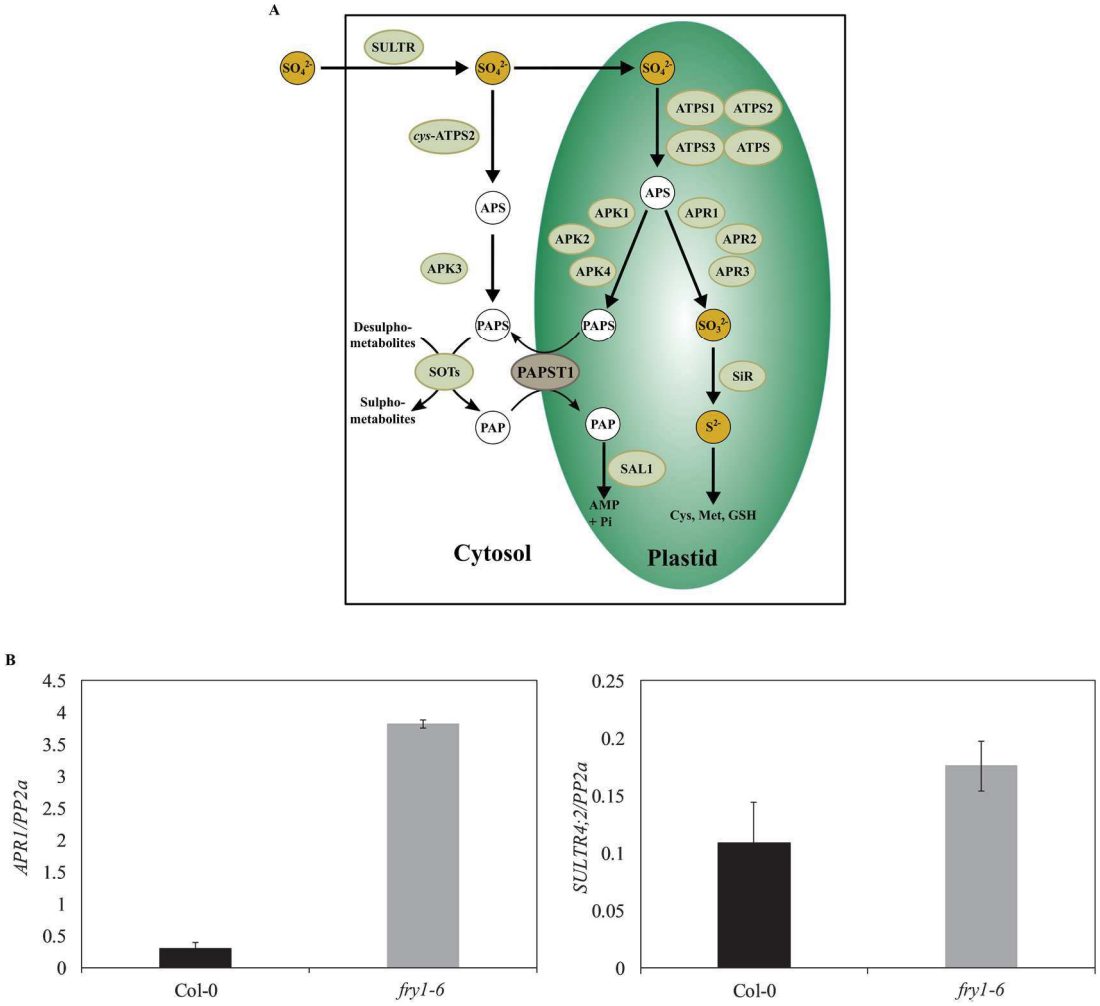

Figure 5.1 Sulfur metabolism in *sal1* mutants. (A) Schematic representation of sulfur metabolism in *Arabidopsis* (Takahashi et al., 2011). Uptake of sulfate (SO_4^{2-}) through the activity of sulfate transporters (SULTR), and subsequent activation of sulfate through synthesis of adenosine 5'-phosphosulfate (APS) by the activity of ATP sulfurylases in the cytoplasm (*cyt*-ATPS) and plastid (ATPS) are shown. Branching to primary sulfur metabolism occurs through the activity of APS reductase (APR) in plastids and the formation of sulfite (SO_3^{2-}). Subsequent reduction to sulfide (S^{2-}) by sulfite reductase (SiR) allows assimilation into cysteine (Cys), methionine (Met) and glutathione (GSH). Secondary sulfur metabolism occurs in plastids and the cytosol through activity of APS kinase (APK) and the formation of 3'-phosphoadenosine-5'-phosphosulfate (PAPS). In the cytoplasm, sulfotransferases (SOT) catalyse sulfation reactions, producing 3'-phosphoadenosine-5'-phosphate (PAP) as byproduct. PAPS transporter 1 (PAPST1) allows movement of PAPS and PAP between cytosol and plastid. SAL1 acts in the plastid to prevent accumulation of PAP. **(B)** Transcript levels for *APR1* (left) and *SULTR4;2* (right) in Col-0 and *fry1-6* in non-sulfate-limiting conditions. Seedlings were grown on 0.5x MS media for 12 days in 12h:12h light:dark cycles under 60 µmol.m^{-2}.s^{-1} white light. Data for each gene were normalised to an internal control (*PP2a*). Error bars indicate standard error of the mean for three technical replicates.

Plants contain four distinct subfamilies of SULTR-type sulfate transporters, bound to the plasma membrane (SULTR1, SULTR2 and SULTR3) and localised in the tonoplast (SULTR4) (Takahashi et al., 2012). Once absorbed, sulfate can be used directly for assimilation or transported into the vacuole for storage (Kopriva et al., 2012). Sulfate is highly stable, and must be activated before assimilation can occur (Kopriva et al., 2012; Takahashi et al., 2011). This is achieved by replacing the pyrophosphate in ATP with sulfate, resulting in adenosine 5'-phosphosulfate (APS) through a reaction catalysed by ATP sulfurylase (ATPS, Figure 5.1a). APS serves as a branching point between primary and secondary sulfate metabolism, with primary metabolites (such as cysteine, methionine, glutathione and co-enzymes) containing the reduced form of sulfur (sulfide or thiol), and secondary metabolites (such as glucosinolates) utilising oxidised sulfur. In the primary assimilation pathway occurring in plastids and chloroplasts, APS is reduced to sulfite (SO_3^2) by APS reductase (APR; Figure 5.1a), which is in turn reduced to sulfide (S^{2-}) by ferredoxin-dependent sulfite reductase (SiR; Figure 5.1a). Sulfide is the form of reduced sulfur incorporated to form cysteine, the first product of primary sulfate assimilation. Cysteine can be used for peptide synthesis, or as a reduced sulfur donor for the biosynthesis of methionine and a large range of co-enzymes and co-factors, including glutathione (GSH). Alternatively, APS can be utilised for secondary sulfur metabolism via phosphorylation by APS kinase (APK; Figure 5.1a) to 3'-phosphoadenosine 5'-phosphosulfate (PAPS). Formation of PAPS occurs mainly through the action of three plastid-localised APK isoforms (APK1, APK2 and APK3), and to a lesser extent in the cytosol through the action of APK3 (Mugford et al., 2009). In the cytosol, PAPS acts as an active sulfate donor for the incorporation of sulfur into a variety of secondary metabolites through sulfation reactions (the transfer of the functional sulfo group to hydroxylated substrates), which is catalysed by sulfotransferases (SOT). The resulting by-product, 3'-phosphoadenosine 5'-phosphate (PAP), is hydrolysed through the activity of SAL1 in chloroplasts, with the movement of PAPS and PAP between plastid and cytosol possibly facilitated by the transporter PAPST1 (Klein and Papenbrock, 2004; Mugford et al., 2009; Gigolashvili et al., 2012).

In the *sal1* mutant allele *fou8*, loss of SAL1 function has been reported to result in lower levels of internal sulfate and gene expression patterns similar to Col-0 plants subjected to sulfate deficiency, even when external sulfate is available (Lee et al., 2012). To confirm the sulfur-deficient phenotype of *sal1* mutants, transcript levels of the plastid-localised APR isoform *APR1* and the tonoplast-localised sulfate transporter *SULTR4;2* were determined in Col-0 and *fry1-6* seedlings in non-sulfate-limiting conditions using qRT-PCR (Figure 5.1b). Both *APR1* and *SULTR4;2* are nuclear-encoded genes for which expression is upregulated in response to sulfur depletion (Nikiforova et al., 2003; Kataoka et al., 2004), and which do not exhibit circadian rhythms in transcript abundance under constant light conditions (Covington and Harmer, 2007). Seedlings were grown on 0.5x MS agar plates for 12 days in 12h:12h light:dark cycles under 60 $\mu mol.m^{-2}.s^{-1}$ white light before harvesting in the late afternoon. Elevated levels of both *APR1* and *SULTR4;2* were observed in *fry1-6* seedlings grown on 0.5x MS agar plates, which corresponds to the upregulation of sulfur starvation-responsive genes previously reported in 5-week old soil-grown *fou8* plants (Lee et al., 2012).

In *Arabidopsis* seedlings, iron (Fe^{2+}) deficiency has been shown to increase circadian period under constant light conditions, while neither the absence nor excess of zinc (Zn^{2+}), copper (Cu^{2+}) or manganese (Mn^{2+}) has any effect on free-running circadian period (Salomé et al., 2012). To determine whether the long period circadian phenotype of *sal1* could be as a result of sulfate deficiency, circadian rhythms in plants grown on sulfate-deficient media were analysed. For experimental controls, MS media was prepared according to the composition for MS basal media, and sulfate-deficient media prepared by replacing all sulfates with chlorides (see Section 2.1.1). qRT-PCR analysis of *APR1* and *SULT4;2* transcript levels was performed to confirm that seedlings grown on sulfate-deficient media were indeed experiencing sulfate starvation. Col-0 and *alx8-1* seedlings were grown on 0.5x MS and 0.5x MS-sulfate agar plates for 12 days in 12h:12h light:dark cycles under 60 $\mu mol.m^{-2}.s^{-1}$ white light before harvesting in the late afternoon. As has been observed for *fou8* (Lee et al., 2012) and *fry1-6* (Figure 5.1b), *alx8-1* seedlings grown in the presence of sulfate exhibited elevated levels of *APR1* and

SULTR4;2 transcripts compared to Col-0 (Figure 5.2a and b). In addition, *APR1* and *SULTR4;2* transcript levels were elevated in both Col-0 and *alx8-1* seedlings grown on MS-sulfate media compared to seedlings grown on control MS media, indicating that growth on MS-sulfate agar plates results in sulfate deficiency stress gene responses (Nikiforova et al., 2003; Kataoka et al., 2004).

With the efficacy of the MS-sulfate media to induce sulfate deficiency stress confirmed, chlorophyll *a* fluorescence imaging was used to analyse circadian rhythms in Col-0 and *alx8-1* grown on sulfate-deficient media under constant blue light. Seedlings were grown on 0.5x MS or 0.5x MS-sulfate agar plates for 12 days in 12h:12h light:dark cycles under 60 $\mu mol.m^{-2}.s^{-1}$ white light before imaging under 20 $\mu mol.m^{-2}.s^{-1}$ constant blue light for ~5 days (Figure 5.2c and d). FFT-NLLS analysis was performed on time series data using BRASS (Millar et al., 2010). As had been observed for seedlings grown on commercially-available 0.5x MS media (Section 4.2.3), F_q'/F_m' fluctuations cycled with robust circadian rhythm in both Col-0 and *alx8-1* seedlings grown on control plates, with *alx8-1* exhibiting a significantly longer period in F_q'/F_m' fluctuations (25.03 ± 0.23 h) compared to Col-0 (23.12 ± 0.25 h; $p<0.001$, Student's T-test). Under sulfate deficient conditions, F_q'/F_m' rhythms remained robust in both Col-0 and *alx8-1*. Although a loss of amplitude in F_q'/F_m' rhythms was observed in *alx8-1* towards the end of the ~5 days free run (Figure 5.2c), no significant difference in RAE was observed in either Col-0 or *alx8-1* under sulfate-deficient conditions compared to control conditions (Figure 5.3d). Circadian period estimates for F_q'/F_m' rhythms revealed a shortening of period in both Col-0 (22.73 ± 0.17 h) and *alx8-1* (24.35 ± 0.30 h) seedlings grown without sulfate compared to their counterparts grown on control media, although this difference in period was not statistically significant (Figure 5.2d). Despite the shortening in period, *alx8-1* seedlings exhibited a longer period in F_q'/F_m' rhythms compared to Col-0 even when grown in the absence of sulfate ($p<0.01$, Student's T-test).

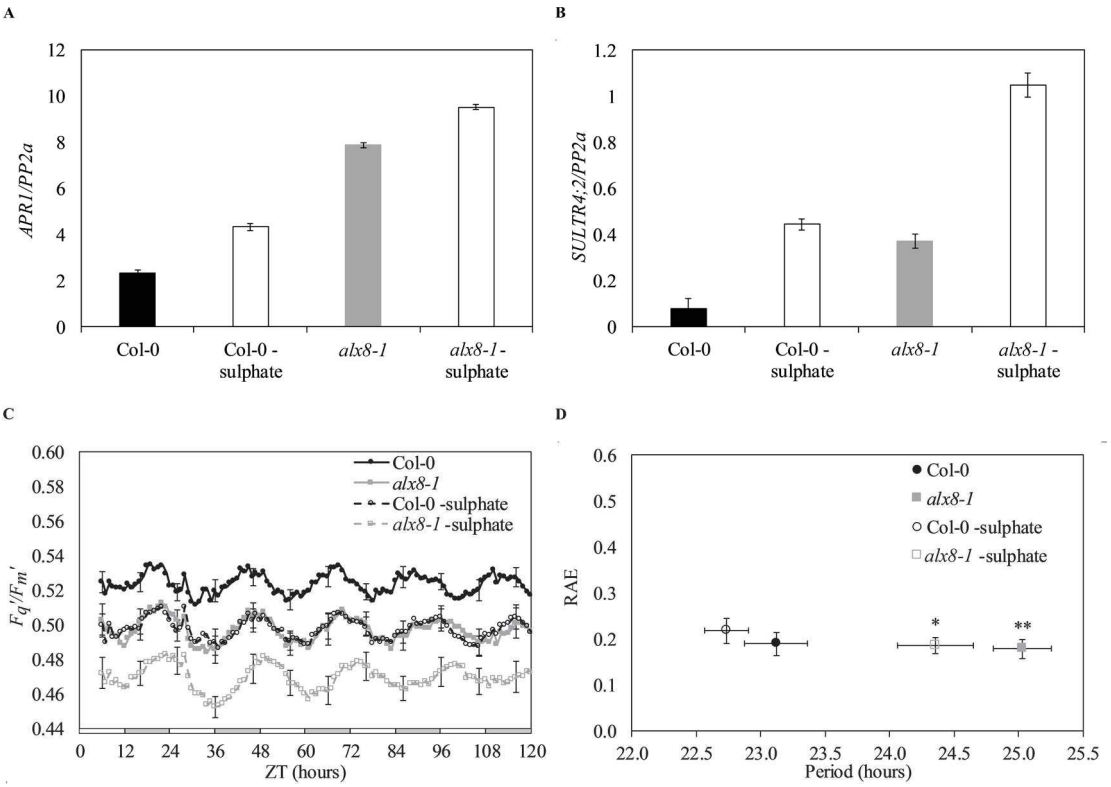

Figure 5.2 Chloroplast rhythms in *sal1* grown under sulfate starvation conditions. (A) Transcript levels for *APR1* and **(B)** *SULTR4;2* in Col-0 and *alx8-1* grown in sulfate-deficient and non-sulfate-deficient control conditions. Seedlings were grown on 0.5x MS or 0.5x MS-sulfate agar plates for 12 days in 12h:12h light:dark cycles under 60 $\mu mol.m^{-2}.s^{-1}$ white light. Data for each gene were normalised to an internal control (*PP2a*). Error bars indicate standard error of the mean for three technical replicates. **(C)** Waveforms and **(D)** circadian period estimates plotted against Relative Amplitude Error (RAE) for F_q'/F_m' oscillations in Col-0 and *alx8-1* grown in sulfate-deficient and non-sulfate-deficient control conditions under constant blue light. Seedlings were grown on 0.5x MS or 0.5MS-sulfate agar plates and entrained in 12h:12h light:dark cycles under 60 $\mu mol.m^{-2}.s^{-1}$ white light for 12 days before imaging under 20 $\mu mol.m^{-2}.s^{-1}$ constant blue light. White bars and grey bars indicate subjective day and subjective night, respectively. Error bars indicate standard error of the mean, with n=8. For waveforms, error bars are shown every 10 hours for clarity. RAE is a measure of rhythmic robustness, with a value of 0 indicating an exact fit to a cosine wave (Plautz et al., 1997). Data from one of three independent experiments are shown. Asterisks indicate statistically significant difference in period compared to Col-0 grown on the comparative medium (** $p<0.001$; * $p<0.01$ Student's T-test).

Since no lengthening in chloroplast rhythms was induced in either Col-0 or *sal1* under sulfate-deficient conditions, the effect of sulfate deficiency on nuclear rhythms was examined by monitoring rhythms in *CCA1* expression under constant blue light. Col-0 *CCA1::LUC2* and *fry1-6 CCA1::LUC2* seedlings were grown on 0.5x MS or 0.5x MS-sulfate agar plates for 12 days in 12h:12h light dark cycle under 60 µmol.m^{-2}.s^{-1} white light, and subsequently imaged under 20 µmol.m^{-2}.s^{-1} constant blue light for ~5 days. As had been observed for F_q'/F_m' rhythms (Figure 5.2c and d), bioluminescence from *CCA1::LUC2* activity cycled with robust circadian rhythm in both Col-0 and *fry1-6* grown on control 0.5x MS plates (Figure 5.3a and b). *CCA1::LUC2* activity peaked shortly after dawn as previously described (Jones et al., 2015), with circadian period estimates determined for *CCA1::LUC2* rhythms (Figure 5.3b) significantly longer in *fry1-6* (26.31 ± 0.10 h) than in Col-0 (24.70 ± 0.11 h; p<0.001, Student's T-test). No effect on amplitude was observed in Col-0 or *fry1-6* grown on sulfate-deficient media (Figure 5.3a). In addition, sulfate deficiency had no effect on period of *CCA1::LUC2* rhythms in Col-0 grown under sulfate-limited conditions, yet shortening of period was observed in *fry1-6* plants grown in sulfate-deficient conditions compare to control conditions (Figure 5.3b). Despite the shortening of period under sulfate deficiency, period of *CCA1::LU2* rhythms remained significantly longer in *fry1-6* (25.57 ± 0.08 h) than in Col-0 (24.76 ± 0.11 h; p<0.001, Student's T-test).

As sulfate deficiency had no effect on rhythms in *CCA1* expression in Col-0, the effect of sulfate deficiency on the expression of other nuclear clock genes was investigated using various luciferase reporter lines. Col-0 expressing the luciferase reporter constructs *CAB2::LUC*, *CCR2::LUC*, *LHY::LUC, PRR7::LUC* or *TOC1::LUC* were grown on 0.5x MS or 0.5x MS-sulfate agar plates for 12 days in 12h:12h light dark cycle under 60 µmol.m^{-2}.s^{-1} white light, and subsequently imaged under 20 µmol.m^{-2}.s^{-1} constant blue light for ~5 days. While a shortening of period was observed in *CAB2::LUC* and *CCR2::LUC* in Col-0 grown without sulfate compared to controls, these differences in period were not significant (Figure 5.3c).

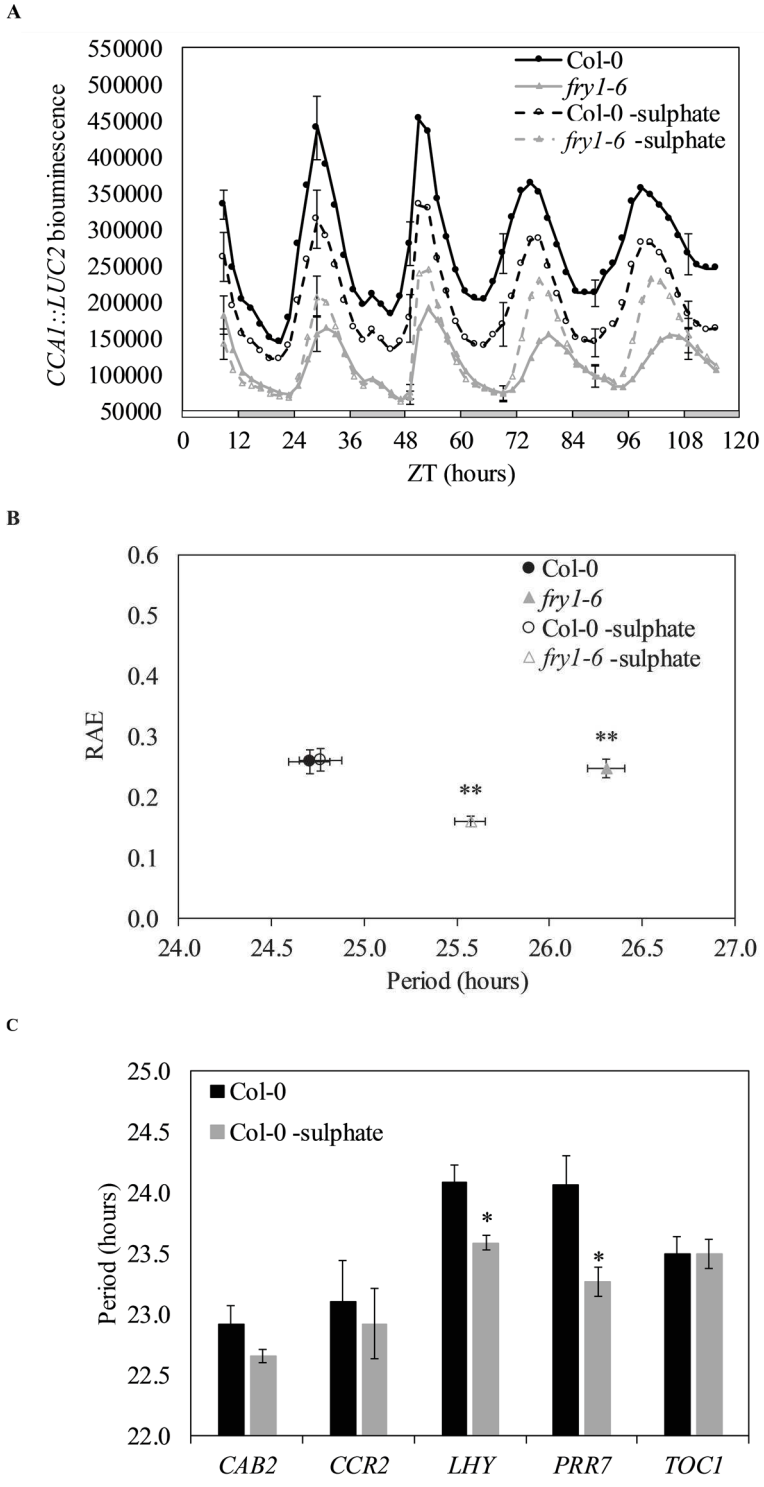

Figure 5.3 Nuclear circadian rhythms in Col-0 and *sal1* grown under sulfate starvation conditions. (A) Waveforms and **(B)** circadian period estimates plotted against Relative Amplitude Error (RAE) for luciferase activity monitored in Col-0 *CCA1::LUC2* and *fry1-6 CCA1::LUC2* seedlings under constant blue light grown under sulfate-deficient and control conditions. **(C)** Period estimates of *CAB2::LUC*, *CCR2::LUC*, *LHY::LUC*, *PRR7::LUC* and *TOC1::LUC* activity in Col-0 grown under sulfur-deficient and control conditions under constant blue light. Seedlings were grown on 0.5x MS or 0.5x MS-sulfate agar plates and entrained in 12h:12h light:dark cycles under 60 $\mu mol.m^{-2}.s^{-1}$ white light for 12 days before imaging under 20 $\mu mol.m^{-2}.s^{-1}$ constant blue light. White bars and grey bars indicate subjective day and subjective night, respectively. Error bars indicate standard error of the mean, with n=10. For waveforms, error bars shown every 10 hours for clarity. RAE is a measure of rhythmic robustness, with a value of 0 indicating an exact fit to a cosine wave (Plautz et al., 1997). Data from one of three independent experiments are shown. Asterisks indicate statistically significant difference in period compared to Col-0 grown on comparative medium (** $p<0.001$; * $p<0.01$ Student's T-test).

However, rhythms in *LHY::LUC* and *PRR7::LUC* were significantly shorter in plants grown in sulfate-deficient media compared to controls (p<0.01; Student's T-test). As had been observed for *CCA1::LUC2* rhythms, no effect on circadian period was observed in *TOC1::LUC* rhythms under sulfate deficiency. Such data suggest that sulfate deficiency may shorten the circadian period reported by specific promoters, although additional work will be necessary to assess this possibility.

5.2.2. Plants with impaired secondary sulfur metabolism do not have a lengthened circadian period

Since total removal of sulfate from media is not an accurate representation of the altered sulfur metabolism observed in *sal1* mutants (Rodriguez et al., 2010; Lee et al., 2012), the effect of impaired secondary sulfur metabolism on circadian rhythms was examined. The *apk1 apk2* double mutant lacks the plastid-localised APS kinase APK1 and APK2 activities, and is inhibited in the production of PAPS (Mugford et al., 2009). The *apk1 apk2* mutant exhibits smaller rosette size and lower levels of aliphatic glucosinolates and sulfated jasmonate, higher levels of the desulfo-precursors of glucosinolates and upregulation of genes involved in glucosinolate synthesis – all phenotypes associated with the *sal1* mutant allele *fou8* (Mugford et al., 2009; Rodriguez et al., 2010; Lee et al., 2012). In addition, introduction of the *fou8* mutation into the *apk1 apk2* mutant background does not rescue these phenotypes, with the *apk1 apk2 fou8* triple mutant exhibiting low levels of aliphatic glucosinolates, higher levels of desulfo- glucosinolate precursors and enhanced glucosinolate synthesis gene expression similar to *apk1 apk2* (Lee et al., 2012). To determine whether impaired secondary metabolism influences circadian rhythms, rhythms in F_q'/F_m' were monitored in Col-0, *fou8, apk1 apk2* and *apk1 apk2 fou8* seedlings under constant blue light. Seedlings were grown on 0.5x MS agar plates for 12 days in 12h:12h light:dark cycles under 60 $\mu mol.m^{-2}.s^{-1}$ white light before imaging under 20 $\mu mol.m^{-2}.s^{-1}$ constant blue light for ~5 days (Figure 5.4a and b).

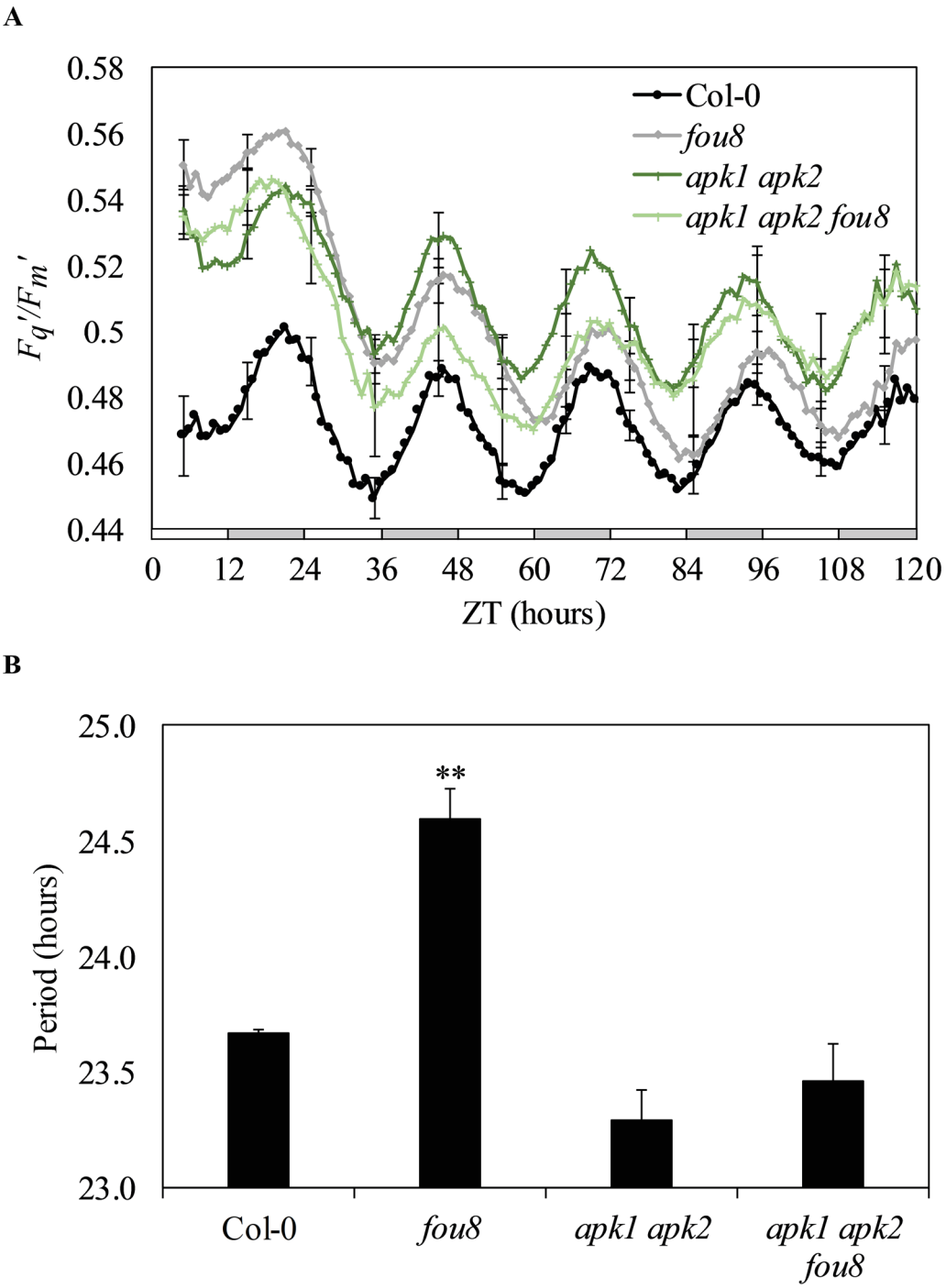

Figure 5.4 Chloroplast rhythms in seedlings deficient in secondary sulfur metabolism under constant blue light. **(A)** Waveforms and **(B)** circadian period estimates plotted against Relative Amplitude Error (RAE) for *F_q'/F_m'* oscillations in Col-0, *fou8, apk1 apk2* and *apk1 apk2 fou8* under conditions under constant blue light. Seedlings were grown on 0.5x MS agar plates and entrained in 12h:12h light:dark cycles under 60 µmol.m^{-2}.s^{-1} white light for 12 days before imaging under 20 µmol.m^{-2}.s^{-1} constant blue light. White bars and grey bars indicate subjective day and subjective night, respectively. Error bars indicate standard error of the mean, with n=8. For waveforms, error bars are shown every 10 hours for clarity. RAE is a measure of rhythmic robustness, with a value of 0 indicating an exact fit to a cosine wave (Plautz et al., 1997). Data from one of three independent experiments are shown. Asterisks indicate statistically significant difference in period compared to Col-0 control (** p<0.001, Student's T-test).

As had been observed for plants grown on sulfate-deficient media (Figure 5.2), F_q'/F_m' rhythms cycled with robust circadian rhythm in Col-0, *fou8*, *apk1 apk2* and *apk1 apk2 fou8*, while no dampening of rhythms was observed over the course of the ~5 days in free-run (Figure 5.4a). Circadian period estimates confirmed the significant long period of F_q'/F_m' rhythms in *fou8* (24.60 ± 0.13 h) compared to Col-0 (23.67 ± 0.07 h; $p<0.001$; Student's T-test), as had been previously observed for *sal1* mutants under constant blue light (Section 4.2.3). However, no long period in F_q'/F_m' rhythms was observed for *apk1 apk2* or *apk1 apk2 fou8* compared to Col-0. While the period of these rhythms tended to be shorter in *apk1 apk2* (23.30 ± 0.13 h) and *apk1 apk2 fou8* (23.46 ± 0.16 h) compared to Col-0, differences were not statistically significant. These data correspond to previous reports that mutation of *fou8* does not rescue the *apk1 apk2* phenotype, and that *APK1* and *APK2* function in the same pathway as *SAL1*. (Lee et al., 2012).

5.2.3. No changes in splicing of core clock transcripts is observed in sal1 mutants under constant blue light

Alternative splicing (AS), particularly intron retention events, has been shown to play an important role in regulating circadian responses to environment changes. To determine whether any intron retention events in core clock transcripts occur in *sal1* mutants grown under constant blue light, full-length transcripts of morning- and evening-phased clock genes were examined using RT-PCR (Figure 5.5). Seedling were grown on 0.5x MS agar plates in 12h:12h light:dark cycles under 60 $\mu mol.m^{-2}.s^{-1}$ white light for 10 days, and subsequently transferred to 20 $\mu mol.m^{-2}.s^{-1}$ constant blue light at subjective dawn. After three days in free-run, seedlings (10-12 per time point) were harvested and RT-PCR analysis performed on extracted total mRNA following DNase treatment. For each clock transcript, the time point with the highest transcript abundance in *sal1* (Figure 4.9) was chosen for analysis. Analysis of transcripts for the morning-phased *LHY* gene, and for the evening-phased genes *PRR5* and *TOC1* showed only a single, clear band corresponding to fully spliced transcripts in Col-0, *alx8-1* and *fry1-6*.

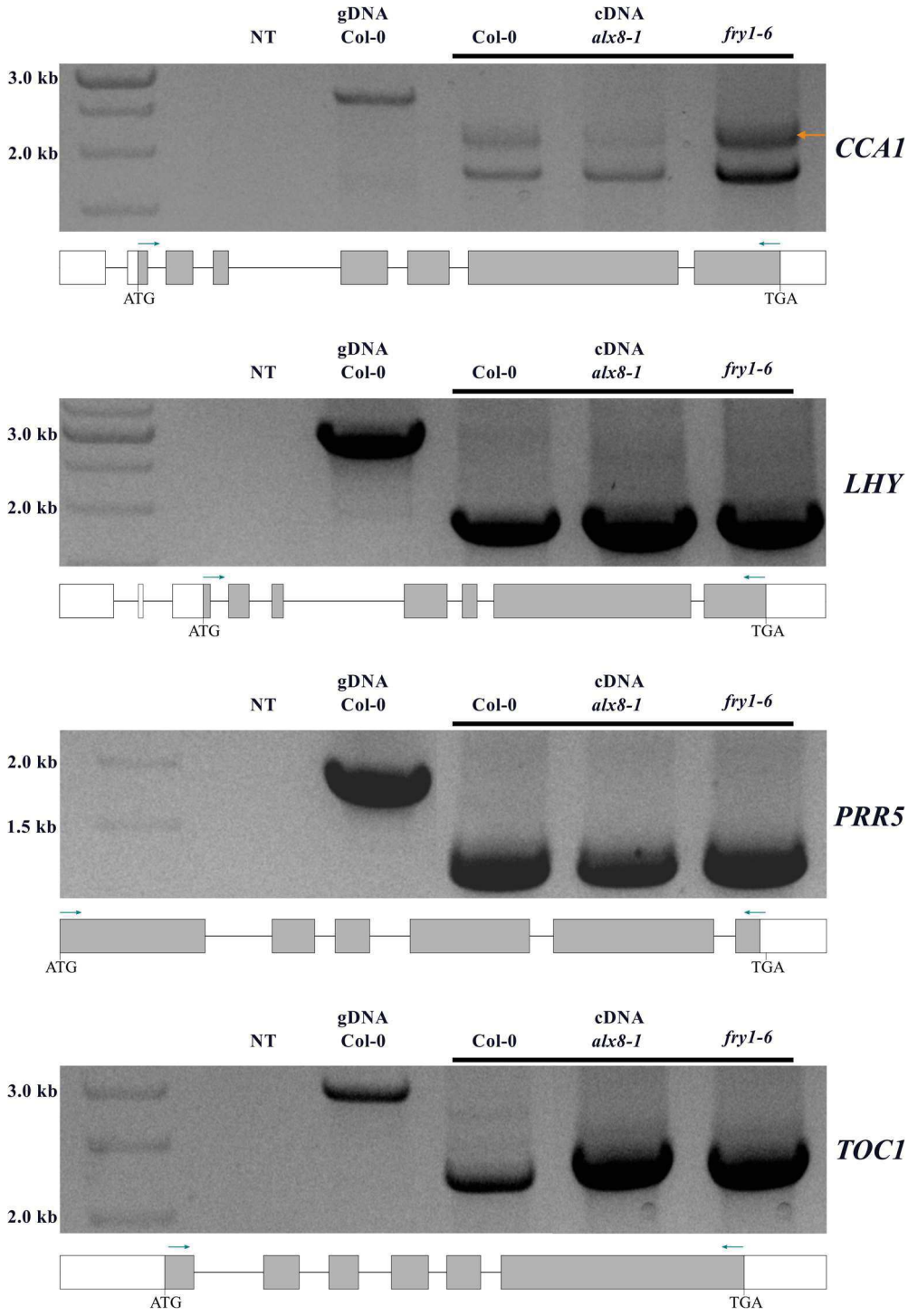

Figure 5.5 Intron retention events in core clock mRNA transcripts in *sal1* mutants under constant blue light. RT-PCR analysis of full-length mRNA transcripts for the core clock genes *CCA1*, *LHY*, *PRR5* and *TOC1*. Simplified gene diagrams indicate position of forward and reverse primer binding near transcription start and stop codons, respectively. Orange arrow indicates bands corresponding to the *CCA1β* mRNA isoform retaining intron 4. NT is non-template control. Seedlings were grown on 0.5x MS agar plates in 12h:12h light:dark cycles under 60 µmol.m^{-2}.s^{-1} white light for 10 days before being transferred to 20 µmol.m^{-2}.s^{-1} constant blue light. 10-12 seedlings were sampled per time point. For each gene, the time point with highest transcript levels in *alx8-1* were chosen. Amplification of transcripts at ZT51 (*CCA1* and *LHY*), ZT57 (*PRR5)* and ZT87 (*TOC1*) are shown.

In contrast, two bands were visible for *CCA1* transcripts in Col-0 and *sal1*mutants, one corresponding to the fully spliced *CCA1* transcript and the other to an mRNA isoform retaining intron 4. This *CCA1* mRNA isoform (*CCA1β*), arising from an intron retention event involving intron 4, has been shown to occur ubiquitously in *Arabidopsis* and plays a role in low temperature and high light responses (Filichkin et al., 2010; James et al., 2012; Seo et al., 2012). Under non-stressed conditions, rhythms in accumulation of the two *CCA1* mRNA isoforms are synchronised, with no difference in period or phase of oscillations (Filichkin et al., 2010; James et al., 2012). To determine whether the retention of *CCA1* intron 4 is affected in *sal1*, rhythms in accumulation of the two *CCA1* mRNA isoforms in constant white light was analysed using qRT-PCR (Figure 5.6). Seedlings were entrained as described for Figure 5.5, and following entrainment were transferred to 60 $\mu mol.m^{-2}.s^{-1}$ constant white light at subjective dawn (ZT0). After 48 hours of free run, 10-12 seedlings per time point were sampled every 3 hours from subjective dawn. As had been observed under constant blue light (Figure 4.2.6), analysis of transcripts amplified by targeting *CCA1* exon 6 reveals circadian oscillations in transcript abundance, with a late phase in peak transcript accumulation in *alx8-1* and *fry1-6* (Figure 5.6a). When targeting the fully spliced mRNA isoform (with forward primer and reverse primer binding to exon 3 and exon 4, respectively), peak transcript accumulation at ZT48 and ZT72 in Col-0, as well as a late phase in *alx8-1* and *fry1-6* are again observed (Figure 5.6b). Similarly, targeting the *CCA1β* isoform (with forward primer and reverse primer binding to intron 4 and exon 4, respectively) reveals transcription level peaks at subjective dawn in Col-0 and a late phase in transcript oscillation in *sal1* mutants (Figure 5.6c). As had been previously reported (Filichkin et al., 2010; James et al., 2012), both mRNA isoforms are synchronised in transcript level oscillations in Col-0, and the same phase in oscillations is obtained when using primers that do not distinguish between the two isoforms (Figure 5.6a). Furthermore, oscillations in abundance of the two RNA isoforms are synchronised in *sal1* as in Col-0, with both *CCA1* mRNA isoforms oscillating with the same late phase in *sal1*.

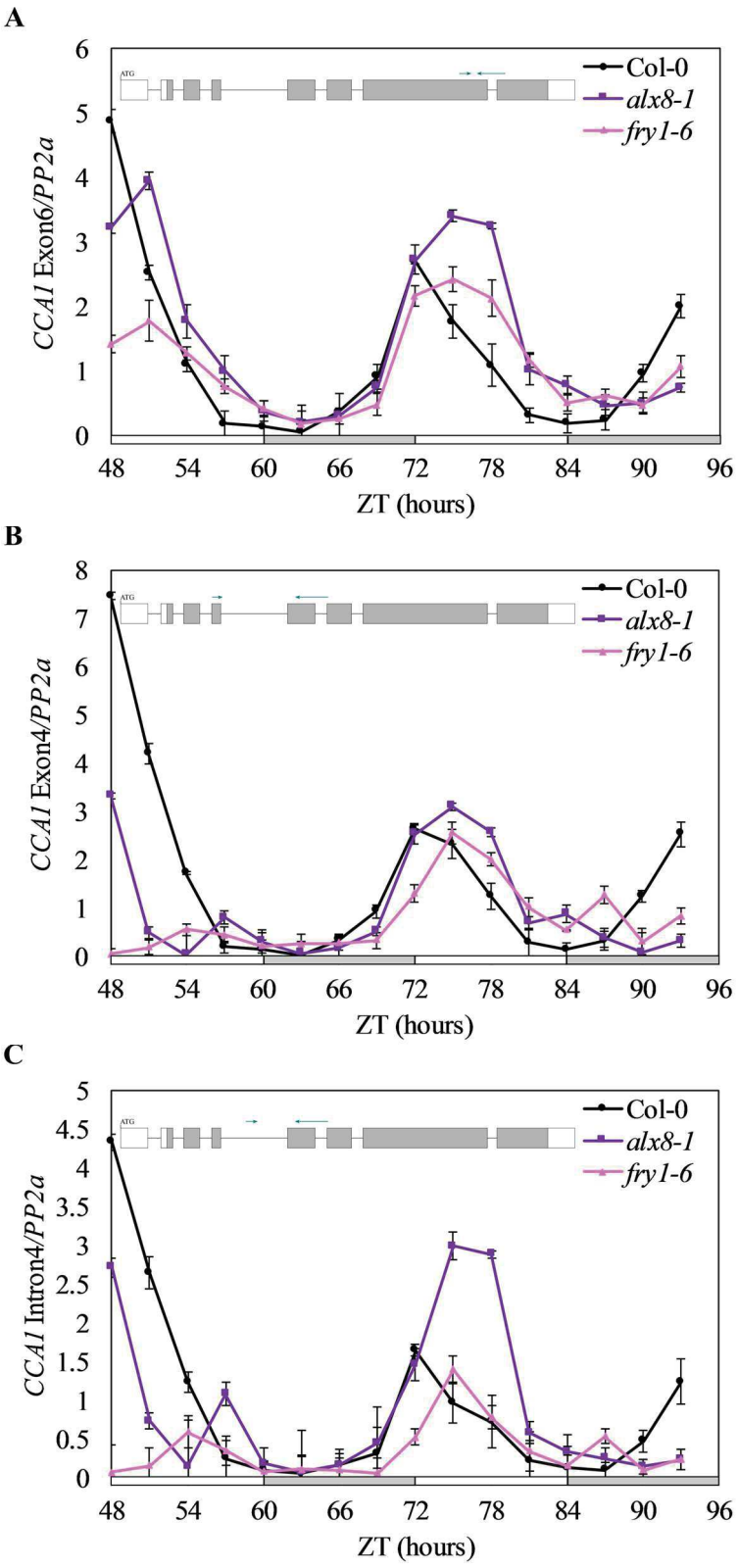

Figure 5.6 Rhythms in transcript accumulation of *CCA1* mRNA isoforms under constant white light. qRT-PCR analysis of accumulation of **(A)** all mRNA isoforms combined, **(B)** fully spliced mRNA isoform and **(C)** alternatively spliced mRNA isoform retaining intron 4 of the morning-phased core clock gene *CCA1* (*CCA1β*). Simplified gene diagrams indicate the positions of primer binding. Seedlings were grown on 0.5x MS agar plates and entrained in 12h:12h light:dark cycles under 60 µmol.m^{-2}.s^{-1} white light for 10 days before being transferred to 60 µmol.m^{-2}.s^{-1} constant white light at subjective dawn. After 48 hours in free-run, 10-12 seedlings were sampled and pooled, with sampling repeated every three hours for two days. White bars and grey bars indicate subjective day and subjective night, respectively. Data for each gene were normalised to an internal control *PP2a,* and are averages of three biological replicates. Error bars indicate standard error of the mean.

5.2.4. Loss of XRN4 activity lengthens circadian period

The broad range of morphological and molecular phenotypes associated with *sal1* mutants has been attributed to the inhibition of 5'→3' exoribonucleases (XRNs) in the absence of SAL1 activity (Gy et al., 2007; Kim and von Arnim, 2009; Chen and Xiong, 2010; Estavillo et al., 2011; Hirsch et al., 2011; Chan et al., 2016a). PAP is known to inhibit XRN activity *in vitro* (Dichtl et al., 1997; Estavillo et al., 2011), and *sal1* mutants share numerous phenotypes with *xrn* mutants (Gy et al., 2007; Chen and Xiong, 2010; Estavillo et al., 2011; Hirsch et al., 2011). The *Arabidopsis* genome contains three XRNs, each structurally similar to the cytoplasmic Xrn2p/Rat1p 5'→3' exoribonuclease ortholog in *Saccharomyces cerevisiae* (Kastenmayer and Green, 2000). XRN2 and XRN3 function in the nucleus, while XRN4 (also called ETHYLENE INSENSITIVE 5, EIN5) is localised in the cytoplasm and acts as a functional homologue of the *S. cerevisiae* Xrn1p (Kastenmayer and Green, 2000). While the mechanisms and exact function of *Arabidopsis* XRNs are not as well characterised as for the yeast homologues, XRNs have been shown to play important roles in numerous RNA processing pathways including miRNA-mediated RNA decay, and also act as suppressors of posttranscriptional gene silencing (PTGS) (Kastenmayer and Green, 2000; Souret et al., 2004; Gy et al., 2007; Zakrzewska-Placzek et al., 2010).

Since RNA stability plays an important role in circadian regulation (Nolte and Staiger, 2015), the effect of reducing XRN activity within the circadian system was investigated. Rhythms in F_q'/F_m' were monitored in the *xrn2-1*, *xrn3-3* and *ein5-1* (*xrn4*) single mutants (Roman et al., 1995; Gy et al., 2007), as well as in the *xrn2-1 xrn3-3 xrn4-6* triple mutant (Hirsch et al., 2011) under constant blue light. *xrn2-1* and *ein5-1* are loss-of-function mutations while *xrn3-3* is hypomorphic, with homozygous complete loss-of-function *xrn3* allele reported as being lethal (Gy et al., 2007). Seedlings were grown on 0.5x MS agar plates for 12 days in 12h:12h light:dark cycles under 60 $\mu mol.m^{-2}.s^{-1}$ white light before imaging under 20 $\mu mol.m^{-2}.s^{-1}$ constant blue light for ~5 days (Figure 5.7a, b and c).

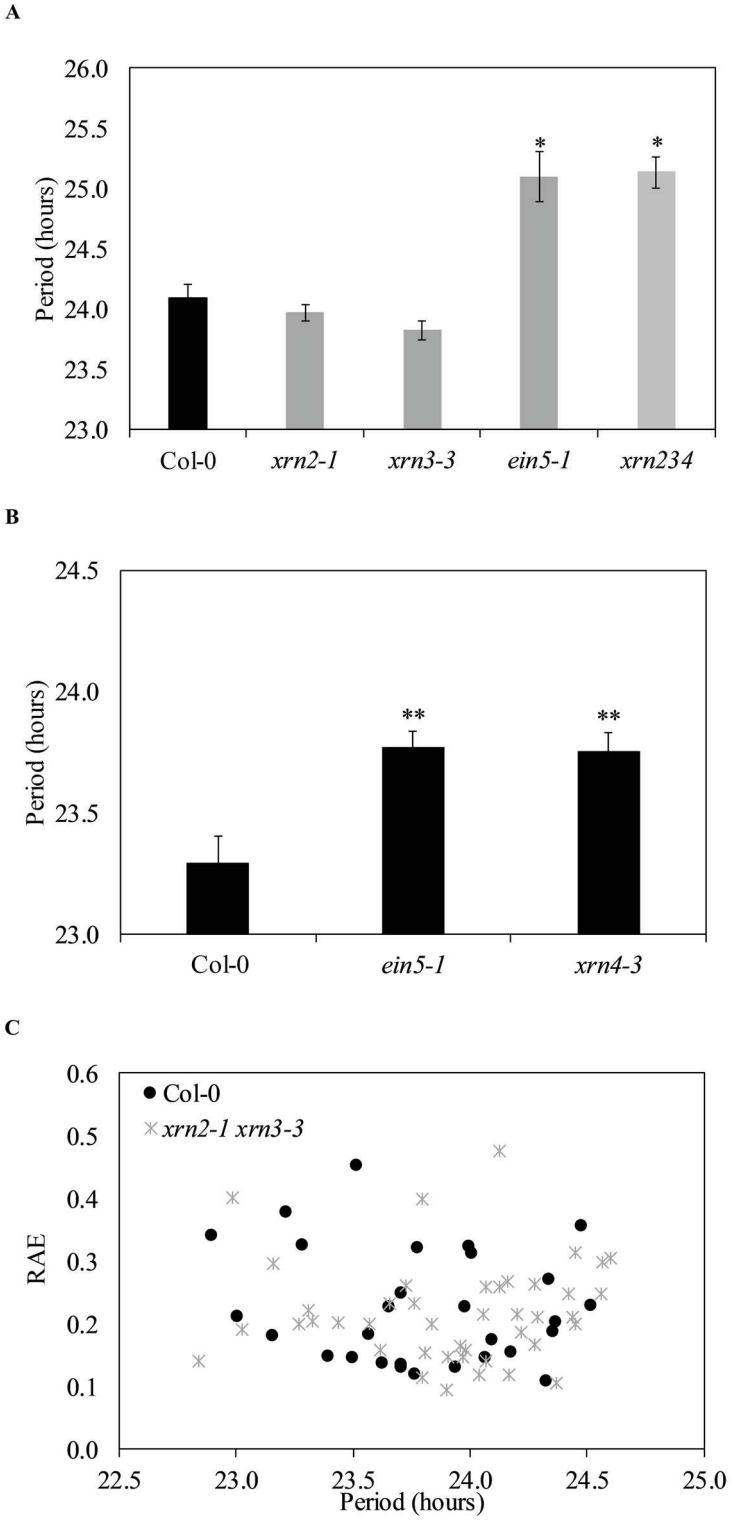

Figure 5.7 Chloroplast rhythms in *xrn* mutants under constant blue light. (A-B) Circadian period estimates and **(C)** circadian period estimates plotted against Relative Amplitude Error (RAE) for F_q'/F_m' oscillations in **(A)** Col-0, *xrn2-1, xrn3-3, ein5-1* single mutants and in the *xrn234* triple mutant, in **(B)** Col-0, *ein5-1* and *xrn4-3*, and in **(C)** individual seedlings from a segregating *xrn2- xrn3-3* double mutant population under constant blue light. Seedlings were grown on 0.5x MS agar plates and entrained in 12h:12h light:dark cycles under 60 $\mu mol.m^{-2}.s^{-1}$ white light for 12 days before imaging under 20 $\mu mol.m^{-2}.s^{-1}$ constant blue light. Error bars indicate standard error of the mean, with n=8. RAE is a measure of rhythmic robustness, with a value of 0 indicating an exact fit to a cosine wave (Plautz et al., 1997). Data from one of three independent experiments are shown. Asterisks indicate statistically significant difference in period compared to Col-0 control (* $p<0.01$, ** $p<0.001$, Student's T-test).

Circadian period estimates indicated no significant difference in period of F_q'/F_m' rhythms in *xrn2* (23.97 ± 0.07 h) or *xrn3* (23.82 ± 0.08 h) compared to Col-0 (24.09 ± 0.12 h; Figure 5.7a). Interestingly, a significantly longer period was observed in both *ein5-1* (25.10 ± 0.21 h) and *xrn234* (25.14 ± 0.13 h) compared to Col-0 (p<0.01; Student's T-test), with no significant difference in period between *ein5-1* and *xrn234* (Figure 5.7a). The significantly lengthened circadian period observed in *ein5-1* was also observed in a second *xrn4* mutant allele, *xrn4-3* (Figure 5.7b).

Since loss of cytoplasmic XRN (XRN4) activity resulted in lengthening of circadian period, the effect of loss of nuclear XRN activity on circadian rhythms was investigated. The nuclear XRNs, XRN2 and XRN3, have overlapping functions (Gy et al., 2007), and therefore rhythms in F_q'/F_m' were monitored in the *xrn2-1 xrn3-3* double mutant (Gy et al., 2007). As the homozygous *xrn2 xrn3* mutant is sterile (Gy et al., 2007; Hirsch et al., 2011), a segregating *xrn2-1*$^{(-/-)}$ *xrn3-3*$^{(-/+)}$ population was used and F_q'/F_m' rhythms monitored in individual seedlings. If the combined total loss of nuclear XRN function lengthened circadian rhythms, ¼ of the segregating *xrn2-1*$^{(-/-)}$ *xrn3-3*$^{(-/+)}$ population would be expected to exhibit long period rhythms in F_q'/F_m'. Upon analysis of 58 individual *xrn2-1 xrn3-3* seedlings and 45 individual Col-0 seedlings, no lengthening in circadian period was observed between the *xrn2 xrn3* double mutant and Col-0 seedlings (24.13 ± 0.24 h average period; Figure 5.7c).

To further analyse the long circadian period observed upon loss of *XRN4* function, the accumulation of nuclear clock gene transcripts were analysed in Col-0 and *ein5-1* under constant white light (Figure 5.8). Seedlings were grown on 0.5x MS agar plates in 12h:12h light:dark cycles under 60 $\mu mol.m^{-2}.s^{-1}$ white light for 10 days and, following entrainment, were transferred to 60 $\mu mol.m^{-2}.s^{-1}$ constant white light at subjective dawn (ZT0). After 48 hours of free run, 10-12 seedlings per time point were sampled from subjective dawn (ZT48) every 3 hours for two days. Rhythmic accumulation was observed for the morning-phased nuclear clock gene transcripts *CCA1* and *LHY*, as well as for the evening-phased *ELF4*, *GI* and *PRR5* transcripts in both Col-0 and *ein5-1* (Figure 5.8).

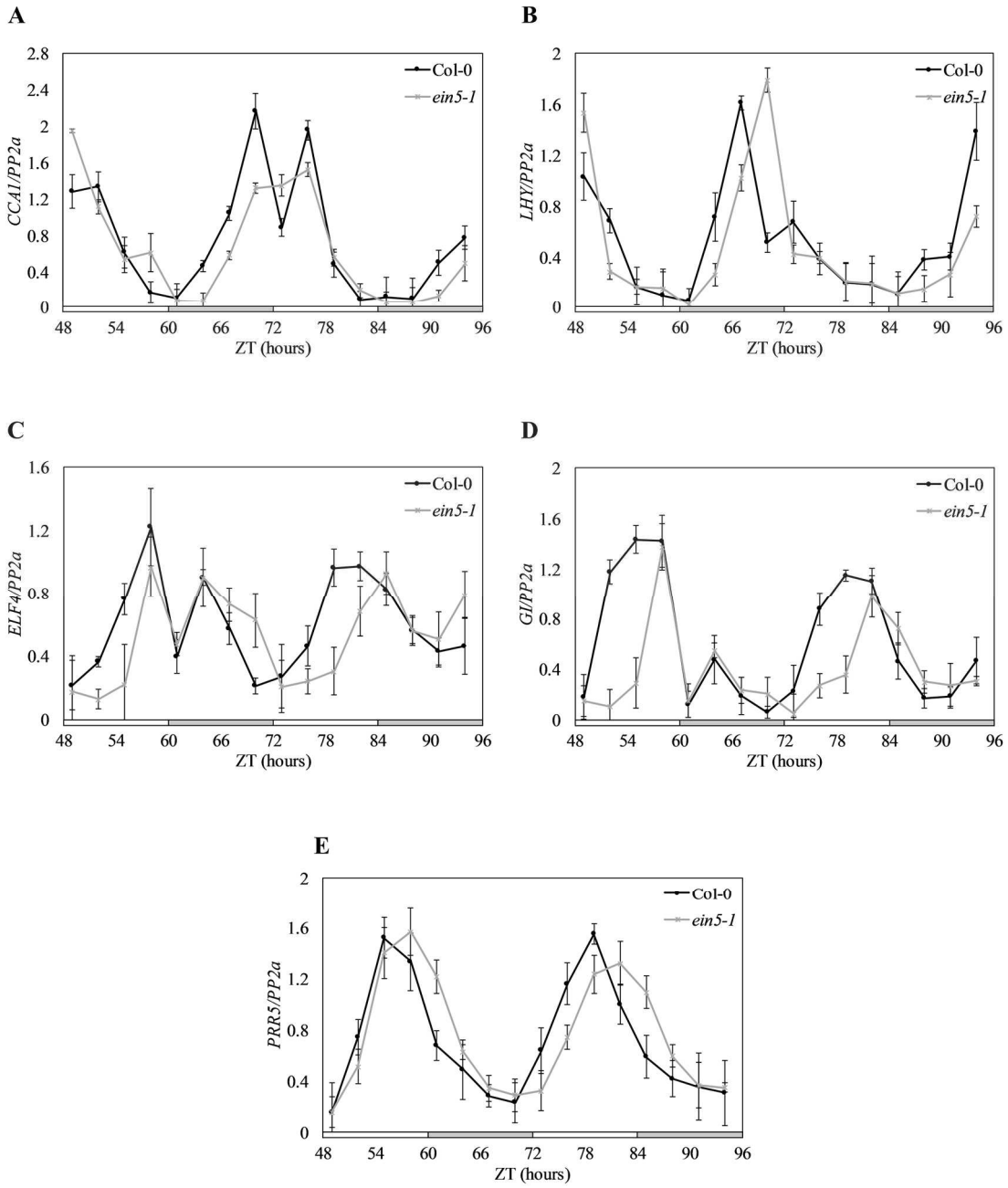

Figure 5.8 Expression of core nuclear circadian clock genes in *ein5-1* mutants under constant white light. qRT-PCR analysis of transcript accumulation for morning-phased core clock genes **(A)** *CCA1* and **(B)** LHY, and evening-phased core clock genes **(C)** *ELF4* **(D)** *GI* and **(E)** *PRR5* in Col-0 and *xrn4* single mutant *ein5-1* under constant white light. Seedlings were grown on 0.5x MS agar plates and entrained in 12h:12h light:dark cycles under 60 µmol.m^{-2}.s^{-1} white light for 10 days before being transferred to 60 µmol.m^{-2}.s^{-1} constant white light at subjective dawn. After 48 hours in free-run, 10-12 seedlings were sampled and pooled, with sampling repeated every three hours for two days. Data for each gene were normalised to an internal control (*PP2a*). White bars and grey bars indicate subjective day and subjective night, respectively. Data are representative of two biological replicates. Error bars indicate standard error of the mean.

A modest late phase (~3 hours) in peak transcript accumulation was observed for analysed clock gene transcripts in *ein5-1* compared to Col-0 (particularly for the evening-phased genes *GI* and *PRR5*), with the phase shift more pronounced on the second day of free-run. Although not as pronounced, this late phase in transcript accumulation corresponded to the long period observed in F_q'/F_m' rhythms in *ein5-1* under constant blue light (Figure 5.7a and b), and support a previous report of long period rhythmic *CCA1* transcription in *ein5-1* under constant light conditions (Hanano et al., 2006).

To determine whether the long period phenotype of *ein5-1* is as a result of mis-regulation of nuclear clock gene transcription under entraining conditions, accumulation of clock gene transcripts under light:dark cycles was analysed in Col-0 and *ein5-1*. Seedlings were entrained on 0.5x MS agar plates in 16h:8h light:dark cycles under 60 $\mu mol.m^{-2}.s^{-1}$ white light for 12 days, and tissue (10-12 seedlings per timepoint) harvested from dawn (ZT0) the following day. Rhythms of transcription of clock genes was as previously reported (Hsu and Harmer, 2014; Millar, 2016), with transcripts of morning-phased components peaking at dawn and transcripts of evening-phased clock components accumulating at highest levels in the afternoon or early evening (Figure 5.9). In Col-0, transcript levels for the morning-phased clock components *CCA1* and *LHY* peak 1 hour after dawn (Figure 5.9a and b). This was followed by a steady decrease in transcript abundance over the course of the day until the lowest levels were reached ~8 hours after dawn, and a subsequent increase in transcript towards the end of the night in anticipation of dawn. Rhythms in *CCA1* and *LHY* transcript accumulation were similar to Col-0 in *ein5-1*, but with a modest (~2 hour) delay in peak transcript abundance compared to Col-0. However, no delay in *CCA1* or *LHY* transcript accumulation was observed in *ein5-1* over the course of the day, with transcripts reaching wild-type levels within 4 hours after dawn and morning-phased transcripts at low levels in both Col-0 and *ein5-1* in the afternoon. A similarly modest late phase in peak transcript abundance was observed for evening-phased *ELF4*, with transcripts peaking at ZT12 in Col-0 and an ~2 hour phase shift observed in *ein5-1* (Figure 5.9d).

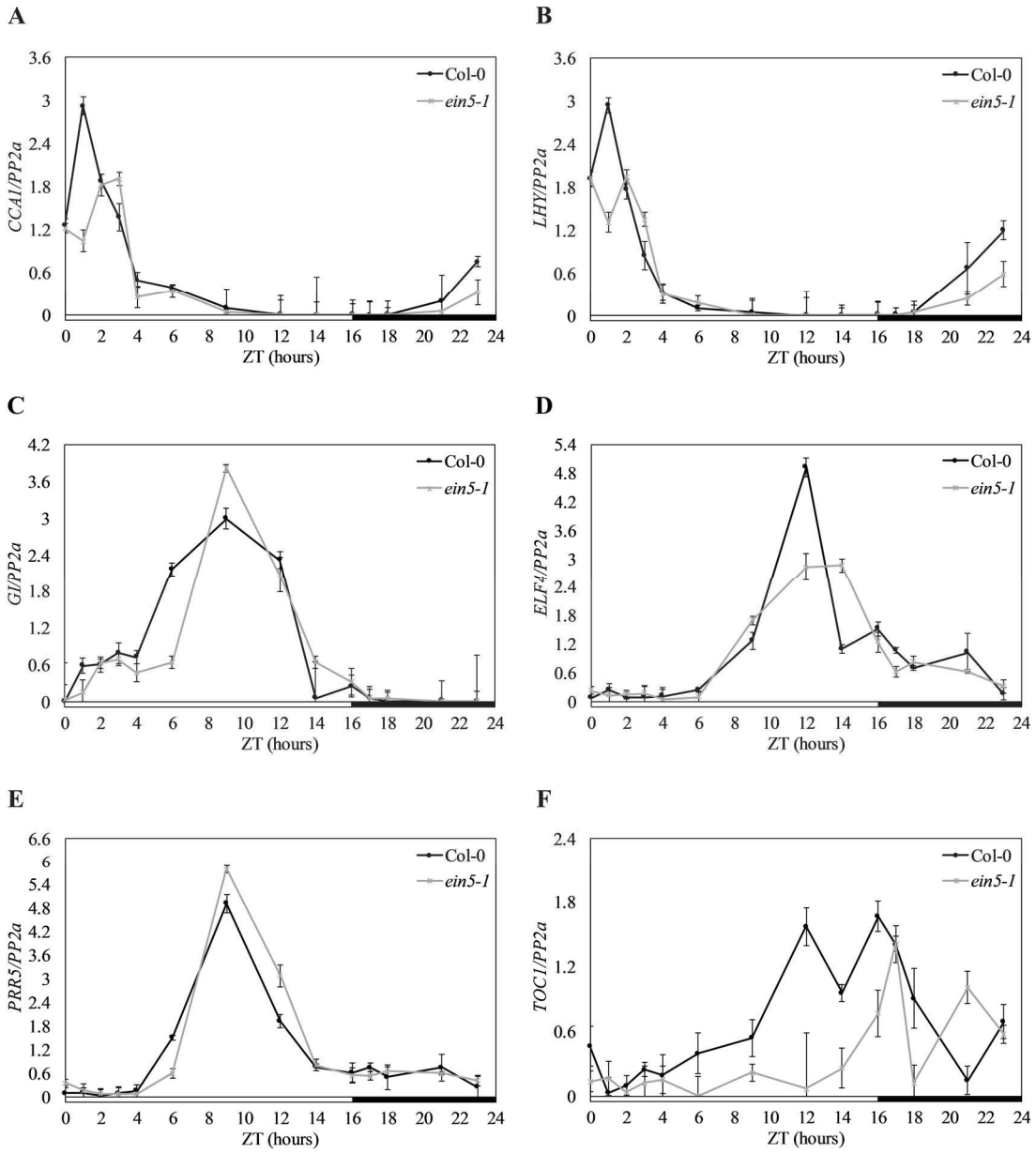

Figure 5.9 Expression of core nuclear circadian clock genes in *ein5-1* mutants under long-day conditions. qRT-PCR analysis of transcript accumulation for morning-phased core clock genes **(A)** *CCA1* and **(B)** LHY, and evening-phased core clock genes **(C)** *GI* **(D)** *ELF4*, **(E)** *PRR5* and **(F)** *TOC1* in Col-0 and *xrn* single mutant *ein5-1* under long-day conditions. Seedlings were grown on 0.5x MS agar plates and entrained in 16h:8h light:dark cycles under 60 µmol.m^{-2}.s^{-1} white light for 12 days before sampling. Data for each gene were normalised to an internal control (*PP2a*). White bars and black bars indicate day and night, respectively. Data are representative of two biological replicates. Error bars indicate standard error of the mean.

No late phase was observed for evening-phased components *GI* and *PRR5* in *ein5-1*, with transcripts peaking at ZT9 (Figure 5.9c and e). Transcripts for evening component *TOC1* were present at lower levels during the day in *ein5-1* compared to Col-0, with a possible late phase in peak transcript abundance observed towards the end of the day in *ein5-1* (Figure 5.9f).

5.2.5. The xrn234 triple mutant mimics the long-period circadian phenotype of sal1 mutants

While the long period observed in the *ein5-1* single mutant suggests that inhibition of XRN4 correlates with lengthened circadian period, previous reports have linked *sal1* phenotypes to the activities of XRN2 and XRN3 (Gy et al., 2007; Estavillo et al., 2011; Kurihara et al., 2012), as well as to XRN4 (Gy et al., 2007). Indeed, a certain level of functional redundancy has been reported among the three *Arabidopsis* XRNs (Kastenmayer and Green, 2000; Gy et al., 2007; Zakrzewska-Placzek et al., 2010). In order to account for the functional redundancy among the XRNs, the *xrn234* mutant was chosen for further analysis into the role of XRN activity in maintaining circadian rhythms. To confirm whether the long circadian period of chloroplast rhythms observed in *sal1* mutants is mimicked in the *xrn234* triple mutant, rhythms in F_q'/F_m' and delayed fluorescence oscillations were monitored in *sal11* and *xrn234* under constant blue light conditions. Seedlings were grown on 0.5x MS agar plates individually (for chlorophyll *a* fluorescence) or in clusters of 10-15 (for delayed fluorescence) and entrained for 10 or 12 days, respectively, in 12h:12h light:dark cycles under 60 $\mu mol.m^{-2}.s^{-1}$ white light before imaging under 20 $\mu mol.m^{-2}.s^{-1}$ constant blue light (Figure 5.10a and b). Chlorophyll *a* fluorescence imaging confirmed the long period phenotype of *alx8-1* and *xrn234* (Figure 5.10 and b), with F_q'/F_m' rhythms robust and exhibiting a significantly longer period in both *alx8-1* (24.97 ± 0.19) and *xrn234* (25.08 ± 0.19) compared to Col-0 (23.86 ± 0.18; $p<0.001$; Student's T-test).

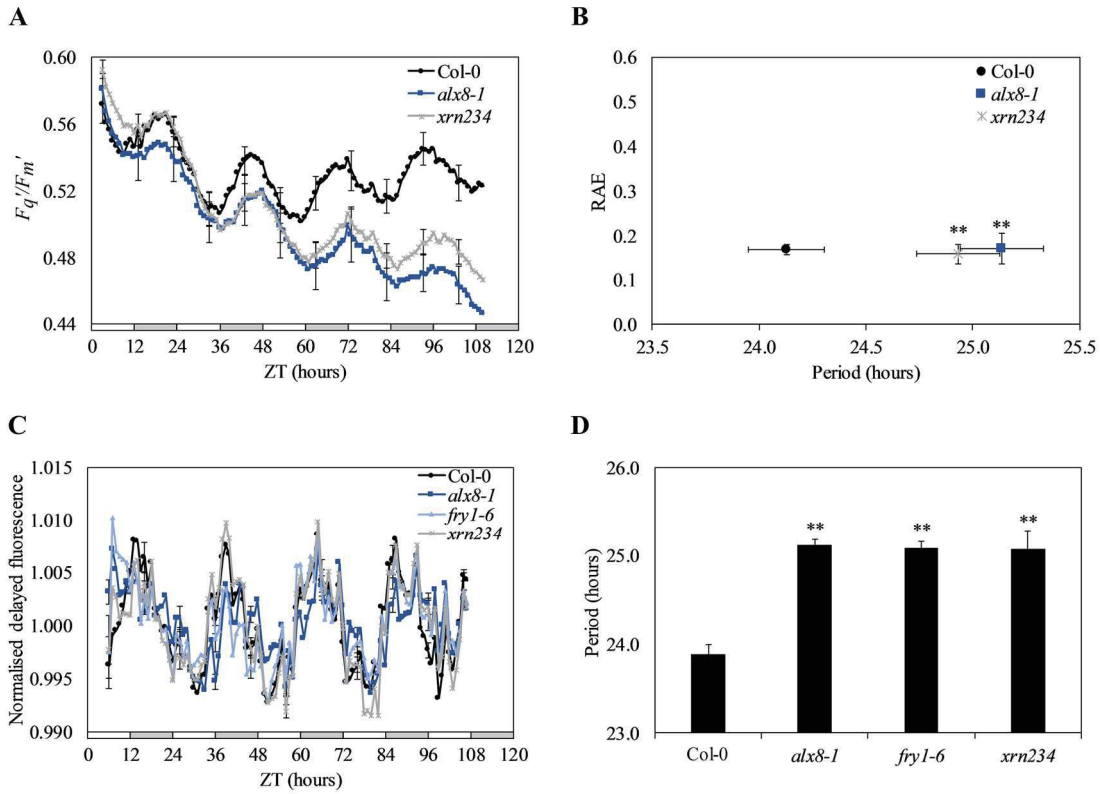

Figure 5.10 Circadian rhythms in chloroplasts of *xrn234* under constant blue light. **(A,C)** Waveforms and **(B,D)** circadian parameter estimates for **(A-B)** F_q'/F_m' and **(C-D)** delayed fluorescence oscillations in Col-0, *sal1* and the *xrn* triple mutant *xrn234*. Seedlings were grown on 0.5x MS agar plates and entrained in 12h:12h light:dark cycles under 60 µmol.m^{-2}.s^{-1} white light for 12 days before imaging under 20 µmol.m^{-2}.s^{-1} constant blue light. White bars and grey bars indicate subjective day and subjective night, respectively. Error bars indicate standard error of the mean, with n=8. For waveforms, error bars are shown every 10 hours for clarity. RAE is a measure of rhythmic robustness, with a value of 0 indicating an exact fit to a cosine wave (Plautz et al., 1997). Data from one of three independent experiments are shown. Asterisks indicate statistically significant difference in period compared to Col-0 control (** p<0.001, Student's T-test).

Similarly, delayed fluorescence rhythms remained robust in Col-0, *alx8-1*, *fry1-6* and *xrn234* (Figure 5.10b and c), with circadian period estimates confirming a significantly longer period in *alx8-1* (25.11 ± 0.34 h), *fry1-6* (25.07 ± 0.26 h) and *xrn234* (25.07 ± 0.18 h) compared to Col-0 (23.88 ± 0.19 h; $p<0.001$, Student's T-test). Furthermore, no difference in period was observed between *sal1* mutants and the *xrn234* triple mutant for either F_q'/F_m' or delayed fluorescence rhythms.

Since long-period chloroplast rhythms were observed in both *sal1* and *xrn234*, circadian regulation of rhythmic transcript accumulation was investigated in *xrn234* under constant blue and constant white light conditions. Seedlings were grown on 0.5x MS agar plates in 12h:12h light:dark cycles under 60 µmol.m^{-2}.s^{-1} white light for 10 days, transferred to 20 µmol.m^{-2}.s^{-1} constant blue light or 60 µmol.m^{-2}.s^{-1} constant white light at subjective dawn (ZT0), and harvested after 48 hours of free run as previously described. As had been previously observed (Section 4.2.6), morning-phased nuclear clock gene transcripts *CCA1* and LHY, and evening-phased *ELF4*, *GI* and *PRR5* transcripts accumulated with circadian rhythm in Col-0 under constant blue light (Figure 5.11). A late phase in peak transcript accumulation for morning- and evening phased transcripts (~3 hours on the first day of free-run, and more pronounced on the second day) was observed for *alx8-1*, *fry1-6* and *xrn234* under constant blue light. This phase shift corresponded to the long-period phenotype of chloroplast rhythms in *sal1* and *xrn234* under constant blue light (Figure 5.10). Interestingly, this late phase in transcript accumulation rhythms was visible, but less pronounced under constant white light than under constant blue light in *sal1* mutant alleles and in *xrn234* for both morning-and evening-phased transcripts (Figure 5.12). Finally, the regulation of clock gene transcription under entraining conditions was investigated in *sal11* and *xrn234*. Col-0, *alx8-1, fry1-6* and *xrn234* seedlings were entrained on 0.5x MS agar plates in 16h:8h light:dark cycles under 60 µmol.m^{-2}.s^{-1} white light for 12 days, and tissue harvested from dawn (ZT0) the following day as previously described.

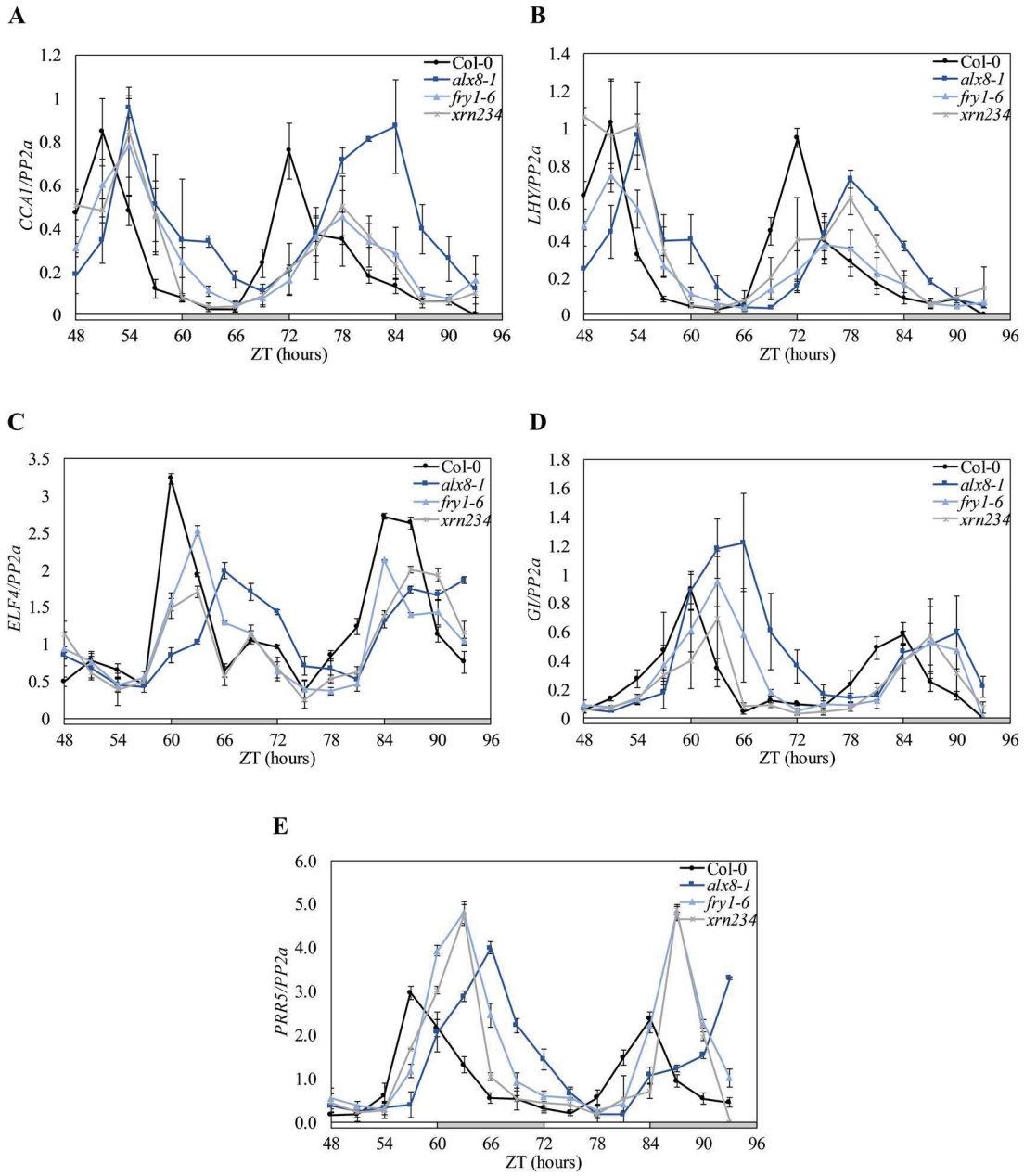

Figure 5.11 Expression of core nuclear circadian clock genes in *sal1* and *xrn234* mutant under constant blue light. qRT-PCR analysis of transcript accumulation for morning-phased core clock genes **(A)** *CCA1* and **(B)** LHY, and evening-phased core clock genes **(C)** *ELF4* **(D)** *GI* and **(E)** *PRR5* in Col-0, *alx8-1*, *fry1-6* and *xrn234* mutants under constant blue light. Seedlings were grown on 0.5x MS agar plates and entrained in 12h:12h light:dark cycles under 60 µmol.m^{-2}.s^{-1} white light for 10 days before being transferred to 20 µmol.m^{-2}.s^{-1} constant blue light at subjective dawn. After 48 hours in free-run, 10-12 seedlings were sampled and pooled, with sampling repeated every three hours for two days. Data for each gene were normalised to an internal control (*PP2a*). White bars and grey bars indicate subjective day and subjective night, respectively. Data are average of three biological replicates. Error bars indicate standard error of the mean.

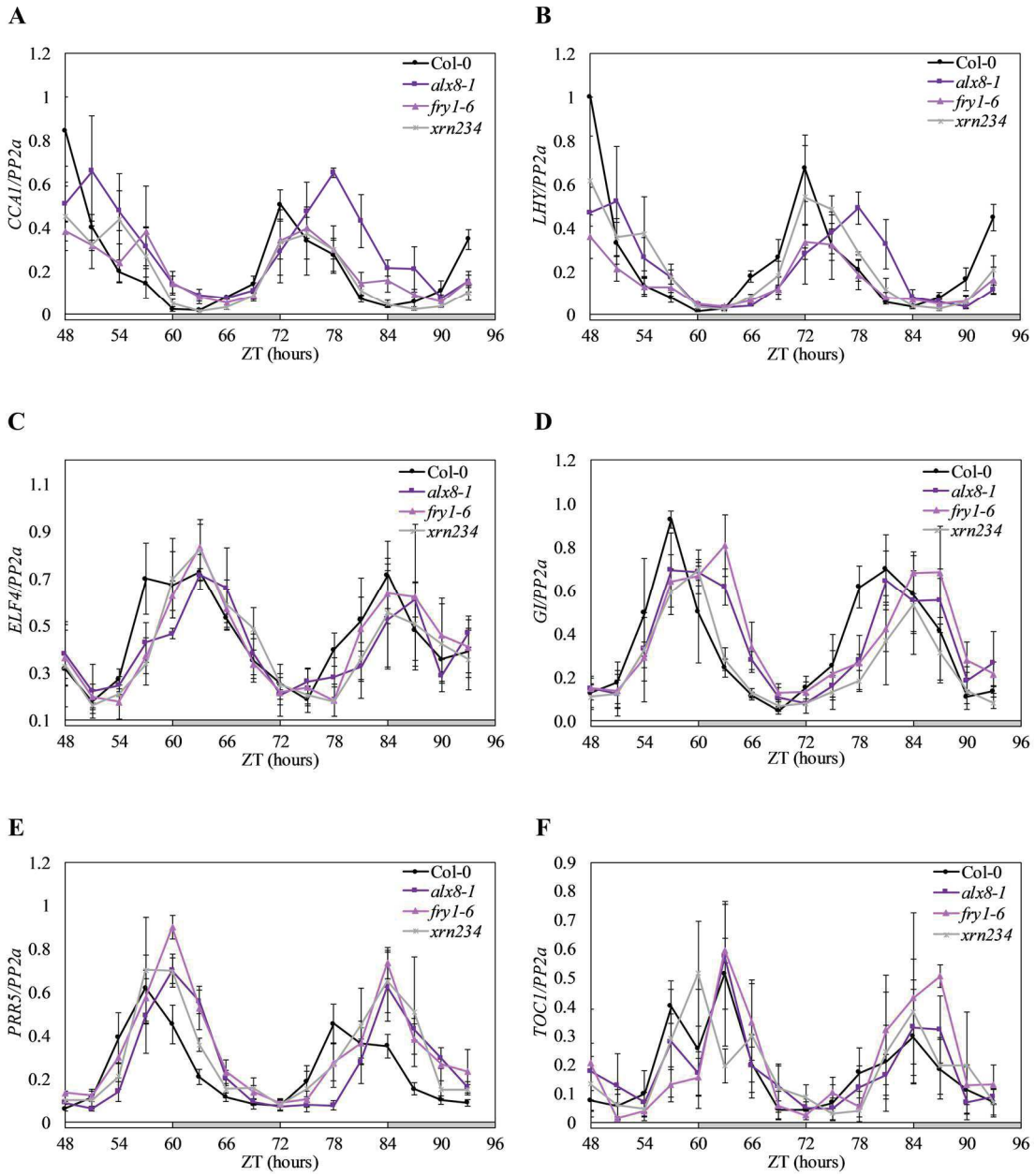

Figure 5.12 Expression of core nuclear circadian clock genes in *sal1* and *xrn234* mutant under constant white light. qRT-PCR analysis of transcript accumulation for morning-phased core clock genes **(A)** *CCA1* and **(B)** LHY, and evening-phased core clock genes **(C)** *ELF4* **(D)** *GI* **(E)** *PRR5* and **(F)** *TOC1* in Col-0, *alx8-1*, *fry1-6* and *xrn234* mutants under constant white light. Seedlings were grown on 0.5x MS agar plates and entrained in 12h:12h light:dark cycles under 60 µmol.m^{-2}.s^{-1} white light for 10 days before being transferred to 60 µmol.m^{-2}.s^{-1} constant white light at subjective dawn. After 48 hours in free-run, 10-12 seedlings were sampled and pooled, with sampling repeated every three hours for two days. Data for each gene were normalised to an internal control (*PP2a*). White bars and grey bars indicate subjective day and subjective night, respectively. Data are average of three biological replicates. Error bars indicate standard error of the mean.

While delayed accumulation of *CCA1* transcript was visible in both *sal1* alleles and *xrn234* (Figure 5.13a), no difference in transcript accumulation rhythms was observed for *LHY* transcripts in *alx8-1*, *fry1-6* or *xrn234* compared to Col-0 (Figure 5.13b). *CCA1* transcripts were present throughout the afternoon in *alx8-1* and *fry1-6,* and detectable until midday in *xrn234*, while these levels were almost undetectable in Col-0 beyond ZT8. A less pronounced delay in transcript accumulation was observed for evening-phased *ELF4*, *GI* and *PRR5* transcripts in *alx8-1*, *fry1-6* and *xrn234* compared to WT (Figure 5.13c, d and e). Furthermore, *ELF4* and *GI* transcripts were present in lower levels throughout the day in *xrn234*, compared to Col-0 and *sal1* mutants (Figure 5.13c and d).

5.2.6. 3' non-coding transcripts and 4CL1 as possible targets for XRN regulation of circadian rhythms

A study of *fry1-6* and *xrn* mutants employing whole genome sequencing (RNA-sequencing and whole-genome tiling array methods) identified the accumulation of several thousand non-coding transcripts mapping to the 3' ends of certain genes in both *fry1-6* and *xrn3-3*, and to a lesser extent in the *xrn2 xrn3* and *xrn3 xrn4* double mutants (Kurihara et al., 2012). These 3' non-coding regions belong to genes that are actively transcribed, occur as separate transcripts (not as a result of extensions of 5'-mRNA), and are thought to arise from mRNA and miRNA precursor transcripts. Analysis of the publicly-available RNA-seq data revealed 3' non-coding transcripts for *ELF4* and *PRR5* had been identified as accumulating in *fry1-6* (Kurihara et al., 2012). As a starting point to determine whether these 3' non-coding transcripts play a role in the long-period circadian phenotype of *sal1* and *xrn234*, qRT-PCR analysis was employed to analyse the levels of 3' non-coding transcripts for *ELF4* and *PRR5* under constant light conditions. Col-0, *alx8-1*, *fry1-6* and *xrn234* seedlings were grown on 0.5x MS agar plates in 12h:12h light:dark cycles under 60 $\mu mol.m^{-2}.s^{-1}$ white light for 10 days, and transferred to 20 $\mu mol.m^{-2}.s^{-1}$ constant blue light or 60 $\mu mol.m^{-2}.s^{-1}$ constant white light at subjective dawn. Under constant blue and constant white light, accumulation of 3' non-coding regions of *ELF4*

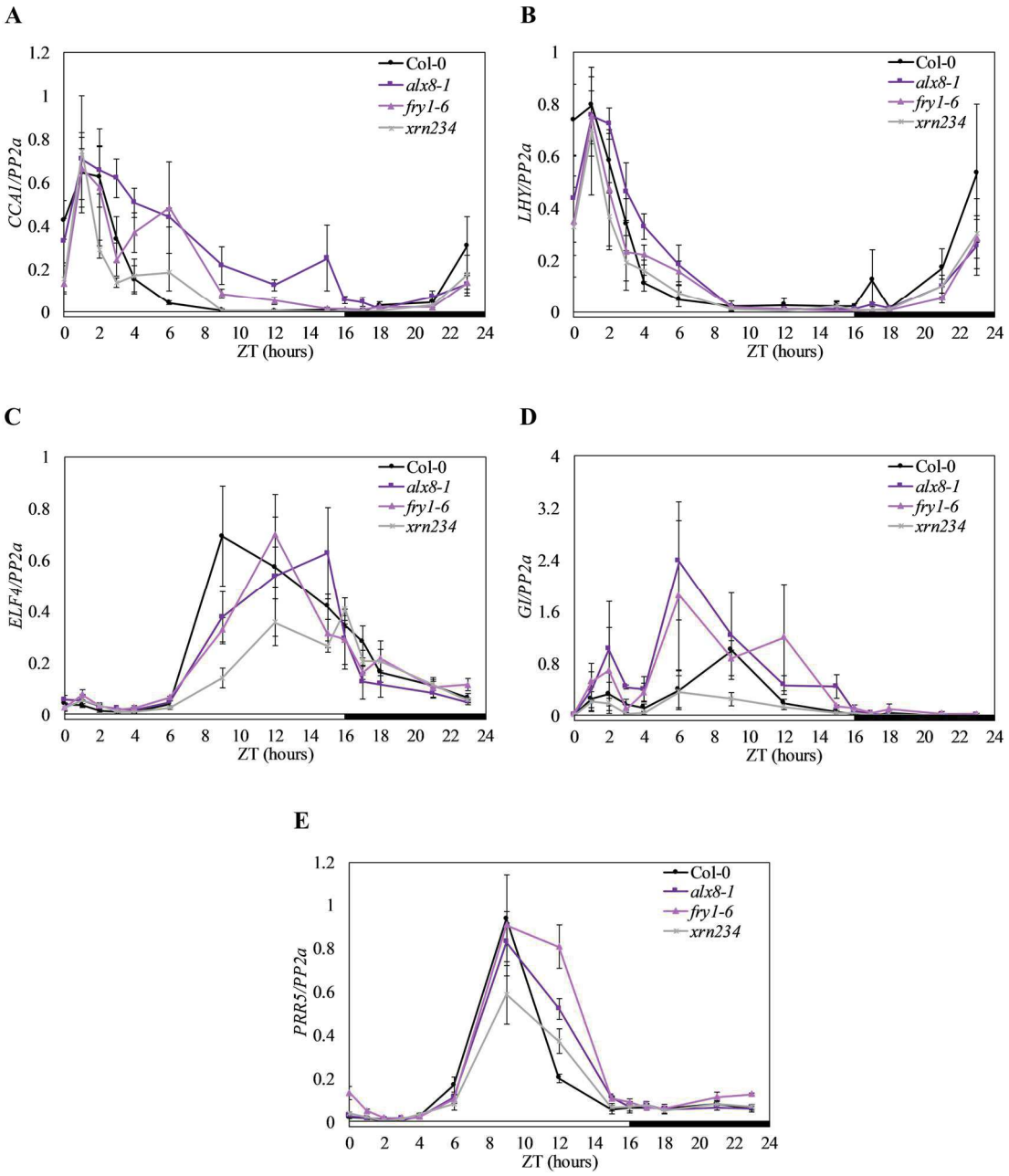

Figure 5.13 Expression of core nuclear circadian clock genes in *sal1* and *xrn234* mutants under long-day conditions. qRT-PCR analysis of transcript accumulation for morning-phased core clock genes **(A)** *CCA1* and **(B)** LHY, and evening-phased core clock genes **(C)** *ELF4* **(D)** *GI* and **(E)** *PRR5* in Col-0, *alx8-1*, *fry1-6* and *xrn234* under long-day conditions. Seedlings were grown on 0.5x MS agar plates and entrained in 16h:8h light:dark cycles under 60 µmol.m^{-2}.s^{-1} white light for 12 days before sampling. Data for each gene were normalised to an internal control (*PP2a*). White bars and black bars indicate day and night, respectively. Data are averages of three biological replicates. Error bars indicate standard error of the mean.

and *PRR5* were detected in both *alx8-1* and *fry1-6* while levels of these transcripts were almost undetectable in Col-0 (Figure 5.14), corresponding to previous reports (Kurihara et al., 2012). In both *alx8-1* and *fry1-6,* accumulation of *ELF4* 3' non-coding transcripts was higher under constant blue light (Figure 5.14a) than under constant white light (Figure 5.14c). Interestingly, 3' non-coding transcripts for *ELF4* or *PRR5* did not accumulate in *xrn234* under constant blue or constant white light (Figure 5.14b and d), suggesting that accumulation of these transcripts is not involved in the long-period circadian phenotype observed in *xrn234*.

Several putative targets of XRN4 have been identified through the use of cDNA microarray analysis comparing *xrn4-5* and Col-0 plants (Souret et al., 2004). Of these possible targets, 4-COUMARATE:COA LIGASE 1 (4CL1), exhibits a 1.9-fold increase in expression in *xrn4-5*, and has been identified through previous microarray studies as being under circadian regulation (Souret et al., 2004; Mockler et al., 2007). In an attempt to identify a possible mechanisms through which XRN4 activity influences circadian rhythms, accumulation of *4CL1* transcript was analysed in Col-0, *sal1* and *xrn* mutants under constant light and long-day conditions (Figure 4.15). For analysis under constant light, seedling were entrained in 12h:12h light:dark cycles and transferred to constant light conditions as previously described. For analysis under long-day conditions, seedlings were entrained for 12 days in 16h:8h light:dark cycles for 12 days as previously described. Despite previous reports to the contrary (Mockler et al., 2007), qRT-PCR analysis of *4CL1* transcripts revealed no circadian rhythm in transcript accumulation under constant white light (Figure 5.15a). Furthermore, no difference in *4CL1* transcript abundance was visible in *ein5-1* or *xrn234* compared to Col-0 under any of light regimes (Figure 5.15a, b and c). These data suggest that *4CL1* is unlikely to be a mechanism through which XRN activity impacts the circadian system.

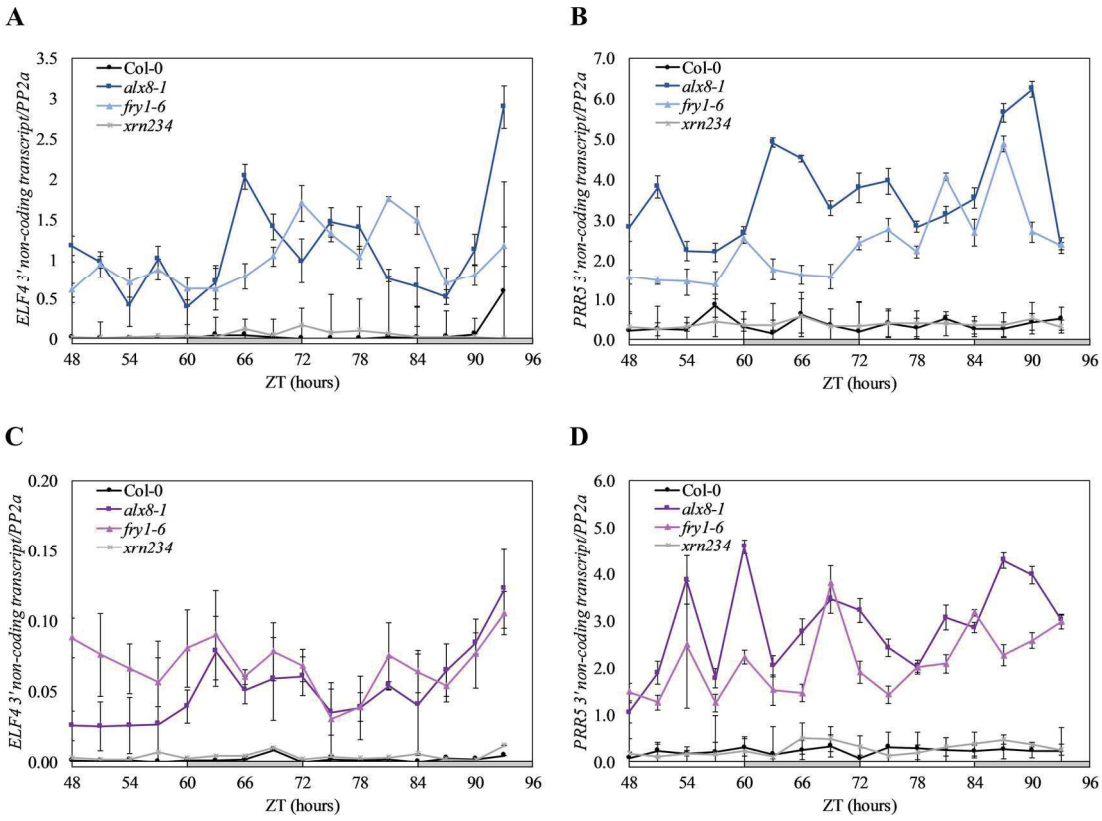

Figure 5.14 Accumulation of 3' non-coding transcripts of core nuclear circadian clock genes in *sal1* and *xrn234* mutants under constant light conditions. qRT-PCR analysis of the accumulation of 3' non-coding transcripts for evening-phased core clock genes **(A,C)** *ELF4* and **(B,D)** *PRR5* in Col-0, *alx8-1*, *fry1-6* and *xrn234* under constant (**A-B**) blue and **(C-D)** white light.. Seedlings were grown on 0.5x MS agar plates and entrained in 12h:12h light:dark cycles under 60 µmol.m^{-2}.s^{-1} white light for 10 days before being transferred to 20 µmol.m^{-2}.s^{-1} constant blue light or 60 µmol.m^{-2}.s^{-1} constant white light at subjective dawn. After 48 hours in free-run, 10-12 seedlings were sampled and pooled, with sampling repeated every three hours for two days. Data for each gene were normalised to an internal control (*PP2a*). White bars and grey bars indicate subjective day and subjective night, respectively. Data are average of three biological replicates. Error bars indicate standard error of the mean.

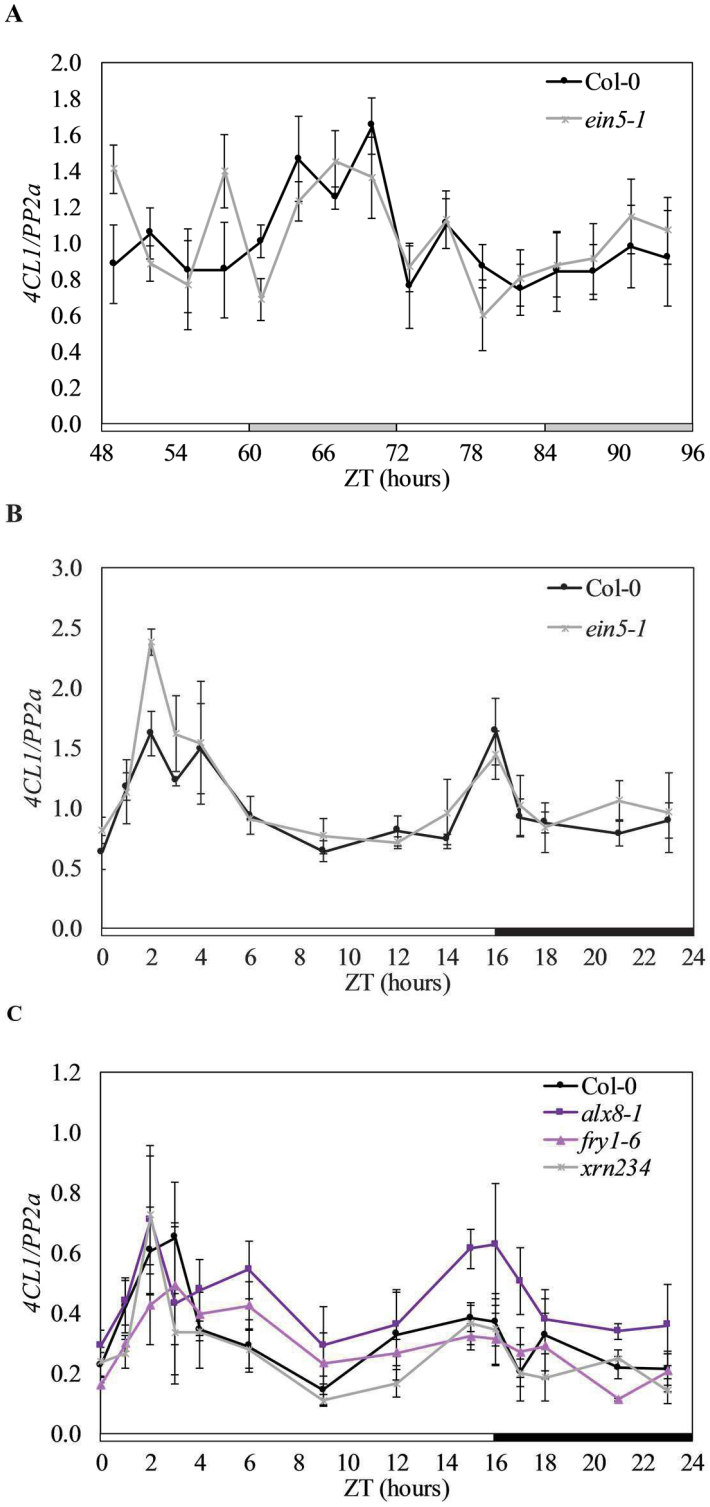

Figure 5.15 Transcription of *4CL1* in *sal1* and *xrn* mutants under constant light and long-day conditions. qRT-PCR analysis of accumulation of *4CL1* transcripts in **(A-B)** Col-0 and *ein5-1*, and in **(C)** Col-0, *alx8-1*, *fry1-6* and *xrn234* under **(A)** constant white light or (**B-C)** long-day conditions. **(A)** Seedlings were grown on 0.5x MS agar plates and entrained in 12h:12h light:dark cycles under 60 µmol.m^{-2}.s^{-1} white light for 10 days before being transferred to 60 µmol.m^{-2}.s^{-1} constant white light at subjective dawn. After 48 hours in free-run, 10-12 seedlings were sampled and pooled, with sampling repeated every three hours for two days. White bars and grey bars indicate subjective day and subjective night, respectively **(B-C)** Seedlings were grown on 0.5x MS agar plates and entrained in 12h:12h light:dark cycles under 60 µmol.m^{-2}.s^{-1} white light for 12 days before harvesting. White bars and black bars indicate day and night, respectively. Data for each gene were normalised to an internal control (*PP2a*). Data are average of three biological replicates. Error bars indicate standard error of the mean.

5.3. Discussion

5.3.1. The long circadian period of sal1 mutants is not due to altered sulfur metabolism

Upon loss of SAL1 function, the accumulation of PAP in *sal1* mutants results in mis-regulation of sulfur metabolism (Rodriguez et al., 2010; Lee et al., 2012). *sal1* mutants exhibit gene expression patterns similar to wild-type plants exposed to sulfate stress, whether in the presence or absence of external sulfate (Figure 5.1, 5.2; Lee et al., 2012). Micronutrients can have an effect on circadian rhythms, as is demonstrated by the long period in rhythmic expression of *CCA1*, *PRR7* and *TOC1* under Fe-starvation conditions (Salomé et al., 2012). In contrast, the micronutrients Cu, Mn and Zn have no effect on circadian period, whether absent or present in excess (Salomé et al., 2012). Very little is known about the effect of sulfur and sulfur metabolism on the circadian system. Previous microarray analysis identifies a small cluster of 5 genes involved in sulfur assimilation that are under circadian control, including genes involved in the uptake and reduction of sulfate and formation of the serine biosynthesis intermediate *O*-acetyl-serine (Harmer et al., 2000). However, analysis of chloroplast and nuclear circadian rhythms in both Col and *sal1* under sulfate starvation conditions did not reveal any lengthening of circadian period under constant light conditions (Figure 5.2 and 5.3). In both Col-0 and *sal1* sulfate starvation either had no effect on circadian rhythm, or resulted in a shortening of period. Similarly the *apk1 apk2* double mutant, in which secondary sulfur metabolism is disrupted (Mugford et al., 2009), does not exhibit a long-period circadian phenotype (Figure 5.4). Rhythms in F_q'/F_m' cycled with a shortened period in *apk1 apk2* compared to Col-0, although this difference was not statistically significant. The observation that sulfate starvation significantly shortens the period of some nuclear rhythms in wild-type (*LHY::LUC* and *PRR7::LUC*), but not others (*CCA1::LUC2*, *CAB2::LUC*, *CCR2::LUC*, and *TOC1::LUC*) needs further investigation. According to the circadian model, a single oscillator can produce rhythmic outputs with different phases, but with only one period (Wood et al., 2001; Hall et al., 2002). Therefore, rhythmic outputs with different periods require different clocks (Wood et al., 2001; Hall et al., 2002). In tobacco, rhythms in cytosolic calcium oscillate

with a shorter period than rhythms of *CAB* expression, while in *Arabidopsis* the rhythmic expression of *PHYB* has an ~1 hour longer free-running period than *CAB* expression (Sai and Johnson, 1999; Hall et al., 2002). It has been suggested that the period difference between *PHYB* and *CAB* expression rhythms is due to regulation by separate copies of the clock mechanism in separate cells that are modified in a tissue-specific manner: *CAB* expression is confined to the mesophyll and guard cells, while *PHYB* is expressed more broadly throughout the aerial organs of the plant (Hall et al., 2002). Distinct, coupled clocks have been reported to occur in the vasculature and mesophyll of *Arabidopsis* (Endo et al., 2014), and it is possible that the different period lengths observed for core clock expression rhythms can be due to tissue-specific effects of sulfate metabolism on oscillators. However, to confirm that the differences in period lengths are significant, circadian rhythms in response to sulfate starvation should be monitored in multiple independent lines for each reporter construct. In addition, investigating the effect of sulfate starvation on rhythms in various clock mutants can shed light on the different roles of specific clock components in rhythmic regulation by sulfur metabolism pathways.

While the exact mechanism underlying the regulation of sulfur metabolism by SAL1 needs further investigation, it has been suggested that the accumulation of PAP may directly inhibit sulfotransferases by shifting the equilibrium towards substrates, thereby leading to reduced efficiency in the sulfation of desulfo-gucosinolates which requires PAPS (Lee et al., 2012). *sal1* shares numerous phenotypes with the *apk1 apk2* double mutant (Rodriguez et al., 2010; Lee et al., 2012). *Arabidopsis* encodes 4 APK isoforms, with APK1, APK2 and APK4 localised in plasmids, and APK3 functioning in the cytosol (Mugford et al., 2009). While single knock-outs of *APK* do not result in visible phenotypical changes, the *apk1 apk2* mutant exhibits a semi-dwarf phenotype and flowers ~1 week later than wild-type, although the wrinkled leaf shape of *sal1* is not present in *apk1 apk2*. Total glucosinolate levels in *apk1 apk2* are reduced to ~20% of wild-type levels, with the greatest reduction occurring in total aliphatic glucosinolates, while indolic glucosinolates are less severely affected. In contrast, the *apk1*

apk4 double mutant contains 30% more glucosinolates than wild-type, while the other *apk* double mutant combinations are not affected (Mugford et al., 2009). Both *sal1* and *apk1 apk2* have lower levels of total glucosinolates (particularly aliphatic glucosinolates) and higher levels of the desulfo-precursors, although this is much more severe in *apk1 apk2* than in *fou8* (Mugford et al., 2009; Lee et al., 2012). Interestingly, quantitative loci mapping of circadian clock outputs have identified quantitative trait loci involved in both circadian regulation and glucosinolate synthesis (Kerwin et al., 2011). The *AOP* locus is linked to natural variation in levels of glucosinolates, and interacts epistatically with two MYB QTLs (MYB28 and MYB19). The natural *AOP2* knockout leads to higher glucosinolate levels compared to Col-0 and exhibits a shortened circadian period (Kerwin et al., 2011). In contrast, the *myb28 myb19* double mutant has lower total glucosinolates and no aliphatic glucosinolates, while also exhibiting a shortened circadian phenotype (Kerwin et al., 2011). These data suggest a possible role for aliphatic glucosinolates in the shortened circadian period observed in *apk1 apk2*, and even sulfate-starved plants.

While the *apk1 fou8*, *apk2 fou8* and *apk3 fou8* double mutants are phenotypically similar to *fou8*, the *apk1 apk2 fou8* triple mutant loses many of the described *fou8* phenotypes and is indistinguishable from *apk1 apk2* in rosette shape and glucosinolate synthesis regulation (Rodriguez et al., 2010; Lee et al., 2012). This pattern was also observed in the analysis of circadian rhythms. No significant difference in the period of F_q'/F_m' rhythms was observed between *apk1 apk2* and *apk1 apk2 fou8* while *fou8* exhibits the characteristically long circadian period of *sal1* mutants (Figure 5.4), suggesting that *SAL1* is epistatic to *APK1* and *APK2*. Furthermore, the absence of a long-period phenotype in *apk1 apk2* or *apk1 apk2 fou8* suggests that the circadian phenotype of *sal1* mutants is not due to a direct perturbation of sulfate metabolism caused by the accumulation of PAP.

5.3.2. Splicing of core clock-regulated transcripts mechanisms remain intact in sal1 mutants

Transcript processing, in particular alternative splicing (AS), plays an important role in circadian regulation. Unproductive alternative splicing is widespread among circadian genes, often producing non-functional transcripts or inducing nonsense-mediated decay (Filichkin and Mockler, 2012; James et al., 2012). In particular, intron retention events in *CCA1*, *LHY,* and *PRR7* transcripts regulate the expression and function of clock components in response to temperature (James et al., 2012). Intact splicing mechanism are needed to maintain circadian rhythms. Mutation in *PROTEIN ARGININE METHYL TRANSFERASE 5* (*PRMT5*), the gene product of which transfers methyl groups to arginine residues present in histones and spliceosomal proteins, changes the levels of unproductive *PRR9* AS transcripts formed through intron retention events, and results in a long period phenotype (Hong et al., 2010; Sanchez et al., 2010). Similarly, mutation in the RNA-binding protein SPLICEOSOMAL TIMEKEEPER LOCUS1 (STIPL1) result in a long period phenotype, possibly as a result of less effective splicing of various clock transcripts, including *CCA1*, *LHY*, *PRR9, GI* and *TOC1* (Jones et al., 2012b). In *sal1* mutants, there was no indication of AS events for *CCA1*, *LHY*, *PRR5* or *TOC1* (Figure 5.5). Only fully spliced transcripts for *LHY, PRR5* and *TOC1* were detected, while the only intron retention event corresponded to the well-conserved and reported retention of intron 4 in *CCA1* (Filichkin et al., 2010). The resulting splice variant, *CCA1β*, encodes a truncated CCA1 form which interferes with CCA1 activity, thereby facilitating a self-regulatory circuit of CCA1 activity involved in temperature regulation of the clock (Seo et al., 2012). In ambient temperatures, oscillation of transcript levels for the two *CCA1* isoforms are synchronised, while *CCA1β* production is repressed under cold temperatures. In *sal1* mutants, oscillations in accumulation of the two *CCA1* isoforms remain synchronised in *sal1* mutants (Figure 5.6), with the same late phase compared to Col-0 that had been observed for other core clock transcripts (Section 4.2.6). These data suggest that the long period phenotype in *sal1* mutants are not as a result of AS in core clock components. This is perhaps not surprising, since the

SAL1/PAP signalling pathway is proposed to act through the inhibition of XRNs, and XRNs are not directly involved in splicing (Nagarajan et al., 2013).

5.3.3. Loss of XRN activity affects the circadian system

While the pleotropic nature of the *sal1* mutation is thought to be due to general inhibition of XRN activities by the accumulation of PAP, identifying the mechanisms through which these phenotypes occur needs further investigation (Hirsch et al., 2011; Estavillo et al., 2011; Chan et al., 2016b). Cells transcribe more RNA than is accumulated and most genomes code a variety of intracellular RNA degrading enzymes, often with functional redundancy (Houseley and Tollervey, 2009; Nagarajan et al., 2013). These RNases occur either as endonucleases that cut RNA internally, as 3' exonucleases that degrade RNA from the 3' end, or as 5' exoribonucleases that degrade RNA from the 5' end (Houseley and Tollervey, 2009). A variety of different types of RNA are degraded in eukaryotes. Almost all RNA species are synthesized as larger precursors that must undergo 3' and/or 5' nuclease processing, while excised rRNA spacer fragments and introns excised from precursor mRNA (pre-mRNA) must also be degraded. Active RNA degradation systems also degrade RNA at the end of its useful life, whether rRNA or as part of the highly regulated turnover of mRNA. In addition, a large number of unstable, non-protein-coding RNAs, as well as defective RNAs are continually identified and degraded (Houseley and Tollervey, 2009; Nagarajan et al., 2013). In eukaryotes, the bulk of mRNA is degraded in the cytoplasm and nucleus by the exosome complex, which has endoribonucleolytic and 3'→5' exoribonuclease activities, as well as by the 5'→3' exoribonuclease activities of cytoplasmic (XRN1) and nuclear (XRN2) XRNs following decapping (Jones et al., 2012a; Houseley and Tollervey, 2009). Through the endonucleolytic pathway, RNA decay is initiated by endonucleolytic cleavage and followed by 3'→5' and 5'→3' exonucleolytic decay of the 5' and 3' cleavage products, respectively (Chiba and Green, 2009). In the decapping/5'→3' pathway, removal of the cap structure produces RNAs with 5' monophosphates, which are the preferred substrates of the 5'→3' exoribonucleases (XRNs)

(Chiba and Green, 2009). In addition to the degradation of mRNA, XRNs also function in other aspects of RNA metabolism, including RNA silencing, rRNA maturation and transcription termination (Nagarajan et al., 2013). The *Arabidopsis* genome codes for three XRN2 orthologs, two of which (XRN2 an XRN3) function in the nucleus, while the third (XRN4) functions in the cytoplasm (Kastenmayer and Green, 2000). The *Arabidopsis* XRNs have distinct identified targets, but also exhibit a degree of functional redundancy which adds to the complexity of XRN activity (Kastenmayer and Green, 2000; Souret et al., 2004; Gy et al., 2007; Rymarquis et al., 2011; Kurihara et al., 2012). While the single null *xrn2* mutation does not result in any visible morphological phenotypes, the homozygous knock-out of *xrn3* is lethal, and the *xrn4* knock-out results in serrated leaves and ethylene insensitivity (Potuschak et al., 2006; Gy et al., 2007; Zakrzewska-Placzek et al., 2010). Analysis of F_q'/F_m' rhythms in *xrn* single, double and triple mutants (Figure 5.7) suggests that activity of the cytoplasmic XRN4, rather than the nuclear XRN2 an XRN3 function within the circadian system. Both the *xrn2* and *xrn3* single mutants, as well as the *xrn2 xrn3* double mutant exhibited wild-type circadian rhythms, yet loss of only XRN4 activity resulted in a significant lengthening of period in the *ein5* mutant (Figure 5.7a, b and c). In addition, no additive effect was observed between *ein5* and the long-period *xrn234* triple mutant (Figure 5.7a).

The long period in chloroplast rhythms of *ein5-1* was echoed in the nuclear rhythms, with a modest late phase in peak transcript accumulation of morning- and evening-phased clock transcripts occurring under constant white light (Figure 5.8). A long circadian period in free-running conditions can manifest as a late phase under entraining conditions (Salomé and McClung, 2005). For example, in the *stipl1* mutant, mutation of the SPLICEOSOMAL TIMEKEEPER LOCUS 1 results in mis-regulation of pre-mRNA splicing and a long circadian period under constant light conditions (Jones et al., 2012b). The long period phenotype of the *stipl1* mutant correlates with delayed accumulation of *CCA1*, *GI, TOC1*, *PRR9* and (to a lesser extent) *LHY* transcripts under long-day light:dark conditions. In the *ein5-1* mutant, a similar

but less severe delay in transcript accumulation is observed in the morning for *CCA1* and *LHY*, and in the afternoon for *ELF4* and *TOC1* transcripts (Figure 5.9).

Previous studies have associated XRN4 function with certain *sal1* mutant phenotypes. *xrn4* and *sal1* have a reduced number of lateral roots, and *sal1* and *xrn4* exhibit reduced sensitivity to IAA in inducing lateral root growth, which is not observed in *xrn2* or *xrn3* single mutants (Chen and Xiong, 2010). Furthermore, microarray analysis revealed a two-fold upregulation of two of the 14 targets of XRN4 in both *alx8-1* and *xrn4-5* mutants (Souret et al., 2004; Wilson et al., 2009). While the *ein5-1* single mutant and the *xrn234* triple mutant mimic the long-period phenotype of *sal1*, the activities of nuclear XRN2 and XRN3 cannot be discounted. In many cases, a combination of XRN2, XRN3 and XRN4 activities seems to be involved in the various *sal1* phenotypes, and studies have attributed *sal1* phenotypes to loss of XRN2 and/or XRN3 activity (Kastenmayer and Green, 2000; Souret et al., 2004; Gy et al., 2007; Estavillo et al., 2011; Nagarajan et al., 2013). Gene expression profiling of *alx8-1* and *xrn2 xrn3* revealed ~4000 and ~2500 transcripts, respectively, that showed a significant change in transcript abundance compared to Col-0 (Estavillo et al., 2011). Of these transcripts, ~50% were coregulated in *alx8-1* and *xrn2 xrn3*. (Souret et al., 2004; Estavillo et al., 2011). In contrast, a much smaller number of transcripts (~150) were significantly altered in *xrn4* compared to Col-0. While null mutation in *XRN2* does not result in morphological changes, *xrn4* mutants have smooth, serrated leaves, and the *xrn3* knock-down mutant exhibits a wrinkled leaf morphology similar to that observed in *sal1* plants (Gy et al., 2007). These morphological characteristics of *xrn3*, including round, crinkled leaves, short petioles, and small rosette size are exacerbated in the *xrn2 xrn3* mutant (Gy et al., 2007). In addition, *xrn2 xrn3*, like *sal1*, has an enhanced response to light in hypocotyl elongation which is not observed in *xrn4* (Kim and von Arnim, 2009; Chen and Xiong, 2011). While null mutation in *XRN2* does not result in late flowering, *xrn4* and *xrn3* single mutants both exhibit moderately delayed flowering, which is more pronounced in *xrn2 xrn3* and *xrn234* (Potuschak et al., 2006; Gy et al., 2007). In *xrn4*, lateral roots exhibit wild-type architecture and a primary root length that is intermediate between Col-

0 and *sal1* primary root lengths (Hirsch et al., 2011). The *xrn234* triple mutant has the same altered lateral root architecture as seen in *sal1*, yet shortened lateral roots are observed in *sal1* but not in *xrn234*. Furthermore, the restoration of fertility in the *xrn234* mutant compared to the infertile *xrn2 xrn3* double mutant suggests that XRN4 can act to suppress XRN2 and XRN3 activity (Hirsch et al., 2011; Kurihara et al., 2012). The varied effects of XRN activities are also observed in plants under stress conditions, and XRN2 and XRN3 (not XRN4) are regarded as playing a role in the negative regulation of stress-responsive genes under drought and high light stress (Estavillo et al., 2011; Chan et al., 2016a). *sal1* mutants survive drought almost 50% longer than wild-type (Wilson et al., 2009), and *xrn2 xrn3* are more drought tolerant than wild-type (but less so than *sal1*) and show similar induction of stress-responsive genes under high light stress (Estavillo et al., 2011). *xrn4* does not exhibit enhanced drought tolerance compared to wild-type (Estavillo et al., 2011), while the *xrn234* is drought tolerant (Hirsch et al., 2011).

The possible overlapping function of XRN2, XRN3 and XRN4 was also observed in circadian regulation. The *xrn234* triple mutant mimics the *sal1* long-period phenotype in chloroplast rhythms (for both chlorophyll *a* fluorescence and delayed fluorescence rhythms, Figure 5.10), while similar late phase patterns in clock-related transcript accumulation are observed in *xrn234* as in *sal1* under constant blue and constant white light conditions (Figure 5.11 and 5.12). Under long-day conditions, however, *sal1* mutants exhibit a clear delay in *CCA1* transcript accumulation, with transcripts present throughout the afternoon in *sal1* (Figure 5.13). This delay also occurs to a lesser extent for *ELF4*, *GI* and *PRR5* transcripts in *sal1*. Similar patterns were observed in the *xrn234* triple mutant, to a lesser extent than in *sal1*, but more pronounced than in *ein5-1* (Figure 5.9). In addition, a dampening of *GI* transcript levels occurs in *xrn234* which is not observed in *xrn4*, further suggesting that the activity of the nuclear XRNs cannot be discounted. Interestingly, in both *sal1* mutant alleles and in *xrn234*, the late phase in clock transcript accumulation is more pronounced under constant blue light than under

constant white light, which would be in agreement with the blue light-specific nature of the *sal1* circadian phenotype.

5.3.4. A mechanism for circadian regulation by XRN activity remains elusive

While these findings shed light on the involvement of individual XRNs in the numerous *sal1* phenotypes, the targets down-stream of XRNs remain elusive. XRNs are known to function as suppressors of post-transcriptional gene silencing (PTGS) (Gazzani et al., 2004; Gy et al., 2007; Rymarquis et al., 2011), and there is strong evidence to suggest that numerous *sal1* phenotypes result from mis-regulation of PTGS arising from the inhibition of XRN2, XRN3 and XRN4 activities (Gy et al., 2007; Chen and Xiong, 2010; Estavillo et al., 2011; Hirsch et al., 2011). PTGS is performed by conserved ARGONAUTE (AGO) proteins to represses gene expression via RNA silencing activity, and is directed in a sequence-specific manner by short, noncoding RNAs called short-interfering RNAs (siRNAs) and microRNAs (miRNAs) (Bartel, 2004; Ambros and Chen, 2007; Peters and Meister, 2007). siRNAs are produced from double-stranded RNA precursors, while miRNAs are generated from RNA hairpins. Both siRNAs and miRNAs associate with protein complexes containing AGO, which cleave target mRNAs that share complementarity to the small RNAs (Bartel, 2004; Ambros and Chen, 2007; Peters and Meister, 2007). The cytoplasmic XRN4 is involved in mRNA degradation by hydrolysing decapped (5' monophosphorylated) mRNA, as well as degrading the 3' intermediate products of smallRNA-directed cleavage, including degradation of the 3' fragment of miRNA-cleaved mRNA (Gazzani et al., 2004; Souret et al., 2004). In the *xrn4* mutant, silencing of a transgene expressed under control of the 35S CaMV promoter is attributed to the accumulation of siRNAs and 5'-decapped mRNA corresponding to transgene sequences (Gazzani et al., 2004). Uncapped mRNAs can be substrates of the RNA-dependent RNA polymerase RDR6 and lead to the formation of double-stranded RNA precursors that are used for siRNA synthesis (Gazzani et al., 2004; Gregory et al., 2008). Interestingly, XRN4 appears to exhibit selectivity among its substrates, as only a select number of miRNA-generated 3' cleavage products

accumulate in *xrn4* (Souret et al., 2004; Rymarquis et al., 2011). The affected 3' cleavage products map to certain functional gene categories, with stamen-associated proteins and hydrolases over-represented among transcripts decreased in *xrn4*, and transcripts encoding nuclear-encoded chloroplast-targeted proteins and nucleic acid–binding proteins over-represented in transcripts that increased in *xrn4* (Rymarquis et al., 2011). One of these targets of XRN4, *4CL1*, provided a promising avenue for further study as its transcript levels are predicted to cycle with circadian rhythm (Souret et al., 2004; Mockler et al., 2007). However, analysis of *4CL1* transcripts in this study indicated no circadian effect, and no change in transcript levels between Col-0 and *xrn* mutants (Figure 5.15). In addition, a more recent analysis of various microarray datasets does not identify *4CL1* as a target of *XRN4* (Rymarquis et al., 2011), further suggesting that XRN4 acts within the circadian system through another mechanism.

A few key studies provide insight into the role of XRN2 and XRN3 in gene silencing, particularly as it pertains to the *sal1* mutant phenotype (Gy et al., 2007; Zakrzewska-Placzek et al., 2010; Estavillo et al., 2011; Kurihara et al., 2012). Like XRN4, the nucleus-localised XRN2 and XRN3 act as suppressors of PTGS, although to a lesser extent than XRN4 (Gy et al., 2007). In addition, XRN2 and XRN3 are also involved in the processing of pre-ribosomal RNA (Zakrzewska-Placzek et al., 2010). Mutation in *xrn2* or *xrn3* restores PTGS in *ago1* mutants defective for PTGS, but less effectively than mutation in *xrn4* (Gy et al., 2007). Importantly, the *sal1* mutation restores PTGS in *ago1* efficiently, likely as a result of the spontaneous inhibition of XRN2, XRN3 and XRN4 activity. Transgene expression in an *ago1* mutant results in high accumulation of transgene mRNA and undetectable levels of transgene siRNAs compared to controls, while *sal1 ago1* mutants have restored transgene mRNA and siRNA accumulation. PTGS is also involved in targeting viral infections, and *sal1* and *xrn4* are hyper-resistant to Cucumber mosaic virus (CMV) infection, exhibiting reduced CMV RNA accumulation and reduced CMV-derived siRNA accumulation than in Col-0. In contrast, mutation in *xrn2* or *xrn3* have no obvious effect on CMV RNA accumulation. As has been

reported for *xrn4*, *sal1* mutants overaccumulate miRNA target 3' cleavage products, but do not exhibit altered accumulation of miRNA-targeted full-length mRNA. This suggests that SAL1 functions during the degradation of intermediates or non-functional end products of small RNA pathways. Excised MIRNA loops (but not stem-loops or partially processed stem loops) derived from DCL1-mediated maturation of miRNA precursors accumulate in *sal1*. This accumulation of MIRNA loops and miRNA cleavage products further suggest impaired exoribonuclease activity in *sal1* mutants. Indeed, MIRNA loops overaccumulate in the hypomorphic *xrn3* single mutant (although to a lesser extent than in *sal1*), while the *xrn2 xrn3* double mutant accumulates MIRNA loops at a higher level than *xrn3* (Gy et al., 2007). Furthermore, the 3' remnants of many DCL1-procesed miRNA precursors also accumulate in *sal1* and *xrn3* mutants (Kurihara et al., 2012).

In addition to MIRNA loops, 3' remnants of miRNA precursors and miRNA cleavage products, *sal1* mutants also accumulate thousands of non-coding transcripts that map to the 3' ends of genes (Kurihara et al., 2012). These 3' non-coding transcripts associate with genes that are actively being transcribed, and SAL1 is suggested to provide general surveillance of these non-coding transcripts, rather than targeting specific gene classes. The accumulation of these transcripts in *sal1* is suggested to be mostly due to the inhibition of XRN3 activity, yet the roles of XRN2 and XRN4 in surveillance of 3' non-coding transcripts needs further investigation. Over 2 000 identified 3' non-coding transcripts are shown to accumulate in *sal1*, with ~500 identified in the hypomorphic *xrn3* mutant. In contrast, ~400 3' non-coding transcripts have been identified in *xrn2 xrn3* and in *xrn3 xrn4*, with only 64 present in *xrn2 xrn4* (Kurihara et al., 2012). Since 3' non-coding transcripts mapping to the core nuclear clock components *ELF4* and *PRR5* were identified as accumulating in *sal1* (Kurihara et al., 2012), these transcripts were investigated as a possible avenue of circadian regulation through XRN activity. While 3' non-coding transcripts for *ELF4* and *PRR5* accumulated to higher level in *sal1* mutant compared to Col-0 under constant light conditions (Figure 5.13), they are unlikely to serve as a mechanism for XRN regulation of the clock in the long-period *sal1* or *xrn* mutants. Firstly, no accumulation

of *ELF4* or *PRR5* 3' non-coding transcripts were observed in *xrn234*, further illustrating the complex nature of overlapping functions between XRN2, XRN3 and XRN4. Secondly, the biological significance of the 3' non-coding transcripts remains a point for debate. These 3' non-coding transcripts are not attached to 5' mRNAs and are not gene transcript extensions (Kurihara et al., 2012). While the possibility exists that these detached 3' non-coding transcripts could function in their capacity as short, non-coding RNAs, the mechanism through which this would occur remains unclear. In addition, while 3' non-coding RNAs map to actively transcribed genes, the 3' non-coding transcripts do not affect the expression levels of their 5' mRNAs (Kurihara et al., 2012), further complicating the question of biological significance of these non-coding transcripts.

The bifunctional nature of the SAL1 enzyme adds yet another level of complexity to an already complicated system that results in the vast array of phenotypes observed in *sal1*mutants. However, data from this chapter strongly suggest that elongation of circadian rhythms in *sal1* occurs through the inhibition of XRN activity rather than through altered sulfur metabolism. These data suggest that the cytoplasmic XRN4, rather than the nuclear XRNs, is involved in circadian regulation, yet the role of XRN2 and XRN3 cannot be discounted. While further study of the exact mechanism of XRN regulation of the clock is needed, it falls beyond the scope of this chapter. In the next chapter, the effect of various environmental inputs on the regulation of circadian rhythms by SAL1 will be investigated.

Chapter 6

Understanding how PAP modulates circadian rhythms in *Arabidopsis*

6.1. Introduction

The inactivation of SAL1 by oxidative stress induces the accumulation of PAP within the cell (Estavillo et al., 2011; Chan et al., 2016). In addition, a number of the broad phenotypes associated with *sal1* mutants correlate with increased endogenous PAP levels (Kim and von Arnim, 2009; Chen et al., 2011; Estavillo et al., 2011; Hirsch et al., 2011). This chapter will investigate the effect of PAP levels on circadian rhythms in Col-0 and *sal1* mutants. The effect of light and osmotic stress on circadian rhythms and PAP accumulation will also be investigated.

6.2. Results

6.2.1. The long-period circadian phenotype of sal1 is light-specific

Analysis of chloroplast and nuclear rhythms in *sal1* mutants had revealed a more pronounced long circadian period phenotype in seedlings grown under constant blue light compared to seedlings grown under constant red or constant white light, suggesting that the circadian phenotype of *sal1* mutants may be dependent upon the wavelength of light (Sections 4.2.3, 4.2.4, 4.3.6 and Section 5.2.5). Furthermore, the shortened hypocotyl phenotype of *sal1* mutants, while observed under both blue and red light (Figure 4.1d), has been reported as being absent in constant darkness (Kim and von Arnim, 2009; Chen and Xiong, 2011). To determine whether the long period circadian phenotype of *sal1* mutants is observed in the absence of light, rhythms in *CCA1* expression was monitored in seedlings grown under constant darkness. Col-

0 *CCA1::LUC2* and *fry1-6 CCA1::LUC2* seedlings were grown on 0.5x MS agar plates supplemented with sucrose for 6 days in 12h:12h light dark cycle under 60 µmol.m^{-2}.s^{-1} white light. Following entrainment, individual seedlings were imaged under constant darkness and time series data subjected to FFT-NLLS analysis. Bioluminescence from *CCA1::LUC2* activity cycled with robust circadian rhythm in Col-0 in constant darkness, with a slightly longer period than normally observed in constant light (25.27 ± 0.16 h; Figure 6.1a and b). The robust circadian rhythm with a period of ~25 hours corresponded to a previous report describing rhythms in *CCR2::LUC* in Col-0 seedlings imaged under constant darkness and in the presence of sucrose (Jones et al., 2012). *CCA1::LUC2* rhythms also cycled with circadian rhythm in *fry1-6*, and no significant difference in period (25.70 ± 0.20 h) compared to Col-0 was observed, indicating that the circadian phenotype of *sal1* is observed only in the presence of light.

To further investigate whether the long period phenotype of *sal1* is affected by the wavelength or fluence rate of light, rhythms in *CCA1* expression was monitored under different fluence rates of constant blue light or constant red light. Col-0 *CCA1::LUC2* and *fry1-6 CCA1::LUC2* seedlings were grown on 0.5x MS agar plates for 6 days in 12h:12h light dark cycle under 60 µmol.m^{-2}.s^{-1} white light. Following entrainment, individual seedlings were imaged under different fluence rates of constant blue light (3, 6, 20 or 40 µmol.m^{2}.s^{-1}) or constant red light (3, 11, 30 or 53 µmol.m^{-2}.s^{-1}) for ~5 days. Bioluminescence from *CCA1::LUC2* activity cycled with circadian rhythm in both Col-0 and *fry1-6* under all 4 fluence rates of constant blue light analysed (Figure 6.2). As had been observed under constant darkness, Col-0 and *fry1-6* seedlings grown under low fluence rates (3 µmol.m^{-2}.s^{-1} or 6 µmol.m^{-2}.s^{-1}) exhibited *CCA1::LUC2* rhythms with period >24 hours (Figure 6.2a and b). However, no significant difference in period was observed in *fry1-6* compared to Col-0 in seedlings grown under either 3 or 6 µmol.m^{-2}.s^{-1} constant blue light (p>0.05, Student's t-test). At higher fluence rates of blue light, rhythms in *CCA1::LUC2* cycled with ~24 hour period in Col-0 (Figure 6.2a, c and d).

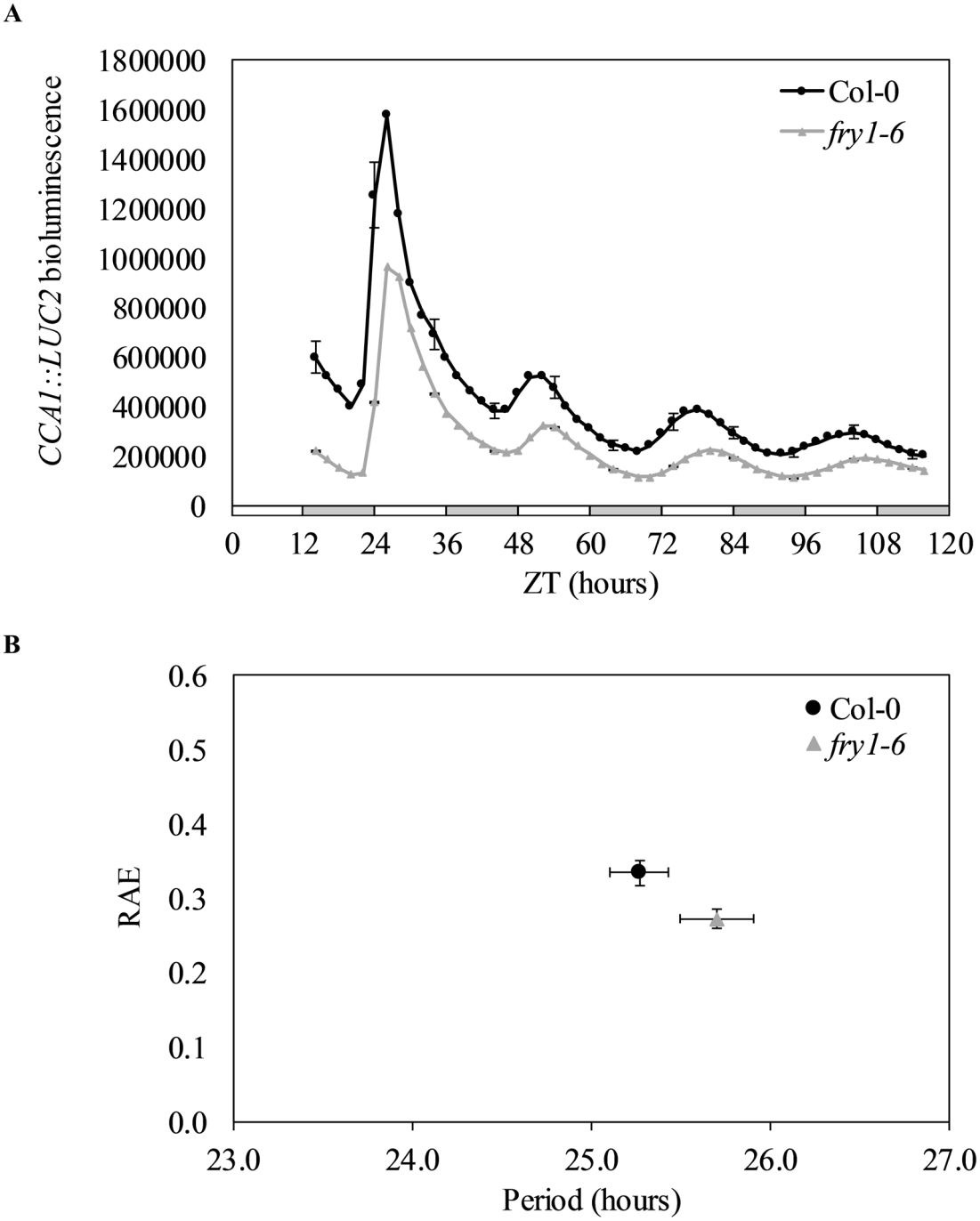

Figure 6.1 Rhythms in *CCA1* expression in *sal1* in constant darkness. **(A)** Waveforms and **(B)** circadian period estimates plotted against Relative Amplitude Error (RAE) for luciferase activity monitored in Col-0 *CCA1::LUC2* and *fry1-6 CCA1::LUC2* seedlings under constant dark conditions. Seedlings were grown on 0.5x MS agar plates supplemented with sucrose, and entrained in 12h:12h light:dark cycles under 60 $\mu mol.m^{-2}.s^{-1}$ white light for 6 days before imaging in constant darkness. White bars and grey bars indicate subjective day and subjective night, respectively. Error bars indicate standard error of the mean, with n=20. For waveforms, error bars are shown every 10 hours for clarity. RAE is a measure of rhythmic robustness, with a value of 0 indicating an exact fit to a cosine wave (Plautz et al., 1997). Data from one of two independent experiments are shown.

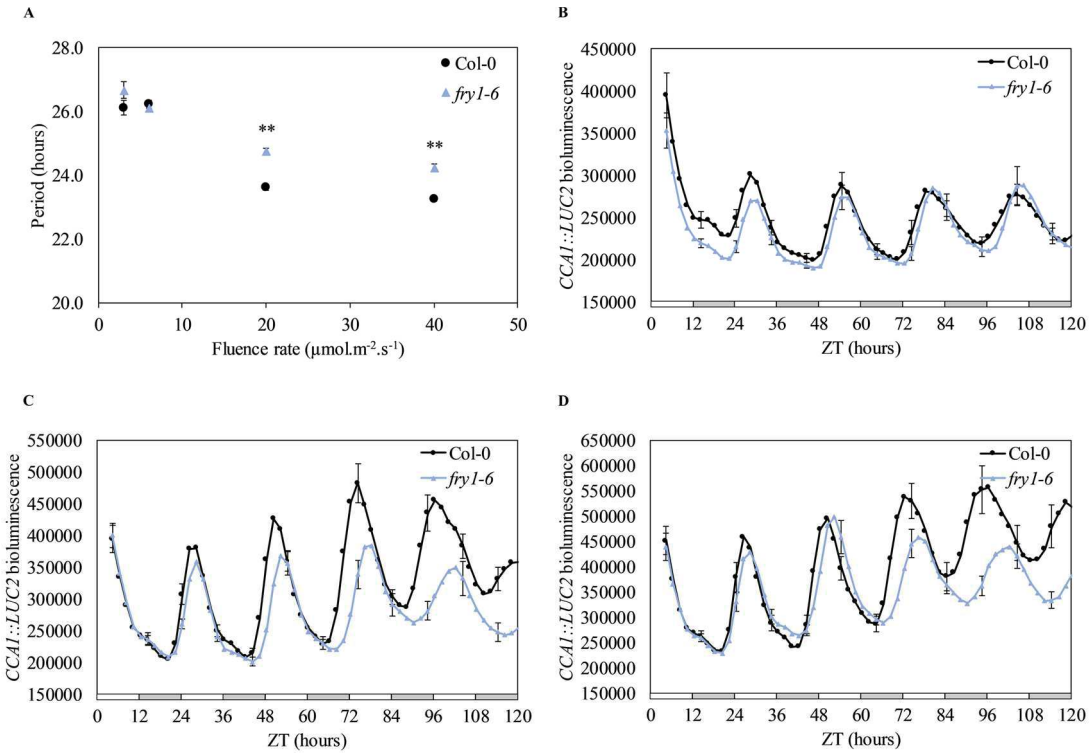

Figure 6.2 Rhythms in *CCA1* expression in *sal1* under different fluence rates of constant blue light. (A) Fluence rate response curve of circadian period estimates for luciferase activity monitored in Col-0 *CCA1::LUC2* and *fry1-6 CCA1::LUC2* seedlings under 3, 6, 20 and 40 µmol.m^{-2}.s^{-1} constant blue light . **(B-D)** Waveforms of luciferase activity monitored in Col-0 *CCA1::LUC2* and *fry1-6 CCA1::LUC2* seedlings under **(B)** 6 µmol.m^{-2}.s^{-1}, **(C)** 20 µmol.m^{-2}.s^{-1} and **(D)** 40 µmol.m^{-2}.s^{-1} constant blue light Seedlings were grown on 0.5x MS agar plates and entrained in 12h:12h light:dark cycles under 60 µmol.m^{-2}.s^{-1} white light for 6 days before imaging under constant blue light. White bars and grey bars indicate subjective day and subjective night, respectively. Error bars indicate standard error of the mean, with n=30. For waveforms, error bars shown every 10 hours for clarity. RAE is a measure of rhythmic robustness, with a value of 0 indicating an exact fit to a cosine wave (Plautz et al., 1997). Data from one of two independent experiments are shown. Asterisks indicate statistically significant difference in period compared to Col-0 control at the comparative fluence rate (** p<0.001, Student's T-test).

Under 20 µmol.m^{-2}.s^{-1}, rhythms in *CCA1:LUC2* cycled with a significantly longer period in *fry1-6* (24.74 ± 0.10 h) compared to Col-0 (23.60 ± 0.09 h; p<0.001, Student's T-test) as had been previously observed (Section 4.2.4). Similarly under 40 µmol.m^{-2}.s^{-1} constant blue light, rhythms in *CCA1::LUC2* cycled with ~1 hour longer period in *fry1-6* (24.22 ± 0.12 h) compared to Col-0 (23.26 ± 0.07 h; p<0.001, Student's T-test).

Under constant red light as under constant blue light, *CCA1::LUC2* activity oscillated with robust rhythms in both *fry1-6* and Col-0 under all 4 different fluence rates (Figure 6.3), with circadian period estimates indicating a period of more than 24 hours in both Col-0 and *fry1-6* under low fluence rates (3 µmol.m^{-2}.s^{-1} or 11 µmol.m^{-2}.s^{-1}), and shorter under higher fluence rates (30 µmol.m^{-2}.s^{-1} or 53 µmol.m^{-2}.s^{-1}). Under 3 µmol.m^{2}.s^{-1} constant red light, *CCA1::LUC2* activity appeared to oscillate with longer circadian rhythm in Col-0 (31.28 ± 0.28 h) compared to rhythms in *fry1-6* (30.25 ± 0.25 h), although this difference was not significant (p>0.05, Student's t-test; Figure 6.3a). Similarly, under 11 µmol.m^{-2}.s^{-1}, *CCA1::LUC2* rhythms observed in Col-0 (27.42 ± 0.15 h) tended towards being longer than in *fry1-6* (26.70 ± 0.16 h), but this was not significant (Figure 6.3a and b). As was observed in DF rhythms in *alx8-1* under constant red light (Section 4.2.3), no significant period lengthening in *CCA1::LUC2* rhythms was observed in *fry1-6* under 30 µmol.m^{-2}.s^{-1} constant red light, with 24.32 ± 0.12 h period in Col-0, and 24.50 ± 0.12 h period in *fry1-6* (Figure 6.3a and c). These data agree with the less severe circadian phenotype observed in chloroplast and transcript accumulation rhythms of *sal1* under 30 µmol.m^{-2}.s^{-1} constant red light compared to 20 µmol.m^{-2}.s^{-1} constant blue light (Sections 4.2.3, 4.2.4 and 4.2.6). Furthermore, no significant difference in period was observed in *CCA1::LUC2* rhythms between *fry1-6* and Col-0 under the highest fluence rate of constant red light (53 µmol.m^{-2}.s^{-1}; Figure 6.3a and d).

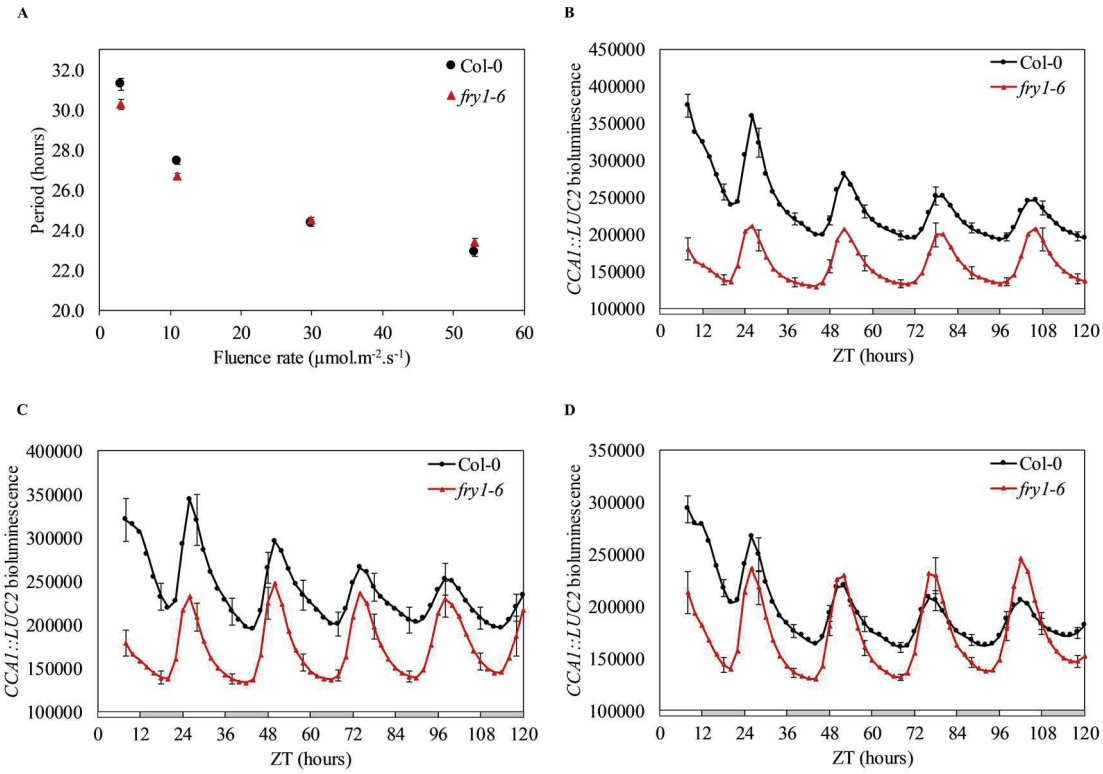

Figure 6.3 Rhythms in *CCA1* expression in *sal1* under different fluence rates of constant red light. (A) Fluence rate response curve of circadian period estimates for luciferase activity monitored in Col-0 *CCA1::LUC2* and *fry1-6 CCA1::LUC2* seedlings under 3, 11, 30 and 53 µmol.m^{-2}.s^{-1} constant red light . **(B-D)** Waveforms of luciferase activity monitored in Col-0 *CCA1::LUC2* and *fry1-6 CCA1::LUC2* seedlings under **(B)** 11 µmol.m^{-2}.s^{-1}, **(C)** 30 µmol.m^{-2}.s^{-1} and **(D)** 53 µmol.m^{-2}.s^{-1} constant red light Seedlings were grown on 0.5x MS agar plates and entrained in 12h:12h light:dark cycles under 60 µmol.m^{-2}.s^{-1} white light for 6 days before imaging under constant red light. White bars and grey bars indicate subjective day and subjective night, respectively. Error bars indicate standard error of the mean, with n=20. For waveforms, error bars shown every 10 hours for clarity. RAE is a measure of rhythmic robustness, with a value of 0 indicating an exact fit to a cosine wave (Plautz et al., 1997). Data from one of two independent experiments are shown. Asterisks indicate statistically significant difference in period compared to Col-0 control at the comparative fluence rate (** p<0.001, Student's T-test).

6.2.2. Circadian rhythms are restored in sal1 mutants overexpressing the SAL1 homologue AHL

Irrespective of the absence or presence of abiotic stresses such as high light, drought or salt stress, *sal1* mutants accumulate higher levels of endogenous PAP than wild-type plants both as seedlings (Chen et al., 2011) and as adult plants (Estavillo et al., 2011; Lee et al., 2012). To confirm that *sal1* mutants accumulate PAP under the experimental conditions used in this study, the PAP content of *fry1-6* seedlings grown under constant light was examined. Col-0 and *fry1-6* seedlings were grown on 0.5x MS agar plates for 12 days in 12h:12h light:dark cycles under 60 µmol.m^{-2}.s^{-1} white light before being transferred to 60 µmol.m^{-2}.s^{-1} constant white light at subjective dawn. After 4 days in constant conditions, ~50 seedlings per genotype (150-300 mg tissue) were harvested at subjective dawn (ZT96), and PAP extracted and quantified using reverse-phase HPLC analysis according to a published method (Bürstenbinder et al., 2007; Estavillo et al., 2011). PAP was present in very low levels in Col-0 seedlings, and a ~10-fold higher PAP content was detected in *fry1-6* seedlings grown under constant white light (9 nmol nmol.g^{-1} FW; p<0.001, Student's T-test; Figure 6.4a). The increased level of PAP in *fry1-6* seedlings under constant white light correlated with the ~3 hour late phase in transcript accumulation for the evening-phased clock component *PRR5* under the constant white light conditions (Figure 6.4b).

In the *fry1-6* mutant, overexpression of the PAP-specific SAL1 paralog AHL has been shown to complement the rosette shape, reduced hypocotyl length, altered root architecture and increased drought tolerance phenotypes of *sal1* (Kim and von Arnim, 2009; Hirsch et al., 2011). To determine whether overexpression of AHL could restore circadian rhythms in a *sal1* mutant, F_q'/F_m' rhythms were monitored in T1 generation *alx8-1* seedlings expressing the cDNA of *AHL* driven by the CaMV 35S promoter (*alx8-1 35S::AHL:GFP,* Appendix II) under 20 µmol.m^{-2}.s^{-1} constant blue light (Figure 6.4c).

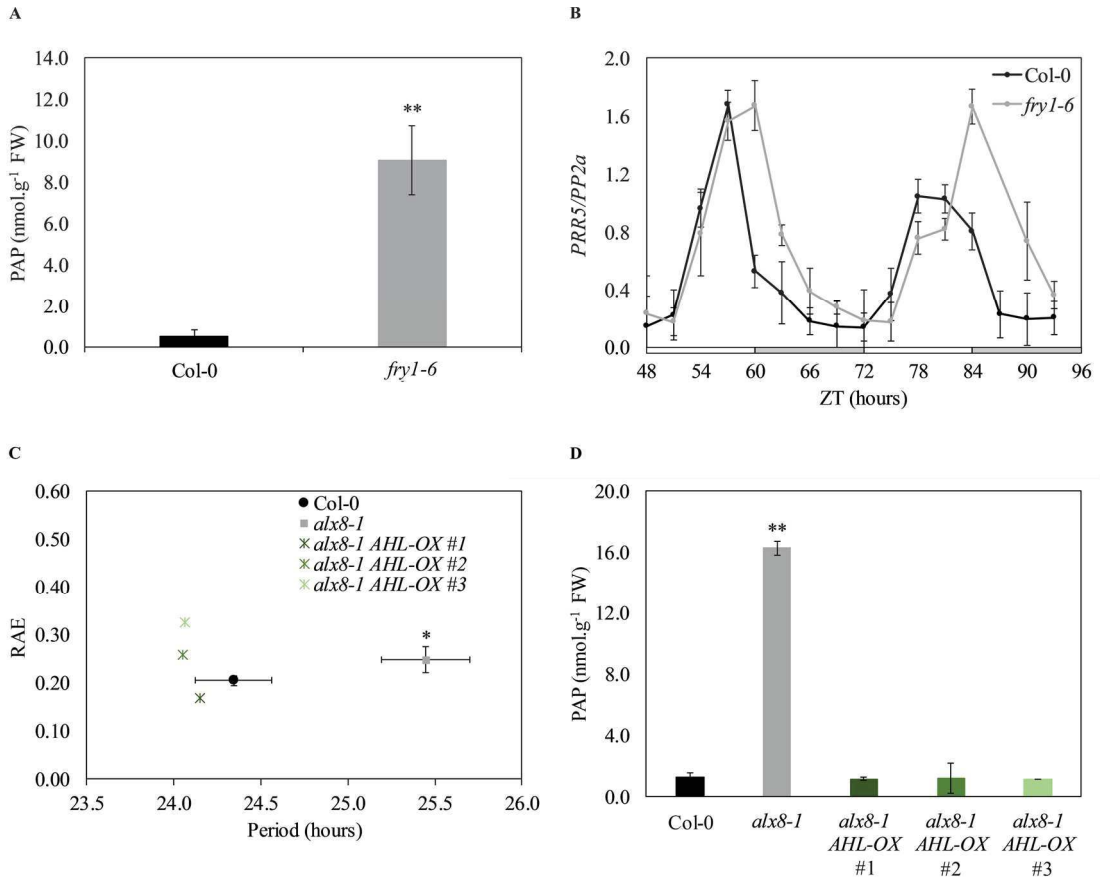

Figure 6.4 PAP accumulation and circadian rhythms in *sal1* mutants under constant light conditions. (A) Quantification of endogenous PAP in Col-0 and *fry1-6* seedlings under constant white light. Seedlings were grown on 0.5x MS agar plates and entrained in 12h:12h light:dark cycles under 60 µmol.m^{-2}.s^{-1} white light for 12 days before transfer to 60 µmol.m^{-2}.s^{-1} constant white light at subjective dawn. Following 4 days in constant conditions, ~50 seedlings per genotype were harvested at subjective dawn (ZT96) and PAP quantified by reverse-phase HPLC as previously described (Bürstenbinder et al., 2007; Estavillo et al., 2011). Error bars indicate standard deviation, with n=4. **(B)** Rhythms in accumulation of the core clock transcript *PRR5* in Col-0 and *fry1-6* seedlings under constant white light. Seedlings were grown on 0.5x MS agar plates and entrained in 12h:12h light:dark cycles under 60 µmol.m^{-2}.s^{-1} white light for 10 days before being transferred to 60 µmol.m^{-2}.s^{-1} constant white light at subjective dawn. After 48 hours in free-run, 10-12 seedlings were sampled and pooled, with sampling repeated every three hours for two days. Data for each gene were normalised to an internal control (*PP2a*). White bars and grey bars indicate subjective day and subjective night, respectively. Data are representative of three biological replicates. Error bars indicate standard error of the mean of three technical replicates. **(C)** Circadian period estimates plotted against RAE of oscillations in *Fq'/Fm'* in Col-0, *alx8-1* and individual seedlings of the T1 generation of three independent *alx8-1 35S::AHL:GFP* (*alx8-1 AHL-OX*). Seedlings were grown on 0.5x MS agar plates and entrained in 12h:12h light:dark cycles under 60 µmol.m^{-2}.s^{-1} white light for 12 days before imaging in 20 µmol.m^{-2}.s^{-1} constant blue light. Error bars indicate standard error of the mean, with n=8. RAE is a measure of rhythmic robustness, with a value of 0 indicating an exact fit to a cosine wave (Plautz et al., 1997). Data from one of two independent experiments are shown. **(D)** Quantification of endogenous PAP in Col-0, *alx8-1* and three independent homozygous *alx8-1 35S::AHL:GFP* lines (*alx8-1 AHL-OX*) under constant blue light. Seedlings were grown on 0.5x MS agar plates and entrained in 12h:12h light:dark cycles under 60 µmol.m^{-2}.s^{-1} white light for 12 days before transfer to 20 µmol.m^{-2}.s^{-1} constant blue light at subjective dawn. Following 4 days in constant conditions, ~50 seedlings per genotype were harvested at subjective dawn (ZT96) and PAP quantified by reverse-phase HPLC as previously described (Bürstenbinder et al., 2007; Estavillo et al., 2011). Error bars indicate standard deviation, with n=4. Asterisks indicate statistically significant difference in **(A,C)** PAP content or **(B)** circadian period, compared to Col-0 control (* p<0.01, ** p<0.001, Student's T-test).

While F_q'/F_m' rhythms in *alx8-1* exhibited a significantly long period (25.45 ± 0.34 h) compared to Col-0 (24.34 ± 0.20 h; $p<0.01$, Student's T-test), the ~1 hour longer period of *alx8-1* was not observed in individual T1 *alx8-1 35S::AHL:GFP,* seedlings (24.15 ± 0.17 h for line #1; 24.05 ± 0.26 h for line #2; 24.06 ± 0.33 h for line #3). To examine the effect of AHL overexpression on PAP accumulation in a *sal1* mutant grown under constant blue light, the level of endogenous PAP was examined in Col, *alx8-1* and homozygous T3 seedlings of three independent *alx8-1 35S::AHL:GFP* lines. Seedlings were grown on 0.5x MS agar plates for 12 days in 12h:12h light:dark cycles under 60 µmol.m^{-2}.s^{-1} white light before being transferred to 20 µmol.m^{-2}.s^{-1} constant blue light at subjective dawn. After 4 days in constant blue light, seedlings were harvested and PAP quantified as described above. As had been observed under constant white light, PAP was present in low levels in Col-0 seedlings (1.2 nmol.g^{-1} FW; Figure 6.4d) under constant blue light. *alx8-1* seedlings accumulated ~13-fold more endogenous PAP than Col-0 seedlings (16.3 nmol.g^{-1} FW; $p<0.001$,Students' T-test), marginally higher than observed for *fry1-6* grown under constant white light (Figure 6.4a). In contrast, overexpression of AHL resulted in a significant decrease in endogenous PAP content in *sal1*, with no significant difference in PAP content between *alx8-1 35S::AHL:GFP* seedlings and Col-0 ($p>0.05$, Student's t-test).

6.2.3. Increase in endogenous PAP content in sal1 is dependent on light intensity

In *sal1* seedlings, the long period circadian phenotype correlates with higher endogenous PAP levels relative to wild-type under 60 µmol.m^{-2}.s^{-1} constant white light or 20 µmol.m^{-2}.s^{-1} constant blue light (Figure 6.4). To determine whether the accumulation of PAP, like circadian period, is affected by the fluence rate of light in *sal1* mutants, endogenous PAP content of *sal1* mutants grown under different fluence rates of constant blue light was examined. Seedlings were grown on 0.5x MS agar plates for 12 days in 12h:12h light:dark cycles under 60 µmol.m^{-2}.s^{-1} white light before being transferred to 5, 20 or 40 µmol.m^{-2}.s^{-1} constant blue light at subjective dawn. After 4 days in constant conditions, seedling were harvested and PAP

extracted and quantified as described for Figure 6.4. PAP was present in very low levels (or undetectable) in Col-0, compared to significantly higher quantities in *fry1-6, alx8-1* and *fou8* under all fluence rates of constant blue light (Figure 6.5a, b and c). This corresponds to previous reports of very low PAP levels in wild-type seedlings, and accumulation of PAP in *sal1* seedlings, under non-stressed conditions (Section 6.2.2; Chen et al., 2011). Furthermore, no difference in PAP content was observed in Col-0 under different fluence rates of constant blue light. Interestingly, PAP accumulated at significantly higher levels under 20 $\mu mol.m^{-2}.s^{-1}$ and 40 $\mu mol.m^{-2}.s^{-1}$ constant blue light compared to 5 $\mu mol.m^{-2}.s^{-1}$ ($p<0.001$, Student's T-test) in *fry1-6* (Figure 6.5a) with no difference in PAP content observed between *fry1-6* seedlings grown under the two highest fluence rates. Similarly, *alx8-1* seedlings accumulated ~6-fold more endogenous PAP when grown under 40 $\mu mol.m^{-2}.s^{-1}$ compared to *alx8-1* seedlings grown under 5 $\mu mol.m^{-2}.s^{-1}$ ($p<0.001$, Student's T-test; Figure 6.5b). The same pattern of increased PAP accumulation under higher fluence rates of constant blue light was observed in *fou8* (Figure 6.5c) with a ~5-fold increase in PAP quantity in seedlings grown under 5 $\mu mol.m^{-2}.s^{-1}$ compared to 40 $\mu mol.m^{-2}.s^{-1}$ constant blue light.

6.2.4. Accumulation of SAL1 is not altered under different light qualities

Since the circadian phenotype and the accumulation of PAP in *sal1* were affected by light conditions, the effect of different wavelengths and fluence rates of constant light on the expression of SAL1 was investigated. Firstly, the transcription of *SAL1* in Col-0 was examined under constant darkness using qRT-PCR. Col-0 seedlings were grown on 0.5x MS agar plates in 12h:12h light:dark cycles under 60 $\mu mol.m^{-2}.s^{-1}$ white light for 10 days, subsequently transferred to constant darkness at subjective dawn, and 10-12 seedlings per time point sampled from subjective dawn (ZT24) every 3 hours for two days. Strong circadian rhythms in transcript accumulation for the evening-phased core clock component *GI* confirmed that gene transcription was still actively taking place in seedlings after three days in constant darkness (Figure 6.6a).

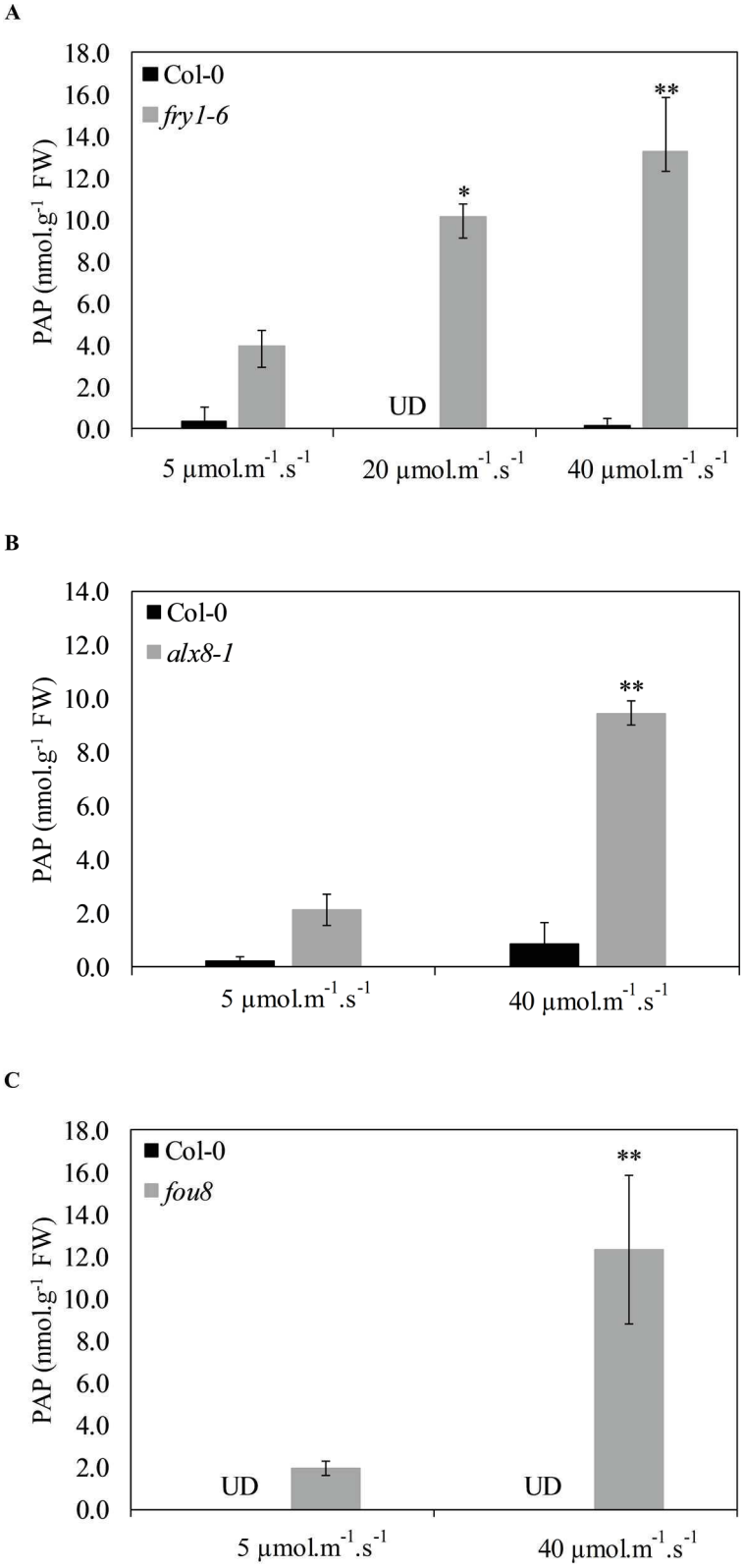

Figure 6.5 Accumulation of PAP in *sal1* under different fluence rates of constant blue light. **(A-C)** Quantification of endogenous PAP in **(A)** Col-0 and *fry1-6* seedlings, in **(B)** Col-0 and *alx8-1* seedlings, and in **(C)** Col-0 and *fou8* seedlings under 5, 20 or 40 µmol.m^{-2}.s^{-1} constant blue light. Seedlings were grown on 0.5x MS agar plates and entrained in 12h:12h light:dark cycles under 60 µmol.m^{-2}.s^{-1} white light for 12 days before transfer to constant blue light at subjective dawn. Following 4 days in constant conditions, ~50 seedlings per genotype were harvested at subjective dawn (ZT96) and PAP quantified by reverse-phase HPLC as previously described (Bürstenbinder et al., 2007; Estavillo et al., 2011). Error bars indicate standard deviation, with n=4. Asterisks indicate statistically significant difference in PAP content compared to comparative *sal1* mutant grown under 5 µmol.m^{-2}.s^{-1} constant blue light (* p<0.01, ** p<0.001, Student's T-test).

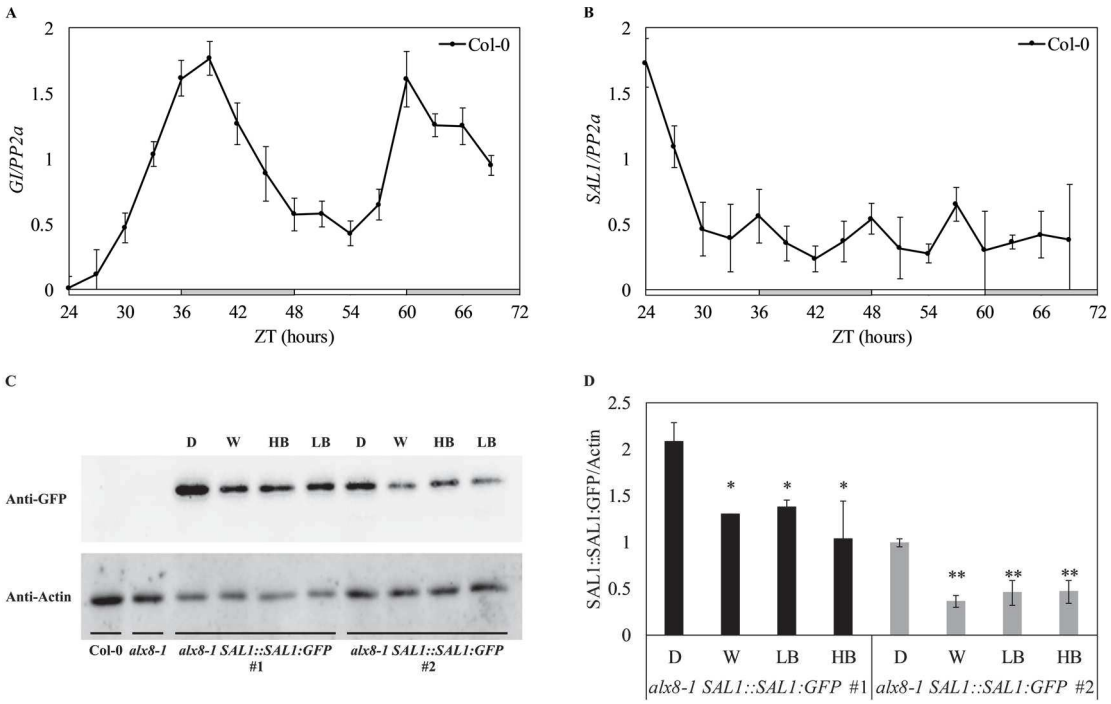

Figure 6.6 Expression of *SAL1* under different light conditions. **(A-B)** Rhythms in accumulation of **(A)** the core clock transcript *GI* and **(B)** *SAL1* in Col-0 and *fry1-6* seedlings under constant darkness. Seedlings were grown on 0.5x MS agar plates and entrained in 12h:12h light:dark cycles under 60 µmol.m^{-2}.s^{-1} white light for 10 days before being transferred to constant darkness at subjective dawn. After 24 hours in free-run, 10-12 seedlings were sampled and pooled, with sampling repeated every three hours for two days. Data for each gene were normalised to an internal control (*PP2a*). White bars and grey bars indicate subjective day and subjective night, respectively. Data are representative of two biological replicates. Error bars indicate standard error of the mean. **(C)** Immunoblot analysis and **(D)** quantification of SAL-GFP levels under constant light conditions using an anti-GFP antibody in Col-0, *alx8-1* and two independent *alx8-1 SAL1::SAL1:GFP* lines, one with higher (#1) and one with lower expression of SAL1-GFP (#2). Anti-Actin antibody was used to detect actin levels for loading control. Seedlings were grown on 0.5x MS agar plates in 12h:12h light:dark cycles under 60 µmol.m^{-2}.s^{-1} white light for 12 days before transfer to constant darkness (D), constant low blue light (5 µmol.m^{-2}.s^{-1} blue light, LB), constant higher blue light (40 µmol.m^{-2}.s^{-1} blue light) or constant white light (60 µmol.m^{-2}.s^{-1} white light). Immunoblots from one of three independent experiments are shown. Protein level quantification data are average of three independent experiments. Data were normalised to internal control (Actin). Error bars indicate standard error of the mean. Asterisks indicate statistical significance of SAL1-GFP protein level compared to level under constant darkness for each independent line (* p<0.01, ** p<0.001, Student's T-test).

No rhythm in transcript accumulation was observed for *SAL1* transcripts (Figure 6.6b), which is similar to transcription patterns of *SAL1* observed under constant light and long-day conditions (Section 4.2.2). Unlike *GI* transcripts, which continue to cycle under constant darkness, transcript levels of *SAL1* were suppressed within 6 hours of transfer to constant darkness. This corresponds to a previous reports of rapid downregulation of *SAL1* transcription within 1 hour of transferring seedlings from light:dark cycles to darkness (Kim and von Arnim, 2006, 2009).

To analyse the accumulation of SAL1 protein under different light conditions, immunoblot analyses was performed on total protein extracts from homozygous T3 seedlings of two independent *alx8-1 SAL1::SAL1:GFP* lines (*alx8-1 SAL1::SAL1:*GFP #1 and #2; Section 4.2.5, Appendix II). Seedlings were grown on 0.5x MS agar plates in 12h:12h light:dark cycles under 60 $\mu mol.m^{-2}.s^{-1}$ white light for 12 days, and subsequently transferred to 60 $\mu mol.m^{-2}.s^{-1}$ constant white light, 40 $\mu mol.m^{-2}.s^{-1}$ constant blue light, 5 $\mu mol.m^{-2}.s^{-1}$ constant blue light or constant darkness. After 3 days in free-running conditions, tissue (12-15 seedlings) was harvested in the subjective afternoon (ZT77). Immunoblot analysis was performed on total protein extracts using an anti-GFP antibody, and intensity of protein bands quantified using ImageJ. SAL1-GFP protein was detected in both independent lines of *alx8-1 SAL1::SAL1:GFP* under all 4 different light conditions (Figure 6.6c and d). Interestingly, quantification of SAL1-GFP revealed significantly higher protein expression accumulation in seedlings grown under constant darkness compared to constant light, despite the suppression of transcript levels under constant darkness (Figure 6.6b). No significant difference in protein levels was observed in seedling grown under 5 or 40 $\mu mol.m^{-2}.s^{-1}$ constant blue light, or 60 $\mu mol.m^{2}.s^{1}$ constant white light (Figure 6.6c and d).

6.2.5. Application of LiCl or exogenous PAP affects circadian period

Since the long period circadian phenotype of *sal1* correlated with increased accumulation of endogenous PAP (Figure 6.4 and 6.5), the effect of exogenous PAP treatments on circadian period was investigated. Loss or inhibition of SAL1 function results in the accumulation of PAP (Estavillo et al., 2011; Chan et al., 2016), and lithium (Li^+) is a known inhibitor of the 3',5'-bisphosphate nucleotidase activity of *Arabidopsis* SAL1 (Quintero et al., 1996; Xiong et al., 2004). To determine whether lithium affects circadian rhythms in Col-0, the rhythmic expression of nuclear clock-controlled components *CAB2, CCA1, LHY, GI* and *TOC1* were examined through imaging of the Col-0 luciferase reporter lines *CAB2::LUC+*, *CCA1::LUC+*, *GI::LUC+*, *LHY::LUC+* and *TOC1::LUC+* treated with LiCl under constant blue light. Seedlings were grown on 0.5x MS agar plates for 6 days in 12h:12h light dark cycle under 60 $\mu mol.m^{-2}.s^{-1}$ white light. Seedling (in clusters of ~5) were subsequently imaged under 20 $\mu mol.m^{-2}.s^{-1}$ constant blue light for 1 day, after which plants were sprayed with LiCl (100 mM, prepared in 0.01% Triton X-100) or a mock control (0.01% Triton X-100) in the subjective afternoon (~ZT30). Luciferase imaging was continued for an additional 5 days, and time series data collected after application of treatments subjected to FFT-NLLS analysis. Application of LiCl had no effect on the robustness of circadian rhythms, but resulted in a significant, >1 h elongation in period for rhythmic expression of *CAB, CCA1* and *GI* in Col-0 compared to mock-treated Col-0 luciferase reporter seedlings ($p<0.001$, Student's T-test; Figure 6.7a). A similar, but less severe (~0.5 h) elongation in period was observed for rhythmic expression of *LHY* and *TOC1* in Col-0 reporter line seedlings treated with LiCl compared to mock controls ($p<0.01$, Student's T-test). To determine whether application of SAL1-inhibiting LiCl affects circadian rhythms in a loss-of-function *sal1* mutant, rhythmic expression of *CCA1* was examined in Col-0 *CCA1::LUC2* and *fry1-6 CCA1::LUC2* treated with LiCl. Individual seedlings were entrained, imaged under constant blue light and treated with LiCl or a mock control as described for Figure 6.7a above.

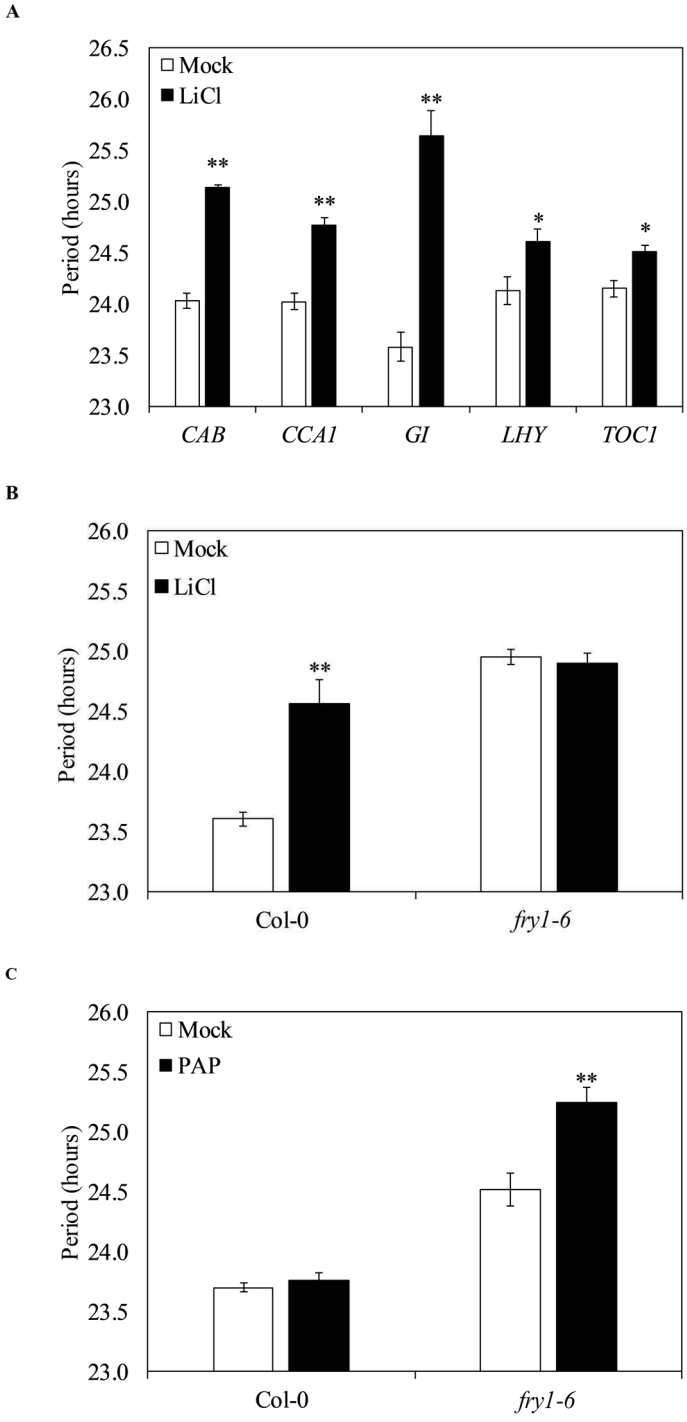

Figure 6.7 Effect of LiCl or exogenous PAP on nuclear circadian rhythms in Col-0 and *sal1* under constant blue light. (A-B) Circadian period estimates for luciferase activity monitored in **(A)** Col-0 *CAB2::LUC+, CCA1::LUC+, GI::LUC+, LHY::LUC+* and *TOC1::LUC+* seedlings, and in **(B)** Col-0 *CCA1::LUC2* and *fry1-6 CCA1::LUC2* seedlings treated with LiCl under constant blue light. **(C)** Circadian period estimates for luciferase activity monitored in Col-0 *CCA1::LUC2* and *fry1-6 CCA1::LUC2* seedlings treated with PAP under constant blue light. Seedlings were grown on 0.5x MS agar plates and entrained in 12h:12h light:dark cycles under 60 $\mu mol.m^{-2}.s^{-1}$ white light for 6 days before imaging in 20 $\mu mol.m^{-2}.s^{-1}$ constant blue light. After 1 day of imaging, seedlings were sprayed with **(A-B)** 100 mM LiCl or **(C)** 1 mM PAP in the subjective afternoon (~ZT30) and imaging continued for ~5 days. Error bars indicate standard error of the mean, with n=20. Data from one of three independent experiments are shown. Asterisks indicate statistical significance in circadian period compared to mock-treated control for each comparative genotype (* $p<0.01$, ** $p<0.001$, Student' T-test).

Bioluminescence from *CCA1::LUC2* activity cycled with robust circadian rhythm in LiCl- and mock-treated seedlings of both genotypes, with a significant, ~1 hour elongation in period observed in Col-0 seedlings treated with LiCl (24.56 27 ± 0.20 h) compared to mock-treated Col-0 seedlings (23.60 27 ± 0.06 h; $p<0.001$, Student's T-test; Figure 6.7b). Interestingly, no significant difference in period was observed between *fry1-6* seedlings treated with LiCl and *fry1-6* seedlings treated with mock control.

In a more direct approach to investigate the effect of increased PAP on circadian period, rhythms in expression of *CCA1* were monitored in Col-0 and *fry1-6* seedlings treated with exogenous PAP. *CCA1::LUC2* and *fry1-6 CCA1::LUC2* seedlings were entrained and imaged under constant blue light as described for Figure 6.7a above. After 1 day of imaging, seedlings were sprayed with PAP (1 mM, prepared in 0.01% Triton X-100) or a mock control (0.01% Triton X-100) in the subjective afternoon (~ZT30). Luciferase imaging was continued for an additional 5 days, and time series data collected after application of treatments subjected to FFT-NLLS analysis. Application of PAP had no effect on circadian rhythms in Col-0, with bioluminescence from *CCA1::LUC2* activity cycling with robust, ~24 h circadian rhythm in PAP- and mock-treated Col-0 seedlings (Figure 6.7c). However, application of exogenous PAP caused a significant period lengthening of ~1 h in *fry1-6*, with *fry1-6* seedlings treated with PAP exhibiting *CCA1::LUC2* rhythms with period of 25.25 ± 0.12 h compared to mock-treated *fry1-6* seedlings (24.52 ± 0.14 h; $p<0.001$, Student's T-test; Figure 6.7c).

6.2.6. Mannitol treatment lengthens circadian period and results in PAP accumulation in Col-0

Under drought stress, adult Col-0 and *sal1* plants accumulate PAP at higher levels than under non-stressed conditions, which correlates with the upregulation of stress-induced genes (Estavillo et al., 2011). In order to investigate whether the accumulation of PAP in response to stress correlates with an effect on circadian rhythms, the effect of mannitol on the endogenous

PAP content and circadian rhythms in Col-0 was investigated. Although not identical to drought treatments, the induction of osmotic stress through the application of mannitol has been used previously to study stress responses in *Arabidopsis* (Xiong et al., 2001; Bray, 2004). Firstly, the effect of mannitol treatment on the endogenous PAP levels of Col-0 and *alx8-1* under constant blue light was examined. Col-0 and *alx8-1* seedlings were grown on 0.5x MS agar plates for 11 days in 12h:12h light:dark cycles under 60 $\mu mol.m^{-2}.s^{-1}$ white light before being transferred to 0.5x MS agar plates substituted with 200 mM mannitol (or to fresh 0.5x MS agar plates as control). After 1 day, plants were transferred to 20 $\mu mol.m^{-2}.s^{-1}$ constant blue light at subjective dawn. Following 4 days in constant conditions, seedlings were harvested, and PAP extracted and quantified as previously described. As observed previously (Figure 6.4 and 6.5), PAP was undetectable in Col-0, but accumulated in *alx8-1* on 0.5x MS control plates (Figure 6.8a). Treatment with mannitol resulted in a significant accumulation of PAP in Col-0 ($p<0.001$, Student's T-test) relative to Col-0 under control conditions, with PAP quantity comparable to that observed in *alx8-1* seedlings grown under control conditions (although values were overall smaller than obtained during previous quantifications of PAP in *sal1* mutants; Figure 6.4 and 6.5). In contrast, no significant increase in PAP was observed in *alx8-1* seedlings treated with mannitol relative to *alx8-1* under control conditions. These data confirm that PAP accumulates in wild-type in response to stress (Estavillo et al., 2011), and indicates that application of stress does not cause accumulation of additional PAP in the *sal1* mutant.

Since mannitol treatment resulted in a significant increase in endogenous PAP content in Col-0 under constant blue light, the effect of mannitol treatment on circadian rhythms in Col-0 was investigated. The expression of nuclear clock-controlled components *CCA1, LHY* and *TOC1* were examined through imaging of the Col-0 luciferase reporter lines *CCA1::LUC+*, *LHY::LUC+* and *TOC1::LUC+* treated with mannitol under constant blue light.

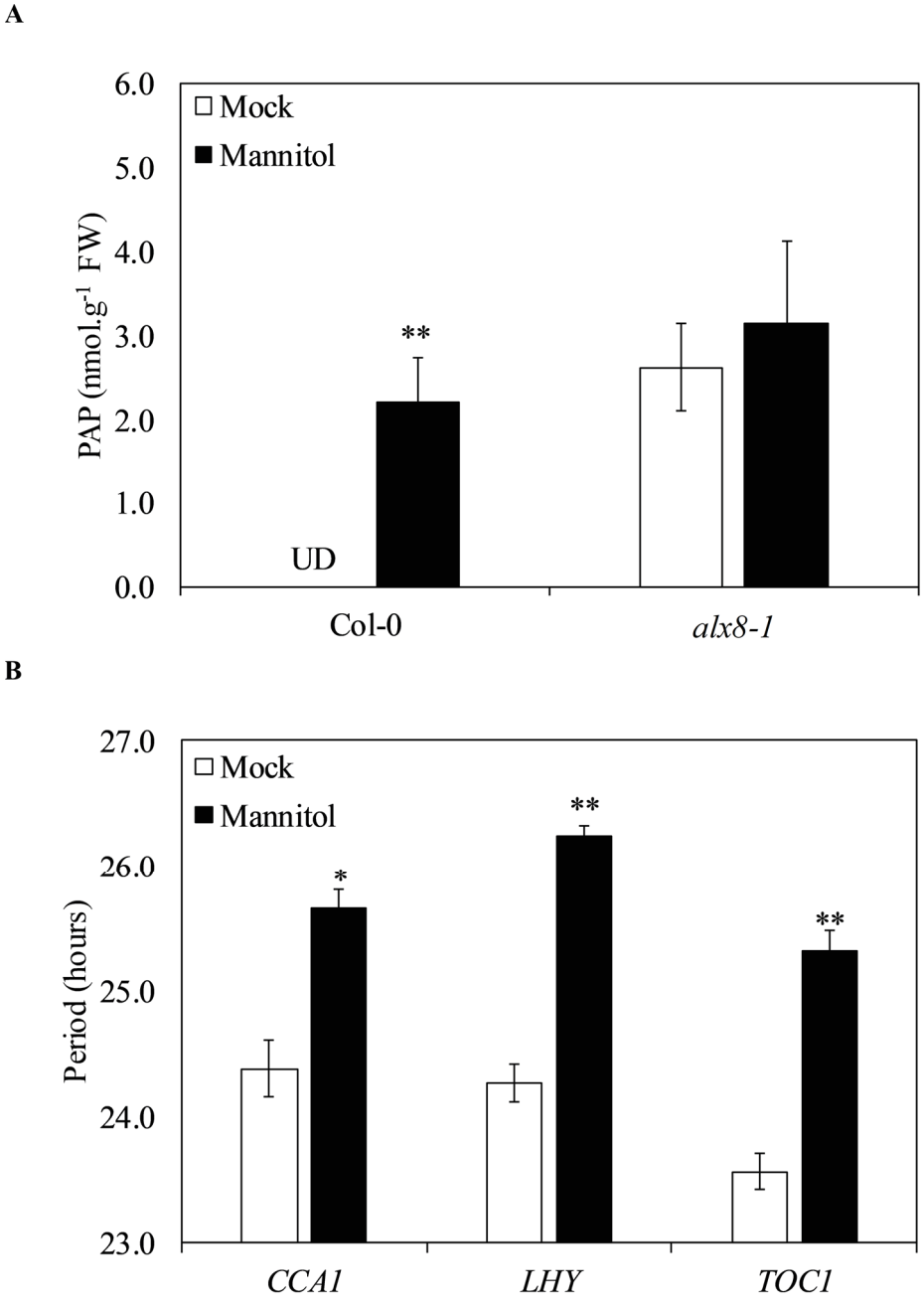

Figure 6.8 Effect of mannitol on PAP accumulation and circadian period under constant blue light. (A) Quantification of endogenous PAP in Col-0 and *alx8-1* seedlings treated with mannitol under constant blue light. Seedlings were grown on 0.5x MS agar plates and entrained in 12h:12h light:dark cycles under 60 µmol.m^{-2}.s^{-1} white light for 11 days before transfer to 0.5x MS plates substituted with 200 mM mannitol (or to 0.5x MS plates as mock treatment). After 1 day, plants were transferred to 20 µmol.m^{-2}.s^{-1} constant blue light at subjective dawn. Following 4 days in constant conditions, ~50 seedlings per genotype were harvested at subjective dawn (ZT96) and PAP quantified by reverse-phase HPLC as previously described (Bürstenbinder et al., 2007; Estavillo et al., 2011). Error bars indicate standard deviation, with n=4. Asterisks indicate statistically significant difference in PAP content compared to comparative genotype grown on 0.5x MS control plates (* p<0.01, ** p<0.001, Student's T-test). **(B)** Circadian period estimates for luciferase activity monitored in Col-0 *CCA1::LUC+, LHY::LUC+* and *TOC1::LUC+* seedlings treated with mannitol under constant blue light. Seedlings were grown on 0.5x MS agar plates and entrained in 12h:12h light:dark cycles under 60 µmol.m^{-2}.s^{-1} white light for 5 days before transfer to 0.5x MS plates substituted with 200 mM mannitol (or to 0.5x MS plates as mock treatment). After 1 day, plants were imaged under 20 µmol.m^{-2}.s^{-1} constant blue light. Error bars indicate standard error of the mean, with n=10. Asterisks indicate statistical significance in circadian period compared to mock-treated control for each comparative genotype (* p<0.01, ** p<0.001, Student' T-test).

Seedlings were grown on 0.5x MS agar plates for 5 days in 12h:12h light dark cycle under 60 $\mu mol.m^{-2}.s^{-1}$ white light before being transferred to 0.5x MS agar plates supplemented with 200 mM mannitol (or 0.5x MS agar plates for control treatments). After one day, seedlings were imaged under 20 $\mu mol.m^{-2}.s^{-1}$ constant blue light for 5 days. While promoter activity of all three clock components analysed oscillated with robust rhythms both in the presence and absence of mannitol, treatment with mannitol resulted in a significant >1 h elongation in circadian period of rhythmic *CCA1*, *LHY* and *TOC1* expression in Col-0 relative to Col-0 seedlings grown on control medium (Figure 6.8b). These data correspond to the previous observations that long circadian period correlates with increased endogenous PAP in *sal1* seedlings (Figure 6.4 and 6.5).

6.3. Discussion

6.3.1. Lengthening of circadian period occurs in sal1 mutants in a light-dependent manner

In the *stipl1* mutant – a mutant with lost function of the putative RNA binding protein SPLICEOSOMAL TIMEKEEPER LOCUS 1 (STIPL) – impaired transcript processing (particularly of circadian-associated transcripts) is associated with a long circadian period phenotype, which is present under both constant light and constant darkness (Jones et al., 2012). Contrary to these findings, the long circadian period observed in *sal1* mutants under constant light is not observed under constant darkness, suggesting a light-dependent element to the circadian phenotype of *sal1* (Figure 6.1). This observation correlates with a previous report which indicates that the shortened hypocotyl phenotype of *sal1* is present under constant light, but not under constant darkness (Kim and Von Arnim, 2009). Interestingly, the loss-of-function *xrn4* mutant *ein5-1* also exhibits a long period circadian phenotype under constant light conditions, but not under constant darkness (Hanano et al., 2006), further suggesting a possible role of SAL1/PAP/XRN4 in regulating circadian rhythm in a light-depended manner. However, the light-specific element of the *sal1* circadian phenotype appears to extend beyond merely the

presence or absence of a light signal. While the shortened hypocotyl phenotype of sal1 is observed both under constant blue and constant red light (Figure 4.1d; Kim and Von Arnim, 2009), the long circadian period of *sal1* is more severe under constant blue light than under constant red light. Previous analysis of delayed fluorescence rhythms and rhythmic transcript accumulation had indicated a wavelength-specific effect, with a more severe long-period phenotype in *sal1* under 20 µmol.m-2.s-1 constant blue light than under 30 µmol.m^{-2}.s^{-1} constant red light (Sections 4.2.3 and 4.2.4). This was confirmed through analysis of *CCA1::LUC2* rhythms in Col-0 and *fry1-6* luciferase reporter lines, with an ~1 h elongation in period observed in *fry1-6* relative to Col-0 under constant blue light, compared to a less severe, ~0.5 h period lengthening under constant red light (Figure 6.2 and 6.3). The circadian period of *sal1* is sensitive not only to the wavelength of light, but also to fluence rate. Under very low levels of constant blue light, as under constant darkness, no long period is observed in *sal1* relative to Col-0. Indeed, the long period phenotype of *sal1* only emerges under comparatively higher levels of constant blue light (20 or 40 µmol.m^{-2}.s^{-1}). Confirming the blue light-specific long period circadian phenotype of *sal1*, the long period of *sal1* is absent under low and higher fluence rate of constant red light tested.

6.3.2. Lengthening of circadian period correlates with PAP levels in sal1 mutants

The numerous *sal1* mutant phenotypes, including morphological characteristics, altered sulfur metabolism, and super-induction of stress-induced genes, correlate with – and are attributed to – the accumulation of PAP, which in turn results in the inhibition of XRN activity (Estavillo et al., 2011; Chen et al., 2011; Lee et al., 2012). The *Arabidopsis* genome contains four genes homologous to *SAL1*, namely *SAL2* (AT5G64000), *SAL3* (AT5G63990), *SAL4* (AT5G09290) and *AHL* (AT5G54390), all of which share >40% amino acid sequence identity to *SAL1* (Quintero et al., 1996; Gil-Mascarell et al., 1999; Xiong et al., 2001; Chen et al., 2011). The *SAL1* homologue genes are located on chromosome V and *SAL1*, *SAL2* and *SAL3* are arranged in tandem on chromosome V, indicating possible duplication from a common ancestor (Chen

et al., 2011). Transcript levels of *SAL1* and *AHL* are at approximately the same level, which is significantly higher than for the remaining *SAL1* homologues (Chen et al., 2011). Of the *SAL1* homologues, *in vitro* enzyme activity data are available only for *SAL1*, *SAL2* and *AHL* (Quintero et al., 1996; Gil-Mascarell et al., 1999; Xiong et al., 2001). Like the yeast HAL2 enzyme, SAL1 and SAL2 are bifunctional enzymes with inositol polyphosphate 1-phosphatase and 3'(2'),5'-bisphosphate nucleotidase activities (Quintero et al., 1996; Gil-Mascarell et al., 1999; Xiong et al., 2001). *In vitro* substrate specificity studies of SAL1 and SAL2 using purified recombinant protein revealed phosphatase activity towards 3'-phosphoadenosine 5'-phosphate (PAP), 2'-PAP and 3'-phosphoadenosine 5'-phosphosulfate (PAPS), but not towards phosphate esters such as ATP or fructose 1,6-bisphosphate. SAL1 and SAL2 also catalyse hydrolysis of inositol 1,4-bisphosphate and inositol 1,3,4-triphosphate (but not inositol 1-phosphate) *in vitro*, with lower activities than towards PAP (Quintero et al., 1996; Gil-Mascarell et al., 1999; Xiong et al., 2001). In contrast, AHL hydrolyses only PAP and PAPS (Gil-Mascarell et al., 1999) *in vitro*. SAL1, SAL2 and AHL all require the presence of Mg^{2+} as cofactor for enzyme activity, and SAL1 exhibits significantly higher activity than SAL2 and AHL towards all substrates (Quintero et al., 1996; Gil-Mascarell et al., 1999; Chen et al., 2011). Despite the presence of functionally redundant homologues, SAL1 is regarded as the main enzyme controlling PAP levels *in vivo* (Chen et al., 2011; Estavillo et al., 2011). Analysis of *Arabidopsis sal1*, *sal2*, *sal3, sal4* and *ahl* null mutants revealed that only *sal1* mutants have significantly higher levels of PAP (Chen et al., 2011). This could be due to the relatively high expression levels of *SAL1* and *AHL* compared to other *SAL1* homologues, combined with the significantly higher enzyme activity of SAL1 towards PAP (Quintero et al., 1996; Gil-Mascarell et al., 1999; Chen et al., 2011).

PAP, not 1,4,5-triphosphate, is regarded as the *in vivo* substrate of SAL1 (Gy et al., 2007; Wilson et al., 2009; Chen and Xiong, 2010; Hirsch et al., 2011; Estavillo et al., 2011). Recombinant SAL1 has a significantly higher affinity towards PAP (K_m of 2-10 µM) than towards IP_3 (K_m of 90 µM), with ~4% activity on IP_3 relative to its activity towards PAP (Gil-

Mascarell et al., 1999; Xiong et al., 2001). Previous reports have attributed the slower germination and changes in postembryonic development, leaf shape, venation patterning and lateral root formation in *sal1* mutants to the accumulation of IP_3 and a subsequent effect on Ca^{2+}-mediated ABA- and auxin signalling (Xiong et al., 2001; Robles et al., 2010; Zhang et al., 2011). The relatively high levels of *SAL1* transcript in buds within the first 4 days of flowering, along with the expression of *SAL1* in seed coats, further suggest a role for SAL1 in seed development, possibly through effect of increased IP3 on *myo*-inositol biosynthesis (Sato et al., 2011; Zhang et al., 2011). However, the studies attributing *sal1* phenotypes to the increased levels of IP_3 only examined SAL1 activity towards polyphosphoinositols and did not investigate PAP levels (Xiong et al., 2001; Xiong et al., 2004; Sato et al., 2011; Zhang et al., 2011). Relative to wild-type, *sal1* mutants accumulate ~20-fold PAP under non-stressed conditions, compared to no increase or a 2-fold increase in IP3 and other polyphosphoinositols (Estavillo et al., 2011; Zhang et al., 2011). In addition, constitutive overexpression of the PAP-specific homologue AHL in *sal1* mutants complements the root and rosette phenotypes of *sal1* and restores hypocotyl elongation in these mutants, indicating that loss of SAL1 3',(2'),5'-bisphosphate nucleotidase activity is responsible for these phenotypes (Kim and von Arnim, 2009; Hirsch et al., 2011). While *in vitro* assays indicate SAL1 activity towards PAPS is comparable to enzyme activity towards PAP (Quintero et al., 1996; Gil-Mascarell et al., 1999), only a small increase in PAPS is observed in a *sal1* mutant compared to wild-type (Estavillo et al., 2011). In addition, SAL1 is localised mainly in the chloroplasts and mitochondria, while PAPS accumulates in the cytosol for utilisation by SOTs (Klein and Papenbrock, 2004; Mugford et al., 2009; Estavillo et al., 2011). These reports suggest that PAP, not PAPS, is the *in vivo* substrate of SAL1. Indeed, the long period phenotype of *sal1* under constant white light conditions correlates with higher PAP levels compared to Col-0 (Figure 6.4a and b). In the current study, overexpression of AHL in *sal1* not only restored circadian rhythms, but also restored PAP levels in *sal1* mutants to wild-type levels (Figure 6.4c and d).

The emergence of the long period circadian phenotype under relatively higher levels of constant blue light correlates with increased accumulation of PAP in *sal1* under these fluence rates (Figure 6.4 and 6.5). *fry1-6* seedlings accumulate >2-fold more PAP under 20 µmol.m^{-2}.s^{-1} than under 5 µmol.m^{-2}.s^{-1} constant blue light, which correlates with an ~1 h period elongation relative to Col-0 under 20 µmol.m^{-2}.s^{-1} and no period lengthening under 5 µmol.m^{-2}.s^{-1}. Furthermore, the absence of a difference in PAP accumulation between *fry1-6* seedlings grown under 20 µmol.m^{-2}.s^{-1} or 40 µmol.m^{-2}.s^{-1} constant blue light correlates with no difference in period between *fry1-6* seedlings under these fluence rates. These relatively small increases in fluence rate also affect PAP accumulation in other *sal1* mutant alleles, with both *alx8-1* and *fou8* accumulating >5-fold more PAP under 40 µmol.m^{-2}.s^{-1} than under 5 µmol.m^{-2}.s^{-1} constant blue light.

While having a significant effect on PAP levels in *sal1*, wavelength and fluence rate of light does not appear to have an effect on SAL1 protein accumulation. No significant difference in SAL1-GFP protein levels were observed in *alx8-1 SAL1::SAL1:GFP* seedlings grown under 60 µmol.m^{-2}.s^{-1} constant white light, 20 µmol.m^{-2}.s^{-1} constant blue light or 20 µmol.m^{-2}.s^{-1} constant blue light (Figure 6.6). These data correspond with the observation that SAL1 protein expression does not change over the course of the day (Section 4.2.2) or in response to stress (Chan et al., 2016), further supporting the proposal that regulation of SAL1 activity, rather than SAL1 protein expression, is important in the SAL1/PAP/XRN signalling pathway (Chan et al., 2016). The downregulation of *SAL1* transcription under constant darkness observed in this study (Figure 6.6b) has been previously reported (Kim and von Arnim, 2006, 2009), but appears to correlate with increased level of SAL1-GFP protein under constant darkness (Figure 6.6c and d). Since SAL1 activity rather than SAL1 protein level is considered to be of importance in SAL1/PAP signalling, the effect of constant darkness on SAL1 expression and PAP signalling needs further investigation.

6.3.3. Inhibition of SAL1 and application of exogenous PAP affects circadian period

In *Arabidopsis* SAL1, as well as in the yeast homologue HAL2 and the mammalian homologue BPntase, 3',(2'),5'-bisphosphate nucleotidase enzyme activity is inhibited by lithium (Murguía et al., 1996; Quintero et al., 1996; Spiegelberg et al., 1999; Xiong et al., 2004). In yeast, HAL2 acts as a target of lithium and salt toxicity, and the application of LiCl results in the accumulation of PAP and the inhibition of sulfur assimilation in yeast cells (Murguía et al., 1996). In this study, application of LiCl resulted in a significant lengthening of circadian period in Col-0, as is evident from the rhythmic expression of both morning- and evening-phased clock components (Figure 6.7a). However, care must be taken when attributing the observed period lengthening to the inhibition of SAL1 activity by LiCl. LiCl is thought to inhibit a range of enzymes, including glycogen synthase kinase-3 (GSK) in plants – a multigene family (with ten GSK genes in the *Arabidopsis* genome) which is involved in numerous different processes, including flower development, NaCl stress and wound responses (Phiel and Klein, 2001; Jonak and Hirt, 2002). Even so, the observation that LiCl causes a significant period lengthening in Col-0 but not in *sal1* (Figure 6.7b) suggests the possible involvement of increased PAP levels resulting from inhibition SAL1 activity. A previous study reported no indication of lithium tolerance in a *sal1* mutant, or indeed any inhibition of SAL1 or accumulation of PAP in Col-0 or *sal1* in response to lithium treatment (Xiong et al., 2004; Chen et al., 2011). However, these lithium treatments were performed by growing plants on media supplemented with, at most, 20 mM LiCl, while previous studies showing inhibition of SAL1 in yeast (Murguía et al., 1996), as well as this study, used a LiCl concentration of 100 mM (although the intracellular LiCl concentration remains unknown). In yeast, HOS2 is thought to confer lithium tolerance by acting as a target for lithium inhibition, with subsequent overexpression of HOS2 resulting in increased 3',(2'),5'-bisphosphate nucleotidase activity and a resulting decrease in intracellular lithium toxicity (Murguía et al., 1996; Quintero et al., 1996). It is therefore possible that, under low LiCl concentration, an increase in SAL1 expression counteracts the effect of lithium toxicity, masking the effect of LiCl on SAL1 activity. Interestingly, the single

nucleotide mutation in the *SAL1* gene of the *Arabidopsis hos2* mutant confers lithium resistance to *hos2* plants and to the hos2 mutant protein, without resulting in loss of 3',(2'),5'-bisphosphate nucleotidase activity. Previous studies have indicated that lithium acts as a non-competitive inhibitor of SAL1 and binds to the Asp288 and Asp134 residues of the enzyme, with the *hos2* mutation resulting in modification of metal binding sites and loss of accessibility to lithium (Spiegelberg et al., 1999; Xiong et al., 2004).

The Li-induced inhibition of SAL1 activity is a crude way of monitoring the effect of increased PAP on circadian rhythms, and the application of exogenous PAP provides a more targeted approach (Figure 6.7c). The significant increase in circadian period upon application of exogenous PAP in *sal1* further supports the correlation between increased PAP accumulation and lengthening of circadian period in *sal1*. No significant difference in period was observed in Col-0 upon application of exogenous PAP, which could be due to the rapid degradation of applied PAP by the highly active wild-type SAL1 enzyme (Quintero et al., 1996; Estavillo et al., 2011; Chan et al., 2016).

6.3.4. Osmotic stress lengthens circadian period possibly through accumulation of PAP in wild-type

Since exogenous PAP could be degraded by the highly active wild-type SAL1 enzyme, and the inhibition of SAL1 by lithium is not specific, studying the effect of PAP accumulation on circadian rhythms in wild-type *Arabidopsis* was problematic. The proposed model of the SAL1/PAP/XRN signalling pathway suggests that the presence of abiotic stresses such as high light or drought results in changes in the redox poise of plastids, which in turn cause inhibition of SAL1 and a subsequent accumulation of endogenous PAP in wild-type (Chan et al., 2016). Indeed, treatment of Col-0 with the osmotic stressor mannitol resulted in the accumulation of endogenous PAP to levels comparable to that observed in *sal1* (Figure 6.8a). This increase in endogenous PAP correlated with a significant period lengthening of > 1 hour in rhythmic

expression of both morning- and evening-phased clock components in Col-0 (Figure 6.8b). These data not only strengthen the correlation between increased PAP accumulation and long circadian period, but also suggest a possible role for SAL1/PAP regulation of the circadian system in response to abiotic stress.

This chapter demonstrated that SAL1 acts on the circadian system in a light-dependent manner, and that lengthening of circadian period directly correlates with the accumulation of PAP *in planta*. Furthermore, a possible link between SAL1/PAP signalling and circadian rhythms under abiotic stress was determined. The implications of these findings and the role of the SAL1/PAP/XRN signalling pathway in the broader context of circadian regulation will be discussed in the final chapter.

Chapter 7

General discussion

7.1. Introduction

Throughout their lifecycle, plants are continuously exposed to various, often challenging, environmental changes, and have developed complex, integrated mechanisms to sense and adapt to these conditions (Millar, 2016; de Souza et al., 2017). Among these environmental changes are rhythmic cues generated by the Earth's rotation and orbit: predictable day-night cycles of light and temperature, and seasonal changes in temperature and day length (Hut and Beersma, 2011; Millar, 2016). Like most organisms, plants have developed an endogenous timing mechanism that serves both to coordinate the various complex biological components of the cell, and to synchronise the organism's responses to environmental rhythms (Golombek and Rosenstein, 2010; Millar, 2016). The circadian system provides plants with adaptive advantages, including synchronisation of organ movement, carbon assimilation and light harvesting to day/night cycles and increasing photosynthesis; accurate timing of starch degradation and growth processes to prevent carbohydrate starvation during the night; and sensing photoperiodic information to time seasonal flowering for optimal survival (Dodd et al., 2005; Graf et al., 2010; Dodd et al., 2014; Song et al., 2015).

The plant circadian clock is entrained most strongly by light which is sensed through a variety of photoreceptors, including receptors that respond to blue light (cryptochromes and LOV-domain photoreceptors), or red and far-red light (phytochromes) (Christie et al., 2015; Millar, 2016). The *Arabidopsis* circadian system is well studied and serves as a model for the transcription-translation feedback loops and post-transcriptional mechanisms that comprise the circadian clock in plants (Hsu and Harmer, 2014; Millar, 2016). At dawn, expression of the MYB-related transcription factors *LHY* and *CCA1* peaks, with CCA1 and LHY inhibiting the

expression of later-phased clock genes including *PSEUDORESPONSE REGULATOR* (*PRR*) genes, *GIGANTEA* (*GI*), and the evening-phased *EARLY FLOWERING 3* (*ELF3*), *ELF4* and *LUX ARRHYTHMO* (*LUX*) (Alabadí et al., 2001; Hazen et al., 2005b; Locke et al., 2006; Herrero et al., 2012; Adams et al., 2015). In turn, PRRs acts sequentially from dawn to limit expression of *CCA1* and *LHY* to a small window in the morning (Matsushika et al., 2000; Nakamichi et al., 2010; Gendron et al., 2012; Huang et al., 2012). The repressive function of the PRRs extend further to include *RVE8*, a MYB-like transcription factor which acts in the afternoon to activate the expression of numerous evening-phased clock components, including *PRR5*, *TOC1*, *PRR3*, *GI*, *LUX* and *ELF4* (Rawat et al., 2011; Hsu et al., 2013). During the early night, ELF3, ELF4 and LUX interact to form a protein complex that acts to repress expression of day- and morning-phased circadian genes during the night (Hazen et al., 2005b; Helfer et al., 2011; Nusinow et al., 2011; Herrero et al., 2012). The oscillations generated by these nuclear feedback loops control a variety of biological processes, including growth, photosynthesis, flowering time and responses to stress (Wang et al., 2011; Hsu and Harmer, 2014; Dodd et al., 2014; Grundy et al., 2015; Song et al., 2015; Millar, 2016). However, overlaps exist among the 'input', 'oscillator' and 'output' components, such as circadian control of expression of the photoreceptors that relay entraining signals to the oscillator, and the ability of metabolic outputs (such as sugar) to in turn regulate the oscillator (Harmer et al., 2000; Hsu and Harmer, 2014; Dodd et al., 2015; Millar, 2016).

In addition to the rhythmic cues of the environment, plants are often exposed to abiotic stressors such as drought, high light or frost, and the circadian clock can allow plants to adapt and predict when these stresses are likely to occur (Jones, 2009; Hsu and Harmer, 2014; Grundy et al., 2015). The oxidative damage caused by environmental stresses are mostly sensed in chloroplasts and mitochondria, and adequate adaptive responses require inter- and intra-cellular cooperation maintained by interorganellar signalling mechanisms (de Souza et al., 2017). Retrograde signalling pathways are often initiated by the action of ROS or Ca^{2+} (signalling "master switches"), and can involve the action of fatty acids or other metabolites that act as

interorganellar signals. One such retrograde signalling pathway is the SAL1-PAP pathway – a ROS-sensitive chloroplast-to-nucleus signalling mechanism that is proposed to alter nuclear expression through XRN activity in response to abiotic stress (Estavillo et al., 2011; Chan et al., 2016a, 2016b). This project examined the role of SAL1 in the circadian system by employing chlorophyll *a* fluorescence imaging and established circadian assays to monitor rhythms in *Arabidopsis* seedlings *in vivo*. In addition, a combination of molecular, imaging and analytical techniques were used to further elucidate the mechanisms through which SAL1 functions within the circadian system. In this final chapter, data from the previous chapters are discussed and possible avenues of further research are suggested.

7.2. Chlorophyll *a* fluorescence imaging allows in vivo monitoring of circadian rhythms and identification of circadian mutants

In vitro and *in vivo* assays have been instrumental in identifying circadian components and their functions in plants, and can provide insight into clock effects under different environmental conditions (Gould et al., 2009; Nagel and Kay, 2012; Millar, 2016). Much of the insight into the workings of the *Arabidopsis* circadian system has been gained through the use of luciferase assays (Gould et al., 2009; Tindall et al., 2015). Clock-controlled promoter-luciferase reporter fusions provide a robust, high-throughput assay to monitor circadian rhythms, and high-resolution luciferase assays can be used to monitor circadian gene activity at tissue- and cellular levels (Millar et al., 1992; Gould et al., 2009; Wenden et al., 2012; Endo et al., 2014). However, luciferase assays are indirect assays that monitor single circadian target genes, are often laborious (requiring the use of transgenics), and are limited to transformable plant species such as *Arabidopsis* (Gould et al., 2009; Tindall et al., 2015). Physiological assays that monitor overall circadian health provide more information about the implications of circadian components (Tindall et al., 2015). Of these, leaf movement assays are robust and easily used across a range of different plant species, but are limited to plants with petioles and often (in species such as *Arabidopsis*) limited to use in young leaves (Edwards and Millar,

2007; Tindall et al., 2015). More recently, delayed fluorescence (DF) was proposed as a simple, high-throughput method that allows monitoring of circadian rhythms in chloroplasts of most – if not all – plant species (Gould et al., 2009). DF is described as the post-illumination emission of light from Photosystem II (PSII) as a result of charge recombination between excited plastoquinone Q_A (the primary quinone acceptor of PSII) and chlorophyll P680 (Rutherford et al., 1984; Gould et al., 2009). The circadian rhythms observed in DF under constant conditions suggest that the composition of the photosynthetic apparatus varies over circadian time, and DF has been proposed as a simple method or probing PSII photochemistry (Gould et al., 2009; Dodd et al., 2014). However, the exact mechanism underlying DF remains unknown (Gould et al., 2009; Tindall et al., 2015). In addition, the signal obtained by DF imaging is weaker than that collected by luciferase imaging and prone to background noise which must be corrected for, and data must be presented as normalised averages for groups of seedlings (Gould et al., 2009). In order to improve on the current methods for studying photosynthetic rhythms, the current study investigated chlorophyll *a* fluorescence (prompt fluorescence) for use as a medium-throughput assay to monitor rhythms in *Arabidopsis* seedlings *in planta*. Chlorophyll *a* fluorescence imaging is a non-invasive method used widely to determine photosynthetic performance in plants and algae, and involves monitoring the light re-emitted by a leaf upon illumination (Butler, 1978; Baker, 2008). Light energy absorbed by the pigment antennae of PSII can be used to drive photochemistry, in which an electron is transferred from chlorophyll P680 to Q_A. However, the excitation energy in the PSII pigment antennae can also be lost as PSII fluorescence or heat. Photochemistry (photochemical quenching), heat loss (non-photochemical quenching) and chlorophyll fluorescence are therefore directly competing processes (Butler, 1978; Baker, 2008). Unlike DF, the relationship between chlorophyll *a* fluorescence parameters and photosynthetic electron transport *in vivo* is well understood (Baker, 2008; Gould et al., 2009). Under non-photorespiratory conditions, these parameters correlate with photosynthetic rates, providing insight into CO_2 assimilation (Baker, 2008). The parameter F_q'/F_m' ($\Delta F/F_m'$; ϕ_{PSII}) represents the PSII operating efficiency of a leaf grown in constant light, and provides an estimate of the efficiency with which light absorbed by the PSII

antennae is used for Q_A reduction. Circadian rhythms of F_q'/F_m' under constant light conditions have previously been reported in individual leaves of the Crassulacean acid metabolism (CAM) plant *Kalanchoë daigremontiana* (Wyka et al., 2005; Malpas and Jones, 2016). The current study confirms that similar circadian oscillations in F_q'/F_m' occur in whole seedlings of wild-type (Col-0) *Arabidopsis thaliana* under constant blue light conditions (Section 3.2.1; Litthauer et al., 2015). Similar to circadian rhythms monitored by DF or luciferase assays (using a *CCA1::LUC2* reporter), rhythms in F_q'/F_m' oscillate with an approximately 24 h free running period (FRP) in *Arabidopsis* seedlings under 20 $\mu mol.m^{-2}.s^{-1}$. However, the phase of DF rhythms peak shortly before subjective dusk (ZT11), while the phasing of peak F_q'/F_m' occurs approximately 10 hours later, shortly before subjective dawn. In addition, circadian rhythms in F_q'/F_m' remain robust across 5 days under constant light conditions, and exhibit a lower Relative Amplitude Error (RAE) than DF rhythms under these conditions (Section 3.2.1; Litthauer et al., 2015).

The mechanism underlying these robust circadian fluctuations in F_q'/F_m' remains unknown (Litthauer et al., 2015). F_q'/F_m' is a ratiometric measurement and therefore not directly affected by chloroplast movement (Brugnoli and Björkman, 1992). Furthermore, these rhythms continue in plants for which leaf movement is restrained, confirming that F_q'/F_m' oscillations occur due to subcellular processes and not as a result of shading artefacts introduced by circadian leaf movement (Litthauer et al., 2015). F_q'/F_m' is affected by a variety of physiological factors, including stomatal conductance (and therefore intercellular CO_2 concentration), and CO_2 assimilation (Baker, 2008). In *K. daigremontiana* leaves, F_q'/F_m' oscillations (peaking at subjective dusk) are antiphasic to rhythms in gas exchange, and continue independent of stomatal regulation (Wyka et al., 2005). The mechanism underlying F_q'/F_m' rhythms in *K. daigremontiana* leaves in which gas exchange is inhibited is explained by circadian activity of phosphoenolpyruvate carboxylase (PEPC). At peaks of PEPC activity, the low internal CO_2 levels are depleted, inhibiting the carboxylase activity of Rubisco and causing a decrease in electron transport rates, which in turn results in troughs of F_q'/F_m'

oscillations. Similarly, downregulation of PEPC leads to improved supply of CO_2 to Rubisco, resulting in increased electron transport rates and peaks of F_q'/F_m' (Wyka et al., 2005). This mechanism of CAM photosynthesis is different to the mechanisms present in *Arabidopsis*, which could explain the difference in phasing of peak F_q'/F_m' in *K. daigremontiana* compared to *Arabidopsis* (Wyka et al., 2005; Litthauer et al., 2015). *Arabidopsis* also exhibits circadian rhythms in stomatal conductance under constant blue light, but rhythms peak during the subjective morning, several hours after peaks in F_q'/F_m' are observed (Litthauer et al., 2015). While this suggests that F_q'/F_m' rhythms do not occur as a direct result of stomatal opening, it is possible that rhythmic stomatal opening contributes to fluctuations in F_q'/F_m' by affecting the rate of photochemistry through alterations in CO_2 availability (Litthauer et al., 2015). Alternatively, feedback mechanisms to the clock from the daily production of starch and sugars might induce alterations in the use of light for photochemistry (Dodd et al., 2015).

While the molecular mechanism underlying F_q'/F_m' circadian oscillations remains elusive, it can be suggested that components of the photosynthetic apparatus vary over the course of the day to limit damage caused by excessive light harvesting, while at the same time maximising energy absorption for efficient photosynthesis (Dodd et al., 2004, 2014; Litthauer et al., 2015). Circadian oscillations in reporters of light harvesting, such as the rate of electron transport, rate of O_2 evolution, or oscillations in post-translational modification of reaction centre proteins, are well reported (Lonergan, 1981; Bonardi et al., 2005; Pesaresi et al., 2009; Dodd et al., 2014). Furthermore, the circadian clock controls photosynthetic processes (such as light harvesting) both at transcriptional and post-transcriptional levels, with many genes required for photosynthesis encoded in the nucleus, while circadian control of a subset of chloroplast gene transcription is driven by rhythms of nuclear gene expression (Dodd et al., 2014; Noordally et al., 2013). Indeed, this study confirms that rhythms in photosynthetic efficiency are controlled by the nuclear circadian system (Section 3.2.2; Litthauer et al., 2015), with short period F_q'/F_m' oscillations observed in the *toc1-4* mutant – a *toc1* null mutant with a short FRP in transcriptional rhythms (Hazen et al., 2005a; Jones and Harmer, 2011; Litthauer et al., 2015).

Similarly, a long period phenotype is observed in the long-period *prr7-3* mutant, while no F_q'/F_m' rhythms are observed in *lux-2* mutants in which no transcriptional circadian rhythms can be detected (Hazen et al., 2005a, 2005b; Litthauer et al., 2015). These findings demonstrate not only that the nuclear clock is required to maintain rhythms of F_q'/F_m' in the chloroplast, but also that chlorophyll *a* fluorescence imaging can potentially be used as a screening assay to identify mutants with altered circadian rhythms. The nuclear regulation of F_q'/F_m' circadian rhythms is not surprising, as the clock is known to regulate approximately one third of the *Arabidopsis* genome, and similar nuclear regulation is observed in DF rhythms (Covington et al., 2008; Gould et al., 2009). Interestingly, analysis of the nuclear-encoded sigma factor SIG5 revealed no effect on the period or amplitude of DF rhythms in *sig5* mutants, despite SIG5 being a known regulator of the blue light-responsive promoter of the chloroplast *psbD* operon (Nagashima et al., 2004; Noordally et al., 2013). *SIG5* expression is circadian regulated and rapidly induced by high light treatment, and it has been suggested that SIG5 is involved in repair of PSII after photoinhibition (Nagashima et al., 2004). It would therefore be interesting to determine whether F_q'/F_m' rhythms are maintained, along with DF rhythms, in *sig5* mutants, or whether the SIG5-mediated mechanism provides a distinction between the two fluorescence phenomena.

While phytochromes, cryptochromes, UVR8 and members of the ZTL protein family entrain the circadian system, a role for phototropin blue light receptors in light input to the clock has not yet been identified (Fankhauser and Staiger, 2002; Hsu and Harmer, 2014; Christie et al., 2015). In addition, a portion of the plant cell's phototropins (both phot1 and phot2) have been shown to localise to the surface of chloroplasts in response to blue light as part of the chloroplast avoidance mechanism (Kong and Wada, 2011; Kong et al., 2013). In order to gain more insight into the mechanism involved in F_q'/F_m' oscillations, this study examined whether phototropin activity is required to maintain rhythms in PSII operating efficiency under constant dim blue light (Section 3.2.3; Litthauer et al., 2015). While loss of phototropin function had no effect on the period or phase of F_q'/F_m' rhythms under 20 $\mu mol.m^{-2}.s^{-1}$ constant blue light, these

rhythms exhibited reduced amplitude in the *p1p2* double mutant, dampening to near arrhythmicity within 4 days of free-run. As is often the case in phototropin-regulated responses, phot1 and phot2 act redundantly to maintain these rhythms, with no effect on F_q'/F_m' circadian oscillations observed in *phot1-5* or *phot2-1* single mutants (Kagawa et al., 2001; Sakai et al., 2001; Higa et al., 2014; Litthauer et al., 2015). Interestingly, no dampening of rhythms was observed in DF oscillations under the same dim blue light conditions either in single *phot* mutants or in the *p1p2* double mutants (Section 3.2.4; Litthauer et al., 2015). DF rhythms tended towards long period in the *p1p2* mutant, but this difference was not statistically significant. These differences observed between F_q'/F_m' and DF rhythms further suggest that the two fluorescence processes are regulated by distinct mechanisms, although further analysis the biological processes is needed.

The mechanism through which phototropins maintain oscillations in PSII operating efficiency remains elusive. While phototropins are known to function in the chloroplast avoidance response in response to blue light, chloroplast movement is not expected to play a role in F_q'/F_m' fluctuations over time due to the ratiometric nature of the F_q'/F_m' parameter (Brugnoli and Björkman, 1992). However, further investigation is needed to determine whether phototropins regulate the turnover of light harvesting complexes, or whether the effect on PSII operating efficiency is an indirect consequence of impaired chloroplast movement or stomatal conductance in the absence of phototropin activity (Litthauer et al., 2015). Previous studies have associated dampening of circadian rhythms under free-run with the weak coupling of individual, self-autonomous clocks that reside in different cells and tissues (Rascher et al., 2001; Wenden et al., 2012). In *K. daigremontiana*, the rapid decline in total leaf F_q'/F_m' occurs as the weakly-coupled patches of tissue, each acting as an individual oscillator, become desynchronised (Rascher et al., 2001). The level of heterogeneity among tissues is influenced by the specific phase of CAM metabolism and is not tissue-type specific, but is rather due to the dynamics of metabolite pools and the limitations of CO_2 diffusion between tightly packed cells (Rascher et al., 2001). In *Arabidopsis*, weak coupling between tissue- and organ-specific

clocks have been reported, while weak intercellular coupling results in desynchronisation of transcriptional rhythms in individual cells (and therefore dampening of overall rhythms) under constant light conditions (Wenden et al., 2012; Endo et al., 2014; Bordage et al., 2016; Millar, 2016). The current study cannot address the patterns of desynchronization that could cause dampening of F_q'/F_m' rhythms in the absence of phototropins, as this would require higher resolution imaging and analysis of PSII operating efficiency at tissue- or cellular level. However, it is unlikely that loss of amplitude in F_q'/F_m' oscillations under constant blue light is due to desynchronization of transcriptional oscillations, as loss of phototropin function has no effect on rhythms of transcript accumulation for either morning- or evening-phased nuclear clock genes (Section 3.2.5; Litthauer et al., 2015, 2016).

While these data imply that the dampening of F_q'/F_m' rhythms under constant blue light is due to processes occurring within the chloroplast, it remains to be determined whether phototropins impact PSII operating efficiency through changes to the light harvesting apparatus, through regulation of photochemistry, or through both (Litthauer et al., 2015, 2016). This study does, however, indicate that maintenance of F_q'/F_m' oscillations under constant blue light does not involve NPH3 (NONPHOTOTROPIC HYPOCOTYL3) – the phototropin-interacting component necessary for phot-dependent phototropism under blue light (Section 3.2.6; Motchoulski and Liscum, 1999; Roberts et al., 2011; Litthauer et al., 2015). Further investigation could provide insight into whether regulation of PSII operating efficiency by phototropins occurs through an alternative cytoplasmic signalling intermediate, or through a phototropin-initiated cascade that allows transmission of signals across the chloroplast membrane (Litthauer et al., 2015). Interestingly, a significant FRP lengthening of F_q'/F_m' rhythms in *p1p2* mutants entrained under short- or long days is observed, which suggests a possible role for phototropins in timing of chloroplast rhythms to regulate photoperiod-sensitive processes (Section 3.2.7). While this study does not provide further insight into the mechanism or function of phototropin regulation of PSII operating efficiency, it does

demonstrate the effectiveness of using chlorophyll *a* fluorescence imaging to monitor circadian rhythms in both wild-type and mutant *Arabidopsis* seedlings.

7.3. SAL1 is a chloroplast-localised protein that acts on the nuclear circadian clock by controlling levels of endogenous PAP

SAL1 is an enzyme with phosphatase activity towards polyphosphoinositols such as inositol 1,4,5-triphosphate (IP_3), and 3'(2')5'-biphosphate nucleotides such as 3'-phosphoadenosine 5'-phosphate (PAP) (Quintero et al., 1996; Xiong et al., 2001; Estavillo et al., 2011). The enzyme is expressed ubiquitously throughout most plant organs, and previous microarray studies have indicated that *SAL1* transcript oscillates in long- and short-day conditions but exhibits less pronounced rhythms under constant light conditions (Xiong et al., 2001; Mockler et al., 2007). The current study confirmed that no discernible rhythms in *SAL1* transcript accumulation are observed under constant white light and that, while *SAL1* transcripts gradually accumulate over the course of the day under entraining conditions, no changes in protein accumulation were apparent in transgenic lines expressing *SAL1-GFP* under control of its native promoter (Section 4.2.2). SAL1 is encoded in the nucleus, but is localised and active mainly in chloroplasts (Chen et al., 2011; Estavillo et al., 2011). Mutations in *SAL1* are highly pleiotropic, with phenotypes including morphological characteristics such as delayed germination and growth, limited root growth, shortened hypocotyls, shortened petioles and rounded leaves, and delayed flowering (Section 4.2.1; Xiong et al., 2001; Kim and Von Arnim, 2009; Wilson et al., 2009; Hirsch et al., 2011); increased tolerance to drought, and hypersensitivity to light and ABA (Xiong et al., 2001; Rossel et al., 2006; Kim and Von Arnim, 2009; Wilson et al., 2009); altered sulfate- and fatty acid metabolism (Rodriguez et al., 2010; Lee et al., 2012); increased RNA silencing triggers (Gy et al., 2007); and increased expression in stress-related genes such as *APX2* (Wilson et al., 2009; Estavillo et al., 2011). As SAL1 accumulates in chloroplasts and mitochondria, this study first used chlorophyll *a* fluorescence imaging to determine whether circadian rhythms in chloroplasts were maintained in the absence of SAL1 activity (Section

4.2.3). Loss of SAL1 function resulted in a significant increase in FRP under constant blue light in the *alx8-1*, *fry1-6* and *fou8* mutant alleles of *sal1* compared to wild-type seedlings. Furthermore, circadian oscillations in F_q'/F_m' were restored in *alx8-1* upon complementation with a wild-type copy of the *SAL1* gene, suggesting that the loss-of-function mutation in *sal1* underlies the observed long period phenotype (Section 4.2.5). Unlike phototropins, which affect the amplitude of rhythms in PSII operating efficiency but not DF (Section 3.2.3, Section 3.2.4; Litthauer et al., 2015), loss of SAL1 activity also resulted in a significant increase in FRP in DF rhythms under constant blue light (Section 4.2.3).

In order to determine whether SAL1 activity also affects circadian rhythms in the nucleus, a *fry1-6 CCA1::LUC2* reporter line was used to study rhythms in *CCA1* activity, and revealed a significantly long FRP in *CCA1* promoter activity in *fry1-6* under 20 $\mu mol.m^{-2}.s^{-1}$ constant blue light (Section 4.2.4). In addition, *alx8-1* and *fry1-6* exhibit a 3-6 hour late phase in peak transcript accumulation for multiple morning- and evening-phased nuclear circadian genes under constant blue light (Section 4.2.6). The observation that the activity of a chloroplast-localised protein (that is absent in the nucleus) has a significant effect on circadian rhythms in the nucleus suggests the involvement of chloroplast-to-nucleus signalling mechanisms. The circadian clock is very closely integrated with photosynthesis and its metabolic products, and metabolites acting as signals to the nuclear circadian system have been reported (Dodd et al., 2007; Haydon et al., 2013; Dodd et al., 2015). Endogenous sucrose acts as a retrograde signal that entrains the circadian clock by respectively repressing and promoting transcription of the morning-active components *PRR7* and *CCA1* (Haydon et al., 2013; Dodd et al., 2015). At dawn, the circadian oscillator is adjusted in response to the low intensity light sensed by cry and phy photoreceptors, after which the activity of sucrose creates a "metabolic dawn" that occurs during the period of higher light intensity occurring after dawn. During this second entraining event, the phase of the oscillator is advanced in response to the rhythmic accumulation of sugars in the morning that results from the daily activation of photosynthesis (Haydon et al., 2013). Photosynthetic electron transport has also been reported to generate a

yet-unidentified retrograde signal that affects alternative splicing of nuclear-encoded transcripts (including transcripts encoding splicing factors) in response to light/dark conditions (Petrillo et al., 2014). In addition, the cytosolic ligand cyclic adenosine diphosphate ribose (cADPR), which promotes the release of Ca^{2+} from internal stores into the cytosol, drives circadian oscillations in cytosolic Ca^{2+} and regulates the nuclear oscillator's transcriptional feedback loops (Dodd et al., 2007).

Although SAL1 has phosphatase activity towards both IP_3 and PAP, PAP is regarded as the enzyme's *in vivo* substrate, with the morphological-, stress tolerance- and gene expression phenotypes observed in *sal1* mutants associated with increased endogenous PAP levels (Kim and von Arnim, 2009; Chen and Xiong, 2010; Hirsch et al., 2011; Estavillo et al., 2011; Lee et al., 2012). *sal1* loss-of-function mutants accumulate up to 20-fold more PAP than wild type, and abiotic stress treatment of wild type plants causes an increase in endogenous PAP and resulting changes in PRANG (plastid redox associated nuclear gene) expression (Estavillo et al., 2011; Chan et al., 2016a). If PAP acts as a signal to relay environmental information sensed in chloroplasts (Chen et al., 2011; Estavillo et al., 2011), modulation of PAP accumulation should be sufficient to lengthen circadian period. Indeed, the current study suggested that the accumulation of endogenous PAP underlies the circadian phenotype observed in *sal1* mutants. The ~3-hour phase shift in transcript accumulation observed in *sal1* mutant seedlings under constant white light correlated with an ~10-fold increase in endogenous PAP compared to wild-type (Section 6.2.2). Furthermore, specifically reducing endogenous PAP levels by constitutive overexpression of the PAP-specific *SAL1* paralog *AHL* (Kim and von Arnim, 2009; Chen and Xiong, 2010; Hirsch et al., 2011) restored both circadian rhythms in F_q'/F_m' and PAP to wild-type levels in a *sal1* mutant under constant blue light, and demonstrates that PAP phosphatase activity is sufficient to complement the *sal1* circadian phenotype (Section 6.2.2). In addition, under constant blue light, application of exogenous PAP was sufficient to further extend the long circadian period of *sal1* mutants that are unable to degrade the metabolite, further suggesting that accumulation of PAP underlies the circadian phenotype in these plants (Section

6.2.5). Previous studies have provided reports of exogenous feeding of metabolites and subsequent responses in plants as supporting evidence that these compounds act as retrograde signals (de Souza et al., 2017). Treatment of adult wild-type *Arabidopsis* plants with the putative retrograde signal β-cyclocitral induces changes in expression of ROS-responsive and defence genes, as well as accumulation of salicylic acid and reduction in ROS production in chloroplasts (Ramel et al., 2012; Lv et al., 2015). Similarly, exogenous application of free linolenic acid or linoleic acid rapidly activates the pathogen-related Rapid Stress Response Element in plants (Walley et al., 2013), and exogenous treatment with the plastid metabolite MEcPP induces a subset of genes involved in the ER Unfolded Protein Response in wild-type plants (Walley et al., 2015). In the current study, exogenous application of PAP to wild-type *Arabidopsis* seedlings had no effect on circadian rhythms (Section 6.2.5). This observation agrees with a previous report that treatment with exogenous PAP does not induce expected changes in stress gene expression in wild-type *Arabidopsis* leaves (Estavillo et al., 2011). This negative result has been attributed to the high catalytic activity of SAL1 towards PAP in chloroplasts (Estavillo et al., 2011; Pornsiriwong et al., 2017). Indeed, the current study confirmed that endogenous PAP levels are very low or undetectable in wild-type under non-stressed conditions (Sections 6.2.2, 6.2.3 and 6.2.6), and showed that constitutive overexpression of SAL1 protein had no effect on circadian rhythms in wild-type seedlings (Section 4.2.7). A recent study circumvented this challenge by including in the exogenous PAP treatments LiCl, for inhibition of native SAL1 activity, and ATP, for outcompeting PAP transport by the ADP/ATP bidirectional transporter TAAC/PAPST1 into plastids where SAL1 is active (Pornsiriwong et al., 2017). However, this approach is unsuitable for use in the current study, as treatment with LiCl lengthened circadian period in Col-0 seedlings (Section 6.2.5), and the effect of exogenous ATP on the circadian system and on ATP-dependent luciferase circadian assays is unknown.

The correlation between endogenous PAP levels and long circadian period was further demonstrated in the light-specific circadian phenotype of *sal1* mutants (Sections 6.2.1 and

6.2.3). Plants with impaired *SAL1* function have previously been reported as being hypersensitive to both red and blue monochromatic light (Kim and von Arnim, 2009), and the current study confirmed that *sal1* mutant seedlings exhibit shortened hypocotyls both under constant blue and constant red light (Section 4.2.1). Since a long circadian period phenotype was observed in *sal1* mutants under constant blue light (Sections 4.2.3 and 4.2.4), the light dependency of the *sal1* circadian phenotype was further examined using the *fry1-6 CCA1::LUC2* luciferase reporter line (Section 6.2.1). The *sal1* mutant phenotype was shown to be light-dependent, with the wavelength and intensity of light influencing the circadian phenotype even under relatively low fluence rates of light (Section 6.2.1). In contrast to the previously reported hypocotyl phenotypes (Kim and Von Arnim, 2009; Section 4.2.1), the current study showed that *sal1* seedlings have a blue light-dependent circadian phenotype. While an ~1-hour period extension was observed under 20 $\mu mol.m^{-2}.s^{-1}$ constant blue light, no significant lengthening in FRP was observed in *sal1* seedlings grown under constant darkness or under constant red light (Section 6.2.1). Similarly, DF rhythms oscillated with an ~1 hour elongated FRP in *sal1* under constant blue light, while FRP of DF rhythms in *sal1* mutants were indistinguishable from wild-type under constant red light (Section 4.2.3). These observations correlated with rhythms in accumulation of core clock transcripts in *sal1* seedlings (Section 4.2.6). A clear shift of 3-6 hours was apparent in the circadian phase of transcript accumulation in *sal1* seedlings transferred to 20 $\mu mol.m^{-2}.s^{-1}$ constant blue light, while a less severe (or no) phase shift was observed in *sal1* seedlings under 30 $\mu mol.m^{-2}.s^{-1}$ constant red light. Similarly, a reduction in the phase difference between *sal1* mutant alleles and wild-type was observed when clock transcript accumulation was monitored under 60 $\mu mol.m^{-2}.s^{-1}$ constant white light (Section 5.2.5). Completion of a fluence rate response curve under constant blue light revealed that the intensity of constant blue light affects the circadian phenotype of *sal1* plants (Section 6.2.1). A pronounced lengthening of FRP is observed in *fry1-6 CCA1::LUC2* seedlings transferred to $\geq 20\ \mu mol.m^{-2}.s^{-1}$ constant blue light, but transfer to very dim blue light ($<5\ \mu mol.m^{-2}.s^{-1}$) had no effect on FRP in these seedlings compared to wild-type. In contrast, different fluence rates of constant red light had no significant effect on FRP

in *fry1-6* seedlings. The light-dependent lengthening of FRP in *fry1-6* under constant blue light correlated with increased endogenous PAP levels at higher fluence rates, and the *alx8-1*, *fry1-6* and *fou8* alleles all accumulated significantly higher endogenous PAP at 20 $\mu mol.m^{-2}.s^{-1}$ than at 5 $\mu mol.m^{-2}.s^{-1}$ constant blue light (Section 6.2.3). These findings suggest that PAP acts to alter FRP via a blue light dependent pathway, but that the blue light-dependent PAP pathway involved in regulating FRP is either not active or insignificant at very low fluence rates.

7.4. A role for the SAL1-PAP pathway in regulating circadian rhythms in response to abiotic stress

According to the SAL1-PAP signalling model, abiotic stresses such as drought or high light induce oxidative stress within chloroplasts, with the change in redox poise in the plastids causing conformational changes in the SAL1 enzyme and subsequent inhibition of SAL1 catalytic activity (Chan et al., 2016a, 2016b). The stress-induced inhibition of SAL1 enzyme activity results in the accumulation of PAP in chloroplasts, and PAP in turn acts as a retrograde signal to affect the expression of stress genes (PRANGs) in the nucleus (Estavillo et al., 2011; Chan et al., 2016b). PAP accumulation is positively correlated with the extent to which SAL1 phosphatase activity is inhibited and with the severity of abiotic stress (Estavillo et al., 2011; Chan et al., 2016a). While PAP accumulates in wild-type plants subjected to either high light or drought, SAL1 activity is particularly inhibited when plants are subjected to drought stress (Estavillo et al., 2011; Chan et al., 2016a). The effect of osmotic stress on PAP levels and circadian period on Col-0 under constant blue light was therefore investigated (Section 6.2.6). Treatment of seedlings with 200 mM mannitol resulted in a significant increase in endogenous PAP in wild-type, while no increase in PAP accumulation was observed in *alx8-1* seedlings in response to osmotic stress treatment. The accumulation of PAP in Col-0 seedlings correlated with a >1 hour lengthening in FRP in nuclear circadian rhythms, suggesting that the SAL1-PAP pathway acts to delay FRP in wild-type seedlings in response to osmotic stress.

A growing body of evidence suggests that the circadian clock contributes to plants' ability to tolerate and acclimate to different types of environmental stress, yet the mechanisms by which the clock couples to stress-response pathways remain elusive (Grundy et al., 2015). The clock controls a broad range of abiotic stress-responsive genes, with over 40% of cold-regulated genes and 50% of genes responsive to heat, osmotic stress, salinity or water deprivation being under circadian control in *Arabidopsis* (Covington et al., 2008; Grundy et al., 2015). The majority of heat-inducible genes are expressed during the day, while the majority of cold-induced genes (including *CRE/DRE-BINDING FACTORs* (*CBF*) 1, 2, and 3, master regulators of the cold acclimation response) peak in the afternoon, a few hours before temperatures drop at night (Harmer et al., 2000; Covington et al., 2008; Grundy et al., 2015). In the evening, heat-repressed genes peak, while genes downregulated by cold peak around dawn, before the daily rise in temperature occurs. Similarly, many drought-induced genes peak around dawn, hours prior to when plants are expected to experience water deficit during the daytime (Harmer et al., 2000; Covington et al., 2008; Grundy et al., 2015). The circadian clock also gates the amplitude of responses to abiotic stress, including maximal cold induction of *CBF1,2,3* in the morning (Fowler et al., 2005; Thomashow, 2010), and maximal drought-induced changes in gene expression at dusk (Wilkins et al., 2010).

Drought and osmotic stress cause changes in the redox state of chloroplast, resulting from the increased generation of reactive oxygen species during photosynthesis (Apel and Hirt, 2004; Chan et al., 2016b). Part of the antioxidant defence system in plants involves the action of peroxiredoxins: thiol-dependent enzymes that decompose peroxides through a three-step process that includes peroxide reduction, thiol resolving, and regeneration to the active form upon transfer of electrons to a donor such as glutathione or ascorbate (Dietz, 2011). The oxidation-reduction cycles that peroxiredoxins undergo oscillate with circadian rhythm under constant light conditions, suggesting an endogenous rhythm in the generation of ROS (Edgar et al., 2012). Indeed, ROS production and scavenging are regulated by light:dark cycles, with peaks in catalase activity and endogenous H_2O_2 around noon and troughs around midnight, and

the majority of ROS-responsive genes exhibiting time-of-day patterns that coincide with rhythms in ROS levels (Lai et al., 2012). ROS homeostasis is also under circadian control, with patterns in H_2O_2 levels and catalase levels apparent under constant light conditions (Lai et al., 2012). A functional clock is required for the time-of-day-specific regulation of ROS production, and the rhythmic expression of *CATALASE* genes under constant light is perturbed in clock mutants (Lai et al., 2012). The circadian regulation of ROS production and scavenging provides a possible mechanism through which the SAL1-PAP pathway could link to the circadian clock. *SAL1* transcript accumulation is not a clock-regulated output, and SAL1 protein levels do not change throughout the course of the day (Section 4.2.2). Furthermore, despite increases in PAP levels in response to drought stress (Estavillo et al., 2011; Chan et al., 2016a), osmotic stress (Section 6.2.6) or high light stress (Estavillo et al., 2011), abiotic stresses have no effect on SAL1 protein accumulation (Chan et al., 2016a). The increase in PAP levels in wild-type in response to drought, high light or oxidative stresses have been attributed to the ROS-induced inhibition of SAL1 activity (Chan et al., 2016a). The ROS-sensitive model of SAL1 regulation could also explain the accumulation of PAP in osmotically-stressed wild-type seedlings, as no significant increase in PAP was observed in a *sal1* mutant following the same treatment (Section 6.2.6). Therefore, while *SAL1* expression is not a clock output, the regulation of SAL1 activity by ROS could allow for interaction between the SAL1-PAP signalling pathway and circadian control of abiotic stress responses. It would be interesting to monitor fluctuations in PAP in wild-type plants over circadian and diurnal time, yet the low (often undetectable) levels of endogenous PAP in wild-type in non-stressed conditions (Estavillo et al., 2011; Sections 6.2.2, 6.2.3 and 6.2.6) would make such analysis difficult. Preliminary analysis of stress gene activation by high light stress in Col-0 and *sal1* under constant light revealed higher activation of stress-responsive genes in both genotypes during the subjective day compared to the subjective night (Appendix III), and investigations into the role of SAL1-PAP in circadian regulation of abiotic stress would be of further interest. One possible avenue of investigation could involve monitoring rhythms in ROS homeostasis in wild-type and *sal1* mutants by using ROS-sensitive biosensors, such as the H_2O_2-sensitive GFP-derived biosensor

HyPer (Exposito-Rodriguez et al., 2013). Attempts to utilise stable transgenic *Arabidopsis* lines expressing HyPer1 were unsuccessful in the current study due to low protein levels and subsequent weak fluorescence signals (Appendix III), possibly as a result of silencing of the transgene (Exposito-Rodriguez et al., 2013). However, alternative ROS-sensitive biosensors (such as HyPer3 or the glutathione-sensitive roGFP2; Schwarzländer et al., 2008; Marty et al., 2009; Bilan et al., 2013) are valuable resources that could be used to investigate the interplay between SAL1-PAP signalling and circadian regulation in abiotic stress responses.

While a direct correlation between FRP and tolerance to abiotic stress is not always clear, a recent study suggests that a delay in the circadian system might improve a plant's survival under abiotic stress conditions by slowing down metabolic processes and conserving energy (Syed et al., 2015). This is consistent with observations that accumulation of endogenous PAP - due to either mutation of *SAL1* or application of osmotic stress - lengthens FRP (Sections 6.2.1, 6.2.3 and 6.2.6), and delays flowering (Wilson et al., 2009). Since higher light intensities are known to accelerate circadian rhythms in plants (Aschoff, 1979), it could be suggested that PAP acts as a light-dependent metabolic 'decelerator', acting to slow clock-regulated metabolic processes under increasing light intensities.

7.5. Regulation of circadian rhythms by SAL1 does not occur as a result of altered sulfate metabolism

PAP is produced in secondary sulfur assimilation as a byproduct in the production of sulfated metabolites (Kopriva et al., 2012). In the cytosol, sulfotransferases (SOT) catalyse sulfation reactions, transfering a functional sulfo group from the sulfate donor (and PAP precursor) 3'-phosphoadenosine 5'-phosphosulfate (PAPS) to the free hydroxyl group of an acceptor substrate (Mugford et al., 2009, 2010). PAPS itself is generated by two pathways: in plastids *via* the action of ATP sulfurylase (ATPS) 1-4 which catalyse the production of adenosine phosphosulfate (APS) from ATP and sulfate, followed by the phosphorylation of APS by APS

kinase (APK) 1, 2, and 4 to form PAPS; or in the cytosol *via* the action of ATPS and APK3. PAPS formed in plastids is exported into the cytosol for utilisation by SOTs through the action of the PAPS/PAP antiporter PAPST1 located in thylakoids and in the plastid envelope, and which also transfers PAP from the cytosol into plastids (Gigolashvili et al., 2012). PAP is also produced to a much lesser extent through the activity of the endoplasmic reticulum-resident tyrosyl protein sulfotransferase (TPST) that activates the low-abundance peptide hormones by sulfonation, although the relative sulfur consumption by TPST is negligible (Chan et al., 2013). The by-product PAP is an 'unfavourable' metabolite that inhibits activity of cytosolic SOTs and of the 5'→3'exoribonucleases (XRNs) located in the cytosol and nucleus (Dichtl et al., 1997; Klaassen and Boles, 1997; Estavillo et al., 2011), and is therefore sequestered in plastids where it is rapidly convered into AMP and P_i by SAL1 (Mugford et al., 2009, 2010). Loss of SAL1 function causes low levels of internal sulfate and total elemental sulfur in the *fou8* mutant which triggers a sulfate deficiency response, as is evident by gene expression patterns that are similar to that observed in wild-type plants subjected to sulfate starvation (Lee et al., 2012). As sulfate assimilation is vital for plant metabolism and photosynthesis (Takahashi et al., 2011), the current study investigated whether *sal1* induces a long period circadian phenotype via the reduced accumulation of sulfate (Section 5.2.1). Growth of Col-0 plants under sulfate-deprived conditions resulted in upregulation of sulfate starvation-responsive genes, yet no FRP lengthening in rhythms of circadian gene promoter activity or F_q'/F_m' was observed under constant blue light. In contrast, FRP in nuclear and chloroplast rhythms tended to be shortened under sulfate-deprived conditions compared to control conditions in both Col-0 and *sal1* (although this change was not always significant), and *sal1* exhibited a longer circadian period compared to Col-0 both under sulfate-deprived and control conditions. Compared to wild-type, the *fou8* mutant has lower levels of glucosinolates and accumulates desulfoglucosinolate precursors. These phenotypes also occur to a greater degree in plants lacking functional APK1 and APK2, the enzymes responsible for the production of PAPS in chloroplasts (Lee et al., 2012). To futher investigate the effect of disrupted sulfate metabolism on circadian rhythms, oscillations in F_q'/F_m' were monitored in *apk* mutants under constant blue light (Section 5.2.2).

The *apk1 apk2* double mutant does not mimic the *fou8* phenotype: PAPS synthesis in chloroplasts is disrupted in the *apk1 apk2* double mutant; a more profound decrease in glucosinolates and consequent increase in desulfoglucosinolates occurs in *apk1 apk2* compared to *fou8*; and severely decreased glucosinolate levels in *apk1 apk2* causes increases in transcript levels of the majority of genes involed in glucosinolate synthesis, while only one gene involved in glucosinolate backbone synthesis (*CYP79F2*) and the three *SOT* genes involved in glucosinolate synthesis are upregulated in *fou8* (Lee et al., 2012). Even so, the *apk1 apk2* mutants provide insight into the effect of disrupted glucosinolate synthesis on circadian rhythms. As was observed in plants grown on sulfate-deficient media, no lengthening in FRP was observed either in the *apk1 apk2* double mutant or in the *apk1 apk2 fou8* triple mutant, with FRP again trending towards being shortened in these mutants.

While the mechanims by which internal sulfate levels are affected in *fou8* is not known, it is clear that the low sulfate content in *fou8* is not due to differences in sulfate uptake or translocation, but rather due to increased sulfate reduction and assimilation into reduced compounds (thols and proteins) (Kopriva et al., 2012; Lee et al., 2012). The disruption in glucosinolate synthesis in *fou8* has been suggested to occur as a result of inhibition of cytosplasmic SOTs activity by accumulated PAP: PAPS accumulates in *fou8* (although to a lesser degree than PAP), and the desulfoglucosinolate sulfotransferase genes *SOT16*, *SOT17* and *SOT18* are upregulated in *fou8* (Chen et al., 2011; Estavillo et al., 2011; Lee et al., 2012). While perturbed secondary sulfate metabolism is not the cause of the long circadian period in *sal1* mutants, the observed acceleration of circadian rhythms in the absence of sulfate or upon disruption of glucosinolate synthesis is an interesting avenue for further investigation. The current study's observations on the effect of altered sulfate metabolism on the circadian system is in agreement with a recent report which demonstrates that perturbed glucosinolate accumulation shortens FRP under combined constant red+blue light (Kerwin et al., 2011). Glucosinolates contribute significantly to the total sulfur pool in plants and are an important sink for the sulfonation reactions that form PAP as byproduct (Chan et al., 2013). Indeed, *SAL1*

is co-regulated with genes involved in glucosinolate synthesis (Mugford et al., 2009; Lee et al., 2012). Not all glucosinolates are affected equally in the *fou8* mutant, with the decrease in total glucosinolates mostly due to lowering in levels of aliphatic glucosinolates, while the indolic glucosinolates are affected to a lesser desgree or unaffected (Lee et al., 2012). The aliphatic glucosinolates decreased in *fou8* - glucoraphanin (4MSOB), its precursor glucoerucin (4MTB), and glucohirsutin 8(MSOO) – are among the most abundant glucosinolates normally present on leaf surfaces in wild-type *Arabidopsis*, and accumulate significantly in plants upon herbivorous feeding by caterpillars (Beekwilder et al., 2008; Lee et al., 2012; Shroff et al., 2015). Similary, the indolic glucosinolates glucobrassicin (I3M) and 4-methoxyglucobrassicin (4MOI3M) accumulate in wild-type in response to herbivory, and are reduced in *fou8* (Beekwilder et al., 2008; Lee et al., 2012). Interestingly, neoglucobrassicin (1MOI3M) is the glucosinolate that shows the greatest increase in wild-type leaves following herbivory, yet levels of this indolic glucosinolate are increased in the *fou8* mutant (Beekwilder et al., 2008; Lee et al., 2012). Studying the role of *SOTs 16-18* and the effects of these indvidual glucosinolates on FRP could provide insight into the role of circadian regulation in biotic stress response. The circadian clock is known to prepare plant defensive mechanisms in anticipation of herbivore activity by regulating jasmonic acid (JA) and salicyclic acid biosynthesis and signalling pathways (Greenham and McClung, 2015). The accumulation of jasmonates and salicylates (which often act antagonistically to jasmonates) are circadian-regulated and antiphasic (Goodspeed et al., 2012). The *Arabidopsis* clock maximises JA signalling and synthesis during the day when cabbage loopers are gated by their own clocks to exhibit feeding activity, thereby maximising the plant's resistance to herbivory (Goodspeed et al., 2012). Plants with disrupted clocks fail to enhance herbivory resistance during the day, and entrainment of *Arabidopsis* and cabbage loopers out of phase with one another (with looper feeding activity at the during the night when the plants were not anticipating attack), devastates plants (Goodspeed et al., 2012). In addition to the sulfate metabolism phenotype discussed, perturbed PAPS metabolism in *fou8* mutants also results in higher levels of JA in undamaged leaves, as well as increased rates of triunsaturated fatty acid (particularly α-linolenic acid [18:3])

oxygenation by lipoxygenases, a reaction which forms part of the JA synthesis pathway in chloroplasts (Rodriguez et al., 2010). Since linolenic acid is reported to act as a chloroplast-to-nucleus retrograde signal that activates the Rapid Stress Response Element in plants (de Souza et al., 2017), the role of altered fatty acid metabolism in the *fou8* long-period circadian phenotype needs further investigation.

According to the SAL1-PAP model, the accumulation of endogenous PAP is attributed to the inhibition of SAL1 catalytic activity, either through mutations in *SAL1* (Chen and Xiong, 2010; Estavillo et al., 2011; Lee et al., 2012), or through ROS-induced inhibition of SAL1 activity in wild type plants (Chan et al., 2016a). However, the current study showed that endogenous PAP levels increase under different fluence rates of constant blue light in *sal1* mutants (Section 6.2.3), which suggest a light-specific effect on PAP production even in non-stressed conditions. The production of the PAP precursor PAPS is mainly through the activity of plastid-localised APK1 and APK2, and to a lesser extent via the action of cytoplasmic APK3 (Kopriva et al., 2012; Lee et al., 2012). Among all six combinations of *apk* double mutants, only the *apk1 apk2* combination results in smaller plants with perturbed gluocosinolate synthesis (Mugford et al., 2009). In addition, the *apk1 apk2 fou8* triple mutant has the same glucosinolate and desulfoglucosinolate levels and similar gene expression patterns as *apk1 apk2*, showing that the mutations affect the same metabolic step (Lee et al., 2012). Furthermore, while the *apk1 apk2 fou8* triple mutant loses many phenotypes visible in *fou8*, the *apk3 fou8* mutant is indistinguishable from *fou8* (Lee et al., 2012). Therefore, focusing on the conditions that induce APK1 and APK2 (and SOT16, SOT17 and SOT18) activity could provide further insight into the mechanisms that result in PAP production and accumulation. APK competes with APS reductase (APR) for the common substrate APS, which serves as the branching point between primary sulfate metabolism and secondary sulfate metabolism, and the activities of APK and APR are redox regulated (Kopriva et al., 2012; Chan et al., 2013). The fine tuning of sulfur partitioning between primary and secondary sulfate metabolism occurs through a combination of regulator circuits that combine competition between APK and APR, PAPS utilisation and

accumulation of PAP (Ravilious et al., 2012; Chan et al., 2013). *APK1* and *APK2* expression are upregulated by methyl jasmonate and by wounding, and treatment with jasmonate increases mRNA levels of *SOT16* and *SOT17* significantly (Kopriva et al., 2012). Interestingly, under prolonged drought, oxidative stress increases APR activity and attentuates APK activity, directing APS into glutahione (GSH) synthesis and away from PAPS synthesis (Ravilious et al., 2012). Furthermore, *SOT16*, *SOT17* and *SOT18* are not affected by drought at transcriptional level and glucosinolates are not assumed to have any role in the drought stress response (Chan et al., 2013).

7.6. Altered hormone signalling and the *sal1* circadian phenotype

The role of altered hormone signalling in the various *sal1* phenotypes, including the circadian phenotype, needs further investigation. As mentioned previously, the *sal1* mutant allele *fou8* exhibits increased rates of oxygenation of triunsaturated fatty acids by lipoxygenases and higher basal JA levels (Rodriguez et al., 2010). The growth phenotype of *fou8* is partly attributed to JA biosynthesis: mutation of *ALLENE OXIDE SYNTHASE* (*AOS*, an enzyme involved in the formation of JA precursors) in the *fou8* background restores petiole length and flowering time, yet the *fou8 aos* mutant has a rosette size only slightly larger than *fou8*. In contrast. the increased fatty acid oxygenation phenotype of *fou8* is dependent entirely on intact JA biosynthesis (Rodriguez et al., 2010). The alterations in fatty acid oxygenation and JA accumulation results from loss of SAL1 activity towards PAP (Mugford et al., 2010; Rodriguez et al., 2010), and it is yet unclear what effect increased JA biosynthesis has on circadian rhythms. Drought stress responses are largely regulated by the phytohormone ABA (Chan et al., 2013), and SAL1 regulates both ABA-dependent and ABA-indepenent drought stress signalling responses (Wilson et al., 2009). The role of ABA in *sal1* circadian rhythms is therefore another avenue of further investigation. ABA modulates several components of sulfate assimilation including sulfate transport, cysteine syntheis and flux of sulfate into primary assimilation (Chan et al., 2013). ABA treatment results in GSH accumualtion in maize,

as well as increased recycling of GSH from GSSG in pea, while ABA conversely also appears to inhibit APR acitivty (Jiang and Zhang, 2001; Contour-Ansel et al., 2006; Chan et al., 2013). *sal1* alleles exhibit reduced sensitivity to auxin, with many of the morphological phenotypes resembling those of auxin resistant mutants, yet (unlike previously reported auxin resistant mutants) *sal1* mutants are ABA hyper-sensitive (Xiong et al., 2001; Chen and Xiong, 2010; Rodríguez et al., 2010). The exogenous application of ABA has been reported to either shorten or extend circadian period, and so it is possible that enhanced ABA sensitivity plays a role in the *sal1* circadian phenotype (Hanano et al., 2006; Liu et al., 2013). In addition, the accumulation of PAP in *sal1* plants up-regulates specific ABA signalling components to induce stomatal closure (Pornsiriwong et al., 2017) and it remains to be determined whether manipulation of these components contribute to the *sal1* circadian phenotype. Furthermore, SAL1 activity towards IP_3 has been shown to affect cytosolic Ca^{2+} levels and directional cell-to-cell auxin transport through the action of polar PIN-FORMED (PIN) auxin efflux transporters (Zhang et al., 2011). Indeed, the *sal1* mutant allele *supo1* is defective in auxin transport and auxin-mediated development, with these phenotypes attributed to the accumulation of IP_3 and subsequent accumulation of cytosolic Ca^{2+} and disruption of PIN localisation (Zhang et al., 2011). Previous reports have identified PAP, not IP_3, as the physiological substrate of SAL1, as IP_3 accumulates to a lesser extent than PAP in *sal1* mutants, and restoration of PAP levels through overexpression of the PAP-specific enzyme AHL complements *sal1* morphological phenotypes (Kim and von Arnim, 2009; Hirsch et al., 2011; Estavillo et al., 2011). Similarly in the current study, the accumulation of PAP corresponded with the lengthening of circadian period in *sal1* and wild-type seedlings, while both endogenous PAP levels and circadian rhythms are restored in *sal1* upon overexpression of AHL, further indicating that SAL1 activity towards PAP, not IP_3, is important for maintaining circadian rhythms. Even so, the effect of IP_3 (and subsequent Ca^{2+} and auxin signalling) on circadian rhythms provides yet another avenue for further investigation. It is possible that changes in plant hormone accumulation, signalling and sensitivity, as well as perturbed sulfate

metabolism in *sal1* mutants jointly contribute to the observed circadian phenotype as part of the global developmental consequences of lost SAL1 activity.

7.7. PAP as a metabolic modulator of circadian rhythms

The action of PAP as a mobile chloroplast-to-nucleus retrograde signal that affects nuclear gene expression in response to stress remains an area of debate and requires further investigation (Xiao et al., 2013; de Souza et al., 2017). The targeting of SAL1 to the nucleus of a *sal1* mutant in the ΔN-SAL1 line results in complete restoration of PAP levels, morphological phenotypes, *APX2* mRNA abundance, and, in the current study, circadian rhythms (Kim and Von Arnim, 2009; Estavillo et al., 2011; Section 4.2.5). The complementation of the *sal1* phenotype in this ΔN-SAL1 line has been proposed as evidence that PAP can be catabolized by either nuclear or chloroplastic targeting of SAL1 (Kim and von Arnim, 2009; Estavillo et al., 2011). Since analysis of isolated chloroplasts has shown that PAP accumulates in chloroplasts (Estavillo et al., 2011), and not in the cytosol, complementation of the *sal1* phenotype in ΔN-SAL1 plants has been used to demonstrates that PAP can move between cellular compartments (Estavillo et al., 2011). However, it must be considered that SAL1 protein in these ΔN-SAL1 results from expression of *SAL1* cDNA lacking the chloroplastic transit peptide, driven by the CaMV 35S promoter, and that the effect of constitutive overexpression of the protein cannot be disregarded. The similar molecular and morphological phenotype of *sal1* and the *xrn2 xrn3* double mutant suggests that PAP accumulation can inhibit the function of nuclear-localised XRNs (Gy et al., 2007; Estavillo et al., 2011). This has been proposed as further evidence that PAP is able to move between cellular compartments, and that degradation of PAP pools in either the chloroplast, mitochondria or nucleus will therefor restore the wild-type phenotype (Estavillo et al., 2011). PAP is synthesised in the cytosol, but degraded in plastids, suggesting that transport of the metabolite across the plastid envelope occurs (Chan et al., 2013). Indeed, the PAPS/PAP antiporter PAPST1 has been proposed as a transporter for PAP and, once in the cytosol, PAP would

diffuse freely into the nucleus through the nuclear pore (as do other nucleotides) (Estavillo et al., 2011; Gigolashvili et al., 2012; Chan et al., 2013). In addition, a recent report has shown that upon exogenous application of defence signals such H_2O_2, chloroplasts produce dynamic tubular extensions (known as stromules) that surround the nucleus and act as a conduit for transport of signals into the nucleus (Caplan et al., 2015). However, the current study showed that loss of function of the cytoplasm-localised XRN4 mimics the light-dependent long circadian period of *sal1* mutants (Section 5.2.4) which, along with reports that cytoplasmic SOT activity is inhibited by PAP in *sal1* mutants (Kopriva et al., 2012; Lee et al., 2012) suggests that the effect of PAP accumulation in the cytosol cannot be discounted. Furthermore, while the proposal of a chloroplast-localised metabolite that moves between cellular compartments to act in the nucleus is an elegant notion, there is no indication whether PAP acts as a compartmentalised, mobile interorganellar signal, or whether the effect of PAP accumulation (or depletion) on nuclear gene expression is merely due to changes in global PAP levels within the cell. This study suggests that the PAP-induced effects on gene transcription could be dose-dependent, as application of exogenous PAP extends circadian period even further in *sal1* mutants that already accumulate intercellular PAP (Section 6.2.5). It remains to be determined whether the effect of PAP on gene expression results from accumulation of intercellular PAP beyond a threshold level, or whether responses are triggered by a fold change. The changes in PAP levels that corresponded to emergence of the long period phenotype in *sal1* mutants were relatively small, with only ~5-fold higher PAP levels in plants grown at 20 $\mu mol.m^{-2}.s^{-1}$ (~10 $nmol.g^{-1}$ FW) compared to plants grown at 5 $\mu mol.m^{-2}.s^{-1}$ (from ~2 $nmol.g^{-1}$ FW). This suggests that even small increases in light intensity at low fluence rates cause enough of an increase in PAP levels to have a significant impact on nuclear gene expression, or that the light-activated pathway affected is not active at very low light levels. Similarly, the significant lengthening of FRP in wild-type seedlings upon treatment with mannitol correlated with a significant 2-fold increase in PAP levels, but PAP levels were once again relatively low (undetectable in control plants, compared to ~2 $nmol.g^{-1}$ FW; Section 6.2.6). That such low levels of endogenous PAP correspond with changes in nuclear gene expression has been

reported before (Estavillo et al., 2011): 30-day old Col-0 plants subjected to 11 days of drought exhibit increased expression of PRANGs and a 30-fold increase in endogenous PAP levels, with droughted adult Col-0 plants containing ~150 nmol.g^{-1} DW; in contrast, 30-day old Col-0 plants exposed to 1 hour of high light treatment exhibit only a 1.5-fold increase and relatively low PAP levels (from 0.6 nmol.g^{-1} to 0.9 nmol.g^{-1} FW), with corresponding changes in PRANG expression still occurring (Estavillo et al., 2011). Together, these findings suggest that PAP is a highly effective molecular signal, capable of impacting nuclear gene expression even at very low levels either in the absence or presence of native SAL1 protein expression. Controlling endogenous PAP levels would therefore be of great importance to the plant cell, and could explain the high catalytic activity and continuous expression of the SAL1 protein regardless of light conditions (Section 6.2.4), presence or absence of stress (Chan et al., 2016a) or the time of day (Section 4.2.2). It has been suggested that, due to the small changes in PAP levels needed for initiation of a response, the regulation of PAP movement and relocation of PAP between compartments within the cell could contribute to the response, although there is currently no evidence to suggest that this is the case (Estavillo et al., 2011; Chan et al., 2013).

7.8. Loss of XRN activity replicates the circadian phenotypes of *sal1* mutants

According to the SAL1-PAP retrograde signalling model, accumulated PAP causes changes in nuclear gene expression by inhibiting 5'→3' exoribonuclease (XRN) activity (Dichtl et al., 1997; Estavillo et al., 2011; Chan et al., 2016a, 2016b). Post-transcriptonal regulation of circadian gene expression plays an important role in responding to environmental changes (Sanchez et al., 2011; Nolte and Staiger, 2015; Millar, 2016): Mis-regulation of RNA processing can lead to alteration in circadian FRP, and alternative splicing of clock components modify circadian rhythms in response to temperature changes and drought (James et al., 2012; Jones et al., 2012; Wang et al., 2012; Perez-Santángelo et al., 2014; Filichkin et al., 2015). The current study therefore examined whether mutation of XRNs, to genetically simulate SAL1-mediated inhibition of XRN activity, was sufficient to alter nuclear circadian rhythms (Sections

5.2.4 and 5.2.5). The *Arabidopsis* genome contains three *XRN* genes: XRN2 and XRN3 function in the nucleas, while XRN4 functions in the cytoplasm (Kastenmayer and Green, 2000; Nagarajan et al., 2013). *xrn2 xrn3* double and *xrn2 xrn3 xrn4* triple mutants exhibit similar developmental defects as *sal1*, including crinkly, rounded leaves, shortened petioles, hypersensitive inhibition of hypocotyl elongation and altered lateral root architecture, as well as delayed flowering (Gy et al., 2007; Kim and von Arnim, 2009; Chen and Xiong, 2010; Hirsch et al., 2011). In the current study, analysis of both chloroplast and nuclear circadian rhythms under constant blue light revealed that the *xrn234* triple mutant mimics the long-period circadian phenoytpe observed in *sal1*mutants: an ~1 hour lengthening in FRP in F_q'/F_m' and DF rhythms was observed in *xrn234* mutants under constant blue light, and the 3-6 hour late phase in circadian transcript accumulation observed in *sal1* mutants was also visible in the *xrn234* triple mutant under constant blue light. Similar to *sal1* mutants, the late phase of clock transcript accumulation was much less pronounced in *xrn234* mutants under constant white light compare to constant blue light.

Action of nuclear-localised XRN2 and XRN3 are thought to play the most important role in SAL1-PAP-XRN-regulated stress responses (Estavillo et al., 2011). More than 50% of the genes with constitutively altered expression in *sal1* and the *xrn2 xrn3* double mutant are coregulated, and *xrn2 xrn3* phenocopies *sal1* in rosette morphology, as well as in drought tolerance and induction of stress-responsive genes under high light stress (Gy et al., 2007; Estavillo et al., 2011). In contrast, no statistically significant overlap in coregulated genes is observed between *xrn4* and *sal1*, and *xrn4* does not exhibit drought tolerance. The role of altered leaf morphology and small rosette shape in the drought tolerance phenotype of *sal1* should be considered, particularly as the *xrn4* mutant exhibits smooth, serrated leaves, but rosette size and shape that resembles wild-type (Gy et al., 2007; Estavillo et al., 2011). However, the drought-tolerant *xrn234* triple mutant exhibits wrinkled leaves with longer petioles and a larger rosette than *sal1*, suggesting that the drought tolerance observed in *sal1* and *xrn234* is not merely linked to reduced leaf biomass, but rather to reduced XRN activity

(Hirsch et al., 2011). Furthermore, mannitol (as well as PAP and LiCl) treatments in this study were performed on seedlings after <14 days of growth, at which stage the visible morphological differences between Col-0 and *sal1* plants are less pronounced than in adult plants, and *sal1* seedlings exhibit fatty acid oxygenation rates comparable to wild-type (Rodriguez et al., 2010; Hirsch et al., 2011; Estavillo et al., 2011). While the activities of nuclear XRN2 and XRN3 are involved in stress-responses nuclear gene expression, the current study suggested that the cytoplasmic XRN4 regulates expression of genes that modulate circadian period (Section 5.2.4). Analysis of chloroplast circadian rhythms in *xrn2*, *xrn3* and *xrn4* single mutants under constant blue light revealed that only the *xrn4* single mutant exhibits the significant lengthening in FRP observed in *sal1* and *xrn234* mutants. Similarly, no lengthening in FRP was observed in segregating *xrn2 xrn3* double mutant seedlings, and no additive effect was observed when comparing FRP of F_q'/F_m' in the *xrn4* single mutant and the *xrn234* double mutant. Interestingly, no pronounced phase shift in core clock transcript accumulation was observed in the *xrn4* mutant under constant white light. This suggest that a similar blue light-specific circadian phenotype observed in *sal1* and *xrn234* mutants is apparent in *xrn4* mutants, although analysis of transcript accumulation and FRP under different wavelengths and fluence rates of light must be investigated in *xrn4*. Indeed, the action of a blue light-specific pathway might explain the lack of overlap reported between transcriptomes of *sal1* and *xrn4* plants grown under white light (Estavillo et al., 2011).

Identifying the targets of XRNs involved in regulation of nuclear gene expression would provide greater insight into how the SAL1-PAP-XRN pathway alters the clock, and how these two mechanisms integrate to regulate stress responses. The substrates of the nuclear-localised partially redundant XRN2 and XRN3 are uncapped RNAs, such as excised hairpin loops that form part of precursor miRNA transcripts, while the cytoplasmic XRN4 degrades 3' cleavage products of miRNA targets (Souret et al., 2004; Gy et al., 2007). Excised mRNA loops accumulate in both *sal1* and the *xrn2 xrn3* double mutant, while the miRNA target cleavage proucts that accumulate in the *xrn4* mutant also accumulate in *sal1*. In addition, XRN2, XRN3,

XRN4 and SAL1 acts as supressors of post-transcriptional gene silencing (Gy et al., 2007). 3'-noncoding transcripts from actively transcribed genes (including for the clock genes *PRR5* and *ELF3*) accumulate in *sal1*, *xrn3* and *xrn2 xrn3* (Kurihara et al., 2012), and were investigated in the current study as a possible mechanism through which circadian rhythms are altered by XRNs (Section 5.2.6). However, 3'-noncoding transcripts were not a consistent consequence of XRN inactivation in *sal1* and *xrn234* mutants, as these transcripts do not accumulate in the *xrn234* mutant under constant blue or constant white light.

7.9. Interactions between the circadian clock and abiotic stress responses

Perturbation of the circadian clock affects tolerance to abiotic stress (Grundy et al., 2015). Overexpression of *LKP2* enhances drought tolerance (Miyazaki et al., 2015), while overexpression of *GI* or *TOC1* results in enhanced salt sensitivity and reduced survival under drought, respectively (Legnaioli et al., 2009; Kim et al., 2013). Conversely, reduced expression of *TOC1* results in improved drought tolerance (Legnaioli et al., 2009), while *gi* mutants show enhanced salt tolerance and improved survival under drought and oxidative stress (Nakamichi et al., 2009; Kim et al., 2013; Fornara et al., 2015). Similarly, *prr5 prr7 prr9* triple mutants show significantly increased tolerance to high salinity, drought and freezing (Nakamichi et al., 2009; Keily et al., 2013), while *gi*, *lux*, *lhy*, *cca1* and *lhy cca1* mutants have reduced tolerance and acclimation to freezing stress (Cao et al., 2005; Espinoza et al., 2010; Dong et al., 2011; Chow et al., 2014). Mutations in core clock components also affect resistance to ROS-producing agents: plants with mutations in *CCA1*, *LHY*, *ELF3*, *ELF4*, *LUX*, *PRR5*, *PRR7* or *PRR9* are hypersensitive to methyl viologen treatment, while plants overexpressing *CCA1* have reduced sensitivity to methyl viologen (Lai et al., 2012). Interestingly, there is often no direct correlation between the effect on FRP and the effect on abiotic stress tolerance in circadian clock mutants (Grundy et al., 2015). For example, clock mutants with long-period phenotypes (*prr9*), short-period phenotypes (*cca1*, *lhy*, *prr5*) or arrhythmia (*efl3*, *elf4*, *lux*) exhibit the same hypersensitivity to methyl viologen (Lai et al., 2012). Short-period *cca1*, *lhy* and *cca1 lhy*

mutants, as well as arrhythmic *elf3* and *elf4* mutants all exhibit higher basal H_2O_2 levels. Similarly, the arrhythmic *lux* mutants and *prr5,7,9* triple mutant have opposing freezing tolerance phenotypes (Nakamichi et al., 2009; Chow et al., 2014). In these cases, FRP of the clock is not the likely primary cause of the altered stress phenotype, but rather direct alteration in the expression of abiotic stress-responsive genes upon mutation of a specific core clock component (Grundy et al., 2015). Some oscillator components have been shown to exhibit dual functions, both in regulating the clock and in directly abiotic stress-responsive genes. For example, *CCA1* specifically regulates responses to oxidative stress and binds directly to the Evening Element and/or CCA1-binding site at the promoter regions of 10 ROS genes involved in transcriptional regulation, including *WRKY11*, *MYB59*, *PAL1*, *ZAT10* and *ZAT12*, to regulate their time-of-day expression (Lai et al., 2012). Similarly, promoters of *CBF1*, *2*, and *3* contain Evening Elements, and CCA1 binds directly to the *CFB1-3* locus, while rhythmic basal expression of *CBF1-3* disrupted in *cca1/lhy* double mutant (Harmer et al., 2000; Dong et al., 2011; Grundy et al., 2015). TOC1 and LUX proteins control correct gating of *CFB3* responses and bind directly to the *CFB3* promoter (Keily et al., 2013), while induction of the cold-inducible genes *CONSTANS-LIKE 1* and *COLD REGULATED GENE 27* requires presence of an Evening Element (Mikkelsen and Thomashow, 2009). While the circadian clock has a clear impact on how plants respond to abiotic and biotic stresses, abiotic stress also has an effect on the circadian system (Grundy et al., 2015). . Differential splicing of a variety of core clock genes occur in response to changes in temperatures and temperature stress (James et al., 2012; Filichkin et al., 2015). In addition, several core clock components are regulated by stress-related transcription factors: the heat shock transcription factor HsfB2b represses transcription of *PRR7* at high temperatures and under drought stress (Kolmos et al., 2014); and binding of CFB1 to the promoter region of *LUX* plays a role in maintaining robust transcriptional rhythms at low temperatures (Chow and Kay, 2013). XRN activity could play a role in mediating both clock gene expression in response to stress and clock-regulated control of genes involved in stress responses. It has long been predicted that changes in mRNA half-life across the circadian cycle contribute to circadian transcript oscillations (Nolte and Staiger, 2015). *CCR-LIKE*

(*CCL*) and *SENESCENCE ASSOCIATED GENE 1* are short-lived transcripts of which mRNA stability changes across the day and is under control of the circadian clock, and disruption of downstream RNA decay of these transcripts leads to circadian defects (Lidder et al., 2005). Furthermore, the stability of *CCA1* transcript is regulated by light, with *CCA1* mRNA relatively stable in the dark and in far-red light, but with a short half-life in red and blue light (Yakir et al., 2007). In the current study, analysis of clock transcript accumulation under entraining conditions revealed a delayed accumulation of *CCA1* transcript visible in *sal1* (despite no changes in *CCA1::LUC2* promoter activity in *sal1* under these conditions, Section 4.2.4), with the delay in accumulation occurring to a lesser extent in *xrn234* (Section 5.2.5). This delay could be due to perturbed mRNA decay resulting from inhibited XRN activity, yet further work is required to determine whether *CCA1* transcript is an XRN target that plays a role in delaying circadian rhythms in response to accumulated PAP. Indeed, no such delay in *CCA1* transcript accumulation was observed in an *xrn4* mutant (Section 5.2.4), suggesting that a more complex mechanism could be involved.

7.10. Final conclusions and future work

Circadian rhythms are integral to plant fitness and survival, playing a key role in regulating growth, metabolism and flowering, and improving readiness of defense mechanisms against biotic and abiotic stress (Dodd et al., 2015; Grundy et al., 2015). Monitoring circadian rhyhtms *in planta* can provide valuable insight into how the clock regulates plant responses under different conditions (Tindall et al., 2015). The curent study proposed that chlorophyll *a* fluorescence imaging can be used as a non-invasive, robust, medium-throughput assay to monitor circadian rhythms in chloroplasts *in planta* and to identify mutants with altered circadian rhythms (Section 3.2.1-3.2.2; Litthauer et al., 2015). Variations in the chlorophyll fluorescence parameter F_q'/F_m' oscillate with circadian rhythm under constant blue light. These rhythms are under control of the nuclear circadian oscillator, and are maintained under constant

blue light by the redundant action of the blue light phototropin receptors, phot1 and phot2 (Section 3.2.2-3.2.3).

Using chlorophyll *a* fluorescence imaging, this study identified *sal1* mutants as exhibiting a long-period circadian phenotype under constant blue light (Section 4.2.3). The chloroplast-localised SAL1 enzyme is reported to act in a chloroplast-to-nucleus retrograde signalling pathway in which nuclear gene expression is controlled through the action of the metabolite PAP in response to abiotic stress (Estavillo et al., 2011; Chan et al., 2016a). Following from the work in this thesis, it is proposed that SAL1 acts within the circadian system, regulating nuclear rhythms via the action of PAP in a blue light-specific mechanism (Sections 4.2.3 -4.2.4; Section 4.2.6; Sections 6.2.1-6.2.3). The blue light-dependend pathways that induce PAP production in the absence of abiotic stress remains to be identified. Analysis of cryptochrome and ZTL pathways by transcriptional analysis and genetic manipulation of signalling components could shed light onto the mechanisms that stimulate PAP production under low light levels and in response to small changes in light. It remains to be seen whether the blue light specificity of the *sal1* circadian phenotype is derived from misregulation of blue light photoreceptor expression, or from disruption of signalling components downstream of photoreceptor transcription or post-tanscriptional RNA processing. The current study demonstrated that PAP is an effective metabolic signal that can alter circadian gene expression upon small changes in low intercellular PAP levels. In addition, this study demonstrated that osmotic stress induces accumulation of PAP at low levels in wild-type, which correlates with a lengthening of circadian period (Section 6.2.6). It is therefore proposed that the inhibition of SAL1 activity under abiotic stress results in the accumulation of PAP in chloroplasts (Chan et al., 2016a), which in turn leads to deceleration of circadian rhythms in response to stress, possibly to improve stress resistance (Syed et al., 2015). Indeed, it would be of interest to analyse the effect of osmotic stress on FRP in *sal1* mutants, and in lines where SAL1 is constitutively overexpressed. An additional avenue of investigation would be to determine whether the stress-induced regulation of circadian timing is conserved in other plant species. It

has been proposed that the redox-sensitive SAL1-PAP pathway can regulate stress gene expression and stress tolerance across monocotyledonous and dicotyledonous plants (Chan et al., 2016a). The redox-responsive cysteine residues of *Arabidopsis* SAL1 are highly conserved across bryophyte, chlorophyte, early angiosperm, eudicot and monocot species. The SAL1 homologue in *Oryza sativa* exhibits the same redox-sensitive inhibition of catalytic activity (Chan et al., 2016a), and virus-induced silencing of the SAL1 homologue in wheat improves drought tolerance (Manmathan et al., 2013). Interestingly, high salinity results in lengthening of circadian period in wheat (Erdei et al., 1998). It would therefore be intriguing to determine whether the SAL1-PAP signalling pathway is involved in circadian regulation of stress responses in agricultural crops.

The SAL1-PAP pathway is proposed to act on nuclear gene expression in response to stress by inhibiting the activity of 5'→3' exoribonuclease (XRN) activity (Estavillo et al., 2011; Chan et al., 2016b). The *Arabidopsis* genome contains three XRNs for which function is often redundant, and accumulated PAP in the *sal1* mutant is reported to simultaneously inhibit all three XRNs (Dichtl et al., 1997; Gy et al., 2007; Estavillo et al., 2011; Nagarajan et al., 2013). The current study demonstrated a possible role for XRN activity in lengthening of circadian period, as loss of XRN function in the *xrn234* mutant results in a blue light-specific long-period circadian phenotype similar to that of *sal1* mutants (Section 5.2.5). While the nuclear-localised XRN2 and XRN3 are regarded as the regulators of stress gene expression in the SAL1-PAP-XRN pathway (Gy et al., 2007; Estavillo et al., 2011), the current study suggests that the cytoplasmic XRN4 regulates the expression of nuclear circadian genes (Section 5.2.4). A role for cytoplasmic XRN activity within the *Chlamydomonas reinhardtii* circadian system has previously been reported, in which case loss of the *XRN4* homologue *XRN1* lengthened circadian rhythm of luciferase activity (Matsuo et al., 2008). *xrn4* alleles have previously been reported as being insensitive to ethylene treatment due to accumulation of *EIN3 BINDING F-BOX PROTEIN1* (*EBF1*) and *EBF2* mRNA (Olmedo et al., 2006; Potuschak et al., 2006), yet ethylene signalling does not contribute to the regulation of circadian rhythms (Thain et al.,

2004; Hanano et al., 2006). Indeed, *xrn4* mutants share similar lateral root defects observed in *sal1* and, while *sal1* mutants are relatively insensitive to ethylene, this lateral root phenotype is not caused by reduced ethylene response (Carrington and Ambros, 2003; Chen and Xiong, 2011). Following from the observations in the current study, it is therefore proposed that XRN4 regulates circadian period through its XRN activity in the cytosol by modulating global changes in circadian transcript abundance and stability, and that loss of this function results in the lengthening of circadian period observed in *xrn4* and *xrn234* mutants. Limiting the role of XRNs to the activity of XRN4 would be a helpful step towards identifying the XRN targets involved in regulating circadian rhythms in response to PAP. As transcripts of the three *XRN*s do not accumulate with daily rhythm (Mockler et al., 2007; Covington et al., 2008), it would be interesting to see whether constitutive overexpression of *XRN4* restores circadian period in a *sal1* mutant. In addition, monitoring RNA-protein interactions through crosslinking-immunoprecipitation (CLIP) combined with sequencing techniques (Licatalosi et al., 2008), could potentially be used to identify the transcripts that act as XRN4 targets in the regulation of circadian rhythms.

While the inhibition of XRN activity by PAP is regarded as the accepted mechanism through which the SAL1-PAP pathway regulates gene expression in response to stress (Estavillo et al., 2011; Chan et al., 2016a, 2016b), the broad range of effects of PAP accumualtion on metabolism (as is evident from the pleiotropic nature of the *sal1* mutation) cannot be disregarded. Indeed, the current study illustrated that *sal1* mutants exhibit delayed accumulation of some circadian transcripts (particularly *CCA1*) under entraining conditions, but that this is less pronounced in *xrn234* and absent in *xrn4* (Sections 5.2.4 and 5.2.45). Similarly, 3'-noncoding transcripts accumulate in *sal1* mutants, but not in the *xrn234* mutants (Section 5.2.6), suggesting the possible involvement of an additional mechanism. Although sulfate deprivation and perturbation of glucosinolate synthesis do not contribute to the long-period circadian phenotype of *sal1* mutants (Sections 5.2.1 and 5.2.2), the effect of PAP accumulation on JA synthesis (Rodriguez et al., 2010), fatty acid oxidation (Rodriguez et al.,

2010; Lee et al., 2012), as well as altered sensitivity to ABA and auxin (Xiong et al., 2001; Chen and Xiong, 2010; Rodriguez et al., 2010) would need further investigation. Interestingly, mutation of the well-defined signalling component *HY5* has been shown to suppress the enhanced light sensitivity in *sal1* hypocotyl elongation and restores lateral root formation (but not leaf morphology) in *sal1* (Chen and Xiong, 2011). HY5 has also been identified as a direct regulator of ABA responses in seed germination, early seedling growth and root development (Chen et al., 2008), and the genetic interaction between HY5 and SAL1 indicates that these two components may act in overlapping pathways to mediate light signalling and root development (Chen and Xiong, 2011). Furthermore, the crossing of *phyB* (or *hy1*) into *sal1* suppresses the light sensitivity of *sal1* and rescues the *sal1* hypocotyl defect, as well as partially rescuing the leaf morphology phenotype of *sal1* (Kim and von Arnim, 2009; Chen and Xiong, 2011). Phytochromes are known to contribute to entrainment of the clock (Jones et al., 2015; Galvão and Fankhauser, 2015), and a role of a phytochrome-dependent factor in chloroplast retrograde signalling has previously been demonstrated (Salomé et al., 2012). It would therefore be interesting to investigate the role of phytochrome signalling in the circadian regulation by the SAL1-PAP pathway. In addition to XRNs, alternative targets of PAP could possibly play a role in regulating circadian rhythms. In addition to its activity on XRNs, PAP is reported to bind to and inhibit nucleoside diphosphate (NDP) kinases (Schneider et al., 1998). NDPKs are a small family of proteins that act as nucleoside phosphotransferases, but are also active in plant responses to environmental cues (Liu et al., 2014). Upregulated protein levels have been detected in plants grown at high salinity, in drought, in polluted soils containing metals, as well as in plants exposed to pathogen elicitors and oxidative stress treatments (Liu et al., 2014). Preliminary data indicates that loss of function of NDPK3 in the *ndpk3* mutant lengthens period of chloroplast circadian rhythms, but to a lesser extent than observed in *sal1* (Appendix IV). The action of NDPK as an alternative to XRN activity in relaying chloroplast signals to the nuclear circadian clock would be an interesting avenue for further research.

References

Adams, S., Manfield, I., Stockley, P., and Carré, I.A. (2015). Revised morning loops of the Arabidopsis circadian clock based on analyses of direct regulatory interactions. PLoS One **10**: e0143943.

Adhikari, N.D., Froehlich, J.E., Strand, D.D., Buck, S.M., Kramer, D.M., and Larkin, R.M. (2011). GUN4-Porphyrin complexes bind the ChlH/GUN5 subunit of Mg-Chelatase and promote chlorophyll biosynthesis in Arabidopsis. Plant Cell **23**: 1449–1467.

Ahmad, M. and Cashmore, A.R. (1993). HY4 gene of A. thaliana encodes a protein with characteristics of a blue-light photoreceptor. Nature **366**: 162–166.

Alabadí, D., Oyama, T., Yanovsky, M.J., Harmon, F.G., Más, P., and Kay, S.A. (2001). Reciprocal regulation between TOC1 and LHY/CCA1 within the Arabidopsis circadian clock. Science **293**: 880–883.

Ambros, V. and Chen, X. (2007). The regulation of genes and genomes by small RNAs. Development **134**: 1635–1641.

Andronis, C., Barak, S., Knowles, S.M., Sugano, S., and Tobin, E.M. (2008). The clock protein CCA1 and the bZIP transcription factor HY5 physically interact to regulate gene expression in Arabidopsis. Mol Plant **1**: 58–67.

Ankele, E., Kindgren, P., Pesquet, E., and Strand, Å. (2007). In vivo visualization of Mg-ProtoporphyrinIX, a coordinator of photosynthetic gene expression in the nucleus and the chloroplast. Plant Cell **19**: 1964–1979.

Apel, K. and Hirt, H. (2004). Reactive oxygen species: metabolism, oxidative stress, and signal transduction. Annu Rev Plant Biol **55**: 373–399.

Arana, M.V., Marín-de la Rosa, N., Maloof, J.N., Blázquez, M.A., and Alabadí, D. (2011). Circadian oscillation of gibberellin signaling in Arabidopsis. Proc Natl Acad Sci U S A **108**: 9292–9297.

Arnold, W. and Davidson, J.B. (1954). The identity of the fluorescent and delayed light emission spectra in Chlorella. J Gen Physiol **37**: 677–684.

Asada, K. (1999). The water-water cycle in chloroplasts: scavenging of active oxygens and dissipation of excess photons. Annu Rev Plant Physiol Plant Mol Biol **50**: 601–639.

Aschoff, J. (1965). Circadian rhythms in man. Science **148**: 1427–1432.

Aschoff, J. (1963). Comparative physiology: diurnal rhythms. Annu Rev Physiol **25**: 581–600.

Atamian, H.S., Creux, N.M., Brown, E.A., Garner, A.G., Blackman, B.K., and Harmer, S.L. (2016). Circadian regulation of sunflower heliotropism, floral orientation, and pollinator visits. Science **353**: 587–590.

Bae, G. and Choi, G. (2008). Decoding of light signals by plant phytochromes and their interacting proteins. Annu Rev Plant Biol **59**: 281–311.

Baker, N.R. (2008). Chlorophyll fluorescence: a probe of photosynthesis in vivo. Annu Rev Plant Biol **59**: 89–113.

Banerjee, R., Schleicher, E., Meier, S., Viana, R.M., Pokorny, R., Ahmad, M., Bittl, R., and Batschauer, A. (2007). The signaling state of Arabidopsis cryptochrome 2 contains flavin semiquinone. J Biol Chem **282**: 14916–14922.

Barajas-López, J. de D., Kremnev, D., Shaikhali, J., Piñas-Fernández, A., and Strand, Å. (2013). PAPP5 Is Involved in the Tetrapyrrole Mediated Plastid Signalling during Chloroplast Development. PLoS One **8**: e60305

Barber, J. (2009). Photosynthetic energy conversion: natural and artificial. Chem Soc Rev **38**: 185–196.

Bartel, D.P. (2004). MicroRNAs: genomics, biogenesis, mechanism, and function. Cell **116**: 281–297.

Batistič, O. and Kudla, J. (2012). Analysis of calcium signaling pathways in plants. Biochim Biophys Acta **1820**: 1283–1293.

Baudry, A., Ito, S., Song, Y.H., Strait, A.A., Kiba, T., Lu, S., Henriques, R., Pruneda-Paz, J.L., Chua, N.H., Tobin, E.M., Kay, S.A., and Imaizumi, T. (2010). F-Box proteins FKF1 and LKP2 act in concert with ZEITLUPE to control Arabidopsis clock progression. Plant Cell **22**: 606–622.

Beekwilder, J., van Leeuwen, W., van Dam, N.M., Bertossi, M., Grandi, V., Mizzi, L., Soloviev, M., Szabados, L., Molthoff, J.W., Schipper, B., Verbocht, H., de Vos, R.C.H., Morandini, P., Aarts, M.G.M., and Bovy, A. (2008). The impact of the absence of aliphatic glucosinolates on insect herbivory in Arabidopsis. PLoS One **3**: e2068.

Belbin, F.E., Noordally, Z.B., Wetherill, S.J., Atkins, K.A., Franklin, K.A., and Dodd, A.N. (2016). Integration of light and circadian signals that regulate chloroplast transcription by a nuclear-encoded sigma factor. New Phytol **213**: 727-738.

Bellafiore, S., Barneche, F., Peltier, G., and Rochaix, J.-D. (2005). State transitions and light adaptation require chloroplast thylakoid protein kinase STN7. Nature **433**: 892–895.

Belousov, V. V, Fradkov, A.F., Lukyanov, K.A., Staroverov, D.B., Shakhbazov, K.S., Terskikh, A. V, and Lukyanov, S. (2006). Genetically encoded fluorescent indicator for intracellular hydrogen peroxide. Nat Methods **3**: 281–286.

Bilan, D.S., Pase, L., Joosen, L., Gorokhovatsky, A.Y., Ermakova, Y.G., Gadella, T.W.J., Grabher, C., Schultz, C., Lukyanov, S., and Belousov, V. V (2013). HyPer-3: A genetically encoded H_2O_2 probe with improved performance for ratiometric and fluorescence lifetime imaging. ACS Chem Biol **8**:535-542.

Binkert, M., Kozma-Bognár, L., Terecskei, K., De Veylder, L., Nagy, F., and Ulm, R. (2014). UV-B-responsive association of the Arabidopsis bZIP transcription factor ELONGATED HYPOCOTYL5 with target genes, including its own promoter. Plant Cell **26**: 4200–4213.

Boden, S.A., Weiss, D., Ross, J.J., Davies, N.W., Trevaskis, B., Chandler, P.M., and Swain, S.M. (2014). EARLY FLOWERING3 regulates flowering in spring barley by mediating gibberellin production and FLOWERING LOCUS T expression. Plant Cell **26**: 1557–1569.

Bohn, A., Geist, A., Rascher, U., and Luttge, U. (2001). Responses to different external light rhythms by the circadian rhythm of crassulacean acid metabolism in Kalanchoe daigremontiana. Plant, Cell Environ **24**: 811–820.

Bonardi, V., Pesaresi, P., Becker, T., Schleiff, E., Wagner, R., Pfannschmidt, T., Jahns, P., and Leister, D. (2005). Photosystem II core phosphorylation and photosynthetic acclimation require two different protein kinases. Nature **437**: 1179–1182.

Bordage, S., Sullivan, S., Laird, J., Millar, A.J., and Nimmo, H.G. (2016). Organ specificity in the plant circadian system is explained by different light inputs to the shoot and root clocks. New Phytol.**121**: 136-149.

Bouly, J.-P., Schleicher, E., Dionisio-Sese, M., Vandenbussche, F., Van Der Straeten, D., Bakrim, N., Meier, S., Batschauer, A., Galland, P., Bittl, R., and Ahmad, M. (2007). Cryptochrome blue light photoreceptors are activated through interconversion of flavin redox states. J Biol Chem **282**: 9383–9391.

Bouvier, F., Rahier, A., and Camara, B. (2005). Biogenesis, molecular regulation and function of plant isoprenoids. Prog Lipid Res **44**: 357–429.

Bowler, C., Montagu, M. V, and Inze, D. (1992). Superoxide dismutase and stress tolerance. Annu Rev Plant Physiol Plant Mol Biol **43**: 83–116.

Bradbeer, J.W., Atkinson, Y.E., Börner, T., and Hagemann, R. (1979). Cytoplasmic synthesis of plastid polypeptides may be controlled by plastid-synthesised RNA. Nature **279**: 816–817.

Bray, E.A. (2004). Genes commonly regulated by water-deficit stress in Arabidopsis thaliana. J Exp Bot **55**: 2331–2341.

Bretzl, H. (1903). Botanische Forschungen des Alexanderzuges (Leipzig).

Briggs, W.R. (2014). Phototropism: some history, some puzzles, and a look ahead. Plant Physiol **164**: 13–23.

Brown, B.A., Cloix, C., Jiang, G.H., Kaiserli, E., Herzyk, P., Kliebenstein, D.J., and Jenkins, G.I. (2005). A UV-B-specific signaling component orchestrates plant UV protection. Proc Natl Acad Sci U S A **102**: 18225–18230.

Brugnoli, E. and Björkman, O. (1992). Chloroplast movements in leaves: Influence on chlorophyll fluorescence and measurements of light-induced absorbance changes related to ?pH and zeaxanthin formation. Photosynth Res **32**: 23–35.

Bunning, E. (1973). The physiological clock: circadian rhythms and biological chronometry (English Universities Press: London).

Burgie, E.S. and Vierstra, R.D. (2014). Phytochromes: an atomic perspective on photoactivation and signaling. Plant Cell **26**: 4568–4583.

Bürstenbinder, K., Rzewuski, G., Wirtz, M., Hell, R., and Sauter, M. (2007). The role of methionine recycling for ethylene synthesis in Arabidopsis. Plant J **49**: 238–249.

Butler, W.L. (1978). Energy distribution in the photochemical apparatus of photosynthesis. Annu Rev Plant Physiol **29**: 345–378.

Candolle, A.P. de (1832). Physiologie Vegetale (Bechet Jeune: Paris).

Cao, S., Ye, M., and Jiang, S. (2005). Involvement of GIGANTEA gene in the regulation of the cold stress response in Arabidopsis. Plant Cell Rep **24**: 683–690.

Caplan, J.L., Kumar, A.S., Park, E., Padmanabhan, M.S., Hoban, K., Modla, S., Czymmek, K., and Dinesh-Kumar, S.P. (2015). Chloroplast stromules function during innate immunity. Dev Cell **34**: 45–57.

Carrington, J.C. and Ambros, V. (2003). Role of microRNAs in plant and animal sevelopment. Science **301**: 336–338.

Casal, J.J. (2013). Photoreceptor signaling networks in plant responses to shade. Annu Rev Plant Biol **64**: 403–427.

Casal, J.J., Candia, A.N., and Sellaro, R. (2014). Light perception and signalling by phytochrome A. J Exp Bot **65**: 2835–2845.

Casal, J.J., Luccioni, L.G., Oliverio, K.A., and Boccalandro, H.E. (2003). Light,

phytochrome signalling and photomorphogenesis in Arabidopsis. Photochem Photobiol Sci **2**: 625–636.

Catalá, R., Medina, J., and Salinas, J. (2011). Integration of low temperature and light signaling during cold acclimation response in Arabidopsis. Proc Natl Acad Sci U S A **108**: 16475–16480.

Cecchini, N.M., Steffes, K., Schläppi, M.R., Gifford, A.N., and Greenberg, J.T. (2015). Arabidopsis AZI1 family proteins mediate signal mobilization for systemic defence priming. Nat Commun **6**: 7658.

Chan, K.X., Mabbitt, P.D., Phua, S.Y., Mueller, J.W., Nisar, N., Gigolashvili, T., Stroeher, E., Grassl, J., Arlt, W., Estavillo, G.M., Jackson, C.J., and Pogson, B.J. (2016a). Sensing and signaling of oxidative stress in chloroplasts by inactivation of the SAL1 phosphoadenosine phosphatase. Proc Natl Acad Sci U S A **113**: E4567-4576.

Chan, K.X., Phua, S.Y., Crisp, P., McQuinn, R., and Pogson, B.J. (2016b). Learning the languages of the chloroplast: retrograde signaling and beyond. Annu Rev Plant Biol **67**: 25–53.

Chan, K.X., Wirtz, M., Phua, S.Y., Estavillo, G.M., and Pogson, B.J. (2013). Balancing metabolites in drought: the sulfur assimilation conundrum. Trends Plant Sci **18**: 18–29.

Chaves, I., Pokorny, R., Byrdin, M., Hoang, N., Ritz, T., Brettel, K., Essen, L.-O., van der Horst, G.T.J., Batschauer, A., and Ahmad, M. (2011). The cryptochromes: blue light photoreceptors in plants and animals. Annu Rev Plant Biol **62**: 335–364.

Chehab, E.W., Kaspi, R., Savchenko, T., Rowe, H., Negre-Zakharov, F., Kliebenstein, D., and Dehesh, K. (2008). Distinct roles of jasmonates and aldehydes in plant-defense responses. PLoS One **3**: e1904.

Chen, D., Xu, G., Tang, W., Jing, Y., Ji, Q., Fei, Z., and Lin, R. (2013a). Antagonistic basic helix-loop-helix/bZIP transcription factors form transcriptional modules that integrate light and reactive oxygen species signaling in Arabidopsis. Plant Cell **25**: 1657–1673.

Chen, H., Wilkerson, C.G., Kuchar, J.A., Phinney, B.S., and Howe, G.A. (2005). Jasmonate-inducible plant enzymes degrade essential amino acids in the herbivore midgut. Proc Natl Acad Sci U S A **102**: 19237–19242.

Chen, H. and Xiong, L. (2010). The bifunctional abiotic stress signalling regulator and endogenous RNA silencing suppressor FIERY1 is required for lateral root formation. Plant Cell Environ **33**: 2180–2190.

Chen, H. and Xiong, L. (2011). Genetic interaction of two abscisic acid signaling regulators, HY5 and FIERY1, in mediating lateral root formation. Plant Signal Behav **6**: 123–125.

Chen, H., Zhang, B., Hicks, L.M., and Xiong, L. (2011). A nucleotide metabolite controls stress-responsive gene expression and plant development. PLoS One **6**: e26661.

Chen, H., Zhang, J., Neff, M.M., Hong, S.-W., Zhang, H., Deng, X.-W., and Xiong, L. (2008). Integration of light and abscisic acid signaling during seed germination and early seedling development. Proc Natl Acad Sci **105**: 4495–4500.

Chen, M. and Chory, J. (2011). Phytochrome signaling mechanisms and the control of plant development. Trends Cell Biol **21**: 664–671.

Chen, S., Zheng, X., Cao, H., Jiang, L., Liu, F., and Sun, X. (2015). A simple and efficient method for extraction of taq dna polymerase. Electron J Biotechnol **18**: 1–4.

Chen, Y.-Y., Wang, Y., Shin, L.-J., Wu, J.-F., Shanmugam, V., Tsednee, M., Lo, J.-C., Chen, C.-C., Wu, S.-H., and Yeh, K.-C. (2013b). Iron is involved in the maintenance

of circadian period length in Arabidopsis. Plant Physiol **161**: 1409–1420.

Chi, W., Feng, P., Ma, J., and Zhang, L. (2015). Metabolites and chloroplast retrograde signaling. Curr Opin Plant Biol **25**: 32–38.

Chiba, Y. and Green, P.J. (2009). mRNA degradation machinery in plants. J Plant Biol **52**: 114–124.

Choi, W.-G., Miller, G., Wallace, I., Harper, J., Mittler, R., and Gilroy, S. (2017). Orchestrating rapid long-distance signaling in plants with Ca^{2+}, ROS and electrical signals. Plant J **90**: 698–707.

Choi, W.-G., Toyota, M., Kim, S.-H., Hilleary, R., and Gilroy, S. (2014). Salt stress-induced Ca^{2+} waves are associated with rapid, long-distance root-to-shoot signaling in plants. Proc Natl Acad Sci U S A **111**: 6497–6502.

Chow, B.Y. and Kay, S.A. (2013). Global approaches for telling time: omics and the Arabidopsis circadian clock. Semin Cell Dev Biol **24**: 383–392.

Chow, B.Y., Sanchez, S.E., Breton, G., Pruneda-Paz, J.L., Krogan, N.T., and Kay, S.A. (2014). Transcriptional tegulation of LUX by CBF1 mediates cold input to the circadian clock in Arabidopsis. Curr Biol **24**: 1518–1524.

Christie, J.M. (2007). Phototropin blue-light receptors. Annu Rev Plant Biol **58**: 21–45.

Christie, J.M., Arvai, A.S., Baxter, K.J., Heilmann, M., Pratt, A.J., O'Hara, A., Kelly, S.M., Hothorn, M., Smith, B.O., Hitomi, K., Jenkins, G.I., and Getzoff, E.D. (2012a). Plant UVR8 photoreceptor senses UV-B by tryptophan-mediated disruption of cross-dimer salt bridges. Science **335**: 1492–1496.

Christie, J.M., Blackwood, L., Petersen, J., and Sullivan, S. (2015). Plant flavoprotein photoreceptors. Plant Cell Physiol **56**: 401–413.

Christie, J.M., Gawthorne, J., Young, G., Fraser, N.J., and Roe, A.J. (2012b). LOV to BLUF: flavoprotein contributions to the optogenetic toolkit. Mol Plant **5**: 533–544.

Christie, J.M., Salomon, M., Nozue, K., Wada, M., and Briggs, W.R. (1999). LOV (light, oxygen, or voltage) domains of the blue-light photoreceptor phototropin (nph1): binding sites for the chromophore flavin mononucleotide. Proc Natl Acad Sci U S A **96**: 8779–8783.

Christie, J.M., Swartz, T.E., Bogomolni, R.A., and Briggs, W.R. (2002). Phototropin LOV domains exhibit distinct roles in regulating photoreceptor function. Plant J **32**: 205–219.

Chun, L., Kawakami, A., and Christopher, D.A. (2001). Phytochrome A mediates blue light and UV-A-dependent chloroplast gene transcription in green leaves. Plant Physiol **125**: 1957–66.

Circolone, F., Granzin, J., Jentzsch, K., Drepper, T., Jaeger, K.-E., Willbold, D., Krauss, U., and Batra-Safferling, R. (2012). Structural basis for the slow dark recovery of a full-length LOV protein from Pseudomonas putida. J Mol Biol **417**: 362–374.

Clarke, J.D. (2009). Cetyltrimethyl ammonium bromide (CTAB) DNA miniprep for plant DNA isolation. Cold Spring Harb Protoc **2009**: pdb.prot5177.

Cloix, C., Kaiserli, E., Heilmann, M., Baxter, K.J., Brown, B.A., O'Hara, A., Smith, B.O., Christie, J.M., and Jenkins, G.I. (2012). C-terminal region of the UV-B photoreceptor UVR8 initiates signaling through interaction with the COP1 protein. Proc Natl Acad Sci U S A **109**: 16366–16370.

Contour-Ansel, D., Torres-Franklin, M.L., Cruz DE Carvalho, M.H., D'Arcy-Lameta,

A., and Zuily-Fodil, Y. (2006). Glutathione reductase in leaves of cowpea: cloning of two cDNAs, expression and enzymatic activity under progressive drought stress, desiccation and abscisic acid treatment. Ann Bot **98**: 1279–87.

Corbesier, L., Vincent, C., Jang, S., Fornara, F., Fan, Q., Searle, I., Giakountis, A., Farrona, S., Gissot, L., Turnbull, C., and Coupland, G. (2007). FT protein movement contributes to long-distance signaling in floral induction of Arabidopsis. Science **316**: 1030–1033.

Covington, M.F. and Harmer, S.L. (2007). The circadian clock regulates auxin signaling and responses in Arabidopsis. PLoS Biol **5**: e222.

Covington, M.F., Maloof, J.N., Straume, M., Kay, S.A., and Harmer, S.L. (2008). Global transcriptome analysis reveals circadian regulation of key pathways in plant growth and development. Genome Biol **9**: R130.

Covington, M.F., Panda, S., Liu, X.L., Strayer, C.A., Wagner, D.R., and Kay, S.A. (2001). ELF3 modulates resetting of the circadian clock in Arabidopsis. Plant Cell **13**: 1305–1315.

Crosson, S. and Moffat, K. (2001). Structure of a flavin-binding plant photoreceptor domain: insights into light-mediated signal transduction. Proc Natl Acad Sci U S A **98**: 2995–3000.

Czeisler, C.A., Weitzman, E. d, Moore-Ede, M.C., Zimmerman, J.C., and Knauer, R.S. (1980). Human sleep: its duration and organization depend on its circadian phase. Science **210**: 1264–1267.

Dai, S., Wei, X., Pei, L., Thompson, R.L., Liu, Y., Heard, J.E., Ruff, T.G., and Beachy, R.N. (2011). BROTHER OF LUX ARRHYTHMO is a component of the Arabidopsis circadian clock. Plant Cell **23**: 961–972.

Dalchau, N., Baek, S.J., Briggs, H.M., Robertson, F.C., Dodd, A.N., Gardner, M.J., Stancombe, M.A., Haydon, M.J., Stan, G.-B., Gonçalves, J.M., and Webb, A.A.R. (2011). The circadian oscillator gene GIGANTEA mediates a long-term response of the Arabidopsis thaliana circadian clock to sucrose. Proc Natl Acad Sci U S A **108**: 5104–5109.

Dally, N., Xiao, K., Holtgräwe, D., and Jung, C. (2014). The B2 flowering time locus of beet encodes a zinc finger transcription factor. Proc Natl Acad Sci U S A **111**: 10365–10370.

Daniel, X., Sugano, S., and Tobin, E.M. (2004). CK2 phosphorylation of CCA1 is necessary for its circadian oscillator function in Arabidopsis. Proc Natl Acad Sci U S A **101**: 3292–3297.

Das, P., Nutan, K.K., Singla-Pareek, S.L., and Pareek, A. (2015). Oxidative environment and redox homeostasis in plants: dissecting out significant contribution of major cellular organelles. Front Environ Sci **2**: 70.

David, K.M., Armbruster, U., Tama, N., and Putterill, J. (2006). Arabidopsis GIGANTEA protein is post-transcriptionally regulated by light and dark. FEBS Lett **580**: 1193–1197.

Dever, L. V., Boxall, S.F., Kneřová, J., and Hartwell, J. (2015). Transgenic Perturbation of the Decarboxylation Phase of Crassulacean Acid Metabolism Alters Physiology and Metabolism But Has Only a Small Effect on Growth. Plant Physiol **167**: 44–59.

Devlin, P.F. (2002). Signs of the time: environmental input to the circadian clock. J Exp Bot **53**: 1535–1550.

Devlin, P.F. and Kay, S.A. (2001). Circadian photoperception. Annu Rev Physiol **63**: 677–

694.

Dichtl, B., Stevens, A., and Tollervey, D. (1997). Lithium toxicity in yeast is due to the inhibition of RNA processing enzymes. EMBO J **16**: 7184–7195.

Dietz, K.-J. (2011). Peroxiredoxins in plants and cyanobacteria. Antioxid Redox Signal **15**: 1129–59.

Dodd, A.N., Belbin, F.E., Frank, A., and Webb, A.A.R. (2015). Interactions between circadian clocks and photosynthesis for the temporal and spatial coordination of metabolism. Front Plant Sci **6**: 245.

Dodd, A.N., Gardner, M.J., Hotta, C.T., Hubbard, K.E., Dalchau, N., Love, J., Assie, J.-M., Robertson, F.C., Jakobsen, M.K., Goncalves, J., Sanders, D., and Webb, A.A.R. (2007). The Arabidopsis circadian clock incorporates a cADPR-based feedback loop. Science **318**: 1789–1792.

Dodd, A.N., Kusakina, J., Hall, A., Gould, P.D., and Hanaoka, M. (2014). The circadian regulation of photosynthesis. Photosynth Res **119**: 181–190.

Dodd, A.N., Parkinson, K., and Webb, A.A.R. (2004). Independent circadian regulation of assimilation and stomatal conductance in the ztl-1 mutant of Arabidopsis. New Phytol **162**: 63–70.

Dodd, A.N., Salathia, N., Hall, A., Kévei, E., Tóth, R., Nagy, F., Hibberd, J.M., Millar, A.J., and Webb, A.A.R. (2005). Plant circadian clocks increase photosynthesis, growth, survival, and competitive advantage. Science **309**: 630–633.

Doi, M., Shigenaga, A., Emi, T., Kinoshita, T., and Shimazaki, K.I. (2004). A transgene encoding a blue-light receptor, phot1, restores blue-light responses in the Arabidopsis phot1 phot2 double mutant. J Exp Bot **55**: 517–523.

Dolata, J., Guo, Y., Ko owerzo, A., Smolinski, D., Brzyzek, G., Jarmo owski, A., and Swiezewski, S. (2015). NTR1 is required for transcription elongation checkpoints at alternative exons in Arabidopsis. EMBO J **34**: 544–558.

Dong, M.A., Farre, E.M., and Thomashow, M.F. (2011). CIRCADIAN CLOCK-ASSOCIATED 1 and LATE ELONGATED HYPOCOTYL regulate expression of the C-REPEAT BINDING FACTOR (CBF) pathway in Arabidopsis. Proc Natl Acad Sci **108**: 7241–7246.

Duanmu, D., Casero, D., Dent, R.M., Gallaher, S., Yang, W., Rockwell, N.C., Martin, S.S., Pellegrini, M., Niyogi, K.K., Merchant, S.S., Grossman, A.R., and Lagarias, J.C. (2013). Retrograde bilin signaling enables Chlamydomonas greening and phototrophic survival. Proc Natl Acad Sci U S A **110**: 3621–3626.

Duek, P.D., Elmer, M. V., van Oosten, V.R., and Fankhauser, C. (2004). The degradation of HFR1, a putative bHLH class transcription factor involved in light signaling, is regulated by phosphorylation and requires COP1. Curr Biol **14**: 2296–2301.

Dunlap, J.C. (1999). Molecular bases for circadian clocks. Cell **96**: 271–290.

Dvornyk, V., Vinogradova, O., and Nevo, E. (2003). Origin and evolution of circadian clock genes in prokaryotes. Proc Natl Acad Sci U S A **100**: 2495–500.

Earley, K.W., Haag, J.R., Pontes, O., Opper, K., Juehne, T., Song, K., and Pikaard, C.S. (2006). Gateway-compatible vectors for plant functional genomics and proteomics. Plant J **45**: 616–629.

Eckel-Mahan, K. and Sassone-Corsi, P. (2015). Phenotyping Circadian Rhythms in Mice. In Current Protocols in Mouse Biology (John Wiley & Sons, Inc.: Hoboken, NJ, USA), pp.

271–281.

Edgar, R.S., Green, E.W., Zhao, Y., van Ooijen, G.,, Olmedo, M., Qin, X., Xu, Y., Pan, M., Valekunja, U.K., Feeney, K.A., Maywood, E.S , Hastings, M.H., Baliga, N.S., Merrow, M., Millar, A.J., Johnson, C.H., Kyriacou, C.P., O'Neill, J.S., and Reddy, A.B. (2012). Peroxiredoxins are conserved markers of circadian rhythms. Nature **485**: 459–464.

Edwards, K.D., Akman, O.E., Knox, K., Lumsden, P.J., Thomson, A.W., Brown, P.E., Pokhilko, A., Kozma-Bognar, L., Nagy, F., Rand, D.A., and Millar, A.J. (2010). Quantitative analysis of regulatory flexibility under changing environmental conditions. Mol Syst Biol **6**: 1–11.

Edwards, K.D. and Millar, A.J. (2007). Analysis of circadian leaf movement rhythms in Arabidopsis thaliana. In, pp. 103–113.

Endo, M., Shimizu, H., Nohales, M.A., Araki, T., and Kay, S.A. (2014). Tissue-specific clocks in Arabidopsis show asymmetric coupling. Nature **515**: 419–422.

Engelke, D.R., Krikos, a, Bruck, M.E., and Ginsburg, D. (1990). Purification of Thermus aquaticus DNA polymerase expressed in Escherichia coli. Anal Biochem **191**: 396–400.

Engelmann, W., Simon, K., and Phen, C.J. (1992). Leaf movement rhythm in Arabidopsis thaliana. Zeitschrift fur Naturforsch **47c**: 925–928.

Erdei, L., Szegletes, Z., Barabás, K.N., Pestenácz, A., Fülöp, K., Kalmár, L., Kovács, A., Tóth, B., and Dér, A. (1998). Environmental stress and the biological clock in plants: changes of rhythmic behavior of carbohydrates, antioxidant enzymes and stomatal resistance by salinity. J Plant Physiol **152**: 265–271.

Espinoza, C., Degenkolbe, T., Caldana, C., Zuther, E., Leisse, A., Willmitzer, L., Hincha, D.K., and Hannah, M.A. (2010). Interaction with diurnal and circadian regulation results in dynamic metabolic and transcriptional changes during cold acclimation in Arabidopsis. PLoS One **5**: e14101.

Estavillo, G.M., Crisp, P.A., Pornsiriwong, W., Wirtz, M., Collinge, D., Carrie, C., Giraud, E., Whelan, J., David, P., Javot, H., Brearley, C., Hell, R., Marin, E., and Pogson, B. (2011). Evidence for a SAL1-PAP chloroplast retrograde pathway that functions in drought and high light signaling in Arabidopsis. Plant Cell **23**: 3992–4012.

Exposito-Rodriguez, M., Laissue, P.P., Littlejohn, G.R., Smirnoff, N., and Mullineaux, P.M. (2013). The use of HyPer to examine spatial and temporal changes in H_2O_2 in high light-exposed plants. Methods Enzymol **571**: 185-201.

Fankhauser, C. and Staiger, D. (2002). Photoreceptors in Arabidopsis thaliana: light perception, signal transduction and entrainment of the endogenous clock. Planta **216**: 1–16.

Farré, E.M. (2012). The regulation of plant growth by the circadian clock. Plant Biol (Stuttg) **14**: 401–410.

Farré, E.M., Harmer, S.L., Harmon, F.G., Yanovsky, M.J., and Kay, S.A. (2005). Overlapping and distinct roles of PRR7 and PRR9 in the Arabidopsis circadian clock. Curr Biol **15**: 47–54.

Farré, E.M. and Liu, T. (2013). The PRR family of transcriptional regulators reflects the complexity and evolution of plant circadian clocks. Curr Opin Plant Biol **16**: 621–629.

Faure, S., Turner, A.S., Gruszka, D., Christodoulou, V., Davis, S.J., von Korff, M., and Laurie, D.A. (2012). Mutation at the circadian clock gene EARLY MATURITY 8 adapts

domesticated barley (Hordeum vulgare) to short growing seasons. Proc Natl Acad Sci U S A **109**: 8328–8333.

Favory, J.-J., Stec, A., Gruber, H., Rizzini, L., Oravecz, A., Funk, M., Albert, A., Cloix, C., Jenkins, G.I., Oakeley, E.J., Seidlitz, H.K., Nagy, F., and Ulm, R. (2009). Interaction of COP1 and UVR8 regulates UV-B-induced photomorphogenesis and stress acclimation in Arabidopsis. EMBO J **28**: 591–601.

Fehér, B., Kozma-Bognár, L., Kevei, É., Hajdu, A., Binkert, M., Davis, S.J., Schäfer, E., Ulm, R., and Nagy, F. (2011). Functional interaction of the circadian clock and UV RESISTANCE LOCUS 8-controlled UV-B signaling pathways in Arabidopsis thaliana. Plant J **67**: 37–48.

Filichkin, S.A., Cumbie, J.S., Dharmawardhana, P., Jaiswal, P., Chang, J.H., Palusa, S.G., Reddy, A.S.N., Megraw, M., and Mockler, T.C. (2015). Environmental stresses modulate abundance and timing of alternatively spliced circadian transcripts in Arabidopsis. Mol Plant **8**: 207–227.

Filichkin, S.A., Priest, H.D., Givan, S.A., Shen, R., Bryant, D.W., Fox, S.E., Wong, W., and Mockler, T.C. (2010). Genome-wide mapping of alternative splicing in Arabidopsis thaliana. Genome Res **20**: 45–58.

Filichkin, S.A. and Mockler, T.C. (2012). Unproductive alternative splicing and nonsense mRNAs: a widespread phenomenon among plant circadian clock genes. Biol Direct **7**: 20.

Flis, A., Sulpice, R., Seaton, D.D., Ivakov, A.A., Liput, M., Abel, C., Millar, A.J., and Stitt, M. (2016). Photoperiod-dependent changes in the phase of core clock transcripts and global transcriptional outputs at dawn and dusk in Arabidopsis. Plant Cell Environ **39**:1955-1981

Folta, K.M. and Kaufman, L.S. (2003). Phototropin 1 is required for high-fluence blue-light-mediated mRNA destabilization. Plant Mol Biol **51**: 609–618.

Folta, K.M., Lieg, E.J., Durham, T., and Spalding, E.P. (2003). Primary inhibition of hypocotyl growth and phototropism depend differently on phototropin-mediated increases in cytoplasmic calcium induced by blue light. Plant Physiol **133**: 1464–1470.

Folta, K.M. and Spalding, E.P. (2001). Unexpected roles for cryptochrome 2 and phototropin revealed by high-resolution analysis of blue light-mediated hypocotyl growth inhibition. Plant J **26**: 471–478.

Fornara, F., de Montaigu, A., Sánchez-Villarreal, A., Takahashi, Y., Ver Loren van Themaat, E., Huettel, B., Davis, S.J., and Coupland, G. (2015). The GI-CDF module of Arabidopsis affects freezing tolerance and growth as well as flowering. Plant J **81**: 695–706.

Fornara, F., Panigrahi, K.C.S., Gissot, L., Sauerbrunn, N., Rühl, M., Jarillo, J.A., and Coupland, G. (2009). Arabidopsis DOF transcription factors act redundantly to reduce CONSTANS expression and are essential for a photoperiodic flowering response. Dev Cell **17**: 75–86.

Fowler, S.G., Cook, D., and Thomashow, M.F. (2005). Low temperature induction of Arabidopsis CBF1, 2, and 3 is gated by the circadian clock. Plant Physiol **137**: 961–968.

Fujiwara, S., Wang, L., Han, L., Suh, S.-S., Salomé, P.A., McClung, C.R., and Somers, D.E. (2008). Post-translational regulation of the Arabidopsis circadian clock through selective proteolysis and phosphorylation of pseudo-response regulator proteins. J Biol Chem **283**: 23073–23083.

Fukuda, H., Nakamichi, N., Hisatsune, M., Murase, H., and Mizuno, T. (2007). Synchronization of plant circadian oscillators with a phase delay effect of the vein network. Phys Rev Lett **99**: 98102.

Galvão, V.C. and Fankhauser, C. (2015). Sensing the light environment in plants: photoreceptors and early signaling steps. Curr Opin Neurobiol **34**: 46–53.

Gawroński, P., Ariyadasa, R., Himmelbach, A., Poursarebani, N., Kilian, B., Stein, N., Steuernagel, B., Hensel, G., Kumlehn, J., Sehgal, S.K., Gill, B.S., Gould, P., Hall, A., and Schnurbusch, T. (2014). A distorted circadian clock causes early flowering and temperature-dependent variation in spike development in the Eps-3Am mutant of einkorn wheat. Genetics **196**: 1253–1261.

Gazzani, S., Lawrenson, T., Woodward, C., Headon, D., and Sablowski, R. (2004). A link between mRNA turnover and RNA interference in Arabidopsis. Science **306**: 1046–1048.

Gendron, J.M., Pruneda-Paz, J.L., Doherty, C.J., Gross, A.M., Kang, S.E., and Kay, S.A. (2012). Arabidopsis circadian clock protein, TOC1, is a DNA-binding transcription factor. Proc Natl Acad Sci U S A **109**: 3167–3172.

Gibon, Y., Bläsing, O.E., Palacios-Rojas, N., Pankovic, D., Hendriks, J.H.M., Fisahn, J., Höhne, M., Günther, M., and Stitt, M. (2004). Adjustment of diurnal starch turnover to short days: depletion of sugar during the night leads to a temporary inhibition of carbohydrate utilization, accumulation of sugars and post-translational activation of ADP-glucose pyrophosphorylase in the followin. Plant J **39**: 847–862.

Gigolashvili, T., Geier, M., Ashykhmina, N., Frerigmann, H., Wulfert, S., Krueger, S., Mugford, S.G., Kopriva, S., Haferkamp, I., and Flügge, U.-I. (2012). The Arabidopsis thylakoid ADP/ATP carrier TAAC has an additional role in supplying plastidic phosphoadenosine 5'-phosphosulfate to the cytosol. Plant Cell **24**: 4187–4204.

Gil-Mascarell, R., López-Coronado, J.M., Bellés, J.M., Serrano, R., and Rodríguez, P.L. (1999). The Arabidopsis HAL2-like gene family includes a novel sodium-sensitive phosphatase. Plant J **17**: 373–383.

Golombek, D. a and Rosenstein, R.E. (2010). Physiology of circadian entrainment. Physiol Rev **90**: 1063–1102.

Goltsev, V., Zaharieva, I., Lambrev, P., Yordanov, I., and Strasser, R. (2003). Simultaneous analysis of prompt and delayed chlorophyll a fluorescence in leaves during the induction period of dark to light adaptation. J Theor Biol **225**: 171–183.

Goodspeed, D., Chehab, E.W., Min-Venditti, A., Braam, J., and Covington, M.F. (2012). Arabidopsis synchronizes jasmonate-mediated defense with insect circadian behavior. Proc Natl Acad Sci U S A **109**: 4674–4677.

Gould, P.D., Diaz, P., Hogben, C., Kusakina, J., Salem, R., Hartwell, J., and Hall, A. (2009). Delayed fluorescence as a universal tool for the measurement of circadian rhythms in higher plants. Plant J **58**: 893–901.

Graf, A., Schlereth, A., Stitt, M., and Smith, A.M. (2010). Circadian control of carbohydrate availability for growth in Arabidopsis plants at night. Proc Natl Acad Sci U S A **107**: 9458–9463.

Green, R.M., Tingay, S., Wang, Z.-Y., and Tobin, E.M. (2002). Circadian rhythms confer a higher level of fitness to Arabidopsis plants. Plant Physiol **129**: 576–584.

Greenham, K. and McClung, C.R. (2015). Integrating circadian dynamics with physiological processes in plants. Nat Rev Genet **16**: 598–610.

Gregory, B.D., O'Malley, R.C., Lister, R., Urich, M.A., Tonti-Filippini, J., Chen, H., Millar, A.H., and Ecker, J.R. (2008). A link between RNA metabolism and silencing affecting Arabidopsis development. Dev Cell **14**: 854–866.

Grieshaber, N.A., Fischer, E.R., Mead, D.J., Dooley, C.A., and Hackstadt, T. (2004). Chlamydial histone-DNA interactions are disrupted by a metabolite in the methylerythritol phosphate pathway of isoprenoid biosynthesis. Proc Natl Acad Sci U S A **101**: 7451–7456.

von Gromoff, E.D., Alawady, A., Meinecke, L., Grimm, B., and Beck, C.F. (2008). Heme, a plastid-derived regulator of nuclear gene expression in Chlamydomonas. Plant Cell **20**: 552–567.

Grundy, J., Stoker, C., and Carré, I.A. (2015). Circadian regulation of abiotic stress tolerance in plants. Front Plant Sci **6**: 648.

Gy, I., Gasciolli, V., Lauressergues, D., Morel, J.-B., Gombert, J., Proux, F., Proux, C., Vaucheret, H., and Mallory, A.C. (2007). Arabidopsis FIERY1, XRN2, and XRN3 are endogenous RNA silencing suppressors. Plant Cell **19**: 3451–3461.

Gyllenstrand, N., Karlgren, A., Clapham, D., Holm, K., Hall, A., Gould, P.D., Källman, T., and Lagercrantz, U. (2014). No time for spruce: rapid dampening of circadian rhythms in Picea abies (L. Karst). Plant Cell Physiol **55**: 535–550.

Hall, A., Kozma-Bognár, L., Bastow, R.M., Nagy, F., and Millar, A.J. (2002). Distinct regulation of CAB and PHYB gene expression by similar circadian clocks. Plant J **32**: 529–537.

Hanano, S., Domagalska, M.A., Nagy, F., and Davis, S.J. (2006). Multiple phytohormones influence distinct parameters of the plant circadian clock. Genes to Cells **11**: 1381–1392.

Harmer, S.L. (2009). The circadian system in higher plants. Annu Rev Plant Biol **60**: 357–377.

Harmer, S.L., Hogenesch, J.B., Straume, M., Chang, H.S., Han, B., Zhu, T., Wang, X., Kreps, J. a, and Kay, S. a (2000). Orchestrated transcription of key pathways in Arabidopsis by the circadian clock. Science **290**: 2110–2113.

Harper, S.M., Christie, J.M., and Gardner, K.H. (2004). Disruption of the LOV-Jalpha helix interaction activates phototropin kinase activity. Biochemistry **43**: 16184–16192.

Harper, S.M., Neil, L.C., and Gardner, K.H. (2003). Structural basis of a phototropin light switch. Science **301**: 1541–1544.

Hastings, J. (2013). Circadian rhythms in Dinoflagellates: what is the purpose of synthesis and destruction of proteins? Microorganisms **1**: 26–32.

Hastings, J.W. (2007). The Gonyaulax clock at 50: translational control of circadian expression. Cold Spring Harb Symp Quant Biol **72**: 141–144.

Hastings, M.H., Reddy, A.B., and Maywood, E.S. (2003). A clockwork web: circadian timing in brain and periphery, in health and disease. Nat Rev Neurosci **4**: 649–661.

Haydon, M.J., Mielczarek, O., Robertson, F.C., Hubbard, K.E., and Webb, A.A.R. (2013). Photosynthetic entrainment of the Arabidopsis thaliana circadian clock. Nature **502**: 689–692.

Hayes, S., Sharma, A., Fraser, D.P., Trevisan, M., Cragg-Barber, C.K., Tavridou, E., Fankhauser, C., Jenkins, G.I., and Franklin, K.A. (2017). UV-B Perceived by the UVR8 Photoreceptor Inhibits Plant Thermomorphogenesis. Curr Biol **27**: 120–127.

Hazen, S.P., Borevitz, J.O., Harmon, F.G., Pruneda-Paz, J.L., Schultz, T.F., Yanovsky, M.J., Liljegren, S.J., Ecker, J.R., and Kay, S.A. (2005a). Rapid array mapping of circadian clock and developmental mutations in Arabidopsis. Plant Physiol **138**: 990–997.

Hazen, S.P., Schultz, T.F., Pruneda-Paz, J.L., Borevitz, J.O., Ecker, J.R., and Kay, S. A. (2005b). LUX ARRHYTHMO encodes a Myb domain protein essential for circadian rhythms. Proc Natl Acad Sci U S A **102**: 10387–10392.

Heijde, M., Binkert, M., Yin, R., Ares-Orpel, F., Rizzini, L., Van De Slijke, E., Persiau, G., Nolf, J., Gevaert, K., De Jaeger, G., and Ulm, R. (2013). Constitutively active UVR8 photoreceptor variant in Arabidopsis. Proc Natl Acad Sci U S A **110**: 20326–20331.

Heijde, M. and Ulm, R. (2013). Reversion of the Arabidopsis UV-B photoreceptor UVR8 to the homodimeric ground state. Proc Natl Acad Sci U S A **110**: 1113–1118.

Helfer, A., Nusinow, D.A., Chow, B.Y., Gehrke, A.R., Bulyk, M.L., and Kay, S.A. (2011). LUX ARRHYTHMO encodes a nighttime repressor of circadian gene expression in the Arabidopsis core clock. Curr Biol **21**: 126–133.

Hennessey, T.L. and Field, C.B. (1991). Circadian rhythms in photosynthesis: oscillations in carbon assimilation and stomatal conductance under constant conditions. Plant Physiol **96**: 831–836.

Herrero, E., Kolmos, E., Bujdoso, N., Yuan, Y., Wang, M., Berns, M.C., Uhlworm, H., Coupland, G., Saini, R., Jaskolski, M., Webb, A., Gonçalves, J., and Davis, S.J. (2012). EARLY FLOWERING4 recruitment of EARLY FLOWERING3 in the nucleus sustains the Arabidopsis circadian clock. Plant Cell **24**: 428–443.

Hetz, C., Chevet, E., and Oakes, S.A. (2015). Proteostasis control by the unfolded protein response. Nat Cell Biol **17**: 829–838.

Higa, T., Suetsugu, N., and Wada, M. (2014). Plant nuclear photorelocation movement. J Exp Bot **65**: 2873–2881.

Hiltbrunner, A., Tscheuschler, A., Viczián, A., Kunkel, T., Kircher, S., and Schäfer, E. (2006). FHY1 and FHL act together to mediate nuclear accumulation of the phytochrome A photoreceptor. Plant Cell Physiol **47**: 1023–1034.

Hirsch, J., Misson, J., Crisp, P.A., David, P., Bayle, V., Estavillo, G.M., Javot, H., Chiarenza, S., Mallory, A.C., Maizel, A., Declerck, M., Pogson, B.J., Vaucheret, H., Crespi, M. Desnos, T., Thibaud, M.-C., Nussaume, L., and Marin, E. (2011). A novel fry1 allele reveals the existence of a mutant phenotype unrelated to 5'->3' exoribonuclease (XRN) activities in Arabidopsis thaliana roots. PLoS One **6**: e16724.

Hoang, N., Bouly, J.-P., and Ahmad, M. (2008). Evidence of a light-sensing role for folate in Arabidopsis cryptochrome blue-light receptors. Mol Plant **1**: 68–74.

Hong, S., Kim, S.A., Guerinot, M. Lou, and McClung, C.R. (2013). Reciprocal interaction of the circadian clock with the iron homeostasis network in Arabidopsis. Plant Physiol **161**: 893–903.

Hong, S., Song, H.-R., Lutz, K., Kerstetter, R.A, Michael, T.P., and McClung, C.R. (2010). Type II protein arginine methyltransferase 5 (PRMT5) is required for circadian period determination in Arabidopsis thaliana. Proc Natl Acad Sci U S A **107**: 21211–21216.

Houseley, J. and Tollervey, D. (2009). The many pathways of RNA degradation. Cell **136**: 763–776.

Hsu, P.Y., Devisetty, U.K., and Harmer, S.L. (2013). Accurate timekeeping is controlled by a cycling activator in Arabidopsis. Elife **2**: e00473.

Hsu, P.Y. and Harmer, S.L. (2014). Wheels within wheels: the plant circadian system. Trends Plant Sci **19**: 240–249.

Hu, W., Franklin, K.A., Sharrock, R.A., Jones, M.A., Harmer, S.L., and Lagarias, J.C. (2013). Unanticipated regulatory roles for Arabidopsis phytochromes revealed by null mutant analysis. Proc Natl Acad Sci U S A **110**: 1542–1547.

Huala, E., Oeller, P.W., Liscum, E., Han, I.S., Larsen, E., and Briggs, W.R. (1997). Arabidopsis NPH1: a protein kinase with a putative redox-sensing domain. Science **278**: 2120–2123

Huang, W., Pérez-García, P., Pokhilko, A., Millar, a. J., Antoshechkin, I., Riechmann, J.L., and Mas, P. (2012). Mapping the core of the Arabidopsis circadian clock defines the network structure of the oscillator. Science **336**: 75–79.

Hut, R.A. and Beersma, D.G.M. (2011). Evolution of time-keeping mechanisms: early emergence and adaptation to photoperiod. Philos Trans R Soc B Biol Sci **366**: 2141–2154.

Imaizumi, T., Schultz, T.F., Harmon, F.G., Ho, L.A., and Kay, S.A. (2005). FKF1 F-box protein mediates cyclic degradation of a repressor of CONSTANS in Arabidopsis. Science **309**: 293–297.

Imaizumi, T., Tran, H.G., Swartz, T.E., Briggs, W.R., and Kay, S.A. (2003). FKF1 is essential for photoperiodic-specific light signalling in Arabidopsis. Nature **426**: 302–306.

Inada, S., Ohgishi, M., Mayama, T., Okada, K., and Sakai, T. (2004). RPT2 is a signal transducer involved in phototropic response and stomatal opening by association with phototropin 1 in Arabidopsis thaliana. Plant Cell **16**: 887–896.

Inoue, S.-I., Kinoshita, T., Matsumoto, M., Nakayama, K.I., Doi, M., and Shimazaki, K.-I. (2008a). Blue light-induced autophosphorylation of phototropin is a primary step for signaling. Proc Natl Acad Sci U S A **105**: 5626–5631.

Inoue, S., Kinoshita, T., Takemiya, A., Doi, M., and Shimazaki, K. (2008b). Leaf positioning of Arabidopsis in response to blue light. Mol Plant **1**: 15–26.

Inoue, S., Matsushita, T., Tomokiyo, Y., Matsumoto, M., Nakayama, K.I., Kinoshita, T., and Shimazaki, K. (2011). Functional analyses of the activation loop of phototropin2 in Arabidopsis. Plant Physiol **156**: 117–128.

Ito, S., Song, Y.H., and Imaizumi, T. (2012). LOV domain-containing F-box proteins: light-dependent protein degradation modules in Arabidopsis. Mol Plant **5**: 573–582.

Izawa, T., Mihara, M., Suzuki, Y., Gupta, M., Itoh, H., Nagano, A.J., Motoyama, R., Sawada, Y., Yano, M., Hirai, M.Y., Makino, A., and Nagamura, Y. (2011). Os-GIGANTEA confers robust diurnal rhythms on the global transcriptome of rice in the field. Plant Cell **23**: 1741–1755.

James, A.B., Monreal, J.A., Nimmo, G.A., Kelly, C.L., Herzyk, P., Jenkins, G.I., and Nimmo, H.G. (2008). The circadian clock in Arabidopsis roots is a simplified slave version of the clock in shoots. Science **322**: 1832–1835.

James, A.B., Syed, N.H., Bordage, S., Marshall, J., Nimmo, G.A., Jenkins, G.I., Herzyk, P., Brown, J.W.S., and Nimmo, H.G. (2012). Alternative splicing mediates responses of the Arabidopsis circadian clock to temperature changes. Plant Cell **24**: 961–981.

Jang, I.-C., Chung, P.J., Hemmes, H., Jung, C., and Chua, N.-H. (2011). Rapid and reversible light-mediated chromatin modifications of Arabidopsis phytochrome A locus.

Plant Cell **23**: 459–470.

Jenkins, G.I. (2009). Signal transduction in responses to UV-B radiation. Annu Rev Plant Biol **60**: 407–431.

Jenkins, G.I. (2014). The UV-B photoreceptor UVR8: from structure to physiology. Plant Cell **26**: 21–37.

Jiang, M. and Zhang, J. (2001). Effect of abscisic acid on active oxygen species, antioxidative defence system and oxidative damage in leaves of maize seedlings. Plant Cell Physiol **42**: 1265–73.

Johanningmeier, U. and Howell, S.H. (1984). Regulation of light-harvesting chlorophyll-binding protein mRNA accumulation in Chlamydomonas reinhardi. Possible involvement of chlorophyll synthesis precursors. J Biol Chem **259**: 13541–13549.

Jonak, C. and Hirt, H. (2002). Glycogen synthase kinase 3/SHAGGY-like kinases in plants: an emerging family with novel functions. Trends Plant Sci **7**: 457–61.

Jones, C.I., Zabolotskaya, M.V., and Newbury, S.F. (2012a). The 5′ → 3′ exoribonuclease XRN1/Pacman and its functions in cellular processes and development. Wiley Interdiscip Rev RNA **3**: 455–468.

Jones, H., Leigh, F.J., Mackay, I., Bower, M.A., Smith, L.M.J., Charles, M.P., Jones, G., Jones, M.K., Brown, T.A., and Powell, W. (2008). Population-based resequencing reveals that the flowering time adaptation of cultivated barley originated east of the Fertile Crescent. Mol Biol Evol **25**: 2211–2219.

Jones, M.A. (2009). Entrainment of the Arabidopsis Circadian Clock. J Plant Biol **52**: 202–209.

Jones, M.A. and Christie, J.M. (2008). Phototropin receptor kinase activation by blue light. Plant Signal Behav **3**: 44–46.

Jones, M.A., Feeney, K.A., Kelly, S.M., and Christie, J.M. (2007). Mutational analysis of phototropin 1 provides insights into the mechanism underlying LOV2 signal transmission. J Biol Chem **282**: 6405–6414.

Jones, M. A. and Harmer, S. (2011). JMJD5 Functions in concert with TOC1 in the Arabidopsis circadian system. Plant Signal Behav **6**: 445–448.

Jones, M.A., Hu, W., Litthauer, S., Lagarias, J.C., and Harmer, S.L. (2015). A Constitutively Active Allele of Phytochrome B Maintains Circadian Robustness in the Absence of Light. Plant Physiol **169**: 814–825.

Jones, M.A., Williams, B.A., McNicol, J., Simpson, C.G., Brown, J.W.S., and Harmer, S.L. (2012). Mutation of Arabidopsis spliceosomal timekeeper locus1 causes circadian clock defects. Plant Cell **24**: 4066–4082.

Kachroo, A., Venugopal, S.C., Lapchyk, L., Falcone, D., Hildebrand, D., and Kachroo, P. (2004). Oleic acid levels regulated by glycerolipid metabolism modulate defense gene expression in Arabidopsis. Proc Natl Acad Sci U S A **101**: 5152–5157.

Kagawa, T., Sakai, T., Suetsugu, N., Oikawa, K., Ishiguro, S., Kato, T., Tabata, S., Okada, K., and Wada, M. (2001). Arabidopsis NPL1: a phototropin homolog controlling the chloroplast high-light avoidance response. Science **291**: 2138–2141.

Kaiserli, E., Sullivan, S., Jones, M.A., Feeney, K.A., and Christie, J.M. (2009). Domain swapping to assess the mechanistic basis of Arabidopsis Phototropin 1 Receptor Kinase activation and endocytosis by blue light. Plant Cell **21**: 3226–3244.

Kamioka, M., Takao, S., Suzuki, T., Taki, K., Higashiyama, T., Kinoshita, T., and Nakamichi, N. (2016). Direct Repression of Evening Genes by CIRCADIAN CLOCK-ASSOCIATED1 in the Arabidopsis Circadian Clock. Plant Cell **28**: 696–711.

Kastenmayer, J.P. and Green, P.J. (2000). Novel features of the XRN-family in Arabidopsis: evidence that AtXRN4, one of several orthologs of nuclear Xrn2p/Rat1p, functions in the cytoplasm. Proc Natl Acad Sci U S A **97**: 13985–13990.

Kataoka, T., Watanabe-Takahashi, A., Hayashi, N., Ohnishi, M., Mimura, T., Buchner, P., Hawkesford, M.J., Yamaya, T., and Takahashi, H. (2004). Vacuolar sulfate transporters are essential determinants controlling internal distribution of sulfate in Arabidopsis. Plant Cell **16**: 2693–2704.

Keily, J., MacGregor, D.R., Smith, R.W., Millar, A.J., Halliday, K.J., and Penfield, S. (2013). Model selection reveals control of cold signalling by evening-phased components of the plant circadian clock. Plant J **76**: 247-257.

Kerwin, R.E., Jimenez-Gomez, J.M., Fulop, D., Harmer, S.L., Maloof, J.N., and Kliebenstein, D.J. (2011). Network quantitative trait loci mapping of circadian clock outputs identifies metabolic pathway-to-clock linkages in Arabidopsis. Plant Cell **23**: 471–485.

Kiba, T., Henriques, R., Sakakibara, H., and Chua, N.-H. (2007). Targeted degradation of PSEUDO-RESPONSE REGULATOR5 by an SCFZTL complex regulates clock function and photomorphogenesis in Arabidopsis thaliana. Plant Cell **19**: 2516–2530.

Kikis, E.A., Khanna, R., and Quail, P.H. (2005). ELF4 is a phytochrome-regulated component of a negative-feedback loop involving the central oscillator components CCA1 and LHY. Plant J **44**: 300–313.

Kim, B.-H. and von Arnim, A.G. (2006). The Early Dark-Response in Arabidopsis thaliana Revealed by cDNA Microarray Analysis. Plant Mol Biol **60**: 321–342.

Kim, B.-H. and von Arnim, A.G. (2009). FIERY1 regulates light-mediated repression of cell elongation and flowering time via its 3'(2'),5'-bisphosphate nucleotidase activity. Plant J **58**: 208–219.

Kim, J., Geng, R., Gallenstein, R.A, and Somers, D.E. (2013a). The F-box protein ZEITLUPE controls stability and nucleocytoplasmic partitioning of GIGANTEA. Development **140**: 4060–4069.

Kim, W.-Y., Fujiwara, S., Suh, S.-S., Kim, J., Kim, Y., Han, L., David, K., Putterill, J., Nam, H.G., and Somers, D.E. (2007). ZEITLUPE is a circadian photoreceptor stabilized by GIGANTEA in blue light. Nature **449**: 356–360.

Kim, W.-Y., Ali, Z., Park, H.J., Park, S.J., Cha, J.-Y., Perez-Hormaeche, J., Quintero, F.J., Shin, G., Kim, M.R., Qiang, Z., Ning, L., Park, H.C., Lee, S.Y., Bressan, R.A., Pardo, J.M., Bohnert, H.J., and Yun, D.-J. (2013). Release of SOS2 kinase from sequestration with GIGANTEA determines salt tolerance in Arabidopsis. Nat Commun **4**: 1352.

Kim, Y., Lim, J., Yeom, M., Kim, H., Kim, J., Wang, L., Kim, W.Y., Somers, D.E., and Nam, H.G. (2013b). ELF4 regulates GIGANTEA chromatin access through subnuclear sequestration. Cell Rep **3**: 671–677.

Kimura, S., Kaya, H., Kawarazaki, T., Hiraoka, G., Senzaki, E., Michikawa, M., and Kuchitsu, K. (2012). Protein phosphorylation is a prerequisite for the Ca^{2+}-dependent activation of Arabidopsis NADPH oxidases and may function as a trigger for the positive feedback regulation of Ca^{2+} and reactive oxygen species. Biochim Biophys Acta **1823**: 398–405.

Kindgren, P., Eriksson, M.-J., Benedict, C., Mohapatra, A., Gough, S.P., Hansson, M., Kieselbach, T., and Strand, A. (2011). A novel proteomic approach reveals a role for Mg-protoporphyrin IX in response to oxidative stress. Physiol Plant **141**: 310–320.

Kindgren, P., Norén, L., López, J. de D.B., Shaikhali, J., and Strand, A. (2012). Interplay between Heat Shock Protein 90 and HY5 controls PhANG expression in response to the GUN5 plastid signal. Mol Plant **5**: 901–913.

Kinoshita, T., Doi, M., Suetsugu, N., Kagawa, T., Wada, M., and Shimazaki, K. (2001). Phot1 and phot2 mediate blue light regulation of stomatal opening. Nature **414**: 656–660.

Kiyosawa, K. (1979). Unequal distribution of potassium and anions within the Phaseolus pulvinus during circadian leaf movement. Plant Cell Physiol **20**: 1621–1634.

Klaassen, C.D. and Boles, J.W. (1997). Sulfation and sulfotransferases 5: the importance of 3'-phosphoadenosine 5'-phosphosulfate (PAPS) in the regulation of sulfation. FASEB J **11**: 404–18.

Klein, M. and Papenbrock, J. (2004). The multi-protein family of Arabidopsis sulphotransferases and their relatives in other plant species. J Exp Bot **55**: 1809–1820.

Kleine, T., Lockhart, P., and Batschauer, A. (2003). An Arabidopsis protein closely related to Synechocystis cryptochrome is targeted to organelles. Plant J **35**: 93–103.

Knight, H., Thomson, A.J.W., and McWatters, H.G. (2008). Sensitive to freezing6 integrates cellular and environmental inputs to the plant circadian clock. Plant Physiol **148**: 293–303.

Kobayashi, Y., Imamura, S., Hanaoka, M., and Tanaka, K. (2011). A tetrapyrrole-regulated ubiquitin ligase controls algal nuclear DNA replication. Nat Cell Biol **13**: 483–487.

Kobayashi, Y., Kaya, H., Goto, K., Iwabuchi, M., and Araki, T. (1999). A pair of related genes with antagonistic roles in mediating flowering signals. Science **286**: 1960-1962.

Kohchi, T., Mukougawa, K., Frankenberg, N., Masuda, M., Yokota, A., and Lagarias, J.C. (2001). The Arabidopsis HY2 gene encodes phytochromobilin synthase, a ferredoxin-dependent biliverdin reductase. Plant Cell **13**: 425–436.

Kolmos, E., Chow, B.Y., Pruneda-Paz, J.L., and Kay, S.A. (2014). HsfB2b-mediated repression of PRR7 directs abiotic stress responses of the circadian clock. Proc Natl Acad Sci U S A **111**: 16172–16177.

Komander, D. (2009). The emerging complexity of protein ubiquitination. Biochem Soc Trans **37**: 937–953.

Kong, S.-G., Suetsugu, N., Kikuchi, S., Nakai, M., Nagatani, A., and Wada, M. (2013). Both phototropin 1 and 2 localize on the chloroplast outer membrane with distinct localization activity. Plant Cell Physiol **54**: 80–92.

Kong, S.-G., Suzuki, T., Tamura, K., Mochizuki, N., Hara-Nishimura, I., and Nagatani, A. (2006). Blue light-induced association of phototropin 2 with the Golgi apparatus. Plant J **45**: 994–1005.

Kong, S.G. and Wada, M. (2011). New insights into dynamic actin-based chloroplast photorelocation movement. Mol Plant **4**: 771–781.

Kopriva, S., Mugford, S.G., Baraniecka, P., Lee, B.-R., Matthewman, C.A., and Koprivova, A. (2012). Control of sulfur partitioning between primary and secondary metabolism in Arabidopsis. Front Plant Sci **3**: 96–105.

Koussevitzky, S., Nott, A., Mockler, T.C., Hong, F., Sachetto-Martins, G., Surpin, M.,

Lim, J., Mittler, R., and Chory, J. (2007). Signals from chloroplasts converge to regulate nuclear gene expression. Science **316**: 715–719.

Krause, G.H. and Weis, E. (1991). Chlorophyll fluorescence and photosynthesis: the basics. Annu Rev Plant Physiol Plant Mol Biol **42**: 313–349.

Kreps, J.A. and Simon, A.E. (1997). Environmental and genetic effects on circadian clock-regulated gene expression in Arabidopsis. Plant Cell **9**: 297–304.

Kropat, J., Oster, U., Rüdiger, W., and Beck, C.F. (1997). Chlorophyll precursors are signals of chloroplast origin involved in light induction of nuclear heat-shock genes. Proc Natl Acad Sci U S A **94**: 14168–14172.

Kuno, N. (2003). The novel MYB protein EARLY-PHYTOCHROME-RESPONSIVE1 is a component of a slave circadian oscillator in Arabidopsis. Plant Cell **15**: 2476–2488.

Kurihara, Y., Schmitz, R.J., Nery, J.R., Schultz, M.D., Okubo-Kurihara, E., Morosawa, T., Tanaka, M., Toyoda, T., Seki, M., and Ecker, J.R. (2012). Surveillance of 3' noncoding transcripts requires FIERY1 and XRN3 in Arabidopsis. G3 (Bethesda) **2**: 487–498.

Laemmli, U.K. (1970). Cleavage of structural proteins during the assembly of the head of bacteriophage T4. Nature **227**: 680–685.

Lai, A.G., Doherty, C.J., Mueller-Roeber, B., Kay, S. a., Schippers, J.H.M., and Dijkwel, P.P. (2012). CIRCADIAN CLOCK-ASSOCIATED 1 regulates ROS homeostasis and oxidative stress responses. Proc Natl Acad Sci U S A **109**: 17129–17134.

Larkin, R.M., Alonso, J.M., Ecker, J.R., and Chory, J. (2003). GUN4, a regulator of chlorophyll synthesis and intracellular signaling. Science **299**: 902–906.

Lau, O.S. and Deng, X.W. (2012). The photomorphogenic repressors COP1 and DET1: 20 years later. Trends Plant Sci **17**: 584–593.

Lau, O.S., Huang, X., Charron, J.-B., Lee, J.-H., Li, G., and Deng, X.W. (2011). Interaction of Arabidopsis DET1 with CCA1 and LHY in mediating transcriptional repression in the plant circadian clock. Mol Cell **43**: 703–712.

Lazaro, A., Valverde, F., Piñeiro, M., and Jarillo, J.A. (2012). The Arabidopsis E3 ubiquitin ligase HOS1 negatively regulates CONSTANS abundance in the photoperiodic control of flowering. Plant Cell **24**: 982–999.

Lee, J., He, K., Stolc, V., Lee, H., Figueroa, P., Gao, Y., Tongprasit, W., Zhao, H., Lee, I., and Deng, X.W. (2007). Analysis of transcription factor HY5 genomic binding sites revealed its hierarchical role in light regulation of development. Plant Cell **19**: 731–749.

Lee, B.-R., Huseby, S., Koprivova, A., Chételat, A.., Wirtz, M., Mugford, S.T., Navid, E., Brearley, C., Saha, S., Mithen, R., Hell, R., Farmer, E.E., and Kopriva, S. (2012). Effects of fou8/fry1 mutation on sulfur metabolism: is decreased internal sulfate the trigger of sulfate starvation response? PLoS One **7**: e39425.

Lee, H., Xiong, L., Ishitani, M., Stevenson, B., and Zhu, J.K. (1999). Cold-regulated gene expression and freezing tolerance in an Arabidopsis thaliana mutant. Plant J **17**: 301–308.

Legnaioli, T., Cuevas, J., and Mas, P. (2009). TOC1 functions as a molecular switch connecting the circadian clock with plant responses to drought. EMBO J **28**: 3745–3757.

Legris, M., Klose, C., Burgie, E.S., Rojas, C.C.R., Neme, M., Hiltbrunner, A., Wigge, P.A., Schäfer, E., Vierstra, R.D., and Casal, J.J. (2016). Phytochrome B integrates light and temperature signals in Arabidopsis. Science **354**: 897–900.

Legris, M., Nieto, C., Sellaro, R., Prat, S., and Casal, J.J. (2017). Perception and signalling of light and temperature cues in plants. Plant J **90**: 683–697.

Leivar, P. and Monte, E. (2014). PIFs: systems integrators in plant development. Plant Cell **26**: 56–78.

Leivar, P. and Quail, P.H. (2011). PIFs: pivotal components in a cellular signaling hub. Trends Plant Sci **16**: 19–28.

León, J. (2013). Role of plant peroxisomes in the production of jasmonic acid-based signals. Subcell Biochem **69**: 299–313.

Li, G., Siddiqui, H., Teng, Y., Lin, R., Wan, X.-Y., Li, J., Lau, O.-S., Ouyang, X., Dai, M., Wan, J., Devlin, P.F., Deng, X.W., and Wang, H. (2011). Coordinated transcriptional regulation underlying the circadian clock in Arabidopsis. Nat Cell Biol **13**: 616–622.

Lian, H.-L., He, S.-B., Zhang, Y.-C., Zhu, D.-M., Zhang, J.-Y., Jia, K.-P., Sun, S.-X., Li, L., and Yang, H.-Q. (2011). Blue-light-dependent interaction of cryptochrome 1 with SPA1 defines a dynamic signaling mechanism. Genes Dev **25**: 1023–1028.

Licatalosi, D.D., Mele, A., Fak, J.J., Ule, J., Kayikci, M., Chi, S.W., Clark, T.A., Schweitzer, A.C., Blume, J.E., Wang, X., Darnell, J.C., and Darnell, R.B. (2008). HITS-CLIP yields genome-wide insights into brain alternative RNA processing. Nature **456**: 464–469.

Lidder, P., Gutiérrez, R.A., Salomé, P.A., McClung, C.R., and Green, P.J. (2005). Circadian control of messenger RNA stability. association with a sequence-specific messenger RNA decay pathway. Plant Physiol **138**: 2374-2385.

Liscum, E. (2016). Blue light-induced intracellular movement of phototropins: functional relevance or red herring? Front Plant Sci **7**: 1–5.

Liscum, E., Askinosie, S.K., Leuchtman, D.L., Morrow, J., Willenburg, K.T., and Coats, D.R. (2014). Phototropism: growing towards an understanding of plant movement. Plant Cell **26**: 38–55.

Liscum, E. and Briggs, W.R. (1995). Mutations in the NPH1 locus of Arabidopsis disrupt the perception of phototropic stimuli. Plant Cell **7**: 473–485.

Litthauer, S., Battle, M.W., and Jones, M.A. (2016). Phototropins do not alter accumulation of evening-phased circadian transcripts under blue light. Plant Signal Behav. **11**: e1126029

Litthauer, S., Battle, M.W., Lawson, T., and Jones, M.A. (2015). Phototropins maintain robust circadian oscillation of PSII operating efficiency under blue light. Plant J **83**: 1034–1045.

Liu, B., Liu, H., Zhong, D., and Lin, C. (2010). Searching for a photocycle of the cryptochrome photoreceptors. Curr Opin Plant Biol **13**: 578–586.

Liu, B., Zuo, Z., Liu, H., Liu, X., and Lin, C. (2011a). Arabidopsis cryptochrome 1 interacts with SPA1 to suppress COP1 activity in response to blue light. Genes Dev **25**: 1029–1034.

Liu, H., Liu, B., Zhao, C., Pepper, M., and Lin, C. (2011b). The action mechanisms of plant cryptochromes. Trends Plant Sci **16**: 684–691.

Liu, H., Weisman, D., Tang, L., Tan, L., Zhang, W. ke, Wang, Z. hua, Huang, Y. he, Lin, W. xiong, Liu, X. ming, and Colón-Carmona, A. (2014). Stress signaling in response to polycyclic aromatic hydrocarbon exposure in Arabidopsis thaliana involves a nucleoside diphosphate kinase, NDPK-3. Planta **241**: 95–107.

Liu, H., Yu, X., Li, K., Klejnot, J., Yang, H., Lisiero, D., and Lin, C. (2008a). Photoexcited CRY2 interacts with CIB1 to regulate transcription and floral initiation in Arabidopsis. Science **322**: 1535–1539.

Liu, L.-J., Zhang, Y.-C., Li, Q.-H., Sang, Y., Mao, J., Lian, H.-L., Wang, L., and Yang, H.-Q. (2008b). COP1-mediated ubiquitination of CONSTANS is implicated in cryptochrome regulation of flowering in Arabidopsis. Plant Cell **20**: 292–306.

Liu, T., Carlsson, J., Takeuchi, T., Newton, L., and Farré, E.M. (2013). Direct regulation of abiotic responses by the Arabidopsis circadian clock component PRR7. Plant J **76**: 101-114..

Liu, X.L., Covington, M.F., Fankhauser, C., Chory, J., and Wagner, D.R. (2001). ELF3 encodes a circadian clock-regulated nuclear protein that functions in an Arabidopsis PHYB signal transduction pathway. Plant Cell **13**: 1293–1304.

Liu, Y., Li, X., Li, K., Liu, H., and Lin, C. (2013). Multiple bHLH proteins form heterodimers to mediate CRY2-dependent regulation of flowering-time in Arabidopsis. PLoS Genet **9**: e1003861.

Locke, J.C.W., Kozma-Bognár, L., Gould, P.D., Fehér, B., Kevei, É., Nagy, F., Turner, M.S., Hall, A., and Millar, A.J. (2006). Experimental validation of a predicted feedback loop in the multi-oscillator clock of Arabidopsis thaliana. Mol Syst Biol **2**: 1–6.

Lonergan, T.A. (1981). A circadian rhythm in the rate of light-induced electron flow in three leguminous species. Plant Physiol **68**: 1041–1046.

Love, J., Dodd, A.N., and Webb, A.A.R. (2004). Circadian and diurnal calcium oscillations encode photoperiodic information in Arabidopsis. Plant Cell **16**: 956–966.

Lu, S.X., Knowles, S.M., Andronis, C., Ong, M.S., and Tobin, E.M. (2009). CIRCADIAN CLOCK ASSOCIATED1 and LATE ELONGATED HYPOCOTYL function synergistically in the circadian clock of Arabidopsis. Plant Physiol **150**: 834–843.

Lu, Y., Gehan, J.P., and Sharkey, T.D. (2005). Daylength and circadian effects on starch degradation and maltose metabolism. Plant Physiol **138**: 2280–2291.

Lv, F., Zhou, J., Zeng, L., and Xing, D. (2015). β-cyclocitral upregulates salicylic acid signalling to enhance excess light acclimation in Arabidopsis. J Exp Bot **66**: 4719–4732.

De Mairan, J.J.. (1729). Observation Botanique. Hist l'Academie R des Sci: 35.

Malpas, K.R. and Jones, M.A. (2016). Natural variation of circadian rhythms in Kalanchoe species. Haseltonia **22**: 35–42.

Mandal, M.K., Chandra-Shekara, A.C., Jeong, R.-D., Yu, K., Zhu, S., Chanda, B., Navarre, D., Kachroo, A., and Kachroo, P. (2012). Oleic acid-dependent modulation of NITRIC OXIDE ASSOCIATED1 protein levels regulates nitric oxide-mediated defense signaling in Arabidopsis. Plant Cell **24**: 1654–1674.

Manmathan, H., Shaner, D., Snelling, J., Tisserat, N., and Lapitan, N. (2013). Virus-induced gene silencing of Arabidopsis thaliana gene homologues in wheat identifies genes conferring improved drought tolerance. J Exp Bot **64**: 1381–1392.

Martin-Tryon, E.L., Kreps, J.A., and Harmer, S.L. (2006). GIGANTEA acts in blue light signaling and has biochemically separable roles in circadian clock and flowering time regulation. PLANT Physiol **143**: 473–486.

Martín, G., Leivar, P., Ludevid, D., Tepperman, J.M., Quail, P.H., and Monte, E. (2016). Phytochrome and retrograde signalling pathways converge to antagonistically regulate a light-induced transcriptional network. Nat Commun **7**: 11431.

Marty, L., Siala, W., Schwarzländer, M., Fricker, M.D., Wirtz, M., Sweetlove, L.J., Meyer, Y., Meyer, A.J., Reichheld, J.-P., and Hell, R. (2009). The NADPH-dependent thioredoxin system constitutes a functional backup for cytosolic glutathione reductase in Arabidopsis. Proc Natl Acad Sci U S A **106**: 9109–9114.

Más, P., Kim, W.-Y., Somers, D.E., and Kay, S.A. (2003). Targeted degradation of TOC1 by ZTL modulates circadian function in Arabidopsis thaliana. Nature **426**: 567–570.

Mathews, S. (2005). Phytochrome evolution in green and nongreen plants. J Hered **96**: 197–204.

Matsuoka, D. and Tokutomi, S. (2005). Blue light-regulated molecular switch of Ser/Thr kinase in phototropin. Proc Natl Acad Sci U S A **102**: 13337–13342.

Matsushika, A., Makino, S., Kojima, M., and Mizuno, T. (2000). Circadian waves of expression of the APRR1/TOC1 family of pseudo-response regulators in Arabidopsis thaliana: insight into the plant circadian clock. Plant Cell Physiol **41**: 1002–1012.

Maxwell, Borland, Haslam, Helliker, Roberts, and Griffiths (1999). Modulation of rubisco activity during the diurnal phases of the crassulacean acid metabolism plant Kalanchoë daigremontiana. Plant Physiol **121**: 849–856.

McClung, C.R. (2006). Plant circadian rhythms. Plant Cell **18**: 792–803.

McWatters, H.G., Bastow, R.M., Hall, A., and Millar, A.J. (2000). The ELF3 zeitnehmer regulates light signalling to the circadian clock. Nature **408**: 716–720.

McWatters, H.G., Kolmos, E., Hall, A., Doyle, M.R., Amasino, R.M., Gyula, P., Nagy, F., Millar, A.J., and Davis, S.J. (2007). ELF4 is required for oscillatory properties of the circadian clock. PLANT Physiol **144**: 391–401.

Michael, T.P., Salomé, P.A., Yu, H.J., Spencer, T.R., Sharp, E.L., McPeek, M.A., Alonso, J.M., Ecker, J.R., and McClung, C.R. (2003). Enhanced fitness conferred by naturally occurring variation in the circadian clock. Science **302**: 1049–1053.

Mikkelsen, M.D. and Thomashow, M.F. (2009). A role for circadian evening elements in cold-regulated gene expression in Arabidopsis. Plant J **60**: 328–339.

Millar, A.J. (2003). A suite of photoreceptors entrains the plant circadian clock. J Biol Rhythms **18**: 217–226.

Millar, A.J. (2004). Input signals to the plant circadian clock. J Exp Bot **55**: 277–283.

Millar, A.J. (2016). The intracellular dynamics of circadian clocks reach for the light of ecology and evolution. Annu Rev Plant Biol **67**: 595–618.

Millar, A., Brown, P.E., and Rand, D.A. (2010). BRASS version 3.

Millar, A.J. and Kay, S.A. (1996). Integration of circadian and phototransduction pathways in the network controlling CAB gene transcription in Arabidopsis. Proc Natl Acad Sci U S A **93**: 15491–15496.

Millar, A.J., Short, S.R., Chua, N.H., and Kay, S.A. (1992a). A novel circadian phenotype based on firefly luciferase expression in transgenic plants. Plant Cell **4**: 1075–1087.

Millar, A.J., Short, S.R., Hiratsuka, K., Chua, N.-H., and Kay, S.A. (1992b). Firefly luciferase as a reporter of regulated gene expression in higher plants. Plant Mol Biol Report **10**: 324–337.

Millar, A.J., Straume, M., Chory, J., Chua, N.H., and Kay, S.A. (1995). The regulation of circadian period by phototransduction pathways in Arabidopsis. Science **267**: 1163–1166.

Mimuro, M., Akimoto, S., Tomo, T., Yokono, M., Miyashita, H., and Tsuchiya, T. (2007). Delayed fluorescence observed in the nanosecond time region at 77 K originates directly from the photosystem II reaction center. Biochim Biophys Acta **1767**: 327–334.

Missra, A., Ernest, B., Lohoff, T., Jia, Q., Satterlee, J., Ke, K., and von Arnim, A.G. (2015). The circadian clock modulates global daily cycles of mRNA ribosome loading. Plant Cell **27**: 2582–2599.

Miyazaki, Y., Abe, H., Takase, T., Kobayashi, M., and Kiyosue, T. (2015). Overexpression of LOV KELCH PROTEIN 2 confers dehydration tolerance and is associated with enhanced expression of dehydration-inducible genes in Arabidopsis thaliana. Plant Cell Rep **34**: 843–852.

Mochizuki, N., Brusslan, J. a, Larkin, R., Nagatani, A., and Chory, J. (2001). Arabidopsis genomes uncoupled 5 (GUN5) mutant reveals the involvement of Mg-chelatase H subunit in plastid-to-nucleus signal transduction. Proc Natl Acad Sci U S A **98**: 2053–2058.

Mochizuki, N., Tanaka, R., Tanaka, A., Masuda, T., and Nagatani, A. (2008). The steady-state level of Mg-protoporphyrin IX is not a determinant of plastid-to-nucleus signaling in Arabidopsis. Proc Natl Acad Sci U S A **105**: 15184–15189.

Mockler, T.C., Michael, T.P., Priest, H.D., Shen, R., Sullivan, C.M., Givan, S.A., McEntee, C., Kay, S.A., and Chory, J. (2007). The DIURNAL project: DIURNAL and circadian expression profiling, model-based pattern matching, and promoter analysis. Cold Spring Harb Symp Quant Biol **72**: 353–363.

Moni, A., Lee, A.-Y., Briggs, W.R., and Han, I.-S. (2015). The blue light receptor Phototropin 1 suppresses lateral root growth by controlling cell elongation. Plant Biol (Stuttg) **17**: 34–40.

Motchoulski, A. and Liscum, E. (1999). Arabidopsis NPH3: A NPH1 photoreceptor-interacting protein essential for phototropism. Science **286**: 961–964.

Moulin, M., McCormac, A.C., Terry, M.J., and Smith, A.G. (2008). Tetrapyrrole profiling in Arabidopsis seedlings reveals that retrograde plastid nuclear signaling is not due to Mg-protoporphyrin IX accumulation. Proc Natl Acad Sci U S A **105**: 15178–15183.

Mugford, S.G., Matthewman, C.A., Hill, L., and Kopriva, S. (2010). Adenosine-5'-phosphosulfate kinase is essential for Arabidopsis viability. FEBS Lett **584**: 119–23.

Mugford, S.G., Yoshimoto, N., Reichelt, M., Wirtz, M., Hill, L., Mugford, S.T., Nakazato, Y., Noji, M., Takahashi, H., Kramell, R., Gigolashvili, T., Flugge, U.-I., Wasternack, C., Gershenzon, J., Hell, R., Saito, K., and Kopriva, S. (2009). Disruption of adenosine-5'-phosphosulfate kinase in Arabidopsis reduces levels of sulfated secondary metabolites. Plant Cell **21**: 910–927.

Müller, L.M., Von Korff, M., and Davis, S.J. (2014). Connections between circadian clocks and carbon metabolism reveal species-specific effects on growth control. J Exp Bot **65**: 2915–2923.

Müller, N.A., Wijnen, C.L., Srinivasan, A., Ryngajllo, M., Ofner, I., Lin, T., Ranjan, A., West, D., Maloof, J.N., Sinha, N.R., Huang, S., Zamir, D., and Jiménez-Gómez, J.M. (2016). Domestication selected for deceleration of the circadian clock in cultivated tomato. Nat Genet **48**: 89–93.

Muramoto, T., Kohchi, T., Yokota, A., Hwang, I., and Goodman, H.M. (1999). The Arabidopsis photomorphogenic mutant hy1 is deficient in phytochrome chromophore biosynthesis as a result of a mutation in a plastid heme oxygenase. Plant Cell **11**: 335–348.

Muranaka, T., Kubota, S., and Oyama, T. (2013). A single-cell bioluminescence imaging system for monitoring cellular gene expression in a plant body. Plant Cell Physiol **54**: 2085–2093.

Murguía, J.R., Bellés, J.M., and Serrano, R. (1996). The yeast HAL2 nucleotidase is an in vivo target of salt toxicity. J Biol Chem **271**: 29029–33.

Murphy, R.L., Klein, R.R., Morishige, D.T., Brady, J.A., Rooney, W.L., Miller, F.R., Dugas, D. V, Klein, P.E., and Mullet, J.E. (2011). Coincident light and clock regulation of pseudoresponse regulator protein 37 (PRR37) controls photoperiodic flowering in sorghum. Proc Natl Acad Sci U S A **108**: 16469–16474.

Nagarajan, V.K., Jones, C.I., Newbury, S.F., and Green, P.J. (2013). XRN 5'-3' exoribonucleases: structure, mechanisms and functions. Biochim Biophys Acta **1829**: 590–603.

Nagashima, A., Hanaoka, M., Shikanai, T., Fujiwara, M., Kanamaru, K., Takahashi, H., and Tanaka, K. (2004). The multiple-stress responsive plastid sigma factor, SIG5, directs activation of the psbD Blue Light-Responsive Promoter (BLRP) in Arabidopsis thaliana. Plant Cell Physiol **45**: 357–368.

Nagashima, Y., Iwata, Y., Ashida, M., Mishiba, K., and Koizumi, N. (2014). Exogenous salicylic acid activates two signaling arms of the unfolded protein response in Arabidopsis. Plant Cell Physiol **55**: 1772–1778.

Nagel, D.H. and Kay, S.A. (2012). Complexity in the wiring and regulation of plant circadian networks. Curr Biol **22**: R648-657.

Nakagawa, T., Ishiguro, S., and Kimura, T. (2009). Gateway vectors for plant transformation. Plant Biotechnol **26**: 275–284.

Nakagawa, T., Kurose, T., Hino, T., Tanaka, K., Kawamukai, M., Niwa, Y., Toyooka, K., Matsuoka, K., Jinbo, T., and Kimura, T. (2007). Development of series of gateway binary vectors, pGWBs, for realizing efficient construction of fusion genes for plant transformation. J Biosci Bioeng **104**: 34–41.

Nakamichi, N. (2011). Molecular mechanisms underlying the Arabidopsis circadian clock. Plant Cell Physiol **52**: 1709–1718.

Nakamichi, N., Kiba, T., Henriques, R., Mizuno, T., Chua, N.H., and Sakakibara, H. (2010). PSEUDO-RESPONSE REGULATORS 9, 7, and 5 are transcriptional repressors in the Arabidopsis circadian clock. Plant Cell **22**: 594–605.

Nakamichi, N., Kita, M., Ito, S., Yamashino, T., and Mizuno, T. (2005). PSEUDO-RESPONSE REGULATORS, PRR9, PRR7 and PRR5, together play essential roles close to the circadian clock of Arabidopsis thaliana. Plant Cell Physiol **46**: 686–698.

Nakamichi, N., Kusano, M., Fukushima, A., Kita, M., Ito, S., Yamashino, T., Saito, K., Sakakibara, H., and Mizuno, T. (2009). Transcript profiling of an Arabidopsis PSEUDO RESPONSE REGULATOR arrhythmic triple mutant reveals a role for the circadian clock in cold stress response. Plant Cell Physiol **50**: 447–462

Nakasako, M., Zikihara, K., Matsuoka, D., Katsura, H., and Tokutomi, S. (2008). Structural basis of the LOV1 dimerization of Arabidopsis phototropins 1 and 2. J Mol Biol **381**: 718–733.

Narusaka, M., Shiraishi, T., Iwabuchi, M., and Narusaka, Y. (2010). The floral inoculating protocol: A simplified Arabidopsis thaliana transformation method modified from floral dipping. Plant Biotechnol **27**: 349–351.

Nassoury, N., Fritz, L., and Morse, D. (2001). Circadian changes in ribulose-1,5-bisphosphate carboxylase/oxygenase distribution inside individual chloroplasts can account for the rhythm in dinoflagellate carbon fixation. Plant Cell **13**: 923–934.

Neeb, C.X. (1952). Hydrodictyon als Objekt einer vergleichenden Untersuchung physiologischer Grossen. Flora **139**: 39–95.

Nikiforova, V., Freitag, J., Kempa, S., Adamik, M., Hesse, H., and Hoefgen, R. (2003). Transcriptome analysis of sulfur depletion in Arabidopsis thaliana: interlacing of biosynthetic pathways provides response specificity. Plant J **33**: 633–650.

Niwa, Y., Yamashino, T., and Mizuno, T. (2009). The circadian clock regulates the photoperiodic response of hypocotyl elongation through a coincidence mechanism in Arabidopsis thaliana. Plant Cell Physiol **50**: 838–854.

Nolte, C. and Staiger, D. (2015). RNA around the clock - regulation at the RNA level in biological timing. Front Plant Sci **6**: 311.

Noordally, Z.B., Ishii, K., Atkins, K.A., Wetherill, S.J., Kusakina, J., Walton, E.J., Kato, M., Azuma, M., Tanaka, K., Hanaoka, M., and Dodd, A.N. (2013). Circadian control of chloroplast transcription by a nuclear-encoded timing signal. Science **339**: 1316–1319.

Nozue, K., Covington, M.F., Duek, P.D., Lorrain, S., Fankhauser, C., Harmer, S.L., and Maloof, J.N. (2007). Rhythmic growth explained by coincidence between internal and external cues. Nature **448**: 358–361.

Nusinow, D.A., Helfer, A., Hamilton, E.E., King, J.J., Imaizumi, T., Schultz, T.F., Farré, E.M., and Kay, S.A. (2011). The ELF4–ELF3–LUX complex links the circadian clock to diurnal control of hypocotyl growth. Nature **475**: 398–402.

O'Neill, J.S., van Ooijen, G., Dixon, L.E., Troein, C., Corellou, F., Bouget, F.-Y., Reddy, A.B., and Millar, A.J. (2011). Circadian rhythms persist without transcription in a eukaryote. Nature **469**: 554–558.

O'Neill, J.S. and Reddy, A.B. (2011). Circadian clocks in human red blood cells. Nature **469**: 498–503.

Olmedo, G., Guo, H., Gregory, B.D., Nourizadeh, S.D., Aguilar-Henonin, L., Li, H., An, F., Guzman, P., and Ecker, J.R. (2006). ETHYLENE-INSENSITIVE5 encodes a 5'-->3' exoribonuclease required for regulation of the EIN3-targeting F-box proteins EBF1/2.. Proc Natl Acad Sci U S A **103**: 13286–13293.

Oelmüller, R., Levitan, I., Bergfeld, R., Rajasekhar, V.K., and Mohr, H. (1986). Expression of nuclear genes as affected by treatments acting on the plastids. Planta **168**: 482–492.

Osterlund, M.T., Hardtke, C.S., Wei, N., and Deng, X.W. (2000). Targeted destabilization of HY5 during light-regulated development of Arabidopsis. Nature **405**: 462–466.

Ostrovsky, D., Diomina, G., Lysak, E., Matveeva, E., Ogrel, O., and Trutko, S. (1998). Effect of oxidative stress on the biosynthesis of 2-C-methyl-D-erythritol-2,4-cyclopyrophosphate and isoprenoids by several bacterial strains. Arch Microbiol **171**: 69–72.

Ostrovsky, D., Kharatian, E., Malarova, I., Shipanova, I., Sibeldina, L., Shashkov, A., and Tantsirev, G. (1992). Synthesis of a new organic pyrophosphate in large quantities is induced in some bacteria by oxidative stress. Biofactors **3**: 261–264.

Ouyang, Y., Andersson, C.R., Kondo, T., Golden, S.S., and Johnson, C.H. (1998). Resonating circadian clocks enhance fitness in cyanobacteria. Proc Natl Acad Sci U S A

95: 8660–8664.

Pal, S.K., Liput, M., Piques, M., Ishihara, H., Obata, T., Martins, M.C.M., Sulpice, R., van Dongen, J.T., Fernie, A.R., Yadav, U.P., Lunn, J.E., Usadel, B., and Stitt, M. (2013). Diurnal changes of polysome loading track sucrose content in the rosette of wild-type arabidopsis and the starchless pgm mutant. Plant Physiol **162**: 1246–1265.

Para, A., Farre, E.M., Imaizumi, T., Pruneda-Paz, J.L., Harmon, F.G., and Kay, S.A. (2007). PRR3 is a vascular regulator of TOC1 stability in the Arabidopsis circadian clock. Plant Cell **19**: 3462–3473.

Park, S.-W., Li, W., Viehhauser, A., He, B., Kim, S., Nilsson, A.K., Andersson, M.X., Kittle, J.D., Ambavaram, M.M.R., Luan, S., Esker, A.R., Tholl, D., Cimini, D., Ellerström, M., Coaker, G., Mitchell, T.K., Pereira, A., Dietz, K.-J., and Lawrence, C.B. (2013). Cyclophilin 20-3 relays a 12-oxo-phytodienoic acid signal during stress responsive regulation of cellular redox homeostasis. Proc Natl Acad Sci U S A **110**: 9559–9564.

Pedmale, U. V and Liscum, E. (2007). Regulation of phototropic signaling in Arabidopsis via phosphorylation state changes in the phototropin 1-interacting protein NPH3. J Biol Chem **282**: 19992–20001.

Pei, Z.M., Murata, Y., Benning, G., Thomine, S., Klüsener, B., Allen, G.J., Grill, E., and Schroeder, J.I. (2000). Calcium channels activated by hydrogen peroxide mediate abscisic acid signalling in guard cells. Nature **406**: 731–734.

Peltier, J.-B., Cai, Y., Sun, Q., Zabrouskov, V., Giacomelli, L., Rudella, A., Ytterberg, A.J., Rutschow, H., and van Wijk, K.J. (2005). The oligomeric stromal proteome of Arabidopsis thaliana chloroplasts. Mol Cell Proteomics **5**: 114–133.

Perez-Santángelo, S., Mancini, E., Francey, L.J., Schlaen, R.G., Chernomoretz, A., Hogenesch, J.B., and Yanovsky, M.J. (2014). Role for LSM genes in the regulation of circadian rhythms. Proc Natl Acad Sci U S A **111**: 15166–15171.

Pesaresi, P., Hertle, A., Pribil, M., Kleine, T., Wagner, R., Strissel, H., Ihnatowicz, A., Bonardi, V., Scharfenberg, M., Schneider, A., Pfannschmidt, T., and Leister, D. (2009). Arabidopsis STN7 kinase provides a link between short- and long-term photosynthetic acclimation. Plant Cell **21**: 2402–2423.

Peters, L. and Meister, G. (2007). Argonaute proteins: mediators of RNA silencing. Mol Cell **26**: 611–623.

Petrillo, E., Godoy Herz, M.A., Fuchs, A., Reifer, D., Fuller, J., Yanovsky, M.J., Simpson, C., Brown, J.W.S., Barta, A., Kalyna, M., and Kornblihtt, A.R. (2014). A chloroplast retrograde signal regulates nuclear alternative splicing. Science **344**: 427–430.

Pfeifer, A., Mathes, T., Lu, Y., Hegemann, P., and Kottke, T. (2010). Blue light induces global and localized conformational changes in the kinase domain of full-length phototropin. Biochemistry **49**: 1024–1032.

Phiel, C.J. and Klein, P.S. (2001). Molecular targets of lithium action. Annu Rev Pharmacol Toxicol **41**: 789–813.

Piques, M., Schulze, W.X., Höhne, M., Usadel, B., Gibon, Y., Rohwer, J., and Stitt, M. (2009). Ribosome and transcript copy numbers, polysome occupancy and enzyme dynamics in Arabidopsis. Mol Syst Biol **5**: 314.

Pittendrigh, C.S. (1992). Circadian Systems: Entrainment. Ann Anat **174**: 383–391.

Pittendrigh, C.S. (1954). On temperature independence in the clock system controlling

emergence time in Drosophila. Proc Natl Acad Sci U S A **40**: 1018–1029.

Pittendrigh, C.S. and Minis, D.H. (1964). The entrainment of circadian oscillations by light and their role as photoperiodic clocks. Am Nat **98**: 261–294.

Plautz, J.D., Straume, M., Stanewsky, R., Jamison, C.F., Brandes, C., Dowse, H.B., Hall, J.C., and Kay, S.A. (1997). Quantitative analysis of Drosophila period gene transcription in living animals. J Biol Rhythms **12**: 204–217.

Pluthero, F.G. (1993). Rapid purification of high-activity Taq DNA polymerase. Nucleic Acids Res **21**: 4850–4851.

Pokhilko, A., Fernández, A.P., Edwards, K.D., Southern, M.M., Halliday, K.J., and Millar, A.J. (2012). The clock gene circuit in Arabidopsis includes a repressilator with additional feedback loops. Mol Syst Biol **8**: 574.

Pokorny, R., Klar, T., Hennecke, U., Carell, T., Batschauer, A., and Essen, L.-O. (2008). Recognition and repair of UV lesions in loop structures of duplex DNA by DASH-type cryptochrome. Proc Natl Acad Sci U S A **105**: 21023–21027.

Pornsiriwong, W., Estavillo, G.M., Chan, K.X., Tee, E.E., Ganguly, D., Crisp, P.A., Phua, S.Y., Zhao, C., Qiu, J., Park, J., Yong, M.T., Nisar, N., Yadav, A.K., Schwessinger, B., Rathjen, J., Cazzonelli, C.I., Wilson, P.B., Gilliham, M., Chen, Z.Hua., and Pogson, B.J. (2017). A chloroplast retrograde signal, 3'phosphoadenosine 5'-phosphate, acts as a secondary messenger in abscisic acid signaling in stomatal closure and germination. Elife **6**: 1–34.

Potuschak, T., Vansiri, A., Binder, B.M., Lechner, E., Vierstra, R.D., and Genschik, P. (2006). The exoribonuclease XRN4 is a component of the ethylene response pathway in Arabidopsis. Plant Cell **18**: 3047–3057.

Prinz, W.A. (2014). Bridging the gap: membrane contact sites in signaling, metabolism, and organelle dynamics. J Cell Biol **205**: 759–769.

Pruneda-Paz, J.L., Breton, G., Para, A., and Kay, S.A. (2009). A functional genomics approach reveals CHE as a component of the Arabidopsis circadian clock. Science **323**: 1481–1485.

Pudasaini, A. and Zoltowski, B.D. (2013). Zeitlupe senses blue-light fluence to mediate circadian timing in Arabidopsis thaliana. Biochemistry **52**: 7150–7158.

Quintero, F.J., Garciadeblás, B., and Rodríguez-Navarro, A. (1996). The SAL1 gene of Arabidopsis, encoding an enzyme with 3'(2'),5'-bisphosphate nucleotidase and inositol polyphosphate 1-phosphatase activities, increases salt tolerance in yeast. Plant Cell **8**: 529–537.

Ramel, F., Birtic, S., Ginies, C., Soubigou-Taconnat, L., Triantaphylidès, C., and Havaux, M. (2012). Carotenoid oxidation products are stress signals that mediate gene responses to singlet oxygen in plants. Proc Natl Acad Sci U S A **109**: 5535–5540.

Ramel, F., Ksas, B., Akkari, E., Mialoundama, A.S., Monnet, F., Krieger-Liszkay, A., Ravanat, J.-L., Mueller, M.J., Bouvier, F., and Havaux, M. (2013). Light-induced acclimation of the Arabidopsis chlorina1 mutant to singlet oxygen. Plant Cell **25**: 1445–1462.

Rascher, U., Hütt, M.T., Siebke, K., Osmond, B., Beck, F., and Lüttge, U. (2001). Spatiotemporal variation of metabolism in a plant circadian rhythm: the biological clock as an assembly of coupled individual oscillators. Proc Natl Acad Sci U S A **98**: 11801–11805.

Ravilious, G.E., Nguyen, A., Francois, J.A., and Jez, J.M. (2012). Structural basis and evolution of redox regulation in plant adenosine-5'-phosphosulfate kinase. Proc Natl Acad Sci U S A **109**: 309–314.

Rawat, R., Schwartz, J., Jones, M. a, Sairanen, I., Cheng, Y., Andersson, C.R., Zhao, Y., Ljung, K., and Harmer, S.L. (2009). REVEILLE1, a Myb-like transcription factor, integrates the circadian clock and auxin pathways. Proc Natl Acad Sci U S A **106**: 16883–16888.

Rawat, R., Takahashi, N., Hsu, P.Y., Jones, M. a, Schwartz, J., Salemi, M.R., Phinney, B.S., and Harmer, S.L. (2011). REVEILLE8 and PSEUDO-REPONSE REGULATOR5 form a negative feedback loop within the Arabidopsis circadian clock. PLoS Genet **7**: e1001350.

Reddy, A.B. and Rey, G. (2014). Metabolic and nontranscriptional circadian clocks: eukaryotes. Annu Rev Biochem **83**: 165–189.

Rizzini, L., Favory, J.-J., Cloix, C., Faggionato, D., O'Hara, A., Kaiserli, E., Baumeister, R., Schäfer, E., Nagy, F., Jenkins, G.I., and Ulm, R. (2011). Perception of UV-B by the Arabidopsis UVR8 protein. Science **332**: 103–106.

Roberts, D., Pedmale, U. V, Morrow, J., Sachdev, S., Lechner, E., Tang, X., Zheng, N., Hannink, M., Genschik, P., and Liscum, E. (2011). Modulation of phototropic responsiveness in Arabidopsis through ubiquitination of phototropin 1 by the CUL3-Ring E3 ubiquitin ligase CRL3(NPH3). Plant Cell **23**: 3627–3640.

Robles, P., Fleury, D., Candela, H., Cnops, G., Alonso-Peral, M.M., Anami, S., Falcone, A., Caldana, C., Willmitzer, L., Ponce, M.R., Van Lijsebettens, M., and Micol, J.L. (2010). The RON1/FRY1/SAL1 gene is required for leaf morphogenesis and venation patterning in Arabidopsis. Plant Physiol **152**: 1357–1372.

Rockwell, N.C., Su, Y.-S., and Lagarias, J.C. (2006). Phytochrome structure and signaling mechanisms. Annu Rev Plant Biol **57**: 837–858.

Rodriguez, V.M., Chetelat, A., Majcherczyk, P., and Farmer, E.E. (2010). Chloroplastic phosphoadenosine phosphosulfate metabolism regulates basal levels of the prohormone jasmonic acid in Arabidopsis leaves. PLANT Physiol **152**: 1335–1345.

Roman, G., Lubarsky, B., Kieber, J.J., Rothenberg, M., and Ecker, J.R. (1995). Genetic analysis of ethylene signal transduction in Arabidopsis thaliana: five novel mutant loci integrated into a stress response pathway. Genetics **139**: 1393–1409.

Rossel, J.B., Cuttriss, A., and Pogson, B.J. (2004). Identifying photoprotection mutants in Arabidopsis thaliana. Methods Mol Biol **274**: 287–299.

Rossel, J.B., Walter, P.B., Hendrickson, L., Chow, W.S., Poole, A., Mullineaux, P.M., and Pogson, B.J. (2006). A mutation affecting ASCORBATE PEROXIDASE 2 gene expression reveals a link between responses to high light and drought tolerance. Plant Cell Environ **29**: 269–281.

Rugnone, M.L., Faigón Soverna, A., Sanchez, S.E., Schlaen, R.G., Hernando, C.E., Seymour, D.K., Mancini, E., Chernomoretz, A., Weigel, D., Más, P., and Yanovsky, M.J. (2013). LNK genes integrate light and clock signaling networks at the core of the Arabidopsis oscillator. Proc Natl Acad Sci U S A **110**: 12120–12125.

Rutherford, A.W., Govindjee, and Inoue, Y. (1984). Charge accumulation and photochemistry in leaves studied by thermoluminescence and delayed light emission. Proc Natl Acad Sci U S A **81**: 1107–1111.

Rymarquis, L.A, Souret, F.F., and Green, P.J. (2011). Evidence that XRN4, an Arabidopsis

homolog of exoribonuclease XRN1, preferentially impacts transcripts with certain sequences or in particular functional categories. RNA **17**: 501–511

Sai, J. and Johnson, C.H. (1999). Different circadian oscillators control Ca^{2+} fluxes and LHCB gene expression. Proc Natl Acad Sci U S A **96**: 11659–11663.

Sakai, T., Kagawa, T., Kasahara, M., Swartz, T.E., Christie, J.M., Briggs, W.R., Wada, M., and Okada, K. (2001). Arabidopsis nph1 and npl1: blue light receptors that mediate both phototropism and chloroplast relocation. Proc Natl Acad Sci U S A **98**: 6969–6974.

Sakai, T., Wada, T., Ishiguro, S., and Okada, K. (2000). RPT2. A signal transducer of the phototropic response in Arabidopsis. Plant Cell **12**: 225–236.

Sakamoto, K. and Briggs, W.R. (2002). Cellular and subcellular localization of phototropin 1. Plant Cell **14**: 1723–1735.

Salomé, P.A. and McClung, C.R. (2005). PSEUDO-RESPONSE REGULATOR 7 and 9 are partially redundant genes essential for the temperature responsiveness of the Arabidopsis circadian clock. Plant Cell **17**: 791–803.

Salomé, P.A., Oliva, M., Weigel, D., and Krämer, U. (2013). Circadian clock adjustment to plant iron status depends on chloroplast and phytochrome function. EMBO J **32**: 511–523.

Salomon, M., Christie, J.M., Knieb, E., Lempert, U., and Briggs, W.R. (2000). Photochemical and mutational analysis of the FMN-binding domains of the plant blue light receptor, phototropin. Biochemistry **39**: 9401–9410.

Salomon, M., Lempert, U., and Rüdiger, W. (2004). Dimerization of the plant photoreceptor phototropin is probably mediated by the LOV1 domain. FEBS Lett **572**: 8–10.

Samach, A., Onouchi, H., Gold, S.E., Ditta, G.S., Schwarz-Sommer, Z., Yanofsky, M.F., and Coupland, G. (2000). Distinct roles of CONSTANS target genes in reproductive development of Arabidopsis. Science **288**: 1613–1616.

Sanchez, S.E., Petrillo, E., Beckwith, E.J., Zhang, X., Rugnone, M.L., Hernando, C.E., Cuevas, J.C., Godoy Herz, M.A., Depetris-Chauvin, A., Simpson, C.G., Brown, J.W.S., Cerdán, P.D., Borevitz, J.O., Mas, P., Ceriani, M.F., Kornblihtt, A.R., and Yanovsky, M.J. (2010). A methyl transferase links the circadian clock to the regulation of alternative splicing. Nature **468**: 112–116.

Sanchez, S.E. and Kay, S.A. (2016). The plant circadian clock: from a simple timekeeper to a complex developmental manager. Cold Spring Harb Perspect Biol **8**: a027748.

Sanchez, S.E., Petrillo, E., Kornblihtt, A.R., and Yanovsky, M.J. (2011). Alternative splicing at the right time. RNA Biol **8**: 954–959.

Sato, Y., Yazawa, K., Yoshida, S., Tamaoki, M., Nakajima, N., Iwai, H., Ishii, T., and Satoh, S. (2011). Expression and functions of myo-inositol monophosphatase family genes in seed development of Arabidopsis. J Plant Res **124**: 385–394.

Satter, R.L., Geballe, G.T., and Galston, A.W. (1974). Potassium flux and leaf movement in Samanea saman. II. phytochrome controlled movement. J Gen Physiol **64**: 431–442.

Savchenko, T., Kolla, V.A., Wang, C.-Q., Nasafi, Z., Hicks, D.R., Phadungchob, B., Chehab, W.E., Brandizzi, F., Froehlich, J., and Dehesh, K. (2014). Functional convergence of oxylipin and abscisic acid pathways controls stomatal closure in response to drought. Plant Physiol **164**: 1151–1160.

Savchenko, T., Walley, J.W., Chehab, E.W., Xiao, Y., Kaspi, R., Pye, M.F., Mohamed, M.E., Lazarus, C.M., Bostock, R.M., and Dehesh, K. (2010). Arachidonic acid: an

evolutionarily conserved signaling molecule modulates plant stress signaling networks. Plant Cell **22**: 3193–3205.

Sawa, M. and Kay, S.A. (2011). GIGANTEA directly activates Flowering Locus T in Arabidopsis thaliana. Proc Natl Acad Sci U S A **108**: 11698–11703.

Sawa, M., Nusinow, D.A., Kay, S.A., and Imaizumi, T. (2007). FKF1 and GIGANTEA complex formation is required for day-length measurement in Arabidopsis. Science **318**: 261–265.

Sayle, R. (1995). RASMOL: biomolecular graphics for all. Trends Biochem Sci **20**: 374–376.

Schaller, A. and Stintzi, A. (2009). Enzymes in jasmonate biosynthesis - structure, function, regulation. Phytochemistry **70**: 1532–1538.

Schlicke, H., Hartwig, A.S., Firtzlaff, V., Richter, A.S., Glässer, C., Maier, K., Finkemeier, I., and Grimm, B. (2014). Induced deactivation of genes encoding chlorophyll biosynthesis enzymes disentangles tetrapyrrole-mediated retrograde signaling. Mol Plant **7**: 1211–1227.

Schneider, B., Xu, Y.W., Janin, J., Veron, M., and Deville-Bonne, D. (1998). 3'-Phosphorylated nucleotides are tight binding inhibitors of nucleoside diphosphate kinase activity. J Biol Chem **273**: 28773–28778.

Scholl, R.L., May, S.T., and Ware, D.H. (2000). Seed and Molecular Resources for Arabidopsis. Plant Physiol **124**: 1477–1480.

Schon, J. (1955). Periodische Schwankungen der Photosynthese und Atmung bei Hydrodictyon. Flora **142**: 347–380.

Schwarzländer, M., Fricker, M.D., Müller, C., Marty, L., Brach, T., Novak, J., Sweetlove, L.J., Hell, R., and Meyer, A. J. (2008). Confocal imaging of glutathione redox potential in living plant cells. J Microsc **231**: 299–316.

Seemann, M., Wegner, P., Schünemann, V., Bui, B.T.S., Wolff, M., Marquet, A., Trautwein, A.X., and Rohmer, M. (2005). Isoprenoid biosynthesis in chloroplasts via the methylerythritol phosphate pathway: the (E)-4-hydroxy-3-methylbut-2-enyl diphosphate synthase (GcpE) from Arabidopsis thaliana is a [4Fe-4S] protein. J Biol Inorg Chem **10**: 131–137.

Seo, P.J. and Mas, P. (2014). Multiple layers of posttranslational regulation refine circadian clock activity in Arabidopsis. Plant Cell **26**: 79–87.

Seo, P.J., Park, M.-J., Lim, M.-H., Kim, S.-G., Lee, M., Baldwin, I.T., and Park, C.-M. (2012). A self-regulatory circuit of CIRCADIAN CLOCK-ASSOCIATED1 underlies the circadian clock regulation of temperature responses in Arabidopsis. Plant Cell **24**: 2427–2442.

Shalitin, D., Yang, H., Mockler, T.C., Maymon, M., Guo, H., Whitelam, G.C., and Lin, C. (2002). Regulation of Arabidopsis cryptochrome 2 by blue-light-dependent phosphorylation. Nature **417**: 763–767.

Shalitin, D., Yu, X., Maymon, M., Mockler, T., and Lin, C. (2003). Blue light-dependent in vivo and in vitro phosphorylation of Arabidopsis cryptochrome 1. Plant Cell **15**: 2421–2429.

Sharrock, R.A. and Clack, T. (2002). Patterns of expression and normalized levels of the five Arabidopsis phytochromes. Plant Physiol **130**: 442–456.

Sheard, L.B., Tan, X., Mao, H., Withers, J., Ben-Nissan, G., Hinds, T.R., Kobayashi, Y., Hsu, F.-F., Sharon, M., Browse, J., He, S.Y., Rizo, J., Howe, G.A., and Zheng, N.

(2010). Jasmonate perception by inositol-phosphate-potentiated COI1-JAZ co-receptor. Nature **468**: 400–405.

Sherf, B.A. and Wood, K. V (1994). Firefly luciferase engineered for improved genetic reporting. Promega Notes Mag: 14–21.

Shroff, R., Schramm, K., Jeschke, V., Nemes, P., Vertes, A., Gershenzon, J., and Svatoš, A. (2015). Quantification of plant surface metabolites by matrix-assisted laser desorption-ionization mass spectrometry imaging: glucosinolates on Arabidopsis thaliana leaves. Plant J **81**: 961–972.

Smale, S.T. (2010). Luciferase assay. Cold Spring Harb Protoc **2010**: pdb.prot5421.

Smith, A.M. and Stitt, M. (2007). Coordination of carbon supply and plant growth. Plant Cell Environ **30**: 1126–1149.

Somers, D.E., Devlin, P.F., and Kay, S.A. (1998a). Phytochromes and cryptochromes in the entrainment of the Arabidopsis circadian clock. Science **282**: 1488–1490.

Somers, D.E., Schultz, T.F., Milnamow, M., and Kay, S.A. (2000). ZEITLUPE encodes a novel clock-associated PAS protein from Arabidopsis. Cell **101**: 319–329.

Somers, D.E., Webb, A.A., Pearson, M., and Kay, S.A. (1998b). The short-period mutant, toc1-1, alters circadian clock regulation of multiple outputs throughout development in Arabidopsis thaliana. Development **125**: 485–494.

Song, H.-R. and Carré, I.A. (2005). DET1 regulates the proteasomal degradation of LHY, a component of the Arabidopsis circadian clock. Plant Mol Biol **57**: 761–771.

Song, Y.H., Estrada, D.A., Johnson, R.S., Kim, S.K., Lee, S.Y., MacCoss, M.J., and Imaizumi, T. (2014). Distinct roles of FKF1, GIGANTEA, and ZEITLUPE proteins in the regulation of CONSTANS stability in Arabidopsis photoperiodic flowering. Proc Natl Acad Sci **111**: 17672–17677.

Song, Y.H., Shim, J.S., Kinmonth-Schultz, H.A., and Imaizumi, T. (2015). Photoperiodic flowering: time measurement mechanisms in leaves. Annu Rev Plant Biol **66**: 441–464.

Souret, F.F., Kastenmayer, J.P., and Green, P.J. (2004). AtXRN4 degrades mRNA in Arabidopsis and its substrates include selected miRNA targets. Mol Cell **15**: 173–183.

de Souza, A., Wang, J.-Z., and Dehesh, K. (2017). Retrograde signals: integrators of interorganellar communication and orchestrators of plant development. Annu Rev Plant Biol **68**: 85–108.

Soy, J., Leivar, P., González-Schain, N., Martín, G., Diaz, C., Sentandreu, M., Al-Sady, B., Quail, P.H., and Monte, E. (2016). Molecular convergence of clock and photosensory pathways through PIF3–TOC1 interaction and co-occupancy of target promoters. Proc Natl Acad Sci **113**: 4870–4875.

Spiegelberg, B.D., Xiong, J.P., Smith, J.J., Gu, R.F., and York, J.D. (1999). Cloning and characterization of a mammalian lithium-sensitive bisphosphate 3'-nucleotidase inhibited by inositol 1,4-bisphosphate. J Biol Chem **274**: 13619–13628.

Strand, A., Asami, T., Alonso, J., Ecker, J.R., and Chory, J. (2003). Chloroplast to nucleus communication triggered by accumulation of Mg-protoporphyrinIX. Nature **421**: 79–83.

Strayer, C., Oyama, T., Schultz, T.F., Raman, R., Somers, D.E., Más, P., Panda, S., Kreps, J.A., and Kay, S.A. (2000). Cloning of the Arabidopsis clock gene TOC1, an autoregulatory response regulator homolog. Science **289**: 768–771.

Suárez-López, P., Wheatley, K., Robson, F., Onouchi, H., Valverde, F., and Coupland, G.

(2001). CONSTANS mediates between the circadian clock and the control of flowering in Arabidopsis. Nature **410**: 1116–1120.

Suetsugu, N. and Wada, M. (2013). Evolution of three LOV blue light receptor families in green plants and photosynthetic stramenopiles: Phototropin, ZTL/FKF1/LKP2 and aureochrome. Plant Cell Physiol **54**: 8–23.

Sullivan, S., Thomson, C.E., Lamont, D.J., Jones, M.A., and Christie, J.M. (2008). In vivo phosphorylation site mapping and functional characterization of Arabidopsis phototropin 1. Mol Plant **1**: 178–194.

Sulzman, F.M., Ellman, D., Fuller, C.A., Moore-Ede, M.C., and Wassmer, G. (1984). Neurospora circadian rhythms in space: a reexamination of the endogenous-exogenous question. Science **225**: 232–234.

Sun, X., Feng, P., Xu, X., Guo, H., Ma, J., Chi, W., Lin, R., Lu, C., and Zhang, L. (2011). A chloroplast envelope-bound PHD transcription factor mediates chloroplast signals to the nucleus. Nat Commun **2**: 477.

Susek, R.E., Ausubel, F.M., and Chory, J. (1993). Signal transduction mutants of Arabidopsis uncouple nuclear CAB and RBCS gene expression from chloroplast development. Cell **74**: 787–799.

Syed, N.H., Prince, S.J., Mutava, R.N., Patil, G., Li, S., Chen, W., Babu, V., Joshi, T., Khan, S., and Nguyen, H.T. (2015). Core clock, SUB1 , and ABAR genes mediate flooding and drought responses via alternative splicing in soybean. J Exp Bot **66**: 7129–7149.

Takahashi, H., Buchner, P., Yoshimoto, N., Hawkesford, M.J., and Shiu, S.-H. (2012). Evolutionary relationships and functional diversity of plant sulfate transporters. Front Plant Sci **2**: 119.

Takahashi, H., Kopriva, S., Giordano, M., Saito, K., and Hell, R. (2011). Sulfur assimilation in photosynthetic organisms: molecular functions and regulations of transporters and assimilatory enzymes. Annu Rev Plant Biol **62**: 157–84.

Takase, T., Nishiyama, Y., Tanihigashi, H., Ogura, Y., Miyazaki, Y., Yamada, Y., and Kiyosue, T. (2011). LOV KELCH PROTEIN2 and ZEITLUPE repress Arabidopsis photoperiodic flowering under non-inductive conditions, dependent on FLAVIN-BINDING KELCH REPEAT F-BOX1. Plant J **67**: 608–621.

Takeda, S., Gapper, C., Kaya, H., Bell, E., Kuchitsu, K., and Dolan, L. (2008). Local positive feedback regulation determines cell shape in root hair cells. Science **319**: 1241–1244.

Takemiya, A. (2005). Phototropins promote plant growth in response to blue light in low light environments. Plant Cell **17**: 1120–1127.

Tan, S.-T., Dai, C., Liu, H.-T., and Xue, H.-W. (2013). Arabidopsis casein kinase1 proteins CK1.3 and CK1.4 phosphorylate cryptochrome2 to regulate blue light signaling. Plant Cell **25**: 2618–2632.

Tanaka, K. and Hanaoka, M. (2013). The early days of plastid retrograde signaling with respect to replication and transcription. Front Plant Sci **3**: 1–5.

Tataroglu, O. and Emery, P. (2014). Studying circadian rhythms in Drosophila melanogaster. Methods **68**: 140–50.

Thain, S.C., Murtas, G., Lynn, J.R., McGrath, R.B., and Millar, A.J. (2002). The circadian clock that controls gene expression in Arabidopsis is tissue specific. Plant Physiol **130**:

102–110.

Thain, S.C., Vandenbussche, F., Laarhoven, L.J.J., Dowson-Day, M.J., Wang, Z.-Y., Tobin, E.M., Harren, F.J.M., Millar, A.J., and Van Der Straeten, D. (2004). Circadian rhythms of ethylene emission in Arabidopsis. Plant Physiol **136**: 3751–3761.

Thomas, B. and Vince-Prue, D. (1997). Photoperiodism in Plants (Academic Press, Inc.: San Diego).

Thomashow, M.F. (2010). Molecular basis of plant cold acclimation: insights gained from studying the CBF cold response pathway. Plant Physiol **154**: 571–577.

Tindall, A.J., Waller, J., Greenwood, M., Gould, P.D., Hartwell, J., and Hall, A. (2015). A comparison of high-throughput techniques for assaying circadian rhythms in plants. Plant Methods **11**: 32.

Tokutomi, S., Matsuoka, D., and Zikihara, K. (2008). Molecular structure and regulation of phototropin kinase by blue light. Biochim Biophys Acta **1784**: 133–142.

Toledo-Ortiz, G., Johansson, H., Lee, K.P., Bou-Torrent, J., Stewart, K., Steel, G., Rodríguez-Concepción, M., and Halliday, K.J. (2014). The HY5-PIF regulatory module coordinates light and temperature control of photosynthetic gene transcription. PLoS Genet **10**: e1004416.

Toledo-Ortiz, G., Kiryu, Y., Kobayashi, J., Oka, Y., Kim, Y., Nam, H.G., Mochizuki, N., and Nagatani, A. (2010). Subcellular sites of the signal transduction and degradation of phytochrome A. Plant Cell Physiol **51**: 1648–1660.

Tossi, V., Lamattina, L., Jenkins, G.I., and Cassia, R.O. (2014). Ultraviolet-B-induced stomatal closure in Arabidopsis is regulated by the UV RESISTANCE LOCUS8 photoreceptor in a nitric oxide-dependent mechanism. Plant Physiol **164**: 2220–2230.

Tsuchida-Mayama, T., Nakano, M., Uehara, Y., Sano, M., Fujisawa, N., Okada, K., and Sakai, T. (2008). Mapping of the phosphorylation sites on the phototropic signal transducer, NPH3. Plant Sci **174**: 626–633.

Turner, A. (2005). The Pseudo-Response Regulator Ppd-H1 Provides Adaptation to Photoperiod in Barley. Science **310**: 1031–1034.

Turner, J.G., Ellis, C., and Devoto, A. (2002). The jasmonate signal pathway. Plant Cell **14 Suppl**: S153-164.

Tuteja, N. and Mahajan, S. (2007). Calcium signaling network in plants: an overview. Plant Signal Behav **2**: 79–85.

Uehlein, N. and Kaldenhoff, R. (2008). Aquaporins and plant leaf movements. Ann Bot **101**: 1–4.

Upchurch, R.G. (2008). Fatty acid unsaturation, mobilization, and regulation in the response of plants to stress. Biotechnol Lett **30**: 967–977.

Untergasser, A., Nijveen, H., Rao, X., Bisseling, T., Geurts, R., and Leunissen, J.A.M. (2007). Primer3Plus, an enhanced web interface to Primer3. Nucleic Acids Res **35**: 71–74.

Valverde, F., Mouradov, A., Soppe, W., Ravenscroft, D., Samach, A., and Coupland, G. (2004). Photoreceptor regulation of CONSTANS protein in photoperiodic flowering. Science **303**: 1003–1006.

Vandenbussche, F., Tilbrook, K., Fierro, A.C., Marchal, K., Poelman, D., Van Der Straeten, D., and Ulm, R. (2014). Photoreceptor-mediated bending towards UV-B in

Arabidopsis. Mol Plant **7**: 1041–1052.

Walley, J., Xiao, Y., Wang, J.-Z., Baidoo, E.E., Keasling, J.D., Shen, Z., Briggs, S.P., and Dehesh, K. (2015). Plastid-produced interorgannellar stress signal MEcPP potentiates induction of the unfolded protein response in endoplasmic reticulum. Proc Natl Acad Sci U S A **112**: 6212–6217.

Walley, J.W., Kliebenstein, D.J., Bostock, R.M., and Dehesh, K. (2013). Fatty acids and early detection of pathogens. Curr Opin Plant Biol **16**: 520–526.

Walter, A., Silk, W.K., and Schurr, U. (2009). Environmental effects on spatial and temporal patterns of leaf and root growth. Annu Rev Plant Biol **60**: 279–304.

Wang, W., Barnaby, J.Y., Tada, Y., Li, H., Tör, M., Caldelari, D., Lee, D., Fu, X.-D., and Dong, X. (2011). Timing of plant immune responses by a central circadian regulator. Nature **470**: 110–114.

Wang, C.-Q., Guthrie, C., Sarmast, M.K., and Dehesh, K. (2014). BBX19 interacts with CONSTANS to repress FLOWERING LOCUS T transcription, defining a flowering time checkpoint in Arabidopsis. Plant Cell **26**: 3589–3602.

Wang, C.-Q., Sarmast, M.K., Jiang, J., and Dehesh, K. (2015). The Transcriptional Regulator BBX19 Promotes Hypocotyl Growth by Facilitating COP1-Mediated EARLY FLOWERING3 Degradation in Arabidopsis. Plant Cell **27**: 1128–1139.

Wang, C. and Dehesh, K. (2015). From retrograde signaling to flowering time. Plant Signal Behav **10**: e1022012.

Wang, L., Fujiwara, S., and Somers, D.E. (2010). PRR5 regulates phosphorylation, nuclear import and subnuclear localization of TOC1 in the Arabidopsis circadian clock. EMBO J **29**: 1903–1915.

Wang, L., Kim, J., and Somers, D.E. (2013). Transcriptional corepressor TOPLESS complexes with pseudoresponse regulator proteins and histone deacetylases to regulate circadian transcription. Proc Natl Acad Sci **110**: 761–766.

Wang, X., Wu, F., Xie, Q., Wang, H., Wang, Y., Yue, Y., Gahura, O., Ma, S., Liu, L., Cao, Y., Jiao, Y., Puta, F., McClung, C.R., Xu, X., and Ma, L. (2012). SKIP is a component of the spliceosome linking alternative splicing and the circadian clock in Arabidopsis. Plant Cell **24**: 3278–3295.

Wang, Y., Wu, J.-F., Nakamichi, N., Sakakibara, H., Nam, H.-G., and Wu, S.-H. (2011). LIGHT-REGULATED WD1 and PSEUDO-RESPONSE REGULATOR9 form a positive feedback regulatory loop in the Arabidopsis circadian clock. Plant Cell **23**: 486–498.

Weller, J.L., Liew, L.C., Hecht, V.F.G., Rajandran, V., Laurie, R.E., Ridge, S., Wenden, B., Vander Schoor, J.K., Jaminon, O., Blassiau, C., Dalmais, M., Rameau, C., Bendahmane, A., Macknight, R.C., and Lejeune-Hénaut, I. (2012). A conserved molecular basis for photoperiod adaptation in two temperate legumes. Proc Natl Acad Sci U S A **109**: 21158–21163.

Wenden, B., Kozma-Bognár, L., Edwards, K.D., Hall, A.J.W., Locke, J.C.W., and Millar, A.J. (2011). Light inputs shape the Arabidopsis circadian system. Plant J **66**: 480–491.

Wenden, B., Toner, D.L.K., Hodge, S.K., Grima, R., and Millar, A.J. (2012). Spontaneous spatiotemporal waves of gene expression from biological clocks in the leaf. Proc Natl Acad Sci U S A **109**: 6757–6762.

Wenkel, S., Turck, F., Singer, K., Gissot, L., Le Gourrierec, J., Samach, A., and

Coupland, G. (2006). CONSTANS and the CCAAT box binding complex share a functionally important domain and interact to regulate flowering of Arabidopsis. Plant Cell **18**: 2971–2984.

Wilkins, O., Bräutigam, K., and Campbell, M.M. (2010). Time of day shapes Arabidopsis drought transcriptomes. Plant J **63**: 715–727.

Wilson, P.B., Estavillo, G.M., Field, K.J., Pornsiriwong, W., Carroll, A.J., Howell, K.A., Woo, N.S., Lake, J.A., Smith, S.M., Harvey Millar, A., von Caemmerer, S., and Pogson, B.J. (2009). The nucleotidase/phosphatase SAL1 is a negative regulator of drought tolerance in Arabidopsis. Plant J **58**: 299–317.

Woelfle, M.A., Ouyang, Y., Phanvijhitsiri, K., and Johnson, C.H. (2004). The adaptive value of circadian clocks: an experimental assessment in cyanobacteria. Curr Biol **14**: 1481–1486.

Wood, N.T., Haley, A., Viry-Moussaïd, M., Johnson, C.H., van der Luit, H.A., and Trewavas, A.J. (2001). The calcium rhythms of different cell types oscillate with different circadian phases. Plant Physiol **125**: 787–96.

Woodson, J.D., Perez-Ruiz, J.M., and Chory, J. (2011). Heme synthesis by plastid ferrochelatase I regulates nuclear gene expression in plants. Curr Biol **21**: 897–903.

Wu, D., Hu, Q., Yan, Z., Chen, W., Yan, C., Huang, X., Zhang, J., Yang, P., Deng, H., Wang, J., Deng, X., and Shi, Y. (2012). Structural basis of ultraviolet-B perception by UVR8. Nature **484**: 214–219.

Wu, J.-F., Tsai, H.-L., Joanito, I., Wu, Y.-C., Chang, C.-W., Li, Y.-H., Wang, Y., Hong, J.C., Chu, J.-W., Hsu, C.-P., and Wu, S.-H. (2016). LWD-TCP complex activates the morning gene CCA1 in Arabidopsis. Nat Commun **7**: 13181.

Wyka, T.P., Duarte, H.M., and Lüttge, U.E. (2005). Redundancy of stomatal control for the circadian photosynthetic rhythm in Kalanchoë daigremontiana Hamet et Perrier. Plant Biol **7**: 176–181.

Xiao, Y., Savchenko, T., Baidoo, E.E.K., Chehab, W.E., Hayden, D.M., Tolstikov, V., Corwin, J.A., Kliebenstein, D.J., Keasling, J.D., and Dehesh, K. (2012). Retrograde signaling by the plastidial metabolite MEcPP regulates expression of nuclear stress-response genes. Cell **149**: 1525–1535.

Xiao, Y., Wang, J., and Dehesh, K. (2013). Review of stress specific organelles-to-nucleus metabolic signal molecules in plants. Plant Sci **212**: 102–107.

Xie, Q., Lou, P., Hermand, V., Aman, R., Park, H.J., Yun, D.-J., Kim, W.Y., Salmela, M.J., Ewers, B.E. Weinig, C., Khan, S.L., Schaible, D.L.P., and McClung, C.R. (2015). Allelic polymorphism of GIGANTEA is responsible for naturally occurring variation in circadian period in Brassica rapa. Proc Natl Acad Sci U S A **112**: 3829–3834.

Xiong, L., Lee, H., Huang, R., and Zhu, J.K. (2004). A single amino acid substitution in the Arabidopsis FIERY1/HOS2 protein confers cold signaling specificity and lithium tolerance. Plant J **40**: 536–545

Xiong, L., Lee Bh, Ishitani, M., Lee, H., Zhang, C., and Zhu, J.K. (2001). FIERY1 encoding an inositol polyphosphate 1-phosphatase is a negative regulator of abscisic acid and stress signaling in Arabidopsis. Genes Dev **15**: 1971–1984.

Yakir, E., Hassidim, M., Melamed-Book, N., Hilman, D., Kron, I., and Green, R.M. (2011). Cell autonomous and cell-type specific circadian rhythms in Arabidopsis. Plant J **68**: 520–531.

Yakir, E., Hilman, D., Hassidim, M., and Green, R.M. (2007). CIRCADIAN CLOCK ASSOCIATED1 transcript stability and the entrainment of the circadian clock in Arabidopsis. Plant Physiol **145**.

Yakir, E., Hilman, D., Kron, I., Hassidim, M., Melamed-Book, N., and Green, R.M. (2009). Posttranslational regulation of CIRCADIAN CLOCK ASSOCIATED1 in the circadian oscillator of Arabidopsis. Plant Physiol **150**: 844–857.

Yang, H.Q., Wu, Y.J., Tang, R.H., Liu, D., Liu, Y., and Cashmore, A.R. (2000). The C termini of Arabidopsis cryptochromes mediate a constitutive light response. Cell **103**: 815–827.

Yang, J., Lin, R., Sullivan, J., Hoecker, U., Liu, B., Xu, L., Deng, X.W., and Wang, H. (2005). Light regulates COP1-mediated degradation of HFR1, a transcription factor essential for light signaling in Arabidopsis. Plant Cell **17**: 804–821.

Ye, J., Coulouris, G., Zaretskaya, I., Cutcutache, I., Rozen, S., and Madden, T.L. (2012). Primer-BLAST: A tool to design target-specific primers for polymerase chain reaction. BMC Bioinformatics **13**: 134.

Yu, J., Rubio, V., Lee, N.-Y., Bai, S., Lee, S.-Y., Kim, S., Liu, L., Zhang, Y., Irigoyen, M.L., Sullivan, J.A., Zhang, Y., Lee, I., Xie, Q., Paek, N., and Deng, X.W. (2008). COP1 and ELF3 control circadian function and photoperiodic flowering by regulating GI stability. Mol Cell **32**: 617–630.

Yu, X., Sayegh, R., Maymon, M., Warpeha, K., Klejnot, J., Yang, H., Huang, J., Lee, J., Kaufman, L., and Lin, C. (2009). Formation of nuclear bodies of Arabidopsis CRY2 in response to blue light is associated with its blue light-dependent degradation. Plant Cell **21**: 118–130.

Zakhrabekova, S., Gough, S.P., Braumann, I., Müller, A.H., Lundqvist, J., Ahmann, K., Dockter, C., Matyszczak, I., Kurowska, M., Druka, A., Waugh, R., Graner, A., Stein, N., Steuernagel, B., Lundqvist, U., and Hansson, M. (2012). Induced mutations in circadian clock regulator Mat-a facilitated short-season adaptation and range extension in cultivated barley. Proc Natl Acad Sci U S A **109**: 4326–4331.

Zakrzewska-Placzek, M., Souret, F.F., Sobczyk, G.J., Green, P.J., and Kufel, J. (2010). Arabidopsis thaliana XRN2 is required for primary cleavage in the pre-ribosomal RNA. Nucleic Acids Res **38**: 4487–4502.

Zerr, D.M., Hall, J.C., Rosbash, M., and Siwicki, K.K. (1990). Circadian fluctuations of period protein immunoreactivity in the CNS and the visual system of Drosophila. J Neurosci **10**: 2749–2762.

Zhang, J.,Vanneste, S.,Brewer, P.B., Michniewicz, M., Grones, P., Kleine-Vehn, J., Löfke, C., Teichmann, T., Bielach, A., Cannoot, B., Hoyerová, K., Chen, X., Xue, H.-W., Benková, E., Zažímalová, E., and Friml, J. (2011). Inositol trisphosphate-induced Ca^{2+} signaling modulates auxin transport and PIN polarity. Dev Cell **20**: 855–866.

Zhang, X., Zhu, Y., Liu, X., Hong, X., Xu, Y., Zhu, P., Shen, Y., Wu, H., Ji, Y.,Wen, X., Zhang, C., Zhao, Q., Wang, Y., Lu, J., and Guo, H. (2015). Suppression of endogenous gene silencing by bidirectional cytoplasmic RNA decay in Arabidopsis. Science **348**: 120–123.

Zhang, X., Chen, Y., Wang, Z.-Y., Chen, Z., Gu, H., and Qu, L.-J. (2007). Constitutive expression of CIR1 (RVE2) affects several circadian-regulated processes and seed germination in Arabidopsis. Plant J **51**: 512–525.

Zhu, J.-Y., Oh, E., Wang, T., and Wang, Z.-Y. (2016). TOC1-PIF4 interaction mediates the circadian gating of thermoresponsive growth in Arabidopsis. Nat Commun **7**: 13692.

Zikihara, K., Iwata, T., Matsuoka, D., Kandori, H., Todo, T., and Tokutomi, S. (2006). Photoreaction cycle of the light, oxygen, and voltage domain in FKF1 determined by low-temperature absorption spectroscopy. Biochemistry **45**: 10828–10837.

Zuo, Z., Liu, H., Liu, B., Liu, X., and Lin, C. (2011). Blue light-dependent interaction of CRY2 with SPA1 regulates COP1 activity and floral initiation in Arabidopsis. Curr Biol **21**: 841–847.

Appendix I

Table 8.1 Primers used for DNA cloning reactions.

clo_AHL genomic F	CAGCTCCTGATAAGAGGTTTTAATATG
clo_AHL genomic R	GAGACTGGAAGATTCCCAAC
clo_FRY1 genomic F	CCCTGCAGCACAAGAACC
clo_FRY1 genomic R	GAGAGCTGAAGCTTTCTCTTGC
clo_FRY1ox_F	CACCATGATGTCTATAAATTGTTTTCG
clo_FRY1ox_R	GAGAGCTGAAGCTTTCTCTTGCC
clo_pGWB4 F	TAATTTCCGTCAATATTTACCTTCC
GW1	GTTGCAACAAATTGATGAGCAATGC
GW2	GTTGCAACAAATTGATGAGCAATGC
pUB-Dest F	CGATTTTCTGGGTTTGATCG
pUB-Dest R	ACTGGTGATTTTTGCGGACT
seq_FRY1 1256R	TTGGAAGATTTACAAAATGGGTTT
seq_FRY1 1879F	CTGAAGGTGGTCCAAATGGT
seq_FRY1 5' into vector	GGCGTGTGAGAGAGCAAA
seq_FRY1 878F	TCTGCAATCAGAAAATGTGAAGA
seq_GFP F	TATATCATGGCCGACAAGCA
seq_GFP R	GAACTCCAGCAGGACCATGT
seq_pEG103_F	GGATTCCATTGCCCAGCTA
seq_pEG103_mGFP_R	CATCCATGCCATGTGTAATCC
seq_pGWB41_F	AGAGAACACGGGGGACTCTAG

DNA oligonucleotides used to prime PCR and DNA sequencing reactions are listed. All primer sequences are given in the 5'-3' orientation.

Table 8.2 Primers used for PCR reactions to analyse splicing of transcripts.

PCR_CCA1_Ex1_F	AAATTCGTCTGGAGAAGATCTGG
PCR_CCA1_Ex7_R	GGAAGCTTGAGTTTCCAACC
PCR_ELF4_3'ext_R	GGTCCAACTAAGAAGAAACAATTTGA
PCR_ELF4_Ex1_F	ATGAAGAGGAACGGCGAGA
PCR_ELF4_Ex1_R	TAAGCTCTAGTTCCGGCAGCA
PCR_LHY_Ex1_F	ATCTGGAGAAGAATTATTAGCTAAGGT
PCR_LHY_Ex7_R	GAAGCTTCTCCTTCCAATCG
PCR_LHY_I5_F	AACGAATTGAAGAACATATTGGGAC
PCR_LHY_I5_R	CCAGTTGATGTTTTCTCAGAGAACG
PCR_PRR5_3'ext_R	TCTAGTTGATGATACAAAATTGAACTG
PCR_PRR5_Ex1_F	GCCACGTCAGCCAATTC
PCR_PRR5_Ex6_R	CTATGGAGCTTGTGTGGATTG
PCR_PRR9_Ex1_F	ATGGGGGAGATTGTGGTT
PCR_PRR9_Ex7_R	ACGAACTGGCCTTTCACTC
PCR_PRR9_I3_F	TTTTGCTCTGCTTGCTTTGG
PCR_PRR9_I3_R	ATGAGCAGTAGGATCATCAC
PCR_TOC1_Ex1_F	ATGGATTTGAACGGTGAGTG
PCR_TOC1_Ex1_R	TCAAGTTCCCAAAGCATCA
PCR_TOC1_I4_F	GAAGTCCCTGTCGTTGTAAAGTG
PCR_TOC1_I4_R	TGTTCCATCAGCACCAAGACC

DNA oligonucleotides used to prime PCR reactions are listed. All primer sequences are given in the 5'-3' orientation.

Table 8.3 Primers used for PCR reactions for screening and genotyping *Arabidopsis* mutants.

apk1-1 LP	TTGGTGGGCCTAATAAATTCC
apk1-1RP	GATTCAAAGCACAAGCCAAAG
apk2-1 LP	CCTTTCAGGTTCTCCCATCTC
apk2-1 RP	ATCATTCACGTGACGAACCTC
fou8_LP	TGCATTGCATCTGTAATTGG
fou8_RP	TCTAATCAGGGACAGGTATAACAAACTGA
FRY1_transgene_F	CATCCATGGCTTACGAGAAAGAG
FRY1_transgene_G	ACTGGTGATTTTTGCGGACTC
fry1-6 LP	CTTCGAATGACTCGAAGAACG
fry1-6 RP	TTTTCGATTCAATCATGACCC
FRY1-OX LP	GAGACCTGATCCAAACTGCTG
FRY1-OX RP	TACAAATGATTGAAGCGGAGC
LB-1	TAGCATCTGAATTTCATAACCAATCTCGATACAC
LB1.3b	ATTTTGCCGATTTCGGAAC
xrn2-1_LB	CATCTCGTATCCGAGGAGGA
xrn2-1_RB	GGATGACCAGAAACTGACCA
xrn3-3_LB	GCCTTCGATTTCAACAGGC
xrn3-3_RB	GAAATCGAACACAAATCCG
xrn4-6_LB	GGGGAATCCACTCTAGTTTGG
xrn4-6_RB	TGTGGGCCTCTATGGTGATGT

DNA oligonucleotides used to prime PCR reactions are listed. All primer sequences are given in the 5'-3' orientation.

Table 8.4 Primers used for qRT-PCR reactions.	
Actin2A	ACCTTGCTGGACGTGACCTTACTGAT
Actin2B	GTTGTCTCGTGGATTCCAGCAGCTT
CCA1 F	CAGCTCCAATATAACCGATCCAT
CCA1 R	CAATTCGACCCTCGTCAGACA
HSFA R	GCTTCTATCTTTCTGAAACCATAAGT
HSFA7	TTGCATTCTTTCTCCACGATTC
PP2a qPCR F	TAACGTGGCCAAAATGATGC
PP2a qPCR R	GTTCTCCACAACCGATTGGT
qPCR GI R	GCTGGTAGACGACACTTCAATAGATT
qPCR_4CL1_F	GCTGTTGTCGCAATGAAAGAA
qPCR_4CL1_R	TTGCTTCACATCATCTTCTGATAACT
qPCR_ACT2_F	CCAAGCAGCATGAAGATTAAGG
qPCR_ACT2_R	GAGATCCACATCTGCTGGAATG
qPCR_APR1_F	GCTTGCTAAGAAGTTAGAGAATGCTT
qPCR_APR1_R	TCTGCACCACTAAATGCAATG
qPCR_APX2 F	CCATTTGTTGAAAAATATGCTG
qPCR_APX2 R	AGCAAACCCGAGTTCTGACA
qPCR_CAB2 F	GCCTCAACAATGGCTCTCTC
qPCR_CAB2 R	GCTTGGCAACAGTCTTCCTC
qPCR_CCA1_5'ext_F	TGATGTTAAGATGGACAAGAATGTAAC
qPCR_CCA1_5'ext_R	TTTCGAGGCTACAAAAGAAACTG
qPCR_CCA1_Ex2-3_F	AGATTGAAGAACATGTAGCAACAAAA
qPCR_CCA1_Ex4_R	ACCTTTAGCTTCAGCCTCTTTCT
qPCR_CCA1_I4_R	ACATCATTTCAAAATTAACCGATTTTA
qPCR_CCR2 F	TCGTTAATGATCTTGGAATCAAT
qPCR_CCR2 R	GTATCGGTGCTTCGTTGGA
qPCR_ELF3_new_F	GATGATGTTGTGGGTATATTAGGTC
qPCR_ELF3_new_R	CAATAAGTTTTTGAACCTTAATCAGTCT
qPCR_ELF4 F new	GGGAGAATCTTGACCGGAAT
qPCR_ELF4 R new	CAAAGCAACGTTCTTCGACA
qPCR_ELF4_3'ext_F	TGACTTTTCACTAGGCTGTGTATTAGA
qPCR_ELF4_3'ext_R	TACTGCAGTTTCTGTTTGCTTTTT
qPCR_FRY1 F	GGTGGCTGAAGAGGACTCAG
qPCR_FRY1 R	TCCTCGGTAGCCAAAGTGTC
qPCR_GI F	ACTAGCAGTGGTCGACGGTTTATC
qPCR_HyPer F	GTGCCACCAGAGAGGAAGAG

qPCR_HyPer R	ATGGTGAACCTGGCCTGTAG
qPCR_LHY F	CAATGCAACTACTGATTCGTGGAA
qPCR_LHY R	GCTATACGACCCTCTTCGGAGAC
qPCR_lux F2	GCACATCATATGGGTATGCAA
qPCR_lux R	GACACCAAGAACCATTTCCAC
qPCR_pEG103GFP_R	CCATCTCGAGCACCACTTTG
qPCR_PRR5 F	ATTCCGAATGAAGCGAAAGGA
qPCR_PRR5 R	TCGTAACGAACCTTTTTCTCATAACAT
qPCR_PRR5_3'ext_F	AAGCTATAGTGAGATCAAAACTTCTGG
qPCR_PRR5_3'ext_R	ATATGTTCATAATCATCTTCTTCGTTT
qPCR_PRR7_F	GAATGTGCTGAGGCGTTCAGA
qPCR_PRR7_R	GGCTGGATTATACCTTGAGAAAGC
qPCR_PRR9 Exon 4 F	ATATCATTCAGATCAAGGAAGTGGTG
qPCR_PRR9 Exon 5 R	TCAAATCCATTGTCACATCAAAAGTT
qPCR_PRR9 F	GTTGAAGAGGAAAGATCGATGCTT
qPCR_PRR9 Intron4-5 R	ATGCAATCTCAAGATGAAAATCTCAC
qPCR_PRR9 R	CTGCTCTGGTACCGAACCTTTT
qPCR_PRR9_newF	GAAACAACGTTGGAGTAGAAGC
qPCR_PRR9_newR	CTCTGGTACCGAACCTTTTTG
qPCR_SAL1_F2	GTTACAGAGGCGGGTGGAATAGT
qPCR_SAL1_R2	GCAACGATAATGCCTGTGTCC
qPCR_SIG5 F	GTGTTGGAGCTAATAACAGCAGACA
qPCR_SIG5 R	TGTCGAATAACCAGACTCTCTTTCG
qPCR_STN7 F	GGACTACAGTGAAGCAGCAAAT
qPCR_STN7 R	AGGCTCTTTCTCCCTGAGTTC
qPCR_SULTR42_F	GCTACGAGAATATGAAGTTGCTATCG
qPCR_SULTR42_R	TGTATGTGACAGGAGACATTTCCA
qPCR_TOC1_newF	AATCCAGCGCAATTTTCTTC
qPCR_TOC1_newR	CGTTAGTTCTAAGGACAGTAGATTTGA
TOC1 F	AATAGTAATCCAGCGCAATTTTCTTC
TOC1 R	CTTCAATCTACTTTTCTTCGGTGCT

DNA oligonucleotides used to prime PCR reactions are listed. All primer sequences are given in the 5'-3'orientation

Appendix II

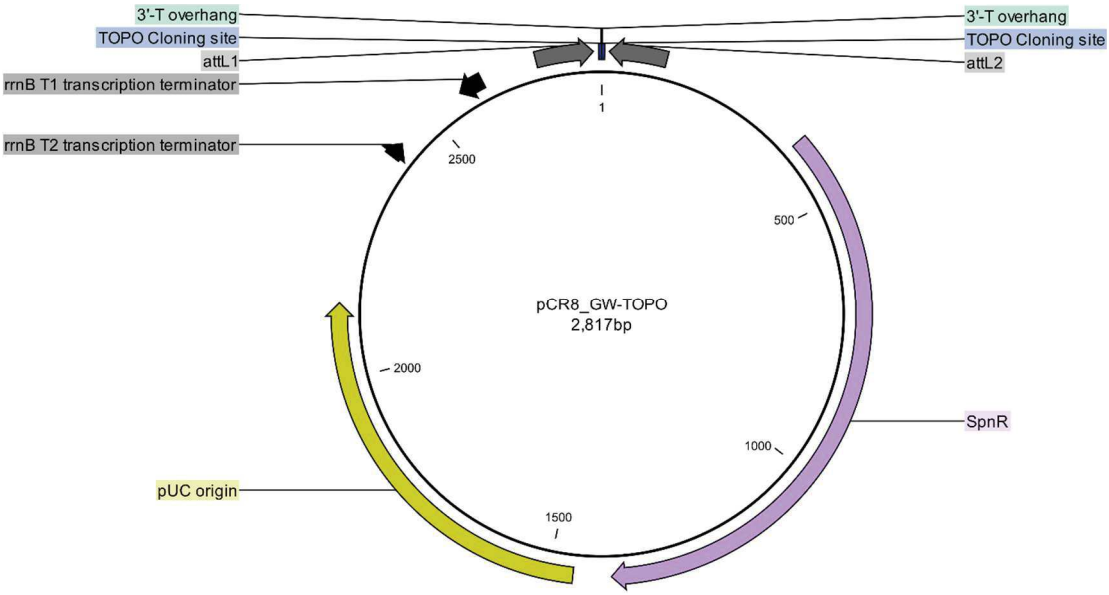

Figure 9.1 Map of the pCR™8/GW/TOPO® entry vector (Invitrogen). TOPO® cloning site with 3'-T overhangs, *att*L1 and *att*L2 regions; pUC origin, *rrnB* T1 and *rrnB* T2 transcription termination sequences, and Spectinoycin resistance gene (SpnR) for bacterial selection are shown**.**

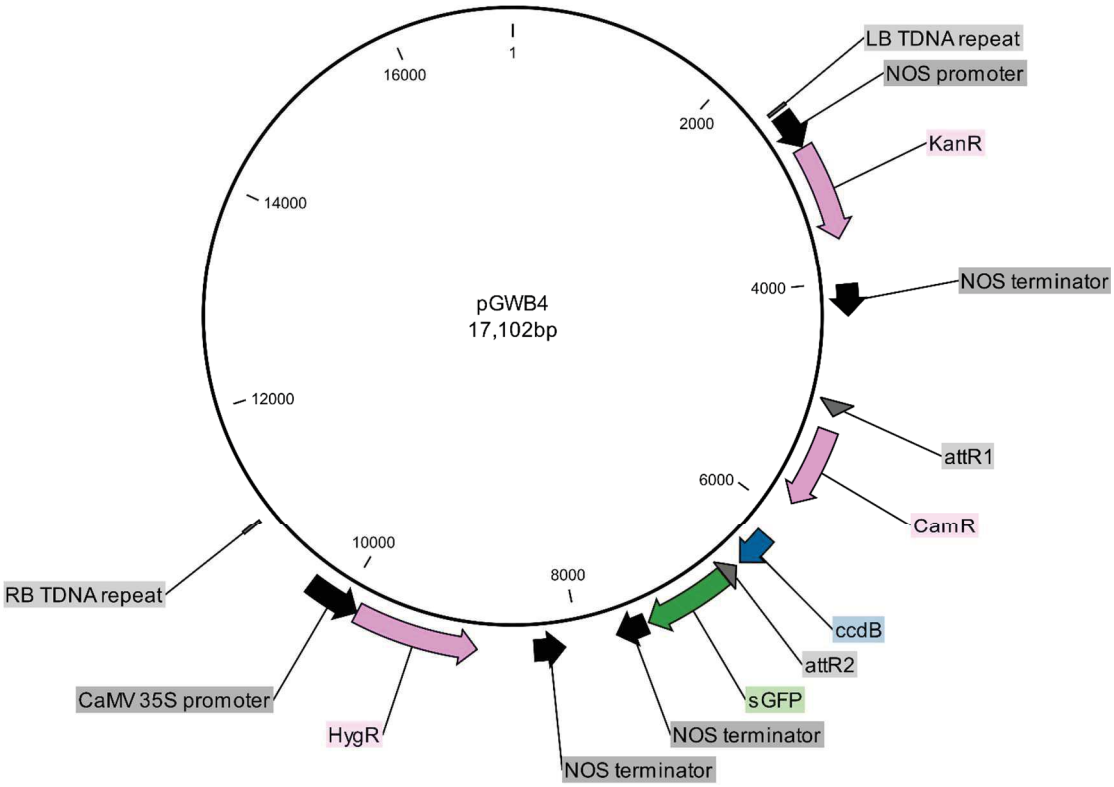

Figure 9.2 Map of the Gateway®-compatible vector pGWB4 (Nakagawa et al., 2007, 2009). Left border (LB) and right border (RB) sequences for *Agrobacterium*-mediated T-DNA transfer; Gateway® cloning cassette with attR1 and attR2 regions, Chlamphenicol resistance gene (CmR), and the *ccdB* killer gene; green fluorescent protein (sGFP) with 6x-Histidine for C-terminal fusion, with NOS terminator region; bacterial Kanamycin resistance gene (Kan) for microbial selection, with NOS promoter and NOS terminator regions; Hygromycin herbicide resistance gene (HygR) with Cauliflower Mosaic Virus 35S promoter (CaMV 35S) and NOS terminator regions for selection of transgenic plants are shown.

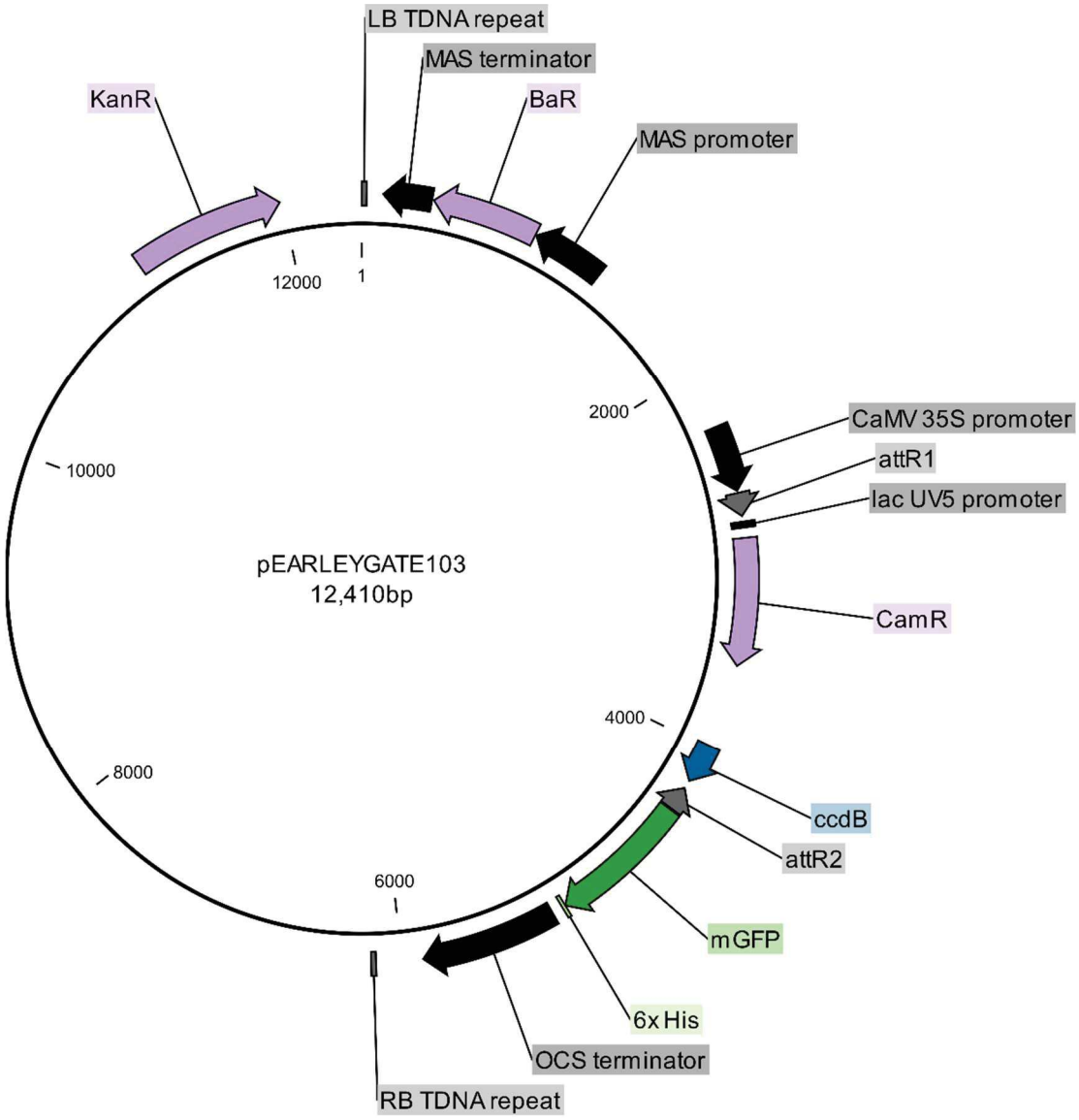

Figure 9.3 Map of the Gateway®-compatible vector pEarleyGate103 (Earley et al., 2006). Left border (LB) and right border (RB) sequences for *Agrobacterium*-mediated T-DNA transfer; Gateway® cloning cassette with attR1 and attR2 regions, lac UV5 promoter, Chlamphenicol resistance gene (CmR), and the *ccdB* killer gene; green fluorescent protein (mGFP) with 6x-Histidine for C-terminal fusion, with OCS terminator region; bacterial Kanamycin resistance gene (Kan) for microbial selection; Basta herbicide resistance gene (BaR) with MAS promoter and MAS terminator for selection of transgenic plants are shown.

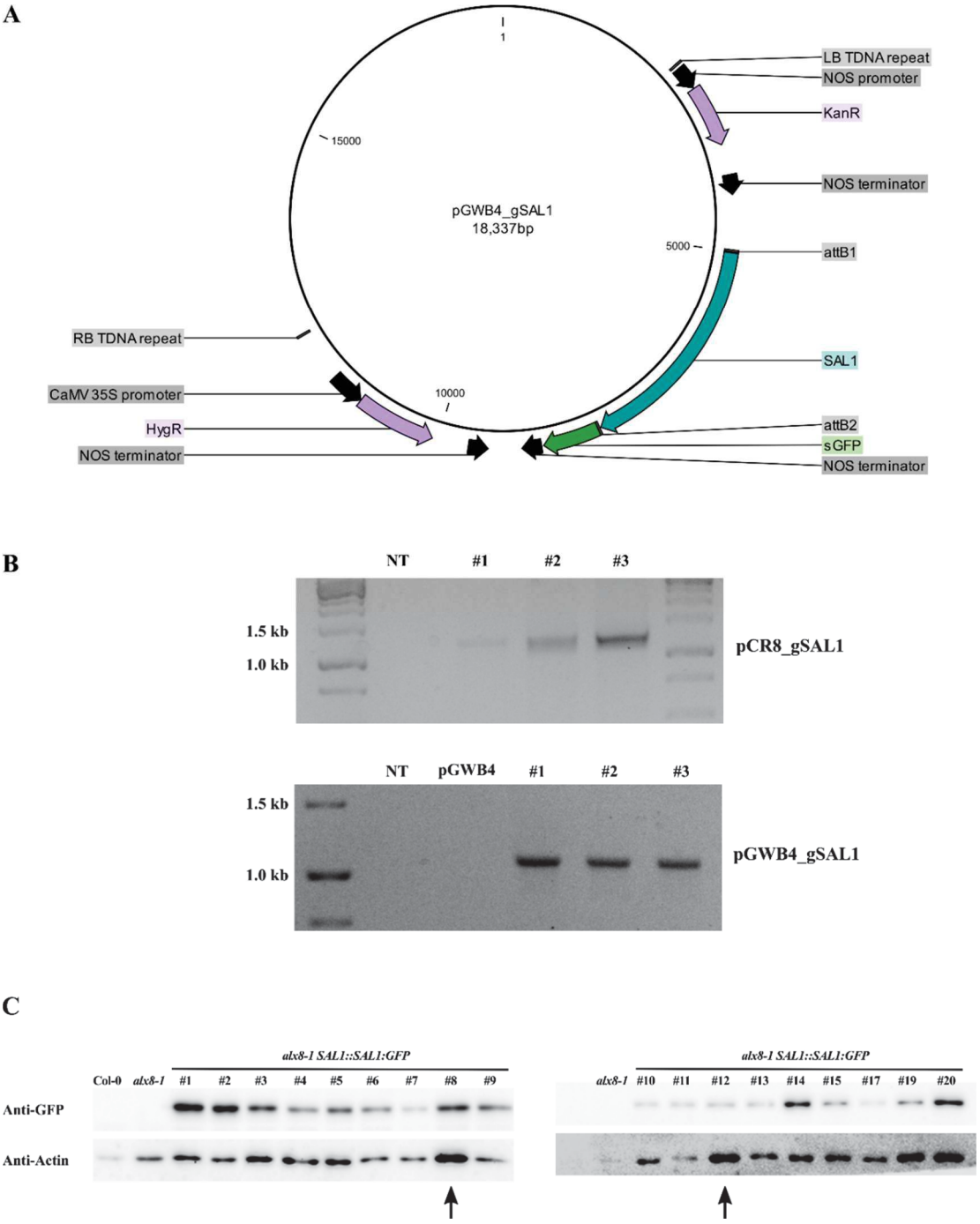

Figure 9.4 Preparation of *alx8-1* SAL1::SAL1-GFP lines (A) Map of vector constructed from Gateway®cloning of SAL1 gDNA into the Gateway® vector pGWB4 (Nakagawa et al., 2007, 2009). Left border (LB) and right border (RB) sequences for *Agrobacterium*-mediated T-DNA transfer; attB1 and attB2 regions; green fluorescent protein (sGFP) with 6x-Histidine for C-terminal fusion, with NOS terminator region; bacterial Kanamycin resistance gene (Kan) for microbial selection, with NOS promoter and NOS terminator regions; Hygromycin herbicide resistance gene (HygR) with Cauliflower Mosaic Virus 35S promoter (CaMV 35S) and NOS terminator regions for selection of transgenic plants are shown. **(B)** PCR amplification of SAL1 gDNA following cloning into the pCR™8/GW/TOPO® entry vector (top) and pGWB4 (bottom) vectors. Reactions using independent clones, empty vector backbones and non-template controls are shown (NT) **(C)** Immunoblot analysis of SAL1 expression levels in independent homozygous T3 ***alx8-1 SAL1::SAL1-GFP*** lines. Arrows indicate lines selected for use in the study.

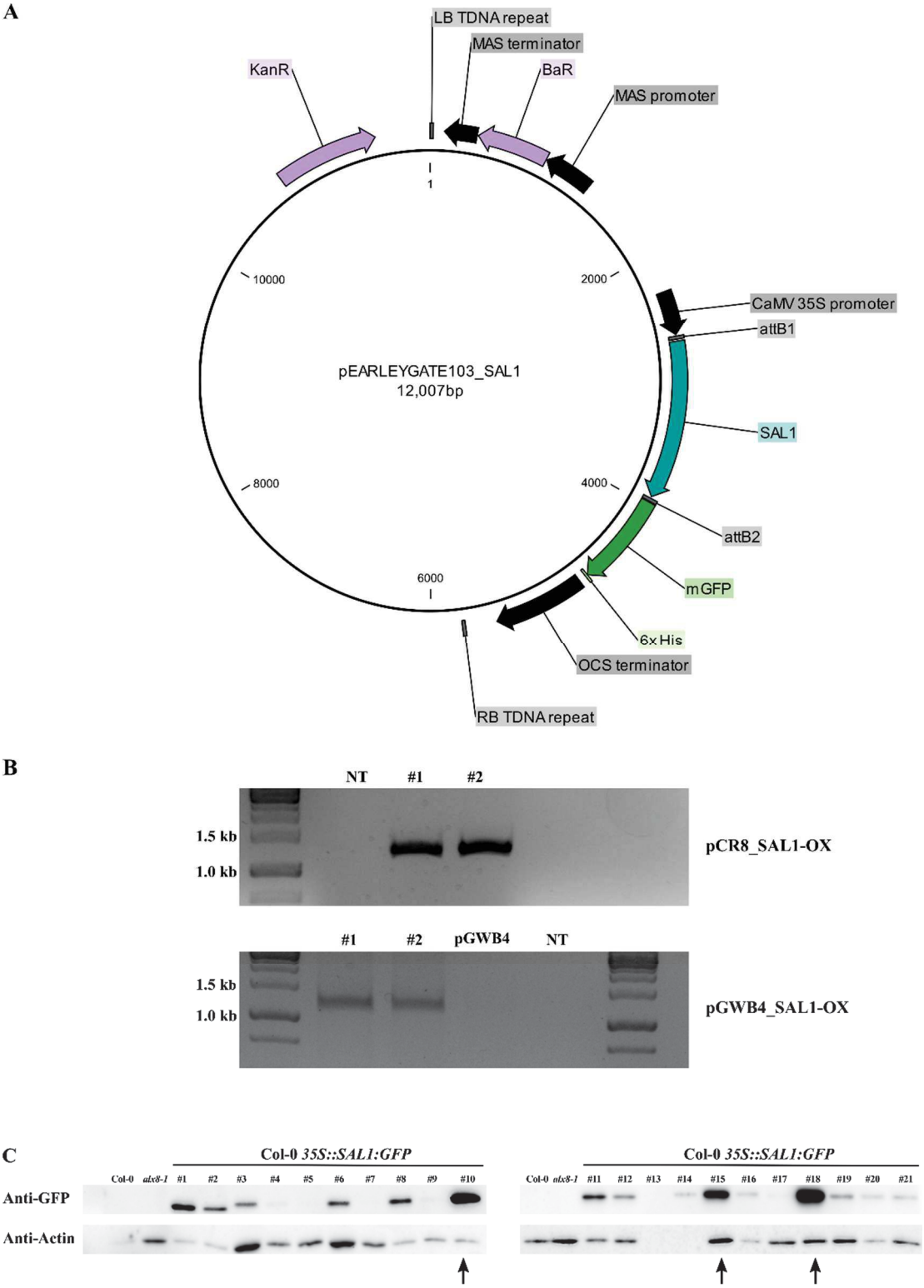

Figure 9.5 Preparation of Col-0 SAL1-OX lines (A) Map of vector constructed from Gateway®cloning of SAL1 cDNA into pEarleyGate103 (Earley et al., 2006). Left border (LB) and right border (RB) sequences for *Agrobacterium*-mediated T-DNA transfer; attB1 and attB2 regions; Cauliflower Mosaic Virus 35S promoter (35S) and OCS terminator regions; SAL1 cDNA; green fluorescent protein (mGFP) with 6x-Histidine for C-terminal fusion; bacterial Kanamycin resistance gene (Kan) for microbial selection; Basta herbicide resistance gene (BaR) with MAS promoter and MAS terminator for selection of transgenic plants are shown. **(B)** PCR amplification of SAL1cDNA following cloning into the pCR™8/GW/TOPO® entry vector (top) and pEarleyGate103 (bottom) vectors. Reactions using independent clones, empty vector backbones and non-template controls are shown (NT) **(C)** Immunoblot analysis of SAL1 expression levels in independent homozygous T2 Col-0 SAL1-OX lines. Arrows indicate lines selected for use in the study.

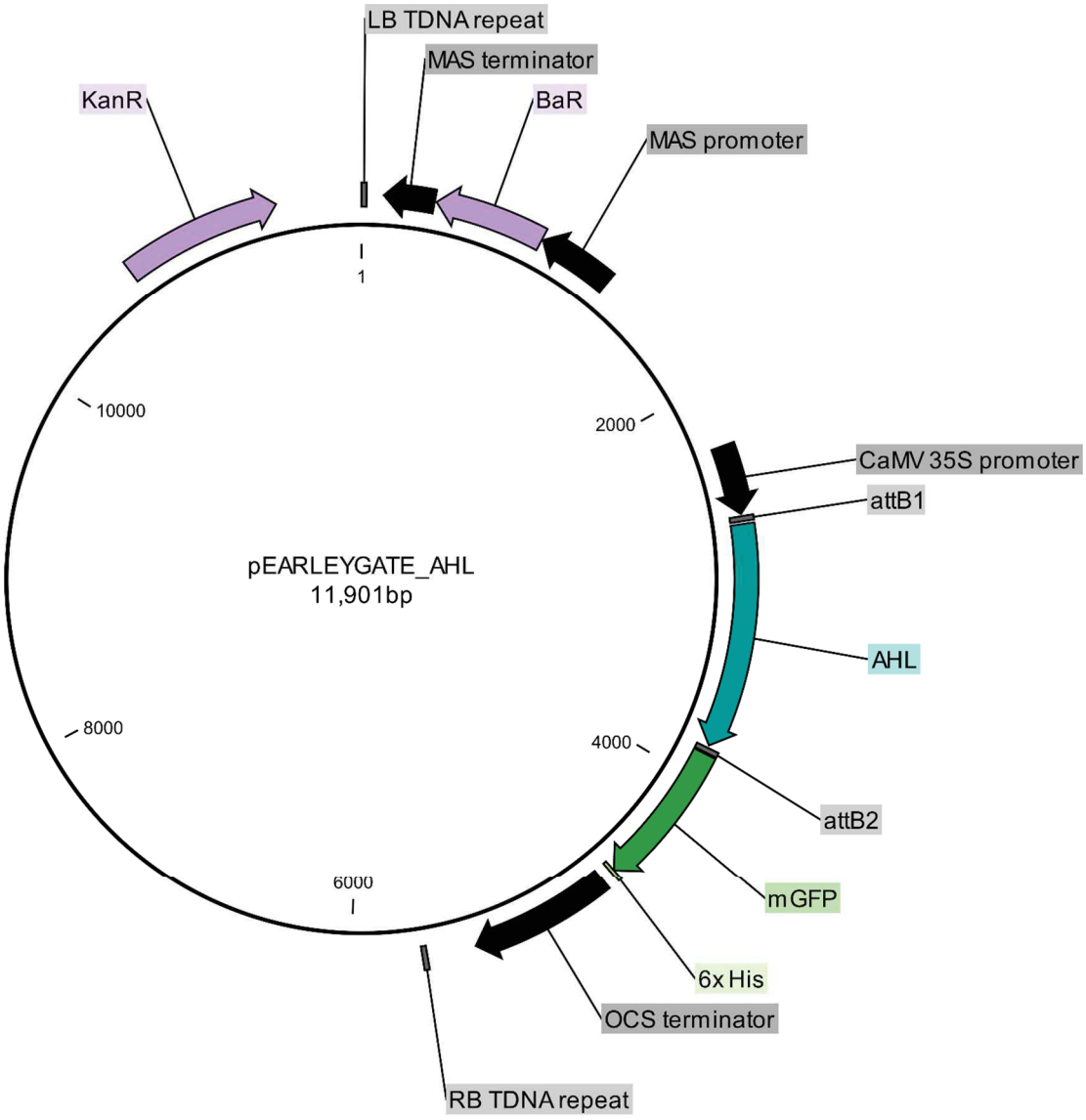

Figure 9.6 Map of vector constructed from Gateway®cloning of AHL cDNA into pEarleyGate103 (Earley et al., 2006). Left border (LB) and right border (RB) sequences for *Agrobacterium*-mediated T-DNA transfer; attB1 and attB2 regions; Cauliflower Mosaic Virus 35S promoter (35S) and OCS terminator regions; AHL cDNA; green fluorescent protein (mGFP) with 6x-Histidine for C-terminal fusion; bacterial Kanamycin resistance gene (Kan) for microbial selection; Basta herbicide resistance gene (BaR) with MAS promoter and MAS terminator for selection of transgenic plants are shown.

Appendix III

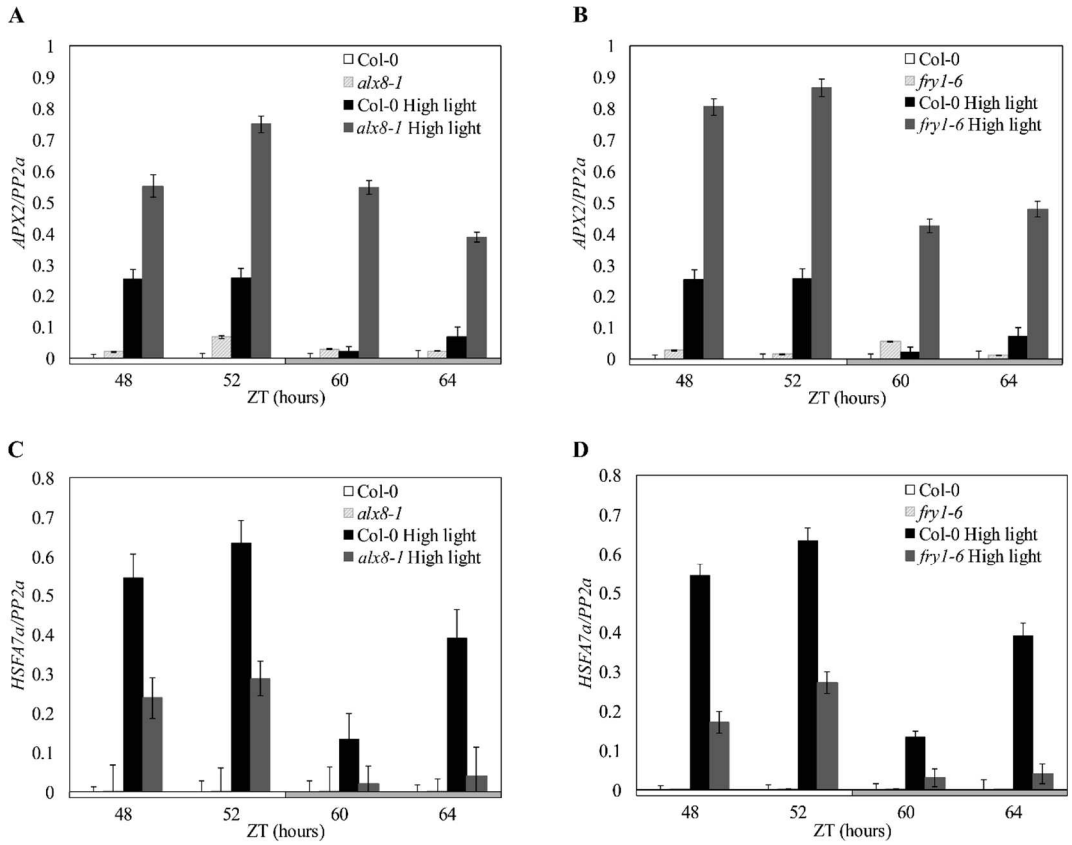

Figure 10.1 Accumulation of stress-gene transcripts following high light treatments at different times of day. Transcript levels for **(A-B)** *APX2* and **(C-D)** *HSFA7* in Col-0, *alx8-1* (left) and *fry1-6* (right) after high light stress treatment was applied at different times of day. Seedlings were grown on 0.5x MS media for 10 days in 12h:12h light:dark cycles under 60 µmol.m^{-2}.s^{-1} white light, before being transferred to constant white light. After 48 hours in free-run, seedlings were treated with 1 000 µmol.m^{-2}.s^{-1} white light for **(A-B)** 60 minutes or **(C-D)** 30 minutes at subjected dawn (ZT48), subjective midday (ZT52), subjective dusk (ZT60) or subjective mid-night (ZT64), using an IsoLight system (Technologica, Essex, UK). Data for each gene were normalised to an internal control (PP2a). and again to highest value for each gene. Error bars indicate standard error of the mean for three technical replicates.

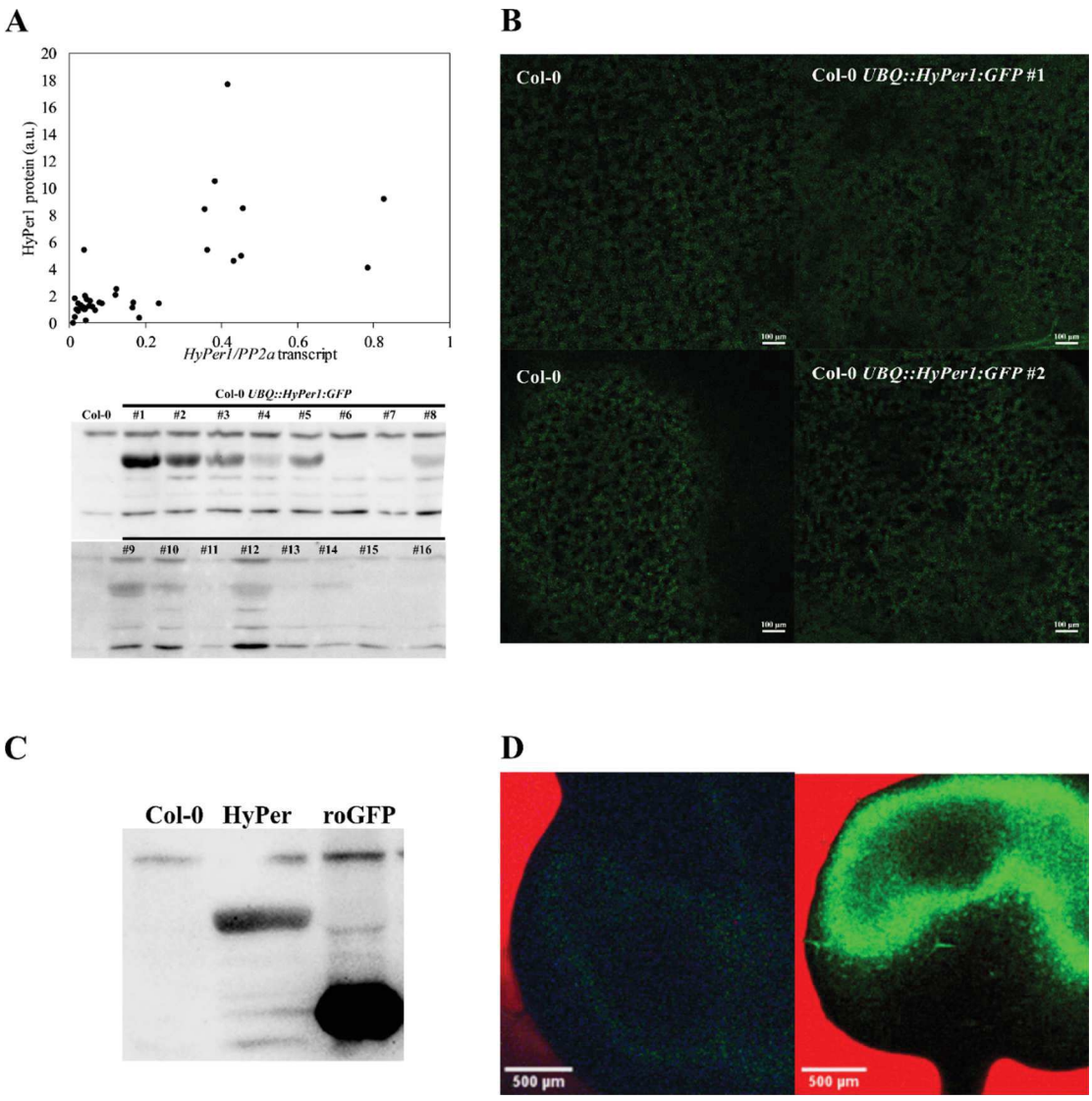

Figure 10.2 Expression of ROS-sensitive biosensors in *Arabidopsis*. (A) Plot showing transcript and protein levels quantified (top) and immunoblot analysis, using Anti-GFP, of protein (bottom) from various independent homozygous T3 lines expressing the *HyPer1* gene (Belousov et al., 2006) under control of the Ubiquitin promoter in a Col-0 background (Col-0 *UBQ::HyPer1:GFP*). **(B)** Confocal laser scanning microscopy images of leaves of Col-0 (left) and 2 independent Col-0 *UBQ::HyPer:GFP* lines showing green (GFP) channel images. **(C)** Immunoblot analysis, using Anti-GFP, of 20 µg protein from Col-0, Col-0 *UBQ::HyPer:GFP* line #1 and *Arabidopsis* expressing roGFP2 (Schwarzländer et al., 2008; Marty et al., 2009). **(D)** Confocal laser scanning microscopy images of leaves of Col-0 (left) and *Arabidopsis* expressing roGFP2 showing green (GFP) channel images. Seedlings were grown on 0.5x MS media in 12h:12h light:dark cycles under 60 µmol.m^{-2}.s^{-1} white light for 12 days before analysis or imaging.

Appendix IV

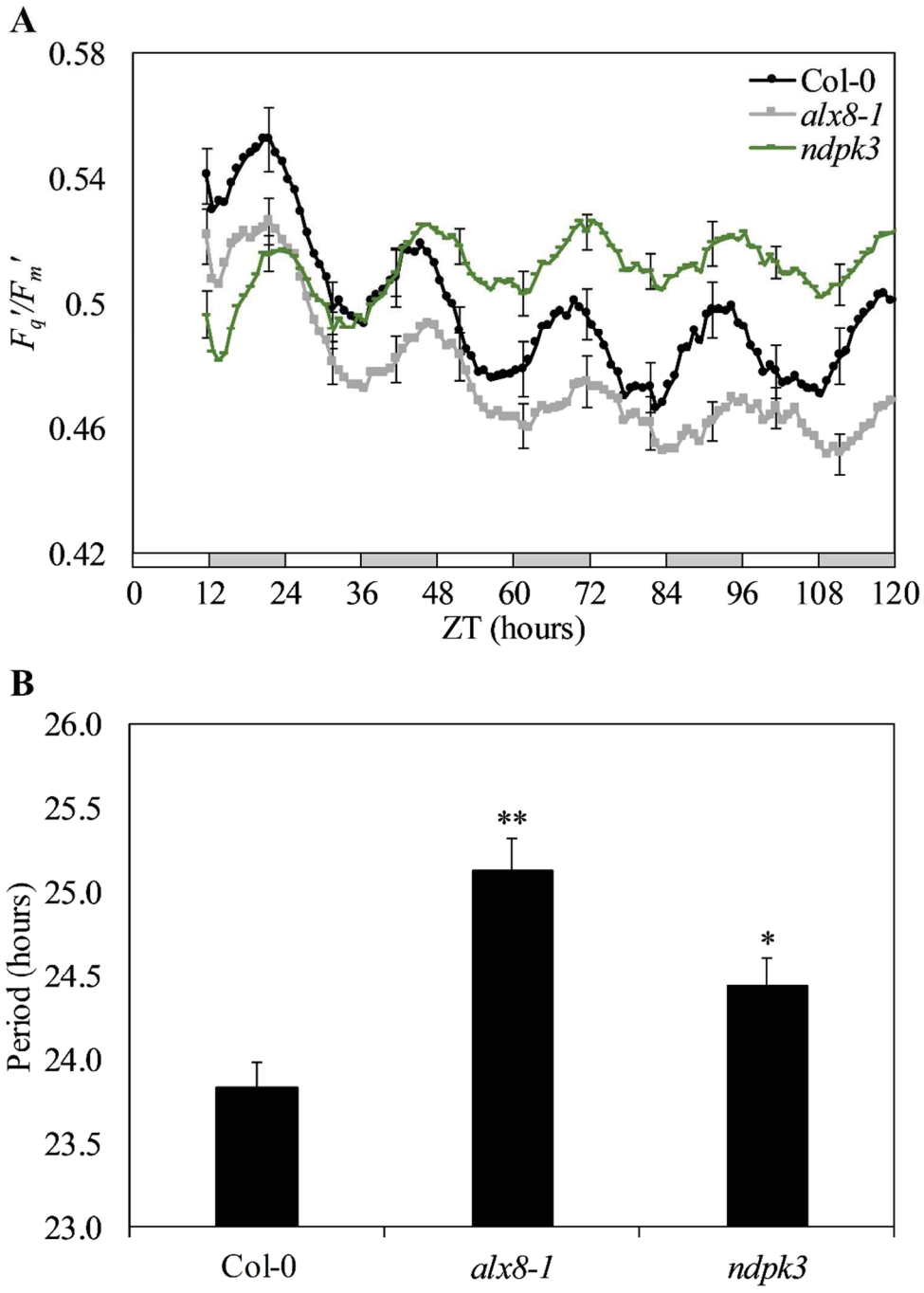

Figure 11.1 F_q'/F_m' rhythms in *sal1* and *ndpk3* mutants under constant blue light. **(A)** Waveforms and **(B)** circadian period estimates for F_q'/F_m' oscillations in Col-0, *alx8-1*, *ndpk3* seedlings under constant blue light. Seedlings were grown on 0.5x MS agar plates and entrained in 12h:12h light:dark cycles under 60 µmol.m^{-2}.s^{-1} white light for 12 days before imaging under 20 µmol.m^{-2}.s^{-1} constant blue light. White bars and grey bars indicate subjective day and subjective night, respectively. Error bars indicate standard error of the mean, with n=8. For waveforms, error bars are shown every 10 hours for clarity. Data from one of two independent experiments are shown. Asterisks indicate statistically significant difference in period compared to Col-0 control (** p<0.001; * p<0.01; Student's T-test).